



# Molecular Recognition of Biotin Derivatives

A thesis submitted for the degree of

Doctor of Philosophy

by

Yu-Lin Jiang B.Sc. (Mas)



**ADELAIDE  
UNIVERSITY**  
AUSTRALIA

The Department of Chemistry  
The University of Adelaide  
November 1999

# Contents

## Abstract

---

## Statement

---

## Acknowledgments

---

## List of Abbreviations

---

## Chapter 1

---

### Introduction

- 1. 1 Model of Action 1
- 1. 2 Hydrogen Bonding and Biotin Binding 6
- 1. 3 Oxyanion Hole and Enzymic Binding 6
- 1. 4 Aims of the Project 9

## Chapter 2

---

### Inter- and Intra-molecular Hydrogen Bonding of Biotin

- 2. 1 Introduction 11
  - 2. 2 Results and Discussion 13
    - 2. 2. 1 Synthesis 13
    - 2. 2. 2 1D NMR and 2D-COSY, NOESY and ROESY NMR of biotin 13
    - 2. 2. 3 Difference of 1D NMR spectrum of biotin (**1**) from biotin derivative Bt-I (**5**) 16
    - 2. 2. 4 NMR of biotin using different ratios of DMSO-d<sub>6</sub>-CDCl<sub>3</sub> 17
    - 2. 2. 5 Variable temperature NMR of biotin and derivatives 19
    - 2. 2. 6 Molecular modelling of the intra-molecular hydrogen bonding of biotin 20
    - 2. 2. 7 Intermolecular hydrogen bonding of biotin and LCQ mass spectroscopy 20
-

## Chapter 3

---

### **Intra-molecular Hydrogen Bonding Promoted Diastereoselective Aminolysis of Biotin Ester**

- 3. 1 Introduction 24
- 3. 2 Results and Discussion 25
  - 3. 2. 1 Synthesis 25
  - 3. 2. 2 Variable temperature NMR of biotin esters and 2D-ROESY and NOESY 26
  - 3. 2. 3 Relationship between intra-molecular hydrogen bonding and  $pK_a$  value 27
  - 3. 2. 4 Chiral aminolysis of biotin esters with arylmethyamines and amino acid esters 29
  - 3. 2. 5 A molecular model for selectively post-translational modification of biotin carboxyl carrier protein by biotin holoenzyme synthetase 37

## Chapter 4

---

### **Intra-molecular Hydrogen Bonding and Molecular Folding of Biotin Peptides: A Structural Approach to Biotin Peptides in Biotin Dependent Enzymes**

- 4. 1 Introduction 40
  - 4. 2 Results and Discussion 41
    - 4. 2.1 Synthesis 41
    - 4. 2. 2 Intra-molecular hydrogen bonding in synthetic peptides 42
    - 4. 2. 3 2D NMR evidences for intra-molecular hydrogen bonding 45
    - 4. 2. 4 Interactions between biotin and aromatics 50
    - 4. 2. 5 Pro-chiral hydrogen differentiation in biotin carboxyl carrier protein unit 53
    - 4. 2. 6 Tentative assignment of pro-chiral hydrogens 58
-

## Chapter 5

---

### Hydrogen Bonding Pair Controlled Molecular Foldings of Biotinylated Nucleobases

- 5.1 Introduction 61
- 5.2 Results 62
  - 5.2.1 Synthesis 62
  - 5.2.1 Intra-molecular hydrogen bonding within biotinylated nucleobases 64
  - 5.2.2 Differentiation and assignment of pro-chiral hydrogens in biotin nucleobases 72
- 5.3 Discussion 76
  - 5.3.1 Introduction of nonpolar aliphatic and aromatic groups into biotinylated nucleobases 76
  - 5.3.2 Hydrogen bonding controlled folding 81
  - 5.3.3 Predicted internal interactions of biotinyl-5'AMP and its geometry on BHS enzyme 85

## Chapter 6

---

### Hydrogen Bonding and $\pi$ - $\pi$ Stacking in DNA Base Pair Triplet Analogues

- 6.1 Introduction 89
- 6.2 Results and Discussion 90
  - 6.2.1 Synthesis 80
  - 6.2.2 Hydrogen bonding in the DNA base pair triplet analogues 81
  - 6.2.3  $\pi$ - $\pi$  Stacking of DNA base pair triplet analogues 85

## Chapter 7

---

### Recognition of Biotin Ester with Synthetic Receptors

- 7.1 Introduction 89
  - 7.2 Results and Discussion 90
    - 7.2.1 Synthesis 90
    - 7.2.2 Molecular recognition of biotin ester 90
    - 7.2.3 Molecular recognition of biotin ester with base pair triplet analogues 96
-

## Chapter 8

---

### Molecular Assembly of Receptors and Complexes with Biotin Esters through Regular Hydrogen Bonding and $\pi$ - $\pi$ Stacking

- 8. 1 Introduction 98
- 8. 2 Results and Discussion 99
  - 8. 2. 1 Synthesis 99
  - 8. 2. 2 Intermolecular hydrogen bonding in compound **79** 99
    - 8. 2. 2. 1 Concentration dependence 99
    - 8. 2. 2. 2 Temperature dependence 101
    - 8. 2. 2. 3 Intra-molecular hydrogen bonding of compound **79** 102
  - 8. 2. 3 Intermolecular  $\pi$ - $\pi$  stacking in compound **79** 103
    - 8. 2. 3. 1 Concentration dependence 103
  - 8. 2. 4 Intermolecular hydrogen bonding of compound **80** 104
    - 8. 2. 4. 1 Concentration dependence 104
    - 8. 2. 4. 2 Temperature dependence 105
  - 8. 2. 5 Intermolecular  $\pi$ - $\pi$  stacking of compound **80** 105
  - 8. 2. 6 Three-centre Hp $\cdots$ N1 $\cdots$ Hp and O $\cdots$ Hp $\cdots$ N intra-molecular hydrogen bonding of compound **80** 106
  - 8. 2. 7 Intermolecular  $\pi$ - $\pi$  stacking interactions in receptors Re-pdigg (**75**), Re-pdigm (**76**) and Re-pdigh (**78**) and their complexes with biotin ester **12** 107
  - 8. 2. 8 Intra-molecular hydrogen bonding in receptors Re-pdigg (**75**), Re-pdigm (**76**) and Re-pdigh (**78**) 108
  - 8. 2. 9 Mass spectrometry 108
  - 8. 2. 10 Helical assembly of compound **79** and **80** 110

## Chapter 9

---

### Molecular Recognition of Biotin Peptides with Synthetic Receptors

- 9. 1 Introduction 112
  - 9. 2 Results and Discussion 112
    - 9. 2. 1 Molecular recognition of biotin amide **33** with receptor **73** 112
    - 9. 2. 2 Binding of biotin peptides with hydrazide receptor **78** 113
    - 9. 2. 3 Molecular recognition of biotin peptides with receptor Re-pdigg (**75**) 116
-

## Chapter 10

---

### Molecular Recognition of Adenine Derivatives with Synthetic Receptors

- 10. 1 Introduction 119
- 10. 2 Results and Discussion 121
  - 10. 2. 1 Synthesis of receptor Re-napha **87** 121
  - 10. 2. 2 Molecular recognition of adenine derivatives with receptor Re-napha **87** 125
  - 10. 2. 3 Molecular recognition of DNA base pair analogous with receptor Re-napha **87** 128
  - 10. 2. 4 Molecular recognition of adenine derivatives with receptor Re-naphdia **93** 131
  - 10. 2. 5 Molecular recognition of DNA by the formation of base pair triplets 132
  - 10. 2. 6 Intra-molecular recognition of nucleobases 133
    - 10. 2. 6. 1 Intra-molecular hydrogen bonding within a DNA base pair and nucleobases 133
    - 10. 2. 6. 2 DNA base pair doublet series 134
    - 10. 2. 6. 3 DNA base pair triplet series 136

## Chapter 11

---

### Recognition of Biotin-5'-AMP Analogues with Synthetic Receptors

- 11. 1 Introduction 140
  - 11. 2 Results and Discussion 141
    - 11. 2. 1 Synthesis of receptors 141
      - 11.2. 1. 1 Synthesis of receptor Re-pt (**133**), Re-pdit (**134**), Re-pu (**135**), Re-pc (**137**), Re-pthiou (**136**) 141
      - 11.2. 1. 2 Synthesis of receptor Re-pau (**141**) 143
    - 11. 2. 2 Molecular recognition of Bt-Ade (**51**) 144
    - 11. 2. 3 Molecular recognition of Bt-Met(D)-Ade (**152**) and Bt-Met(L)-Ade (**153**) 148
    - 11. 2. 4 Molecular recognition of Bt-Ade (**51**) with other receptors 151
-

## Chapter 12

---

### Molecular Reception Catalysis and Biotin Action Mechanisms

- 12. 1 Introduction 153
- 12. 2 Results and Discussion 154
  - 12. 2. 1 Synthesis 154
  - 12. 2. 2 Molecular recognition of imidazolidinone (**155**) and carboethoxyimidazolidinone (**156**) 154
  - 12. 2. 3 Crystal structure of carboethoxyimidazolidinone (**156**) 155
  - 12. 2. 4 Hydrogen bonding induced distortion of biotin derivatives 158
  - 12. 2. 5 Receptor catalysis of the decarboxylation of carboxyimidazolidinone 162
  - 12. 2. 6 Molecular recognition of biotin and aliphatic acids 163
  - 12. 2. 7 Molecular recognition of inorganic substrates  $\text{H}_2\text{PO}_4^-$ ,  $\text{HCO}_3^-$ ,  $\text{CO}_3^{2-}$  and acetate 163
  - 12. 2. 8 Binding of bicarbonate  $\text{HCO}_3^-$  by biotin and biotin derivatives 164
  - 12. 2. 9 A model for the mechanism of formation of biotin-5'-AMP 167
  - 12. 2. 10 A model for the mechanism of the formation of carboxyphosphate 168
  - 12. 2. 11 A model for the mechanism of the carboxylation of biotin by carboxyphosphate 169
  - 12. 2. 12 A model for the mechanism of the transdecarboxylation of carboxybiotin and carboxylation of a substrate with the retention of configuration 170

### Conclusions 173

---

## Chapter 13

---

### Experimental 174

### Bibliography 218

### Appendix

---

## Abstract

In *Escherichia coli*, biotin dependent carboxylase catalyses the first step of the acetyl-CoA carboxylase reaction, which is the first committed step of fatty acid biosynthesis. In its functional cycle the biotin carboxyl carrier protein (BCCP) participates in three heterologous protein-protein interactions, depending on its state of post-translational modification. Athappilly and co-worker revealed the internal multiple biotin-mediated interactions in the crystal structure of the biotinylated BCCP of the acetyl CoA carboxylase (Athappilly, F. K.; Hendrickson, W. A. *Structure* **1995**, *3*, 1407). However, the results were clouded by the later finding of the absence of observable biotin-protein interactions in the dilute solution of the 1.3 subunit of transcarboxylase (Reddy, D. V.; Shenoy, B. C.; Carey, P. R.; Sonnichsen, F. D. *Biochemistry* **1997**, *36*, 14676). Biotin is attached via an amide linkage to a specific lysine residue of the biotin dependent enzymes by the intermediate BirA-biotinyl-5'-AMP. However, chemically, the interactions between biotin and the various proteins, between biotin and nucleic acids and between different biotin dependent enzymes are not well documented.

The intra-molecular hydrogen binding of biotin in the mixed organic solvent  $\text{CDCl}_3$ -DMSO- $d_6$  was initially revealed by multiple NMR techniques and provided a support for the proposed mechanism (Goodall, G. J.; Prager, R.; Wallace, J. C.; Keech, D. B. *FEBS Lett.* **1983**, *163*, 6) and preferential carboxylation at N-1' of biotin (Fry, D. C.; Fox, T.; Lane, M. D.; Dilavan, A. S. *Ann. N. Y. Acad. Sci.* **1985**, *447*, 140). The intra-molecular hydrogen bonding in biotin esters was investigated as well as the aminolysis of active biotin esters. For various biotin peptides, intra-molecular hydrogen bonding networks were observed, which resulted in the pro-chiral vicinal hydrogen differentiation of side chain methylenes and hydrophobic interactions between biotin and aromatic side chains. During the investigation of biotin nucleobases, Bt-Ade (**51**), Bt-Cyt (**52**), Bt-Thy (**53**), Bt-Ura (**54**) and Bt-Thioura (**55**), the nucleobases, cytosine, adenine, thymine and uracil form hydrogen bonding pairs with the NHb and carbonyl group of biotin, however, thiouracil preferentially formed a hydrogen bonding pair with the NHa and the carbonyl group of biotin.

A series of potential receptors for biotin derivatives based on the 2, 6-pyridinedicarboxamide motifs were investigated. The three-centred intra-molecular hydrogen bonds gave rise to a planar conformation, which also resulted in efficient intermolecular  $\pi$ - $\pi$  stacking interactions. Efficient bindings were observed between these receptors and biotin esters and between these receptors and biotin peptides.

---



Receptors were designed for the recognition of adenine through efficient hydrogen bonding and  $\pi$ - $\pi$  stacking interactions. Receptor **73** was used to bind DNA base pair doublet and triplet analogues by hydrogen bonding and  $\pi$ - $\pi$  stacking interactions. DNA base pair interactions and Watson-Crick and Hoogsteen hydrogen bonding, were also observed within a series of artificial base pair doublets and triplets.

The crystal structure of carboethoxyimidazolidinone, and structures on the conformation of biotin derivatives and various receptors provided support for a literature mechanism (Kluger, R.; Tsao, B. *J. Am. Chem. Soc.* **1993**, *115*, 2089) for decarboxylation of carboxybiotin. Tetrapeptide receptor **73** was used to investigate the binding of free biotin, and inorganic substrates such as hydrogen phosphate, bicarbonate, carbonate and organic acetate anion which are the basic materials used in the carboxylation of biotin. The binding interactions between various biotin peptides and bicarbonate were also investigated.

Based on the above information, models were proposed for the formation of biotin-5'-AMP and carboxyphosphate, the carboxylation of biotin by carboxyphosphate and the transdecarboxylation of carboxybiotin and carboxylation of malonyl with retention of configuration.

---

## Statement

This work contains no material which has been accepted for the award of any other degree or diploma in any university or other tertiary institution and, to the best of my knowledge and belief, contains no material previously published or written by another person, except where due reference has been made in the text.

I give consent to this copy of my thesis, when deposited in the University Library, being available for loan and photocopying.

Yu-Lin Jiang

24 / 11 / 1999

Date

## Acknowledgments

I would like to express sincere thanks and gratitude to my supervisor Dr Geoff Crisp for his enthusiasm and support over the past three and half years. I would also like to thank him for his effort in assisting with the writing of this thesis in the last half of the year. Furthermore, I would like to give thanks to him for assisting me to obtain a post-doctoral position at the Center for Advanced Research in Biotechnology at the University of Maryland, USA.

I would like to thank all the Staff of the Department of Chemistry for their help, especially: Phil Clements (NMR), Dr Edward Tiekink (X-Ray), Tom Blumenthal (Mass Spectrometry), Jeff Borkent (Computing) and John Cameron (Store).

I would also like to thank my research group for being friends and to work with, in particular Peter Turner for having done some correction of research reports in the initial three years.

Acknowledgment must also go to the Australian Research Council for providing me with an Overseas Postgraduate Research Scholarships and The University of Adelaide and The Department of Chemistry for giving me the opportunity to learn, work and enjoy a new life in Australia.

---

## List of Abbreviation

A	Adenosine
AAT	Adenine Adenine Thymine
Ac	Acetyl
Ade	Adenine
Adenos	Adenosine
ADP	Adenosine diphosphate
Ahx	6-Aminohexanoic acid
APA	Adenyl adenyl phosphate
ATP	Adenosine triphosphate
BCCP	Biotin carboxyl carrier protein
Bct	Biotinyl lysine
BHS	Biotin holosynthetase
Bt	Biotin
COSY	Correlated Spectroscopy
CPS	Carbamoyl phosphate synthetase
Cyt	Cytosine
DCC	<i>N, N'</i> -Dicyclohexyl carbodimide
DCU	<i>N, N'</i> -Dicyclohexyl urea
DMA	Dimethyl acetamide
DMF	Dimethyl formamide
DMSO	Dimethyl sulfoxide
EI	Electron Impact
eq	Equivalents
FAB	Fast Atom Bombardment
Ghmbc	Gradient Suppression Heteronuclear Multiple-Bond Coherence
Ghmqc	Gradient Suppression Heteronuclear Multiple-Quantum Coherence
Glu	Glutamic acid
Gly	Glycine
HECTOR	Heteronuclear Chemical-Shift Correlation
His	Histidine
HMBC	Heteronuclear Multiple-Bond Coherence
HMQC	Heteronuclear Multiple-Quantum Coherence

---

II	Iso-leucine
IR	Infrared Spectrum
LCQ	Liquid Chromatography Quadrupole
LSIMS	Liquid Secondary Ionisation Mass Spectroscopy
Lys	Lysine
Met	Methionine
mp	melting point
NBS	N-Bromo Succinimide
NHS	N-Hydroxy Succinimide
NMR	Nuclear Magnetic Resonance
NOESY	Nuclear Overhauser Effect Spectroscopy
Phala	Phenylalanine
ppm	parts per million
py	pyridine
ROESY	Rotating Frame Overhauser Effect Spectroscopy
TAA	Thymine Adenine Adenine
TAT	Thymine Adenine Thymine
THF	Tetrahydrofuran
Thioura	Thiouracil
tlc	thin layer chromatography
TNF	Tumor Necrosis Factor
Trp	Tryptophan
Tyr	Tyrosine
U	Uridine, deoxyuridine
Ura	Uracil
VT	Variable Temperature NMR

---

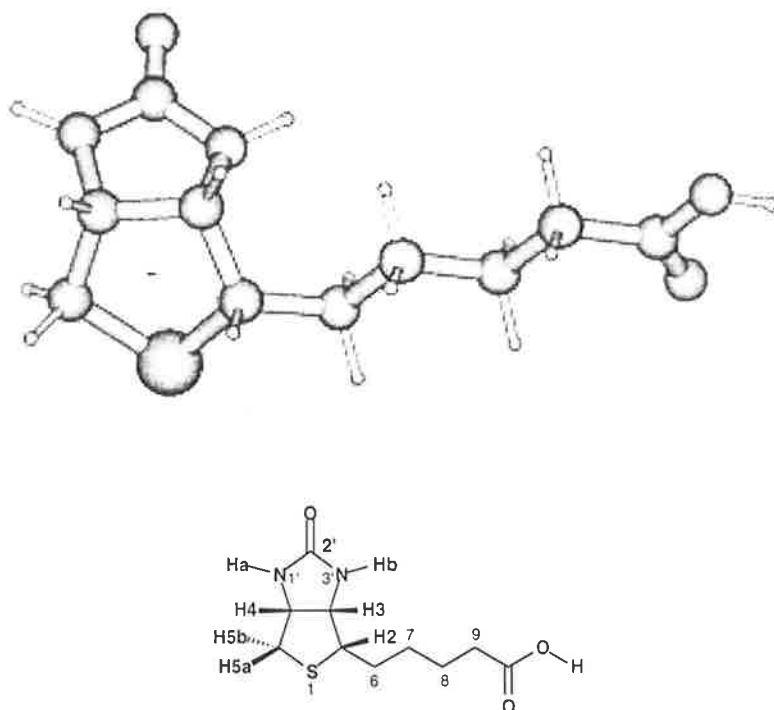


# Chapter 1

## Introduction

### 1. 1 Mode of Action

Biotin, or Vitamin H, is an essential vitamin and a component of many enzymes.<sup>1</sup> Structurally, it is composed of a 5-membered ureido ring and a tetrahydrothiophene ring containing a pentanoic acid side chain (Figure 1).

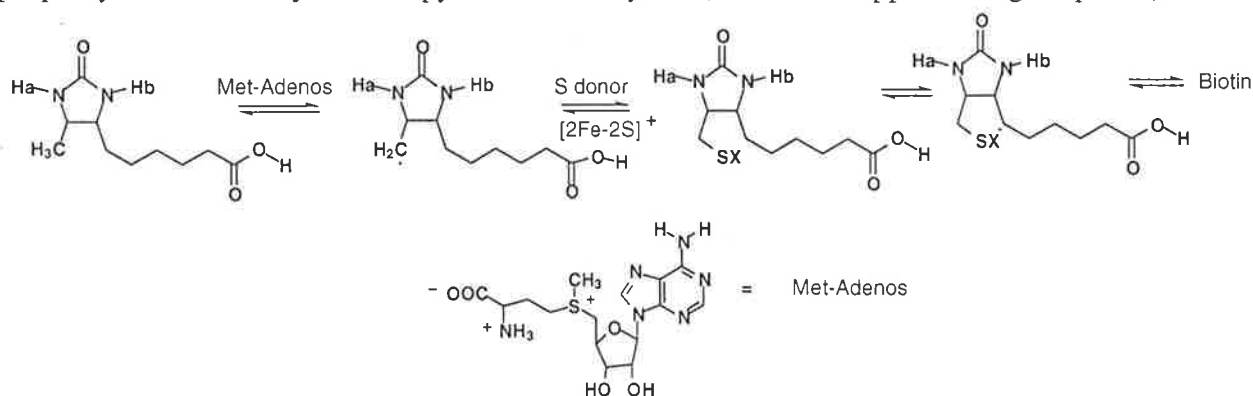


**Figure 1.** Molecular modelling structure with extended conformation and numbering of *d*-(+)-biotin .

The biosynthesis of biotin has been studied in *Escherichia coli* biotin synthase.<sup>2-4</sup> The formation of the tetrahydrothiophene ring involves a radical mechanism with homolytic cleavage of a C-H bond as the initial step, followed by the incorporation of sulfur from a donor (most probably a  $[2\text{Fe}-2\text{S}]^+$  cluster) and another cleavage of the  $\alpha$ -C-H bond and connection of the sulfur into the side chain (Scheme 1). It is believed that methionine-adenosine (Met-Adenos) plays an important role in the synthesis.

Biotin containing enzymes play crucial roles in lipogenesis, gluconeogenesis and amino acid metabolism in all living systems.<sup>5</sup> Biotin is involved in the transfer of carbon dioxide during carboxylation, decarboxylation and transdecarboxylation reactions. The four biotin-dependent

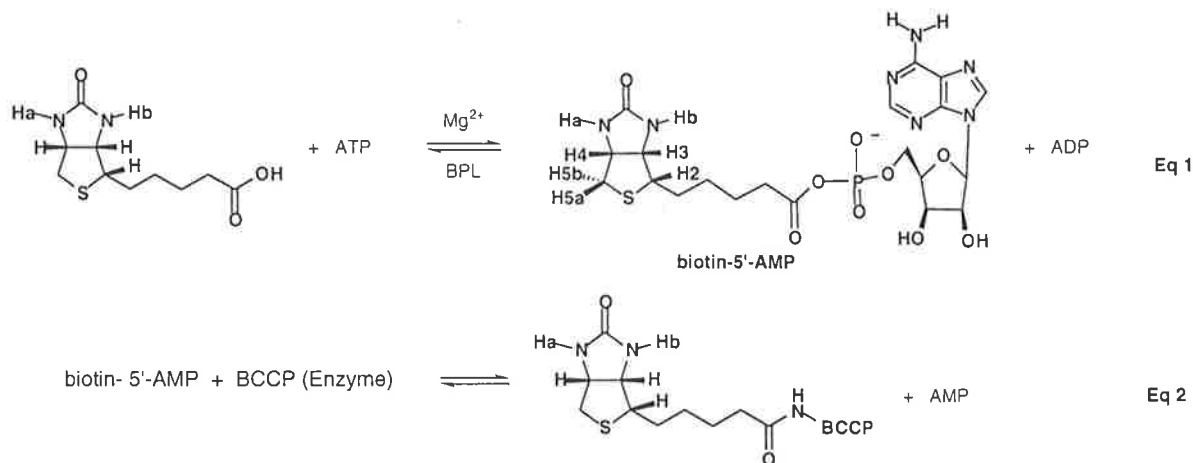
carboxylases found in mammals are acetyl-CoA carboxylase, methylcrotonyl-CoA carboxylase, propionyl-CoA carboxylase and pyruvate carboxylase (which also appear in higher plants).<sup>6</sup>



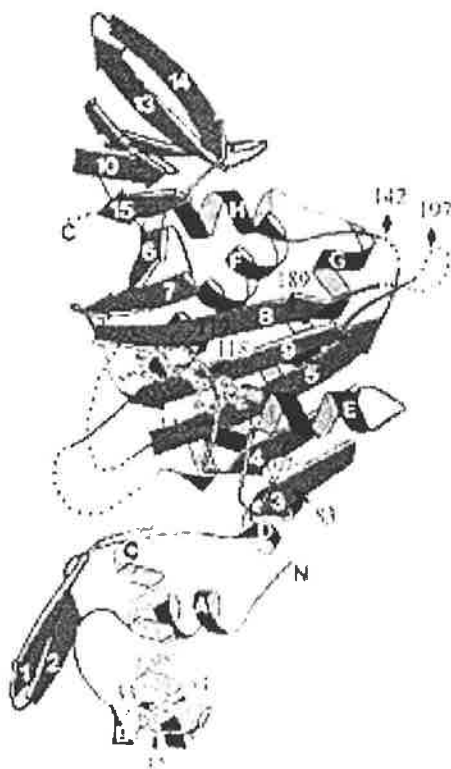
**Scheme 1.** Biosynthesis of biotin.

Commercially, biotin is a dietary additive for the food of human babies, cattle and poultry.<sup>7-9</sup> Recently, biotinylated antibodies, avidin and streptavidin have been applied to the targeting of tumours and for *in vivo* diagnosis and radioimmunotherapy in cancer patients. The presence of both biotinylated human tumor necrosis factor  $\alpha$  (bio-TNF) on the cell surface and cell-bound bio-TNF can trigger cytolytic effects *in vitro* and antitumor effects *in vivo*.<sup>10-12</sup>

Biotin coenzyme has biological activity only when it is covalently attached to a class of important metabolic enzymes, the biotin carboxylases and decarboxylases.<sup>13-14</sup> The biotinyl group is attached post-translationally by the action of a biotinyl protein ligase (BPL, also known as biotin holoenzyme synthase and BirA), which catalyses the formation of an amide linkage between the carboxyl group of the biotin and the  $N^{\epsilon}$ -amino group of a specific lysine residue in biotin carboxyl carrier protein (BCCP). The first two steps are summarized below (Eq. 1 and 2).<sup>15-16</sup> It is believed that BPL collects biotin and ATP together for the formation of biotinylated intermediate BPL-biotinyl-5'-AMP, which then binds to biotin carboxyl carrier protein for the subsequent post-translational biotinylation.<sup>17-18</sup> According to the literature, biotin occupies a portion of the  $\beta$ -sheet face that is exposed to the solvent in domain II, and makes contacts with parts of three  $\beta$ -strands, the N-terminus of helix E and the main-chain atoms of residues 114-118 of BirA.<sup>19</sup> The biotin binding pocket has hydrophobic sides with a more hydrophilic center, the biotin carbonyl and ureido protons interact via hydrogen bonding with the hydrophilic interior of the cavity, while the hydrophobic tail and tetrahydrothiophene ring interact with the hydrophobic sides of the pocket (Figure 2).



It is suggested that the ATP binding site is spatially close to the biotin to permit the formation of biotinyl-5'-AMP and that biotin binding will order the N-terminal portion of the presumed phosphate-binding loop.<sup>19</sup>



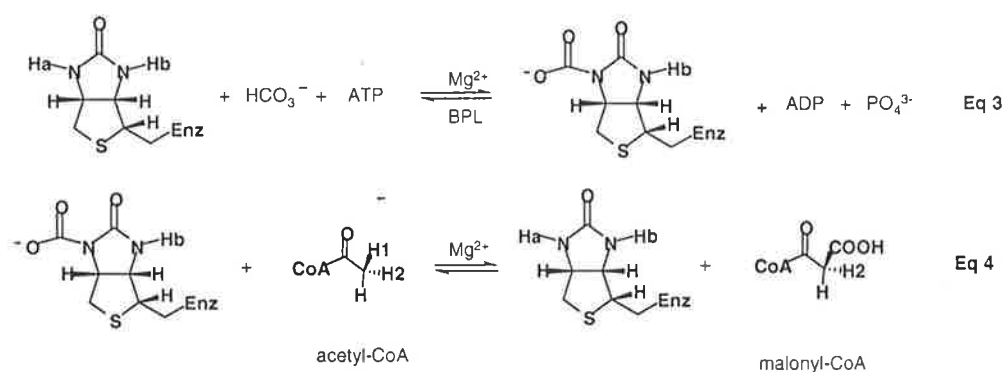
**Figure 2.** Ribbon drawing showing the overall topology of biotin repressor BirA. The relationship between the DNA recognition helix and biotin is depicted.

The post-translational modification of BCCP occurs with extraordinary specificity as it is reported that BPL recognizes this protein out of 4000 different protein species of *Escherichia coli*. BCCP is one of the four protein species that comprise acetyl-CoA carboxylase, the enzyme

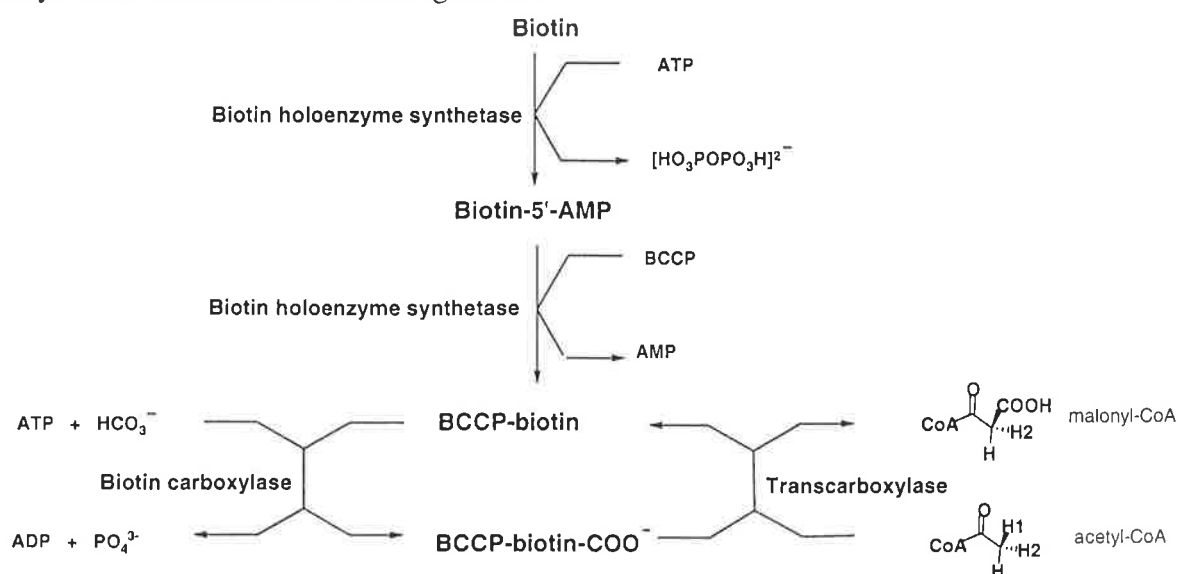


catalysing the first committed step of fatty acid biosynthesis, the conversion of acetyl-CoA to malonyl-CoA.<sup>20</sup>

The biotin carboxyl carrier protein BCCP engages heterologous protein-protein interactions not only with the biotin holoenzyme synthetase, BirA, which results in the post-translational attachment of biotin to an essential lysine residue on BCCP, but also with the biotin carboxylase subunit. This latter reaction leads to the carboxylation of biotin by the electrophilic substitution of the proton Ha on N-1' by a carboxyl group. Finally, the carboxybiotinylated BCCP interacts with transcarboxylase in the conversion of acetyl-CoA to malonyl-CoA with the retention of configuration and the completion of the first committed step of fatty acid synthesis (Eq 3 and Eq 4). The general mechanism is shown as follows.<sup>21-24</sup>



All these reactions are summarized in Figure 3, including the conversion of biotin to biotin-5'-AMP, BCCP-biotin and BCCP-biotin-COO<sup>-</sup> and finally carboxylation of acetyl-CoA to malonyl-CoA with retention of configuration.



**Figure 3.** Schematic representation of the conversion of biotin to its derivatives and final carboxylation of acetyl-CoA to malonyl-CoA with retention of configuration involving biotin carboxyl carrier protein (BCCP), biotin holoenzyme synthetase, biotin carboxylase and transcarboxylase of acetyl-CoA carboxylase.

Although the three-dimensional structure of the biotinylated form of the biotin domain of *E. coli* BCCP has been determined by both NMR spectroscopy and X-ray crystallography, giving essentially identical structures, it is not clear whether the biotin is involved in the interactions of BCCP with BPL, or with carboxylase or carboxyl transferase subunits of acetyl-CoA carboxylase.<sup>21, 25</sup> The molecular recognition study of BCCP with acetyl carrier protein does not show the direct involvement of the biotin or biocytin (biotinyl lysine).<sup>16</sup> There is some suggestion that the B-domain of the biotin carboxylase subunit of acetyl-CoA carboxylase is involved in the interaction with BCCP and acts as a "lid" that closes down on the active site when biotin,  $Mg^{2+}$ -ATP, and  $HCO_3^-$  are positioned for catalysis.<sup>24</sup> Therefore, the internal interactions between the biotin (biocytin) unit with other residues of BCCP are possible in order to promote the formation of carboxybiotin (Eq 3). The three dimensional structure of holo-BCCP shows that seven amino acid residues (Tyr-92, Thr-94, Pro-95, Ser-96, Pro-97, Ile-117 and Met-124) are located within 4.0 Å of the biotin moiety and side-chain and the main-chain oxygen atoms of Thr-94 form hydrogen bonds respectively with the ureido carbonyl and Ha of biocytin<sup>25</sup> (Figure 4).

Interestingly, Goodall et al provided a mechanism for the transfer of the carboxyl group from N-1'-carboxybiotin to acceptor substrates, in which a base positioned adjacent to the N-3' of the carboxybiotin abstracts a proton from the N-3' and the resulting enolate ion and acceptor substrate undergo a concerted reaction resulting in carboxyl group transfer with retention of configuration. The carboxyl group is added to the same face of the molecule from which the  $\alpha$ -proton was removed. However, the evidence for the mechanism remains to be collected with respect to the presence of the interaction between Hb and a base residue.<sup>26</sup> Probably, the necessary base exists among the seven amino acid residues which are so close to the biotin moiety in holo-BCCP. Hydrogen bonding may play a role as a bridge for the interactions and promotion of the reactions (Scheme 2).

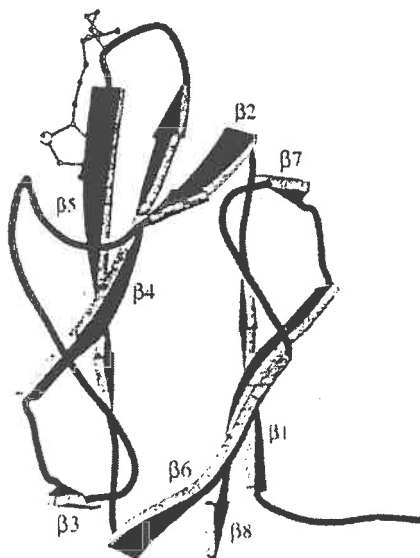
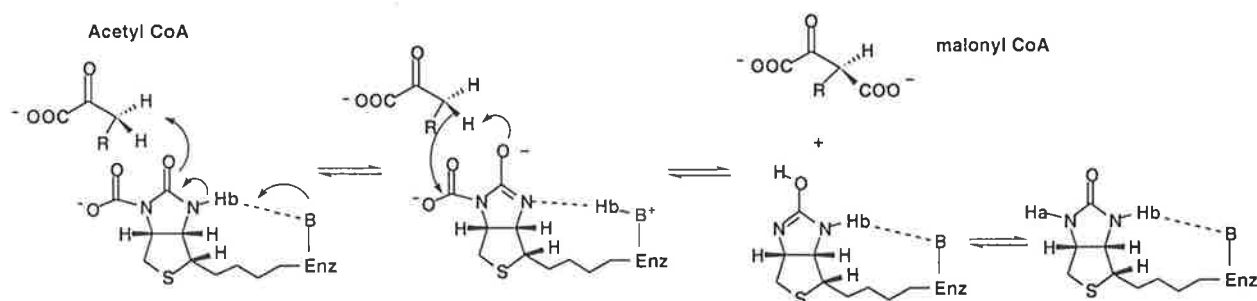


Figure 4. Overall folding of BCCPsc with ball-and-stick representation of the side chain of biocytin.



**Scheme 2.** Goodall's mechanism with retention of configuration during the transfer of carboxyl group from carboxybiotin to acetyl-CoA to form malonyl-CoA.

## 1.2 Hydrogen Bonding and Biotin Binding

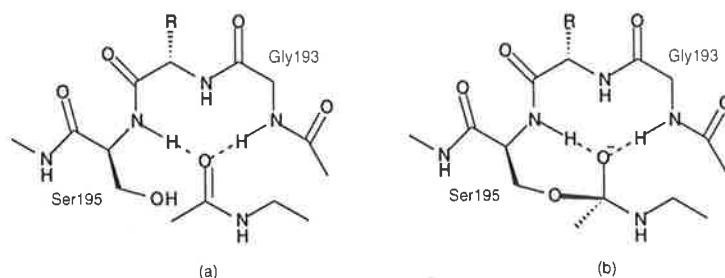
Hydrogen bonding is a non-covalent interaction that varies in strength,<sup>27</sup> depending on the length of the hydrogen bond and the angle between the donor group and the hydrogen acceptor.<sup>28-30</sup> Between polar amino acids, both hydrogen bonding and van der Waals interactions are important. The marginal stabilities of proteins arise from these interactions,<sup>31</sup> as well as the stabilities of the nucleic acids DNA and RNA. Intra-molecular hydrogen bonding has been proposed to play an important role in peptide conformations,<sup>32</sup> protein folding<sup>33-40</sup> and reactions.<sup>41</sup> During enzymatic reactions, enzymes tend to adjust their secondary and tertiary structures automatically to generate an active site for binding by various weak forces, such as hydrogen bonding, and bring neighboring groups into the correct orientation in order for the reactions to be most effective and stereoselective.<sup>42-47</sup> Hydrogen bonding can also be the stereocontrolling element in reactions such as free-radical C-allylation,<sup>48</sup> catalytic addition of hydrogen cyanide to benzaldehyde<sup>49</sup> and chiral solvation.<sup>50</sup>

Biologically, biotin can be extremely tightly bound to streptavidin and avidin by multiple interactions in the active binding site.<sup>51</sup> These interactions include an extensive hydrogen bonding network and hydrophobic and van der Waals interactions.<sup>52, 53</sup> This is why biotin is widely and commercially applied as a label for oligonucleotides in the identification of a variety of viral infections in human beings and plants such as HIV, HCV, HTLV and hepatitis C.<sup>54-57</sup>

## 1.3 Oxyanion Hole and Enzymic Binding

It is reported that many protease enzymes possess characteristic features such as an "oxyanion hole" to carry out enzymatic reactions. For example, the amide-NH group of Ser-195 and Gly-193 form two hydrogen bonds with the substrate amide carbonyl of chymotrypsin (Figure 5).<sup>58</sup> In the hydrolysis process, the activated and fixed carbonyl group is then attacked by the adjacent serine hydroxyl to produce a tetrahedral intermediate oxyanion, which is stabilized further by the

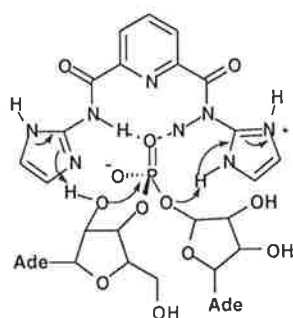
binding pocket (Figure 5b). The self-adjustment of the binding pocket and the stabilisation of reactive intermediate or transition state compared to the starting amide substrate is necessary in order to produce effective catalysis.<sup>59</sup>



**Figure 5.** “Oxyanion hole” in chymotrypsin.

Frey and co-workers suggested hydrogen bonds are formed between the His-57 and Asp-102 residues of the active site of chymotrypsin, as the reaction proceeds to form the tetrahedral intermediate necessary to hydrolyze the peptide bond.<sup>60-62</sup> A good model for the Asp-His dyad of the active site in the serine protease was provided by Neuvonens.<sup>63</sup> The importance of hydrogen bonding was also reported in lysozyme-catalysed hydrolysis,<sup>64-66</sup> metalloenzyme-mediated hydrolysis,<sup>67-68</sup> and ribonuclease catalysed cleavage of RNA.<sup>69-70</sup>

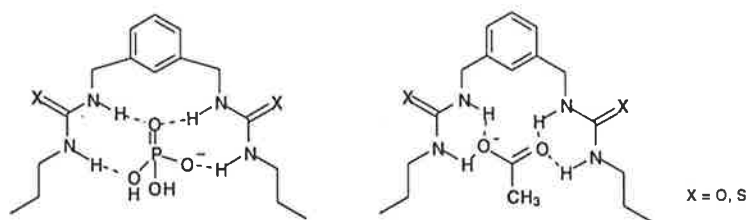
The function of an “oxyanion hole” can also be seen in the cleavage of adenylyl (3’-5’) adenosine (APA) of RNA by dipicolinyl compound.<sup>70</sup> As reported, the degradation of APA proceeds via nucleophilic attack of the 2’-hydroxy group of ribose on a phosphodiester by intramolecular assistance of the receptor. The 2’, 3’-cyclic phosphate is then formed, followed by hydrolysis to yield the 3’-phosphate of adenosine (Figure 6).



**Figure 6.** Recognition of adenylyl phosphate with dipicolinyl receptor.

In carbamoyl-phosphate synthase (CPS) and glutathione synthetase, ADP-forming ligases are reported to undergo a conformational change and serve as a lid for the active site upon nucleotide binding. Presumably, the active site in the enzymes is also the so-called “oxyanion hole” which would provide the necessary binding required during the enzymatic reactions.<sup>71-73</sup>

Chemically, bis-urea and bis-thiourea hosts, simple compounds with “oxyanion holes” were reported to bind dihydrogenphosphate and acetate by the formation of multiple hydrogen bonds (Figure 7).<sup>74</sup>

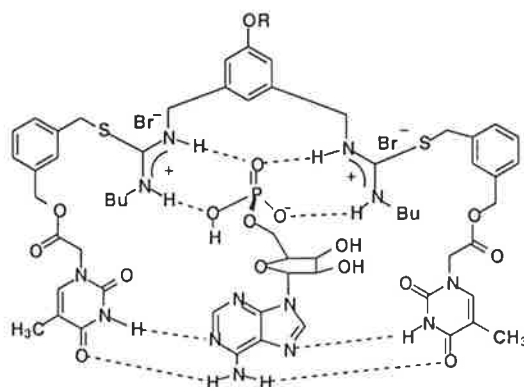


**Figure 7.** The binding of phosphate and carbonate with synthetic receptors.

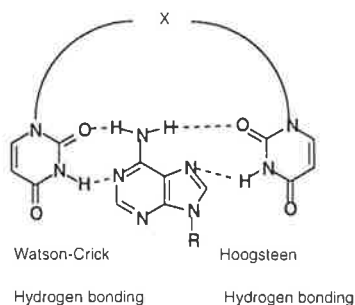
Although there are reported receptors with “oxyanion holes” that bind imidazolidinone and its derivatives as mimics for biotin, no receptor has been reported that directly interacts with biotin derivatives.<sup>75-76</sup>

Biotinyl-5'-AMP is the intermediate for the biotinylation of apo-enzymes during the first committed step of fatty acid synthesis. The BPL binds not only ATP and biotin but also the resulting biotinyl-5'-AMP to form BPL-biotinyl-5'-AMP complex by multiple hydrogen bonds.<sup>19</sup> The binding site for the biotin unit is thought to be an “oxyanion hole” formed by the amino acids residues that form the binding pocket, although details of the binding are not known.

Recently, an artificial thiuronium-thymine conjugate receptor was reported to bind and possibly transport 5'-AMP, which could interact with both phosphate and adenine moieties as shown in Figure 8.<sup>77</sup> Recognition is thought to involve the binding of the phosphate unit with an “oxyanion hole” (Figure 5)<sup>74</sup> and the interaction of adenine with double thymine moieties to form a DNA base pair triplet.<sup>78</sup> The artificial double uridine receptors for binding adenine have also been reported in the literature,<sup>79</sup> with Watson-Crick and Hoogsteen hydrogen bonding (Figure 9).



**Figure 8.** Proposed structure of complex of 5'-AMP with the receptor.



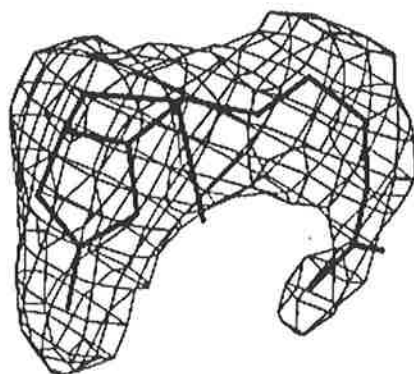
**Figure 9.** DNA base pair triplet and recognition with different DNA hydrogen bonds.

## 1.4 Aims of the Project

This research is driven by a desire to understand the mode of action and biosynthetic pathways of biotin enzymes related to *Escherichia coli*. The details of how the biotin dependent enzymes form active sites, interact with DNA and RNA and other enzymes to carry out a series of enzymatic reactions need be elucidated.

It is reported that the biotin valeric acid side chain in the carboxylase curls back towards the bicyclic biotin ring system rather than adopting an external conformation (Figure 10).<sup>19, 80, 81</sup> This project will examine the intra-molecular hydrogen bonding of biotin and attempt to rationalise possible catalytic roles for biotin based on these conformations.

Probably, because of the considerable flexibility of biotin dependent enzyme proteins, their structures and those of their complexes are not readily detected.<sup>24, 82</sup> It is reported that there have been some difficulties in carrying out substrate binding studies on biotin carboxylase<sup>24</sup> in the crystalline state and the assignment of binding active sites for ATP are still tentative.<sup>82</sup>



**Figure 10.** Difference electron density map corresponding to the  $\text{Ag}^+$ /biotin complex in the biotin-containing acetyl-CoA carboxylase.

The biotinylation intermediate, biotinyl-5'-AMP is essential for connection of biotin onto biotin dependent enzymes, yet the real nature of the selective binding and transport to target enzymes by BPL enzyme is not clear. The understanding of the interactions between biotinyl-5'-AMP and enzymes would be useful in the design of effective inhibitors and drugs for human diseases caused by *Escherichia coli*, such as *Escherichia coli* meningitis, herpes simplex virus type 1 and varicella-zoster virus, persistent bladder and urinary tract infection and infective bacteria for children.<sup>83-85</sup>

## Chapter 2

### Inter- and Intra-molecular Hydrogen Bonding of Biotin

#### 2.1 Introduction

The three dimensional crystal structure of free *d*-(+)-biotin shows that the valeryl chain of biotin in the solid state is severely twisted from the maximally extended all-trans conformation (Figure 11).<sup>86</sup> The electron density map of Ag<sup>+</sup>/biotin in biotin carboxylase in water solution shows that the valeric acid side chain curls backward toward the bicyclic ring system rather than adopting the extended conformation (Figure 10).<sup>19, 80, 81</sup> The distortions in this case may result from coordination to the Ag<sup>+</sup> ion.

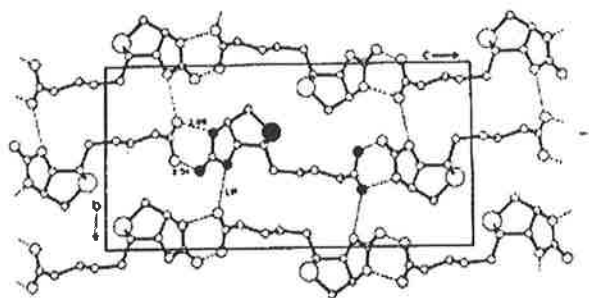


Figure 11. Crystal structure of biotin.<sup>86</sup>

Proton-exchange measurements on biotin in aqueous solution suggested intra-molecular hydrogen bonding between the carboxylate group and NHb (Figure 12a).<sup>87</sup> A similar proposal was reported for biotin in DMSO-*d*<sub>6</sub> (Figure 12b and Figure 12c).<sup>88</sup> However, the experiments carried out by Reddy and co-workers did not show any evidence for intra-molecular hydrogen bonding of free biotin in aqueous solution.<sup>89</sup> Intra-molecular hydrogen bonding in biotin of the type shown in Figure 12 is really expected to promote not only the H-D exchange rate of its ureido protons<sup>88</sup> but also enzymic reactions.<sup>26</sup> The carboxylic acid proton in biotin is also expected to be a chelating element during binding.<sup>19, 80, 81</sup>

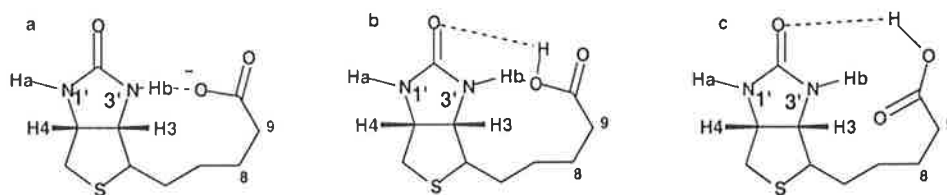


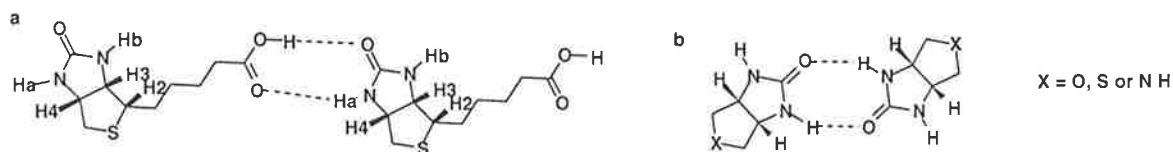
Figure 12. Intramolecular hydrogen bonding suggested in the literatures, (a) biotin anion form in water solution.<sup>87</sup> (b) and (c) free biotin in DMSO-*d*<sub>6</sub>.<sup>88</sup>



It is well known that the enzymatic substitution of the biotin prosthetic group always occurs on N-1' (NHa is exchanged).<sup>90</sup> One possible explanation for this selectivity is the steric effect from the valeryl side chain, which makes the approach of catalytic groups from the enzyme to the N-3' less favorable.<sup>88</sup> However, the steric effect could hardly explain the different NMR chemical shifts of NHa and NHb of biotin as shown in the literatures.<sup>87-89</sup>

Goodall and co-workers proposed an enolate-ion relay mechanism for the retention of configuration about the  $\alpha$ -carbon of the substrate molecule, the carboxyl group was added to the same face of the molecule from which the  $\alpha$ -proton was removed (Scheme 2) (Chapter 1).<sup>26</sup> The intra-molecular hydrogen bonding of Hb with electron donor groups from the side chain of biotin enzyme would promote this process. Therefore, the intra-molecular hydrogen bonding between Hb and the carbonyl group of the carboxyl of biotin possibly results in the differentiation of the NMR peaks of Ha from Hb. However, evidence remains to be collected for the presence of the interaction between Hb with a base residue on the enzyme.

The crystal structure of free *d*-(+)-biotin also shows that the carboxyl group in the valeryl chain of biotin in the solid state is involved in an intermolecular hydrogen bond with its ureido neighbour (Figure 11).<sup>86</sup> The interactions can be written as a dimer of biotin as shown in Figure 13a. However, when there is no carboxyl proton, ureido moieties of such compounds will adopt the amide-amide hydrogen bonding pair as shown in Figure 13b.<sup>91</sup>



**Figure 13** Structures of biotin and its analogues in the crystalline state.

## 2.2 Results and Discussion

### 2.2.1 Synthesis

In order to investigate the intra-molecular hydrogen bonding in biotin in detail, compounds **2**, **3**, and **4** were prepared as previously described (Figure 14).<sup>92-94</sup> Compound Bt-I (**5**) was synthesized by the nucleophilic substitution of compound **4** by sodium iodide in acetone at rt as shown in Scheme 3.

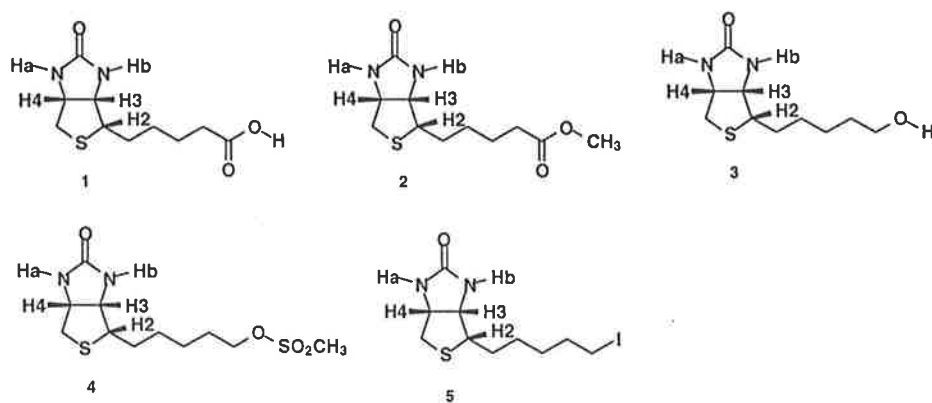
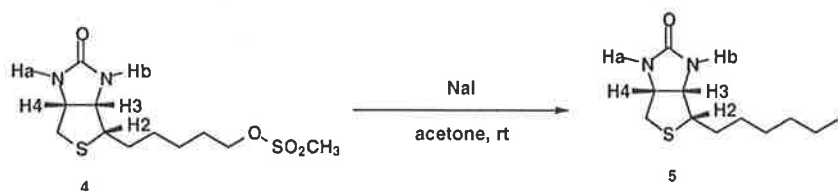


Figure 14. Biotin and biotin derivatives.



Scheme 3. Conversion of compound 4 to Bt-I (5).

### 2. 2. 2 NMR spectra of biotin

Biotin does not dissolve significantly in  $\text{CDCl}_3$  and so added  $\text{DMSO-d}_6$  was used in the preparation of homogeneous and stable solutions. Figure 15 shows the 1D proton NMR spectrum of biotin at 5 mM in a mixed solvent of 10%  $\text{DMSO-d}_6$  and 90%  $\text{CDCl}_3$  at rt. In order to assign all the protons of biotin, 2D-COSY and ROESY NMR spectra were also recorded at 5 mM in a mixed solvent of 10%  $\text{DMSO-d}_6$  and 90%  $\text{CDCl}_3$  at rt, and which are shown in Figure 16 and Figure 17 respectively. The protons and chemical shifts ( $\delta$ , ppm) for the NMR spectrum of biotin were H7 (1.465, m, 2 H); H6b + H8 (1.642, m, 3 H); H6a (1.737, m, 1 H); H8 (2.292, t,  $J = 7.2$  Hz, 2 H); H5b (2.756, d,  $J = 13.2$  Hz, 1 H); H5a (2.888, dd,  $J = 13.2$  Hz, 4.8 Hz, 1 H); H2 (3.148, m, 1 H); H3 (4.275, m, 1 H); H4 (4.466, m, 1 H); Hb (5.586, s, 1 H); Ha (5.681, s, 1 H).

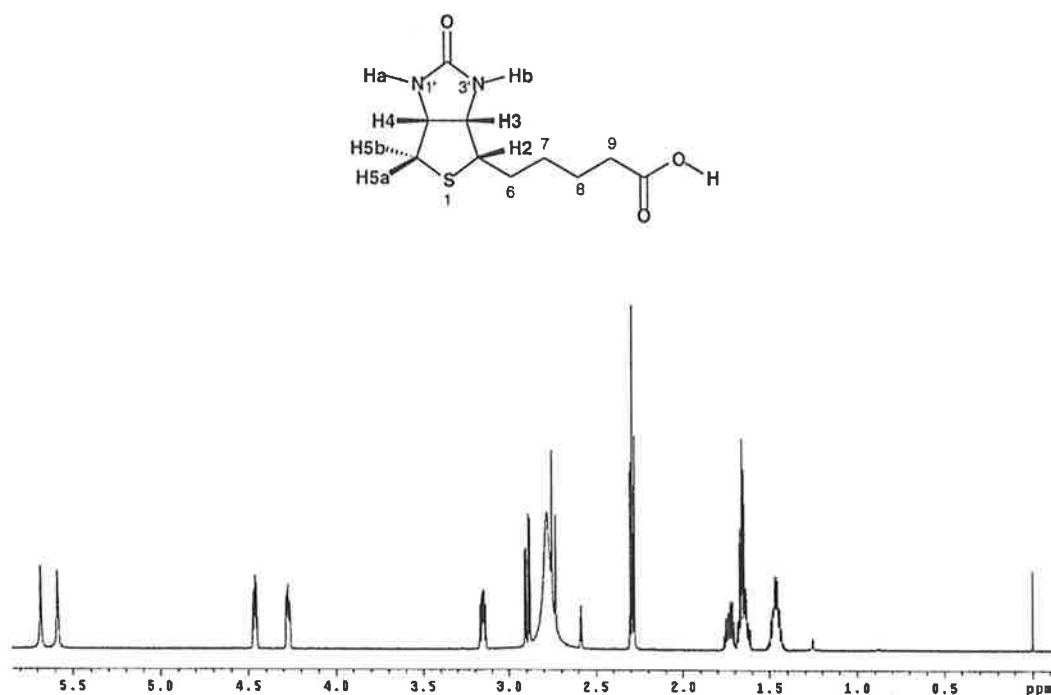


Figure 15. 1D proton NMR spectrum of biotin at 5 mM in 10% DMSO- $d_6$  and 90%  $CDCl_3$  solvent at rt.

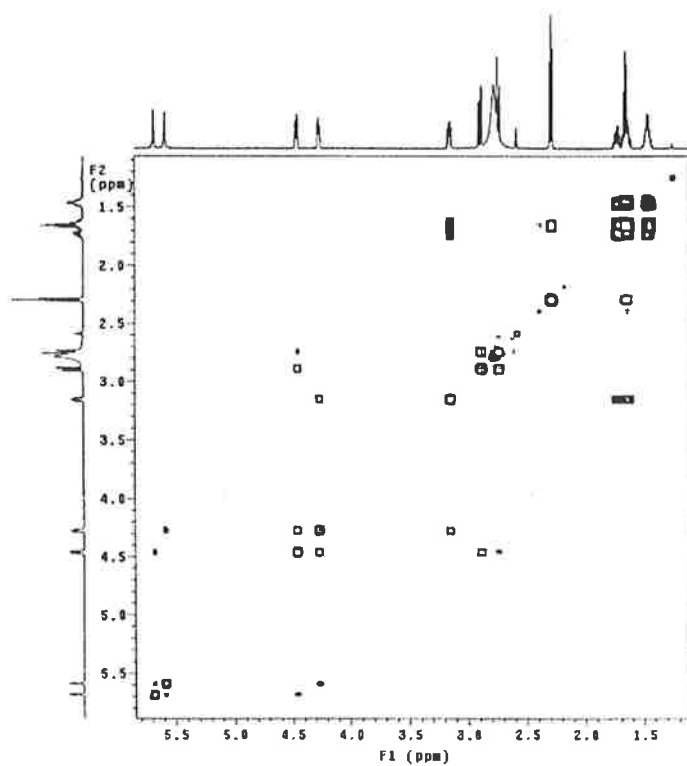
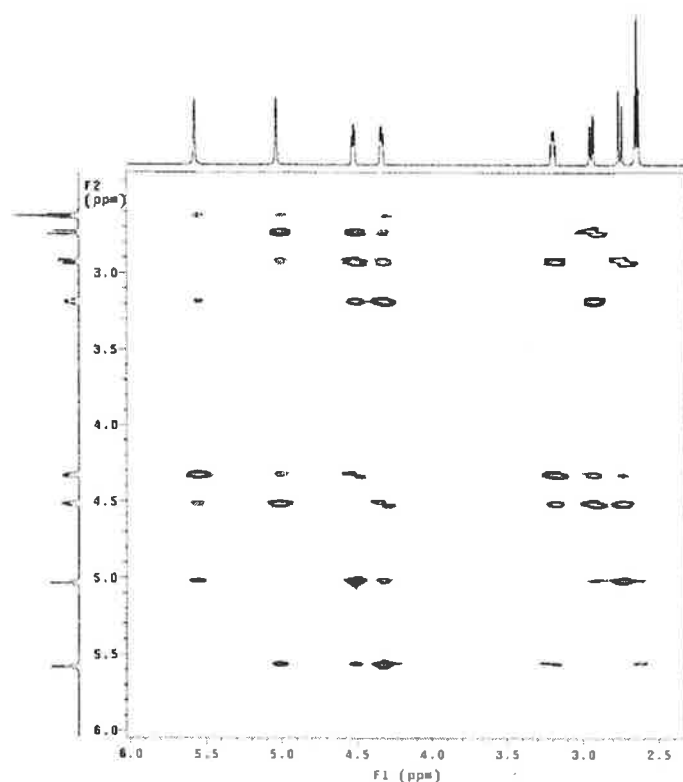
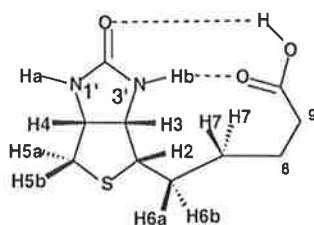


Figure 16. 2D-COSY NMR spectrum of biotin at 5 mM in 10% DMSO- $d_6$  and 90%  $CDCl_3$  solvent at rt.



**Figure 17.** 2D-ROESY NMR spectrum of biotin at 5 mM in 10% DMSO- $d_6$  and 90%  $CDCl_3$  solvent at rt.

As shown in the 2D-ROESY NMR spectrum of biotin in Figure 17, cross peaks were observed between H3 and H7, and between H2 and H7, indicating their close proximity in space. In the spectrum, the cross peaks of Hb with H7 were also significant, along with the cross peaks of Hb with H6a and H6b. The ROESY NMR spectrum suggested the conformation shown in Figure 18 and indicates the likely formation of an intra-molecular hydrogen bond between NHb and the carboxyl group of biotin.



**Figure 18.** Possible conformation of biotin in 10% DMSO- $d_6$  and 90%  $CDCl_3$  solvent.

The geometry of biotin in 10% DMSO- $d_6$  and 90%  $CDCl_3$  solvent at 5 mM solution at rt was also probed by carrying out homonuclear NOESY experiments. Irradiation of the H3 signal revealed a close contact with H7 (0.85%), H6a (0.34%) but no contact with H6b on the side chain protons (Table 1), supporting the conformation of biotin with intra-molecular hydrogen bonding in Figure 18.

The other important NOESY experiments were the irradiation of H2, where NOEs were observed with H2 to H7 (4.95%), H6a (3.34%), H6b + H8 (5.06%) and H9 (1.05%) in the side chain of biotin (Table 3), further suggesting the conformation as shown in Figure 18.

**Table 1.** NOESY Data for Biotin.<sup>a</sup>

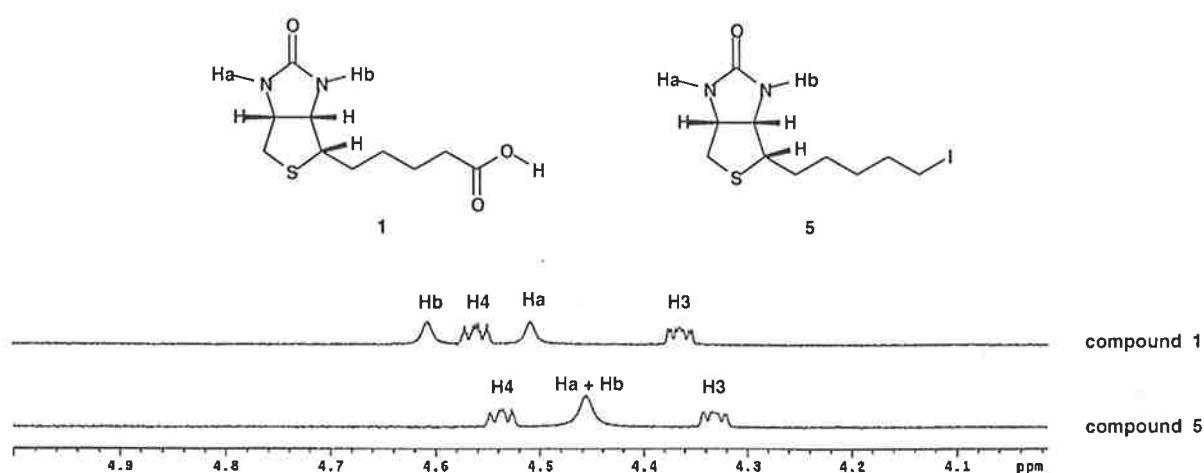
proton irradiated	NOEs observed (%)			
	H7	H6a	H6a + H8	H9
H3	0.85	0.34		
H2	4.95	3.34	5.06	1.05

<sup>a</sup> Experiments carried out in 10% DMSO-d<sub>6</sub> and 90% CDCl<sub>3</sub> solvent at rt.

### 2. 2. 3 Difference of 1D NMR spectrum of biotin (1) from biotin derivative Bt-I (5)

Figure 19 shows the selected NMR spectra of biotin (1) and biotin derivative Bt-I (5). The spectra are different, although both compounds possess the ureido moiety. Steric effects are not likely to explain the difference in the spectra.<sup>95</sup>

In biotin, a carboxyl group is connected to the ureido moiety by a valeryl chain. In compound 5, the iodine atom is not expected to form an intra-molecular hydrogen bond with NHb. However, the carboxyl group is highly likely to be involved in an intra-molecular hydrogen bond with the ureido moiety.<sup>88</sup> Therefore, the difference of the NMR spectra of biotin from compound 5 provides evidence for the intra-molecular hydrogen bonding in biotin concerning NHb and the carboxyl group.



**Figure 19.** Difference of proton NMR peak patterns of compound 1 and 5.

## 2. 2. 4 NMR of biotin using different ratios of DMSO-d<sub>6</sub>-CDCl<sub>3</sub>

Figure 20 shows the accumulated NMR spectra of biotin as a 5 mM solution in CDCl<sub>3</sub> with various amounts of DMSO-d<sub>6</sub> at room temperature. Figure 21 shows the possible free intermolecular and intra-molecular hydrogen-bonded states of biotin in the mixed organic solvent CDCl<sub>3</sub>-DMSO-d<sub>6</sub>.

As can be seen from Figure 20, when the proportion of DMSO-d<sub>6</sub> in the mixed organic solvent CDCl<sub>3</sub>-DMSO-d<sub>6</sub> was 4.0%, the NHb chemical shift of biotin was much more downfield than that of NHa, indicating that NHb was involved in intra-molecular hydrogen bonding as shown in Scheme 4 (**I**). When the proportion of DMSO-d<sub>6</sub> increased from 4.0% to 5.3%, the NMR resonance of NHb moved up-field, which would be consistent with intra-molecular hydrogen bonding being gradually broken as in state **III** (Scheme 4). However, the NMR resonance of NHa moved downfield, which is consistent with NHa in **I** and **III** being hydrogen bonded with DMSO-d<sub>6</sub>.<sup>96</sup> When the DMSO-d<sub>6</sub> content was 6.0%, the chemical shifts of both NHa and NHb moved downfield and became coincident, which indicates that NHa and NHb are hydrogen bonded further to form states **II** and **V**. When the proportion of DMSO-d<sub>6</sub> was increased further, both of the chemical shifts of NHa and NHb moved further downfield. When the proportion of DMSO-d<sub>6</sub> was 6.6% to 20.0%, the NMR resonances of NHa moved further downfield than those of NHb. This probably indicated that NHa in **III** was hydrogen bonded in form **IV**, which causes the NMR resonance of NHa to move further downfield. Previous literature NMR assignments for biotin have usually assumed that NHb was always further downfield compared to NHa.<sup>87-89</sup> These present results have highlighted the need to be cautious in assigning which resonance is which, since NHb can be up-field of NHa depending on the solvent composition.

When the proportion of DMSO-d<sub>6</sub> was 26.7%, the NMR chemical shifts of NHa and NHb again coincide, indicating a predominance of **IV** and **V** (Scheme 4). When the proportion of DMSO-d<sub>6</sub> was 33.3% or more, structures **V** and **II** were likely to be major contributors for the more downfield of NHb than NHa even in 100% DMSO-d<sub>6</sub>.<sup>88</sup>

In the crystalline state, free biotin can form intermolecular hydrogen bonding as shown in Figure 13. This interaction is also expected to appear in solutions of water or DMSO-d<sub>6</sub> at high concentration. At room temperature, no intermolecular amide-amide hydrogen bonding was detectable in a 1 mM solution of peptides in non-polar (halogen) solvents, such as CD<sub>2</sub>Cl<sub>2</sub> and CDCl<sub>3</sub>.<sup>30</sup> When relatively polar solvents were used, such as CH<sub>3</sub>CN, the concentration of peptides could be raised to 10 mM for the non-intermolecular hydrogen-bonded state.<sup>30</sup> Therefore, solutions of biotin at concentrations of 5 mM or less in a mixed solvent of CDCl<sub>3</sub> and DMSO-d<sub>6</sub> used in this research were expected to be free of intermolecular hydrogen bonding.

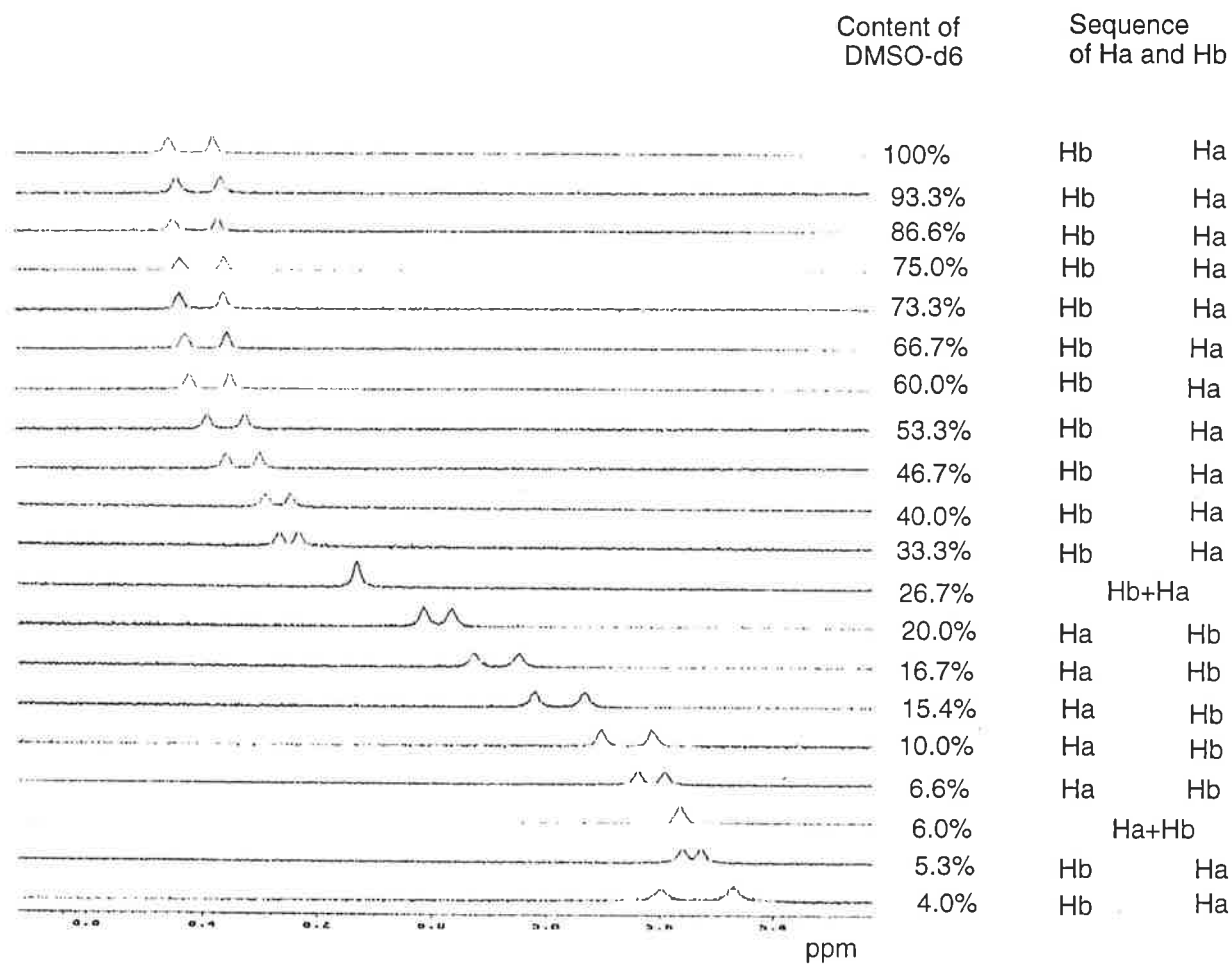
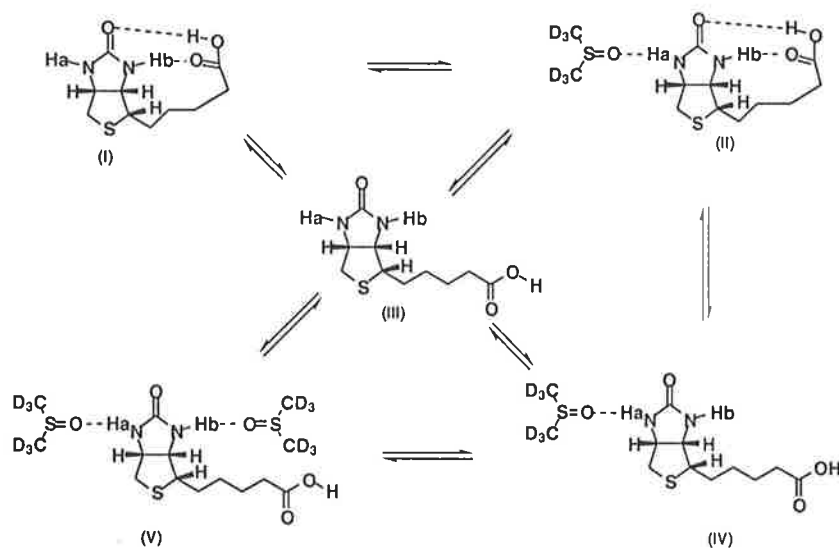


Figure 20. Proton NMR spectra of biotin in DMSO-d<sub>6</sub>-CDCl<sub>3</sub> with different ratios.



Scheme 4. Possible hydrogen bonded states of biotin in DMSO-d<sub>6</sub>-CDCl<sub>3</sub>.

### 2. 2. 5 Variable temperature NMR of biotin and derivatives

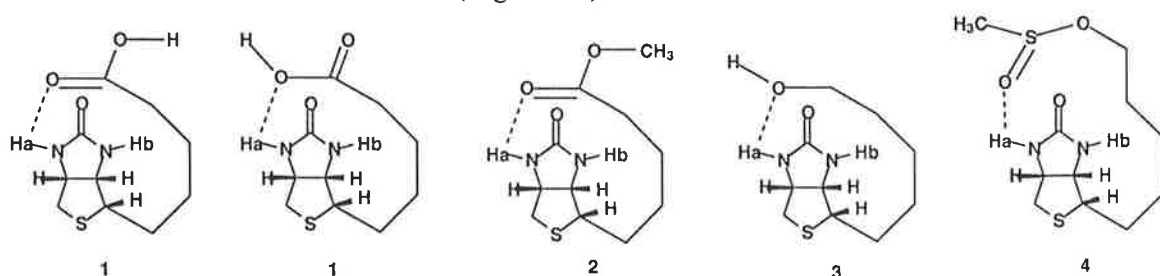
The temperature dependencies of amide protons, the  $\Delta\delta\text{NH}/\Delta T$  value, provide an indication of the efficiency of intra-molecular hydrogen bonding. Non-hydrogen bonded amide protons generally show small temperature dependencies,  $< 3$  ppb/K.<sup>30, 97</sup> In order to confirm the extent of intra-molecular hydrogen bonding of biotin, the temperature dependencies of biotin (in 2 % DMSO- $d_6$  and 98%  $\text{CDCl}_3$ ), biotinol **3**, methyl biotin ester **2**, biotinyl methanesulfonate **4** and biotinyl iodide **5** were measured at 1 mM in  $\text{CDCl}_3$  and are shown in Table 2.

As the data in Table 2 show, for compounds **1-4**,  $\Delta\delta\text{NH}/\Delta T$  values for NHb are much higher than 3 ppb/K, indicating that the protons are involved in strong intra-molecular hydrogen bonding. The  $\Delta\delta\text{NH}/\Delta T$  values for NHa and NHb in compound **5** were 3.8 ppb/K, which indicated that the protons were not involved in intra-molecular hydrogen bonding. The  $\Delta\delta\text{NH}/\Delta T$  value of compound **5** was used as a control, since the value 3.8 ppb/K indicated no intra-molecular hydrogen bonding. Compound **3** shows a significantly higher  $\Delta\delta\text{NH}/\Delta T$  value for NHb compared to **1**, **2** and **4**, indicating a particularly favorable hydrogen bonding.

**Table 2.** Intra-molecular Hydrogen Bonding in Biotin and Its Derivatives and Temperature Dependencies  $\Delta\delta\text{NH}/\Delta T$  (ppb/K).

	<b>1</b>	<b>2</b>	<b>3</b>	<b>4</b>	<b>5</b>
Ha	7.9	5.7	7.6	5.8	3.8
Hb	11.7	9.1	21.1	11.4	3.8

Table 2 also shows the temperature dependencies of NHa for compounds **1-4**, which are all larger than 3.8 ppb/K and indicative of NHa being involved in intra-molecular hydrogen bonding as well, although this interaction was not as significant as the hydrogen bonding involving NHb because of less favorable orientations (Figure 21).



**Figure 21.** Possible intra-molecular hydrogen bonding involving NHa.



The three-dimensional crystal structure of biotin showed the intermolecular hydrogen bonding between the ureido group of one molecule and protonated carboxyl group of the valeryl side chain of a symmetry-related, neighboring molecule.<sup>86</sup> In the present work, the strong intra-molecular hydrogen bonding of the ureido moiety of biotin with the protonated carboxyl group of the valeryl side chain was observed and confirmed. This intra-molecular hydrogen bonding will make proton exchange at N-3' difficult but promote that at N-1', hence, promote the substitution of the proton and the carboxylation at N-1'.<sup>87</sup> Therefore, the intra-molecular hydrogen bonding would be a reasonable explanation for the active side of biotin being N-1' for the enzymatic carboxylation, decarboxylation and transcarboxylation reactions.

### 2. 2. 6 Molecular modelling of the intra-molecular hydrogen bonding of biotin

The molecular modelling programme SPARTAN was used in determining the minimum energies. The conformations of the structures (Figure 22) were consistent with intra-molecular hydrogen bonding and their corresponding energies (Figure 23). The pattern **P1** is believed to be the most favorable for intra-molecular hydrogen bonding pair involving NHb and the ureido carbonyl with the carboxyl group. Structure **P2** is also thought to be energetically favorable, but **P3** is high in energy and so less favored.

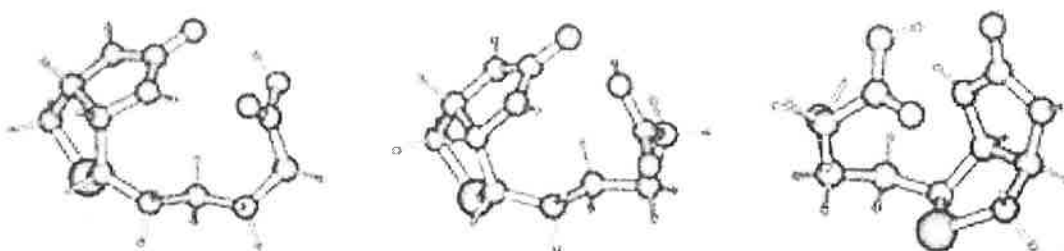


Figure 22. Molecular modelling structures of biotin with intra-molecular hydrogen bonding.

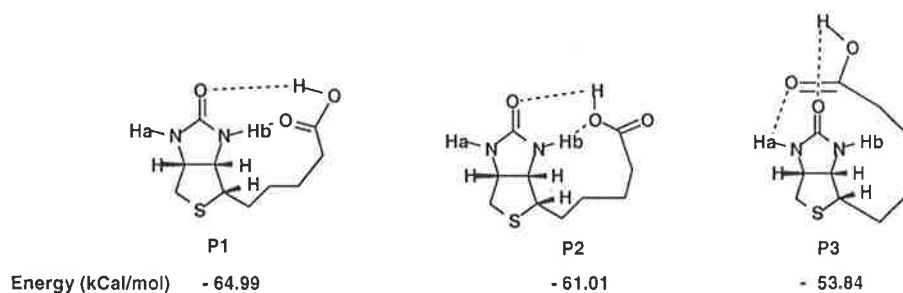


Figure 23. Energies of intramolecular hydrogen bonding patterns.

### 2. 2. 7 Intermolecular hydrogen bonding of biotin and LCQ mass spectrometry

In order to study the formation of dimers and higher oligomers of biotin compounds at higher concentration or in the solid state, mass spectrometry was applied to compounds **1-3** (Table 3). The dimer ( $2M + H^+$ ) of compound **1** at 489.1 with a 40.0% relative abundance to the base peak

(sodiumated dimer at 511.1) was observed. The protonated monomer, trimer and tetramer of compound **1** were found at 245.1 (30.0%), 732.9 (12.0%) and 976.7 (4.0%). The sodiumated monomer, trimer and tetramer of compound **1** were observed at 267.0 (4.0%), 754.9 (76.0%) and 998.7 (23.0%).

**Table 3** . L-CQ Mass Spectrometry Results of Compounds **1**, **2** and **3** (Relative Abundance %).

compound	monomer	dimer	trimer	tetramer
1 + H <sup>+</sup>	245.1 (30.0)	489.1 (40.0)	732.9 (12.0)	976.7 (74.0)
1 + Na <sup>+</sup>	267.0 (4.0)	511.1 (100)	754.0 (76.0)	998.7 (23.0)
2 + H <sup>+</sup>	259.2 (9.0)	517.0 (12.0)		
2 + Na <sup>+</sup>	281.1 (6.5)	538.9 (100)	796.6 (36.0)	1054.1 (4.0)
3 + H <sup>+</sup>	231.1 (31.8)	460.3 (15.9)		
3 + Na <sup>+</sup>	253.0 (15.6)	482.9 (100)	713.0 (40.0)	

As for compound **2**, the protonated dimer was observed at 517.0 (12%), relative to base peak-sodiumated dimer at 538.9. The protonated monomer and sodiumated monomer, trimer and tetramer of compound **2** were found at 259.2 (9.0%), 281.1 (6.5%), 796.6 (36.0%) and 1054.1 (4.0%). Table 3 also shows protonated dimer at 460.3 with 15.9% relative abundance to sodiumated dimer at 482.9 (100%). The protonated monomer, sodiumated monomer and trimer were at 231.1 (31.8%), 253.0 (15.6%) and 713.0 (40.0%).

The results in Table 3 reflecting the relative abundances of protonated monomer of compounds **1-3** are consistent with the temperature dependencies of the compounds in Table 2. The stronger the intra-molecular hydrogen bonding, the higher the relative abundance of the molecular ions. Therefore, intra-molecular hydrogen bonding might stabilize the molecular ion in the gas phase.<sup>98,99</sup>

More importantly, the relative abundance of protonated dimer of compound **1** appears much greater than that of **2** or **3**, which is indicative that the dimer of **1** is more stable than that of **2** or **3**. The intermolecular hydrogen bonding of the carboxylic groups of biotin would account for the dimerization and stabilization.<sup>100-103</sup>

The most likely structure of a biotin dimer in either the gas phase or non-polar solvents is shown in Figure 24 with six hydrogen bonds, including two intermolecular hydrogen bonding pairs between the two carboxyl groups and between the two ureido moieties concerning NHa and NHb in adjacent molecules.

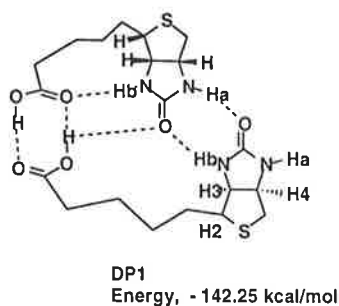


Figure 24. Dimer of biotin and its energy.

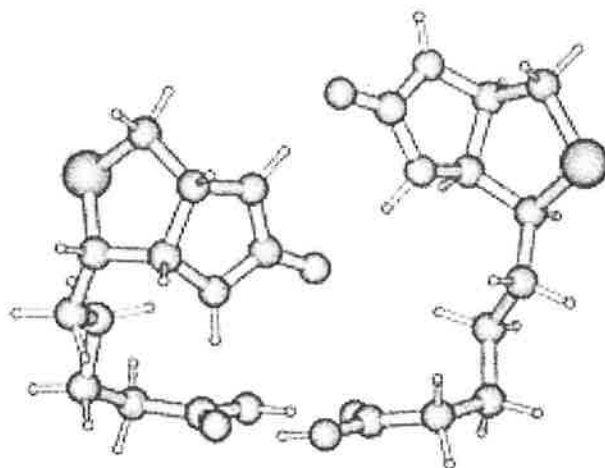


Figure 25. Molecular modelling structure of dimer of biotin with both intra- and inter-molecular hydrogen bonding.

The dimer pattern of biotin **DP1** has the lowest energy among all the possible motifs for the dimerization (Figure 24 and Figure 26). The motif **DP2** contains four hydrogen bonds including two hydrogen-bonding pairs between the carboxyl and ureido moiety involving NHb. Both motifs **DP3** and **DP4** possess a hydrogen bonding pair involving the carboxyl groups and ureido moieties involving NHb respectively.

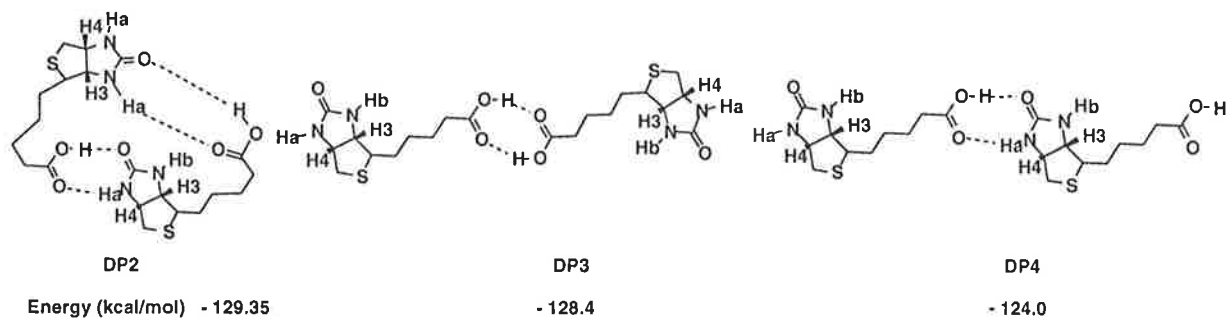


Figure 26. Energies of dimer motifs of biotin in gas phase with intermolecular hydrogen bonding.

With the stabilisation from the intermolecular and intra-molecular hydrogen bonding, the protonated trimer and tetramer of compound **1** are more likely than those of **2** or **3**, as are the sodiated trimer and tetramer of compound **1**. The proposed dimers of compound **2**, **3** and **4** are shown in Figure 27.

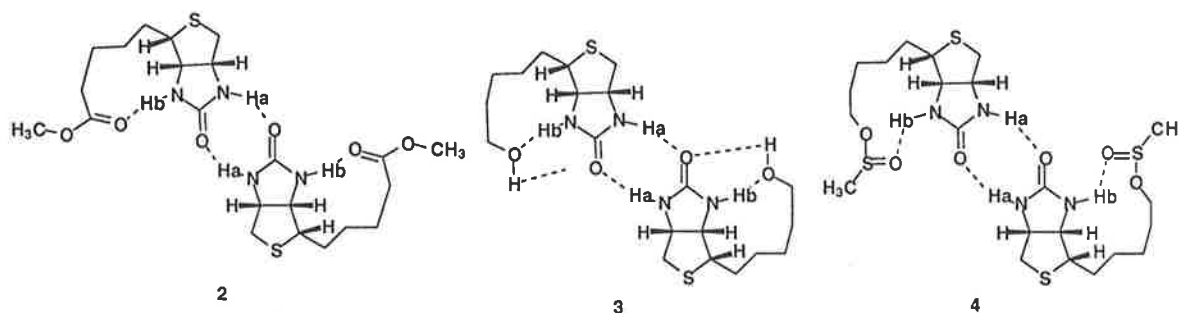


Figure 27. Dimers of biotin derivatives **2**, **3** and **4**.

---

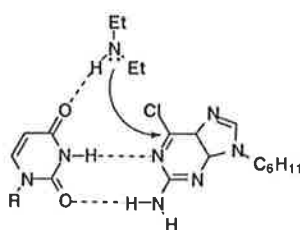
## Chapter 3

---

# Intra-molecular Hydrogen Bonded Promoted Diastereoselective Aminolysis of Biotin Ester

### 3.1 Introduction

Hydrogen bonding has been shown to play a very important role in various enzymatic reactions. For the hydrolysis of a peptide bond by serine protease, Frey and co-workers proposed that a low energy hydrogen bond was formed between His-57 and Asp-102.<sup>60-62</sup> A good model for the Asp-His dyad of this active site in the serine protease was provided by the Neuvonens.<sup>63</sup> Hydrogen bonding was seen in lysozyme-catalysed hydrolysis of peptides,<sup>64-66</sup> metalloenzyme-mediated hydrolysis of peptides<sup>67-68</sup> and ribonuclease catalysed cleavage of RNA.<sup>69-70</sup> Very recently, hydrogen bonding interactions of DNA base pairs were observed to accelerate the aminolysis of 6-chloropurine derivatives by uracil moiety (Figure 28).<sup>104</sup>



**Figure 28.** Possible ternary complex between 2-amino-6-chloropurine and uracil derivative.<sup>104</sup>

There is now strong evidence that intra-molecular hydrogen bonding is the dominant force for protein folding<sup>33-40</sup> as well as for rate accelerations in enzyme catalysis.<sup>105</sup> Intra-molecular hydrogen bonding also promotes the scaffolding of proteins, which collect active sites together for binding a substrate by polyvalent interactions.<sup>106</sup> The individual hydrogen bonds may be very weak, however, many individual interactions combine and the resultant polyvalent interactions are often strong and significant.

During enzymatic reactions, the enzyme tends to adjust its secondary and tertiary structure automatically to generate an active site for binding using various weak forces and bringing various neighboring groups into the correct orientation in order for the reaction to be most effective and often stereoselective.<sup>42-47</sup> Hydrogen bonding can be a stereo-controlling element in the reaction such as free-radical C-allylation,<sup>107</sup> catalytic addition of hydrogen cyanide to benzaldehyde<sup>49</sup> and chiral solvating reactions.<sup>50</sup>

The main feature of Goodall's mechanism for biotin-catalysed carboxylation<sup>26</sup> is that the configuration of the  $\alpha$ -carbon of the substrate molecule is retained, i.e. the carboxyl group is added to the same face of the molecule from which the  $\alpha$ -proton was removed (Scheme 2). Therefore, the reactions catalysed by biotin containing enzymes such as pyruvate carboxylase,<sup>108</sup> propionyl-CoA carboxylase<sup>109</sup> and transcarboxylase<sup>110</sup> produce chiral compounds. The active site of the enzyme in these reactions contains a biotin moiety. In order to establish the molecular basis for the rapid, regio-selective and stereo-selective biosynthesis of biotin-L-lysine residues in the biotin carboxyl carrier protein, exploit the utility of biotin moiety and confirm its specific function in enzymatic reactions, reactive biotin esters **12**, **13**, **14**, and **15** were investigated as mimics of biotin-5'-AMP to carry out aminolysis with arylmethylamine and amino acid esters.

## 3. 2 Results and Discussion

### 3. 2. 1 Synthesis

Compounds **12**, **15**, **20-23** and **25** were available commercially (Figure 29-30). Compounds **5-9**, **16**, **19**, **24** and **26-30** were prepared according to literature procedures (Figure 29-30).<sup>54, 92-94, 111-114</sup>

Compounds **10**, **11**, **13**, **14**, **17** and **18** were prepared in a similar manner to the example described in Scheme 5 for the reaction of biotin with an appropriate phenol and DCC in DMF. Compounds **17** and **18** were prepared using a similar procedure for biotin ester as shown in Scheme 6 except that the solvent was dichloromethane and the carboxylic acid reagent was caproic acid (Scheme 6).

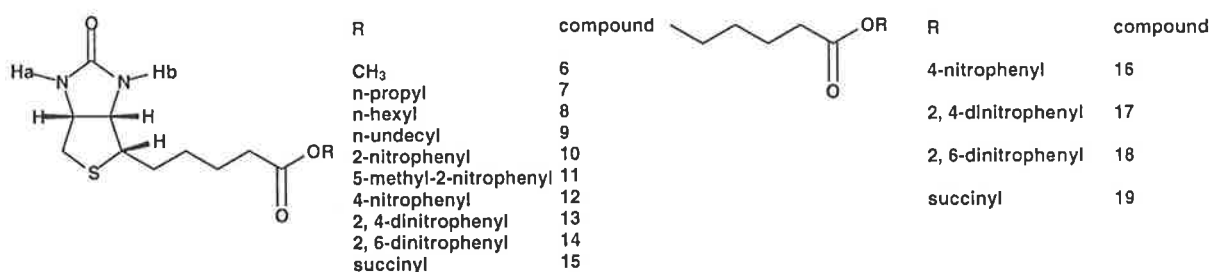


Figure 29. Biotin and caproic acid esters.

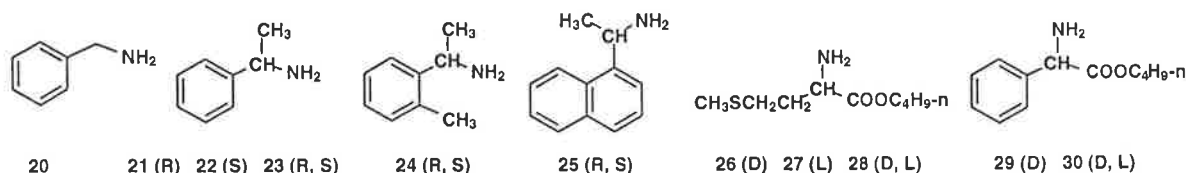
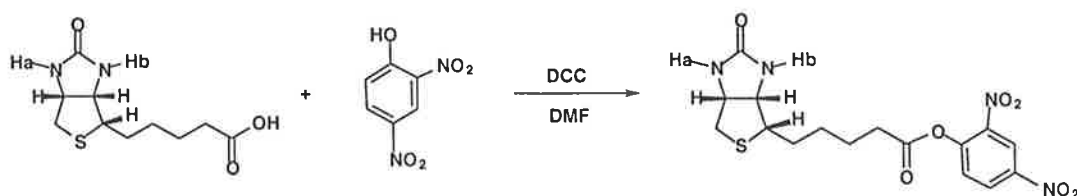
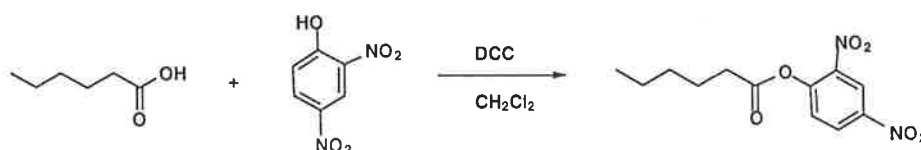


Figure 30. Amino compounds for aminolysis.



Scheme 5. Synthesis of biotin ester.



Scheme 6. Synthesis of caproic acid ester.

### 3. 2. 2 Variable temperature NMR of biotin esters and 2D-ROESY and NOESY.

In order to confirm the intra-molecular hydrogen bonding of biotin esters and exclude any contribution from intermolecular hydrogen bonding, the temperature dependencies of compounds **6**, **7**, **8**, **9**, **12** and **5** were measured at 1 mM in  $\text{CDCl}_3$  and are shown in Table 4. As the data in Table 4 show for compounds **6-9** and **12**,  $\Delta\delta\text{NH}/\Delta T$  values for NHb are much higher than 3.8 ppb/K (value for **5**, side chain containing no ester, but a pentyl iodide), which indicated that the protons were involved in intra-molecular hydrogen bonding (Figure 31a). The  $\Delta\delta\text{NH}/\Delta T$  value of compound **5** for NHa and NHb (3.8 ppb/K) represents a control for the significance of intra-molecular hydrogen bonding in biotin esters **6-9** and **12**.<sup>30</sup> According to the  $\Delta\delta\text{NH}/\Delta T$  value of NHa, this proton appears also to be involved in intra-molecular hydrogen bonding (Figure 31b), although to a much smaller amount.

Table 4. Temperature Dependencies of Biotin Esters **5-9** and **12**  $\Delta\delta\text{NH}/\Delta T$  (ppb/K).

Compound	<b>6</b>	<b>7</b>	<b>8</b>	<b>9</b>	<b>12</b>	<b>5</b>
Ha	5.7	6.2	7.0	6.6	4.6	3.8
Hb	9.1	10.2	9.9	10.2	9.2	3.8

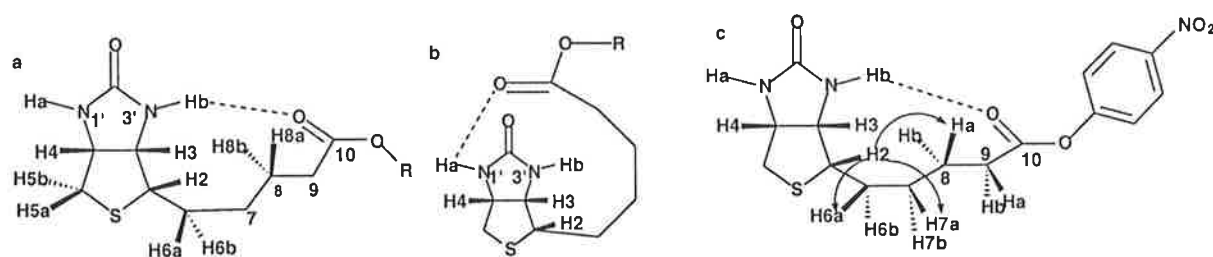
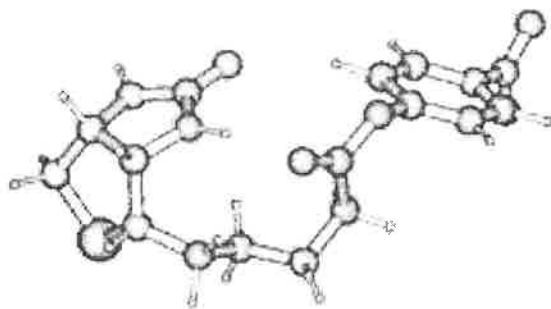


Figure 31. Intra-molecular hydrogen bonding in biotin ester (a) and (b) and possible conformation of biotin ester **12** in  $\text{CDCl}_3$  (c).



**Figure 32.** 3D structure of biotin ester **12** with intra-molecular hydrogen bonding.

The observation of intra-molecular hydrogen bonding in biotin esters continues to support Goodall's mechanism and the preference for carboxylation of the N-1' position. The conformation of intra-molecular hydrogen-bonded biotin provides a template for the design of artificial enzymes described in later Chapters. The geometry of biotin ester **12** in  $\text{CDCl}_3$  solvent at 20 mM solution was probed by carrying out homonuclear NOESY experiments. Irradiation of H3 revealed a close contact with H8b (0.46%) and H7a (0.48%) (Table 5). NOE data were observed between H2 and H8a (1.94%), H7a (2.10%) and H6 (1.31%), suggesting the conformation shown in Figure 31c.

**Table 5.** NOEs data for biotin ester **12**.<sup>a</sup>

proton irradiated	NOE data (%)			
	H6	H7a	H8a	H8b
H2	1.31	2.10	0.94	
H3		0.48		0.46

<sup>a</sup> Experiments were carried out at 20 mM in  $\text{CDCl}_3$  at room temperature

The 2D-ROESY spectrum of biotin ester **12** in  $\text{CDCl}_3$  at room temperature is shown in Figure 33 with cross peaks observed between Hb and H9 and between H3 and H9, supporting the conformation in Figure 31c. As shown in Figure 32, additional cross peaks between Hb and H2, Ha and H5a, Ha and H5b were also observed.



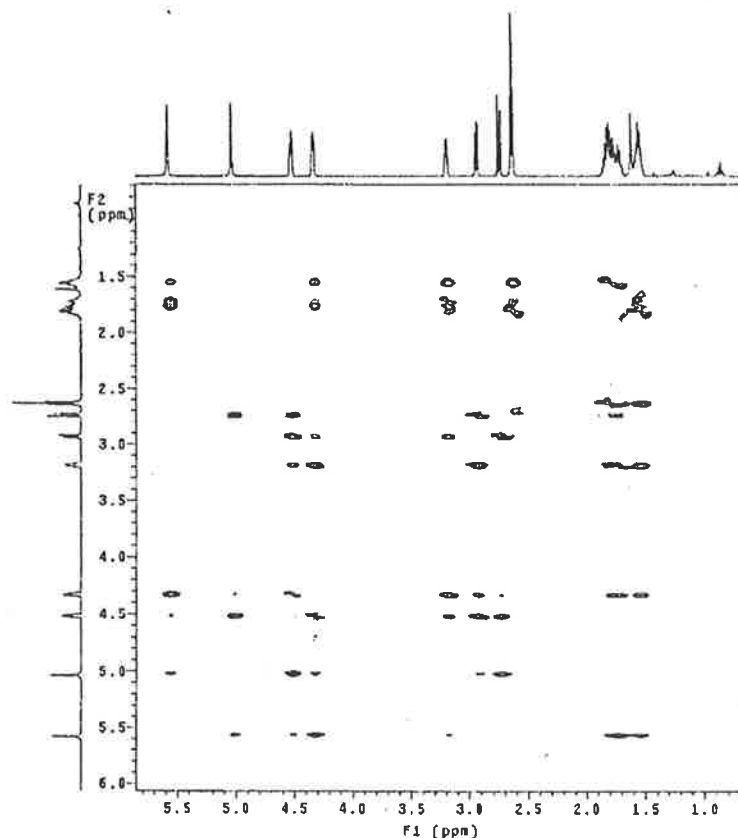


Figure 32. ROESY NMR spectrum of biotin ester **12** in  $\text{CDCl}_3$  at room temperature.

### 3. 2. 3 Relationship between intra-molecular hydrogen bonding and $pK_a$ value.

The proton NMR chemical shifts of Ha and Hb in selected biotin esters at 1 mM at room temperature in  $\text{CDCl}_3$  are shown in Table 6. Basically, there is a linear relationship between the chemical shift of Hb and the acidity of the corresponding phenol. Electron-withdrawing groups on the phenyl ring tend to increase the intra-molecular hydrogen bonding by an inductive effect through the ester carbonyl. In contrast, an electron-donating group (e. g. methyl) on the phenyl ring decreased the stability of the hydrogen bonding between Hb and the carbonyl group. Therefore there is a relationship between the  $pK_a$  value of different phenols and the strength<sup>115</sup> or distance<sup>116</sup> of the intra-molecular hydrogen bond.

Table 7. Proton NMR Chemical Shifts of Ha and Hb in Biotin Esters **10-14** (ppm) and  $pK_a$  Values from the Literature.<sup>117, 118</sup>

Compound	chemical shifts (ppm)		$pK_a$ of phenol derivatives
	Ha	Hb	
Bt-OPh-5-Me-2-nitro ( <b>11</b> )	4.451	4.653	6.94
Bt-OPh-2-nitro ( <b>10</b> )	4.476	4.686	6.88
Bt-OPh-2, 4-dinitro ( <b>13</b> )	4.528	4.715	4.09
Bt-OPh-2, 6-dinitro ( <b>14</b> )	4.498	4.718	3.73

### 3.2.4 Chiral aminolysis of biotin esters with arylmethylamines and amino acid esters.

As mentioned above, enzymatic reactions proceed through the formation of an enzyme-substrate complex and subsequent intermediates.<sup>119</sup> For examples, the hydrolysis of peptides by enzymatic catalysis e.g. serine protease proceed by the catalytic pathway of tetrahedral intermediates.<sup>120</sup> The aminolysis of esters by amines will also take place by the way of a tetrahedral intermediate.<sup>121-124</sup>

The ability of biotin to assist in the aminolysis of the side-chain ester was investigated in order to elucidate the pathway of enzymatic reactions. The determination of the order of aminolysis of biotin esters involved two separate experiments in which the initial concentration of biotin ester was kept constant and the initial concentration of the amine was set at two different values,  $[A]_{01}$  and  $[A]_{02}$ . For both conditions, the initial velocities  $u_{01}$  and  $u_{02}$  were measured graphically as product concentration versus time. The slopes of the linear plots were used to obtain the initial velocities. The initial rate ( $u_0$ ) is proportional to the initial concentration raised to the appropriate order (Eq 5).

$$U_0 = k[A_0]^a[B_0]^b \quad \text{Eq 5}$$

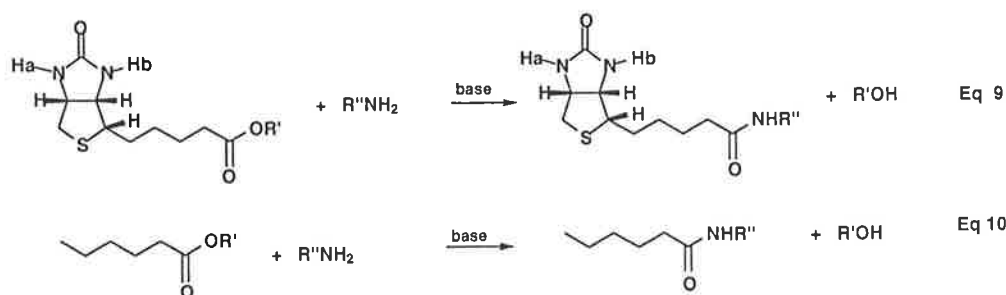
The order for the biotin ester may be calculated by using the following expression (Eq 6).

$$a = \log(u_{01}/u_{02})/\log([A]_{01}/[A]_{02}) \quad \text{Eq 6}$$

With this manner of determination, the order for biotin ester is proximately one, that for amine is also very close to one. Therefore the initial rate  $u_0$  of aminolysis of biotin ester can be fitted to the second order equation, consistent with the results reported in the literatures (Eq 7).<sup>122, 123</sup>  $[A]$  is the concentration of amine and  $[B]$  is that of biotin ester. The reaction constants of the aminolysis of biotin esters by amines (Eq 9) were then calculated from the equation (Eq 8).<sup>122, 123</sup>

$$U_0 = k[A][B] \quad \text{Eq 7}$$

$$-d[B]/dt = k[A_0][B_0] \quad \text{Eq 8}$$



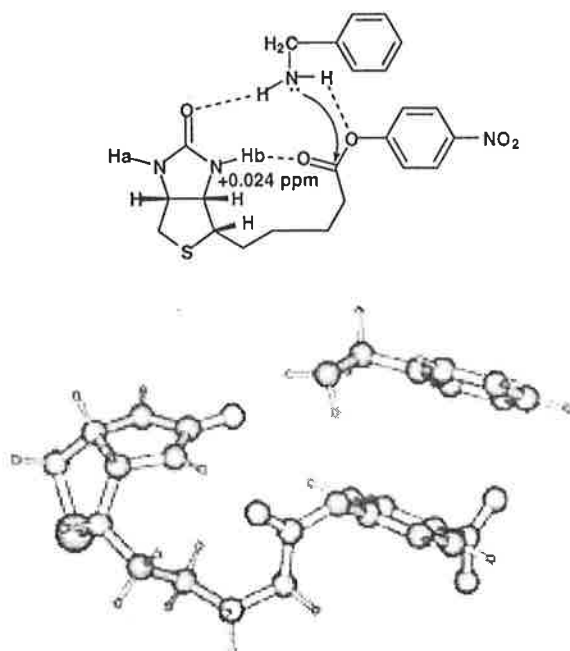
The reaction constants for the aminolysis of caproic esters by amines (Eq 10) were also measured by this method. All the reaction constants are listed in Table 7 and Table 8. Benzylamine, (*S*)- $\alpha$ -methylbenzylamine, (*R*, *S*)- $\alpha$ -methylbenzylamine and (*S*)-methionine butyl ester were used as amines in the aminolysis. As shown in Table 7, the reactivity of the biotin esters was much greater than that of the corresponding caproic acid ester. One explanation for this rate enhancement is the formation of a ternary complex such as proposed in Figure 33. By undergoing intramolecular hydrogen bonding and simultaneously hydrogen bonding to the amine nucleophile a rate enhancement would be expected.

Tentative evidence for the formation of the ternary complex was that the  $^1\text{H}$  NMR chemical shift of Hb moved downfield by + 0.024 ppm, compared to that in the free state of biotin ester **12** under the same concentrations (10 mM) and at the same temperature (20 °C) (Figure 33). The downfield movement of the chemical shift of the proton NHb would be indicative for complexation by multiple hydrogen bonding interactions. The hydrogen-bonding network in Figure 33 is expected to improve the affinity of the amine to the ester group and promote the reaction. This hydrogen-bonding network is also expected to stabilize the transition state of the aminolysis as shown in Figure 34.

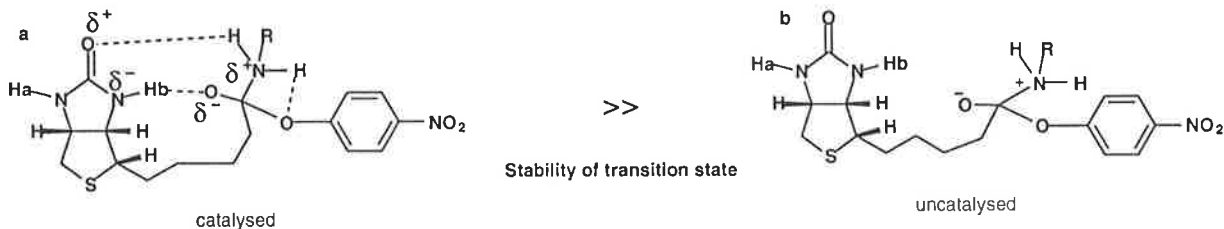
**Table 7.** Second Order rate Constants ( $\times 10^3 \text{ M}^{-1} \text{ s}^{-1}$ ) for the Reactions of Biotin Esters and Caproic Acid Esters with Amines (Eq 9 and 10).

R''NH <sub>2</sub>	R'	biotin ester	caproic acid
PhCH <sub>2</sub> NH <sub>2</sub>	succinyl <sup>a</sup>	567	103
PhCH <sub>2</sub> NH <sub>2</sub>	4-nitrophenyl <sup>b</sup>	1.3	0.29
S-PhCH(CH <sub>3</sub> )NH <sub>2</sub>	succinyl <sup>a</sup>	250	72
( <i>R</i> , <i>S</i> )-PhCH(CH <sub>3</sub> )NH <sub>2</sub>	succinyl <sup>a</sup>	255	
S-PhCH(CH <sub>3</sub> )NH <sub>2</sub>	4-nitrophenyl <sup>c</sup>	156	44
S-PhCH(CH <sub>3</sub> )NH <sub>2</sub>	4-nitrophenyl <sup>d</sup>	106	
L-CH <sub>3</sub> SCH <sub>2</sub> CH <sub>2</sub> CH(NH <sub>2</sub> )COOC <sub>4</sub> H <sub>9-n</sub>	2, 4-dinitrophenyl <sup>e</sup>	5.64	0.69
L-CH <sub>3</sub> SCH <sub>2</sub> CH <sub>2</sub> CH(NH <sub>2</sub> )COOC <sub>4</sub> H <sub>9-n</sub>	2, 6-dinitrophenyl <sup>e</sup>	0.78	

<sup>a</sup> equiv. NEt<sub>3</sub> and 0.6% DMSO-d<sub>6</sub> in CDCl<sub>3</sub>; <sup>b</sup> 1.3% DMSO-d<sub>6</sub> in CDCl<sub>3</sub>; <sup>c</sup> equiv. NEt<sub>3</sub> and 4.0% DMSO-d<sub>6</sub> in CDCl<sub>3</sub>; <sup>d</sup> 2.0% DMSO-d<sub>6</sub> in CDCl<sub>3</sub>; <sup>e</sup> 2 equiv. NEt<sub>3</sub> in CDCl<sub>3</sub>.



**Figure 33.** The possible complex of aminolysis of biotin ester **12** (10 mM) and benzylamine (10 mM) in  $\text{CDCl}_3$  at room temperature and molecular modelling structure of the complex.



**Figure 34.** Possible transition-state stabilization by intra-molecular hydrogen bonding interactions.

**Table 8.** Second order rate constants ( $\times 10^3 \text{ M}^{-1} \text{ s}^{-1}$ ) and diastereomeric excess for the reactions of biotin esters and caproic acid esters with amines in presence of  $\text{NEt}_3$  in  $\text{CDCl}_3$  at 20 °C.

$\text{R}''\text{NH}_2$	$\text{R}'$	biotin ester		caproic acid	
		k	de $\pm 0.1$ (%)	k	de $\pm 0.1$ (%)
(D, L)- $\text{CH}_3\text{SCH}_2\text{CH}_2\text{CH}(\text{NH}_2)\text{COOC}_4\text{H}_9\text{-n}$	2, 4-dinitrophenyl	8.9	4.4	2.2	
(D, L)- $\text{CH}_3\text{SCH}_2\text{CH}_2\text{CH}(\text{NH}_2)\text{COOC}_4\text{H}_9\text{-n}$	2, 6-dinitrophenyl	3.4	9.6	1.4	
(R, S)- $\text{PhCH}(\text{CH}_3)\text{NH}_2$	2, 4-dinitrophenyl	80.0	7.5	33.3	
(R, S)- $\text{PhCH}(\text{CH}_3)\text{NH}_2$	2, 6-dinitrophenyl	37.0	7.0	15.0	

The complexation of biotin ester **12** with benzylamine could also be observed by mass spectrometry. Table 9 lists the relative abundances of ions for complexes between biotin esters

and amines and those of the products (biotin amides (Eq 9) and their dimers. The ester and amine were mixed immediately prior to injection into the mass spectrometer.

The observation of the complexes by NMR and mass spectrometry confirmed that the aminolysis takes place stepwise and the formation of complexes is essential for the reactions. The complexation also reflects the binding ability of biotin ureido moiety, which is involved in biotin-containing enzymatic reactions. The formation of the complex facilitates the further aminolysis, which could be regarded as intra-molecular aminolysis as shown in Figure 33. The intra-molecular hydrogen bonding brings the hydrophilic sites together for binding, and the double intermolecular hydrogen bonds stabilise the complex (Figure 33).<sup>60</sup>

**Table 9.** Mass Spectrometry Results of Aminolysis of Esters with Benzylamine to **39** ( $[M + H]^+$ , 334; Dimer ( $[2M + H]^+$ , 667) and N-benzyl Hexamide ( $[M + H]^+$ , 206; Dimer ( $[2M + H]^+$ , 411).

active ester	relative abundance (%)		
	complex	product	dimer of product
Bt-O-succinyl ( <b>15</b> )	7.6	15.9	11.4
Bt-OPh-2-nitro ( <b>12</b> )	48.5	2.8	4.2
Bt-OPh-2, 6-dinitro ( <b>14</b> )	40.0	65.8	36.4
Bt-OPh-2, 4-dinitro ( <b>13</b> )	39.3	75.7	38.3
Cap-O-succinyl ( <b>19</b> )	15.6	28.1	9.5
Cap-OPh-2-nitro ( <b>16</b> )	10.4	25.4	12.1

Menger's seminal study of bimolecular aminolysis of activated esters showed that, in a non-polar medium, the aminolysis proceeds by a general base-catalysed mechanism.<sup>121-124</sup> Thus the formation of intra-molecular hydrogen bonding of Hb with the carbonyl group oxygen should enhance the basicity of the oxygen atom, which further polarizes the amine and increases its nucleophilicity to the ester carbonyl, which is activated by an intra-molecular hydrogen bond as well because of improvement of electron deficiency of carbonyl carbon. The intermolecular hydrogen bonding of the amine proton with the oxygen of the phenoxy group also increases the reaction rate by accelerating the collapse of the tetrahedral intermediate.<sup>125</sup>

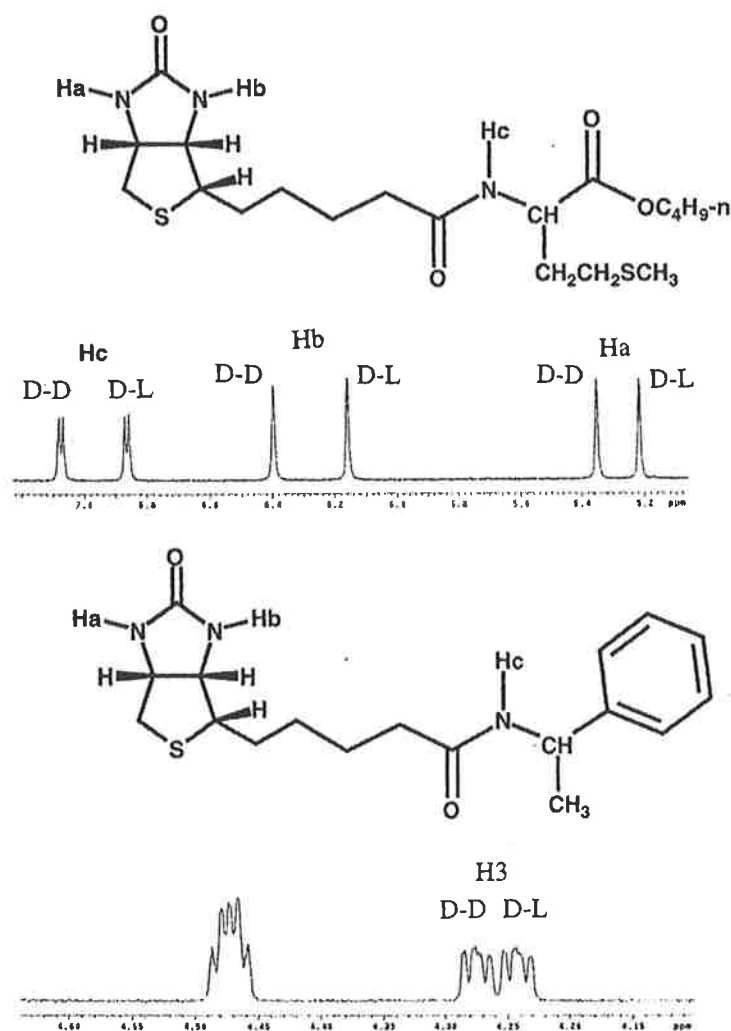
The hydrogen bonding based nitrophenol-arylmethylamine complex was observed in the non-polar solvent, as shown by the yellow color of the reaction mixture.<sup>126, 127</sup> Therefore, a proton-transferred complex  $[\text{PhO} \cdot \text{HN}^+\text{R}_3]_{\text{solv}}$  existed in the reaction mixture as well as hydrogen bonded complex  $[\text{PhOH} \cdot \text{NR}_3]_{\text{solv}}$ . Therefore the amine proton in Figure 33 is expected to form an intermolecular hydrogen bond with the phenoxy oxygen and help to remove the amine proton.

The relative rates of aminolysis of biotin esters and benzylamine were also reflected in the gas phase as shown in Table 9. In the gas phase, **39** could be produced rapidly, which appeared at 333 in the mass spectrum. According to the relative abundances of the molecular ions from

different reactions, the reaction rate sequence was **13** > **14** > **12**, which is consistent with that for reactions in solution. Intermolecular and intra-molecular hydrogen bonding has been reported in gas phase molecular recognition with intermolecular hydrogen bonding being dominant.<sup>98, 128</sup>

Enzymes are very useful for catalytic asymmetric syntheses because of their high catalytic efficiencies and their enantiospecificity.<sup>128-132</sup> The enzymatic aminolysis catalysed by *Candida antarctica component B* lipase with acceptable stereo-selectivity was reported by Unelius and co-workers.<sup>133</sup> However, only very recently have systematic investigations begun to appear on a complementary approach, namely the use of synthetically obtained chiral peptides as catalysts in asymmetric organic reactions.<sup>134-139</sup> It is reported that biotin containing enzymes catalyse the asymmetric carboxylation of pyruvate because of the unsymmetrical biotin unit.<sup>108-110</sup> Unlike most enzymes, biotin enzymes have a very flexible structure according to the electron micrograph, and this could explain why biotin enzymes are so effective in catalysis.<sup>1</sup>

**Table 8** lists the diastereomeric excess of biotin amides with L(*S*) configuration. The formation of the L(*S*) diastereomer by aminolysis was preferred to the D(*R*) diastereomer, which is consistent with that reported in the literature and results in an L(*S*)-excessive biotin amide and D(*R*)-excessive amine (amino acid ester) during the reaction.<sup>140-142</sup> The diastereomer L(*S*) and D(*R*) can be separated and characterized by <sup>1</sup>H NMR spectroscopy,<sup>50, 143, 144</sup> by using synthetic L(*S*) or D(*R*) diastereomers to assign NMR resonances in the reaction mixture. The integration of peaks in the NMR spectra was used to determine the diastereomeric excess (Figure 35).

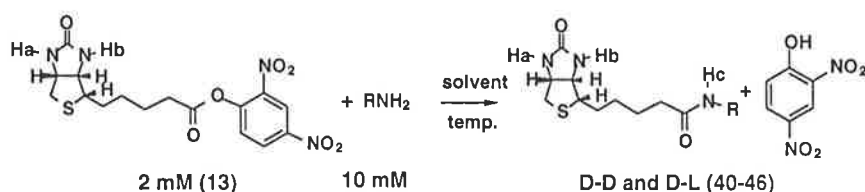


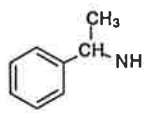
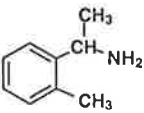
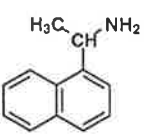
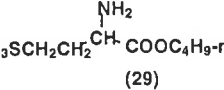
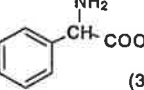
**Figure 35.**  $^1\text{H}$  NMR spectra of 1:1 mixture of D(*R*) (in front) and L(*S*) of biotin amide (a) Bt-Met (37 + 38) and (b) Bt-MBA (42).

The asymmetric induction during the aminolysis of biotin esters was also investigated in different solvents and temperatures. As shown in Table 10, there was a small increase in diastereoselectivity, when the reaction temperature was lowered. The addition of toluene- $d_6$  to  $\text{CDCl}_3$  decreases the polarity of the solvent and increased the diastereoselectivity. However, only 1.6% DMSO- $d_6$  in  $\text{CDCl}_3$  will dramatically reduce the diastereoselectivity. Therefore, both intra-molecular and intermolecular hydrogen bonding are involved in the asymmetric aminolysis of biotin esters. The intra-molecular hydrogen bonding will not prevail in the very polar solution, and DMSO will destroy intra-molecular hydrogen bonding. Therefore, intra-molecular hydrogen bonding may play a role in controlling conformational mobility,<sup>48</sup> and promote remote (1, 8) and (1, 9) asymmetric induction.

Stereo-control over more than four atoms is rare in any system.<sup>145-149</sup> To date, there has been no report on 1, 9-asymmetric induction, although there has been one report on a 1, 8-asymmetric induction<sup>150</sup> and some reports on 1, 7-, 1, 6, 1, 5- and 1, 4-asymmetric inductions.<sup>150-154</sup> Furthermore, almost all of the remote asymmetric inductions were achieved by using metal chelation to fix the conformation and position. The stereo-controlling groups should be as near as possible to the reactive centre. During the investigation of aminolysis of biotin esters with racemic amines (arylmethylamines and amino acid esters) in  $\text{CDCl}_3$  at room temperature, the intra-molecular hydrogen bonding of Hb with the carbonyl oxygen was observed as a stereo-controlling element.

**Table 10.** The Effects of Solvent and Temperature on Diastereomer Excess of Aminolysis of Biotin Ester 13.



R <sup>n</sup> NH <sub>2</sub>	product	solvent	reaction temperature (K)	R/S <sup>a</sup> (%)	de <sup>b</sup> (%)
 (23)	40 (R)	$\text{CDCl}_3$	293	44.7/55.3	10.6
	41 (S)	$\text{CDCl}_3$	273	44.4/55.6	11.2
		$\text{CDCl}_3$ -Toluene- $d_8$	293	42.7/57.3	14.6
		$\text{CDCl}_3$ + 1.6%-DMSO- $d_6$	293	49.1/50.9	1.8
 (24)	43 (R)	$\text{CDCl}_3$	293	47.1/52.9	5.8
	43 (S)	$\text{CDCl}_3$	273	47.0/53.0	6.0
 (25)	44 (R)	$\text{CDCl}_3$	293	45.0/55.0	10.0
	44 (S)	$\text{CDCl}_3$	273	43.4/56.6	13.2
 (29)	37 (D)				
	38 (L)	$\text{CDCl}_3$	293	48.3/51.7	3.4
 (30)	45 (D)				
	46 (L)	$\text{CDCl}_3$	293	44.6/55.4	10.8

<sup>a</sup> R or S configuration of amine portion of product, <sup>b</sup> diastereomeric excess of D-L epimer.

The origin of the stereo-selectivity in the aminolysis is the unsymmetric biotin unit, which controls the diastereo-selectivity. The intra-molecular hydrogen bonding in biotin esters is capable of providing the diastereo-control by preferentially arranging the S enantiomer of the amine for aminolysis (Figure 33). According to molecular modeling and 2D-NOESY (Figure



32), biotin ester adopts a hemi-spheric structure. The biotin ureido moiety and side chain ester group will form a hydrophilic side and the rest of the molecule will form the hydrophobic side. During the formation of the complex for aminolysis, any large group tends to avoid entering the hemi-sphere. Protons H5b, H6b and H8b are all on the same face of the molecule and will form a steric barrier to large groups. Therefore, the amine nucleophile with *S*-configuration will form the complex with the least steric repulsion between the aliphatic group and hydrogens H5b, H6b or H8b (Figure 36). The *S*-amine derived complex will be more stable than the *R*-amine derived complex because of accessible hydrogen bonds. The proximity of the 2, 4-dinitrophenyl group to the phenyl (amino acid ester group) may also be a result of  $\pi$ - $\pi$  stacking in the stabilization of the complex.<sup>155, 156</sup>

The molecular modelling structures of both complexes between biotin ester **12** and *R* or *S*- $\alpha$ -methylbenzylamine are shown in Figure 37, showing the intermolecular and intra-molecular hydrogen bonding interactions and stacking interactions. The energy of the *S* complex is 26.22 kcal/mol, that for *R* is 28.54 kcal/mol, which also indicates that the former complex is more stable than the latter one.

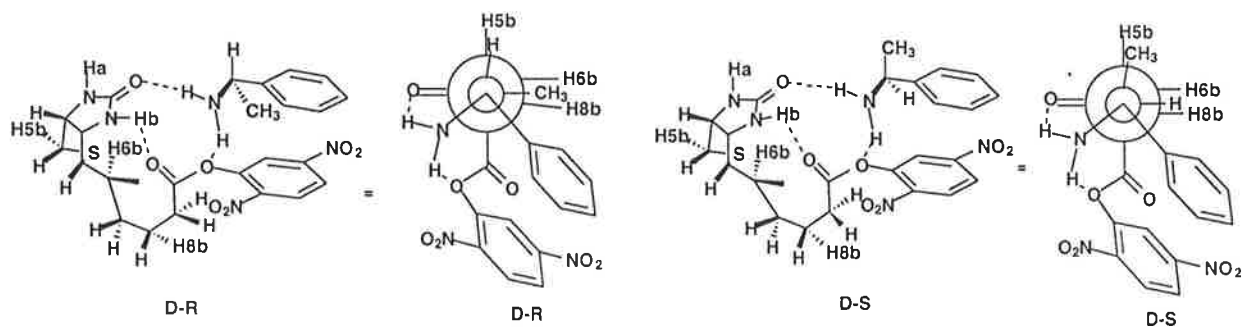
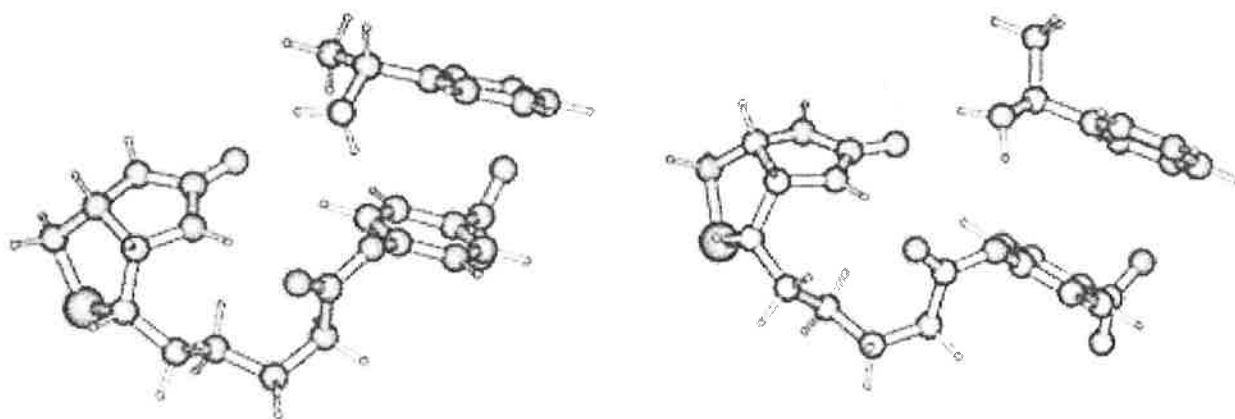


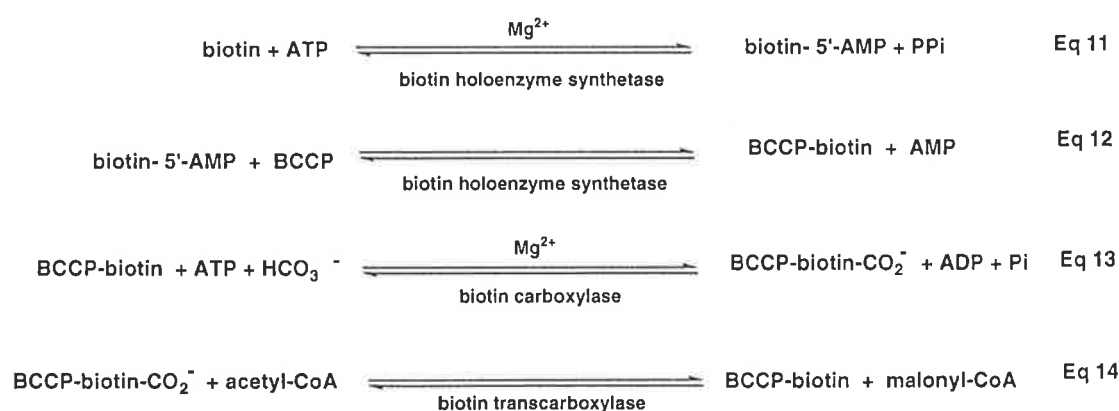
Figure 36. The assumed complex structure of biotin ester **13** with *R*- or *S*- $\alpha$ -methylbenzylamine.



**Figure 37.** Molecular modelling structures of the complexes between biotin ester 12 and *R* or *S*- $\alpha$ -methylbenzylamine

### 3. 2. 5 A molecular model for selective post-translational modification of biotin carboxyl carrier protein by biotin holoenzyme synthetase.

Acetyl-CoA carboxylase catalyses the first committed and one of the regulated steps in the fatty acid biosynthesis.<sup>21, 22</sup> The enzyme and co-enzyme biotin, found in all animals, plants, and bacteria, mediate the biotin-dependent carboxylation of acetyl-Co-A to yield malonyl-CoA with retention of configuration during the reactions.<sup>1, 26</sup> The four step reaction mechanism is summarized and shown as follows.<sup>15, 21, 24</sup>

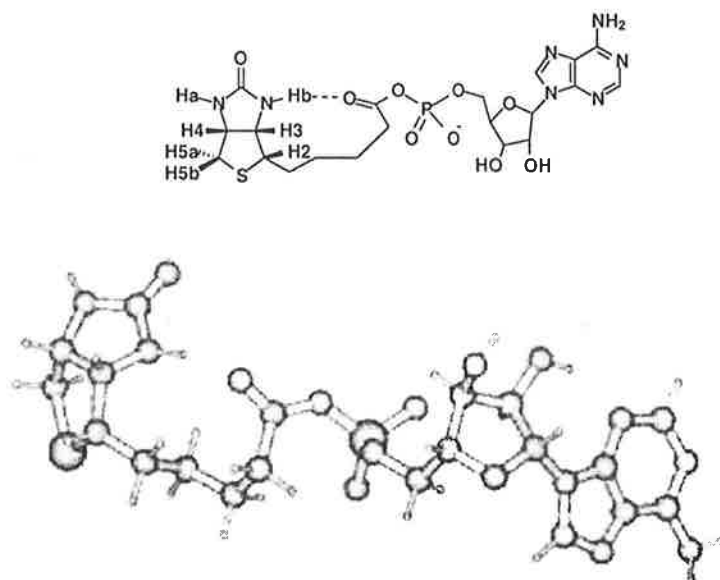


The mechanism includes the activation of the carboxyl group of biotin by reaction with ATP to form biotin-5'-AMP and elimination of pyrophosphate (PPi) (Eq 11), followed by the selective post-translational attachment to a target lysine residue at the tip of the  $\beta$ -turn in the biotin carboxyl carrier protein (BCCP) and release of AMP (Eq 12), catalysed by the biotin holoenzyme synthetase. The third step is the interaction of the biotinylated BCCP with biotin carboxylase, which results in the carboxylation of the biotin moiety with bicarbonate (Eq 13).

Finally, interaction of carboxybiotinylated BCCP with transcarboxylase leads to transfer of the carboxylate group to acetyl-CoA to yield malonyl-CoA (Eq 14).

The intra-molecular hydrogen bonding of biotin has been summarized in Figure 31. The hydrogen bonds are now proposed to assist the activation of the carboxyl group of biotin, together with the biotin holoenzyme synthetase.<sup>17, 22</sup> The hydrogen bonding of Hb with the carboxyl carbonyl oxygen tends to increase the acidity of carboxyl proton and the hydrogen bonding of the carboxyl proton with biotin ureido carbonyl. This is likely to help the deprotonation of the carboxyl proton to produce a carboxyl oxygen anion, which is environmentally active for the following nucleophilic attack of ATP to form biotin-5'-AMP. The formation of intra-molecular hydrogen bonding is likely to preclude the solvation of the substrate biotin-5'-AMP and place the nucleophilic reaction in a desolvated environment by direct contact. Therefore, the biotin ureido moiety has the ability to carry out internal catalysis with a proximity effect.

Based on the observation of intra-molecular hydrogen bonding in biotin ester (Figure 31) and molecular modeling, the biotin-5'-AMP probably adopts the intra-molecular hydrogen bonding of Hb with the carbonyl oxygen in side chain as follows in Figure 38. Such interaction can potentially contribute significantly to the stability of the intermediate biotin-5'-AMP,<sup>157</sup> activation of the carbonyl group for the following formation of tetrahedral intermediate<sup>121</sup> and release of AMP to yield biotinylated BCCP. The energy for the hydrogen bonded biotin-5'-AMP is - 53.43 kcal/mol, that for non-hydrogen bonded one is - 39.17 kcal/mol, indicating the contribution to the stability of the intermediate from intra-molecular hydrogen bonding as shown in Figure 38.



**Figure 38.** Proposed intra-molecular hydrogen bonding and molecular modelling structure of biotin-5'-AMP.

The intra-molecular hydrogen bonding of Hb with the carbonyl group in the side chain of biotin ester also exists in these complexes. The implication is that the bindings of biotin and biotin-5'-AMP to biotin holoenzyme synthetase at active site(s)<sup>17, 22</sup> is reversible, which is necessary for the enzyme to perform its catalytic role. The disassociation of the intra-molecular hydrogen bond of Hb with the carbonyl oxygen in the side chain of biotin may orient the biotin for complexation with the synthetase. The formation of an intra-molecular hydrogen bond of Hb with the carbonyl group in the side chain of biotin in biotin-5'-AMP not only promotes the covalent linkage of biotin to a specific lysine residue of apo-BCCP, but also helps the release of the reaction product biotinylated BCCP for the next complexation with biotin carboxylase. It could further play a role as a stereo-controlling element to orient the biotinylation on the lysine residue in apo-BCCP with *S*-configuration. Therefore, the enzymatic reactions possess not only the catalytic role of a high rate but also high regio-selectivity and stereo-selectivity. The intra-molecular hydrogen bonding undoubtedly plays a very important role as a determinant<sup>21</sup> in the enzymatic catalysis. The concepts described herein are of general interest and should find applications for drug design and a clearer understanding of the enzymatic catalysis process.

---

## Chapter 4

---

# Intra-molecular Hydrogen Bonding and Molecular Folding of Biotin Peptides: A Structural Approach to Biotin Peptides in Biotin Dependent Enzymes

### 4.1 Introduction

The structural similarity between various biotin-containing enzymes and their similarity to ADP-forming peptide synthetase, e.g. G. Hase DD-ligase and tRNA synthase have been related to a common evolutionary past.<sup>13, 158</sup> Furthermore, mechanistic details of the mode of action of biotin carboxylase and transcarboxylase have not been developed any further due to a lack of structural information concerning enzyme-substrate complexes.<sup>24</sup>

Recently, the crystal structure of biotinylated BCCP was determined to 1.8 Å resolution by Athappilly and Hendrickson, and internal biotin-mediated hydrogen bonding interactions were observed.<sup>25</sup> However, the biotin-protein interactions were not observable in the related biotinylated 1.3S subunit of transcarboxylase.<sup>89</sup> Biotin is co-valently attached to the  $\epsilon$ -amino group of the lysine residue in both enzyme subunits as a post-translational modification to form the basic biotin carboxyl carrier unit Ala-Met-Bct-Met-Glu (Bct: Bt-Lys), which is the conserved region of the biotinyl subunit.<sup>1</sup>

The intra-molecular hydrogen bonding of biotin and biotin esters has been observed (Chapter 3) and provides support for Goodall's mechanism for biotin action and a rationalization for the preferential reaction of the N-1' of biotin.<sup>87</sup> Intra-molecular hydrogen bonding was proposed for rate enhancements in biotin aminolysis (Chapter 3).

In order to probe the potential interactions of side chain amino acids with biotin in biotin-containing enzymes, Bt-Lys(L)-Met(L) (**47**), Bt-Lys(L)-Met(D) (**48**), Bt-Ahx-Met(L) (**49**) and Bt-Ahx-Met(D) (**50**) were prepared. These compounds were used to elucidate the possible intra-molecular hydrogen bonding interactions, folding and the formation of active sites of the peptides and a mechanism for the catalytic cycle involving the release of biotinylated BCCP and subsequent attachment to biotin carboxylase then transcarboxylase. These compounds should also provide evidence for a mechanism whereby holo-BCCP enzymes can distinguish pro-chiral hydrogens during biotin promoted carboxylations.

## 4.2 Results and Discussion

### 4.2.1 Synthesis

Biotin amides and peptides **31-46** were prepared by a common procedure involving biotin *N*-hydroxysuccinimide ester and the corresponding amine or amino acid ester in DMF at rt (Figure 39 and Scheme 7-8). For the preparation of **34-38**, **45** and **46**,  $\text{NEt}_3$  was required in order to generate free amine from the corresponding hydrochloride salt.

During the synthesis of the biotin peptide Bt-Lys(L)-Met(D) (**47**), biotinyl lysine was initially prepared by the amidation of biotin *N*-hydroxysuccinimide ester with free *N*-*t*-Boc-L-lysine in pyridine- $\text{NaOH}$ - $\text{H}_2\text{O}$  solution as shown in Scheme 7. The biotinyl lysine was then converted into its *N*-hydroxysuccinimide ester, which was amidated with butyl D-methionine ester hydrochloride in the presence of  $\text{NEt}_3$  to give **47**. Compound Bt-Lys(L)-Met(L) (**48**), Bt-Ahx-Met(D) (**49**) and Bt-Ahx-Met(L) (**50**) were prepared in a similar manner.

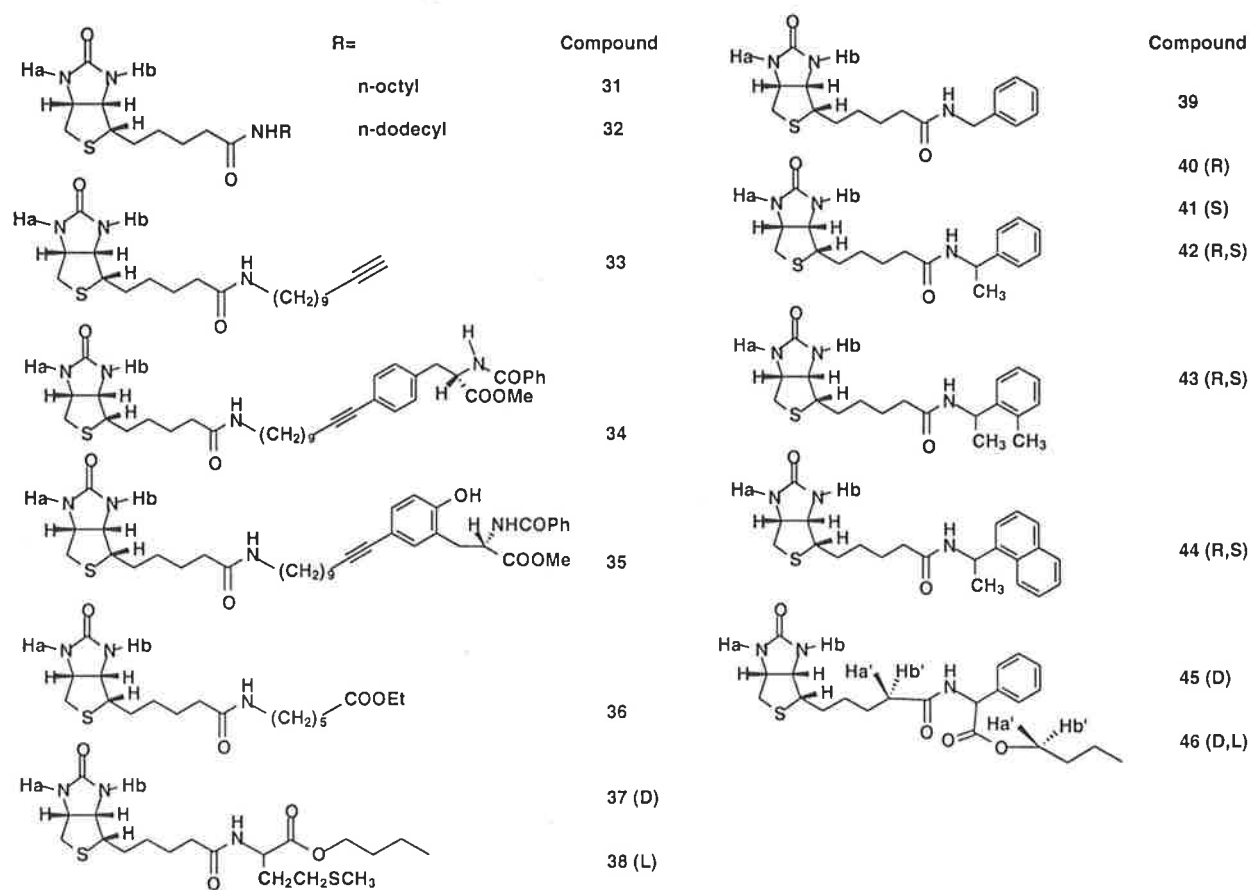


Figure 39a. Synthetic biotin peptides

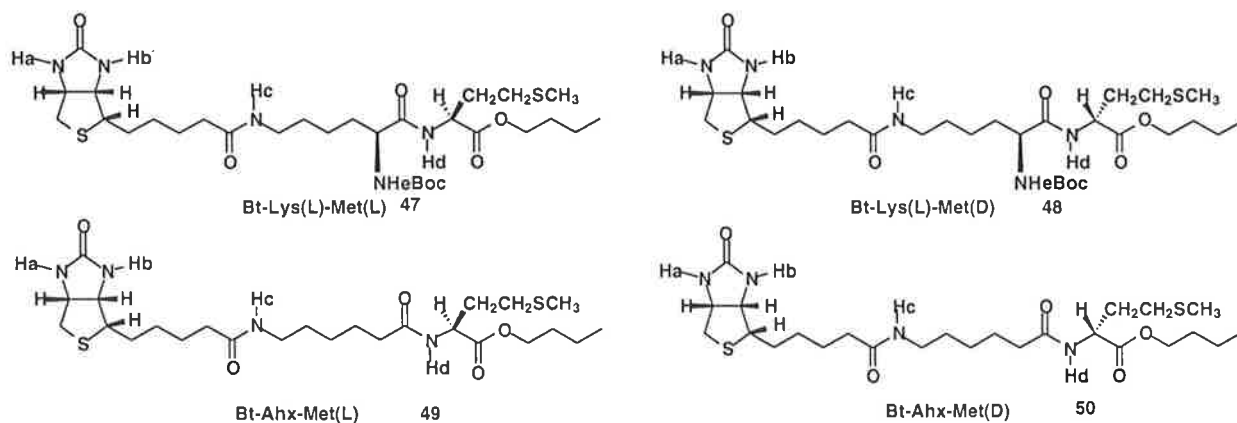
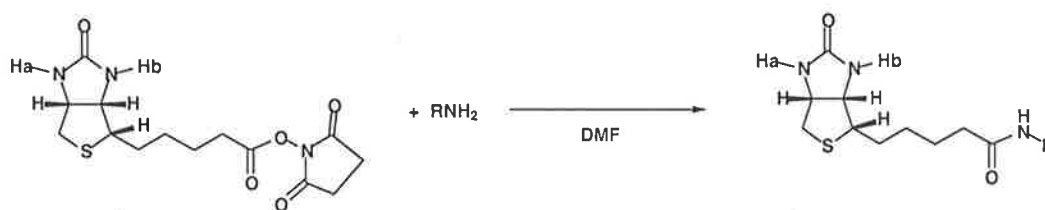
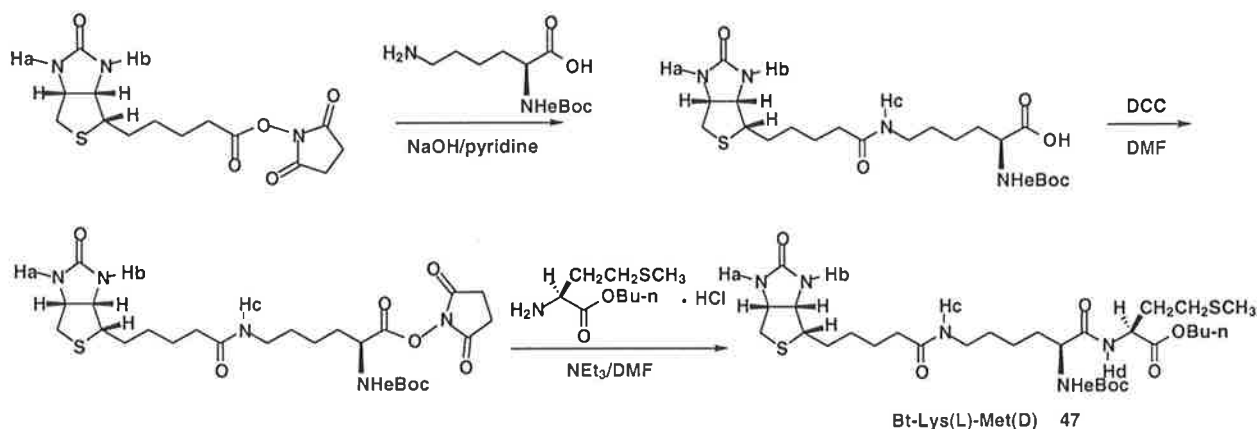


Figure 39b. Synthetic biotin peptides.



Scheme 7. Synthesis of biotin amides and peptides.



Scheme 8. Synthesis of biotin peptide 47.

#### 4. 2. 2 Intra-molecular hydrogen bonding in synthetic peptides

Table 11 shows the temperature dependencies of the various active NH protons in the synthetic biotin peptides **31-35** in  $\text{CDCl}_3$  (all samples 1 mM). According to the literature, for similar model peptides in chlorocarbon solvents, an intra-molecular hydrogen bonded amide NH proton exhibits temperature dependency,  $\Delta\delta_{\text{NH}}/\Delta T$ , greater than 4 ppb/K,<sup>97</sup> while a free NH proton gives a value around 3.0 ppb/K.<sup>159</sup> Gellman and co-workers have reported that for a flexible diamide,  $\Delta\delta_{\text{NH}}/\Delta T$  values for the completely hydrogen-bonded state is about 5.0 ppb/K.<sup>30</sup> The temperature dependence of the amide NH proton chemical shifts has become a useful tool in the

study of peptide conformation.<sup>160</sup> However, one must be careful with the interpretation of the data because changes in both solvent and structure of the peptide will cause deviations in the  $\Delta\delta\text{NH}/\Delta\text{T}$  values.<sup>161, 162</sup> In order to exclude the possible contribution to the temperature dependence from intermolecular hydrogen bonding, compound **5** was used as a control, since this compound cannot exhibit intra-molecular hydrogen bonding and exhibited the same value of 3.8 ppb/K for both Ha and Hb.

According to the data in Table 11,  $\Delta\delta\text{NH}/\Delta\text{T}$  values for NHb in the biotin peptides **31-33** were as high as 16 ppb/K, which indicated that NHb was significantly involved in intra-molecular hydrogen bonding with the carbonyl group in the side chain of biotin peptides. An intra-molecular hydrogen bond between NHa with the carbonyl group was also evident, but it was less significant (Figure 40). Likewise,  $\Delta\delta\text{NH}/\Delta\text{T}$  values for NHc of around 6 ppb/K are significant and indicative of an intra-molecular hydrogen bond between NHc and the carbonyl group of biotin (Table 11).

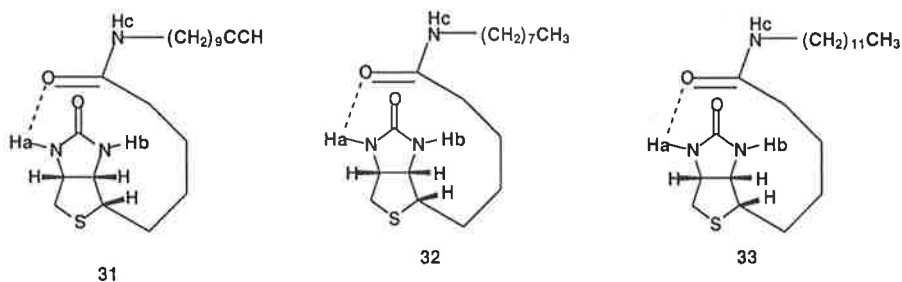


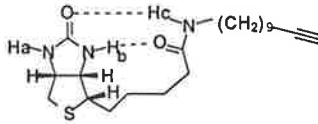
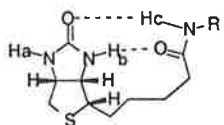
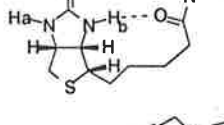
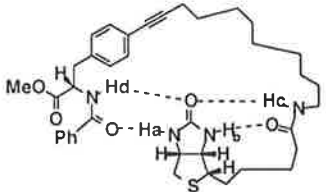
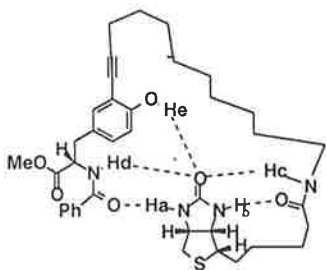
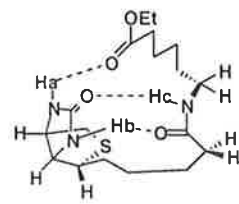
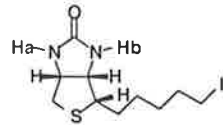
Figure 40. Intramolecular hydrogen bonding involving NHa in **31-33**.

As for biotin peptide **34**, the  $\Delta\delta\text{NH}/\Delta\text{T}$  value for NHb was 15.4 ppb/K and that for NHc was 6.9 ppb/K, indicating that NHb and NHc were both involved in intra-molecular hydrogen bonding (Table 11). Furthermore, the  $\Delta\delta\text{NH}/\Delta\text{T}$  value for NHa was 10.5 ppb/K, one of the highest values for this NH group. Therefore, Ha is likely to be involved in intra-molecular hydrogen bonding with the carbonyl group of the amide of the phenyl alanine methyl ester as shown in Table 11. Likewise, the  $\Delta\delta\text{NH}/\Delta\text{T}$  value for NHd was 4.7 ppb/K, suggesting a weak intra-molecular hydrogen bond with the carbonyl of biotin.

The larger  $\Delta\delta\text{NH}/\Delta\text{T}$  values for NHa and NHb for compound **35** compared to **34** suggested stronger hydrogen-bonding interactions (Table 11). The  $\Delta\delta\text{NH}/\Delta\text{T}$  values for NHc, NHd and He all suggest a simultaneous polyvalent interaction or an average of individual interactions that is collectively much stronger than the corresponding monovalent interaction.<sup>106, 163</sup> Compound **36**, showed the highest  $\Delta\delta\text{NH}/\Delta\text{T}$  values for NHb, NHb and NHc, indicating a likely cooperative effect of the hydrogen bonding interactions (Table 11).



**Table 11.**  $^1\text{H}$  NMR Chemical Shift Temperature Dependencies (ppb/K) of NH Protons in Biotin Peptides in  $\text{CDCl}_3$  at 1 mM.

biotin peptide	name	Ha	Hb	Hc	Hd	He
	33	8.8	15.7	6.1		
	31 (R = n-octyl)	6.5	16.3	6.1		
	32 (R = n-dodecyl)	9.2	16.2	6.1		
	34 (Bt-Phe)	10.5	15.4	6.9	4.7	
	35 (Bt-Tyr)	10.2	17.2	10.4	6.8	11.6
	36 (Bt-Ahx)	13.3	21.8	10.6		
	5 (Bt-I)	3.8	3.8			

According to the structure of biotin carboxylase,<sup>13, 82, 158</sup> the valeric acid side chain of biotin is in close proximity to the bicyclic ring system.<sup>19, 80, 81</sup> The observation of strong intra-molecular hydrogen bonding of Hb with the carbonyl group may be one explanation for the observed conformation of biotin attached to peptides.

According to our observation of intramolecular hydrogen bonding concerning Ha and the ureido carbonyl oxygen atom in biotin peptides **33** and **34**, the folding<sup>164, 165</sup> of biotin carboxylase and stabilization of biotin-enzyme complex<sup>165</sup> could be due to a cooperative hydrogen bonding. Intramolecular hydrogen bonding has been well recognized as a dominant force in the folding of

peptides and proteins,<sup>33-40</sup> such as circular WW protein.<sup>105</sup> Intra-molecular hydrogen bonding also promotes the scaffolding of proteins, showing that co-operativity in hydrogen bonding can be much stronger and more effective than the corresponding monovalent interactions.

### 4. 2. 3 2D NMR evidence for intra-molecular hydrogen bonding

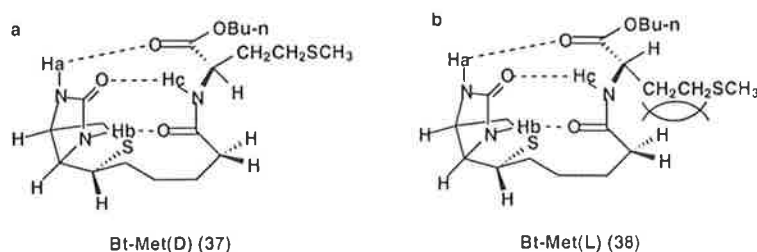
In the conserved tetrapeptide Ala-Met-Bct-Met of biotin enzymes, Met-88 has been placed in an important position for the transferring of a carboxyl group from the enzyme to substrate. The replacement of methionine at position 88 either by hydrophobic or hydrophilic residues significantly altered the enzyme activity.<sup>166</sup> In order to elucidate the structural basis for the specific function of methionine in the conserved tetrapeptide, both enantiomers of methionine butyl ester were reacted with biotin *N*-hydroxysuccinimide to give biotin peptides **37** and **38**.

The variable temperature <sup>1</sup>H NMR data for Ha, Hb and Hc in biotin peptide Bt-Met(D) (**37**) and Bt-Met(L) (**38**) in CDCl<sub>3</sub> at 1 mM concentration are shown in Table 12. All three NH protons Ha, Hb and Hc in **37** show larger temperature dependencies than those of **38**. The  $\Delta\delta_{\text{NH}}/\Delta T$  value for Hb of compound Bt-Met(D) (**38**) was close to that of compound **36**, however,  $\Delta\delta_{\text{NH}}/\Delta T$  values for Ha and Hc were much larger than the corresponding values in compound **31-36** (Table 11). Molecular modelling showed low energy conformations for hydrogen bonded structure Bt-Met(D) (**37**) (Figure 42).

Molecular models of compounds **38** showed that steric repulsion between the side chain of methionine (CH<sub>2</sub>CH<sub>2</sub>SCH<sub>3</sub>) and the methylene hydrogens in the 9 position of the valeric chain of biotin in Bt-Met(L) (**38**) reduces intra-molecular hydrogen bonding for Hb, Hc and Ha, compared to that in Bt-Met(D) (**37**).

**Table 12.** Temperature Dependence of Proton NMR Resonances of NH in Biotinylated Methionine Butyl Ester **37** and **38** for 1 mM in CDCl<sub>3</sub> ( $\Delta\delta_{\text{NH}}/\Delta T$ , ppb/K).

Compound	Ha	Hb	Hc
Bt-Met(D) ( <b>37</b> )	14.1	21.4	17.6
Bt-Met(L) ( <b>38</b> )	10.9	15.0	10.5



**Figure 41.** Intra-molecular H-bonding in biotin peptide Bt-Met(D), (a) (**37**) and Bt-Met(L) (b) (**38**) in CDCl<sub>3</sub>.

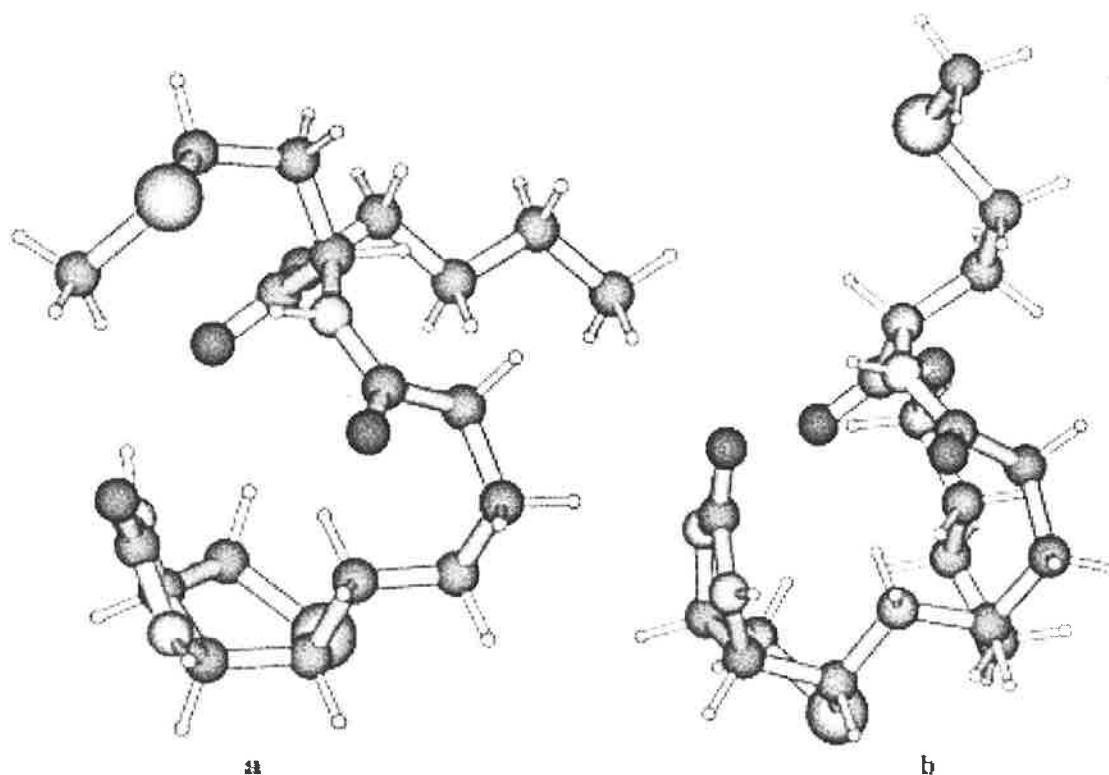


Figure 42. 3D structures of compounds **37** (a) and **38** (b) by molecular modelling.

The geometry of biotin peptides Bt-Met(D) (**37**) and Bt-Met(L) (**38**) in  $\text{CDCl}_3$  solvent at 25 mM solution was probed by 2D-ROESY experiments. Part of the 2D ROESY spectrum for Bt-Met(D) (**37**) is shown in Figure 43 and shows that the cross peaks are very strong between Hb and Hc, and between Ha and Hc, which are indicative for their proximity. The cross peaks in the 2D-ROESY spectrum for Bt-Met(D) (**37**) were much stronger than those for Bt-Met(L) (**38**), which is consistent with the result derived from the variable temperature experiments and  $\Delta\delta_{\text{NH}}/\Delta T$  values.

Cross peaks were observed between H9 and Hm11-14 (butyl group) and between Hm4 and H6, H7, Hc and Hb, confirming the spatial proximity of the butyl group in the ester to C9 in the valeric side chain of biotin and side chain of methionine  $\text{CH}_2\text{CH}_2\text{SCH}_3$  to Hc, Hb, C6 and C7 in the valeric side chain of biotin (Figure 45). The cross peaks support the conformation of Bt-Met(D) (**37**) predicted by molecular modelling as shown in Figure 41. As for Bt-Met(L) (**38**) (Figure 44), although the cross peaks between Hb and Hc, Ha and Hc and Hm4 and Hc were observed and so confirmed the intra-molecular hydrogen bonds as described in Figure 41, cross peaks between protons on C9 of the valeric side chain of biotin and those in the butyl ester were not obvious. Cross peaks of H9 with Hm2, Hm3a and Hm3b were observed (Figure 46), showing their spatial proximity and confirming the geometry in Figure 41.

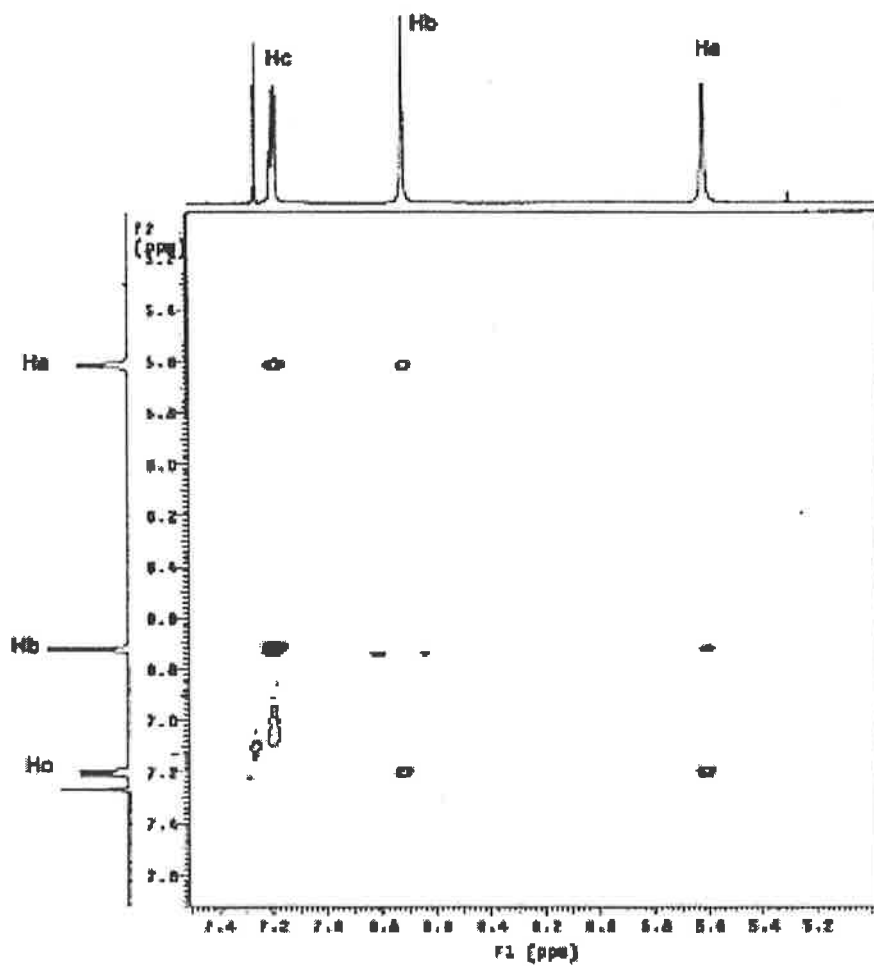
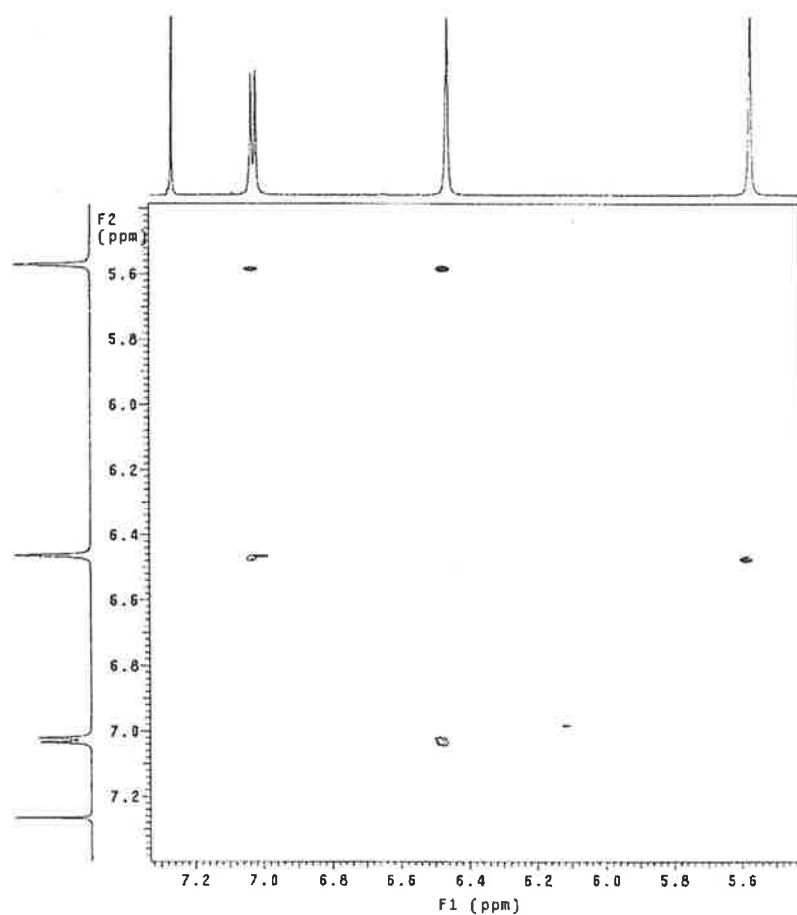
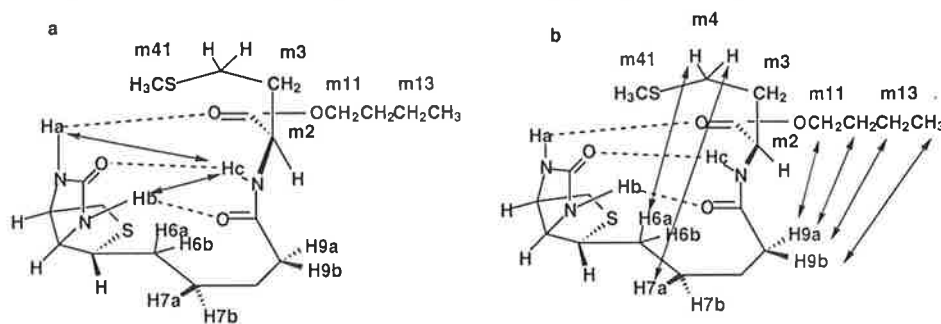


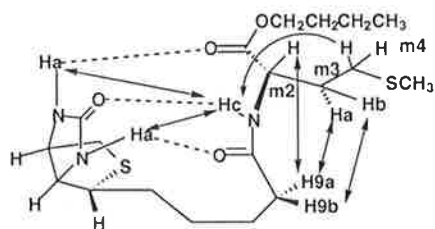
Figure 43. 2D-ROESY spectrum of Bt-Met(D) (37) in  $\text{CDCl}_3$  at 25 mM at rt.



**Figure 44.** 2D-ROESY spectrum of Bt-Met(L) (**38**) in  $\text{CDCl}_3$  at 25 mM at rt.



**Figure 45.** Cross peaks between Hc and Ha and Hb (a) and between Hm4 and H6 and H7, and between Hm11, Hm12, Hm13 and Hm14 and H9 (b) in NMR ROESY spectrum of Bt-Met(D) (**37**).

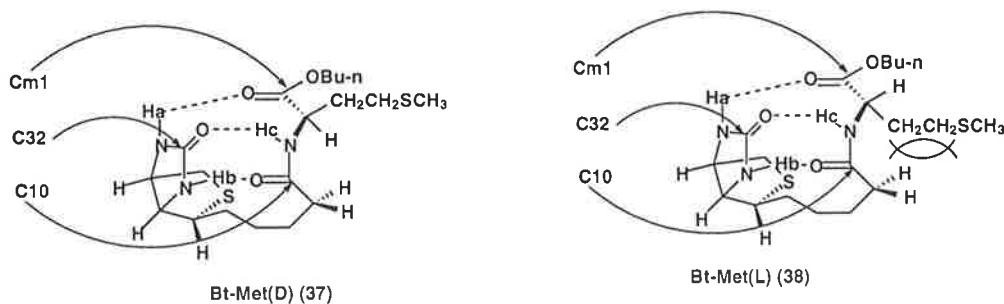


**Figure 46.** Cross peaks of Bt-Met(L) (**38**) in ROESY spectrum between Hc and Ha, Hb and Hm4, between H9 and Hm2, Hm3a and Hm3b.

Tables 13 and 14 show the  $^{13}\text{C}$  and  $^1\text{H}$  NMR chemical shifts for the carbonyl carbons and NH protons in Bt-Met(D) (**37**) and Bt-Met(L) (**38**) in  $\text{CDCl}_3$  at 25 mM and 20 °C. All of the carbons of the carbonyl groups and NH protons in Bt-Met(D) (**37**) were downfield, compared to those of Bt-Met(L) (**38**). This is consistent with the carbonyl groups in Bt-Met(D) (**37**) being involved in more efficient intra-molecular hydrogen bonding than those of Bt-Met(L) (**38**).

**Table 13.**  $^{13}\text{C}$  NMR Chemical Shifts (ppm) of the Carbonyl Carbons in Bt-Met(D) (**37**) and Bt-Met(L) (**38**) in  $\text{CDCl}_3$  at 25 mM and 20 °C.

Compound	C32	C10	Cm1
Bt-Met(D) ( <b>37</b> )	164.08	173.13	173.31
Bt-Met(L) ( <b>38</b> )	163.97	172.95	173.26
$\Delta\delta$ $^{13}\text{C}$ (D-L)	0.11	0.18	0.05



Therefore, 2D-ROESY NMR experiments together with variable temperature proton as well as carbon NMR experiments (Table 13) confirm the intra-molecular hydrogen bonding in biotin peptide Bt-Met(D) (**37**) and Bt-Met(L) (**38**). The compound Bt-Met(L) (**38**) contains the natural enantiomers for biotin and methionine, whereas Bt-Met(D) (**37**) contains the unnatural amino acid. The strong intra-molecular hydrogen bonding within both peptides Bt-Met(D) (**37**) and Bt-Met(L) (**38**) would be important for the folding of peptides containing these groups. Although Bt-Met(D) (**37**) showed stronger intra-molecular hydrogen bonding compared to Bt-Met(L) (**38**), the enzyme active site will contain additional hydrogen bonding and hydrophobic interactions that may be more favorable for biotin peptide derivatives with the L configuration. Additionally, the orientation of groups in the active site may require this specific configuration to optimize catalytic activity.

**Table 14.**  $^1\text{H}$  NMR Chemical Shifts of NH Protons in **37** and **38** in  $\text{CDCl}_3$ , 1 mM and at rt.

Compound	Hc	Hb	Ha
Bt-Met(D) ( <b>37</b> )	7.20	6.72	5.62
Bt-Met(L) ( <b>38</b> )	7.02	6.46	5.57
$\Delta\delta$ $^1\text{H}$ (D-L)	0.18	0.26	0.05

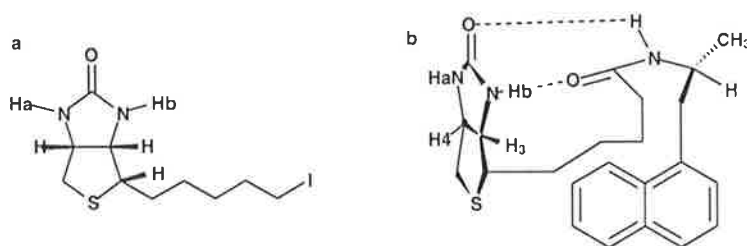
#### 4.2.4 Interactions between biotin and aromatics

It is well known that biotin can be bound by avidin extremely tightly,<sup>167-169</sup> which explains the toxic effect of ingested uncooked egg white in animals,<sup>170</sup> since it renders biotin unavailable for use in enzymes.<sup>1,171</sup> Avidin has been widely applied to the study of biotin-dependent enzymes, because of its specific ability to bind tightly to biotin. However, the nature of this binding is still not clear. According to the literature, four tryptophan residues in each subunit interact directly with biotin.<sup>167</sup> Very recently, Wilchek and co-worker used avidin to displace low affinity ligands to show the high affinity of avidin with the aromatic amino acid residues Trp-97, Trp-70, Phe-79, Tyr-33, Lys-111 and Trp-110.<sup>169</sup>

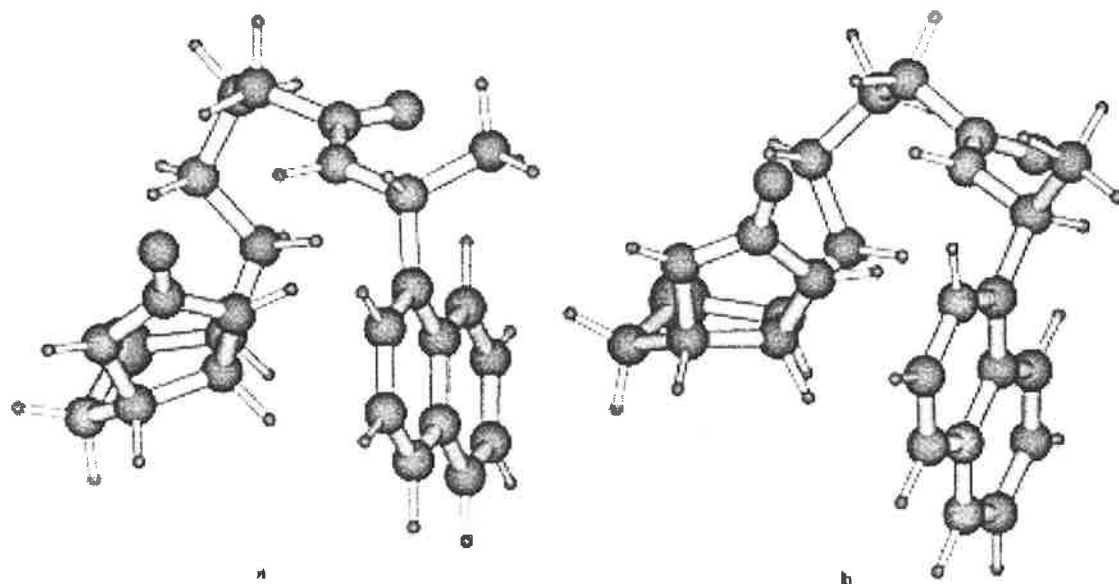
The chemical shifts of H3 in compounds **5**, **40**, **41**, **45** and **44** are shown in Table 15 in CDCl<sub>3</sub> at 1 mM and room temperature. The introduction of an aromatic ring into biotin peptides resulted in an upfield shift of the proton NMR resonance of H3. The biotin ring system does allow the aromatic ring to lie under, or endo to the fused rings. The H3 of compound **44** was greatly shielded (0.202 ppm), compared to compound **5**, the latter compound containing no aromatic ring in the side-chain. The absolute value of the change is much larger than 0.05 ppm, a value used to judge the significance of the change of chemical shifts and effectiveness of interactions.<sup>166</sup> The upfield movement of the proton NMR resonance of H4 is 0.073 ppm, which is smaller than 0.202 ppm and reflects the fact that H3 (D-L) is closer to the aromatic ring than H4.

**Table 15.** Proton NMR Resonance of H3 in Compounds **5**, **40**, **41**, **45** and **44** in CDCl<sub>3</sub> at rt at 1 mM and 10 mM, except **44** at 6.7 mM in Saturated Solution (ppm).

compound	<b>5</b>	<b>40</b>	<b>41</b>	<b>45</b>	<b>44</b>
1mM	4.357	4.310	4.296	4.290	4.155
10mM	4.335	4.258	4.244	4.250	4.108



**Figure 47.** Structures of compound **5** (a) and **44** (R) with possible stacking contacts of naphthyl group with H3 and H4 in biotin unit.



**Figure 48.** 3D-structures of the diastereomers *R* (a) and *S* (b) of compound **44** with intra-molecular hydrogen bonding interactions and stacking interactions between H3 and naphthyl ring.

There are seven atoms which separate biotin from the aromatic (naphthyl) ring, so the intra-molecular hydrogen bonding within biotin amides promotes the proximity of the biotin ring system and the aromatic ring. The evidence for the intra-molecular hydrogen bonding are the temperature dependencies of protons Ha, Hb and Hc in biotin peptides **39-41** and **45** shown in Table 16, all the values are larger than 3.8 ppb/K. According to Table 16, for the diastereomeric compounds **40** (Bt-mbn(*R*)) and **41** (Bt-mbn(*S*)), the  $\Delta\delta_{\text{NH}}/\Delta T$  values for Hc and Hb were very similar, however, the value for Ha in **41** was larger than **40**.

**Table 16.**  $^1\text{H}$  NMR Resonance Temperature Dependency for Biotin Peptides **39**, **40**, **41** and **45** in  $\text{CDCl}_3$  at 1 mM (ppb/K).

Compound	Ha	Hb	Hc
<b>39</b>	7.2	20.3	10.5
<b>40</b>	8.5	20.2	11.9
<b>41</b>	10.5	21.6	11.9
<b>45</b>	16.3	22.2	18.8

Furthermore, as for naphthyl compound **44**, the chemical shifts of H3 for the diastereomers *R* (4.280 ppm) and *S* (4.155 ppm) were quite different. A possible explanation for this difference (0.125 ppm) is that the *S* isomer experiences a stronger hydrophobic interaction between the biotin ring system and the aromatic ring. The minimum energy calculated for the conformation *S* (- 29.48 kcal/mol) and *R* (- 23.29 kcal/mol) (Figure 48), showed that the *S* conformation was more stable than *R*. As a result, the hydrophobic interaction in *S* is more likely than *R*. As an implication, the biotin aromatic (naphthyl) interaction is significant and the interactions of



biotin-aromatic in the enzyme-substrate complex or in the biotin-avidin (tryptophan) are contributory to the stabilization during the enzymatic reactions.

Table 17 lists the chemical shifts of Hb for the *S* and *R* diastereomers for **42-44** in CDCl<sub>3</sub> at rt and 1 mM. The naphthyl group of **44** makes the largest difference to the shift of Hb in the NMR spectrum between *R* and *S*, confirming that Hb is in the shielding area of the aromatic ring.

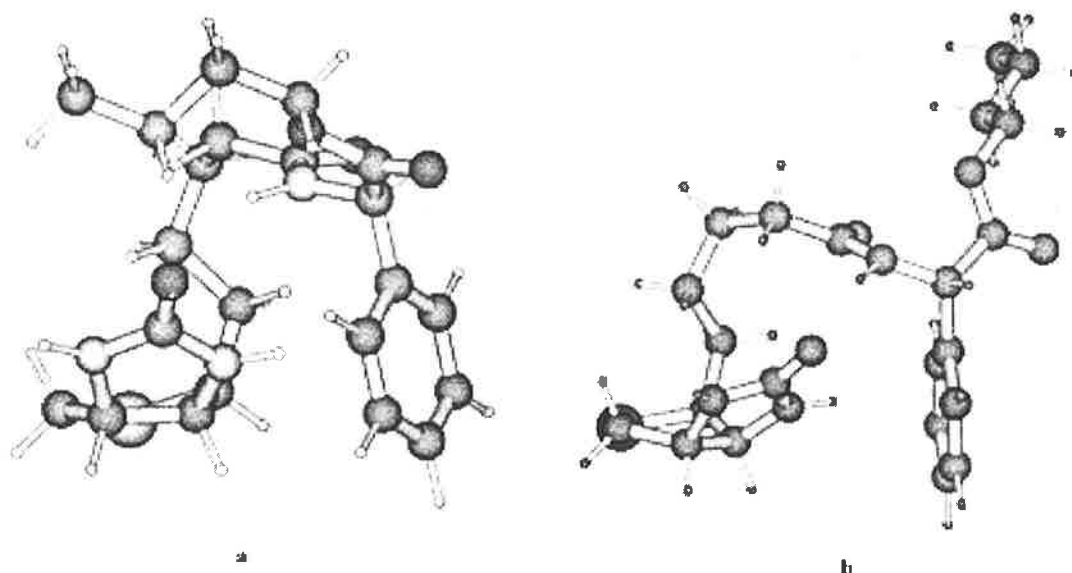
**Table 17.** Proton NMR Chemical Shifts of Hb in Compounds **42**, **43** and **44** in CDCl<sub>3</sub> at 1 mM and rt (ppm).

Compound	<b>42</b>	<b>43</b>	<b>44</b>
S	4.93	4.97	4.90
R	4.99	5.04	5.05
$\Delta\delta$ (R-S)	0.07	0.07	0.16

**Table 18.** Proton NMR Resonance of Protons in Diastereomers D and L of **45** in CDCl<sub>3</sub> at 1 mM and rt (ppm).

Diastereomer	H3	Ha	Hb	Hc
D	4.282	4.68	5.29	6.75
L	4.323	4.61	5.38	6.70
$\Delta\delta$ (D-L)	-0.041	+0.07	-0.09	+0.05

For compounds **45** and **46**, whose molecular modelling structures are shown in Figure 49, the D diastereomer is geometrically favoured for the hydrophobic interaction. The calculated energy of the D diastereomer was - 10.40 kcal/mol, that for L was only - 7.49 kcal/mol. Since the D configuration is favourable for intramolecular hydrogen bonding, the shielding of NHb causes an upfield movement of the proton NMR resonance. The favourable hydrogen bond of Ha and Hc causes a downfield movement of their chemical shifts.



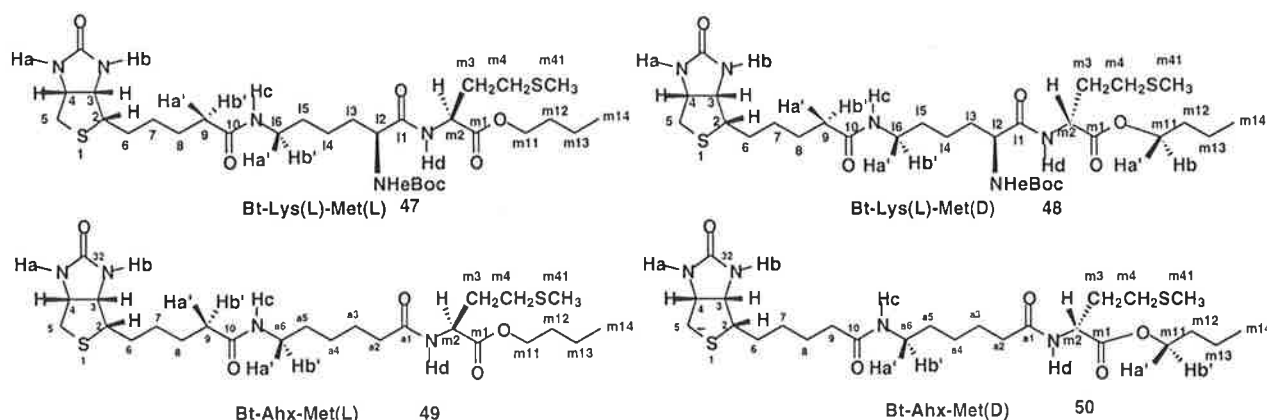
**Figure 49.** 3D structures of Bt-Phala (46) with D (a) and L (b) configurations with intramolecular hydrogen bonding interactions and hydrophobic interactions.

#### 4. 2. 5 Pro-chiral hydrogen differentiation in biotin carboxyl carrier protein unit

According to the literature,<sup>166</sup> all of the biotin enzymes contain the naturally occurring peptide Bt-Lys(L)-Met(L). The Met-88 residue plays a catalytically critical role in the overall transcarboxylation. Waldrop and co-workers reported that the protein in biotin carboxylase was asymmetric and adopts an  $\alpha$ -helical conformation.<sup>24</sup> There are abundant evidences that the biotin enzyme catalysed carboxylations of pyruvate with carboxybiotin occurs with retention of configuration about the  $\alpha$ -carbon of the substrate.<sup>108-110</sup> A two-step mechanism has been proposed<sup>26</sup> and supported by experimental evidences<sup>172-177</sup> in which proton H<sub>b</sub> is first abstracted from the ureido moiety of biotin by a base on the enzyme to generate an enolate-anion. A cyclic reaction then occurs including the abstraction of a proton from pyruvate and translocation of the carboxyl group from carboxybiotin to pyruvate (Scheme 2). In this mechanism, the binding of the acceptor substrate to the active reaction site induces a conformational change in the enzyme favorable for the further approach of the carboxybiotin to complete transcarboxylation. Therefore, the conformational change of acceptor substrate and approach of the carboxybiotin are essential for the reaction. Enzymes have been well documented to adequately control the stereo-chemical discrimination for hydrogen removal from methylene.<sup>172-177</sup>

A question arises as to how the enzyme can differentiate the two protons of the methylene. Chemically, chiral chemical shift reagents can distinguish the enantiotopic nuclei of enantiomers, and change the enantiotopic nuclei of a meso isomer into diastereotopic nuclei.<sup>178</sup> An adjacent aromatic ring in the shift reagent is essential for the observation,<sup>179, 180</sup> because of its efficient shielding.

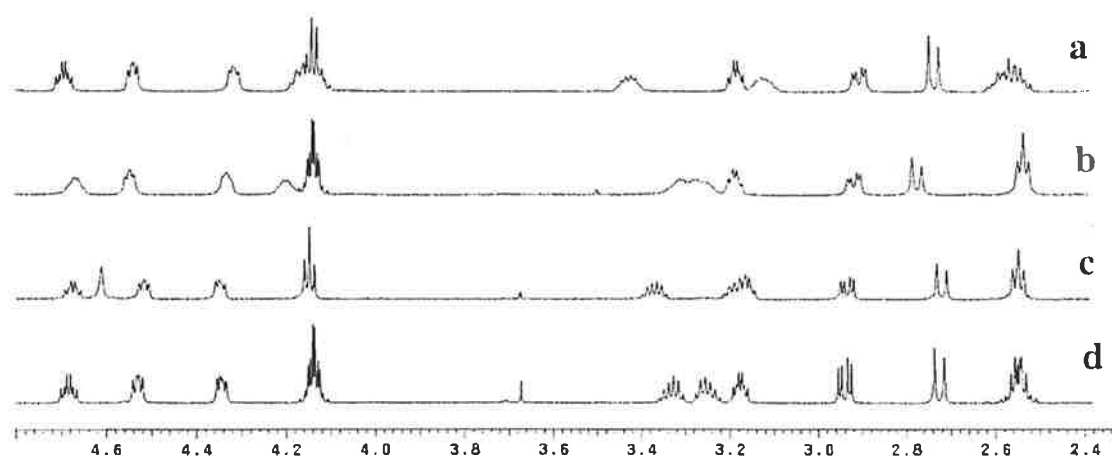
In order to help disclose the specific function of biotin enzymes in the asymmetric carboxylation of pyruvate, biotin peptide analogues Bt-Lys(L)-Met(L) (**47**), Bt-Lys(L)-Met(D) (**48**), Bt-Ahx-Met(L) (**49**) and Bt-Ahx-Met(D) (**50**) were studied in detail. The temperature dependencies of the active NH protons in the four peptides in CDCl<sub>3</sub> at 1 mM are listed in Table 19 and their hydrogen-bonded structures shown in Figure 50 according to molecular modelling. Shown in Figure 51 are the accumulated proton NMR spectra of the peptides **47-50** in CDCl<sub>3</sub> at 1 mM and rt from 2.4-4.8 ppm.



**Figure 50.** Numbering and pro-chiral hydrogen differentiation of methylene groups of compounds **47-50**.

According to Figures 51 and 52, the vicinal protons Ha' and Hb' in the a6 position of Bt-Ahx-Met(L) (**49**) have been separated with an absolute difference of 0.176 ppm (Ha', Hb'; 3.365 ppm, 3.189 ppm). As for compound Bt-Ahx-Met(D) (**50**), each of the three vicinal protons Ha and Hb in positions 9, a6 and m11 are differentiated, 0.015 ppm (Ha', Hb'; 2.557 ppm, 2.542 ppm), 0.071 ppm (Ha', Hb'; 3.326 ppm, 3.255 ppm) and 0.006 ppm (Ha', Hb'; 4.146 ppm, 4.140 ppm) respectively. In compound Bt-Lys(L)-Met(L) (**47**), the vicinal protons Ha' and Hb' in position 9 and a6 are separated with an absolute difference of 0.025 ppm (Ha', Hb' 2.577 ppm, 2.552 ppm) and 0.293 ppm (Ha', Hb'; 3.418 ppm, 3.125 ppm) respectively. In biotin peptide Bt-Lys(L)-Met(D) (**48**), the vicinal protons Ha' and Hb' in position a6 and m11 were also separated with an absolute difference 0.005 ppm (Ha', Hb'; 4.129 ppm, 4.134 ppm) and 0.042 ppm (Ha', Hb'; 3.308 ppm, 3.266 ppm) respectively.

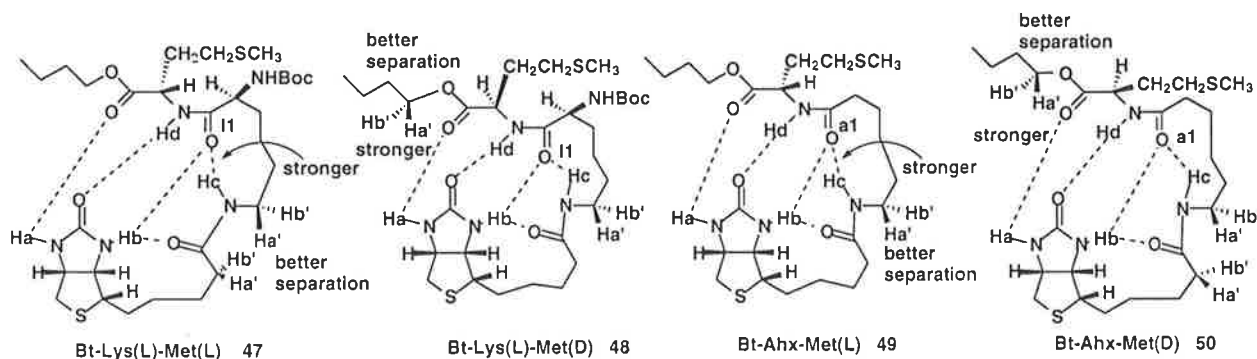
According to the temperature dependencies of the active NH protons of peptides **47-50**, they are all involved in intra-molecular hydrogen bonding except NHe, whose  $\Delta\delta_{\text{NHe}}/\Delta T$  value is only 3.41 ppb/K for Bt-Lys(L)-Met(D) (**48**) and 2.58 ppb/K for Bt-Lys(L)-Met(L) (**47**). Both values are low and can be used a control to judge the significance of intra-molecular hydrogen bonding for the other protons Ha, Hb, Hc and Hd.



**Figure 51.** Accumulated proton NMR spectra of biotin peptides Bt-Lys(L)-Met(L) (47) (c), Bt-Met(L)-Met(D) (48) (d), Bt-Ahx-Met(L) (49) (a) and Bt-Ahx-Met(D) (50) (b) (from top to bottom) in  $\text{CDCl}_3$  at 1 mM and rt.

**Table 19.**  $^1\text{H}$  NMR Chemical Shift Temperature Dependencies of NH Protons in Biotin Peptides 47-50 (ppb/K).

Compound	Ha	Hb	Hc	Hd	He
Bt-Lys(L)-Met(L) (47)	8.9	12.4	10.4	10.6	2.6
Bt-Lys(L)-Met(D) (48)	10.8	13.2	9.4	6.8	3.4
Bt-Ahx-Met(L) (49)	5.9	11.2	8.0	13.6	
Bt-Ahx-Met(D) (50)	8.0	7.7	7.2	11.1	



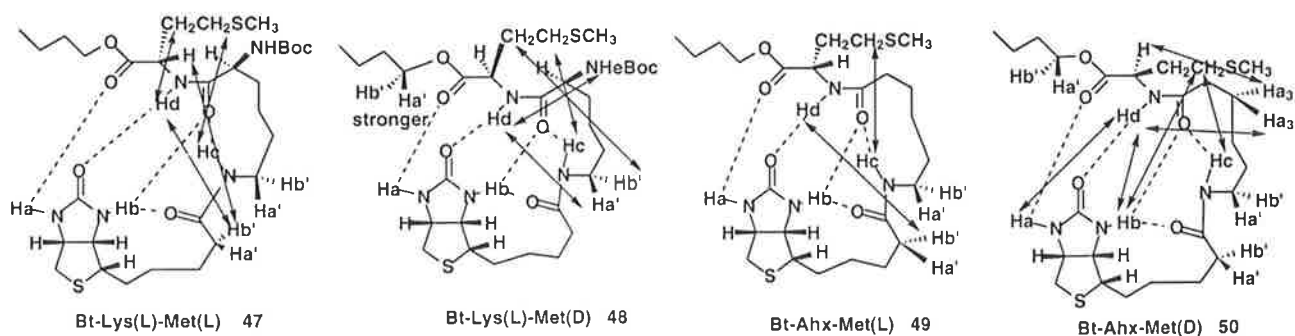
**Figure 52.** Intra-molecular hydrogen bonding in biotin peptides and pro-chiral hydrogen separation.

According to molecular modelling and 2D-COSY and ROESY NMR spectra for all the four peptides in  $\text{CDCl}_3$  at rt and 5 mM, the possible intra-molecular hydrogen bonding and molecular geometry are shown in Figure 52. The cross peaks of the protons of the four peptides are listed in Table 20, or Figure 53, and support the proposed structures.

According to Figures 51 and 52 and Table 19, the better separation of Ha' and Hb' in Bt-Ahx-Met(L) (**49**) in the a6 position is probably due to stronger intra-molecular hydrogen bonding concerning Hc in **49** compared to **50**, since the  $\Delta\delta\text{NH}/\Delta T$  value for Hc (**49**) is 8.0 ppb/K, while that for **50** was 7.2 ppb/K. The  $\Delta\delta\text{NH}/\Delta T$  value of Ha for Bt-Ahx-Met(D) (**50**) was 8.0 ppb/K, which was larger than 5.9 ppb/K for Bt-Ahx-Met(L) (**49**), as a result, the vicinal protons Ha' and Hb' in the m11 position are differentiated. This preferential conformation and hydrogen bonding allows long range differentiation of pro-chiral hydrogens and represents one of the longest spatial differentiations reported for relatively simple molecules. Therefore, the intra-molecular hydrogen bonding promotes the differentiation of vicinal protons Ha' and Hb' in biotin peptides and could also occur in biotin containing enzymes. According to the literatures, the differentiation of pro-chiral hydrogens can be observed when there is an adjacent chiral center.<sup>180, 181</sup> Therefore, the intra-molecular hydrogen bonding in the biotin peptides **47-50** may play a role as a bridge, which brings the chiral center close to the vicinal hydrogens enabling the differentiation. Intra-molecular hydrogen bonding could then play an important role in the binding of the acceptor substrate in the correct orientation at the active site, and allow differentiation of the vicinal protons so that subsequent proton abstraction and carboxylation would result in retention of configuration during the biotin-dependent enzyme catalytic carboxylation.

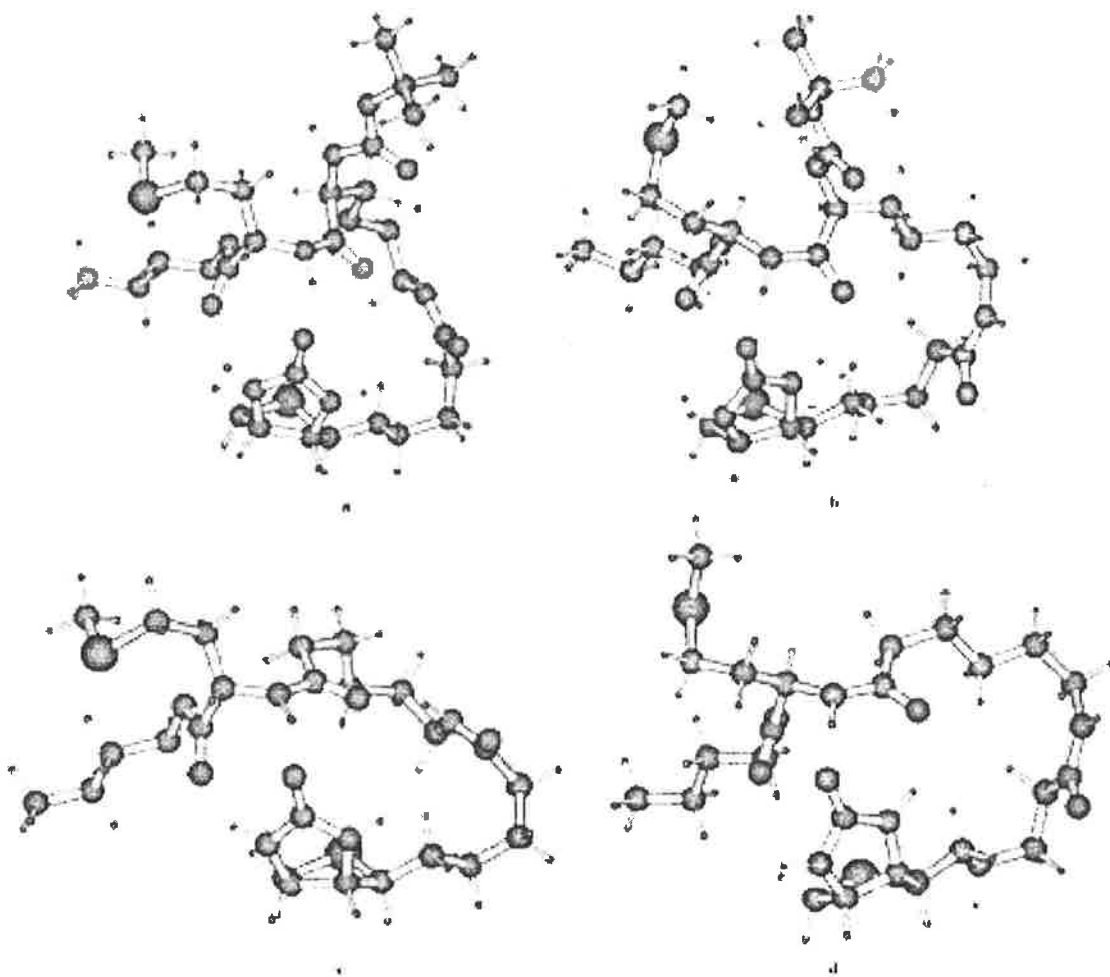
**Table 20.** Selected Cross Peaks between Protons in 2D-ROESY Spectra of Biotin Peptides **47-50** in CDCl<sub>3</sub> at 5 mM and rt.

Bt-Lys(L)-Met(L) ( <b>47</b> )	Bt-Lys(L)-Met(D) ( <b>48</b> )	Bt-Ahx-Met(L) ( <b>49</b> )	Bt-Ahx-Met(D) ( <b>50</b> )
Hc-Hm4	Hc-Hm4	Hc-Hm4	Ha-Hd
Hd-H9	Hd-He	Hd-Ha2	Hb-Hd
Hd-Hm3a, Hm3b	Hd-H9	Hd-Hm3b	Hc-Hm4
Hm2-H9	Hd-Hm3a, Hm3b	Hd-H9	Hd-Ha3
Hm4-Hm12	Hm11-H9	Hm4-H6, H7, H8	Hd-Hm3a, Hmsb
	H9-Hm3a, Hm3b		Hm2-Ha2
			Hm4-Hb
			Hm4-H9



**Figure 53.** Cross peaks of Bt-Lys(L)-Met(L) (**47**), Bt-Lys(L)-Met(D) (**48**), Bt-Ahx-Met(L) (**49**) and Bt-Ahx-Met(D) (**50**) in 2D NMR ROESY spectra.

The intra-molecular hydrogen bonding networks for compounds **47-50** are shown in Figure 52. The molecular modelling structures in Figure 54 show a distance of  $O_{11}$ -Hc of 2.24 Å for **47** and 4.87 Å for **48**, indicating that the intra-molecular hydrogen bonding,  $O_{a1}$ -Hc, in **47** is significant. The corresponding distance of  $O_{a1}$ -Hc in compound **49** and **50** are 2.17 Å and 4.86 Å respectively, which also suggest that the hydrogen bonding in **49** is significant.



**Figure 54.** Molecular modelling structures of compounds **47(a)**, **48(b)**, **49(c)** and **50(d)** with intra-molecular hydrogen bonding networks.

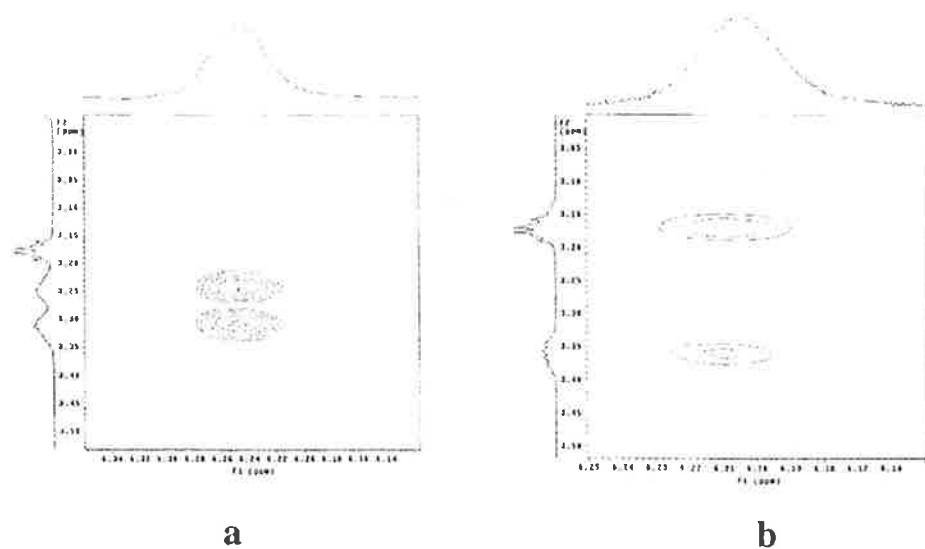
Furthermore, intra-molecular hydrogen bonding brings the active sites together to form a hydrophilic side to the biotin peptide, which is on the top of the hemisphere structures (Figure 52). The hydrophobic side is formed from the aliphatic chains of biotin, aminohexanoic acid (lysine) and the butyl group. This kind of formation is consistent with the spheric structure of the active site of the biotin carboxylase subunit of acetyl-CoA carboxylase,<sup>24</sup> which is reported to bind phosphate and two water molecules. Biotin peptides **47-50** with a hemisphere structure,

resemble the active site pocket of the enzyme including His-209, Glu-211, His-236, Glu-241, Glu-276, IL-287, Glu-296 and Arg-338. These amino acid residues are involved in hydrogen bonding on the hydrophilic side and van der Waals and stacking interactions on the hydrophobic side.<sup>165</sup> With this effective contact, the formation of carboxy-biotin by the reaction of biotin with carboxy-phosphate attached to the active site and abstraction of pro-chiral hydrogen from pyruvate and translocation of the carboxyl group from carboxy-biotin to pyruvate then occurs with regi-selectivity and stereoselectivity.<sup>182, 183</sup>

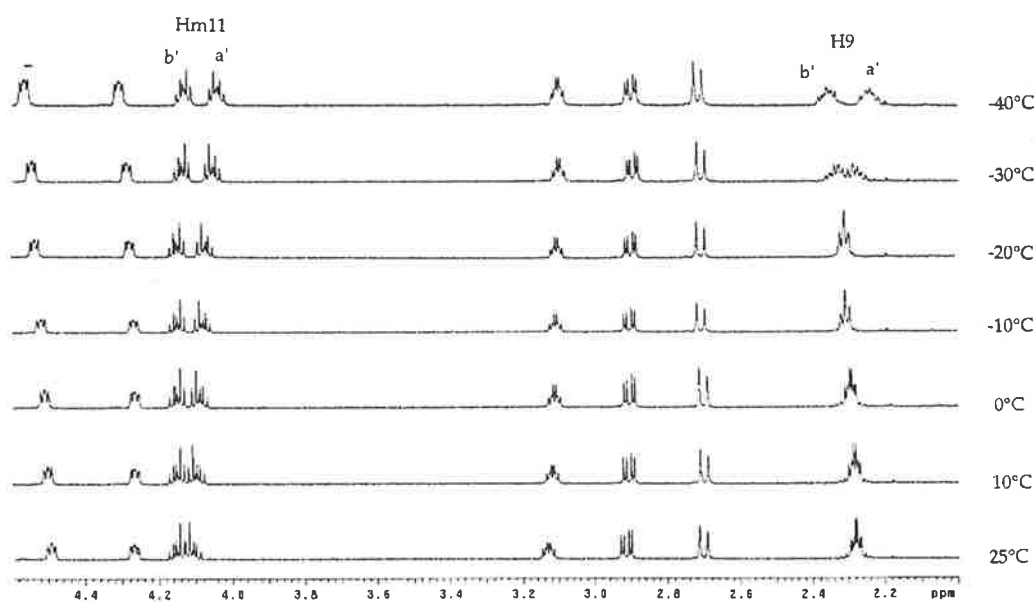
#### 4. 2. 6 Tentative assignment of pro-chiral hydrogens

Figure 56 shows the good separation of protons Ha' and Hb' in the a6 and l6 positions. The effective intra-molecular hydrogen bonding is expected to play an important role in this differentiation. According to the 2D-ROESY spectrum of compound Bt-Lys(L)-Met(d) (**48**) in Figure 55, Hc is closer to Ha' (3.313 ppm) in position l6 than Hb' (3.247 ppm). However, in compound Bt-Lys(L)-Met(L) (**47**), Hc is closer to Hb' in position l6 than Ha'. A possible explanation for this observation is that strengthening the intra-molecular hydrogen bond of Hc with the methionine carbonyl group from compound Bt-Lys(L)-Met(D) (**48**) to Bt-Lys(L)-Met(L) (**47**) (Table 19) shortens the length of the hydrogen bond<sup>29</sup> and enlarges the N-Hc...O angle, which results in rotation of the carbon in position l6 thus forcing Hb' closer to Hc than Ha'. The structure of Bt-Lys(L)-Met(D) (**48**) in Figure 54 showed the distances of Hc to Ha' as 2.42 Å, that of Hc to Hb' as 3.01 Å. However, the structure of Bt-Lys(L)-Met(L) (**47**) showed the distances of Hc to Ha' and Hb' as 2.96 Å and 2.67 Å respectively. Therefore, Ha' in position l6 is the pro-*S* hydrogen and Hb' is the pro-*R* hydrogen. Both 2D-ROESY experiments of Bt-Lys(L)-Met(L) at 5 mM and 25 mM show the same results, that is, Hc is closer to Hb' than Ha'.

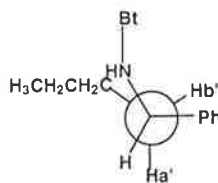
As to vicinal protons Ha' and Hb' in m11 position, their separation could not be seen in any of biotin peptides Bt-Met(D) or Bt-Met(L), but was observable in biotin peptide Bt-Phala (**45**). Both the differentiation of Ha' and Hb' in position m11 and 9 became apparent at low temperature - 40 °C (Figure 56). Therefore, the phenyl group in Bt-Phala (**45**) probably plays an important role in the differentiation through shielding.<sup>180, 181</sup>



**Figure 55.** 2D-ROESY NMR spectra of Bt-Lys(L)-Met(D) (**48**) (a) and Bt-Lys(L)-Met(L) (**47**) (b) with cross peaks of Hc with Ha' and Hb' in I6 position.



**Figure 56.** Variable temperature NMR experiments of Bt-Phala (**45**) at 1 mM in  $\text{CDCl}_3$ .

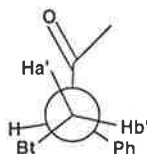


**Figure 57.** The preferred conformation of Bt-Phala(D) (**45**) in position m11, in which the ester linkage is omitted.



According to the Mosher model and 3D structure of Bt-Pha (D) (**45**), the preferred Newman projection of the biotin peptide Bt-Phala (D) (**45**) is shown in Figure 57, where Hb' eclipses the phenyl ring and the corresponding chemical shift will move upfield<sup>184</sup> compared to Ha' of the diastereomer which eclipses a hydrogen atom. Therefore, Ha' is assigned a chemical shift of 4.152 ppm and Hb' is 4.043 ppm at -60 °C in CDCl<sub>3</sub>. Ha' is then the pro-*S* and Hb' is the pro-*R* hydrogen.

As to vicinal protons Ha' and Hb' in the 9 position, they will adopt the conformation as shown in Figure 58, in which the intra-molecular hydrogen bonds lock the conformation at low temperature (-40 °C). Therefore, Hb' eclipses the phenyl group and will occur up-field compared to the proton Ha' of the diastereomer which eclipses the carbonyl group.



**Figure 58.** The interlocked conformation of Bt-Phala (*R*) (**45**) in position 9 in which the amide linkage is omitted.

Analysis of the <sup>1</sup>H NMR spectrum of Bt-Phala (*R*) (**45**) in CDCl<sub>3</sub> at -40 °C and 1 mM revealed that the signal Ha' appeared at a chemical shift of 2.35 ppm and Hb' at 2.26 ppm. Ha' is therefore the pro-*R* and Hb' is the pro-*S* hydrogen.

---

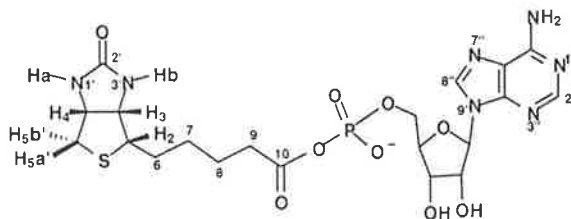
## Chapter 5

---

# Hydrogen Bonding Pairs Controlled Molecular Foldings of Biotinylated Nucleobases

## 5.1 Introduction

Biologically, biotin can be extremely tightly bound to streptavidin and avidin by multiple interactions in the active binding site.<sup>51</sup> These include an extensive hydrogen bonding network, hydrophobic and van der Waals interactions.<sup>52, 53</sup> Therefore, biotin is widely applied as a label for oligo-nucleotides and oligo-deoxyribonucleotides for the identification of a variety of viruses in human beings and plants such as HIV, HCV, HTLV and hepatitis.<sup>54-57</sup> In addition, biotin can also be bound to the *Escherichia Coli* biotin operon repressor, BirA, serving both as a biotin activation enzyme and a transcriptional regulator.<sup>185, 186</sup> This enzyme catalyses the formation of biotinyl-5'-AMP (Figure 59) from biotin and ATP and transfers biotin to a specific lysine residue on the biotin carboxyl carrier protein (BCCP), a subunit of acetyl CoA carboxylase.<sup>187, 188</sup> BirA represses transcription when all the biotin accepting protein in the cell has been biotinylated, and the BirA-biotinyl-5'-AMP complex accumulates and binds to DNA to form BirA-biotinyl-5'-AMP-DNA complex.<sup>187-190</sup> However, the possible internal interaction between biotin and nucleoside bases such as adenine has not been reported, although there are some reports concerning the interaction of DNA with a tripeptide dimer,<sup>191</sup> proteins<sup>192</sup> and imide receptors<sup>193,194</sup> by hydrogen bonding and  $\pi$ - $\pi$  stacking interactions. In order to establish a structural basis for the possible interaction of biotin and nucleobases in biotinyl oligonucleotides and oligodeoxyribonucleotides, analogues of biotinyl-5'-AMP (Figure 59) and BirA-biotinyl-5'-AMP-DNA were prepared. These analogues were Bt-Ade (**51**), Bt-Cyt (**52**), Bt-Thy (**53**), Bt-Ura (**54**) and Bt-Thioura (**55**). Their hydrogen-bonding and hydrophobic interactions were studied by NMR spectroscopy.



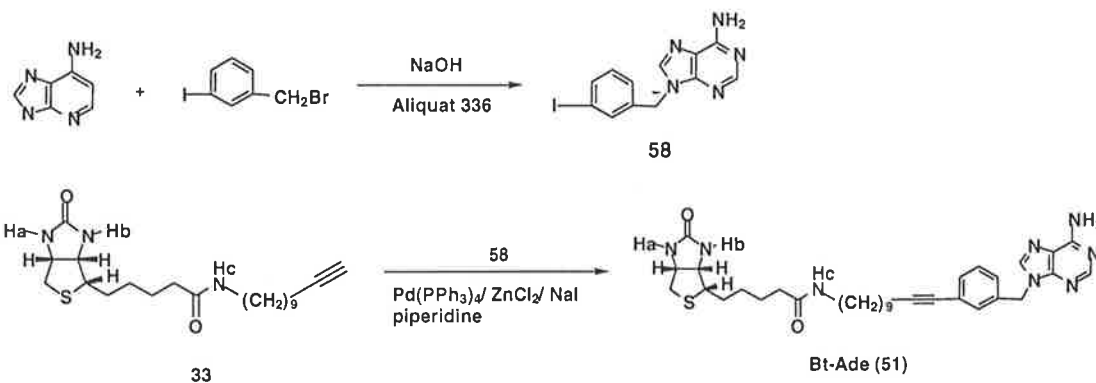
**Figure 59.** Structure of biotinyl-5'-AMP and numbering of biotin and adenine moieties.

## 5.2 Results

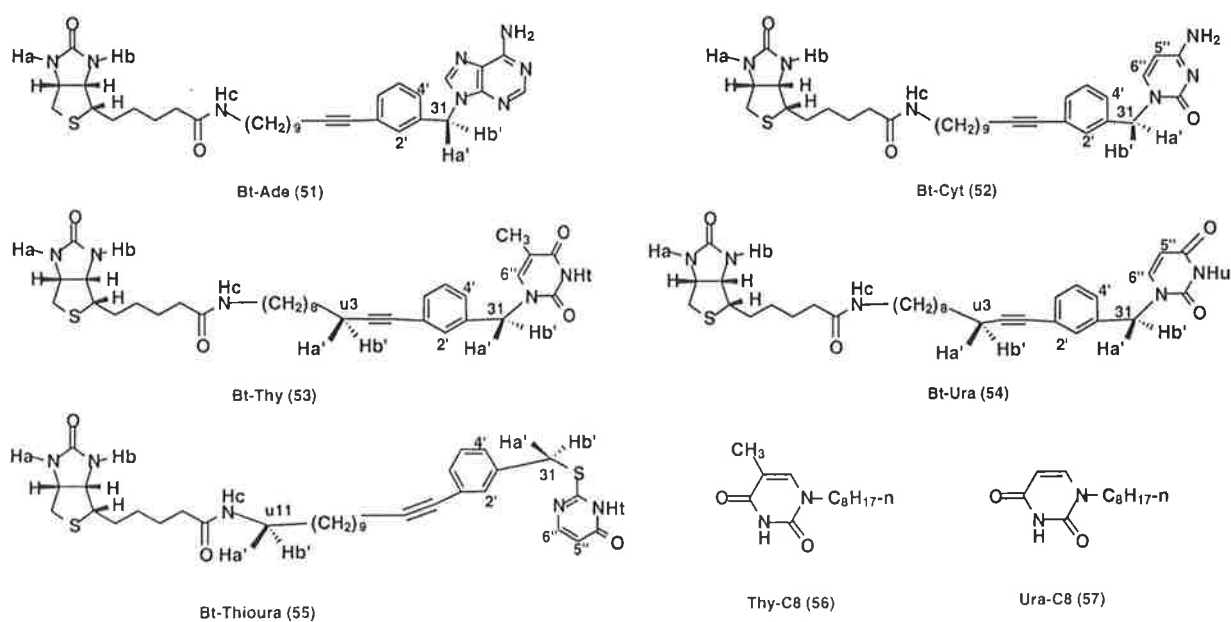
### 5.2.1 Synthesis

The biotinylated nucleobases examined here are shown in Figure 60, along with the common precursor biotinyl amide Bt-Uyne (**33**). Bt-Uyne (**33**) was prepared according to the literature.<sup>54</sup> The nucleobases were synthesized by a standard palladium catalysed coupling reaction of Bt-Uyne (**33**) with nucleobase aryl iodide derivatives.

Typically, adenine was alkylated at the 9-position with 3-iodobenzylbromide, which was coupled to biotinyl amide Bt-Uyne (**33**) in the presence of Pd(PPh<sub>3</sub>)<sub>4</sub>, ZnCl<sub>2</sub> and NaI in piperidine at reflux (Scheme 9).<sup>195</sup> Other similar compounds (**52-55**) were prepared by a same route. Compounds **56** and **57** were prepared by direct alkylation of thymine and uracil with 1-bromooctane in the presence of potassium carbonate in DMF.<sup>196</sup>



**Scheme 9.** Synthesis of the biotin nucleobase Bt-Ade (**51**) (an example for the nucleobases).



**Figure 60.** Biotinylated nucleobases and related compounds.

In the trials to find stronger intra-molecular hydrogen bonding and better pro-chiral methylene proton differentiation, the biotin peptide containing adenine derivatives Bt-Met(D)-Ade (**152**) and Bt-Met(L)-Ade (**153**) were also prepared (Figure 62) together with biotin peptides **82** and **83** (Figure 61). During the synthesis of precursors **82** and **83**, biotinyl methionine Bt-Met(D)-acid (**146**) was prepared by the amidation of biotin *N*-hydroxysuccinimide ester (**143**) with free *D*-methionine (**144**) in pyridine-NaOH-H<sub>2</sub>O solution as shown in **Scheme 10**. Compound **146** was then converted into its *N*-hydroxysuccinimide ester (**148**), which was amidated with amine **154** to give product **82**. Compound Bt-Met(L)-C9 (**83**) was prepared in a similar manner to the initial amidation of **143** with free *L*-methionine (**145**) to give compound **147**, which was esterified to give *N*-hydroxysuccinimide derivative **149**, followed by a second amidation with **154** to give **83**.

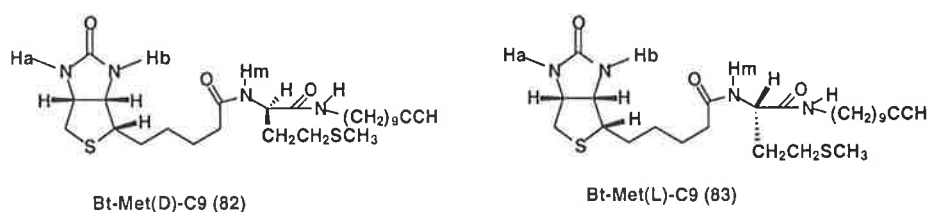
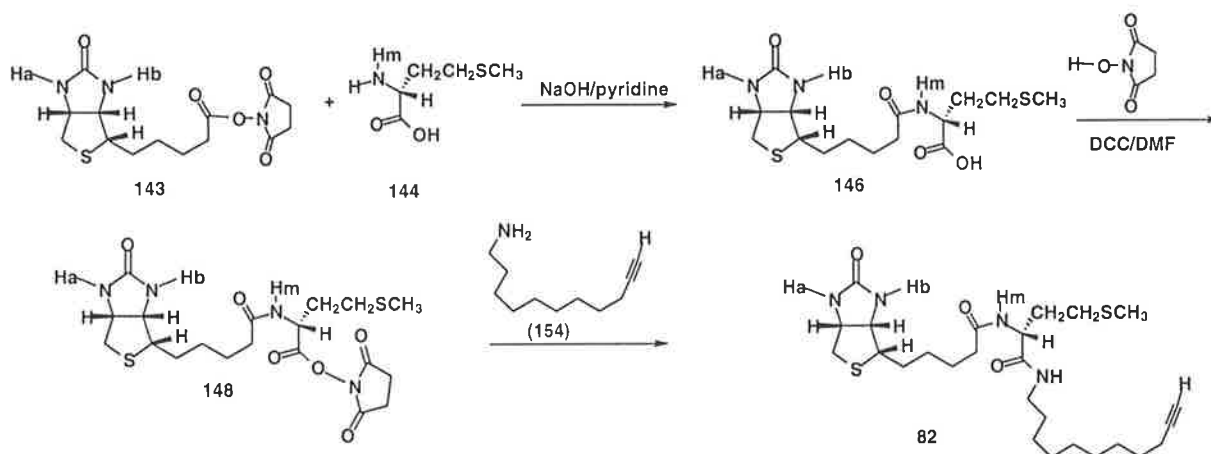


Figure 61. Biotin peptides **82** and **83**.

The compound Bt-Met(D)-Ade (**152**), was prepared by the coupling reaction with compound **58** in the presence of Pd(PPh<sub>3</sub>)<sub>4</sub> (**Scheme 11**). Compound Bt-Met(L)-Ade (**153**) was prepared in a similar manner.



Scheme 10. Preparation of Bt-Met(D)-acid (**146**) and synthesis of Bt-Met(D)-C9 (**82**).

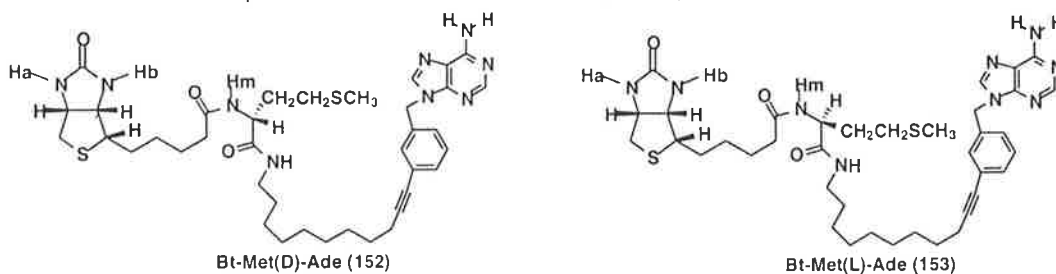
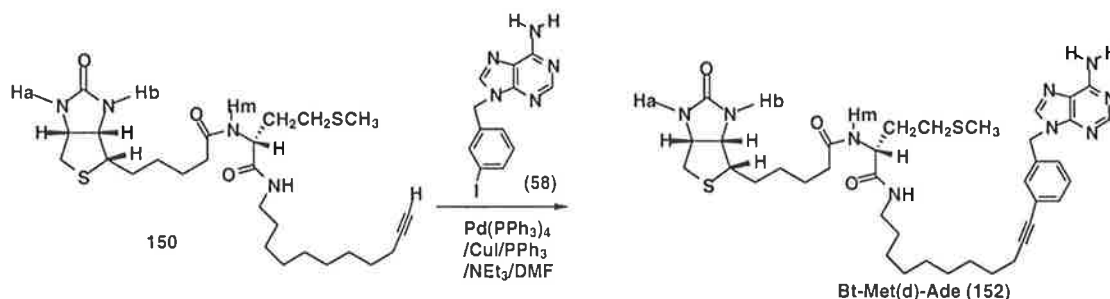


Figure 62. Bt-Met(D)-Ade (**152**) and Bt-Met(L)-Ade (**153**).



Scheme 11. Synthesis of substrate Bt-Met(D)-Ade (152).

### 5. 2. 1 Intra-molecular hydrogen bonding in biotinylated nucleobases

The  $^1\text{H}$  NMR chemical shift temperature dependencies of the active NH protons in the synthetic biotinylated nucleobases at 1 mM in  $\text{CDCl}_3$  are shown in Table 21. Also shown in Table 21 are the  $\Delta\delta_{\text{NH}}/\Delta T$  values for 1 mM samples of biotinyl amide Bt-Uyne (33) and biotinyl iodide Bt-I (5). As mentioned in the previous Chapters, in order to exclude the possible contributions to the temperature dependence of intermolecular hydrogen bonding, compound Bt-I (5) was used as a control (3.8 ppb/K). According to the data in Table 21, all of the biotinylated nucleobases were involved in significant intra-molecular hydrogen bonding concerning NHa and NHb, including biotinyl amide Bt-Uyne (33), which was the precursor of all the biotinylated nucleobases. Also shown in the previous Chapters, NHb in Bt-Uyne (33) was significantly involved in intra-molecular hydrogen bonding with the carbonyl group in the valeryl side chain of biotin. Therefore, compound Bt-Uyne (33) can function as a standard to judge the effect of the introduction of nucleobases on biotinyl amides.

Table 21.  $^1\text{H}$  NMR Chemical Shift Temperature Dependencies of NH Protons in Biotin Nucleobases in  $\text{CDCl}_3$  at 1 mM (ppb/K).

compound	Ha	Hb	Hc	others
Bt-Ade (51)	13.2	28.3	10.2	Hd: 18.2 (NH <sub>2</sub> ) He: 10.9 (NH <sub>2</sub> )
Bt-Cyt (52)	4.7	10.9	4.7	
Bt-Thy (53)	10.1	13.7	9.8	Ht: 25.2
Bt-Ura (54)	9.2	12.3	8.3	Hu: 20.7
Bt-Thioura (55)	6.0	10.3	7.5	
Bt-Uyne (33)	8.7	15.7	6.1	
Bt-I (5)	3.8	3.8		

Shown in Table 22 are the differences ( $\Delta\text{Ha}$  and  $\Delta\text{Hb}$ ) of  $^1\text{H}$  NMR chemical shifts of NHa and NHb between biotinylated nucleobases and 33 at 1 mM and 20 °C in  $\text{CDCl}_3$ . The differences  $\Delta(\Delta\text{Hb}-\Delta\text{Ha})$  between  $\Delta\text{Hb}$  and  $\Delta\text{Ha}$  are also listed in Table 22. The values of  $\Delta\text{Ha}$  and  $\Delta\text{Hb}$  represent the changes in the NMR shifts of NHa and NHb due to the introduction of nucleobases to the biotinyl amide, based on intra-molecular hydrogen bonding and stacking interactions. As reported previously,  $^1\text{H}$  NMR resonances of NHa and NHb in Bt-I (5) appear at the same

chemical shift (4.44 ppm in  $\text{CDCl}_3$  at 1 mM and 20 °C). The chemical shifts of NHa and NHb in Bt-Uyne (**33**) appear at 4.51 ppm and 4.99 ppm respectively and the difference in the chemical shifts of NHa and NHb between Bt-Uyne (**33**) and Bt-I (**5**) reflects the efficiency of intra-molecular hydrogen bonding. Intra-molecular hydrogen bonds involving NHc of the side chain amide and the carbonyl group are expected to exist together with the interactions involving biotin and nucleobase. As shown in Table 22, the largest value of  $\Delta(\Delta\text{Hb}-\Delta\text{Ha})$  is + 1.95 ppm, and for  $\Delta\text{Hb}$  is + 1.93 ppm, for compound Bt-Cyt (**52**) and indicates that NHb is more likely to interact intra-molecularly with the cytosine moiety than NHa. There is little effect on the chemical shift of NHa with the introduction of cytosine into Bt-Uyne (**33**),  $\Delta\text{Ha}$  is - 0.02 ppm. Bt-Ade (**51**) exhibits intra-molecular hydrogen bonding involving NHb (**51a**) rather than NHa (**51b**), since its structure is similar to cytosine and the data in Table 22 shows the preference for NHb in the formation of intra-molecular hydrogen bonds. Compound Bt-Thy (**53**) and Bt-Ura (**54**) appeared to adopt a conformation favoring an intra-molecular hydrogen bond with NHb rather than NHa. However, the  $\Delta\text{Ha}$  value for Bt-Thioura (**55**) is 1.69 ppm which is larger than  $\Delta\text{Hb}$  (1.37 ppm), the  $\Delta(\Delta\text{Hb}-\Delta\text{Ha})$  value is negative (- 0.31 ppm), indicating that Bt-Thioura (**55**) adopts a conformation favoring intra-molecular hydrogen bond between the thiouracil ring and NHa (**55b**) (Figure 63).

**Table 22.** Differences of proton NMR Chemical Shifts of NH Protons Between Biotinylated Nucleobase and Biotinyl Amide Bt-Uyne in  $\text{CDCl}_3$  at 1 mM and 20 °C (ppm).

compound	$\Delta\text{Ha}$	$\Delta\text{Hb}$	$\Delta\text{Hc}$	$\Delta(\Delta\text{Hb}-\Delta\text{Ha})$
Bt-Ade ( <b>51</b> )	0.14	0.71	0.10	0.58
Bt-Cyt ( <b>52</b> )	-0.02	1.93	0.77	1.95
Bt-Thy ( <b>53</b> )	0.34	0.74	0.26	0.40
Bt-Ura ( <b>54</b> )	0.47	0.86	0.37	0.39
Bt-Thioura ( <b>55</b> )	1.69	1.37	0.51	-0.31

Molecular modelling studies showed that for Bt-Ade (**51**) (Figure 64), conformation **51a** was more stable than **51b**, since the energy for **51a** was - 9.08 kcal/mol and that for **51b** was - 2.26 kcal/mol. However, the conformation **55a** for Bt-thioura (**55**) (Figure 67) was less stable than **55b**, since the energy for **55a** was - 130.80 kcal/mol and that for **55b** was - 138.80 kcal/mol. Therefore, molecular modelling probing the lowest energy conformation of compounds in Figures 64-67 suggested the intra-molecular hydrogen bonding interactions within the biotin nucleobases could be formed with either NHa or NHb.

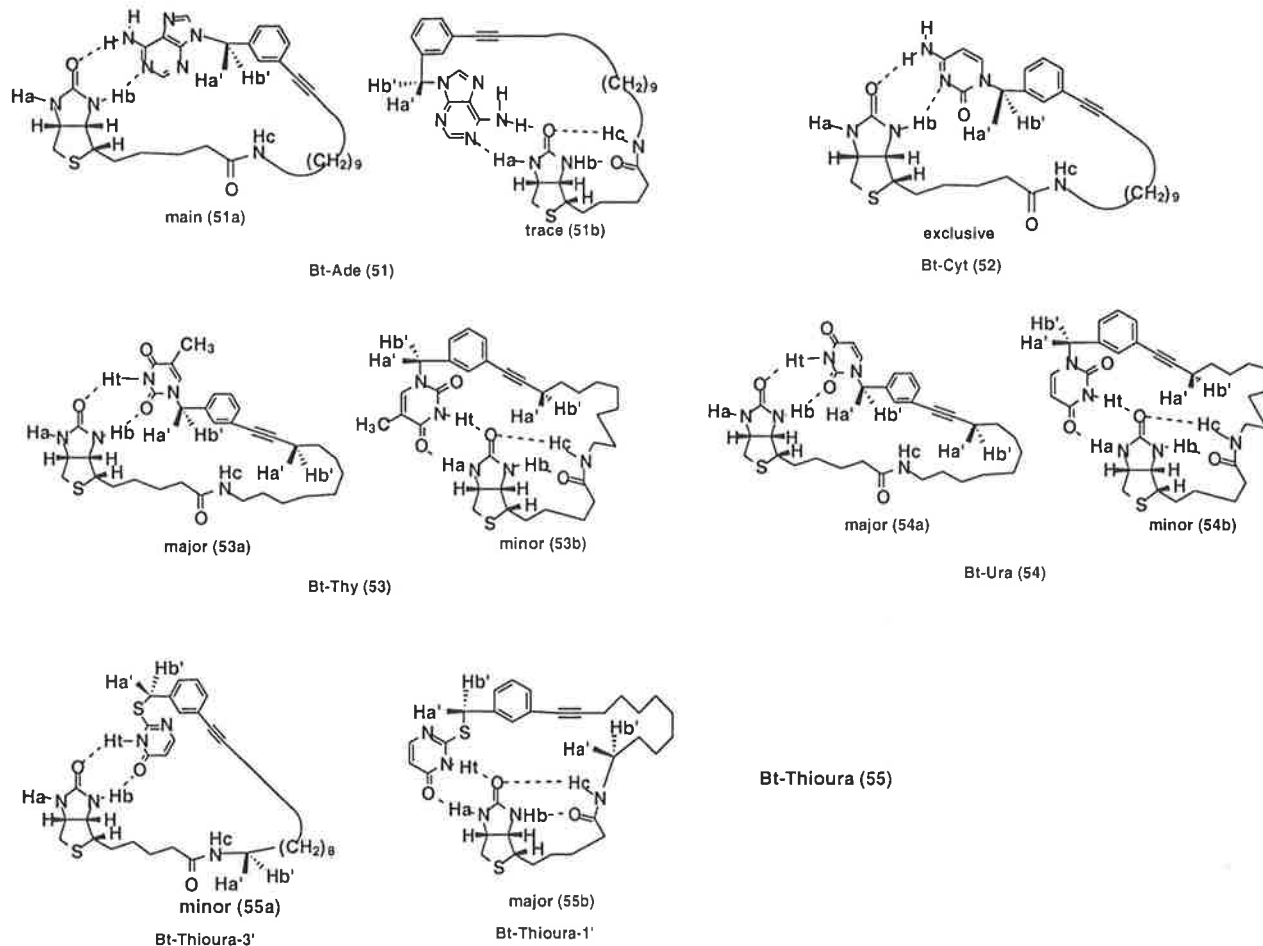


Figure 63. Possible hydrogen bonding pairs of biotin and nucleobases.

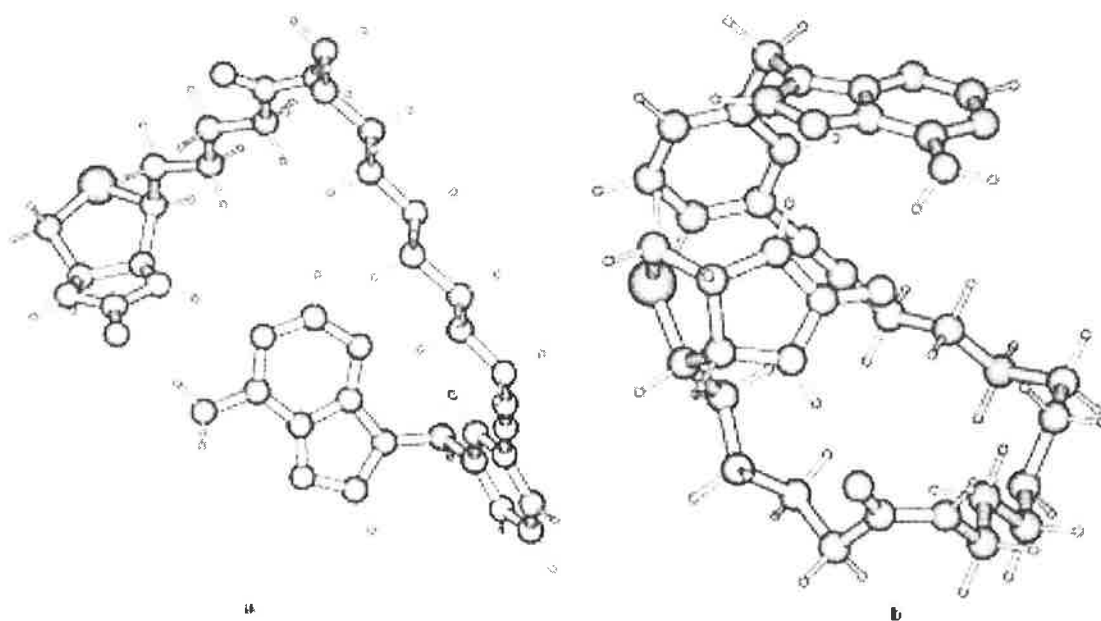


Figure 64. Structures of Bt-Ade (51) with the differing arrangements 51a and 51b.

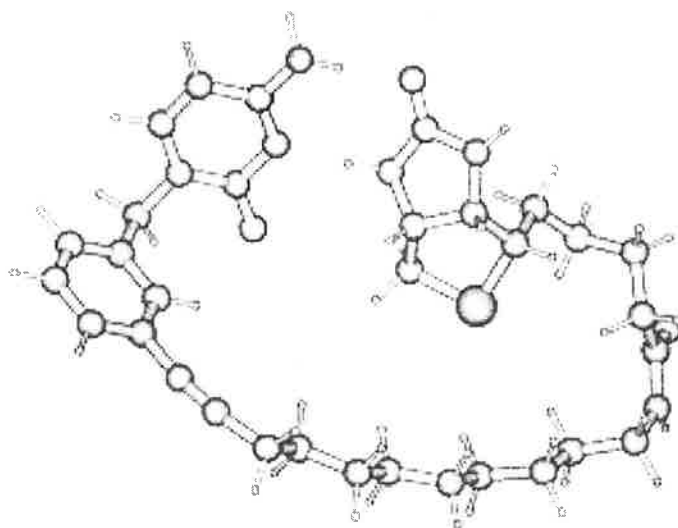


Figure 65. Preferential structure of Bt-Cyt (52).

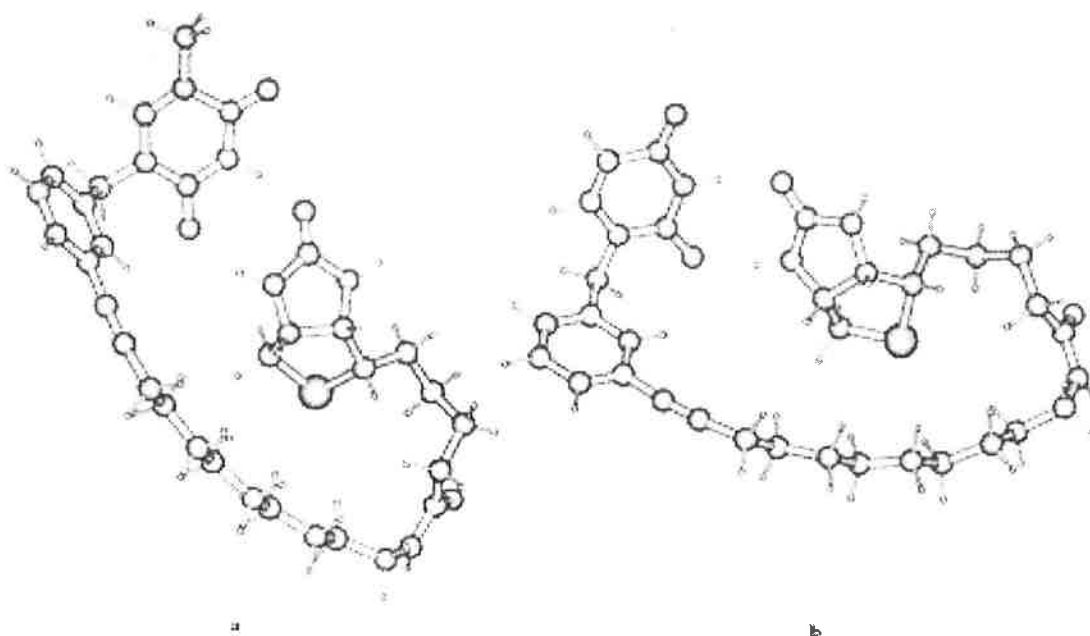


Figure 66. Preferential structures of Bt-Thy (53) and Bt-Ura (54).



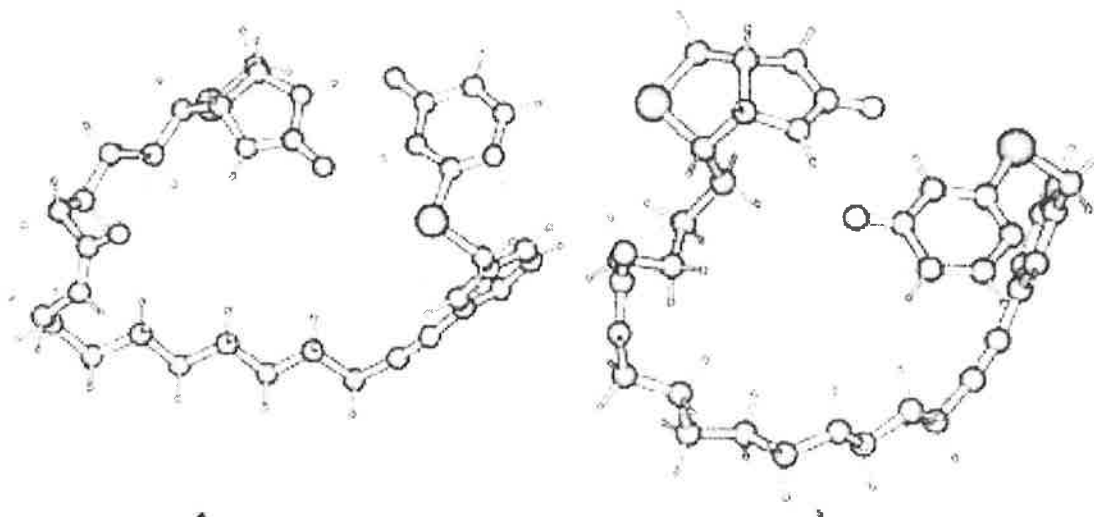
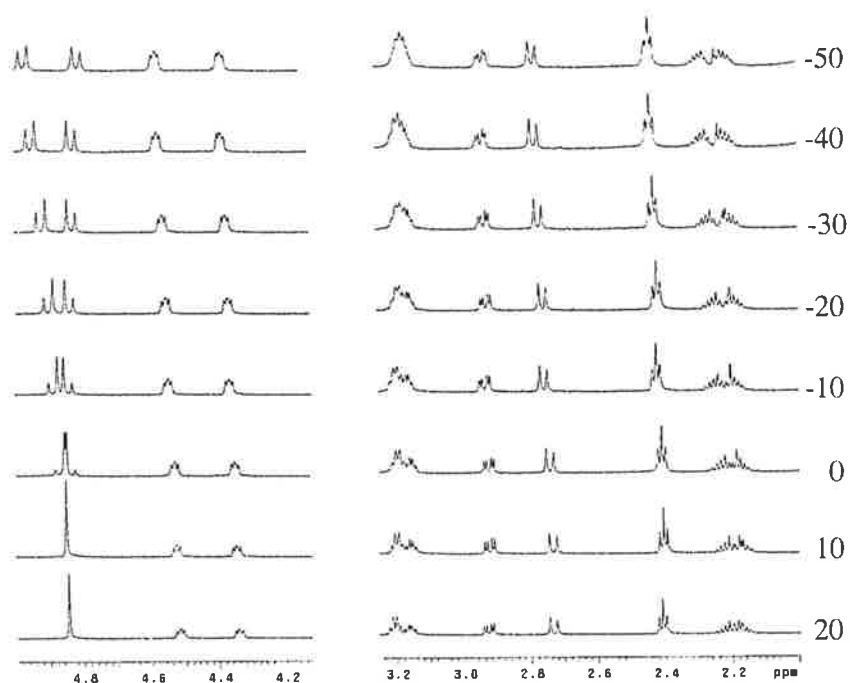


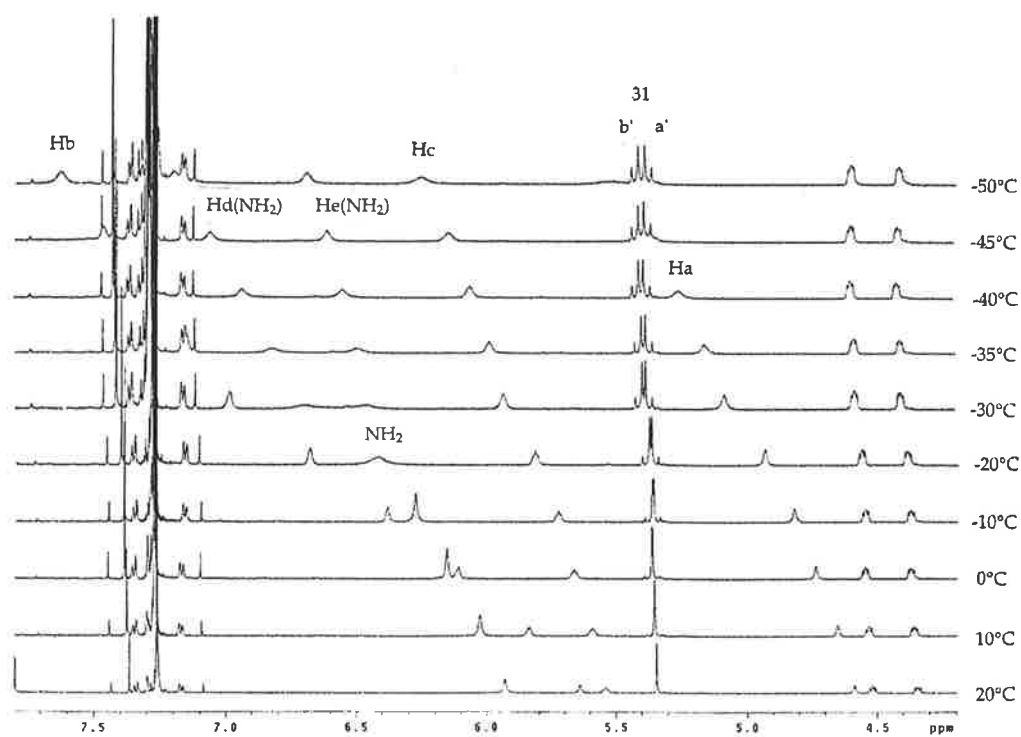
Figure 67. Structures of Bt-Thiourea (**55**) with different arrangements **55a** and **55b**.

The evidence for intra-molecular hydrogen bonding between biotin and nucleobases is the temperature dependencies of their NH protons. The  $\Delta\delta_{\text{NH}}/\Delta T$  values for protons in the ureido moiety of biotin in Bt-Ade (**51**) were 13.2 ppb/K and 28.4 ppb/K for Ha and Hb, respectively. The value for Hb in Bt-Ade (**51**) was the largest among the biotinylated nucleobases, so was the difference (15.13 ppb/K) between Hb and Ha. The  $\Delta\delta_{\text{NH}}/\Delta T$  values for the protons in nucleobase **53** was 25.2 ppb/K (Ht) and for **54** was 20.7 ppb/K (Hu). The  $\Delta\delta_{\text{NH}}/\Delta T$  values for *N*-(*n*-octy)thymine (**56**) and *N*-(*n*-octyl)uracil (**57**) were 4.7 ppb/K and 7.4 ppb/K respectively, indicating a component of intermolecular hydrogen bonding. This would indicate that intermolecular hydrogen bonding is possible at 1 mM for some of the compounds.

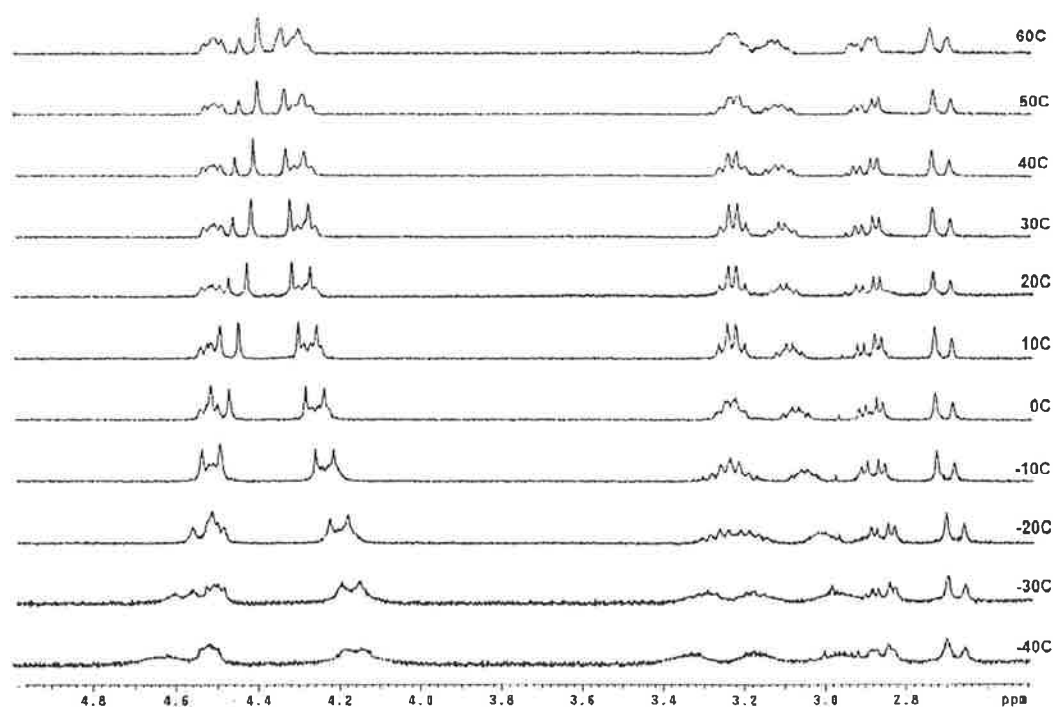
Furthermore, according to the NMR spectra of Bt-Ade (**51**) at different temperatures in  $\text{CDCl}_3$  at 1 mM (Figure 69), two different signals for the NH resonances of adenine were observed below -30 °C. Based on the temperature dependencies of the two protons, one signal at 7.20 ppm was attributed to hydrogen Hd with 18.2 ppb/K temperature dependence, which is bonded with the biotin ureido moiety as shown in Figure 63, while the other at 6.69 ppm was attributed to the relatively unbound proton He with 10.9 ppb/K temperature dependence at -50 °C. The inequivalence of these two amino protons is due to a slow rotation about the carbon-nitrogen  $\sigma$ -bond on the NMR time scale at -50 °C, caused by the intra-molecular hydrogen bonding. Therefore, the result provides further support for the intra-molecular hydrogen bonding between adenine and the biotin ureido moiety.



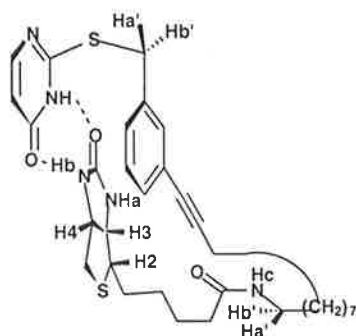
**Figure 68.** Accumulated NMR spectra of Bt-Thy (**53**) with temperature from 20 °C to - 50 °C at 1 mM and in CDCl<sub>3</sub> (600 MHz).



**Figure 69.** Accumulated NMR spectra of Bt-Ade (**51**) with temperature from 20 °C to - 50 °C at 1 mM and in CDCl<sub>3</sub> (600 MHz).



**Figure 70.** Accumulated NMR spectra at temperatures from 60 °C to - 40 °C for Bt-Thioura (**55**) at 1 mM and in CDCl<sub>3</sub> (300 MHz).



**Figure 71.** Possible hydrophobic interaction of biotin bicycle ring with phenyl group in Bt-Thioura (**55**).

Table 23 shows the differences in the <sup>1</sup>H NMR chemical shifts for H3 and H4 between biotinylated nucleobases and biotin amide (**33**) at 1 mM and 20 °C in CDCl<sub>3</sub>. The largest value for ΔH3 was observed for Bt-Cyt (**52**) and probably resulted from a deshielding of the bridgehead protons by the aromatic ring. In contrast, Bt-Thioura (**55**) shows a negative value for ΔH3, suggests that H3 was situated in a shielding region of the aromatic ring.

**Table 23.** Differences of  $^1\text{H}$  NMR Chemical Shifts of H3 and H4 between Biotinylated Nucleobases and Biotinyl Amide Bt-Uyene (**33**) in  $\text{CDCl}_3$  at 1 mM and 20  $^\circ\text{C}$  (ppm).

compound	$\Delta\text{H3}$	$\Delta\text{H4}$
Bt-Ade ( <b>51</b> )	+0.005	+0.008
Bt-Cyt ( <b>52</b> )	+0.051	-0.009
Bt-Thy ( <b>53</b> )	+0.014	+0.018
Bt-Ura ( <b>54</b> )	+0.010	+0.010
Bt-Thioura ( <b>55</b> )	-0.062	+0.012

The accumulated variable temperature NMR spectra of Bt-Thy (**53**) are shown in Figure 68, and those of Bt-Thioura (**55**) are shown in Figure 70 (both 1 mM samples in  $\text{CDCl}_3$ ). Figure 70 shows that protons associated with the biotin ring system move upfield with a decrease in temperature from 60  $^\circ\text{C}$  to -40  $^\circ\text{C}$ . No obvious pattern is discernible in Figure 68 for Bt-Thy (**53**). These changes are summarised for **51-55** in Table 24 and show the significant up-field movement of H2 and H3 for Bt-Thioura (**55**). However, the changes in  $^1\text{H}$  NMR chemical shifts for protons H2, H3, H4, H5a' and H5b' in Bt-Ade (**51**) with a decrease in temperature are positive and significant (larger than 0.05 ppm). Therefore, the data in Table 24, together with the spectra in Figure 70 are indicative that the biotin ring in Bt-Thioura (**55**) is involved in a stacking interaction and the hydrogen bonding pair in Bt-Thioura (**55**) is quite different from that of Bt-Ade (**51**). There is no indication of involvement of hydrophobic interaction in other biotinylated nucleobases. The formation of a hydrogen bonding pair in Bt-Thioura (**55**) facilitates the hydrophobic interaction. Conversely, the observation of the hydrophobic interaction is consistent with the formation of a hydrogen bonding pair concerning NHa and the carbonyl group of biotin ureido moiety. According to molecular modelling, only this kind of hydrogen bonding pair concerning NHa is possible for the hydrophobic interaction between the biotinyl ring system and the phenyl group. Therefore, the left side of biotin ureido moiety containing NHa (Figure 63) is likely to preferentially bind nucleobase-thiouracil, however, the right side of the biotin ureido moiety containing NHb mainly interacts with adenine, cytosine, thymine and uracil.

**Table 24.** Changes in  $^1\text{H}$  NMR Chemical Shifts for Protons on the Biotin Ring of **51-55** at Temperatures from 20  $^\circ\text{C}$  to -60  $^\circ\text{C}$  at 1 mM and in  $\text{CDCl}_3$  (ppm).

compound	H2	H3	H4	H5a	H5b
Bt-Ade ( <b>51</b> ) <sup>a</sup>	+0.050	+0.072	+0.086	+0.029	+0.066
Bt-Cyt ( <b>52</b> )	+0.013	+0.042	+0.056	+0.020	+0.052
Bt-Thy ( <b>53</b> ) <sup>a</sup>	+0.010	+0.061	+0.067	+0.024	+0.052
Bt-Ura ( <b>54</b> )		+0.042	+0.071	+0.020	+0.048
Bt-Thioura ( <b>55</b> ) <sup>b</sup>	-0.169	-0.132	-0.002	-0.049	-0.046

<sup>a</sup>20  $^\circ\text{C}$  to -50  $^\circ\text{C}$  for compound **51** and **53**; <sup>b</sup>20  $^\circ\text{C}$  to -40  $^\circ\text{C}$  for compound **55**.

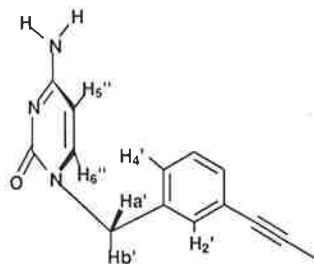
### 5. 2. 2 Differentiation and assignment of pro-chiral hydrogens in biotin nucleobases

The accumulated variable temperature NMR spectra of Bt-Thy (**53**) are shown in Figure 68 and those for Bt-Thioura (**55**) are arranged in Figure 70, in CDCl<sub>3</sub> at 1 mM. According to Figure 68, the double vicinal protons Ha' and Hb' at positions 31 and u3 are separated at - 50 °C. As to compound Bt-Thioura (**55**), the separation of pro-chiral hydrogens occurs at room temperature as shown in Figure 70. In compound Bt-Ura (**54**) in CDCl<sub>3</sub> and at 1 mM, the vicinal protons Ha' and Hb' in position 31 are separated at - 60 °C. In biotinylated nucleobase Bt-Ade (**51**) at 1 mM, the separation of vicinal protons in the 31 position in CDCl<sub>3</sub> is observable at - 20 °C and better at - 50 °C (Figure 69). As to Bt-Cyt (**52**) in CDCl<sub>3</sub> and at 1 mM, the differentiation of pro-chiral hydrogens at position 31 occurred at room temperature (Figure 63). All the data are arranged in Table 25.

**Table 25.** Proton NMR Signal Differentiation of Pro-Chiral Hydrogens in Biotin Nucleobases at 1 mM in CDCl<sub>3</sub> (ppm).

Compound	temperature	31			u3			u11			9		
		Ha'	Hb'	(Hb'-Ha')	Ha'	Hb'	(Hb'-Ha')	Ha'	Hb'	(Hb'-Ha')	Ha'	Hb'	(Hb'-Ha')
Bt-Ade ( <b>51</b> )	-50	5.395	5.420	0.025									
Bt-Cyt ( <b>52</b> )	20	4.782	5.072	0.290									
Bt-Thy ( <b>53</b> )	-50	4.834	4.964	0.128	2.232	2.284	0.052						
Bt-Ura ( <b>54</b> )	-60	4.841	4.890	0.049									
Bt-Thioura ( <b>55</b> )	20	4.148	4.622	0.474				3.175	3.330	0.155			
Bt-Met(D)-Ade ( <b>152</b> )	20	5.326	5.361	0.035							2.502	2.531	0.029
Bt-Met(L)-Ade ( <b>153</b> )	20	5.334	5.362	0.028							2.516	2.546	0.030

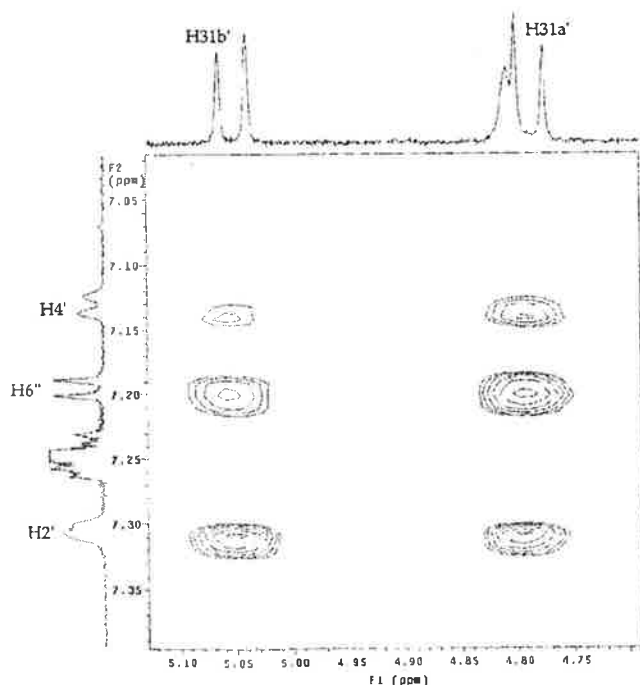
The differentiation of the vicinal protons at u11 of the biotinylated nucleobases was only observed in Bt-Thioura (**55**) at 300 MHz, which is presumably the result of the intra-molecular hydrogen bonding of Hc with the carbonyl group of the ureido moiety and the proximity of those hydrogen atoms to the biotin ring system and confirms the preferential hydrogen bonding pair concerning Ha and the carbonyl as shown in Figure 63.



**Figure 72.** The preferred conformation of Bt-Cyt (**52**) with least steric repulsion. The alkyl group and biotin moiety are omitted for clarity.

According to the 2D NMR spectra of Bt-Cyt (**52**) at 1 mM in CDCl<sub>3</sub> at 40 °C (for better solubility) (Figure 73), Ha' in position 31 is close to H4' and Hb' is close to H2' and Ha' is close to H6''. According to molecular modelling, Bt-Cyt (**52**) tends to adopt the low energy

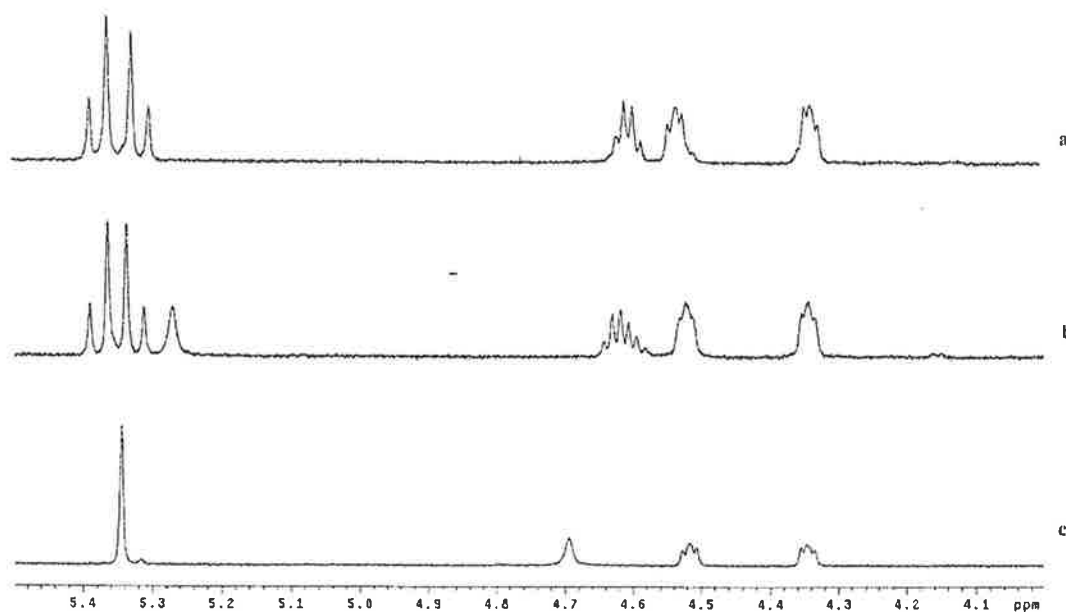
conformation shown in Figure 72. Ha' is expected to be in the same plane with H6'', and Hb' in the same plane as H2', while Hb' is expected to be in contact with the carbonyl group of cytosine.<sup>197</sup> The evidence for the possible contact of Hb' with the carbonyl group of the cytosine ring is the temperature dependence of Hb' in position 31. The effective interaction of Hb' with the carbonyl group results in the downfield movement of the NMR resonance of the proton. The <sup>1</sup>H NMR chemical shift temperature dependence for Ha' was - 0.59 ppb/K, that for Hb' was +1.10 ppb/K from 20 °C to - 60 °C. Furthermore, the temperature dependencies of Ha' and Hb' in Bt-Thy were - 0.40 ppb/K and 2.08 ppb/K respectively at 1 mM in CDCl<sub>3</sub> from 0 °C to - 50 °C, which is indicative for the interaction of Hb' with the carbonyl group in thymine. Therefore, Ha' was assigned as pro-R with a chemical shift of 4.782 ppm, and Hb' as pro-S with a shift 5.072 ppm in Bt-Cyt (**55**) in CDCl<sub>3</sub> at 1 mM and room temperature.



**Figure 73.** Selected 2D-ROESY spectrum of Bt-Cyt (**52**) at 1 mM and 40 °C in CDCl<sub>3</sub> (600 MHz).

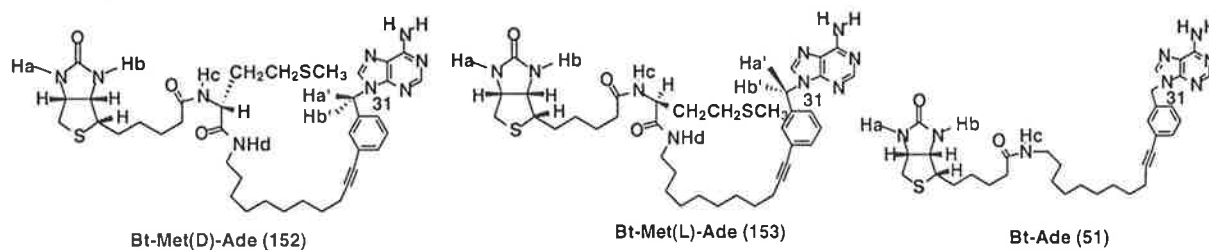
Furthermore, the biotin peptide nucleobases **152** and **153** were also studied for the differentiation of pro-chiral methylene protons and intra-molecular hydrogen bonding interactions (Figure 75). Figure 74 shows the accumulated NMR spectra of compounds **152** and **153** together with Bt-Ade (**51**) at rt and 1 mM in CDCl<sub>3</sub>. The differentiation of pro-chiral hydrogens at position 31 and 9 were observed at room temperature (Figure 74 and Table 25). These results suggest that the conformation adopted by **152** and **153** allows for a better separation of pro-chiral methylene protons at the 31 position in **152** and **153** compared to **51** (Table 26). The intra-molecular hydrogen bonding interactions were also expected to be much stronger for **152** and **153** compared to **51**, since all the proton NMR resonances for NH<sub>2</sub>, Ha, Hb and Hc (Table 26) in compounds **152** and **153** were further downfield for compound **51**. According to the data in

Table 26, the chemical shifts of Hc and NH<sub>2</sub> in **153** are greater than those in compound **152**, which indicates that the natural occurring amino acid residue L-methionine is important for the involvement of intra-molecular hydrogen bonding by the amino group of adenine. Proton Hc in compound **153** is more likely to be involved in the intra-molecular hydrogen bonding than **152**. Therefore, intra-molecular hydrogen bonding networks in both **152** and **153** indicated the structures as shown in Figure 75 with molecular modelling of the hydrogen bonds as shown in Figure 76. The computer modelling showed the energy for the conformation of **153** was - 26.69 kcal/mol which is much lower than that for **152** (4.15 kcal/mol) (Figure 76). The results suggest that compound **153** is more likely to be involved in the intra-molecular hydrogen bonding interactions concerning adenine.

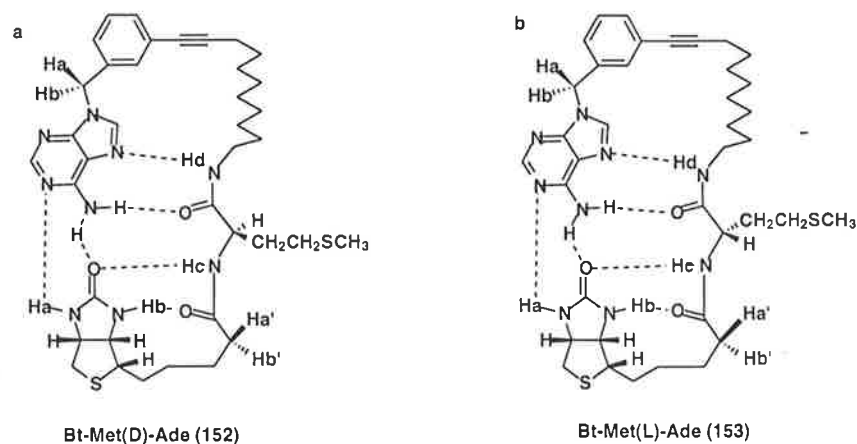


**Figure 74.** Accumulated NMR spectra of biotinylated nucleobases **52** (c), **152** (a) and **153** (b) in CDCl<sub>3</sub> at 1 mM and 20 °C.

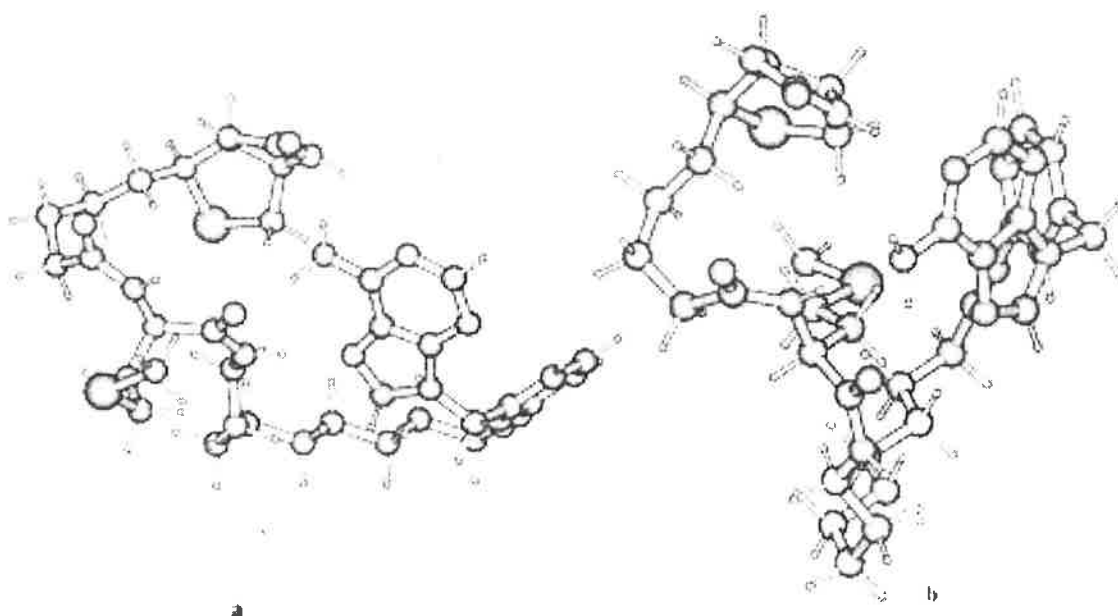
**Table 26.**  $^1\text{H}$  NMR Chemical Shifts of Protons in Biotinylated Nucleobases **52**, **152** and **153** in  $\text{CDCl}_3$  at 1 mM and  $20^\circ\text{C}$  (ppm) and Pro-chiral Differentiation of Methylene Hydrogens at the 31 Position.



compound	Bt-Met(D)-Ade ( <b>152</b> )	Bt-Met(L)-Ade ( <b>153</b> )	Bt-Ade ( <b>51</b> )
NH <sub>2</sub>	6.16	6.41	5.97
Ha	5.78	5.23	4.69
Hb	6.66	6.53	5.74
Hc	6.84	7.10	5.61
Hd	7.49	7.35	



**Figure 75.** Possible hydrogen bonding networks of **152** (a) and **153** (b) in  $\text{CDCl}_3$  at 1 mM and  $20^\circ\text{C}$ .



**Figure 76.** Molecular modelling structures of **152** (a) and **153** (b) with hydrogen bonding networks.



## 5.3 Discussion

### 5.3.1 Introduction of nonpolar aliphatic and aromatic groups into biotinylated nucleobases

In *Escherichia coli*, biotin carboxyl carrier protein (BCCP) is a subunit of acetyl coenzyme A and catalyses the first committed step of fatty acid synthesis.<sup>21</sup> The BCCP is first post-translationally modified in the reaction catalysed by the biotin holoenzyme (BHS).<sup>24</sup> During the reaction, both biotin and ATP are expected to be attached to the BHS enzyme, the intermediate biotinyl-5'-AMP (Figure 59) is then produced "intra-molecularly" by the proximity effect, and biotin is connected to the target lysine residue of the BCCP enzyme.<sup>15, 17</sup>

In biotinylated BCCP, biocytin (biotin lysine) is located at a type I'  $\beta$  turn of the N-terminal and C-terminal halves of biotinylated BCCP. The turn is stabilised by three hydrogen bonds. Tyr-92 is one of the seven amino acid residues within 4.0 Å of the biotin moiety.<sup>25</sup> In the streptavidin-biotin complex, biotin is bound by hydrogen bonding and hydrophobic interactions, Tyr-43 directly contacts the streptavidin by these interactions. Therefore, a nonpolar undecynyl group and aromatic phenyl group were introduced into the biotinyl-5'-AMP analogue Bt-Ade (**51**) (Figure 63).

### 5.3.2 Hydrogen bonding controlled folding

Although the intra-molecular hydrogen bonding and  $\pi$ - $\pi$  stacking interaction are important in the folding of polypeptides, protein and nucleic acids in aqueous and polar solutions,<sup>198</sup> for the relatively small biotinylated nucleobases Bt-Ade (**51**), Bt-Cyt (**52**), Bt-Thy (**53**), Bt-Ura (**54**), Bt-Thioura (**55**), Bt-Met(D)-Ade (**152**) and Bt-Met(L)-Ade (**153**), the nonpolar solvent CDCl<sub>3</sub> was necessary to evaluate the folding and internal interactions of the molecules. In order to eliminate possible intermolecular hydrogen bonding and stacking interactions between biotinylated nucleobases in CDCl<sub>3</sub>, the concentrations of the compounds were kept to 1 mM. According to the results in Tables 21 to 26, the N-3' side of biotin involving NHb forms hydrogen bonding pairs with nucleobases-adenine, cytosine, thymine and uracil (Figure 63).

However, in Bt-Thioura (**55**) the preferred hydrogen bonding pair involved NHa and thiouracil. Remarkably, the strikingly hydrophobic interaction between the biotin and phenyl groups is observed at the same time. Both of the interactions are expected to be important in the folding of biotinylated nucleobase Bt-Thioura (**55**), which is different from the folding in Bt-Ade (**51**), Bt-Cyt (**52**), Bt-Thy (**53**) and Bt-Ura (**54**). The hydrogen bonding and hydrophobic interactions are consistent with the interactions observed in the crystal structure of streptavidin-biotin complex,<sup>199</sup> in which Tyr-43 is believed to directly contact the biotin by hydrogen bonding and hydrophobic interactions.

### 5.3.3 Predicted internal interactions of biotinyl-5'-AMP and its geometry on BHS enzyme

Recently, both Watson-Crick and Hoogsteen type base pair hydrogen bonds have been experimentally observed by application of NMR techniques, e. g. (Figure 78).<sup>200</sup> Accordingly, imides are widely used as hosts to bind with adenine derivatives through hydrogen bonding and  $\pi$ - $\pi$  stacking interactions.<sup>193, 194, 201, 202</sup> Therefore, the possible hydrogen bonding pair in biotinyl-5'-AMP is structurally similar to the DNA base pair A·T and A·U.

According to the crystal structure of BHS enzyme or BirA, ATP will bind adjacent to the biotin. Biotin tends to orient the binding of ATP on the binding loop and affect the activity of the binding to the loop.<sup>19</sup> According to the model suggested by Hoagland and coworkers,<sup>17, 19</sup> ATP and amino acid were bound on the synthetase, followed by the formation of the intermediate for amidation. Therefore, biotin bound on the BHS enzyme, probably promotes the following binding of ATP on the BHS enzyme by the hydrogen bonding interaction and then enhances the reactivity of ATP by placing the ATP close to biotin on BHS enzyme and promoting the following intra-molecular reaction. Secondly, with the formation of the hydrogen bonding pair as shown in Figure 77 for biotinyl-5'-AMP, both biotin and adenine are expected to be in the same plane for the maximisation of hydrogen bonding. After the formation of biotinyl-5'-AMP on the BHS enzyme, the formation of the hydrogen bonding pair in Figure 77 is also expected to promote the detachment of the intermediate from the BHS enzyme for the following attachment to BCCP enzyme. It is understood that the closed form of the flexible intermediate biotinyl-5'-AMP (Figure 77) takes advantage of its small entropy loss upon the complexation on enzymes due to the self-preorganization by the hydrogen bonding pair.<sup>79</sup>

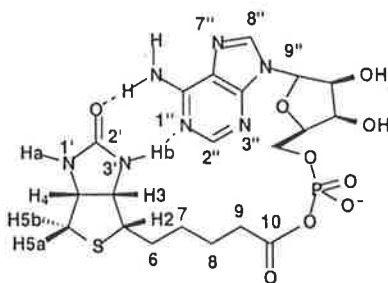
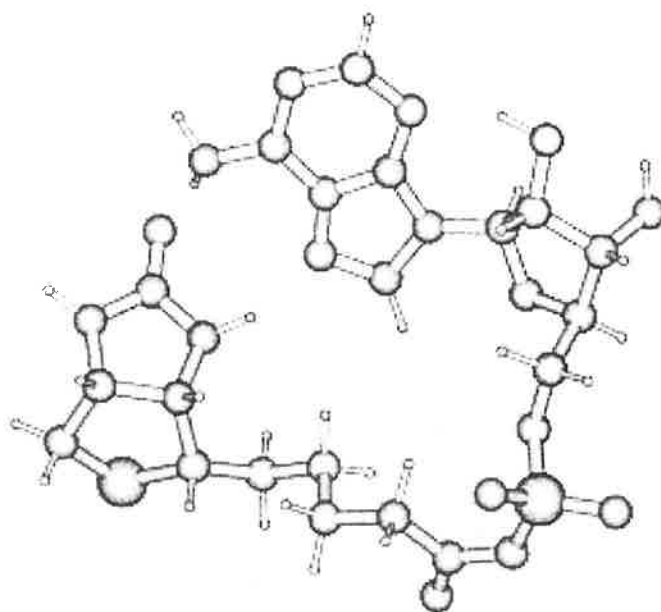
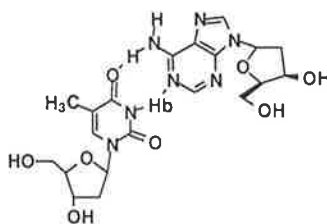


Figure 77a. Possible hydrogen bonding pair in biotinyl-5'-AMP.



**Figure 77b.** Molecular modelling structure of biotinyl-5'-AMP with intra-molecular hydrogen bonding pair.



**Figure 78.** Watson-Crick type hydrogen bonding pair A·T.<sup>200</sup>

As shown in Figures 68 to 70, vicinal protons in position 31 of biotinylated nucleobases are differentiated. The hydrogen bonding accounts for the separation, which locks the conformation and makes the vicinal protons in different chemical environments. The formation of hydrogen bonding pairs results in the asymmetric hemispheric structure, which is structurally favorable for further binding of biotinyl-5'-AMP in the specific biotin binding loop of BCCP enzyme.<sup>21</sup>

## Chapter 6

### Hydrogen Bonding and $\pi$ - $\pi$ Stacking in DNA Base Pair Triplet Analogues

#### 6.1 Introduction

The molecular recognition of DNA is of great interest in the potential design of new drug compounds to regulate gene expression<sup>203,204</sup> and the selective cleavage of DNA.<sup>205</sup> The specific hydrogen bonding including Hoogsteen and Watson-Crick type interactions are dominant in the recognition of single base pairs,<sup>204-208</sup> along with  $\pi$ - $\pi$  stacking which is important in the stabilization of DNA and DNA-receptor complexes.<sup>203,209</sup> The DNA triplet motif is common in biology,<sup>203,210-215</sup> however, little has been reported on model compounds which have the potential to recognize DNA triple helices. It is known that thymine can interact with adenine and thymine to form a TAT base pair triplet.<sup>206,208</sup> The crystallographic results for adenosine derivatives have suggested the formation of the base pair triplet TAA.<sup>216,217</sup> Adenine can also recognize the AT base pair to form an AAT base pair triplet.<sup>218</sup> The protonated cytosine could complex with two adenines to form an AC\*A base pair triplet<sup>78</sup> as shown in Figure 79a. Using this motif, an analogue was designed and prepared with one pyridine and two adenine units as shown in Figure 79b. The intra-molecular hydrogen bonding and  $\pi$ - $\pi$  stacking interactions of a series of adenine complexes was investigated.

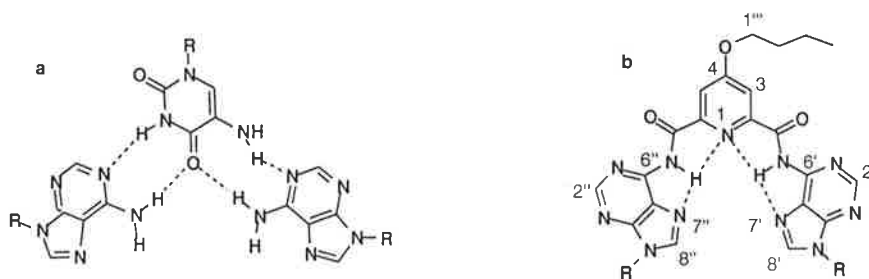


Figure 79. DNA base pair triplet (a) and its analogue (b).

Recently, a preorganized crossed-linked scaffold was prepared by Chaudhuri and co-workers based on adenine and possessing considerable stability with strong Watson-Crick and Hoogsteen hydrogen bonding as well as  $\pi$ - $\pi$  stacking interactions (Figure 80).<sup>219</sup>

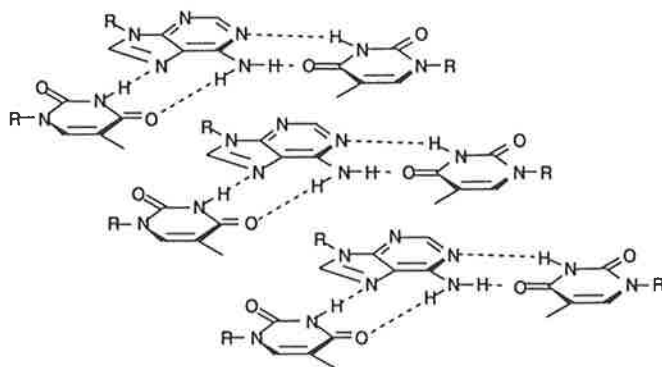
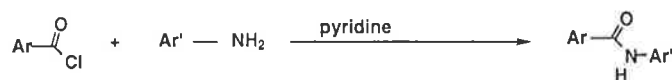


Figure 80.  $\pi$ - $\pi$  Stacking interactions of DNA base pair triplets.

## 6.2 Results and Discussion

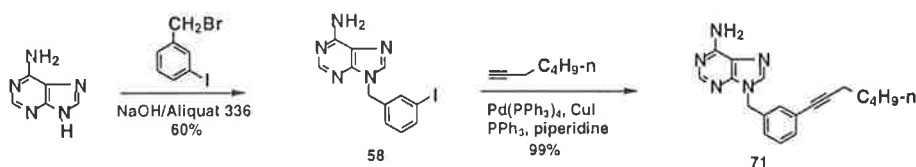
### 6.2.1 Synthesis

In order to investigate the complex intra- and intermolecular interactions expected for complex **69**, sample analogues **58-68** (Figure 81) were prepared by acylation using the appropriate acyl chloride and the corresponding amine in pyridine<sup>220</sup> as shown in Scheme 12. In this way the individual hydrogen bonding and  $\pi$ - $\pi$  stacking properties could be characterised (Figure 81).

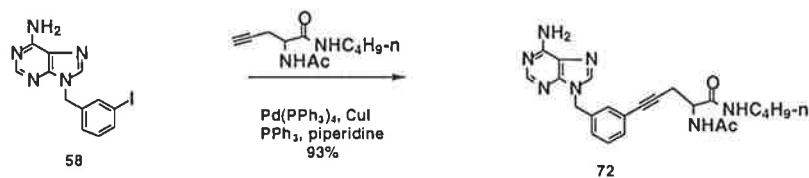


Scheme 12. Synthesis of amides.

9-Butyladenine was synthesized by the direct butylation of adenine with 1-iodobutane in the presence of Aliquat 336. Adenine was benzylated with 3-iodobenzyl bromide to form compound **58**, and compounds **71** and **72** were subsequently prepared by the palladium mediated coupling reactions with 1-heptyne and 1-(*N*-butyl)-2-(*N*-acetyl)-2-propargyl glycine amide respectively (Schemes 13 and 14).<sup>221</sup>



Scheme 13. Synthesis of adenine derivatives.



Scheme 14. Synthesis of adenine derivatives.

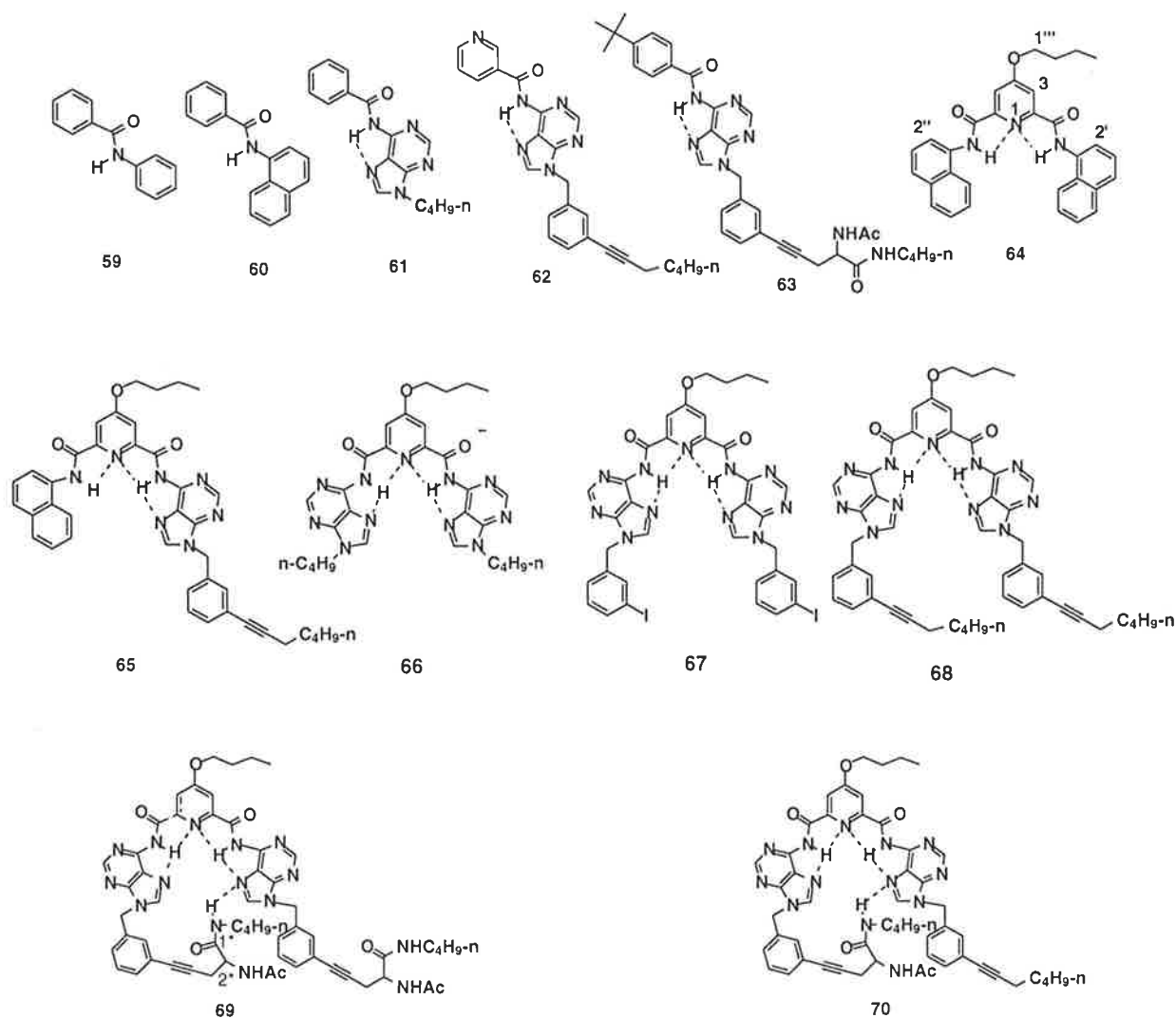
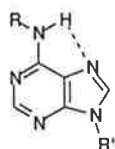


Figure 81. DNA base pair triplet analogues and related compounds.

### 6.2.2 Hydrogen bonding in the DNA base pair triplet analogues

The NMR and FT-IR data for amides **59-68** in 1.9 mM  $\text{CDCl}_3$  solution are listed in Table 27. Compounds **59** or **60** cannot display an intra-molecular hydrogen bond so their  $^1\text{H}$  NMR chemical shifts and infrared frequency for their NH serve as baseline. Compounds **61-63** can form intra-molecular hydrogen bonds with the N-7 in adenine, since the chemical shifts of NH in the compounds **61**, **62** and **63** are larger than those in **59** and **60**. The infrared absorption for the

N-H bond in compounds **61-63**, move to lower wavenumbers compared to **59** or **60**, suggesting the intra-molecular hydrogen bonding of N-H with nitrogen in adenine (Figure 82).



**Figure 82.** Intra-molecular hydrogen bonding of adenine in DNA.

The chemical shift of the amide protons in compound **64** is much larger than that in **59** as well as **61-63**, but the infrared absorption of the NH bond is much smaller than that of **59** and **60**, these results confirm the existence of an intra-molecular hydrogen bonding of NH with the nitrogen in pyridine in compound **64**. Furthermore, the  $^1\text{H}$  NMR chemical shifts of NH in compounds **66-68** also shift downfield considerably, based on FT-IR data of compounds **59-64**. This data indicate that the N-H in compounds **66-68** forms stable hydrogen bond with both of the nitrogens in adenine and pyridine. Interestingly, one N-H in compound **65** formed one intra-molecular hydrogen bond with the nitrogen in the pyridine ring, however, the other N-H formed a three-centre intra-molecular hydrogen bond with the nitrogen atoms of both the pyridine and adenine (Figure 81).

Literature reports indicate that if the amide NH proton was involved in intra-molecular hydrogen bonding, the absorption would appear as a broad peak between  $3300\text{-}3400\text{ cm}^{-1}$ , while an amide NH with no internal hydrogen bond would appear as a sharp absorption between  $3400\text{-}3500\text{ cm}^{-1}$ .<sup>79,159</sup> The amide NH infrared absorbances of compounds **61-68** are all in the range of  $3300\text{-}3400\text{ cm}^{-1}$ .

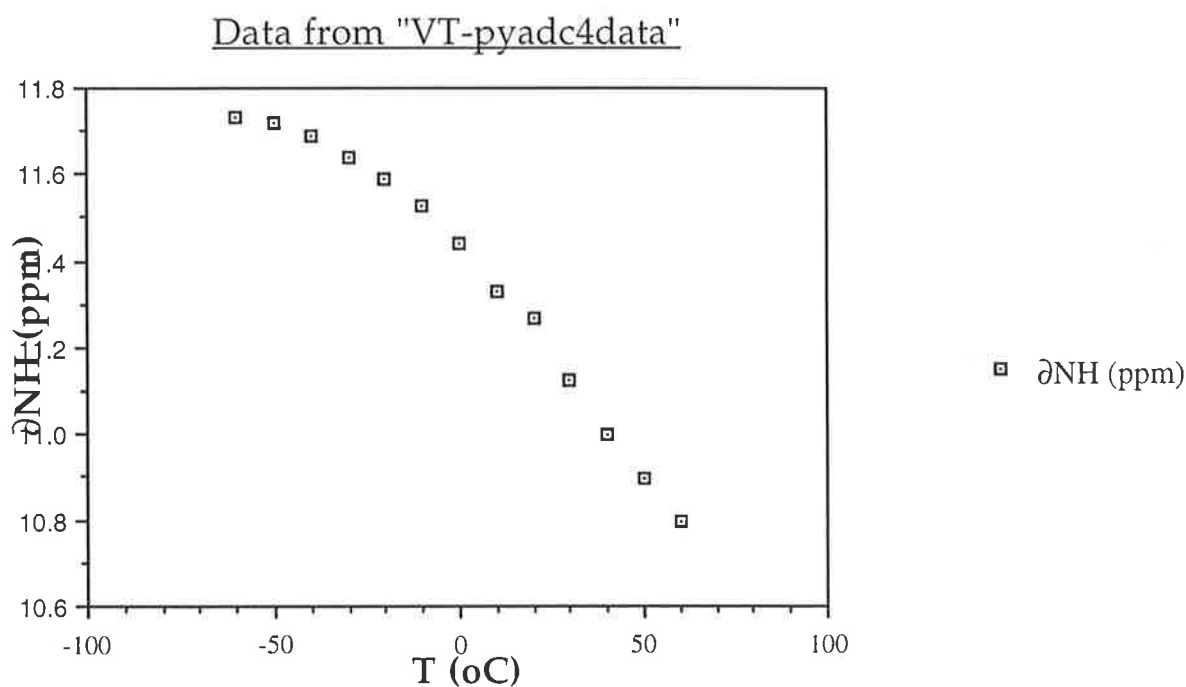
**Table 27.** NMR and FT-IR Data for Compounds **59-68** in  $\text{CDCl}_3$  (1.9 mM).

Compound	$\delta$ NH (ppm)	$\nu$ max ( $\text{cm}^{-1}$ )
<b>59</b>	7.78	3437
<b>60</b>	8.19	3434
<b>61</b>	8.88	3409
<b>62</b>	8.91	3399
<b>63</b>	8.91	3414
<b>64</b>	10.32	3389
<b>65</b>	11.05, 10.40	3370
<b>66</b>	11.08	3359
<b>67</b>	11.07	3359
<b>68</b>	11.04	3360

To characterise further the intra-molecular hydrogen bonding of the amide NH protons in compounds **66**, **67** and **69**, the values for the temperature dependencies of the chemical shifts ( $\Delta\delta\text{NH}/\Delta\text{T}$ ) were measured. The  $\Delta\delta\text{NH}/\Delta\text{T}$  values for the amide NH proton in CONH-purinyll

of compounds **66**, **67** and **69** were 10.5 ppb/K, 11.4 ppb/K and 10.2 ppb/K, respectively, indicating efficient three-centered intra-molecular hydrogen bonds (Figure 81).

Figure 83 shows the changes of chemical shifts of NH of **66** with temperatures. According to Figure 83, as the temperature is lowered, the intra-molecular hydrogen bonding increases until approximately -60 °C when no further change was observed.



**Figure 83.** Changes of chemical shifts of amide protons of compound **66** (1.9 mM) with temperatures.

The selected NMR data of compounds **69**, **70** and the control compound **63** are listed in Table 28. As we can see from Table 28, the difference in chemical shift of the amide protons in  $\text{CONH}^*\text{C}_4\text{H}_9\text{-n}$  from compound **63** to **70** is + 0.45 ppm, and the change  $\Delta\delta'$ **63-70** of chemical shift of the proton in NHAc from **63** to **70** is + 0.17 ppm. These results reveal that both protons are involved in intra-molecular hydrogen bonding, but the former one is more likely than the latter, because  $\Delta\delta$ **63-70** (0.45 ppm) is larger than  $\Delta\delta'$ **63-70** (0.17 ppm).  $\Delta\delta$ **63-69** is 0.62 ppm, but  $\Delta\delta'$ **63-69** is 0.28 ppm, so that  $\Delta\delta$ **63-69** >  $\Delta\delta$ **63-70** and  $\Delta\delta'$ **63-69** >  $\Delta\delta'$ **63-70**. These results indicate that all the protons of compound **69** in the amino acid amide moiety could form intra-molecular hydrogen bonds with the nitrogens on the purinyl rings (Figure 81). Also, the proton in the  $\text{CONH}^*\text{C}_4\text{H}_9\text{-n}$  moiety is more likely to form hydrogen bonds than those in  $\text{NH}^*\text{Ac}$ , and the intra-molecular hydrogen bonding in compound **69** is much stronger than that in compound **70**. With the intra-molecular hydrogen bonding of the amino acid amide with nucleobases, the amino acid amide moieties will fold back onto the structure (Figure 85).

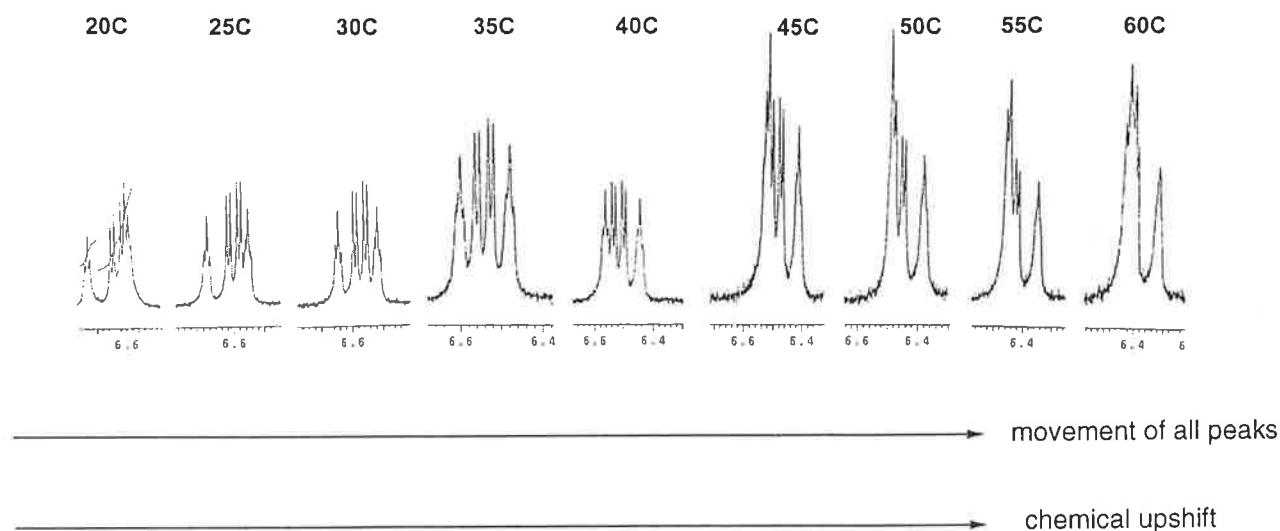


**Table 28.** Proton (\*) NMR Data of Amino Acid Amide in Compounds **63**, **69** and **70** in CDCl<sub>3</sub> (1.9 mM) at rt (ppm).

compound	<b>63</b>	<b>70</b>	<b>69</b>
CONH*C <sub>4</sub> H <sub>9</sub> -n	6.11	6.56	6.73
NH*Ac	6.36	6.53	6.64
CH*(NHAc)CONH	4.54	4.64	4.67

All the temperature coefficient values of NH protons in the amino acid amides of **69** were 8.4/6.2 ppb/K (CONHBu) and 5.7/5.6 ppb/K (NHAc), which are much larger than the standard value (3 ppb/K), indicating the presence of intra-molecular hydrogen bonding.<sup>79, 159</sup> However,  $\Delta\delta_{\text{NH}}/\Delta T$  value of proton in CONHC<sub>4</sub>H<sub>9</sub> is much larger than that in NHAc, the difference indicating that the former proton is more likely to form intra-molecular hydrogen bonding than the latter.

Figure 84 shows the movements of amide peaks in compound **69** with an increase of temperature from 20 °C to 60 °C. Clearly, the proton **I** in CONHBu moved upfield more quickly than the proton **III** in NHAc with the increase of temperature. This result suggested that proton **I** in CONHBu is more likely to form the intra-molecular hydrogen bonding than proton **III** in NHAc. The increase of temperature on NMR promoted the resolution of peaks of the amino acid amide in compound **69**. The best resolution was obtained at 30 °C and 35 °C. There are clear four peaks **I**, **II**, **III** and **IV**. Two different amide proton peaks **I** and **II** in CONHBu suggested that **I** could form the internal H-bond firstly, then the possible second one **II** during the folding back (Figure 85).

**Figure 84 .** Changes of proton NMR peaks of amide NH in compound **69** with temperatures at 1.9 mM in CDCl<sub>3</sub>.

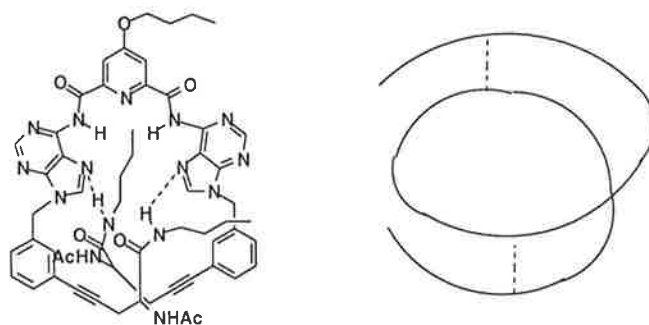


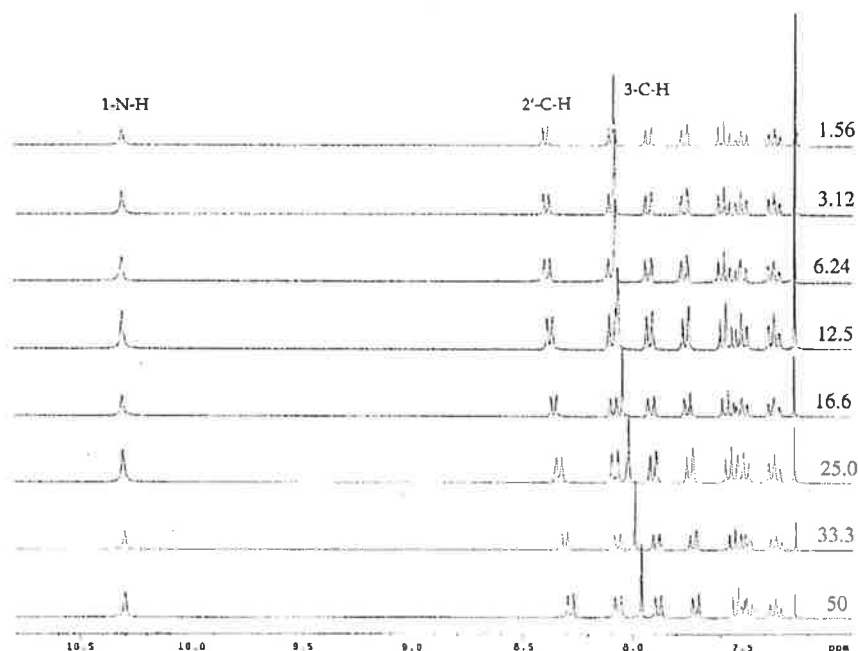
Figure 85. Folding of molecule in compound 69.

### 6. 2. 3 $\pi$ - $\pi$ Stacking of DNA base pair triplet analogues

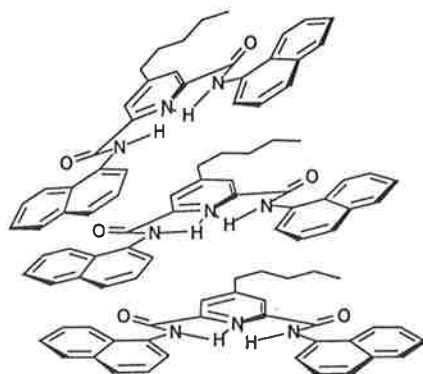
NMR dilution experiments for compounds **61**, **64** and **68** were carried out in  $\text{CDCl}_3$  at room temperature (Figure 86). Some selected results are shown in Table 29. As shown in Figure 86 for compound **64**, as the concentration was increased, there was a gradual up-field shift for the protons, indicating intermolecular  $\pi$ - $\pi$  stacking. Furthermore at higher concentration, intermolecular hydrogen bonding would occur. However, there was little change in the NH chemical shift as the concentration increased, indicating the stability of the intra-molecular hydrogen bonding (Figure 81) of the NH with nitrogen in pyridine ring of compound **64**. The intra-molecular hydrogen bonds in compounds **64** (Figure 81) is expected to ensure a planar arrangement for the pyridine and adenine rings. The pyridine rings would overlap each other as would the naphthyl ring. The intra-molecular hydrogen bonding of the adenine N-H to the N-1 in the pyridine ring would promote  $\pi$ - $\pi$  stacking,<sup>222</sup> because the pyridine ring becomes progressively electron-poor with the formation of the intra-molecular hydrogen bonding. The butoxyl group in the pyridine ring will aggregate together by van de Waals interactions.<sup>223</sup> Therefore compound **64** could be involved in regular assembly by  $\pi$ - $\pi$  stacking interactions as shown in Figure 87.

Table 29. Selected Changes of Proton Chemical Shifts of Compounds **64**, **68** and **61** from Dilution Experiments in  $\text{CDCl}_3$  at rt (ppm).

compound	concentration change (mM)	N-H	3-C-H	8'-C-H	4-O-C-H
<b>64</b>	50.0 to 1.56	+0.02	+0.183	+0.166 (2'-H)	+0.121
<b>68</b>	64.1 to 1.14	+0.05	+0.031	+0.061	+0.016
<b>61</b>	461 to 18.4	-0.94		+0.099	

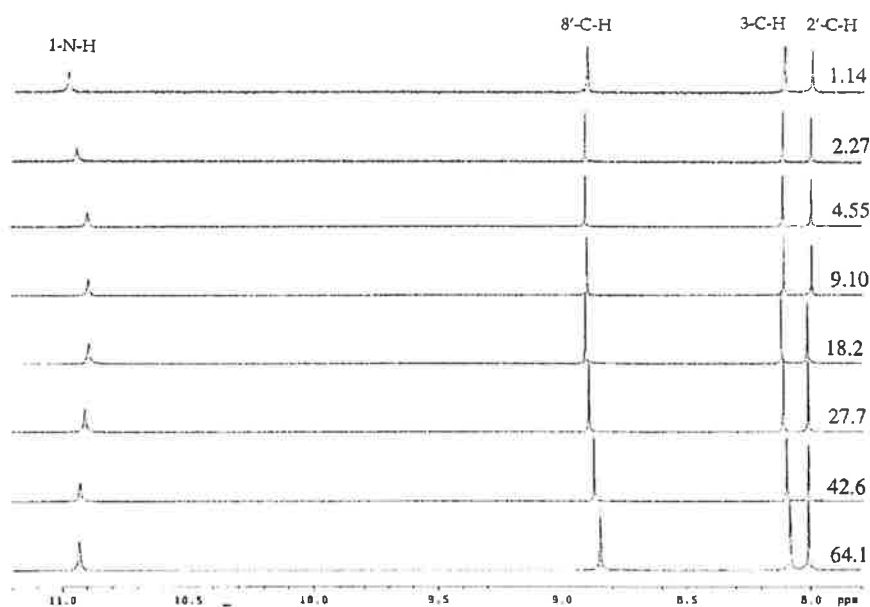


**Figure 86.** NMR spectra of compound **64** from high to low concentrations (mM) in  $\text{CDCl}_3$  at rt.



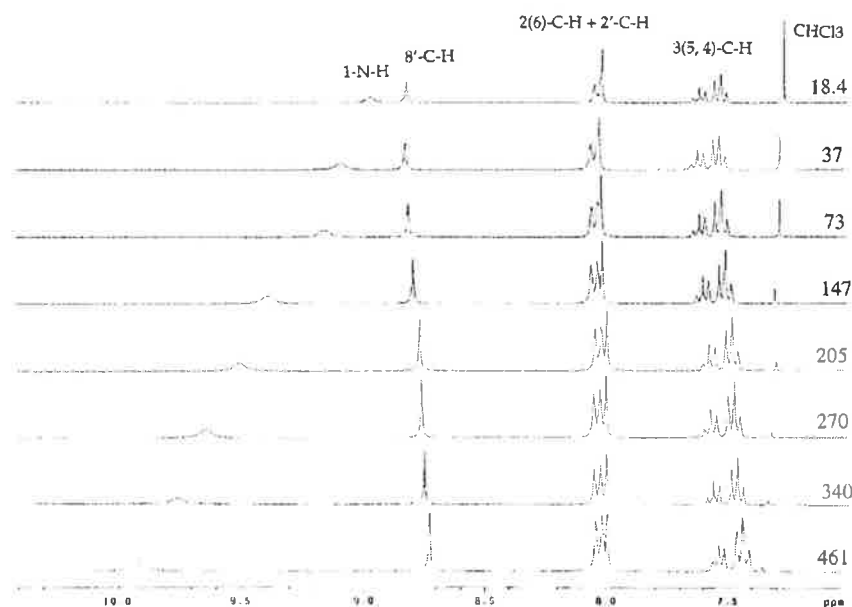
**Figure 87.**  $\pi$ - $\pi$  Stacking of compound **64**.

NMR experiments also confirmed that compound **61** could form strong intermolecular hydrogen bonds with the amide moiety at high concentration, as shown in Table 29. The change of chemical shift of N-H in compound **61** was - 0.94 ppm, while the concentration was reduced from 461 to 18.4 mM. The result for compound **61** in Table 29 and the movement of peaks in Figure 88 also indicate the efficient intermolecular  $\pi$ -stacking at relatively higher concentrations, since all the resonances moved downfield except the N-H, when the concentration was decreased. In dilution experiments of 9-butyladenine and 9-(3-(1-heptynyl)benzyl)adenine **71** using NMR spectroscopy, little or no chemical shift change ( $\pm 0.003$  ppm) for 8-C-H or 2-C-H in adenine was observed at constant temperature.

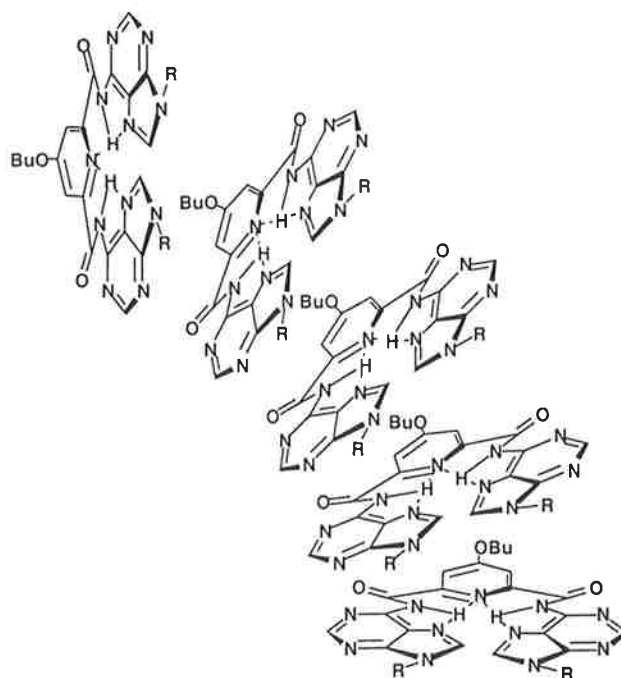


**Figure 88.** NMR spectra of compound **61** from high to low concentrations (mM) in  $\text{CDCl}_3$  at rt.

The NMR dilution experiments for compound **68** were also carried out from 64.1 mM to 1.14 mM. All the NMR spectra from 11.40 ppm to 7.60 ppm were arranged in Figure 89. The chemical shift change ( $\Delta\delta$ ) of 8'-C-H in adenine was about + 0.061 ppm, and that of 3-C-H of pyridine was + 0.031 ppm, indicating the  $\pi$ - $\pi$  stacking interactions in the assembly state at higher concentration. The possible chemical and computer modelling structures are shown in Figure 90, in which this assembly possesses helicity.



**Figure 89.** NMR spectra of compound **68** from high to low concentrations (mM) in  $\text{CDCl}_3$  at rt.



**Figure 90.** Chemical and molecular modelling structures of **68** showing  $\pi$ - $\pi$  stacking.

---

## Chapter 7

---

### Recognition of Biotin Ester with Synthetic Receptors

#### 7.1 Introduction

As well as functioning as a co-enzyme of carboxylase, biotin also plays an important role in the metabolism of amino acids and sugars. Biotin selectively and tightly binds to avidin and streptavidin<sup>224</sup> through numerous van der Waals interactions involving stacking with tryptophan, an extensive pattern of hydrogen bonds involving the ureido group, polar interactions between the biotin sulfur and the hydroxyl group of threonine residues in the proteins and hydrogen bonded interactions of the valeryl carboxyl group with asparagine residues. Biotin is situated in a flexible loop of the protein which provides an "oxyanion pocket" that contributes protons to bind biotin and isolate biotin from surrounding water molecules. As a result, the protein forms three hydrogen bonds with the oxygen of the ureido moiety.<sup>80</sup> The strong affinity of avidin and streptavidin for biotin allows the protein to be used to isolate biotin-containing enzymes and purify biotinyl proteins and oligo-nucleotides.

Biotin has biological activity only when covalently attached to an enzyme. Biotin is post-translationally connected to a specific lysine residue of the enzyme by biotin protein ligase (BPL) (Figure 3). The BPL binds not only ATP and biotin by multiple hydrogen bonds but also the resultant biotinyl-5'-AMP to form BPL-biotinyl-5'-AMP complex.<sup>19</sup> The binding site for biotin is presumably the oxyanion hole formed by the surrounding amino acid residues, although details are not known.

In the functional cycle of enzymatic reactions, the biotin carboxyl carrier protein (BCCP), a subunit of acetyl-CoA carboxylase, engages heterologous protein-protein interactions not only with BPL, but also with the biotin carboxylase subunit, which leads to the carboxylation of biotin by the electrophilic substitution of the proton Ha on N-1' by a carboxyl group. Finally, the carboxybiotinylated BCCP interacts with transcarboxylase in the conversion of acetyl-CoA to malonyl-CoA with the completion of the first committed step of fatty acid synthesis. The general mechanism is shown in Eq 3 and Eq 4 (Chapter 1).<sup>17, 21-24</sup>

Although the three-dimensional structure of the biotinylated form of the biotin domain of *E. coli* BCCP has been determined by both NMR and X-ray crystallography, giving essentially identical structures, it is not clear whether the biotin is involved in the interactions of BCCP with BPL, or with carboxylase or carboxyl transferase subunits of acetyl-CoA carboxylase.<sup>21, 25</sup> The molecular

recognition study of BCCP with acetyl carrier protein does not show the direct involvement of biotin or biocytin (biotinyl lysine).<sup>16</sup> There is some suggestion that the B-domain of the biotin carboxylase subunit of acetyl-CoA carboxylase is involved in the interaction with BCCP and acts as a “lid” that closes down on the active site when biotin,  $Mg^{2+}$ -ATP, and  $HCO_3^-$  are positioned for catalysis.<sup>24</sup> The experimental evidence that confirms this interaction is not available, although the biotin dependent-enzymes are very likely to possess an oxyanion hole, because BPL, BCCP and acetyl-CoA carboxylase are related and have similar structures.<sup>13, 82, 158</sup>

## 7.2 Results and Discussion

### 7.2.1 Synthesis

In order to approach the biological process of biotin dependent enzymes and chemically understand the reaction mechanisms and molecular interactions, a series of biotin derivatives and appropriate receptors were prepared. The receptors possessing an “oxyanion hole” were based on picolinyl derivatives (**73** and **75-78**) and prepared according to Scheme 12 (Chapter 6) by the reactions of picolinyl diacid chloride with the appropriate corresponding hydrazides or diamino acid amide esters in pyridine (Figure 91).

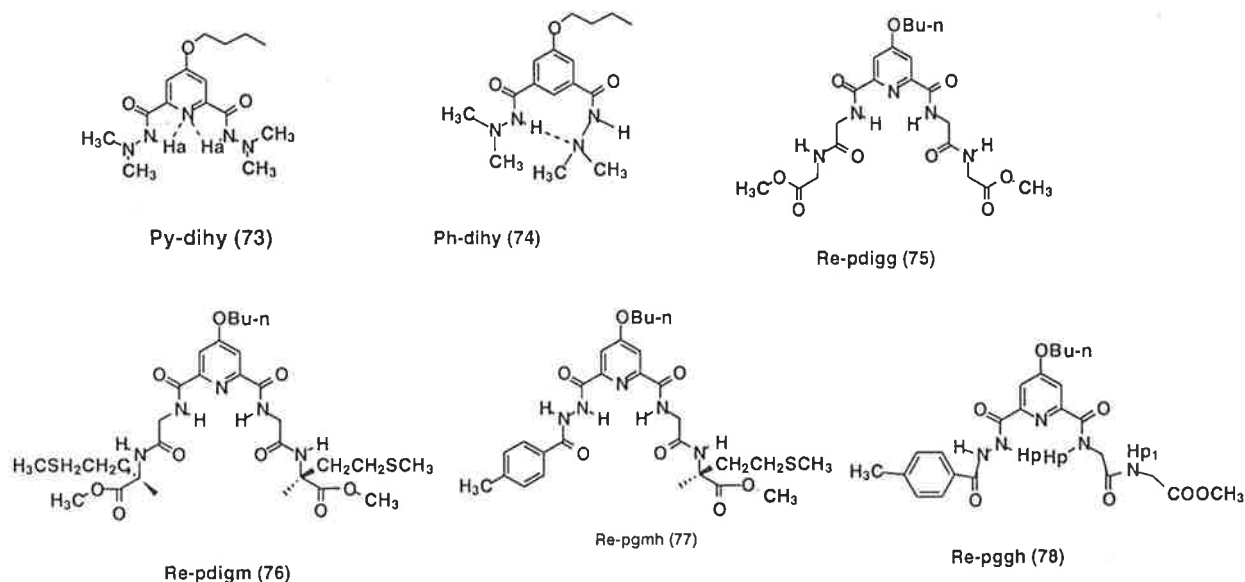
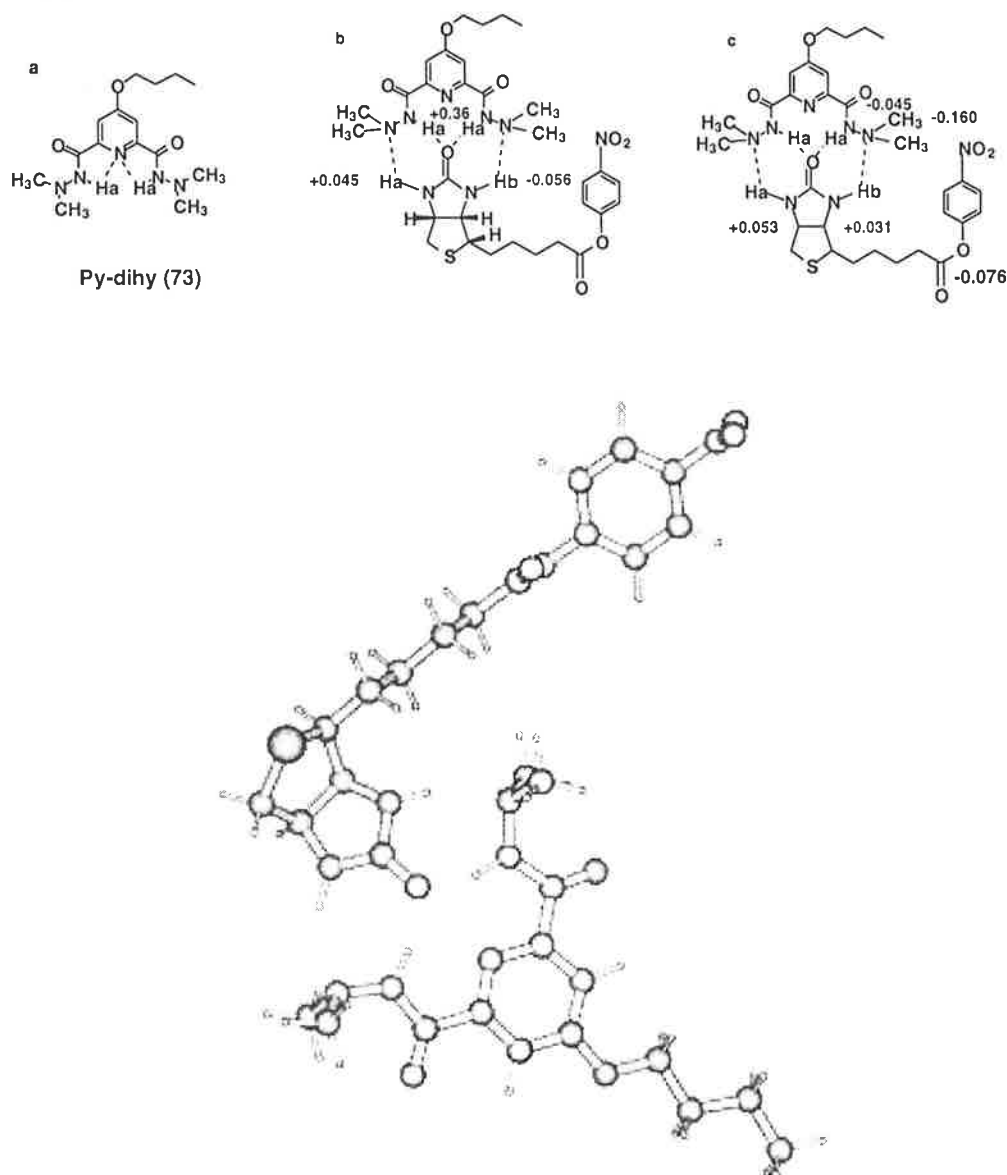


Figure 91. Receptors based on “oxyanion hole” motif.

### 7.2.2 Molecular recognition of biotin ester

Receptor py-dihy (**73**) possesses two intra-molecular hydrogen bonds, resulting in a planar conformation. When the receptor **73** is bound to the biotin ureido moiety, two amide protons of the receptor will interact with the carbonyl oxygen atom in the biotin ureido moiety, and two hydrazine nitrogen atoms with electron lone pairs will form intermolecular hydrogen bonding with Ha and Hb in the biotin ureido moiety. The biotin ester **12** was used as a soluble model in

the molecular recognition studies. The possible complex of the receptor **73** and biotin ester **12** is shown in Figure 92.



**Figure 92.** Intra-molecular hydrogen bonds within receptor Re-dihy (**73**) (a), and changes of proton (b) and carbon (c) NMR resonances in the complex with biotin ester **12**; [**73**] = 20 mM, [**12**] = 20 mM at rt and in  $\text{CDCl}_3$  (ppm).

Figure 92b shows the changes of  $^1\text{H}$  NMR shifts of the amide protons in receptor Py-dihy (**73**) and biotin ester **12** in  $\text{CDCl}_3$  at 20 mM with molar ratio 1:1. The large down field shift of receptor amide proton NH was indicative of an interaction between the protons with the carbonyl oxygen in the biotin ester **12** (Figure 92b). Furthermore, the chemical shifts of Ha in biotin moiety moved downfield, suggesting the efficient interaction of Ha with the nitrogen lone pair of receptor Py-dihy (**73**) (Figure 92b). However, the proton NMR resonance of Hb moved up-field,




suggesting that the intra-molecular hydrogen bonding of Hb with the carbonyl ester of the side chain was stronger than the intermolecular hydrogen bonding of Hb with the nitrogen of Py-dihy (**73**) (Figure 92b).

Changes in the  $^{13}\text{C}$  NMR resonances of the complex between **73** and **12** are also shown in Figure 92c. The carbon chemical shift of the N-methyl carbon of the receptor moved up-field, consistent with hydrogen bonding involving the corresponding nitrogen.<sup>225</sup> The association of aliphatic amines with hydrogen halide resulted in the up-field movement of  $^{13}\text{C}$  NMR resonances of carbons which were adjacent to the nitrogen atom.<sup>226</sup>

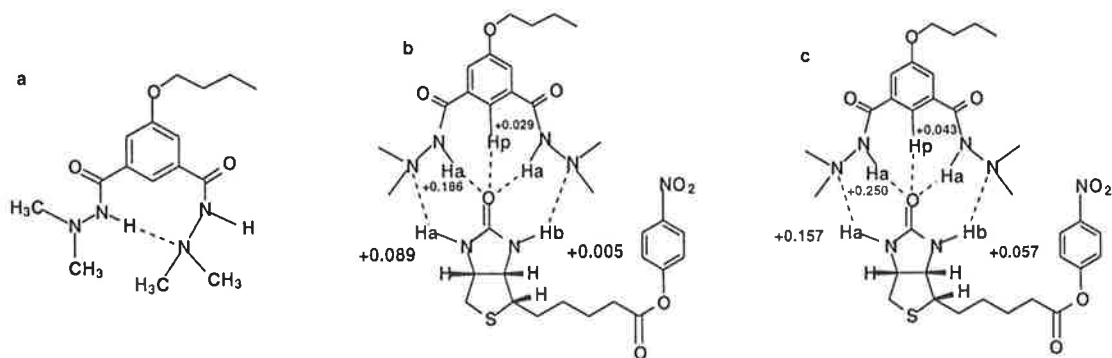
Figure 92c also shows the up-field movement of the  $^{13}\text{C}$  NMR resonance of C-10 in the carbonyl group of the side chain in biotin ester **12**. It reflects the breaking of the intra-molecular hydrogen bonding, which will cause a downfield shift of the  $^{13}\text{C}$  NMR resonance of the carbon in the carbonyl group.

**Table 30.**  $^{13}\text{C}$  NMR Resonance of Carbon adjacent to the Nitrogen in Organic Solvent.<sup>226</sup>

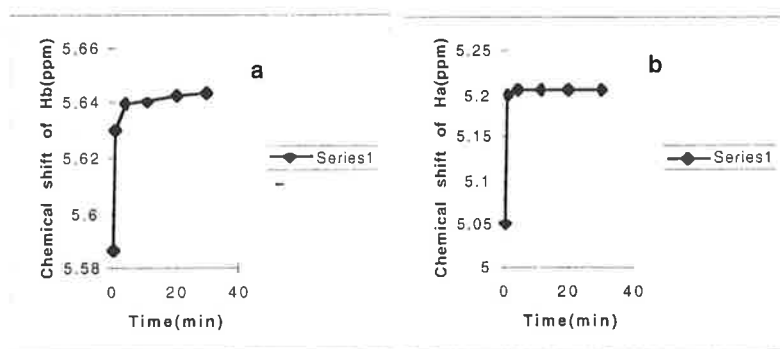
amine	carbon chemical shifts (ppm)	
	amine	amine-HCl
$\text{CH}_3\text{CH}_2\text{CH}_2\text{NH}_2$	44.07	40.20
$(\text{CH}_3\text{CH}_2)_2\text{NH}$	44.05	42.49
$(\text{CH}_3\text{CH}_2)_3\text{N}$	46.99	46.05
 $\text{CH}_2\text{NHCH}_2\text{CH}_2\text{CH}_3$	55.21	50.87
	51.91	47.68

The receptor Ph-dihy (**74**) also formed a complex with biotin ester **12**. Receptor **74** is likely to exhibit an intra-molecular hydrogen bond as shown in Figure 93a. The selected complexation-induced changes in  $^1\text{H}$  NMR chemical shifts for the complex of biotin ester **12** and receptor Ph-dihy **74** in  $\text{CDCl}_3$  at 10 mM and 20 mM are shown in Figure 93b and Figure 93c. The change in Hb at 10 mM is insignificant, suggesting that the inter- and intra-molecular hydrogen bonds are similar in strength (Figure 93). Furthermore, the change of chemical shift for Hb was significant at relative higher concentration (20 mM), also indicating that Hb formed intermolecular hydrogen bonds with the hydrazine nitrogen (Figure 93c).

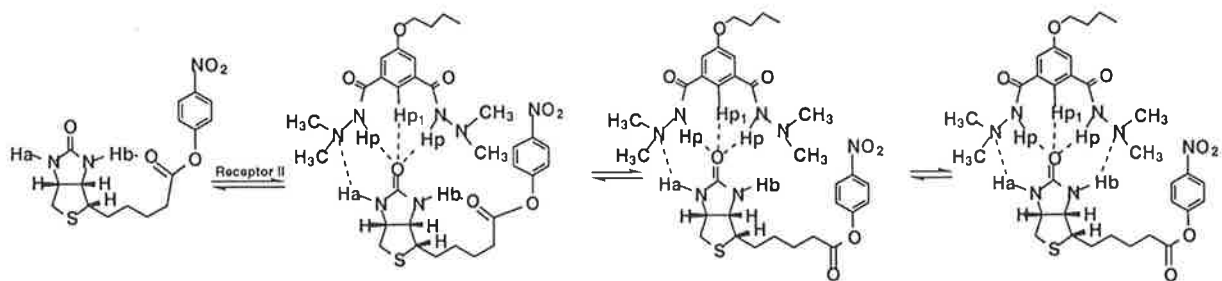
As shown in Figure 94 (b), the change of NMR chemical shift for Ha was completed rapidly within 1 minute. However, the change of NMR chemical shift for Hb was much slower (Figure 94a). The changes of  $^1\text{H}$  NMR chemical shift of the protons in the receptor were complete within 1 minute. Therefore Ha is bound initially to receptor Ph-dihy (**74**) then Hb. This process is summarised in Scheme 15.



**Figure 93.** Receptor Ph-dihy (**74**) (a) with the intra-molecular hydrogen bonding between amide proton and hydrazine nitrogen, and selected changes of proton NMR resonance in the complex with **12** in  $\text{CDCl}_3$  at room temperature and 10 mM (b) and 20 mM (c).



**Figure 94.** Ureido proton NMR resonances of biotin ester **12** in the complex with Ph-dihy (**74**) in  $\text{CDCl}_3$  at room temperature (20 mM) as a function of time Hb (a) and Ha (b).

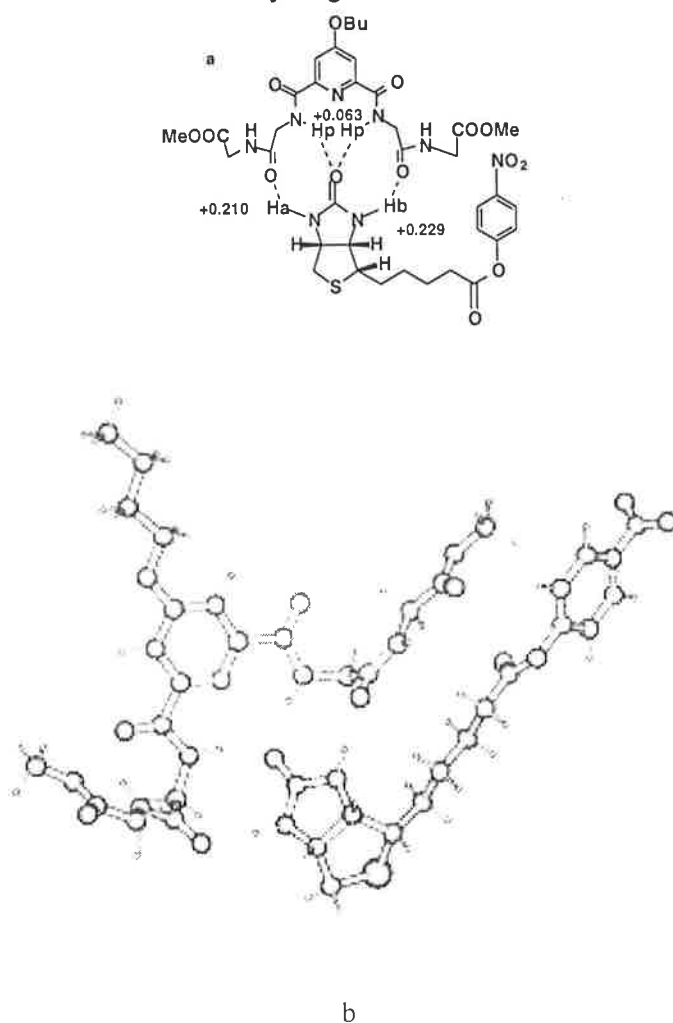


**Scheme 15.** The molecular recognition process of biotin ester **12** with receptor Ph-dihy (**74**).

Biotin ester **12** can be bound by receptors Py-dihy (**73**) and Ph-dihy (**74**) by sequential formation of the intermolecular hydrogen bonds of Ha and Hb with the hydrazine nitrogens. This concept may also be applicable for the molecular recognition of biotin-containing enzymes by natural or artificial receptors. With the different stability of hydrogen bonds to Ha and Hb with receptors, intra-molecular hydrogen bonding of Hb with the carbonyl group in the side chain of biotin would control the complexation patterns and enzymatic reactions. The stronger the intra-

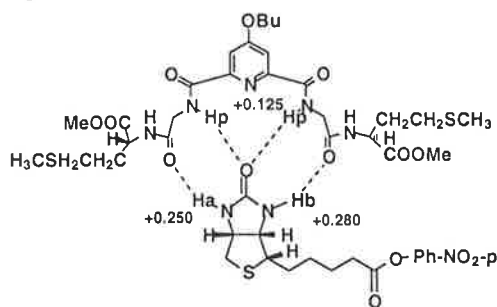
molecular hydrogen bonding, the weaker the intermolecular hydrogen bonds in complexes. Enzymes will associate with a substrate to form a complex by weak interactions such as hydrogen bonding. The formation of the initial complex  $(E \cdot R)_1$  between biotin and a receptor is followed by the production of a second intermediate  $(E \cdot R)_2$ . Reactions within  $(E \cdot R)_2$ , including formation and dissociation of covalent or non-covalent bonds then lead to the ternary complex of enzyme and product(s)  $(E \cdot P)_3$ . Release of the product(s) regenerates free enzyme and the sequence continues.<sup>227</sup> Therefore the formation of intra-molecular hydrogen bonds in biotin-containing enzymes will not only control secondary and tertiary structures but also play an important role in the enzymatic reactions.

The binding of biotin ester **12** to tetra-amide receptor Re-pdigg (**75**) involves four intermolecular hydrogen bonds, including two between the ureido oxygen of biotin and two amide protons of the receptor and two between the ureido protons and the amide carbonyl groups in the receptor (**75**). Figure 95 shows the changes of chemical shifts of the NH protons in both receptor (**75**) and biotin ester **12** and confirms the four hydrogen bonds involved.



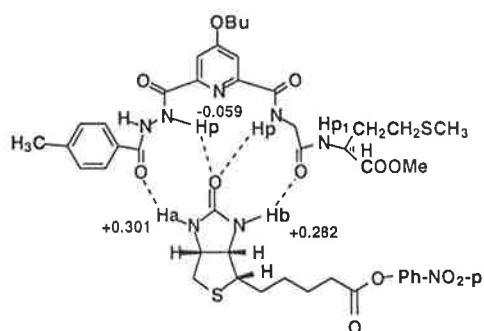
**Figure 95.** The complex of receptor Re-pdigg (**75**) with biotin ester **12** (a) and molecular modelling structure of the complex (b),  $[75] = 1.0 \text{ mM}$ ,  $[12] = 1.0 \text{ mM}$  at rt and in  $\text{CDCl}_3$  (ppm).

Biotin ester **12** could also be bound by receptor Re-dipgm(D) (**76**) through four intermolecular hydrogen bonds. The changes in the chemical shifts of the NH protons observed for receptor Re-dipgm (**76**) are shown in Figure 96.



**Figure 96.** The complex of receptor Re-dipgm (**76**) with biotin ester **12**, [**76**] = 1.0 mM, [**12**] = 1.0 mM at rt and in  $\text{CDCl}_3$  (ppm).

Complex formation of biotin ester **12** with the receptor Re-pgmh (**77**) is shown in Figure 97 and the chemical shift changes for the biotin NH protons indicate strong intermolecular hydrogen bonds.

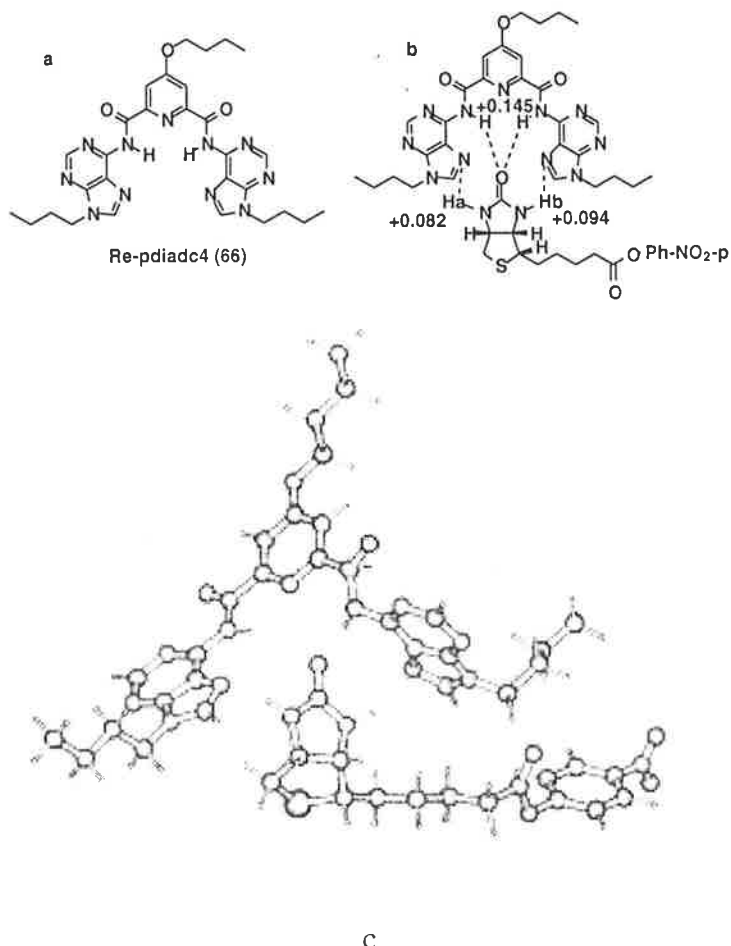


**Figure 97.** The complex of receptor Re-pgmh (**77**) with biotin ester **12**, [**77**] = 1.0 mM, [**12**] = 1.0 mM at rt and in  $\text{CDCl}_3$  (ppm).

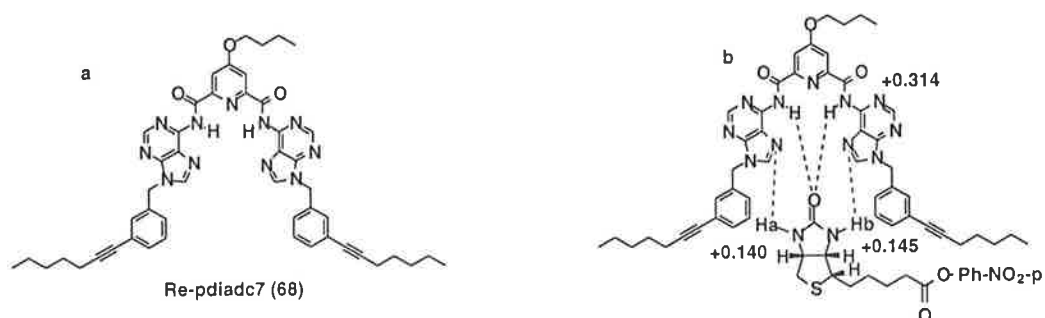
### 7. 2. 3 Molecular recognition of biotin ester with base pair triplet analogues

In order to investigate the binding of biotin with DNA, the base pair triplet analogues Re-pnadc7 (**65**), Re-pdiadc4 (**66**) and Re-diadc7 (**68**) were used in the complexation with biotin ester **12**. As shown in Figure 98, the chemical shift changes of biotin ester **12** ureido protons were + 0.084 ppm and + 0.092 ppm respectively for Ha and Hb, when it was bound to Re-pdiadc4 (**66**). The NMR signal for protons in Re-pdiadc4 (**66**) moved downfield by as much as + 0.145 ppm. The binding of Re-pdiadc7 (**68**) with biotin ester **12** was more effective than Re-piadc4 (**66**), when the butyl groups were replaced by 3'-alkynyl benzyl groups. As shown in Figure 99, the chemical shifts for the ureido protons Ha and Hb moved downfield by as much as 0.140 ppm and 0.145 ppm respectively. At the same time, the chemical shift of the amide protons in receptor Re-piadc7 (**68**) shifted downfield by 0.314 ppm. However, the binding between

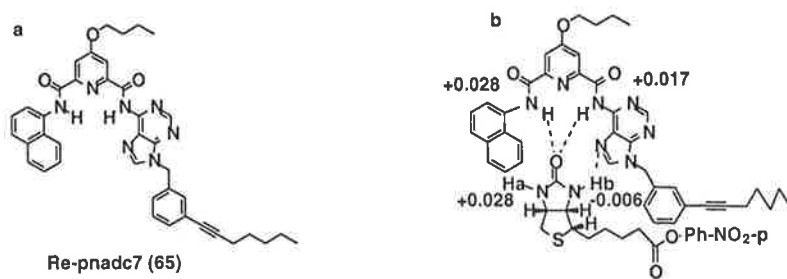
receptor Re-pnadc7 (**65**) and biotin ester **12** was insignificant (Figure 100). Therefore, the two adenine units of the base pair triplet analogues **66** and **68** and a planar structure were necessary to bind biotin ester **12** efficiently.



**Figure 98.** Receptor Re-pdiadc4 (**66**) (a) and the complex (b) of biotin ester **12** with it and molecular modelling structure of the complex (c), [**66**] = 1.0 mM, [**12**] = 1.0 mM at rt and in CDCl<sub>3</sub> (ppm).



**Figure 99.** Receptor Re-pdiadc7 (**68**) (a) and the complex (b) with biotin ester **12**, [**68**] = 1.0 mM, [**12**] = 1.0 mM at rt and in CDCl<sub>3</sub> (ppm).



**Figure 100.** Receptor Re-pnadc7 (65) (a) and the complex (b) with biotin ester 12, [65] = 1.0 mM, [12] = 1.0 mM at rt and in CDCl<sub>3</sub> (ppm).

---

## Chapter 8

---

# Molecular Assembly of Receptors and Complexes with Biotin Esters through Regular Hydrogen Bonding and $\pi$ - $\pi$ Stacking

## 8.1 Introduction

It is well known that single nucleic acids adopt helical structures. Double and triple helices of DNA<sup>200, 212, 215</sup> are formed by Hoogsteen-type and Watson-Crick type hydrogen bonds<sup>228</sup> and  $\pi$ - $\pi$  stacking<sup>203, 209</sup> between complementary deoxyribonucleic acid strands. Both single strands and dimers of oligomeric  $\beta$ - amino acids and  $\beta$ - peptides can adopt stable helical conformations with multiple and regular amide-amide hydrogen bonding<sup>33, 229, 230</sup> as shown in Figure 101. Furthermore, proteins are able to interact with DNA to form peptide-DNA complexes<sup>191, 231-233</sup> by hydrogen bonding and extensive van der Waals contacts between the peptide and the floor and walls of the minor groove of DNA.

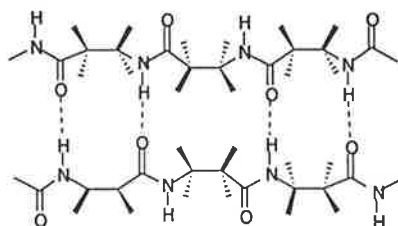


Figure 101. Regular hydrogen bonding in  $\beta$ -peptides.

Recently, the self-assembly of molecules into helices has attracted great interest as a fundamental property of biologically important compounds. The non-covalent forces responsible for these are believed to be hydrogen bonding,  $\pi$ - $\pi$  stacking, steric interactions and van der Waals interactions.<sup>107, 234-239</sup>

Molecular assembly is common in the solid state through regular hydrogen bonding and  $\pi$ - $\pi$  stacking.<sup>240-243</sup> In addition, some compounds with peptide bonds, such as glycopeptide antibiotics<sup>37, 196, 244</sup> and capsule molecules,<sup>245, 246</sup> tend to dimerize by stable amide-amide hydrogen bonds in solution.

In Chapter 6, the efficient intra-molecular hydrogen bonding and intermolecular  $\pi$ - $\pi$  stacking (Figure 81 and Figure 87) in pyridine base receptors was observed. In this Chapter the intermolecular and intra-molecular interactions of receptors based on the DNA triplet motif are examined.

## 8.2 Results and Discussion

### 8.2.1 Synthesis

In order to examine the molecular assembly properties of diacylhydrazides and their complexes in solution, compounds **79** and **80** (Figure 102) were prepared by the amidation of the corresponding aryl carbonyl chlorides with isobutyryl hydrazide (Scheme 12 in Chapter 6).

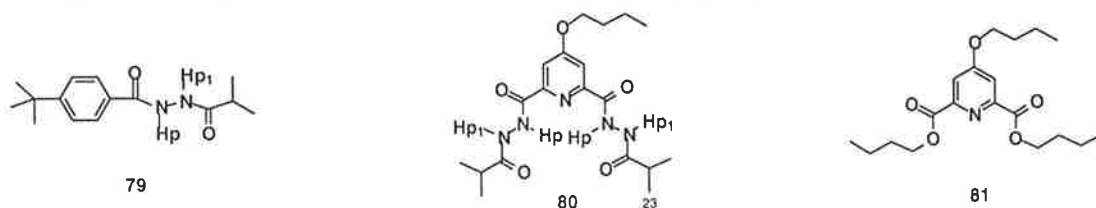


Figure 102. Hydrazides and related compound.

### 8.2.2 Intermolecular hydrogen bonding in compound 79

#### 8.2.2.1 Concentration dependence

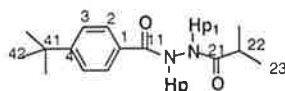
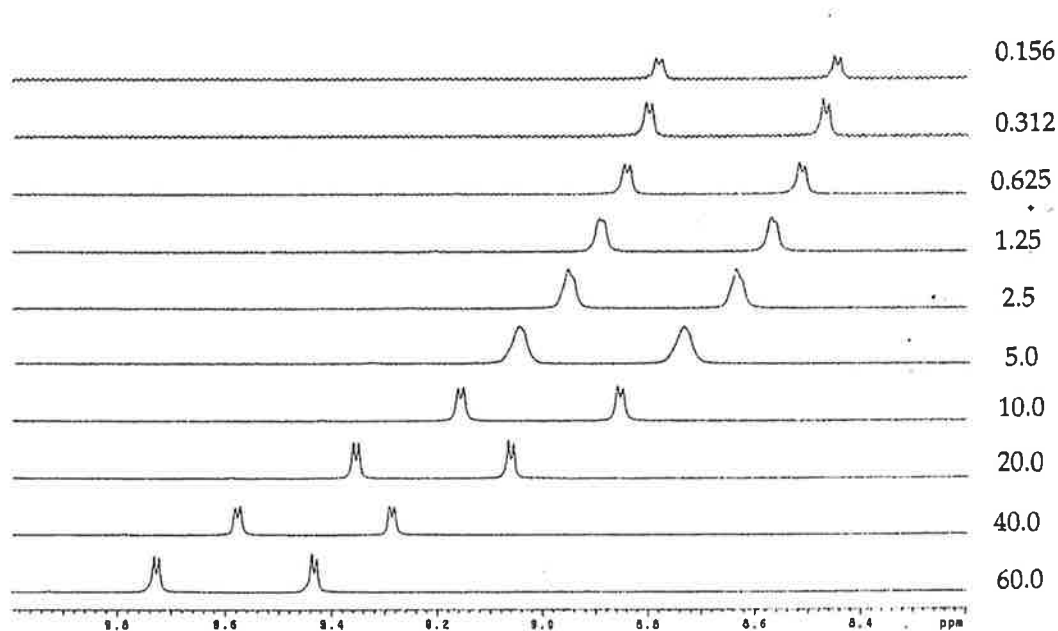


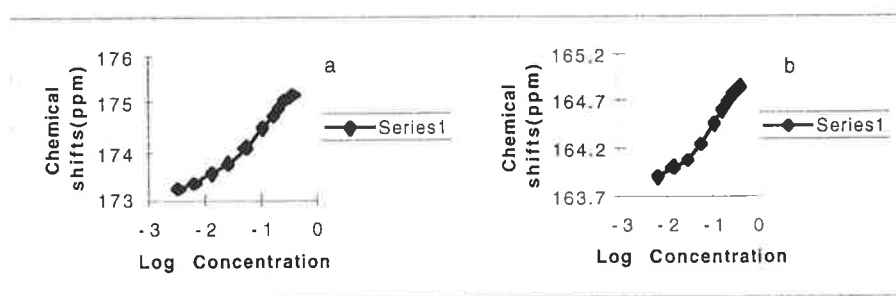
Figure 103 shows the concentration dependence of proton NMR chemical shifts of the hydrazyl protons of compound **79** with variation in concentration from 73 mM to 0.156 mM. The dilution experiments show that the proton NMR resonances for Hp and H1 in **79** are downfield at relatively high concentration (> 5 mM). When the concentration was decreased, the proton NMR chemical shifts of Hp and Hp1 moved up-field. At very low concentration, there was little or no intermolecular hydrogen bonding, and the proton NMR chemical shifts did not change significantly.<sup>30, 161, 247-249</sup> The concentration dependence of the proton NMR resonances for Ha and Hb reflects the significant intermolecular hydrogen bonding of compound **79** at high concentration.

The dependence of the carbon NMR resonances of the carbonyl groups in compound **79** with respect to concentration are shown in Figure 104. The higher the concentration of compound **79**, the greater the carbon NMR chemical shifts for both carbonyl C11 and C21. Intermolecular hydrogen bonding tends to decrease the electron density on carbon C11 and C21 by partial protonation of oxygen O11 and O21. Therefore, the concentration dependence of carbon NMR chemical shifts suggest that carbonyl groups C11=O11 and C21=O21 are involved in intermolecular hydrogen bonding.<sup>250</sup>



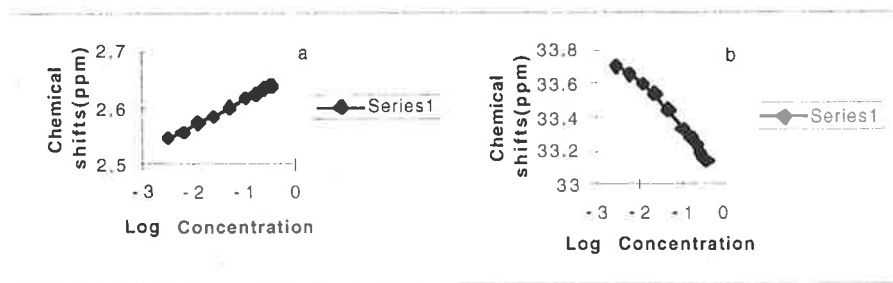
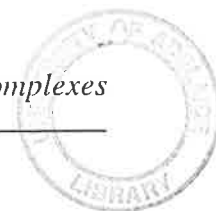


**Figure 103.** Hydrazyl proton NMR chemical shifts of compound **79** (left, Hp1; right, Hp) from 70 mM to 0.156 mM.



**Figure 104.** Amide carbon NMR chemical shifts of C21 (a) and C11 (b) of compound **79** in  $\text{CDCl}_3$ , as a function of the logarithm of concentration (3 mM to 335 mM).

Furthermore, Figure 105 shows the dependencies of proton and carbon NMR chemical shifts for H22 and C22 with concentration from 3 mM to 335 mM in  $\text{CDCl}_3$ . An increase in the concentration of **79**, caused an increase in the proton NMR resonance for H22 (Figure 105a), which suggested the involvement of an intermolecular hydrogen bond  $\text{C22-H22}\cdots\text{O}$ . The corresponding carbon NMR chemical shift of C22 (Figure 105b) moved up-field as the concentration was increased.



**Figure 105.** Proton and carbon NMR chemical shifts of C22 (b) and H22 (a) in C22-H22 of compound **79**, as a function of the logarithm of concentration.

Recently, C-H $\cdots$ O hydrogen bonding has been well documented,<sup>251</sup> and recognized as an important component in molecular recognition. Derewenda and co-workers reported that the C-H $\cdots$ O hydrogen bonding of the  $\alpha$ -hydrogen in peptide residues and the oxygen on an adjacent strand of  $\beta$ -sheets were common.<sup>252, 253</sup>

**Table 31.** Selected Changes of Chemical Shifts of Protons of Compound **79** from 6 mM to 335 mM (ppm).

Hp	Hp1	H22	H3	H42
1.174	1.203	0.081	-0.125	-0.045

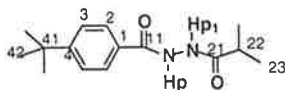
**Table 32.** Changes of Carbon Chemical Shifts of Compound **79** from 6 mM to 335 mM (ppm).

C11	C21	C22	C3	C4	C41	C42
0.971	1.828	-0.516	-0.410	-0.554	-0.183	-0.076

The changes of NMR chemical shifts for selected protons and carbons in compound **79** are shown in Tables 31 and 32. It can be seen that the intermolecular hydrogen bonding between molecules of **79** resulted in a downfield movement of the resonances for proton Hp (1.174 ppm), Hp1 (1.203 ppm), H22 (0.081 ppm) and carbon C11 (0.971 ppm) and C21 (1.828 ppm). The up-field movement of carbon C22 (-0.516 ppm) was possibly due to the increase of electron density of C22 by intermolecular hydrogen bonding C22-H22 $\cdots$ O. The results suggest that each of the protons Hp, Hp1 and H22 is involved in intermolecular hydrogen bonding at higher concentration.

### 8. 2. 2. 2 Temperature dependence

The temperature dependencies of the amide proton NMR chemical shifts of protons Hp and Hp1 in **79** at 1.79 mM, 27.9 mM and 47.9 mM are shown in Table 33. Also shown in Table 34 are the carbon  $\Delta\delta C/\Delta T$  values from carbon C11, C21 and C22 in compound **79** at 47.9 mM and 200 mM in CDCl<sub>3</sub>.



**Table 33.** Selected Proton NMR Chemical Shift Temperature Dependencies  $\Delta\delta\text{H}/\Delta\text{T}$  (ppb/K) for **79** in  $\text{CDCl}_3$  at Different Concentrations (mM).

concentration	1.79 <sup>a</sup>	27.9 <sup>a</sup>	47.9 <sup>b</sup>	200 <sup>b</sup>
Hp	7.5	9.83	3.70	5.58
Hp1	9.95	13.88	4.05	6.78

<sup>a</sup>333 K-222 K. <sup>b</sup>333 K-293 K.

**Table 34.** Selected Carbon NMR Chemical Shift Temperature Dependencies  $\Delta\delta\text{C}/\Delta\text{T}$  (ppb/K) for **79** in  $\text{CDCl}_3$  from 333 K-293 K.

concentration (mM)	C11	C21	C22
47.9	1.05	3.60	
200	0.95	5.33	-2.08

According to Table 33, both the resonances Hp and Hp1 are downfield at low temperatures as indicated by high  $\Delta\delta\text{H}/\Delta\text{T}$  values which indicate a cooling-induced strengthening of the intermolecular hydrogen bonding. Table 34 shows the increase in carbon NMR chemical shifts for carbons in C11=O11 and C21=O21 with a decrease in temperature, which suggests that the oxygens O11 and O21 are likely to be involved in intermolecular hydrogen bonding at low temperatures.<sup>250</sup> Furthermore, the proton shift values for Hp1 in Table 33 indicate that Hp1 forms a stronger intermolecular hydrogen bond than Hp. The carbon  $\Delta\delta\text{C}/\Delta\text{T}$  value in Table 34 indicates that O21 in C21=O21 is involved in a stronger intermolecular hydrogen bond than O11 in C11=O11.<sup>306, 307</sup>

The data in Table 33 also show that at high concentration, heating the solution tended to disrupt the intermolecular hydrogen bonding (200 mM). When the concentration was low e. g. (1.79 mM), cooling the solution promoted the formation of hydrogen bonds.

### 8. 2. 2. 3 Intramolecular hydrogen bonding of compound 79

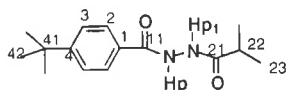
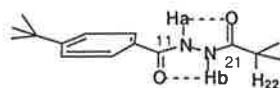


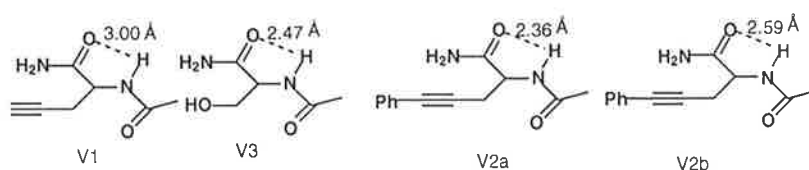
Figure 103 also shows the change of peak patterns for both Hp and Hp1 in the proton NMR spectrum with the decrease in the concentrations of **79** from 60 mM to 0.156 mM in  $\text{CDCl}_3$  at room temperature. The peaks appeared as a doublet at 60 mM but were broadened when the concentration was decreased. At a concentration of 5 mM, both of the peaks appeared as

singlets. However, when the concentration was further reduced, the singlet peaks diverge to form doublets at 0.625 mM. The broadening of peaks at 5 mM is presumably due to an equilibrium between intermolecular hydrogen bonding and intra-molecular hydrogen bonding<sup>254</sup> in a C<sub>5</sub>-conformation as shown in Figure 106.<sup>30, 255</sup>

When the concentration is very low (< 2 mM), intra-molecular hydrogen bonding will be dominant.<sup>30</sup> The C<sub>5</sub>-conformation of intra-molecular hydrogen bonds, although weak, is very important in polypeptides and proteins.<sup>96, 255, 256</sup> This interaction can also be observed from single crystal structures for some synthetic amino acid amides, with the C<sub>5</sub>-type intra-molecular hydrogen bonding lengths around 2.36-3.00 Å (Figure 107).<sup>257-259</sup> The distances are consistent with the formation of intra-molecular hydrogen bonds between the amide N-H with amide C=O.<sup>252</sup>



**Figure 106.** The intra-molecular hydrogen bonds (C<sub>5</sub>-conformation) of compound **79**.



**Figure 107.** The solid state structures of compounds **V1**, **V2** and **V3**. The C<sub>5</sub>-conformation intra-molecular N-H...O=C hydrogen bonding is indicated by the dotted line.

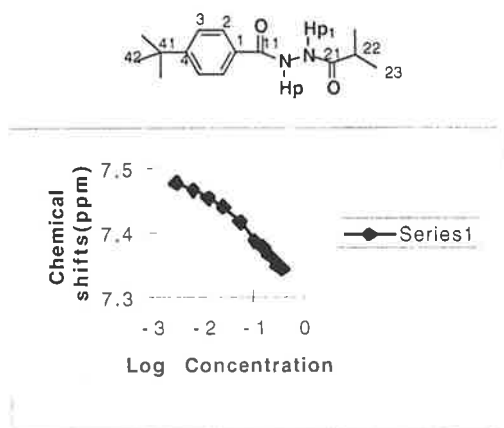
The  $-\Delta\delta\text{H}/\Delta\text{T}$  values for H<sub>p</sub> and H<sub>p1</sub> of **79** at 1.79 mM are listed in Table 33. Both of the values (7.50 for H<sub>a</sub>, 9.95 for H<sub>b</sub>) are much larger than 3 ppb/K,<sup>30, 247</sup> which indicate the effective intra-molecular hydrogen bonds C11=O11...H<sub>b</sub> and C21=O21...H<sub>a</sub> as shown in Figure 106.<sup>96</sup>

### 8. 2. 3 Intermolecular $\pi$ - $\pi$ stacking in compound **79**

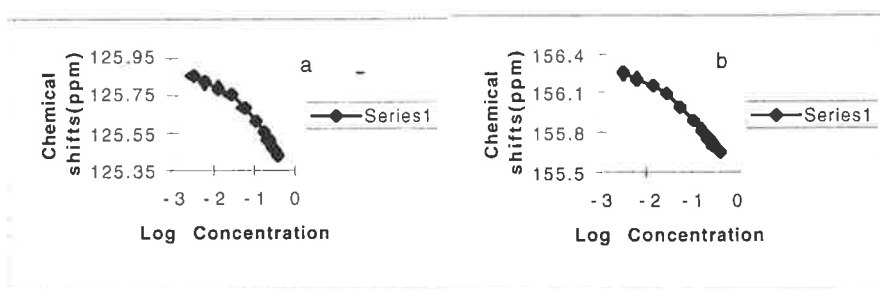
#### 8. 2. 3. 1 Concentration dependence

The decrease in the proton NMR resonance for H<sub>3</sub> with an increase in concentration from 6 mM to 335 mM in CDCl<sub>3</sub> at room temperature is shown in Figure 108. The maximum change was -0.125 ppm (Table 31) and a corresponding decrease (-0.40 ppm) in the chemical shift of carbon C<sub>3</sub> with an increase in concentration from 6 mM to 335 mM in CDCl<sub>3</sub> at room temperature was also observed (Figure 109a). Similarly, the resonance for C<sub>4</sub> also moved up-field (-0.554 ppm) with an increase in concentration. In conclusion, the phenyl group in **79** undergoes aromatic  $\pi$ - $\pi$  stacking as the concentration increased. The  $\pi$ - $\pi$  stacking also caused an up-field shift of

proton H42 (ca. 0.045 ppm), carbon C41 (- 0.183 ppm) and C42 (- 0.076 ppm) in the *t*-butyl group.



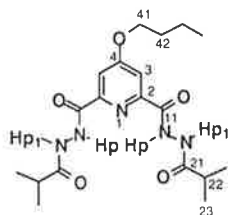
**Figure 108.** Aromatic hydrogen C3-H3 NMR chemical shifts of compound **79**, as a function of the logarithm of concentration.



**Figure 109.** Aromatic carbon C3 (a) and C4 (b) chemical shifts of compound **79**, as a function of the logarithm of concentration.

## 8. 2. 4 Intermolecular hydrogen bonding of compound 80

### 8. 2. 4. 1 Concentration dependence



When the concentration of compound **80** was increased from 0.009 mM to 27.9 mM at room temperature, the resonance for proton Ha moved downfield by 0.183 ppm, proton Hb moved downfield by 0.641 ppm and proton H3 moved upfield by 0.218 ppm. When the concentration of **80** was increased from 1.5 mM to 43 mM, the carbon NMR resonance for C11 moved up-field by 0.781 ppm, carbon C21 moved downfield by 1.764 ppm but carbon C22 moved up-field by 0.516 ppm. The results suggest that **80** forms strong intermolecular hydrogen bonding at higher concentration.<sup>250</sup>

### 8. 2. 4. 2 Temperature dependence

Table 35 shows the temperature dependencies of the proton NMR chemical shifts for Hp and Hp1 and H3 at the three different concentrations (1.79 mM, 13 mM and 27.9 mM) in CDCl<sub>3</sub>. The  $\Delta\delta C/\Delta T$  data for selected carbons at different concentrations (1.79 mM, 13.9 mM, 20.0 mM and 27.9 mM) are listed in Table 36.

As shown in Table 35, there was little change in the proton NMR chemical shifts of Hp with an increase in temperature at 13.0 mM and 27.9 mM. However, the resonance for proton Hp1 moved up-field significantly with temperature at 13.0 mM and 27.9 mM. The  $\Delta\delta C/\Delta T$  values for C21 were as high as 10.23 (13.0 mM) and 13.4 (27.9 mM) (Table 36), however those for C11 were - 13.65 and - 12.20 ppb/K.

**Table 35.** Selected Proton NMR Chemical Shift Temperature Dependencies (ppb/K) for Compound **80** in CDCl<sub>3</sub> at Different Concentrations (mM).

concentration	Ha	Hb	H3
1.79	3.42 <sup>a</sup>	6.67 <sup>b</sup>	-5.85 <sup>b</sup>
13.0	1.23	9.74 <sup>d</sup>	-5.71
20.0 <sup>e</sup>	0.65	7.21	-5.55
27.9	0.83	9.21 <sup>d</sup>	-5.30

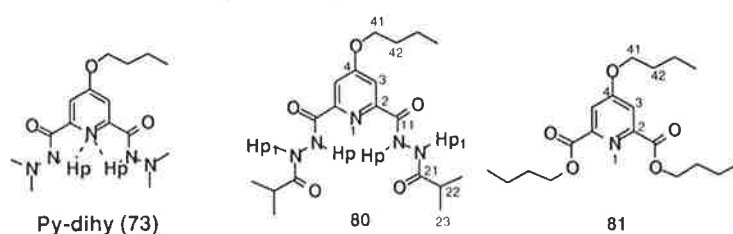
<sup>a</sup>333 K-233 K; <sup>b</sup>333 K-243 K; <sup>c</sup>333 K-223 K; <sup>d</sup>333 K-253 K; <sup>e</sup>333 K-273 K.

**Table 36.** Selected Carbon NMR Chemical Shift Temperature Dependencies (ppb/K) for Compound **80** in CDCl<sub>3</sub> at Different Concentrations (mM).

concentration	C11	C21	C3	C22
13.0 <sup>a</sup>	-13.65	10.23		
20.0 <sup>b</sup>	-12.20	13.40	-10.87	-6.50

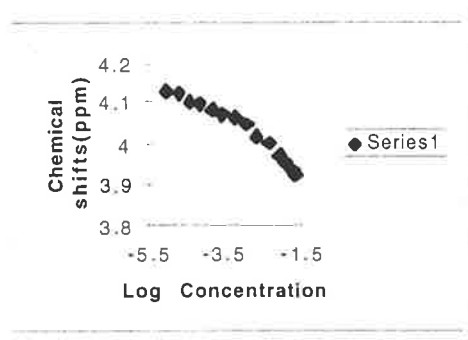
<sup>a</sup>333 K-293 K; <sup>b</sup>333 K-273 K.

### 8. 2. 5 Intermolecular $\pi$ - $\pi$ stacking of compound **80**



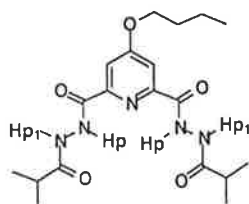
As shown in Figure 110, the proton NMR resonance of H3 decreased with an increase in the concentration of compound **80**. The maximum change in the H3 NMR resonance was - 0.723

ppm. However, there was little change in the H3 NMR chemical shift of compound **73** (- 0.004 ppm) and **81** (no change) with an increase in concentration. Therefore there was significant intermolecular  $\pi$ - $\pi$  stacking of molecules of compound **80**.<sup>260-262</sup>



**Figure 110.** Proton NMR chemical shifts of H3 of compound **80** at room temperature in  $\text{CDCl}_3$ , as a function of the logarithm of concentration.

### 8. 2. 6 Three-centre $\text{Hp}\cdots\text{N1}\cdots\text{Hp}$ and $\text{O}\cdots\text{Hp}\cdots\text{N}$ intra-molecular hydrogen bonding of compound **80**



The proton NMR chemical shifts of proton Ha in compounds **73**, **79** and **80** were determined at 1.79 mM in  $\text{CDCl}_3$  at room temperature as 8.29 ppm, 8.53 ppm and 10.26 ppm respectively. In these solutions, little or no intermolecular hydrogen bonding between molecules was expected and only intra-molecular hydrogen bonding should be important. Therefore, the proton NMR resonance of Hp in compound **80** (10.26 ppm) was much larger than that of compound **79** (8.53 ppm), which indicated that Hp of compound **80** was involved in an intra-molecular hydrogen bonding with N-1' in pyridine ring. When both Hp protons in compound **80** were hydrogen bonded, the three-centre intra-molecular hydrogen bonding arrangement  $\text{Hp}\cdots\text{N1}\cdots\text{Hp}$  resulted (Figure 111).

According to Table 35, the  $-\Delta\delta\text{H}/\Delta\text{T}$  values of Hp in compound **80** at 13.0 mM, 20.0 mM and 27.9 mM were 1.23, 0.65 and 0.83 ppb/K. It is reported that the  $-\Delta\delta\text{H}/\Delta\text{T}$  values for protons in amide bonds are directly related to the mobility of the hydrogen.<sup>263</sup> Therefore, these small values indicate that the three-centre intra-molecular hydrogen bonding is very stable (Figure 111). The formation of the three-centre  $\text{Hp}\cdots\text{N1}\cdots\text{Hp}$  induces the two carbonyl groups and pyridine ring to be in the same plane, which in turn promotes  $\pi$ - $\pi$  stacking.

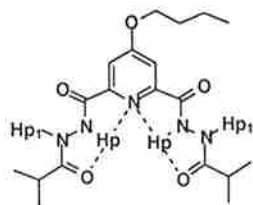


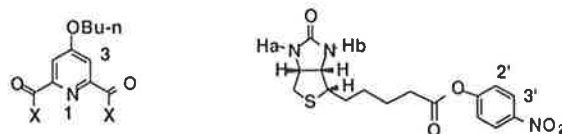
Figure 111. Three-centre intra-molecular hydrogen bonding of compound **80**.

It can be seen from Table 35, the  $-\Delta\delta H/\Delta T$  value for compound **80** at 1.79 mM concentration in  $CDCl_3$ , was 3.42, larger than those at higher concentrations (13.0 mM, 1.23 ppb/K; 20.0 mM, 0.65 ppb/K; 27.9 mM, 0.83 ppb/K). The larger value can be explained by the formation of the  $N\cdots Hp\cdots O$  three-centre hydrogen bonding as shown in Figure 111.<sup>41, 253</sup>

### 8. 2. 7 Intermolecular $\pi$ - $\pi$ stacking interactions in receptors Re-pdigg (**75**), Re-pdigm (**76**) and Re-pdigh (**78**) and their complexes with biotin ester **12**

Table 37 shows the  $\Delta\delta H/\Delta T$  values for proton H3 of receptors, Re-pdigg (**75**), Re-pdigm (**76**) and Re-pdigh (**78**), and their complexes with biotin ester **12**. The greatest changes for Re-pdigh, Re-pdigm and Re-pdigg were - 0.114, - 0.100 and - 0.055 ppm respectively when the temperature was reduced by 40 K. Table 37 also shows the positive  $\Delta\delta H/\Delta T$  values for proton H3' on the phenyl group of biotin ester **12**. These results suggest that the pyridinyl group with H3 forms a significant  $\pi$ - $\pi$  stacking interactions in the complexed and uncomplexed forms. Furthermore, the  $\Delta\delta H/\Delta T$  value for H3 in the receptor is very close to its value in the complex with biotin ester **12**, which suggests the stacking interactions in the receptor are very similar to those in the complex.

Table 37. Proton NMR Chemical Shift Temperature Dependencies  $\Delta\delta H/\Delta T$  (ppb/K) of H3 in the Receptors and Their Complexes with Biotin Ester **12** and H3' of **12** in  $CDCl_3$  at 1 mM from 333 K-293 K.



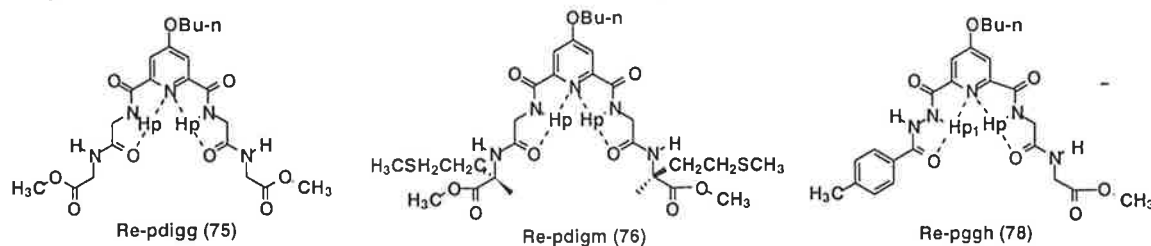
compound	H3 (substrate)	H3 (complex)	H3'
Re-pdigg ( <b>75</b> )	-1.32	-1.50	0.47
Re-pdigm ( <b>76</b> )	-2.50	-2.96	0.40
Re-pdigh ( <b>78</b> )	-2.85	-2.85	0.33



### 8.2.8 Intra-molecular hydrogen bonding in receptors Re-pdigg (75), Re-pdigm (76) and Re-pdigh (78)

The temperature dependencies for proton NMR resonances of amide protons Hp in the receptors Re-pdigg (75), Re-pdigm (76) and Re-pdigh (78) and their complexes with biotin ester **12** are shown in Table 38. All the values are small, which suggests the low mobility of the hydrogen Hp and the three-centre intra-molecular hydrogen bonding interactions  $N \cdots Hp \cdots O$ .<sup>263</sup> The intra-molecular hydrogen bonding is important in maintaining a planar conformation for the self-assembly of the receptors and their complexes. Furthermore, the  $\Delta\delta H/\Delta T$  value of Hp in the uncomplexed receptor is very close to its value in the complex, which also suggests the similar assembly of the complex with biotin ester **12**.

**Table 38.** Proton NMR Chemical Shift Temperature Dependencies  $\Delta\delta H/\Delta T$  (ppb/K) of Amide Proton Hp in the Receptors and Their Complexes with Biotin Ester **12** in  $CDCl_3$  at 1 mM from 333 K-293 K.



compound	Re-pdigg (75)	Re-pdigm (76)	Re-pdigh (78)
substrate	3.3	4.8	0.9
complex	3.6	5.2	0.7

### 8.2.9 Mass spectrometry

Mass spectrometry results for the intermolecular complexes are listed in Table 39. The positive-ion FAB mass spectra of compounds **79** and **80** show a dimer for **79** at 525 (3.3%) and a dimer for **80** at 816 (51%), besides the molecular ion  $[M+H]^+$  peaks at 408 and 263. The dimer for **73** was observed at 647 but the intensity was very low (0.33%).

**Table 39.** L-CQ and FAB Mass Spectrometry Results (Relative Abundance %).

compound	LC-Q				FAB
	monomer	dimer	trimer	tetramer	dimer
<b>73</b> + $H^+$	324.20 (100)				647 (0.33)
<b>73</b> + $Na^+$	346.20 (3.28)	668.73 (0.60)			
<b>79</b> + $H^+$	263.07 (100)	524.93 (60.78)			525 (3.30)
<b>79</b> + $Na^+$	285.13 (45.59)	547.07 (79.72)	808.60 (2.18)		
<b>80</b> + $H^+$	408.33 (100)	815.13 (80.5)	1222.0 (23.8)	1628.93 (8.3)	816 (5.0)
<b>80</b> + $Na^+$	430.33 (430)	837.20 (1106)	1243.87 (268)	1650.67 (120)	

Furthermore, the results from LCQ mass spectrometry are significant and indicate the efficient assembly between molecules of compounds **79** and **80** (Figure 112). As for protonated oligomers for **73**, no evidence for aggregation was found in the protonated form by LCQ mass spectrometry. However, there was a dimer  $[2M+H]^+$  for compound **79** at 524.93 with 60.78% relative abundance to the molecular ion at 263.07. The protonated monomer, dimer, trimer and tetramer of compound **80** were found at 408.33 (100%), 815.13 (80.5%), 1222.0 (23.8%) and 1628.93 (8.3%).

The sodiated aggregates for both **79** and **80** were observed at 285.13 (45.59%) and 430.33 (440%), dimer at 547.07 (79.72%) and 837.20 (1106%) and trimer at 808.60 (2.18%) and 1243.87 (268%) respectively. The tetramer of compound **80** was also observed at 1650.67 (120%).

The mass spectrometry results confirmed the existence of stable aggregates of compounds **79** and **80**. Sodium ions tend to stabilize higher aggregates for compounds **79** and **80**. The results from the FAB experiments were very similar to those from LCQ. Multiple hydrogen bonding in the aggregate state would account for the stability of oligomers of compounds **79** and **80**.<sup>264, 265</sup>

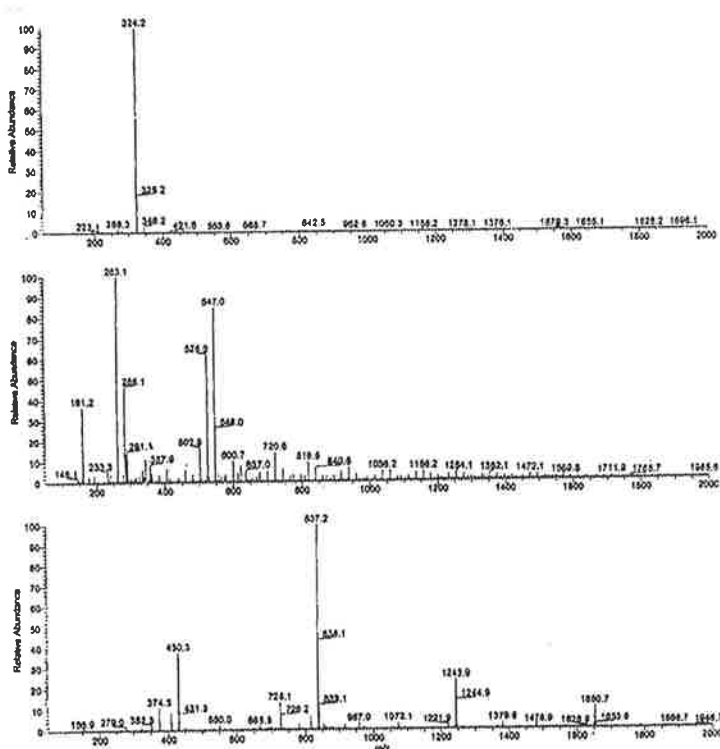
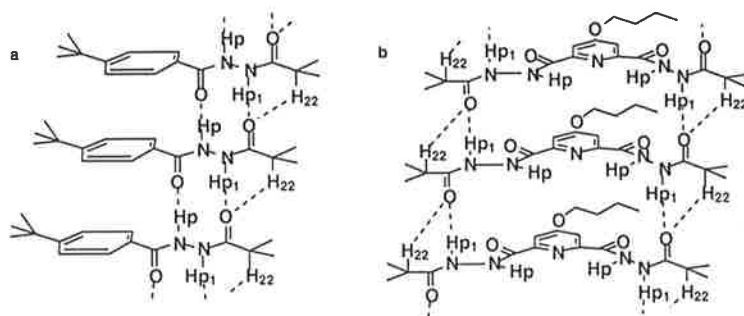


Figure 112. L-CQ spectra of compounds **73** (a), **79** (b) and **80** (c).

### 8. 2. 10 Helical assembly of compounds 79 and 80

Based on the observation of hydrogen bonding and  $\pi$ - $\pi$  stacking interactions in **79** and **80** at higher concentration and low temperature, the possible structures of these aggregates are described below (Figure 113).

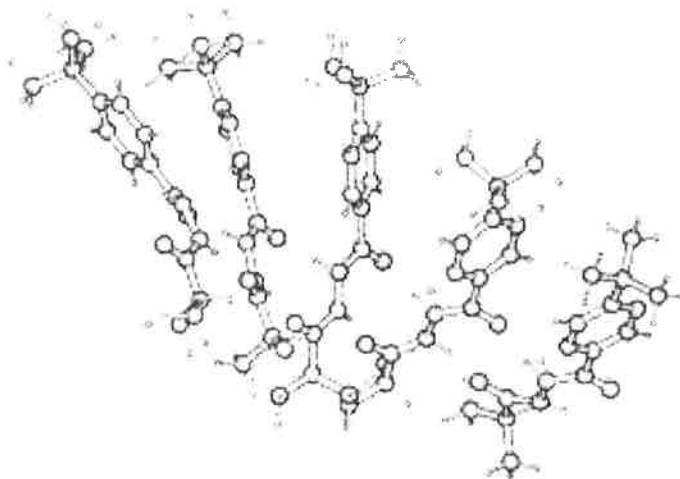
Hydrogen Hp and oxygen O21 of one molecule will form hydrogen bonds with O11' and Hb' in another molecule and the O11 and Hp1 from this molecule will interact with Hp'' and O21'' in another molecule. The intermolecular hydrogen bondings adopt a *trans* configuration around the HN-NH unit consistent with literature structures of diacyl hydrazide.<sup>266-268</sup> At the same time, the phenyl group of compound **79** tends to form  $\pi$ - $\pi$  stacking which is promoted by the intermolecular hydrogen bonding. A consequence of this type of interaction for **79** would be the formation of helices since there is a *gauche* torsional angle around N11 bond,<sup>266-268</sup> and the steric interactions of the side groups (*t*-butyl and isopropyl). Both factors promote the assembly of molecules of **79** in the same direction to form either left- or right-handed helices.<sup>107, 234-239</sup> The *t*-butyl group tends to impede the  $\pi$ - $\pi$  stacking of phenyl groups, consequently, the phenyl rings tend to overlap in a crossed manner.



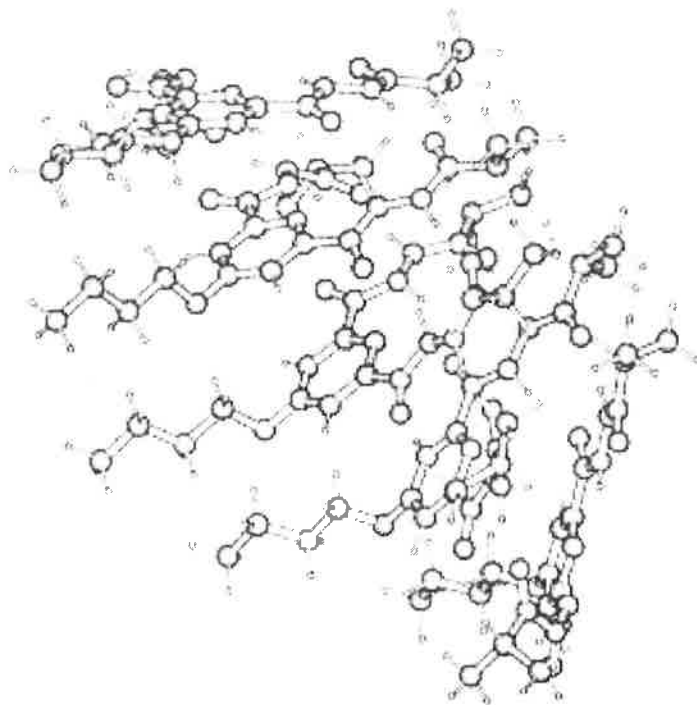
**Figure 113.** Assembly structures of compounds **79** (a) and **80** (b) with expected hydrogen bonding and  $\pi$ - $\pi$  stacking.

As for compound **80**, there are two Hp1 protons and related carbonyl groups C21=O21. As expected, both Hp1 protons and carbonyl groups C21=O21 can be involved in intermolecular hydrogen bonds as shown in Figure 113b. The amide proton N21-Hp1 on the right side could be involved in an intermolecular hydrogen bond with the oxygen O21''=C21'' from another molecule, the oxygen atom of the amide C21=O21 on the right side will form a hydrogen bond with a neighboring molecule. The same arrangement would apply for O21=C21 and N21''-Hp1''. A consequence of this type of interaction would be the formation of terraces. There would then be a displacement of one bond length in the horizontal direction for each ring in the terrace. Furthermore, proton Hp will form an intra-molecular hydrogen bond with nitrogen N1 in the pyridine ring, which results in the planar conformation for compound **80**. This conformation favors  $\pi$ - $\pi$  stacking interactions, and in order to maintain vertical  $\pi$ - $\pi$  stacking of the pyridine rings, the assembly proceeds in a helical manner with right- and left-handed helices.

In order to provide evidence for these possibilities, molecular modelling was applied to the assemblies of the both **79** and **80** using minimum energy conformation in Spartan. The proposed helicity of compounds **79** and **80** appears as expected from these calculations as shown in Figure 114 and Figure 115. Since compounds **79** and **80** have no chiral centre, the helices would occur in both the right-hand and left-hand forms.



**Figure 114.** Computer modelling structures of assembly of compound **79** showing right-handed helicity.



**Figure 115.** Computer modelling structures of assembly of compound **80** showing right-handed helicity.

---

## Chapter 9

---

# Molecular Recognition of Biotin Peptides with Synthetic Receptors

## 9.1 Introduction

In biotin carboxyl carrier protein (BCCP), the biotin-lysine residue is well placed to act as a swinging arm becoming carboxylated and passing on the carboxyl group at the active site of the biotin carboxylase.<sup>15</sup> The protein-protein interactions are crucial for the orientation and activation during the carboxylation process, since the biotin accepting domain of BCCP has to be functionalized by undergoing complexation with the active sites of carboxylase and subsequently transferase. Although the BCCP biotin-accepting domain has been identified, the details of carboxylation and decarboxylation of biotin in the active site are not known.<sup>16</sup>

## 9.2 Results and Discussion

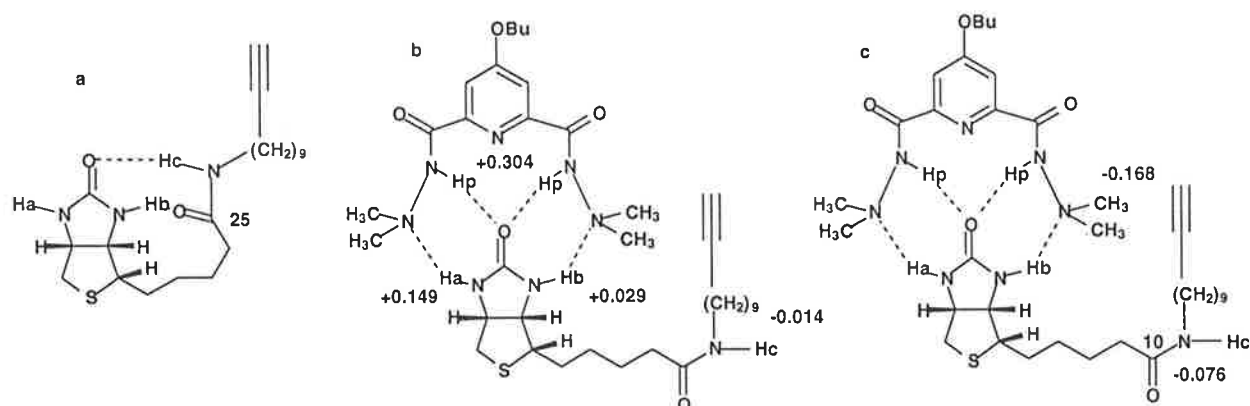
### 9.2.1 Molecular recognition of biotin amide **33** with receptor **73**

Receptor **73** (Figure 91 in Chapter 8) possesses two intra-molecular hydrogen bonds, resulting in a planar conformation. When one equivalent of receptor **73** and biotin amide **33** are mixed in CDCl<sub>3</sub> at 10 mM, changes occur in the proton NMR resonances. The complex of **73** and biotin amide **33** is proposed as shown in Figure 116, which shows the changes in proton NMR resonances for the amide protons in receptor **73** and biotin amide **33** in CDCl<sub>3</sub> at 10 mM on the structures. The downfield shift of the NH proton on **73** (0.304 ppm) is indicative of an interaction between the hydrazine protons with the carbonyl oxygen in biotin amide **33**. Furthermore, the chemical shift of Ha in biotin moves downfield + 0.149 ppm, suggesting the efficient interaction of Ha with the N(CH<sub>3</sub>)<sub>2</sub> group of receptor **73**. However, the proton NMR resonance of Hb moves only slightly downfield (+ 0.029 ppm). A possible explanation for this is that the intra-molecular hydrogen bond between Hb and the carbonyl group in the side chain of biotin amide **33** is still present. The fact that Hc moves only slightly up-field (0.014 ppm) in the complex is consistent with the existence of the intra-molecular hydrogen bond.

Figure 116c shows the changes in the <sup>13</sup>C NMR resonances for the N(CH<sub>3</sub>)<sub>2</sub> of the receptor and amide C=O of the biotin side chain and these moved upfield by 0.168 ppm and 0.076 ppm respectively, indicating that the nitrogen was involved in the intermolecular hydrogen bonding but the carbonyl group was released from intra-molecular hydrogen bonding. As mentioned previously, the association of secondary and tertiary amines with hydrogen halides results in the

upfield movement of  $^{13}\text{C}$  NMR resonances for carbons which are attached to the nitrogen atom.

225, 226

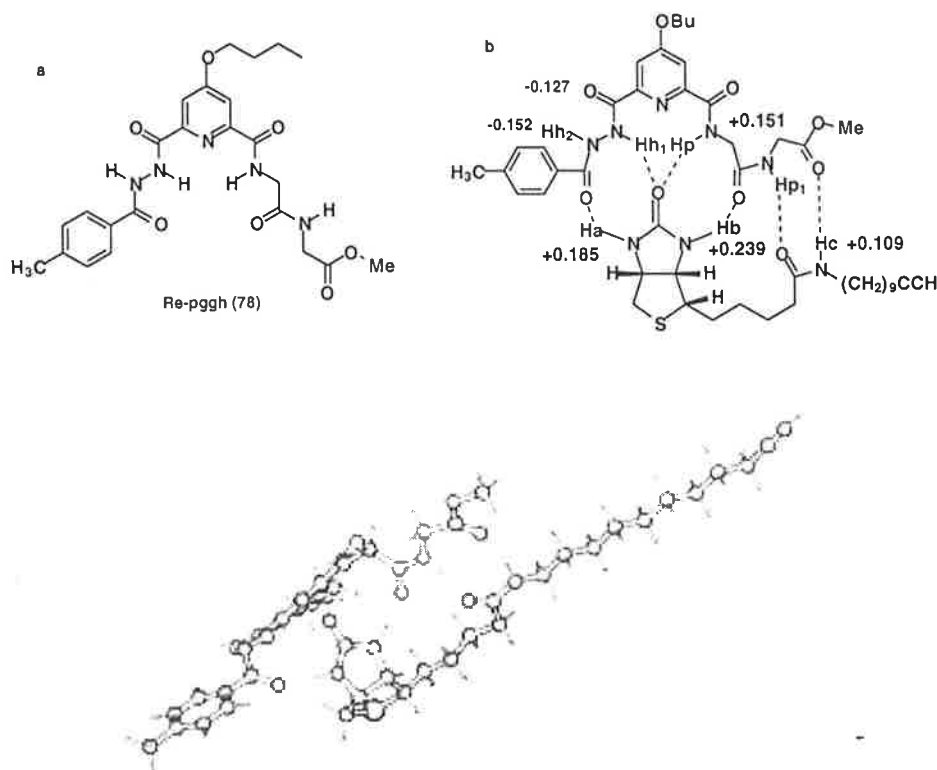


**Figure 116.** Substrate biotin amide Bt-C9 (**33**) (a) and the complex of biotin amide Bt-C9 (**33**) with receptor Re-pdihy,  $[\mathbf{73}] = 20.0 \text{ mM}$ ,  $[\mathbf{12}] = 20.0 \text{ mM}$  at rt and in  $\text{CDCl}_3$  (ppm).

The molecular recognition of a biotin amide with receptor **73** serves as a prototype for the complexation of biotin with peptides in the active site of enzymes by effective hydrogen bonding. A typical hydrogen bond may contribute as much as 2-3 kcal/mol toward binding. If the strength of a given hydrogen bond in the transition state is stronger than that in the ground state, the hydrogen bond lowers the energy barrier for the enzymic reaction by solvating the high-energy transition-state species. Strong hydrogen bonds therefore have the potential to contribute to enzymic catalysis by stabilising the initial complex  $(\text{E-S})_1$  of enzyme and substrate or the intermediate  $(\text{E-S})_2$ .<sup>227</sup>

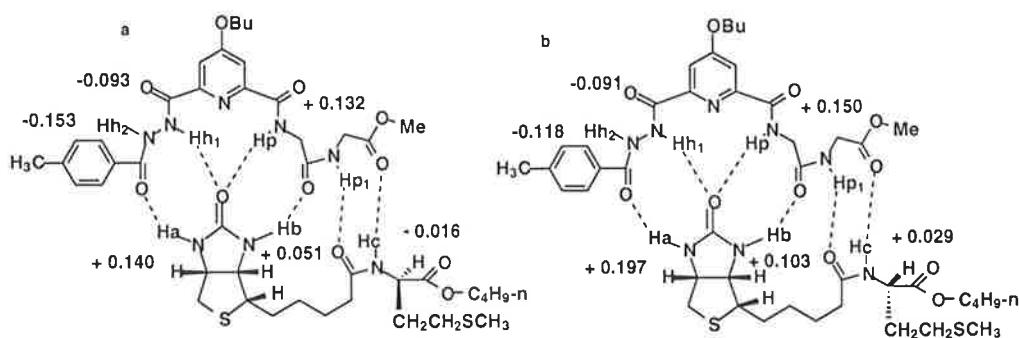
### 9.2.2 Binding of biotin peptides with hydrazide receptor **78**

In order to increase the binding ability of the hydrazide receptors the extended structure Re-phgg (**78**) was prepared. As shown in Figure 117, the changes in the proton chemical shifts of the various NH groups indicate an efficient hydrogen-bonding interaction, with NHa, NHb and Hpc all shifting downfield significantly. The change in proton shift for Hc was + 0.109 ppm, indicating a hydrogen bonding interaction (Figure 117). However, the changes in the chemical shifts of protons NHh1 and NHh2 were both negative, indicating a disruption to the intermolecular hydrogen bonding of the receptor to itself.



**Figure 117.** Receptor Re-phgg (a) and the complex of biotin aimde Bt-C9(b) (33) with receptor Re-pggh (78) and molecular modelling structure of the complex (c), [78] = 1.0 mM, [33] = 1.0 mM at rt and in  $\text{CDCl}_3$  (ppm).

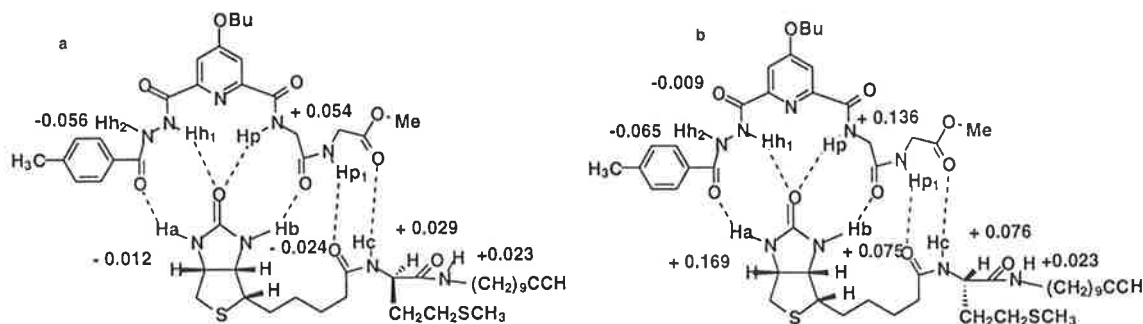
Figure 118 shows the changes in NH chemical shifts for receptor Re-phgg (78) and biotin peptides Bt-Met(D) (37) and Bt-Met(L) (38). Both ureido NH protons move downfield in the presence of receptor Re-pggh (78), with Bt-Met(L) (38) causing larger changes than Bt-Met(D) (37).



**Figure 118.** Complexes of biotin peptide Bt-Met(D) (37) (a) and Bt-Met(L) (38) (b) with receptor Re-pggh (78), [37 or 38] = 1.0 mM, [12] = 1.0 mM at rt and in  $\text{CDCl}_3$  (ppm).

The changes in the chemical shifts of NH protons for receptor Re-pggh (78) in the presence of biotin peptides Bt-Met(D)-C9 (82) and Bt-Met(L)-C9 (83) are shown in Figure 119. In this case, the receptor causes a significant change in  $^1\text{H}$  NMR shifts for Bt-Met(L)-C9 (83) but not Bt-

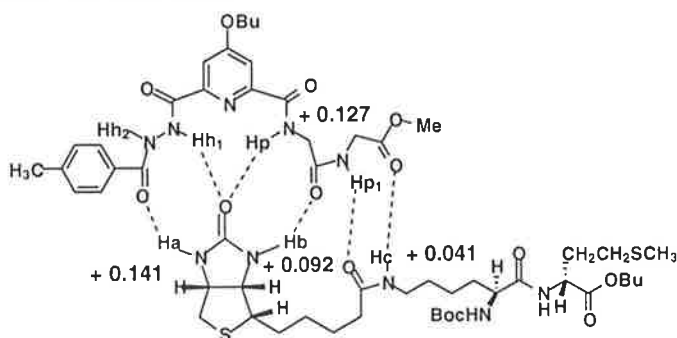
Met(D)-C9 (**82**). These results, together with those in Figure 118 indicate that the receptor Re-pggh (**78**) can selectively recognize Bt-Met(L)-C9 (**83**) compared to Bt-Met(D)-C9 (**82**).



**Figure 119.** The complexes of biotin peptide Bt-Met(D)-C9 (**82**) (a) and Bt-Met(L)-C9 (**83**) (b) with receptor Re-pggh (**78**), [**82** or **83**] = 1.0 mM, [**78**] = 1.0 mM at rt and in  $\text{CDCl}_3$  (ppm).

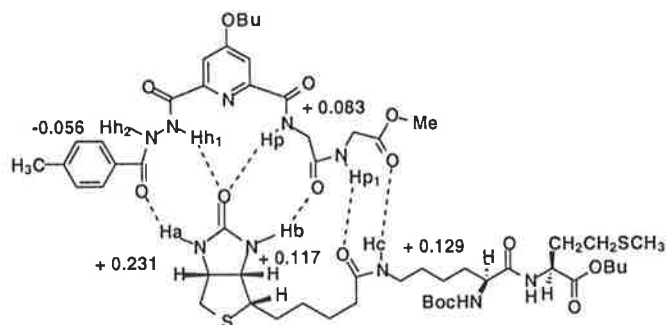
The binding of the receptor Re-pggh with biotin peptides Bt-Lys(L)-Met(D) (**48**), Bt-Lys(L)-Met(L) (**47**) and Bt-Ahx-Met(D) (**50**) and the changes in the chemical shifts of the NH protons are shown in Figure 120, 121 and 122 respectively. The biotin peptide Bt-Lys(L)-Met(L) (**47**) is the basic unit of biotin dependent enzymes. The results show the receptor could bind to Bt-Lys(L)-Met(D) (**48**) more efficiently than the other biotin peptides.

Furthermore, the better binding of the receptor Re-pggh (**78**) with Bt-Lys(L)-Met(L) (**47**) also demonstrates the better co-operativity of the binding and intermolecular hydrogen bonding within the complex than other complexes. As shown in Figure 121, the change in  $^1\text{H}$  NMR shift for Hc in the complex of Re-pggh (**78**) with Bt-Lys(L)-Met(L) (**47**) is the largest among the three complexes in Figures 120, 121 and 122.

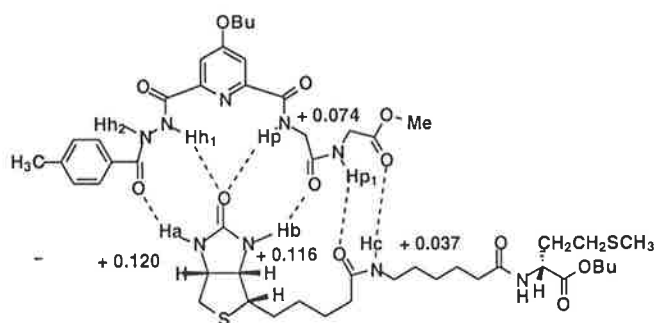


**Figure 120.** The complex of biotin peptide Bt-Lys(L)-Met(D) (**48**) with receptor Re-pggh (**78**), [**48**] = 0.50 mM, [**78**] = 0.50 mM at rt and in  $\text{CDCl}_3$  (ppm).





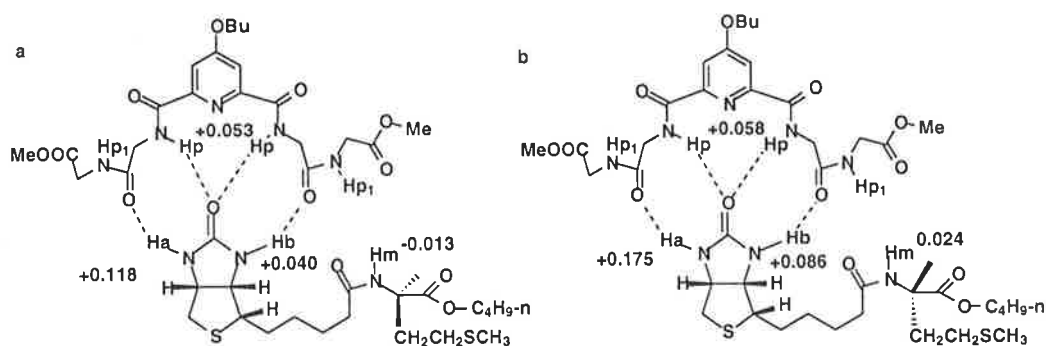
**Figure 121.** The complex of biotin peptide Bt-Lys(L)-Met(L) (**47**) with receptor Re-pggh (**78**), [**47**] = 0.50 mM, [**78**] = 0.50 mM at rt and in CDCl<sub>3</sub> (ppm).



**Figure 122.** The complex of biotin peptide Bt-Ahx-Met(D) (**50**) with receptor Re-pggh (**78**), [**50**] = 0.50 mM, [**78**] = 0.50 mM at rt and in CDCl<sub>3</sub> (ppm).

### 9. 2. 3 Molecular recognition of biotin peptides with receptor Re-pdigg (**75**)

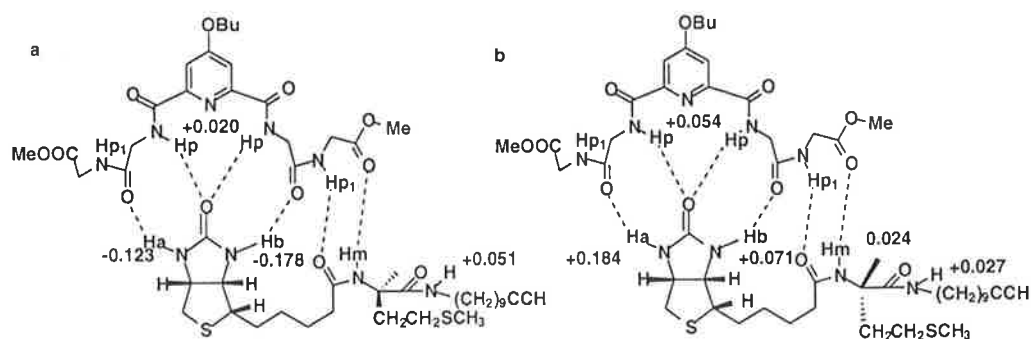
The changes in the proton chemical shifts for Bt-Met(D) (**37**) and Bt-Met(L) (**38**) in the presence of receptor Re-pdigg **75** are shown in Figure 123. The changes in chemical shifts, are consistent with binding of (**37**) and (**38**). The receptor's binding pocket appears to bind both to the ureido oxygen and ureido NH protons, by the formation of intermolecular hydrogen bonds. The changes of chemical shifts of protons Hp and Hp1 in receptor Re-pdigg (**75**) in the presence of Bt-Met(D) (**37**) and Bt-Met(L) (**38**) are very similar. However, changes in the shifts for the ureido protons were not similar with Ha and Hb of compound Bt-Met(L) (**38**) being larger than those of Bt-Met(D) (**37**). Compound Bt-Met(D) (**37**) has been shown in Chapter 4 to form stronger intra-molecular hydrogen bonds than Bt-Met(L) (**38**).



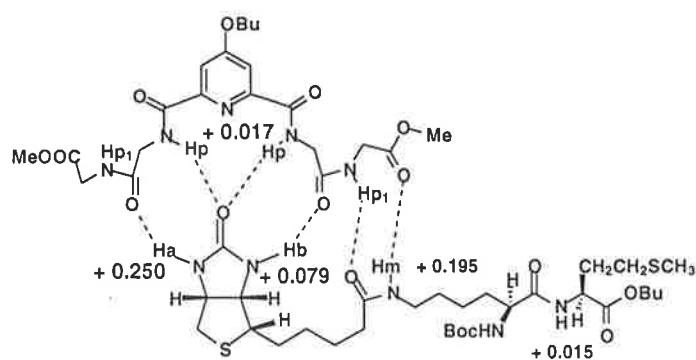
**Figure 123.** The complexes of biotin peptide Bt-Met(D) (**37**) (a) and Bt-Met(L) (**38**) (b) with receptor Re-pdigg (**75**),  $[75] = 1.0 \text{ mM}$ ,  $[37 \text{ or } 38] = 1.0 \text{ mM}$  at rt and in  $\text{CDCl}_3$  (ppm).

The proposed binding of receptor Re-pdigg (**75**) with biotin peptides is presented in Figure 124 along the changes in the proton chemical shifts for NH. The binding of Bt-Met(L)-C9 (**83**) with the receptor Re-pdigg is stronger than Bt-Met(D)-C9 (**82**), suggesting that the receptor can selectively recognize Bt-Met(L)-C9 (**83**) from Bt-Met(D)-C9 (**82**).

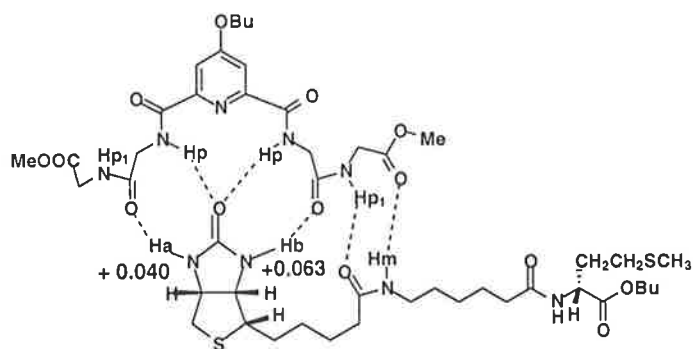
The binding of Bt-Lys(L)-Met(L) (**47**) with receptor Re-pdigg (**75**) and the changes in the chemical shifts of NH protons are shown in Figure 125. Figure 126 also shows the binding of Bt-Ahx-Met(D) (**50**) with the receptor Re-pdigg **75** and the changes of chemical shifts which were observed from the relevant NMR spectra. The results show the binding of Bt-Lys(L)-Met(L) (**47**) with the receptor is much better than Bt-Ahx-Met(D) (**50**).



**Figure 124.** Receptor Re-pdigg (a) and the complex of biotin peptide Bt-Met(D)-C9 (**82**) (a) and Bt-Met(L)-C9 (**83**) (b) with Receptor Re-pdigg (**75**),  $[82 \text{ or } 83] = 1.0 \text{ mM}$ ,  $[75] = 1.0 \text{ mM}$  at rt and in  $\text{CDCl}_3$  (ppm).



**Figure 125.** The complex of biotin peptide Bt-Lys(L)-Met(L) (**47**) with receptor Re-pdigg (**75**),  $[47] = 0.50$  mM,  $[78] = 0.50$  mM at rt and in  $\text{CDCl}_3$  (ppm).



**Figure 126.** The complex of biotin peptide Bt-Ahx-Met(D) (**50**) with receptor Re-pdigg (**75**),  $[50] = 0.50$  mM,  $[75] = 0.50$  mM at rt and in  $\text{CDCl}_3$  (ppm).

## Chapter 10

# Molecular Recognition of Adenine Derivatives with Synthetic Receptors

## 10.1 Introduction

The molecular recognition of DNA and nucleobases has potential applications in the selective cleavage of DNA. The fundamental interactions of DNA and proteins are important to an understanding of human and animal development. It is reported that proteins can directly interact with DNA, resulting in the extrusion of a nucleobase, e.g. uracil, by a pinch-push-pull mechanism.<sup>269</sup> The interactions are generally hydrogen bonding between proteins and phosphates or nucleobases. The Watson-Crick hydrogen bonding and Hoogsteen hydrogen bonding types are very common for the interactions between DNA and between protein and nucleic acid base pairs as outlined in Figure 127.<sup>200, 228</sup>

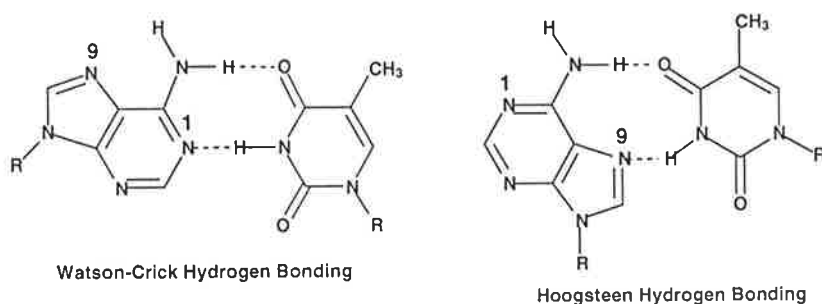


Figure 127. DNA Watson-Crick hydrogen bonding and Hoogsteen hydrogen bonding.

DNA base pairs can also form  $\pi$ - $\pi$  stacking interactions, besides Watson-Crick and Hoogsteen hydrogen bonding. As shown in Figure 128, thymine can form  $\pi$ - $\pi$  stacking interactions with adenine.<sup>228</sup> This  $\pi$ - $\pi$  stacking is the result of  $\pi$ - $\sigma$  attractions that overcome  $\pi$ - $\pi$  repulsions ( $\sigma$ -framework,  $\pi$ -electrons).<sup>209</sup>

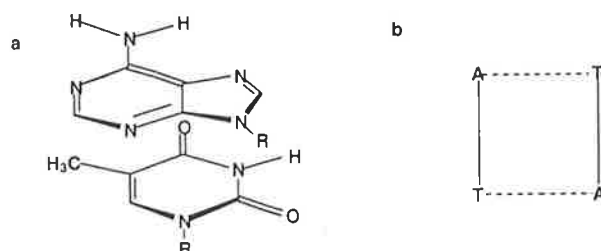
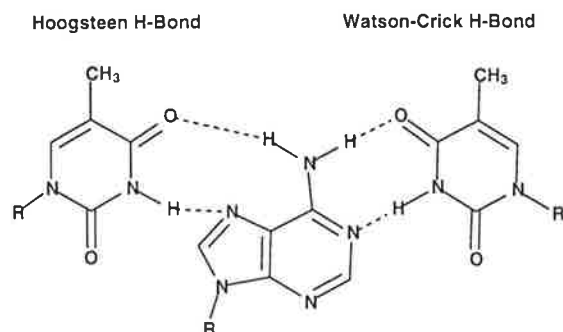


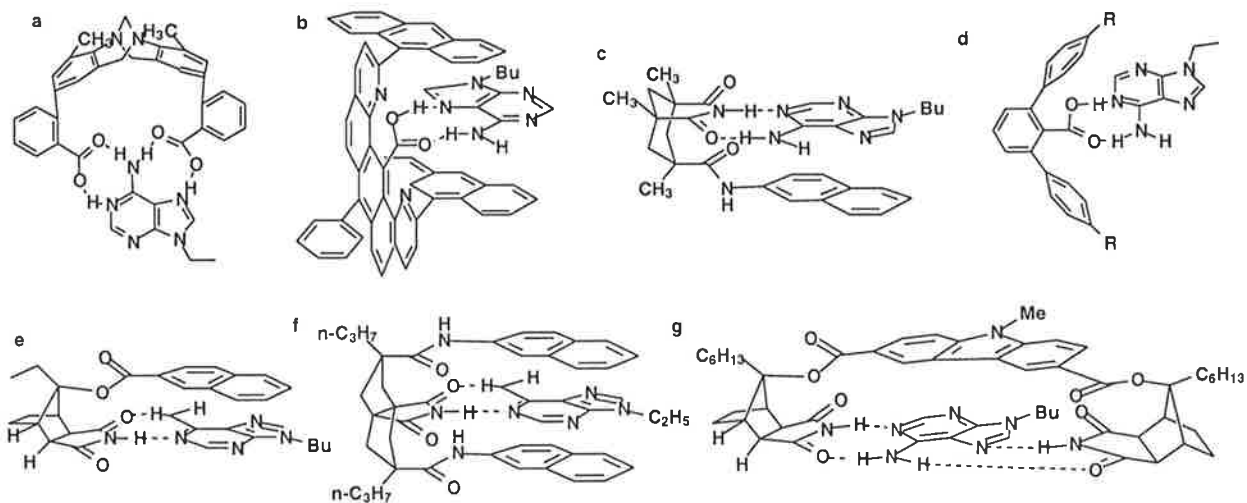
Figure 128. DNA  $\pi$ - $\pi$  stacking interaction. (a)  $\pi$ - $\pi$  stacking of adenine with thymine, (b)  $\pi$ - $\pi$  stacking of base pair A-T with T-A.

Nucleic acids can also form base pair triplets, such that both Watson-Crick and Hoogsteen hydrogen bonding are possible to an adenine unit at the same time as shown in Figure 129.



**Figure 129.** DNA Watson-Crick hydrogen bonding and Hoogsteen hydrogen bonding in a DNA base pair triplet.

Based on the concept of Watson-Crick and Hoogsteen hydrogen bonding in the molecular recognition of adenine, flexible receptors containing two uracil moieties connected through alkyl spacers to an adenosine derivative to form base pair triplets as shown in Figure 9 have been reported.<sup>79</sup> A number of receptors that are capable of binding adenine have been reported, including those illustrated in Figure 130 a-g.<sup>201, 270-274</sup>



**Figure 130.** Receptors for the bonding of an adenine unit with  $\pi$ - $\pi$  stacking and hydrogen bonding.

Data on the molecular structure of DNA base pair doublets and triplets is extensive. The DNA base doublet adopts a propeller twist conformation as shown in Figure 131a with an average length of the base pair being about 13 Å (Figure 131b).<sup>233</sup>

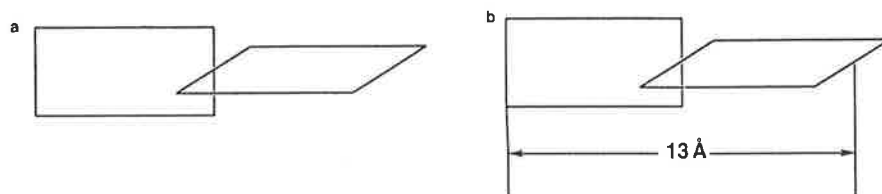


Figure 131. Propeller twist structure of DNA base pair (a) and the average length of the base pair (b).

The distance between stacked base pairs in DNA is between 3-4 Å (Figure 132a) and roll angles (about 30°) and distances (6.7 Å) (Figure 132b).

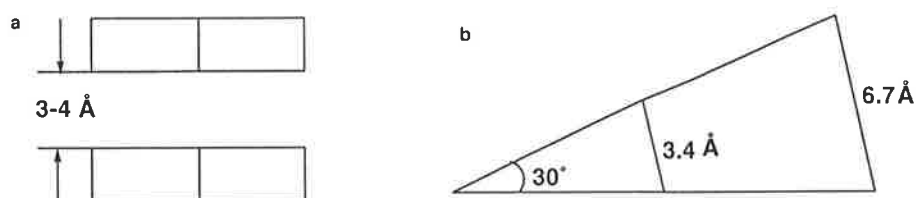
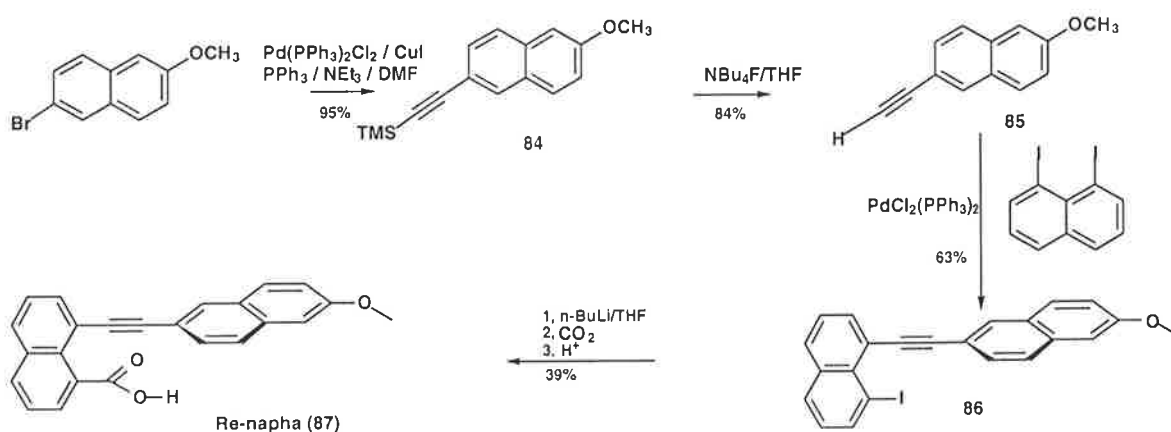


Figure 132. DNA space distances between base pairs (a) and roll angles and distances between base pairs (b).

## 10.2 Results and Discussion

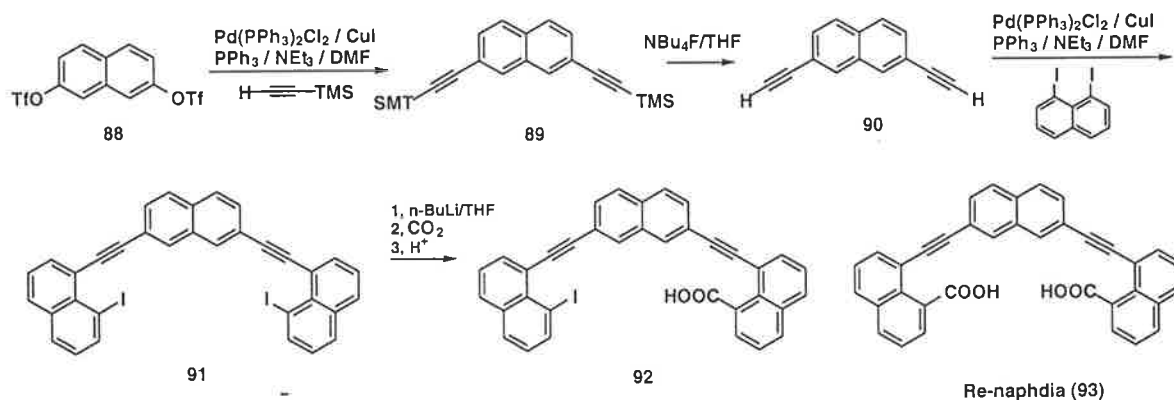
### 10.2.1 Synthesis of receptor Re-napha 87

A series of receptors for adenine were prepared containing both rigid and flexible linker arms. Initially, 6-bromo-2-methoxynaphthalene was converted into **84** by palladium mediated coupling involving trimethylsilylacetylene in the presence of  $\text{PdCl}_2(\text{PPh}_3)_2$ . Subsequent hydrolysis of **84** with wet tetrabutylammonium fluoride in THF gave **85**, which could be selectively coupled with 1, 8-diiodonaphthalene in the presence of  $\text{PdCl}_2(\text{PPh}_3)_2$  to give **86**. Compound **86** was converted into the final receptor **87** by lithiation with butyl lithium in THF, carboxylation and acidification (Scheme 16a). The structure of the receptor was confirmed by  $^1\text{H}$ ,  $^{13}\text{C}$ , COSY, NOESY and  $^1\text{H}$ - $^{13}\text{C}$  NMR spectroscopy and mass spectrometry.



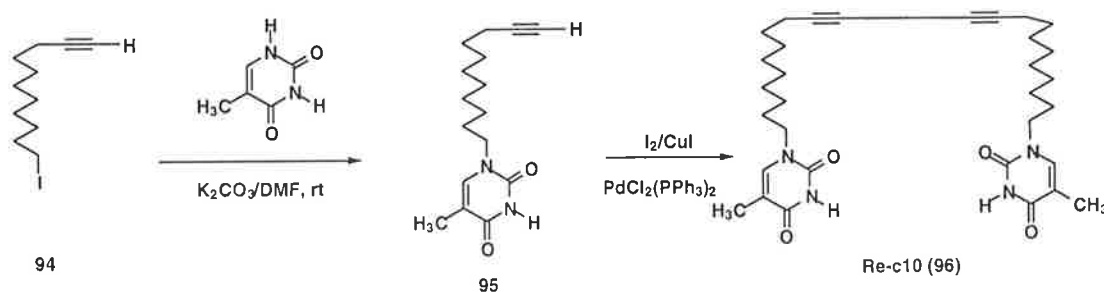
Scheme 16a. Synthesis of receptor Re-napha (87).

A more elaborate and rigid receptor, Re-naphdia **93** was then prepared according to the route in Scheme 16b. Bistriflate **88** was coupled with two equivalents of trimethylsilylacetylene in the presence of  $\text{PdCl}_2(\text{PPh}_3)_2$ , and the resultant product **89** desilylated with tetrabutylammonium fluoride to give **90**. Coupling of **90** with 1, 8-diiodonaphthalene by the  $\text{PdCl}_2(\text{PPh}_3)_2$  catalysed reaction, followed by the lithiation of compound **91**, carboxylation and acidification gave receptor Re-naphdia **93** (Scheme 16b).



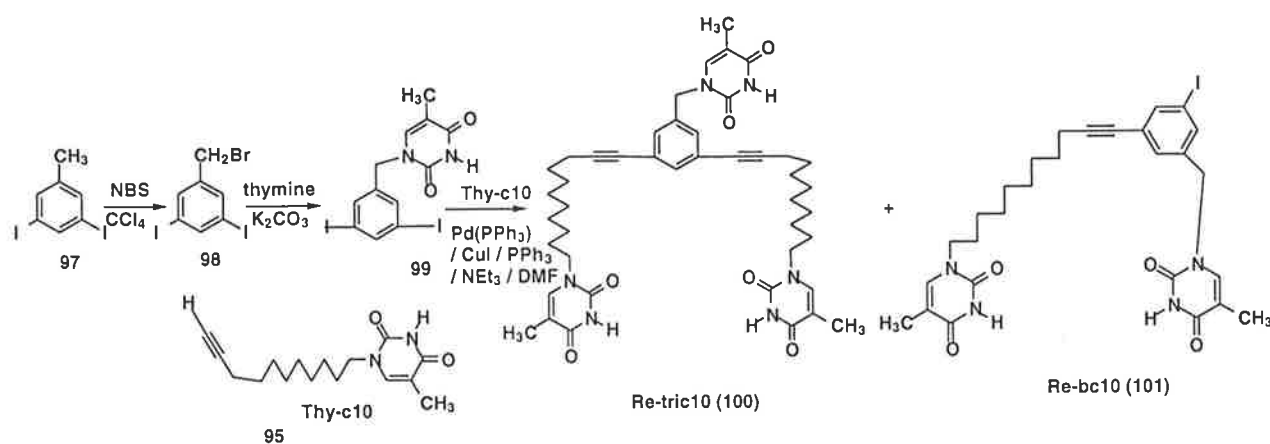
Scheme 16b. Synthesis of receptor Re-naphdia (**93**).

Receptor Re-c10 (**96**) was prepared by the homo-coupling reaction of compound **95** in the presence of  $\text{PdCl}_2(\text{PPh}_3)_2$ , copper (I) iodide, iodine and diisopropylamine.<sup>275</sup> Compound **95** was prepared by the alkylation of thymine in DMF with 11-iododec-1-yne (**94**) and potassium carbonate (Scheme 17).



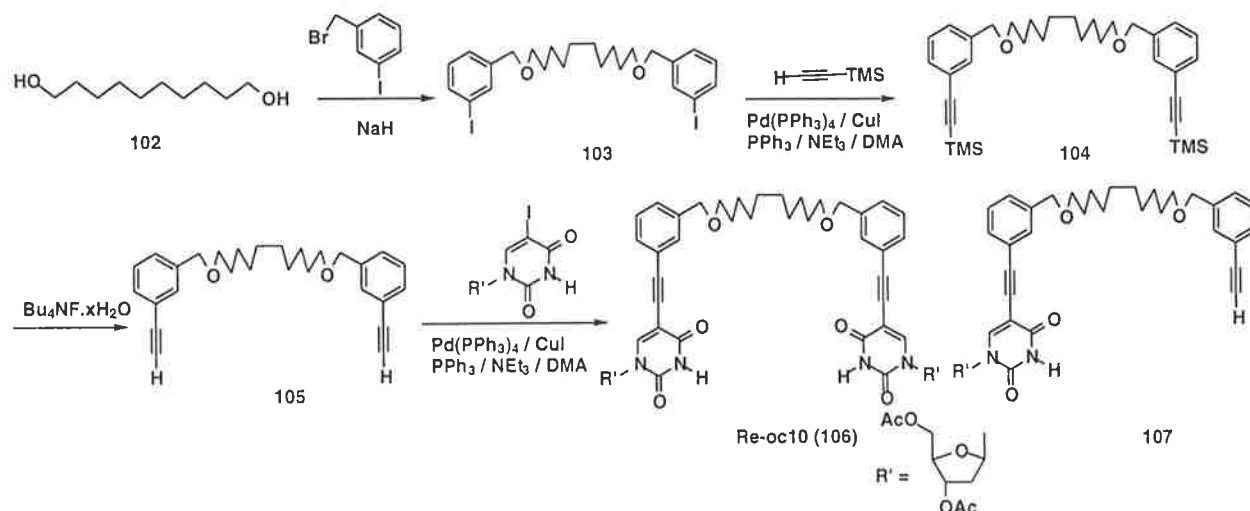
Scheme 17 Synthesis of receptor Re-c10 (**96**).

The preparation of receptors Re-tric10 (**100**) and Re-bc10 (**101**) commenced with the bromination of 3, 5-diiodotoluene (**97**) with NBS in  $\text{CCl}_4$  to give **98** which was alkylated with thymine in DMSO in the presence of potassium carbonate to give intermediate **99**. The palladium catalysed coupling of **99** with Thy-c10 (**95**) gave a mixture of Re-tric10 (**100**) and Re-bc10 (**101**) (Scheme 18).



Scheme 18. Synthesis of receptors Re-tric10 (**100**) and Re-bc10 (**101**).

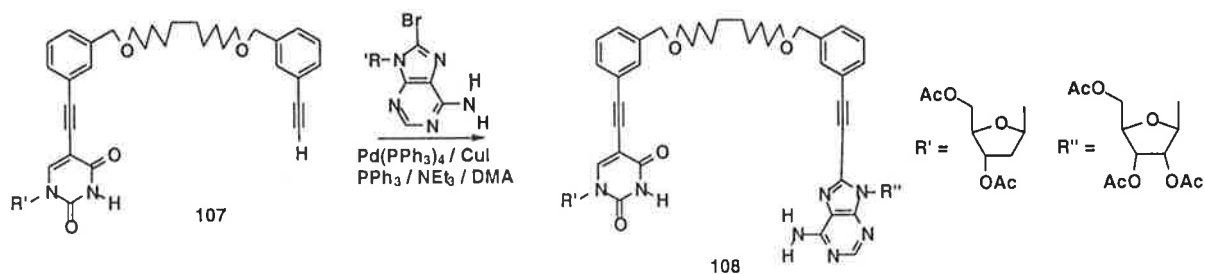
For the preparation of receptor Re-oc10 (**106**), 1, 10-didodecanediol (**102**) was firstly alkylated with 3-iodobenzylbromide in the presence of sodium hydride to give diiodo compound **103**, which was coupled with trimethylsilylacetylene in the presence of Pd(PPh<sub>3</sub>)<sub>4</sub> and CuI to give **104** which was desilylated with tetrabutylammonium fluoride to give **105**. Palladium catalysed coupling of **105** with diacetyl 5-iododeoxyuridine gave the final product **106**, together with by-product **107** (Scheme 19).



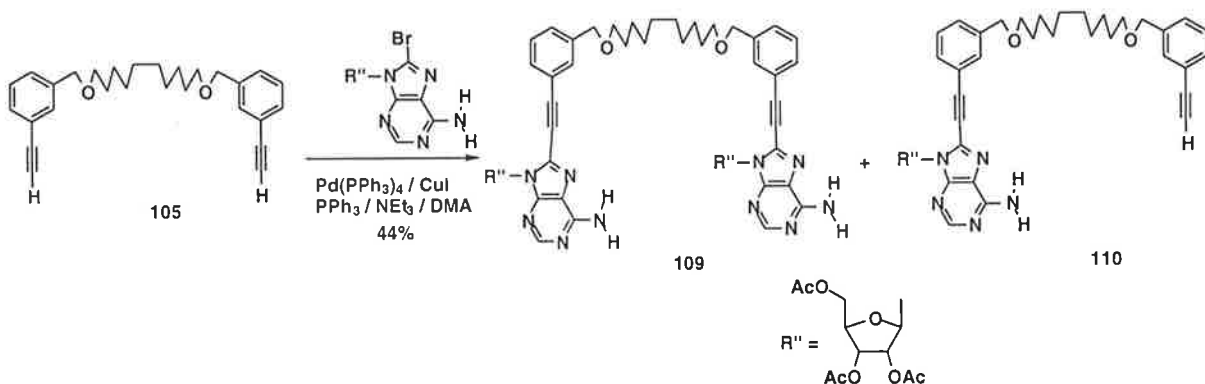
Scheme 19. Synthesis of receptor Re-oc10 (**106**).

The monocoupled product **107** was used for the preparation of a DNA base pair doublet by the Pd(PPh<sub>3</sub>)<sub>4</sub> catalysed coupling with triacetyl 8-bromoadenosine as shown in Scheme 20.

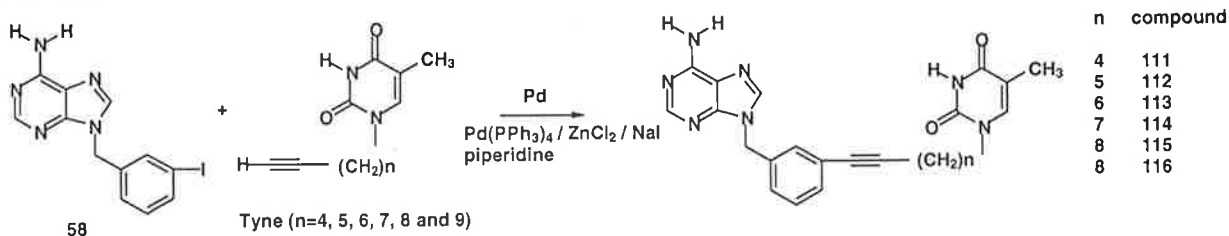


Scheme 20. Synthesis of DNA base pair **108**.

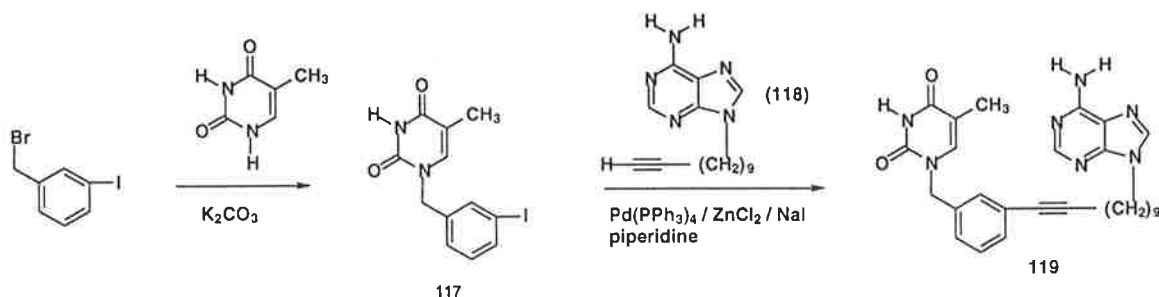
Compound **105** was also converted into **109** and **110** by palladium catalysed coupling with 8-bromoadenosine (Scheme 21).

Scheme 21. Synthesis of compound **109**.

Adenine derivative **58** was coupled with **154-159** (Tyne,  $n = 4, 5, 6, 7, 8$  and  $9$ ) (Scheme 22) in the presence of  $\text{Pd}(\text{PPh}_3)_4$ ,  $\text{ZnCl}_2$  and  $\text{NaI}$  in piperidine to give the corresponding compounds **111-116**.

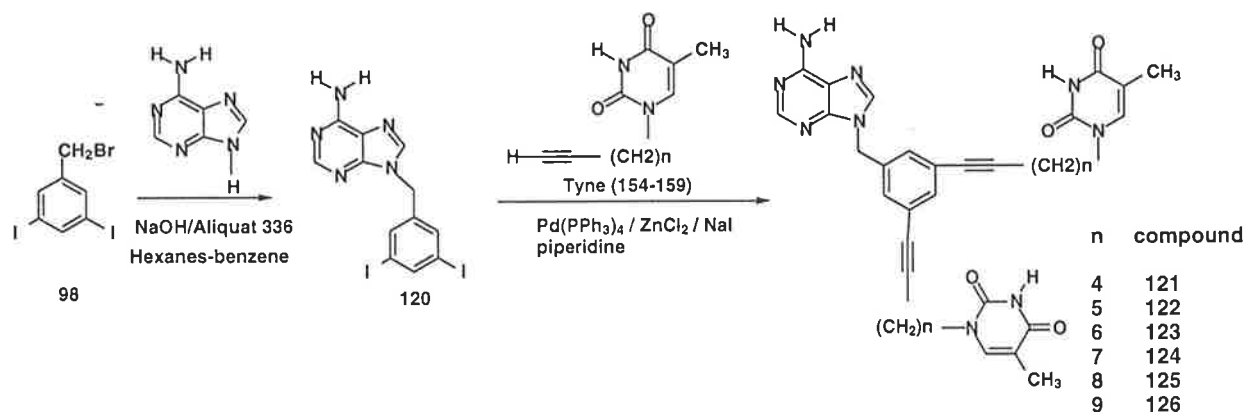
Scheme 22. Synthesis of DNA base pair doublets **111-116**.

The complementary **117** was prepared based on the Scheme 23. Thymine was firstly benzylated in DMF by 3-iodobenzyl bromide in the presence of potassium carbonate to give compound **117**, which was applied in the palladium catalysed reaction to give DNA base pair doublet **119**.



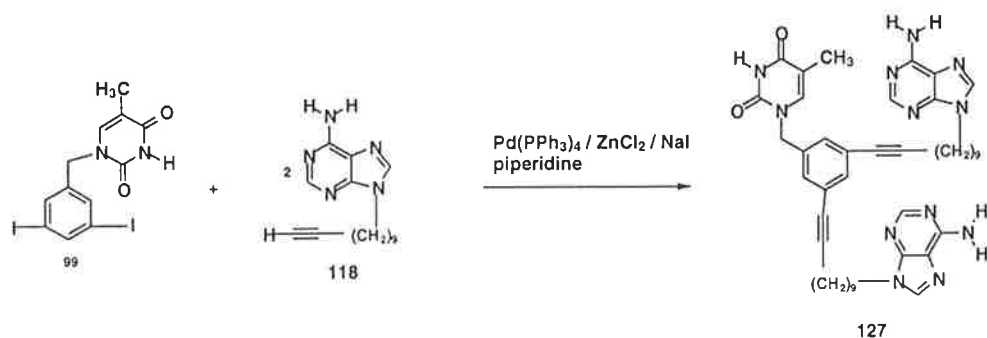
Scheme 23. Synthesis of DNA base pair doublet 119.

The preparation of DNA base triplets started with the alkylation of adenine with 3, 5-diiodobenzyl bromide (**98**) in aqueous NaOH in the presence of Aliquat 336 with mixed solvent hexanes-benzene to give intermediate **120**. The palladium ( $\text{Pd}(\text{PPh}_3)_4$ ) catalysed coupling reactions between **120** and Tyne (**154-159**) then gave DNA base pair triplets **121-126** (Scheme 24).



Scheme 24. Synthesis of DNA base pair triplets 121-126.

The complementary compound **127** was prepared by the reaction of compound **99** with adenine derivative **118** in the presence of a palladium catalyst as shown in Scheme 25.



Scheme 25. Synthesis of DNA base pair triplet 127.

### 10. 2. 2 Molecular recognition of adenine derivatives with receptor Re-napha 87

Titration of a solution of Re-napha **87** with increasing amounts of 9-butyladenine showed a gradual downfield movement of the adenine NH protons and up-field movement of the aromatic signals in the  $^1\text{H}$  NMR spectrum (Figure 133). A solution of 1.0 mM Re-napha **87** and 1.0 mM 9-butyl adenine showed changes in the proton NMR shifts as shown in Figure 134. The downfield shift for the NH proton of adenine (1.20 ppm) was consistent with intermolecular hydrogen bonding while the up-field shift for the adenine aromatic and butyl protons as well as the methoxy protons were consistent with  $\pi$ - $\pi$  stacking.<sup>201</sup>

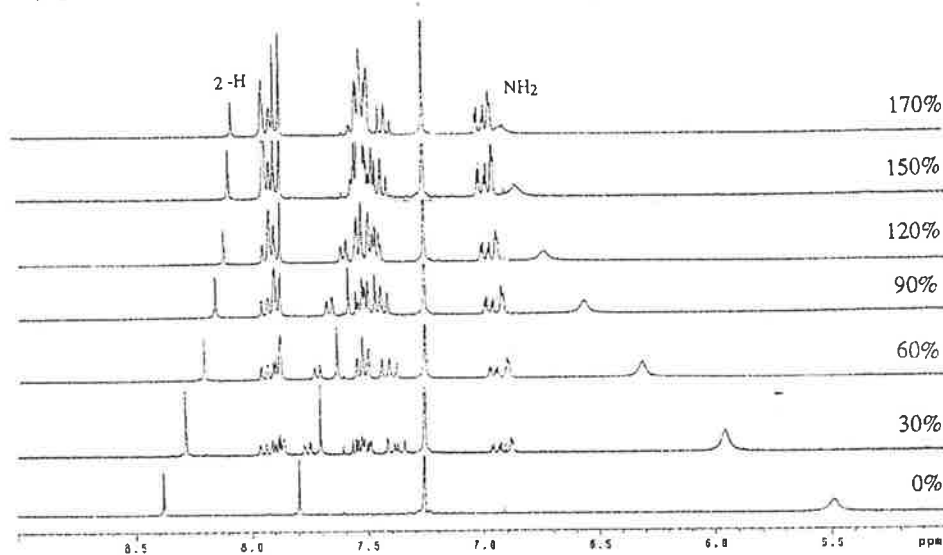


Figure 133. Titration of substrate 9-butyladenine with receptor Re-napha (**87**) in  $\text{CDCl}_3$  at rt.

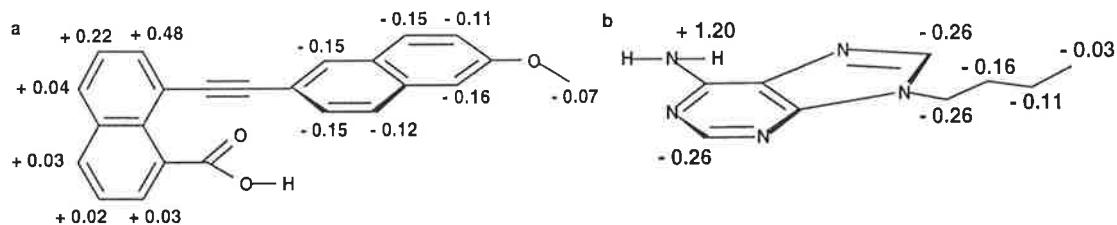


Figure 134. The changes of chemical shifts of receptor Re-napha (**87**) (a) and substrate 9-butyladenine (b), [**87**] = 1.0 mM, [butyladenine] = 1.0 mM at rt and in  $\text{CDCl}_3$  (ppm).

Both **Job plots** (Figure 135) and **Molar ratio plots** (Figure 136) show the 1:1 complexation between receptor Re-napha (**87**) and 9-butyladenine with an **association constant** of  $K_a = 1633 \text{ M}^{-1}$ .

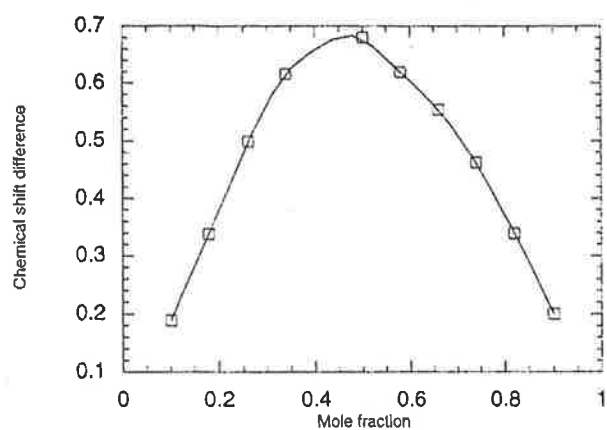


Figure 135. Job plot for complexation of receptor Re-napha (87) and 9-butyladenine.

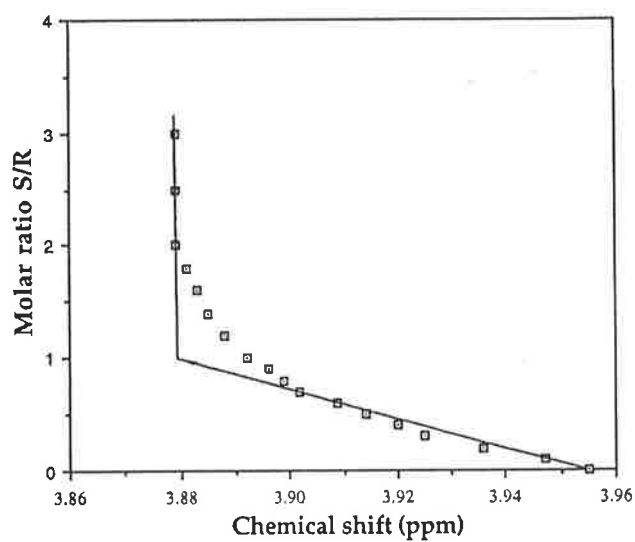


Figure 136. Molar ratio plots of the complexation of receptor Re-napha (87) and 9-butyladenine.

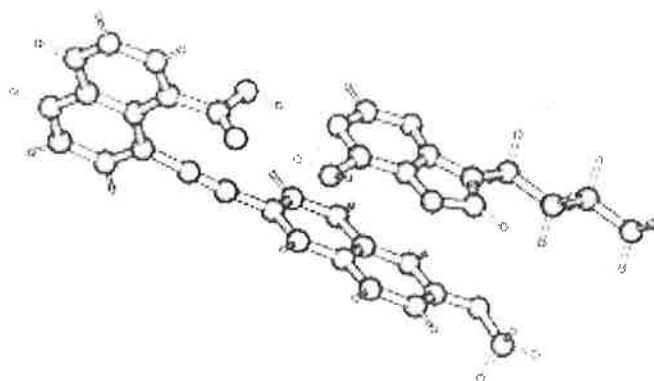
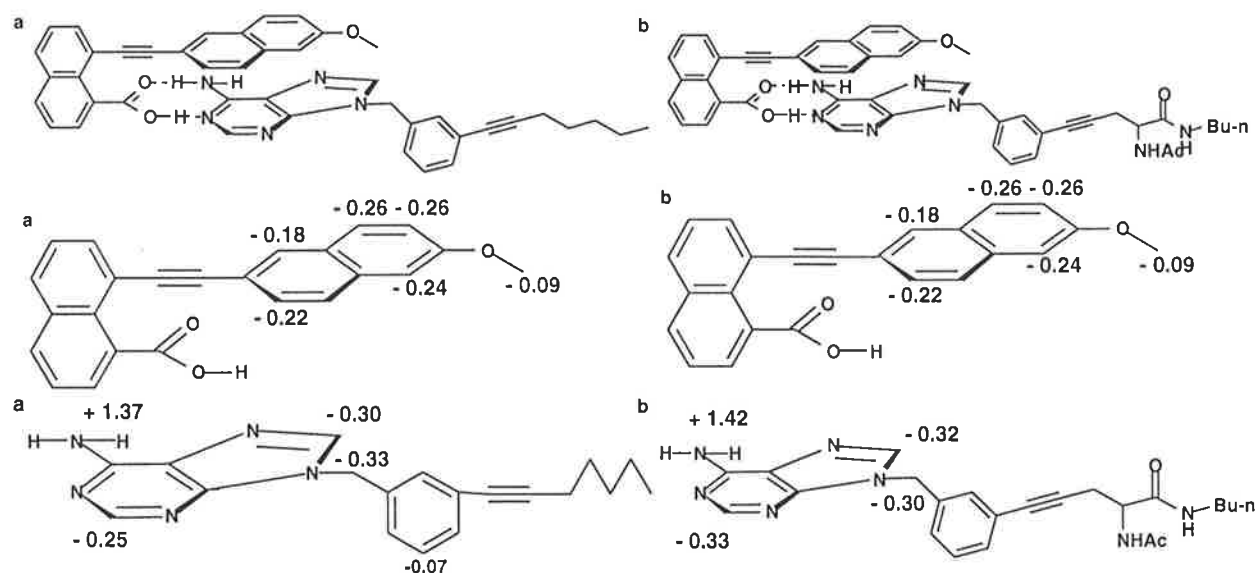


Figure 137. Molecular modelling structure of the complex between receptor Re-naphtha (87) and 9-butyladenine.

Receptor Re-napha (**87**) could also bind to adenine derivatives 3-(1'-pentynyl)-benzenemethyladenine (**71**) and **72**. The relevant chemical shift changes are shown in Figures 138 and 139. Both of these complexes showed the same downfield shift of the NH protons of the adenine and the upfield shift of the aromatic signals as for Re-napha (**87**).

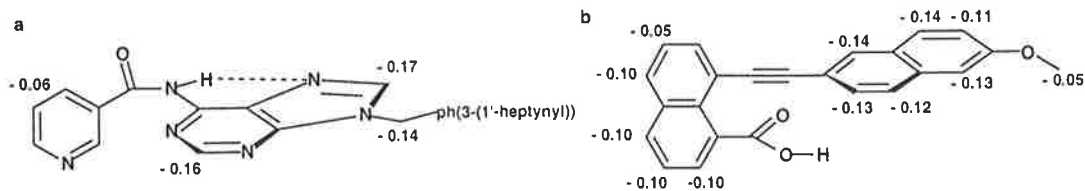


**Figure 138.** The possible complexes of receptor Re-napha (**87**) with adenine derivatives 3-(1'-pentynyl)-benzenemethyladenine (**71**) (a) or adeny amino acid diamide (**72**) (b). The changes of chemical shifts of receptor Re-napha (**87**) and substrate 3-(1'-pentynyl)-benzenemethyladenine (**71**) in their complex (a) and Re-napha (**87**) and adeny amino acid diamide (**72**) in their complex (b), [**87**] = 1.0 mM, [**71** or **72**] = 1.0 mM at rt and in  $\text{CDCl}_3$  (ppm).

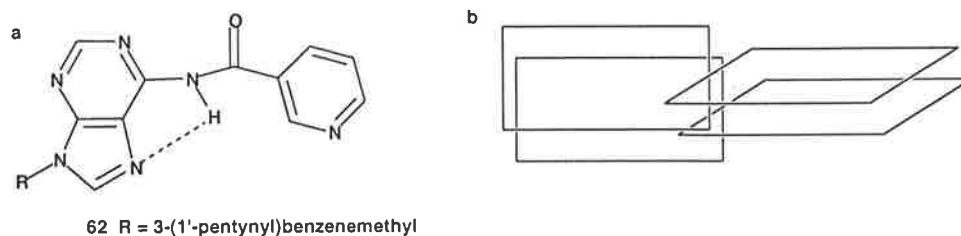
### 10.2.3 Molecular recognition of DNA base pair analogous with receptor Re-napha **87**

Figure 139a shows the changes of  $^1\text{H}$  NMR shifts for the 1:1 complex of **62** and **87** at 1 mM in  $\text{CDCl}_3$  at rt. Figure 139b shows the changes of  $^1\text{H}$  NMR shifts of receptor Re-napha (**87**) for [**87**] = 0.2 mM, [**62**] = 0.8 mM. The results suggest aromatic ring  $\pi$ - $\pi$  stacking (nicotinyl ring with naphthyl ring with carboxyl group; adeny ring with naphthyl with methoxy group) and accessible hydrogen bonding (carboxyl group with adenine).

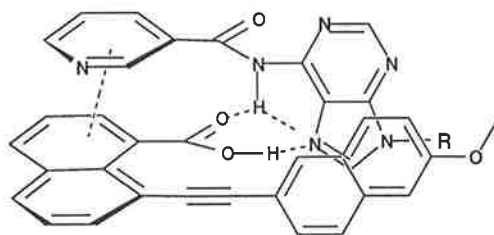
As discussed in Chapter 6, the base pair doublet analogue **62** (adenyl nicotinamide) can form an intra-molecular hydrogen bond as shown in Figure 140. DNA base pairs adopt a propeller twist structure, a consequence of Watson-Crick and Hoogsteen type hydrogen bonding and  $\pi$ - $\pi$  stacking interactions. The interactions between **62** and **87** involving both hydrogen bonds and  $\pi$ - $\pi$  stacking would then appear as outlined in Figure 141.



**Figure 139.** The changes of chemical shifts of substrate adenyl nicotinamide (**62**) (a) and receptor Re-natha (**87**) (b) after the binding in  $\text{CDCl}_3$  at rt. Specific conditions for (a)  $[\mathbf{87}] = 1.0 \text{ mM}$ ,  $[\mathbf{62}] = 1.0 \text{ mM}$ , for (b)  $[\mathbf{87}] = 0.2 \text{ mM}$ ,  $[\mathbf{62}] = 0.8 \text{ mM}$ .

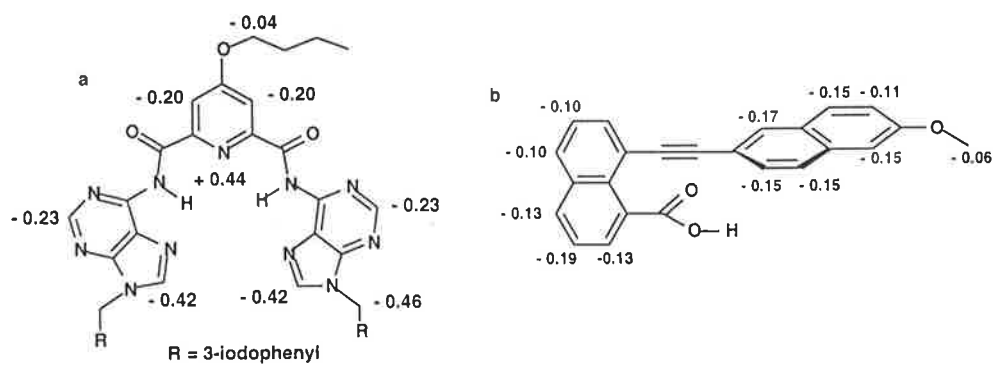


**Figure 140.** DNA base pair doublet analogue (**62**) (a) and the expected recognition model for the analogue (b).

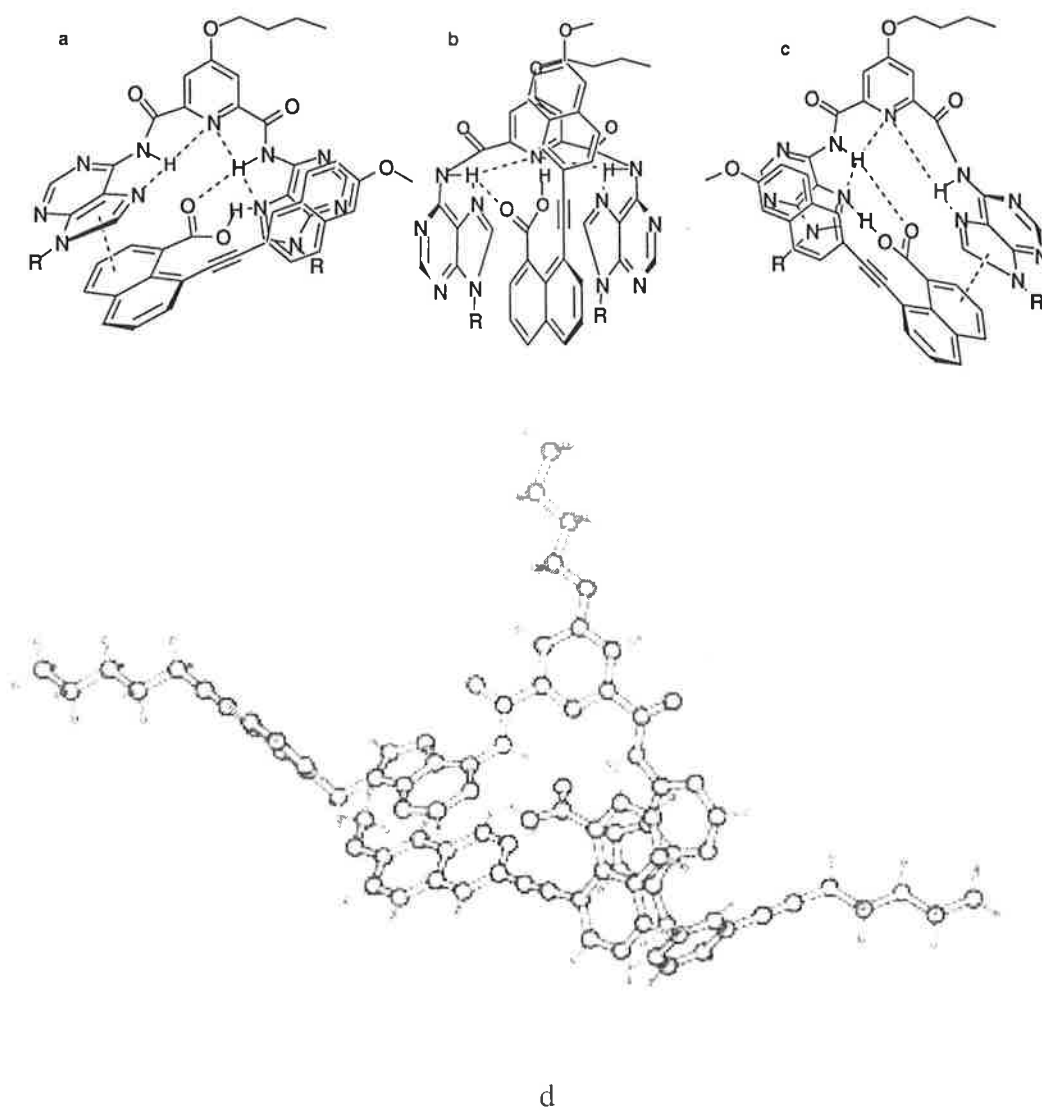


**Figure 141.** The expected molecular recognition of DNA base pair doublet analogue **62** by receptor Re-napha (**87**) with hydrogen bonding and  $\pi$ - $\pi$  stacking interactions.

Figure 142 shows the changes in  $^1\text{H}$  NMR resonances of receptor Re-napha (**87**) and **67** when mixed in a 1:1 ratio in dilute solution. The downfield shift in the NH resonances and the up-field shift in the aromatic resonances were consistent with hydrogen bonding and  $\pi$ - $\pi$  stacking. Three alternative arrangements reflecting this hydrogen bond and  $\pi$ - $\pi$  stacking are shown in Figure 143. The interactions between **69** and receptor Re-phtha **87** were hydrogen bonding between the carboxyl group and adenine NH and  $\pi$ - $\pi$  stacking between the methoxy naphthyl ring and adenine, as well as between the carboxyl naphthyl ring and adenine.

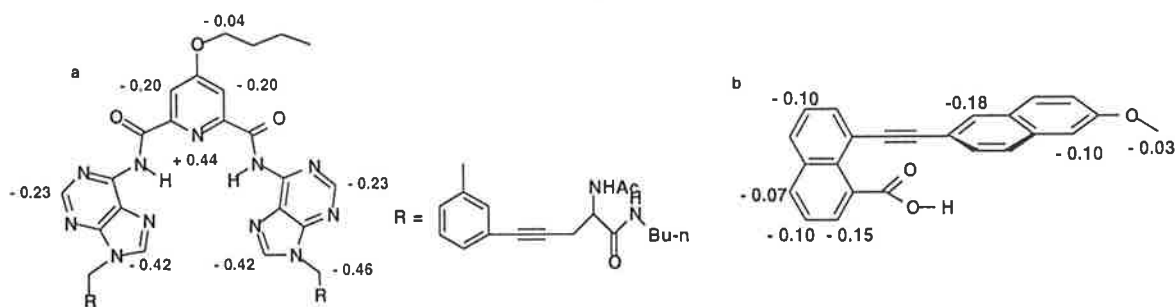


**Figure 142.** The changes of chemical shifts of substrate DNA base pair triplet analogue (R = 3-iodophenyl) (**67**) (a) and receptor Re-natha (**87**) (b) after the binding in  $\text{CDCl}_3$  at rt and  $[\text{R}] = 1.0 \text{ mM}$ ,  $[\text{S}] = 1.0 \text{ mM}$ .



**Figure 143.** Three different arrangements of the complexes between DNA base pair triplet analogues and the receptor Re-napha (**87**) (a, b and c) and molecular modelling of the complex (d).

Figure 144 shows the changes of chemical shifts for binding between synthetic receptor **69**, which is a modified amino acid diamide nucleic acid derivative, and **87** in a 1:1 ratio.



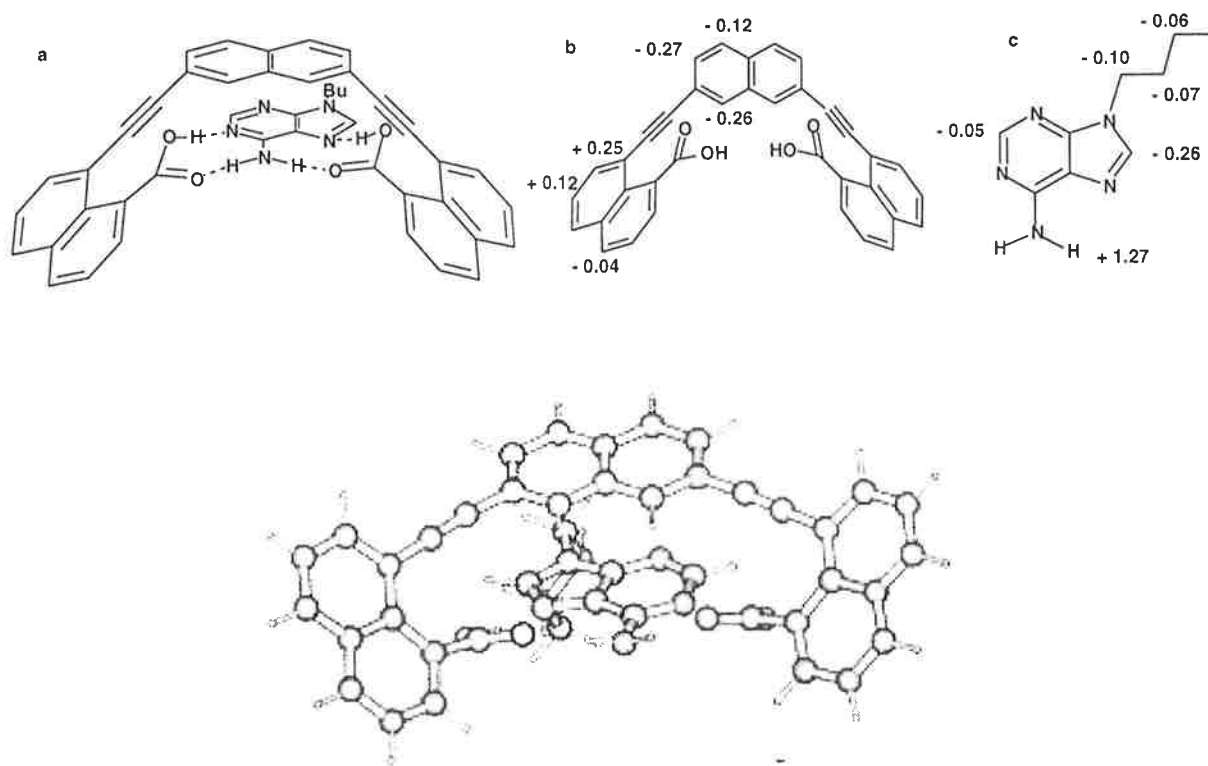
**Figure 144.** The changes of chemical shifts of **69** (a) and Re-napha (**87**) (b) after the binding in  $\text{CDCl}_3$  at rt and  $[\mathbf{87}] = 1.0 \text{ mM}$ ,  $[\mathbf{69}] = 1.0 \text{ mM}$ .

As shown above the receptor Re-napha (**87**) was a suitable receptor for binding adenine derivatives to a variety of substrates by  $\pi$ - $\pi$  stacking and Watson-Crick or Hoogsteen hydrogen bonding.

#### 10.2.4 Molecular recognition of adenine derivatives with receptor Re-naphdia **93**

The changes in proton NMR resonances for the receptor Re-naphdia (**93**) and 9-butyladenine in a 1:1 ratio in  $\text{DMSO-d}_6$  and  $\text{CDCl}_3$  are shown in Figure 145. Receptor **93** was not soluble in  $\text{CDCl}_3$  alone, so  $\text{DMSO-d}_6$  had to be added. The receptor was initially dissolved in  $\text{DMSO-d}_6$  then  $\text{CDCl}_3$  added. The NMR experiments also showed the broadening of the signals in the aromatic region on the diethynyl naphthalene when the binding of 9-butyladenine occurred. These results suggest the formation of both Watson-Crick and Hoogsteen hydrogen bonding and  $\pi$ - $\pi$  stacking interactions (Figure 145).



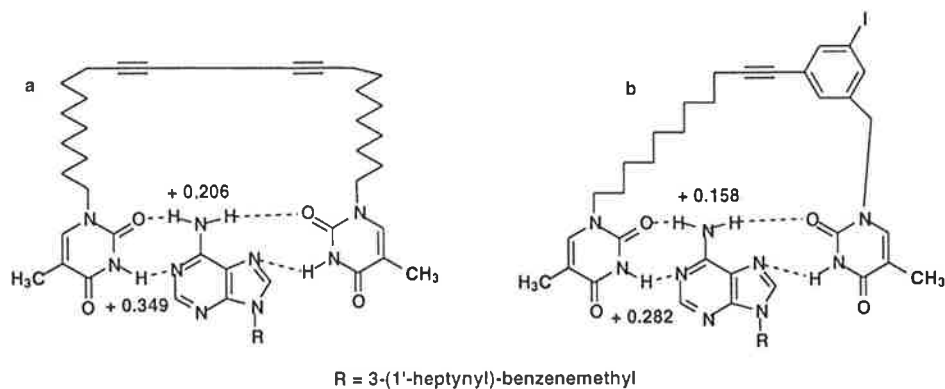


**Figure 145.** Molecular recognition of an adenine unit with both Watson-Crick hydrogen bonding (left) and Hoogsteen hydrogen bonding (right) and  $\pi$ - $\pi$  stacking interaction of the adenine ring with the diethynyl naphthyl ring. The changes of chemical shifts of receptor Re-naphdia (**93**) (b) and substrate 9-butyladenine (c) after the binding in 3.7% DMSO- $d_6$  in  $CDCl_3$  at rt and  $[93] = 1.0$  mM,  $[9\text{-butyladenine}] = 1.0$  mM, and molecular modelling of the complex.

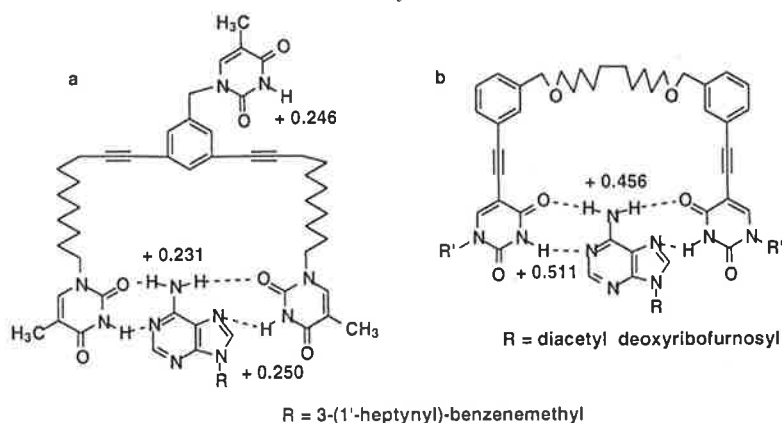
### 10.2.5 Molecular recognition of DNA by the formation of base pair triplet

Adenine can form a base pair triplet with uracil in DNA, such that both Watson-Crick and Hoogsteen hydrogen bonding are possible. Based on this model, the four receptors Re-c10 (**96**), Re-bc10 (**101**), Re-tric10 (**100**) and Re-oc10 (**106**) were prepared and their binding to adenine derivatives was investigated. The binding and the complex structures between the receptors and corresponding adenine derivatives are shown in Figure 146 and Figure 147.

As shown in the Figures 146 and Figure 147, the changes of proton chemical shifts are indicative of both Watson-Crick and Hoogsteen hydrogen bonding. The interaction of the adenine unit with both uracil units in Re-c10 (**96**) would be expected to be stronger than for Re-bc10 (**101**), due to the steric effect during the formation of complexes. This expectation was confirmed by the changes in proton chemical shifts shown in Figure 146. The largest changes in proton chemical shifts were shown by a 1:1 mixture of **106** and **97**, indicating that this combination provides the optimum arrangement for hydrogen bonding.



**Figure 146.** The proposed complexes between (a) **96** and **71** and (b) **101** and **71**. The changes in proton chemical shifts from  $[\mathbf{96}] = 1.0 \text{ mM}$ ,  $[\mathbf{71}] = 1.0 \text{ mM}$  for (a) and  $[\mathbf{101}] = 0.65 \text{ mM}$ ,  $[\mathbf{71}] = 0.65 \text{ mM}$  and (b) at rt and in  $\text{CDCl}_3$  (ppm).



**Figure 147.** The proposed complexes between (a) **100** and **71** and (b) **106** and triacetyl adenosine. The changes in proton chemical shifts from  $[\mathbf{100}] = 0.80 \text{ mM}$ ,  $[\mathbf{71}] = 0.80 \text{ mM}$  for (a) and  $[\mathbf{106}] = 0.75 \text{ mM}$ ,  $[\text{triacetyl adenosine}] = 0.75 \text{ mM}$  for (b) at rt and in  $\text{CDCl}_3$  (ppm).

## 10.2.6 Intra-molecular recognition of nucleobases

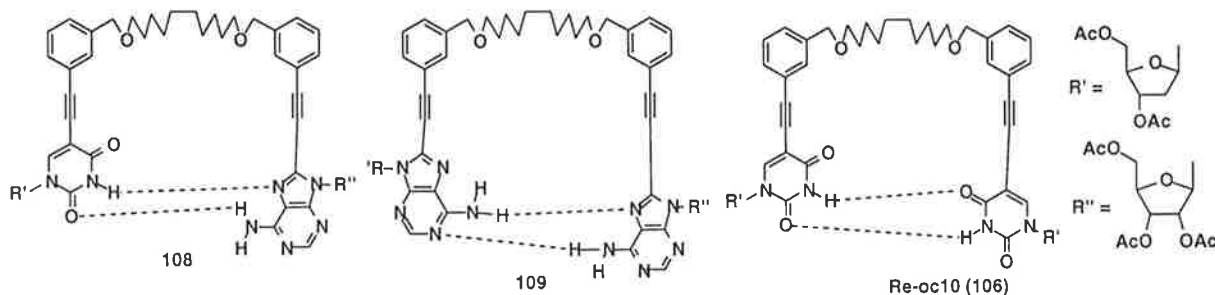
### 10.2.6.1 Intra-molecular hydrogen bonding within a DNA base pair and nucleobases

As shown in Table 40, the chemical shift for the NH proton of thymine in C10-2U (Re-oc10) (**106**) was 8.86 ppm at 1 mM and rt in  $\text{CDCl}_3$ , which was larger than the corresponding value 8.05 ppm for compound C10-1U (**107**), indicating that Re-oc10 (**106**) forms a stronger intra-molecular hydrogen bond (Figure 148). The value for C10-U-A (**108**) was 9.65 ppm, which reflects a stronger intra-molecular hydrogen bond for this complex (Figure 148). The proton chemical shift of the NH group of adenine derivative C10-1A (**110**) at 1 mM at rt in  $\text{CDCl}_3$  was 5.66 ppm, that for C10-2A (**109**) was 5.89 ppm, which was indicative that the double adenine units in this compound **109** form intra-molecular hydrogen bonding (Figure 148). The  $\Delta\delta_{\text{NH}}/\Delta T$  values for the NH protons were obtained by variable temperature NMR experiments from  $-60 \text{ }^\circ\text{C}$

to 60 °C. Compounds **106**, **108** and **109** were investigated for intra-molecular hydrogen bonding interactions. As for compound C10-1A-1U (**108**), the temperature dependency of the NH in thymine was as high as 42.6 ppb/K, which was much larger than the corresponding value for **106** (23.2 ppb/K) (Table 40). Furthermore, the  $\Delta\delta_{\text{NH}}/\Delta T$  value for the amino group of adenine in **108** was 21.1 ppb/K, while compound **109** was only 9.6 ppb/K also indicating an efficient hydrogen bond with thymine. The  $\Delta\delta_{\text{NH}}/\Delta T$  values for compounds **109** show that DNA bases will be involved in hydrogen bonding with themselves if placed in a suitable conformation.

**Table 40.** Chemical Shifts (ppm) at rt (Temperature Dependencies (ppb/K)) of NHe Protons in Thymine (NH) and Adenine (NH<sub>2</sub>) at 1mM in CDCl<sub>3</sub>.

Compound	NH	NH <sub>2</sub>
C10-1U ( <b>107</b> )	8.05	
C10-2U (Re-oc10 ( <b>106</b> ))	8.86 (23.2)	
C10-1A ( <b>110</b> )		5.66
C10-2A ( <b>109</b> )		5.89 (9.6)
C10-1A-1U ( <b>108</b> )	9.65 (42.6)	5.66 (21.1)



**Figure 148.** Possible intramolecular hydrogen bonding in synthetic DNA base pair doublet (**108**), receptor Re-oc10 (**106**) and compound **110**.

### 10. 2. 6. 2 DNA base pair doublet series

Figure 149 shows the NMR spectra of compounds **111-116** as 5 mM solutions in CDCl<sub>3</sub>. These spectra show the effect of varying the distance between the adenine and thymine rings and the proton NMR shifts. For all the compounds, the signals for the aromatic proton on thymine appeared at the same position, however, the peaks for H-2 and H-8 of adenine were quite different with different chain length. When *n* varied from 5 to 9, the positions of the peaks for H-2 did not change significantly. However, the signal for H2 shifted up-field in compound **111**

and the signal for H8 shifted downfield, which suggests that both the amino group and 8-H of adenine in compound **111** are involved in efficient Hoogsteen type intra-molecular hydrogen bonding (Figure 150). Further evidence for intra-molecular hydrogen bonding was the chemical shift of the amino group of compound **111**, which at 8.151 ppm was further downfield than **112-116**. When  $n$  was odd, strong hydrogen bonding and the formation of a DNA base pair was observed, whereas when  $n$  was even hydrogen bonding was not as favored.

The changes in the chemical shifts of H2, H8 and NH<sub>2</sub> in compound **116** are shown in Figure 151 and show the effect of introducing a thymine group to the terminus of the aliphatic chain. The data suggest that H8 is more likely to be involved in the DNA base pair doublet interactions than H2, since the change of <sup>1</sup>H NMR resonance for H8 is very significant but not for H2. Therefore, the Hoogsteen type hydrogen bonding was preferred in forming the base pair doublet in this molecule.

Compound **119** was also applied to the study of the formation of a DNA base pair doublet. Figure 152 shows the changes in the chemical shifts of H2, H8 and NH<sub>2</sub> in compound **119**, compared to compound **118** with the same adenine unit. The data are compatible with the formation of a DNA base pair doublet and the preferential formation of the Hoogsteen-type hydrogen bonding, since the change of the proton H8 is more significant than H2. Molecular modelling showed the energy (- 45.667 kcal/mol) for the conformation of the DNA base pair doublet with Hoogsteen type hydrogen bonding was lower than that with Watson-Crick type hydrogen bonding (- 43.44 kcal/mol) (Figure 153).

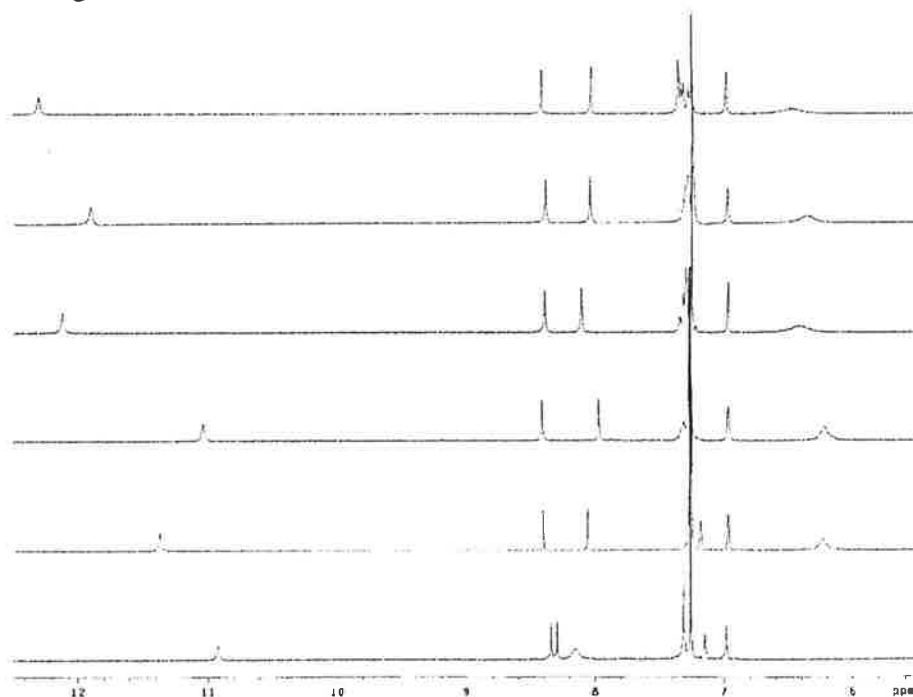
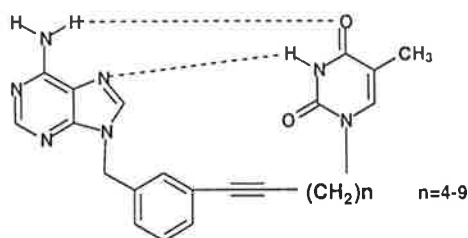
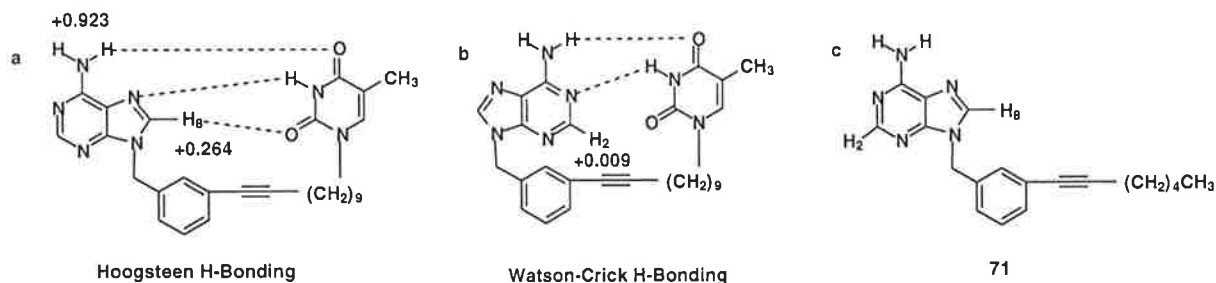


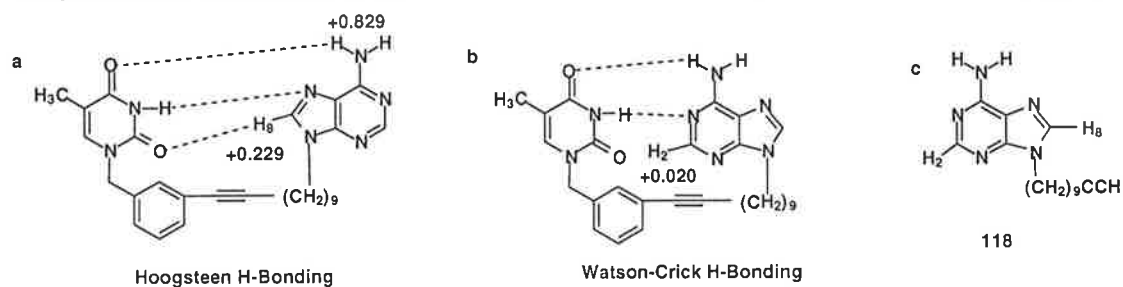
Figure 149. The accumulated NMR spectra of compounds **111-116** from bottom to top at 5 mM and rt in CDCl<sub>3</sub>.



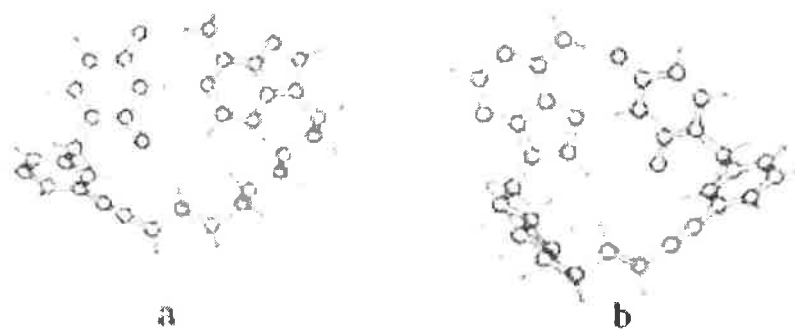
**Figure 150.** Possible intra-molecular hydrogen bonding DNA base pair doublets for **111-116**.



**Figure 151.** DNA base pair doublets with Hoogsteen H-bonding (a) and Watson-Crick H-bonding (b) in compound **116**. The changes of chemical shifts are referenced to **71**, 2 mM at rt and in CDCl<sub>3</sub> (ppm).



**Figure 152.** DNA base pair doublets with Hoogsteen H-bonding (a) and Watson-Crick H-bonding (b) in compound **119** and compound **118** with similar structure. The changes of chemical shifts are referenced to compound **118** with the same adenine unit at 2 mM and rt and in CDCl<sub>3</sub> (ppm).



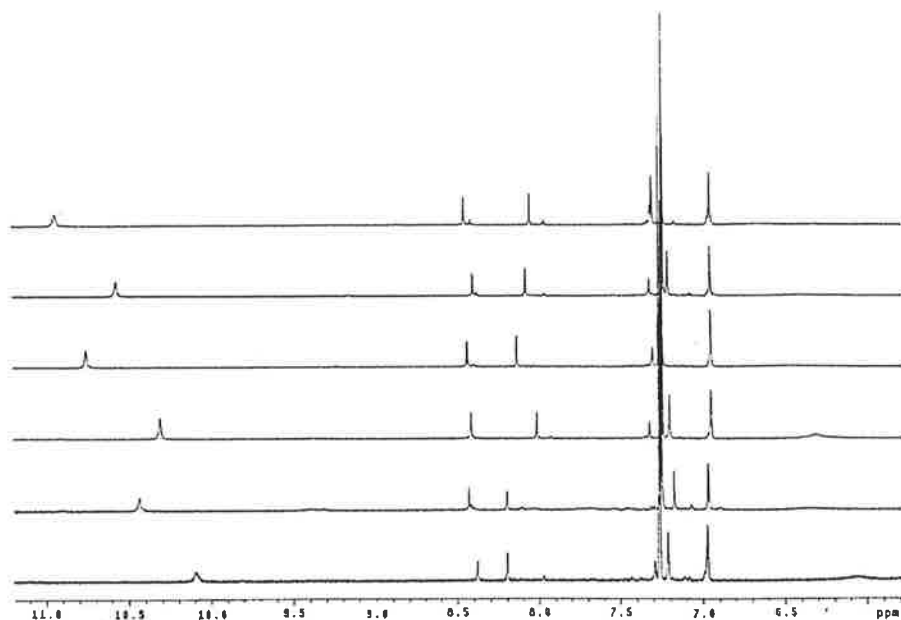
**Figure 153.** Molecular modelling structures of the conformations with Hoogsteen and Watson-Crick types hydrogen bonding interactions in compound **119**.

### 10. 2. 6. 3 DNA base pair triplet series

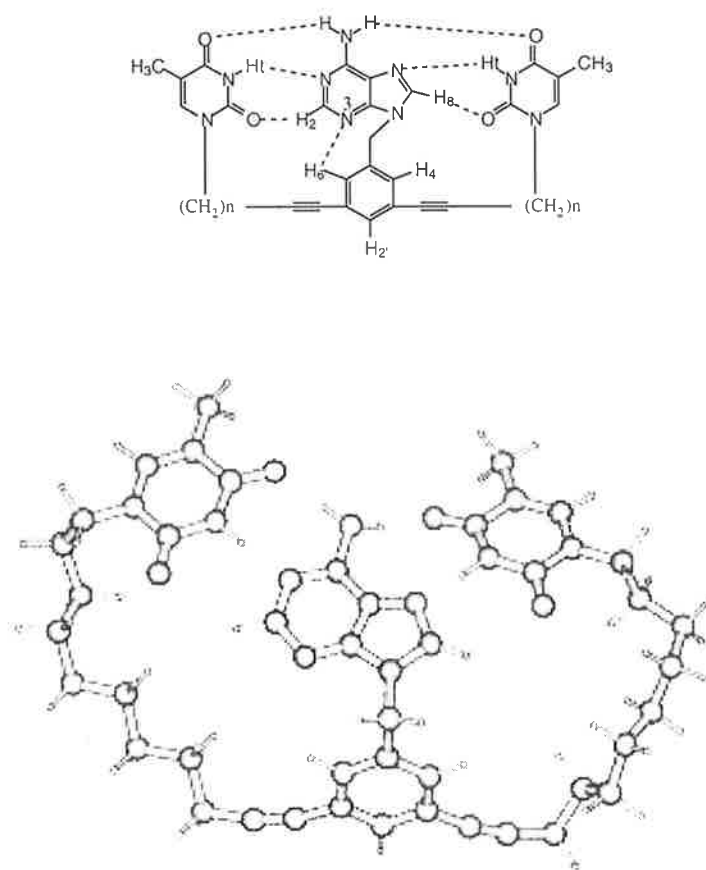
Figure 154 shows the accumulated NMR spectra of compounds **121-126** from 5.8-11.2 ppm. The  $^1\text{H}$  NMR signals of the aromatic protons on thymine and the 2 position of the phenyl group appear almost at the same position from compounds **121** to **126**, however, the chemical shifts of the aromatic protons of adenine H2 and H8 and phenyl protons H4 and H6 are very different for different  $n$  number. The greatest change of chemical shift for H8 was + 0.083 ppm from  $n = 4$  to  $n = 9$ , that for H2 was - 0.174 ppm from  $n = 4$  to  $n = 6$  and that for H4 and H6 were 0.147 ppm from  $n = 5$  to  $n = 9$ , which indicate these protons are in the shielding or deshielding areas and suggest they are in the environment of the formation of base pair triplets between one adenine and two thymine units. The protons H2 and H8 of adenine should be involved in efficient Watson-Crick and Hoogsteen type hydrogen bonding respectively (Figure 155). The proton H6 of the phenyl group is likely to have effective contact with the nitrogen atom (N-3) of adenine, since molecular modelling of the base pair triplet also shows the distance between the atoms was 2.8 Å (Figure 155).

The evidence for the formation of base pair triplets can also be observed from the alternating downfield movement of protons Ht of thymine and the amino proton of adenine from  $n = 4$  to  $n = 9$ . The results show the DNA base pair triplets are more likely to form when the  $n$  number is greater and the aliphatic chain is longer. Figure 154 also shows when  $n$  was odd, the conformations of the compounds were favorable for the stronger base pair triplets and hydrogen bonding interactions. This result is consistent with that from the base pair doublets as shown in Figure 149.

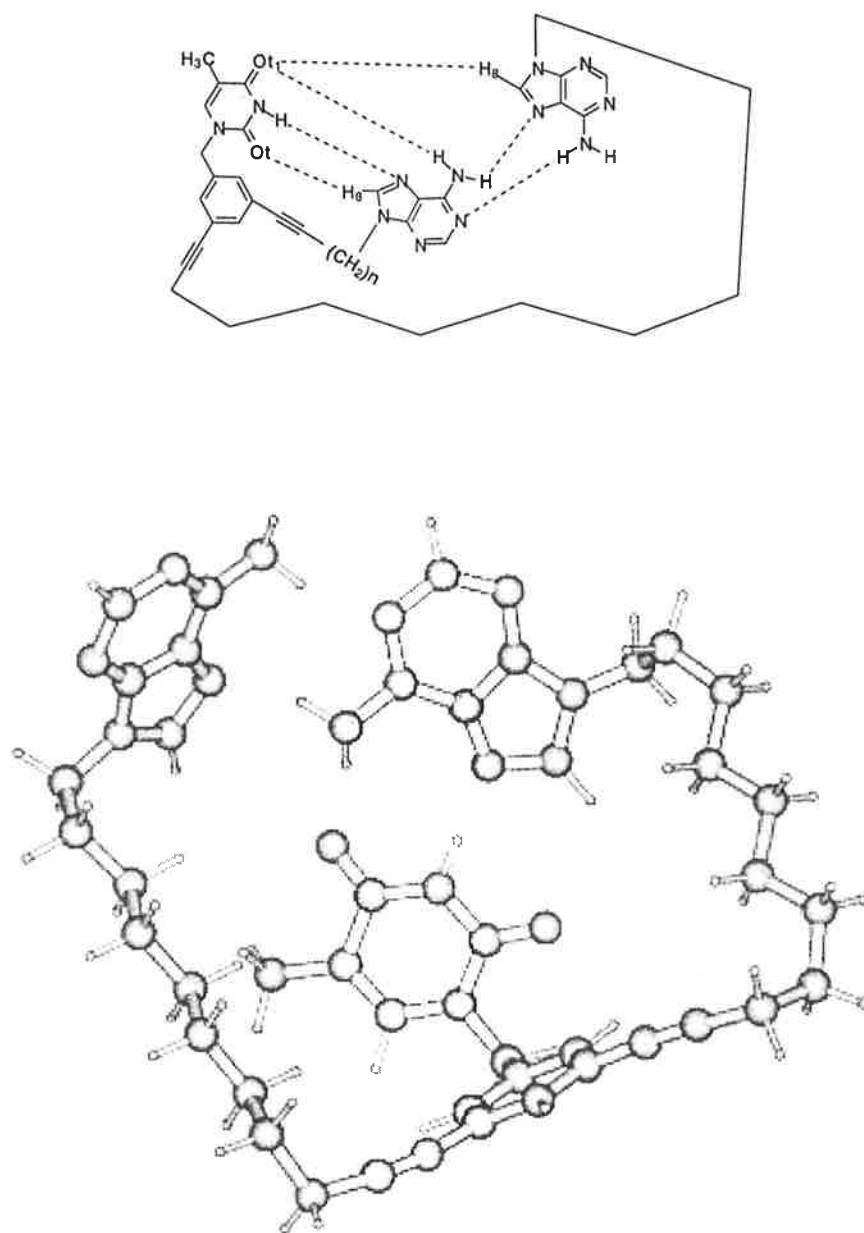
The DNA base pair triplet between two adenine and one thymine units was also observable in compound **127** (Figure 156), by comparing the  $^1\text{H}$  NMR chemical shifts of relevant protons in compound **119** (Figure 152) in  $\text{CDCl}_3$  at 2 mM and rt. The chemical shift of NHt in thymine of compound **119** was 12.45 ppm, that for **127** was 13.18 ppm, which showed that the thymine proton was involved in a stronger hydrogen bond in compound **127** compared to **119**. Furthermore the chemical shift of adenine proton H8 in compound (**127**) was 7.918 ppm, the corresponding proton in compound **118** was 7.788 ppm, the difference was + 0.130 ppm, which is due to the binding effect caused by the thymine and suggests that this proton is involved in the interaction with both Ot and Ot1 as shown in Figure 156. Molecular modelling of compound **127** showed the distance between H8 and Ot1 was 3.5 Å, which is less than 4 Å and suggestive for the involvement of a weak interaction. However, the change of the chemical shift of proton H2 of adenine is + 0.006 ppm, so this downfield movement is not significant. Therefore, the formation of the Hoogsteen type hydrogen bonding interactions also have preference over Watson-Crick type hydrogen bonding in the DNA base pair triplet as shown in Figure 156.



**Figure 154.** The accumulated NMR spectra of compounds **121-126** from bottom to top at 2 mM and rt in  $\text{CDCl}_3$ .



**Figure 155.** Possible intra-molecular hydrogen bonding DNA base pair triplets for compounds **121-126** (a) and its molecular modelling structure (b) for **126**.



**Figure 156.** Possible intra-molecular hydrogen bonding for the DNA base pair triplet of **127** (a) and its molecular modelling structure.



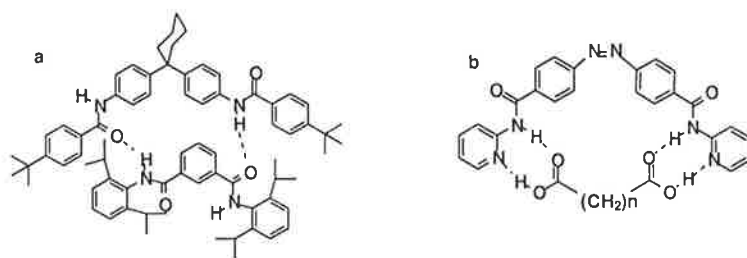
## Chapter 11

# Recognition of Biotin-5'-AMP Analogues with Synthetic Receptors

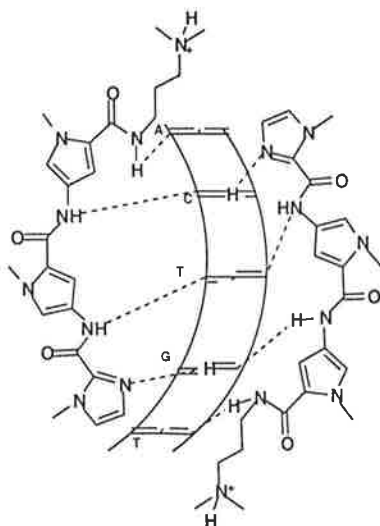
### 11.1 Introduction

Biotin-5'-AMP is the intermediate formed in the post-translational modification of biotin dependent-enzymes, BCCP, during the first committed step of the biosynthesis of aliphatic acids.<sup>21</sup> The biotin operon repressor, BirA, serves both as the biotinylation activating enzyme and a transcriptional regulator. It binds biotin together with ATP and catalyzes the formation of biotin-5'-AMP. It then assists the transfer of the intermediate and biotinylation of a specific lysine residue on the carboxyl carrier protein, a subunit of acetyl-CoA carboxylase. If all the BCCP in the cells have been biotinylated, the BirA-biotinyl-5'-AMP complex accumulates and binds to the 40-base-pair bio-operator, repressing transcription of the biotin biosynthetic genes.<sup>19</sup> However, the structural details of binding in the complex of BirA-biotin-5'-AMP still remains an open question, although the nature of the biotin- and DNA-binding domains have been proposed.<sup>19</sup> Recent findings on the interactions of BirA with biotin containing enzyme holo-BCCP did not show any specific involvement of the biotin unit at all.<sup>16</sup>

In biology complex systems bind together through multiple, simultaneous molecular interactions, and display unique collective properties that are stronger than the corresponding monovalent interactions.<sup>106</sup> Hunter and co-workers reported the cooperative binding of a substrate by a receptor with two binding sites (Figure 157a).<sup>276</sup> Hydrogen bonding induced configurational locking of a photoresponsive receptor was also reported for a dicarboxylic acid through two binding sites as shown in Figure 157b. Recently, Dervan and co-workers reported the hairpin polyamide binding model based on the multiple hydrogen bonding interactions between the pyrrole-imidazole polyamide receptor and oligo-nucleotide substrate 5'-TGTTA-3' as shown in Figure 158.



**Figure 157.** Molecular recognition of substrates with multiple binding sites by receptors (a) and (b).



**Figure 158.** Hairpin polyamide binding model for the complex formed between pyrrole-imidazole polyamide receptor and oligo-nucleotide substrate.

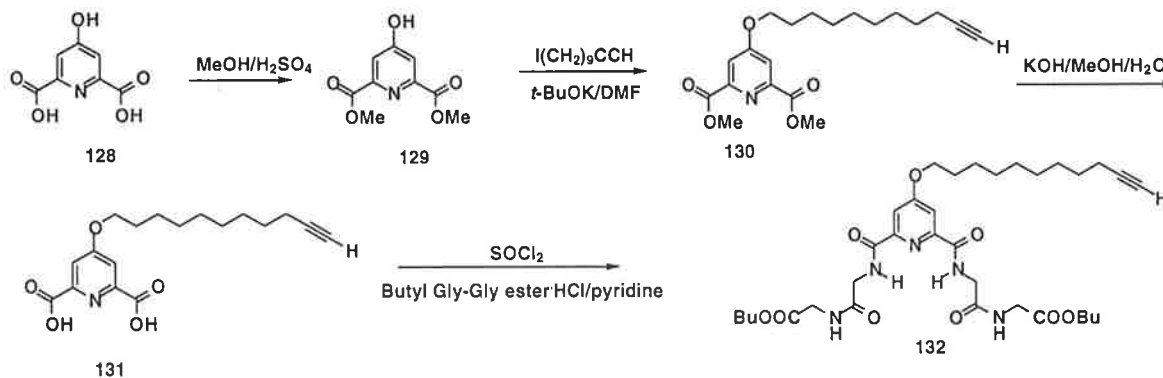
## 11.2 Results and Discussion

### 11.2.1 Synthesis of receptors

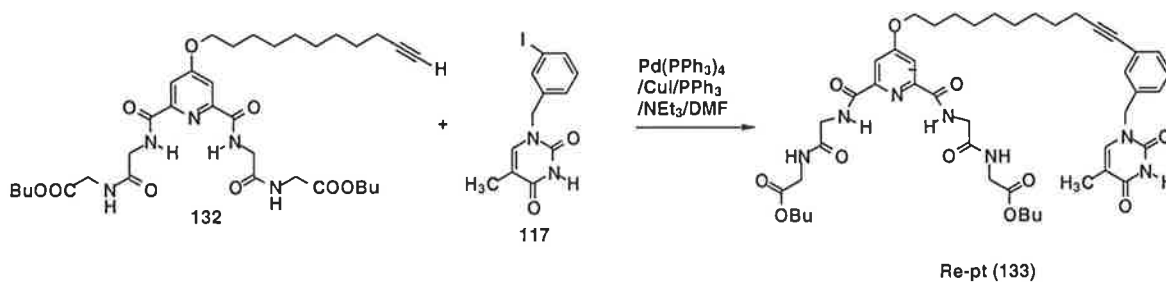
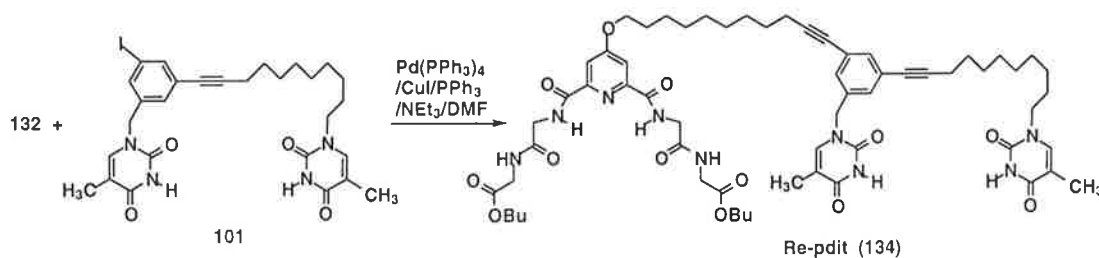
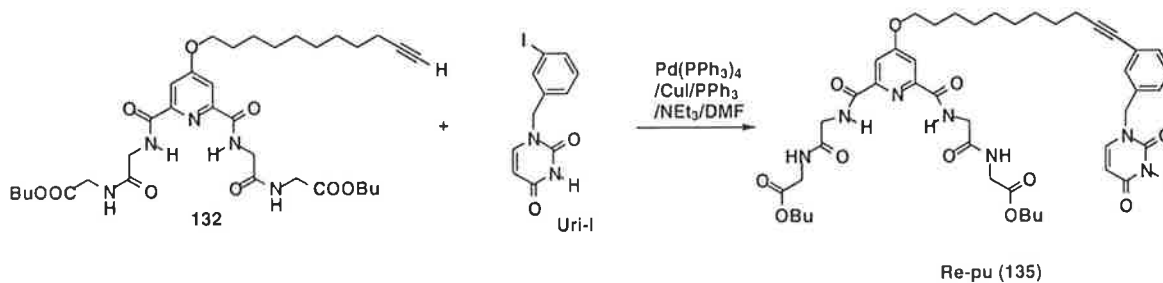
#### 11.2.1.1 Synthesis of receptors Re-pt (133), Re-pdit (134), Re-pu (135), Re-pc (137) and Re-pthiou (136)

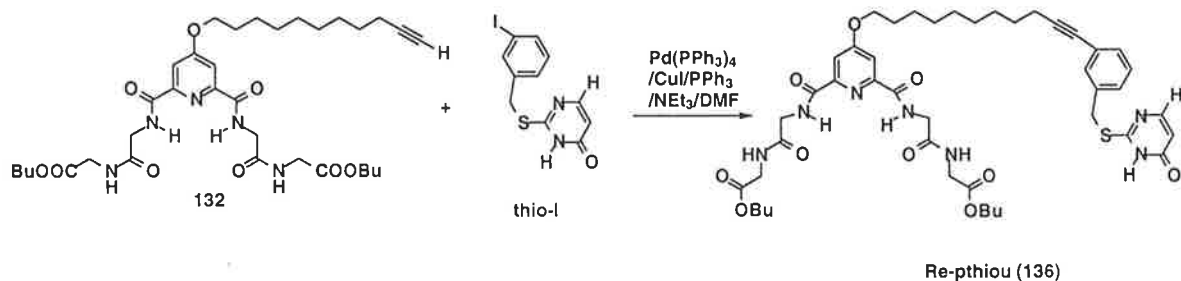
In order to establish a model for the binding of biotin-5'-AMP with BirA, the receptors Re-pt (133), Re-pdit (134), Re-pu (135), Re-pc (137), Re-pthiou (136) and Re-pau (142) were synthesized and were expected to show multiple, intermolecular hydrogen bonding and  $\pi$ - $\pi$  stacking interactions.

The synthesis of the receptors began with the preparation of the common unit **132**. 4-Hydroxy-2,6-pyridinedicarboxylic acid was esterified with methanol in the presence of sulfuric acid and product **129** was isolated after removal of methanol and neutralization with saturated sodium bicarbonate solution. Alkylation of **129** was accomplished with *t*-BuOK and 11-iodo-1-undecyne in DMF and **130** was isolated. The hydrolysis of compound **130** required hot potassium hydroxide in methanol with a small amount of water. The common unit **132** was prepared by the established procedure discussed previously for pyridinedicarboxamides in Scheme 26.

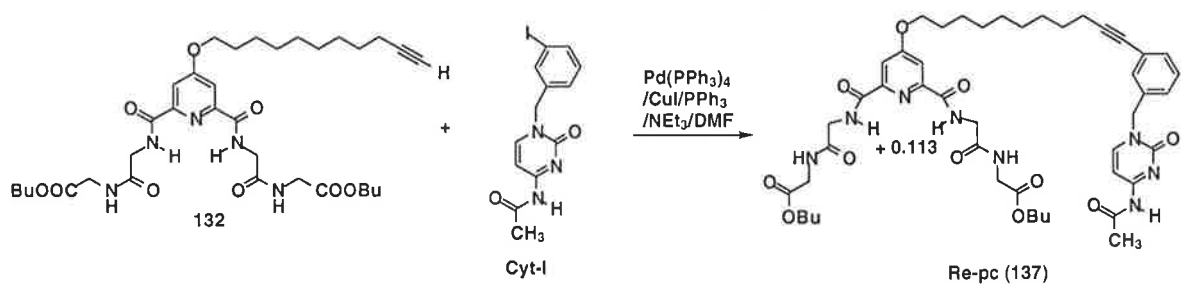
Scheme 26. Synthesis of acetylene precursor **132**.

The receptors Re-pt (**133**), Re-pdit (**134**), Re-pu (**135**), Re-pc (**137**), Re-pthiou (**136**) were prepared by the  $\text{Pd}(\text{PPh}_3)_4$  catalysed coupling reactions involving precursor **132** and the corresponding iodo compounds, **117**, **101**, **Uri-I**, **Cyt-I** and **Thio-I**, as shown in Schemes 27-31.

Scheme 27. Synthesis of receptor Re-pt (**133**).Scheme 28. Synthesis of receptor Re-pdit (**134**).Scheme 29. Synthesis of receptor Re-pu (**135**).



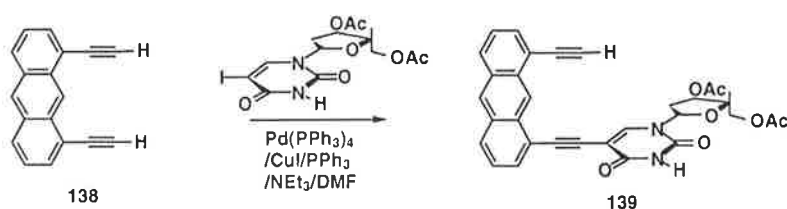
Scheme 30. Synthesis of receptor Re-ptiou (136).



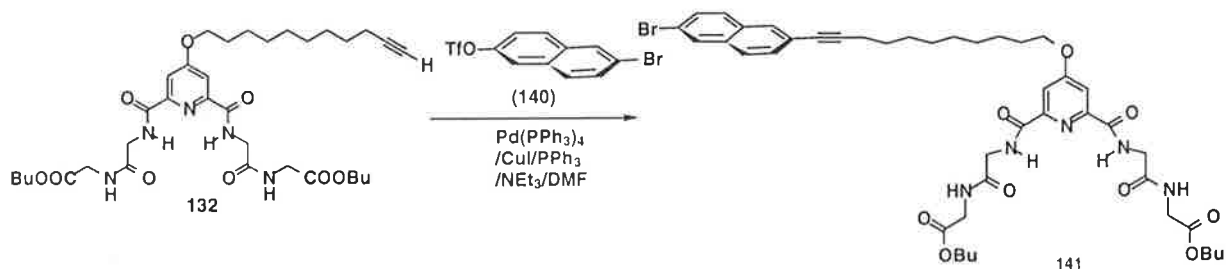
Scheme 31. Synthesis of receptor Re-pc (137).

### 11.2. 1. 2 Synthesis of receptor Re-pau (142)

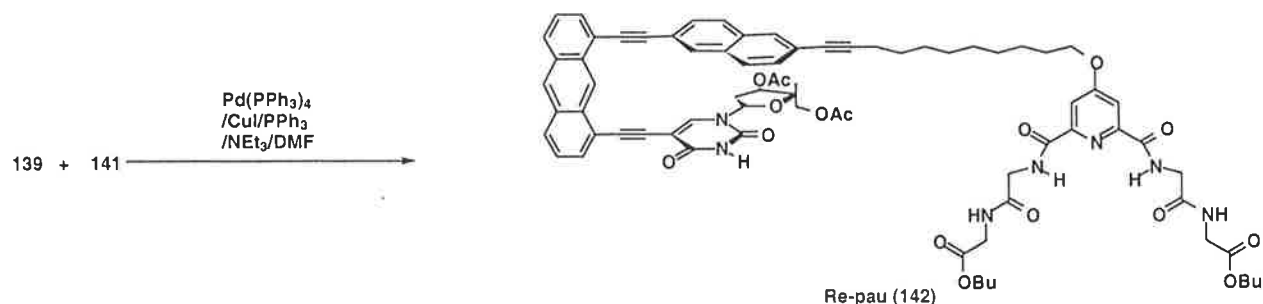
The preparation of receptor Re-pau (142) is outlined in Schemes 32-34. The palladium catalysed coupling reaction of 1, 8-diethynylantracene with triacetyl 8-iodo-deoxyuridine resulted in the formation of compound 139, and that of 132 with 140 resulted in the formation of 141. The following coupling reaction was then carried out by the reaction of precursors 139 and 141 in the presence of palladium catalyst Pd(PPh<sub>3</sub>)<sub>4</sub> to give 142 (Scheme 34).



Scheme 32. Preparation the precursor 139.



Scheme 33. Preparation the precursor 141.



Scheme 34. Synthesis of receptor Re-pau (142).

### 11. 2. 2 Molecular recognition of Bt-Ade (51)

The binding of biotinyl adenine Bt-Ade (**51**), an analogue of biotin-5'-AMP, with receptor Re-pt (**133**) is shown in Figure 159. The changes in the  $^1\text{H}$  NMR chemical shifts of protons on both receptor and substrate are listed in Figure 159a. The molecular modelling structure of the complex between **133** and **51** is shown in Figure 159b. Figure 160 shows the  $^1\text{H}$  NMR chemical shift changes for biotinyl adenine Bt-Ade (**51**) in the binding with receptor Re-pdig (**75**), which is a structurally simpler version of receptor **133**. As shown in Figure 159, the receptor Re-pt (**133**) can bind to Bt-Ade (**51**) by the formation of up to 8 hydrogen bonds. Figure 160 shows the binding of the receptor Re-pdig (**75**) with biotinyl adenine Bt-Ade (**51**) and the changes in proton chemical shifts for the NH groups and indicates hydrogen bonding with the tetrapeptide unit of **75**. In the complex of receptor Re-pt (**133**) with Bt-Ade (**51**), the tetrapeptide unit can bind to the biotin and amide side chain, and the binding between them becomes much stronger than that in the complex of Re-pdig (**75**) with Bt-Ade (**51**). The binding of adenine with thymine in the complex of Re-pt (**133**) with Bt-Ade (**51**) promotes the binding of the biotin unit with the tetrapeptide of the receptor **133**. A comparison of the changes of proton chemical shifts in Figures 159 and 160 show the cooperative effect of the additional hydrogen bonding possible for receptor **133**.

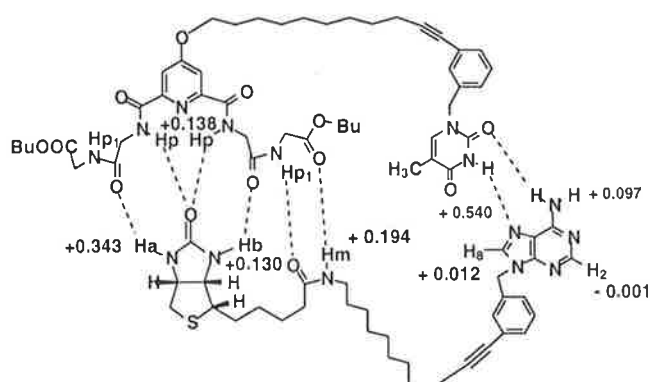
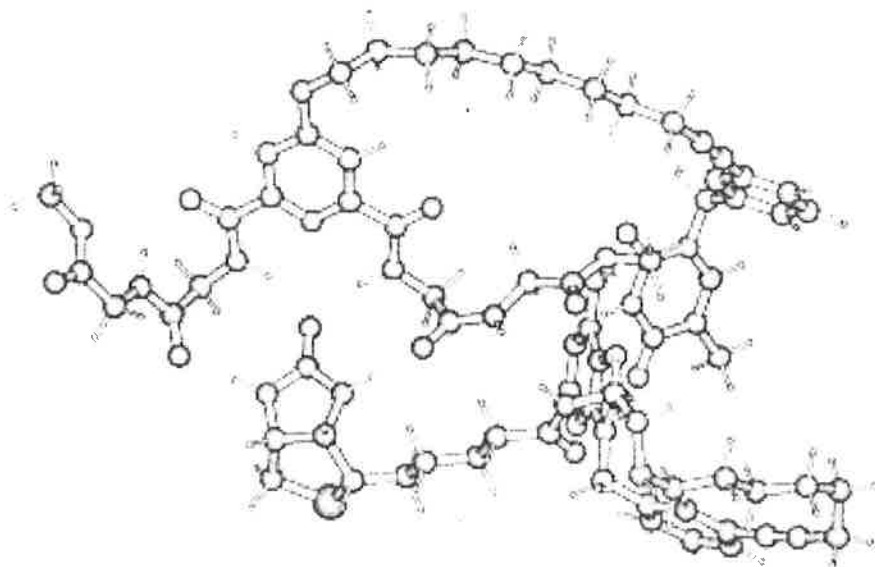
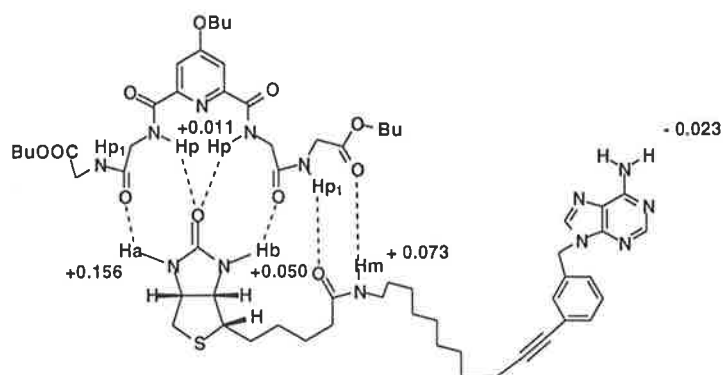


Figure 159a. The complex of biotinyl adenine Bt-Ade (**51**) with receptor Re-pt (**133**), [**133**] = 1.0 mM, [**51**] = 1.0 mM at rt and in  $\text{CDCl}_3$  (ppm).

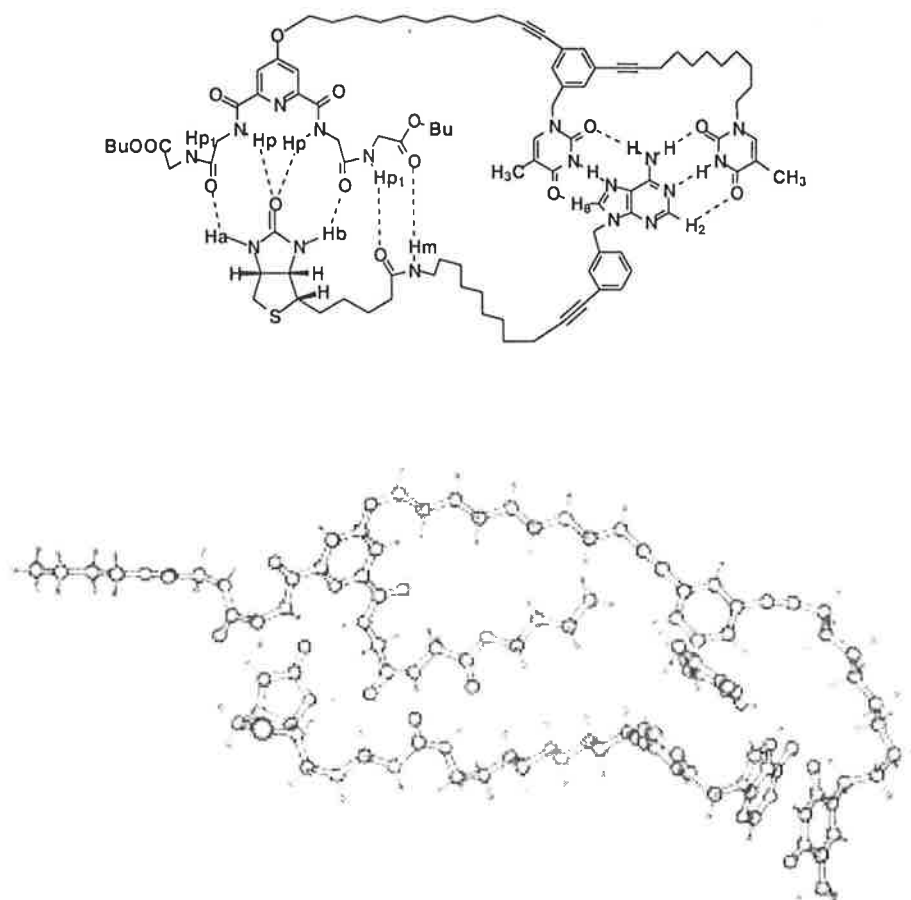


**Figure 159b.** Molecular modelling structure of the complex of biotinyl adenine Bt-Ade (**51**) with receptor Re-pt (**133**).

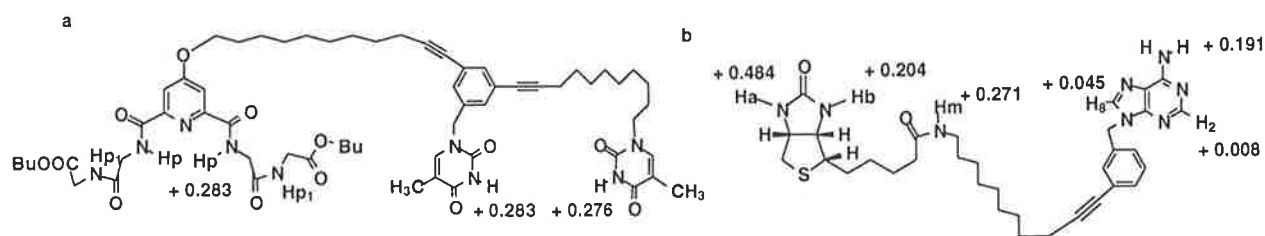


**Figure 160.** Proton chemical shift changes for the complex of biotinyl adenine Bt-Ade (**51**) with receptor Re-pdigg (**75**), [**51**] = 1.0 mM, [**75**] = 1.0 mM at rt and in  $\text{CDCl}_3$  (ppm).

Figure 162 shows the changes in the proton chemical shifts for a 1:1 mixture of Re-pdit (**134**) and Bt-Ade (**51**) after the binding, which are indicative that this binding is much stronger than that in the complex between Re-pt (**133**) with Bt-Ade (**51**), as the individual change in chemical shifts of the NH protons in **51** and **134** after the binding were much larger than the corresponding values for **51** and Re-pt (**133**). The molecular modelling structure of the complex between **134** and **51** is also shown in Figure 162. In the complex of Re-pdit (**134**) with Bt-Ade (**51**), the adenine unit of Bt-Ade (**51**) can form a DNA base pair triplet with the two thymine units, promoting the binding of the biotin amide unit with the tetrapeptide unit.

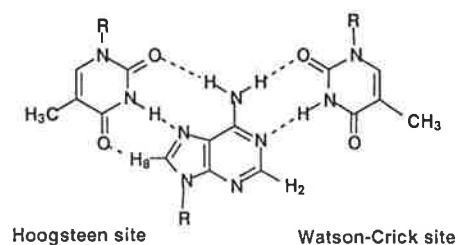


**Figure 161.** The complex of biotinyl adenine Bt-Ade (**51**) with receptor Re-pdit (**134**).



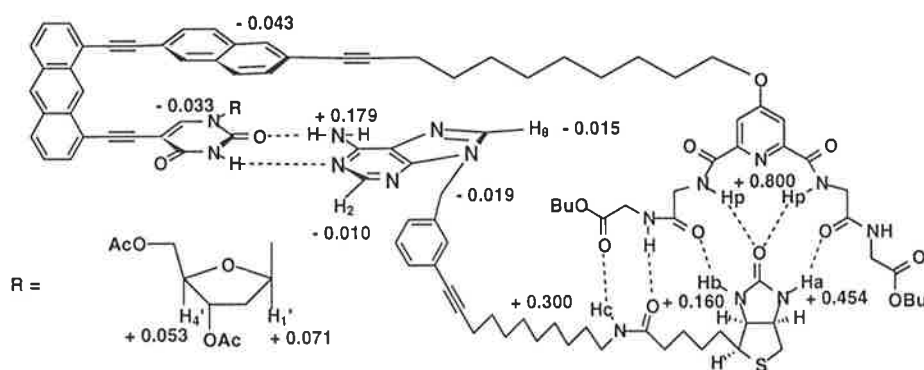
**Figure 162.** The changes of chemical shifts of Re-pdit (**134**) (a) and Bt-Ade (**51**) (b),  $[134] = 1.0 \text{ mM}$ ,  $[51] = 1.0 \text{ mM}$  at rt and in  $\text{CDCl}_3$  (ppm).

Furthermore, the aromatic proton (8-H) in the adenine unit of Bt-Ade (**51**) is likely to be involved in the hydrogen bonding with the carbonyl groups of the thymines in the receptor Re-pdit (**134**) as a consequence of the interactions among DNA base pair triplets as shown in Figure 161. Five hydrogen bonds (Figure 163) (involving both the Watson-Crick site and the Hoogsteen site) within the DNA base pair triplet greatly improves its stability.<sup>277</sup> As shown in Figure 172b, the change of  $^1\text{H}$  NMR chemical shift for 2-H is as high as + 0.045 ppm, which is larger than the corresponding values shown in Figure 159 (+ 0.012 ppm for 2-H).



**Figure 163.** Possible hydrogen bonding in DNA base pair triplet.

Figure 164a shows the binding of the receptor Re-pau (**142**) with biotinyl adenine Bt-Ade (**51**) with up to 8 hydrogen bonds and  $\pi$ - $\pi$  stacking interactions between the naphthyl ring and the adenine ring. Figure 164b shows the structure from molecular modelling of the complex between **142** and **51**. As shown in Figure 164a, the proton NMR resonances of the aromatic protons involved in the  $\pi$ - $\pi$  stacking interactions have all moved upfield. Furthermore, the amide protons H<sub>p</sub> of the tetrapeptide unit are also in the deshielding area, which indicates that the proton is involved in the hydrogen bonding with the biotin unit of the substrate Bt-Ade (**51**).



**Figure 164a.** Proton chemical shift changes for the complex of biotinyl adenine Bt-Ade (**51**) with receptor Re-pau (**142**), [51] = 1.0 mM, [142] = 1.0 mM at rt and in CDCl<sub>3</sub> (ppm).



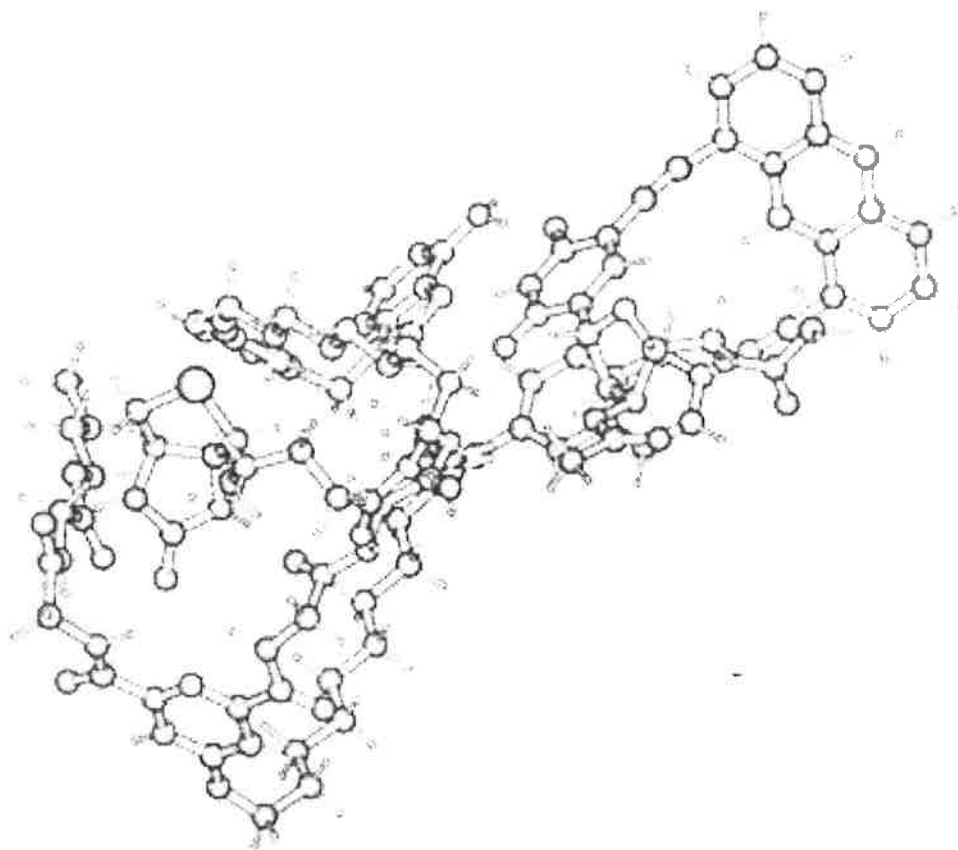


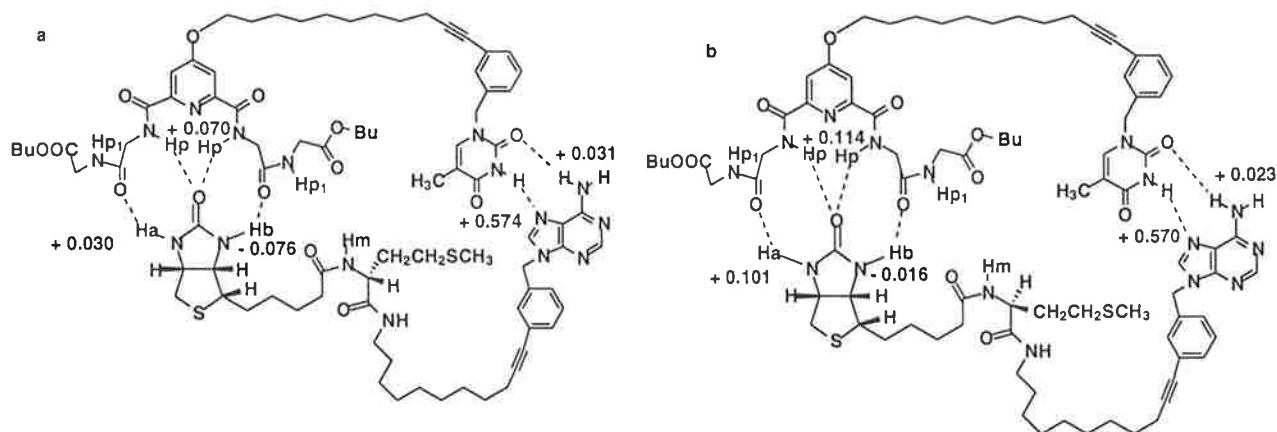
Figure 164b. Molecular modelling of the complex between **142** and **51**.

As to biotinyl adenine Bt-Ade (**51**), the changes in  $^1\text{H}$  NMR chemical shifts after the binding are also arranged in Figure 164. In this case the 2-H and 8-H of the adenine unit are in the shielding region; their chemical shift changes are  $-0.015$  ppm and  $-0.010$  ppm, the chemical shift change for the methylene protons in the benzyl group is also  $-0.019$  ppm, which suggests that the adenine unit form  $\pi$ - $\pi$  stacking interaction with the naphthyl group of the receptor Re-pau (**142**). The changes of chemical shifts of protons Ha, Hb and Hc in the biotin amide unit are  $+0.454$  ppm,  $+0.160$  ppm and  $+0.300$  ppm respectively, which reflect that these three protons are involved in inter-molecular hydrogen bonding with receptor Re-pau (**142**).

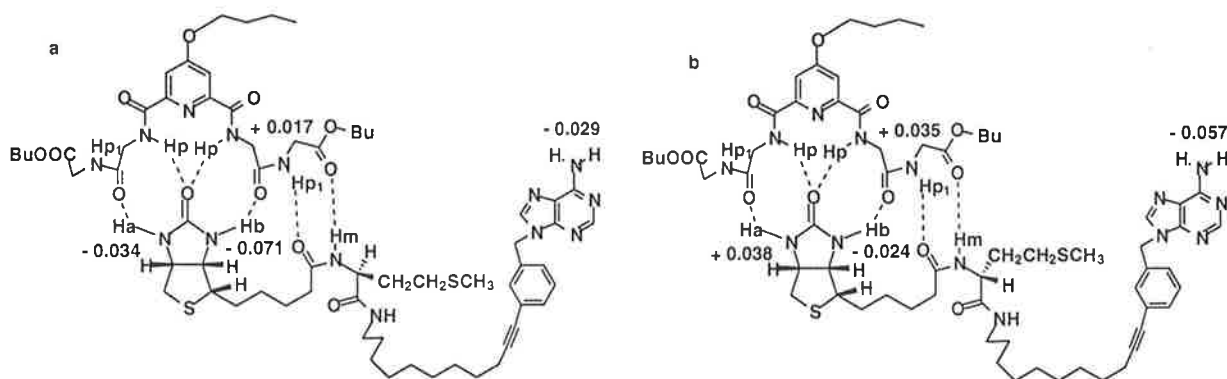
### 11. 2. 3 Molecular recognition of Bt-Met(D)-Ade (**152**) and Bt-Met(L)-Ade (**153**)

The intermolecular interactions between receptor Re-pt (**133**) and Bt-Met(D)-Ade (**152**) and Bt-Met(L)-Ade (**153**) are shown in Figure 165. The changes in the proton chemical shifts after binding are also shown in Figure 165. The results show that the binding of biotin in both Bt-Met(D)-Ade (**152**) and Bt-Met(L)-Ade (**153**) with the tetrapeptide unit in receptor Re-pt (**133**)

was stronger than that with receptor Re-pdigg (**75**) (Figure 166). The binding of Bt-Met(L)-Ade (**153**) with Re-pt (**133**) appears to be stronger than that for Bt-Met(D)-Ade (**152**), on the basis of the chemical shift changes in the NH signals.

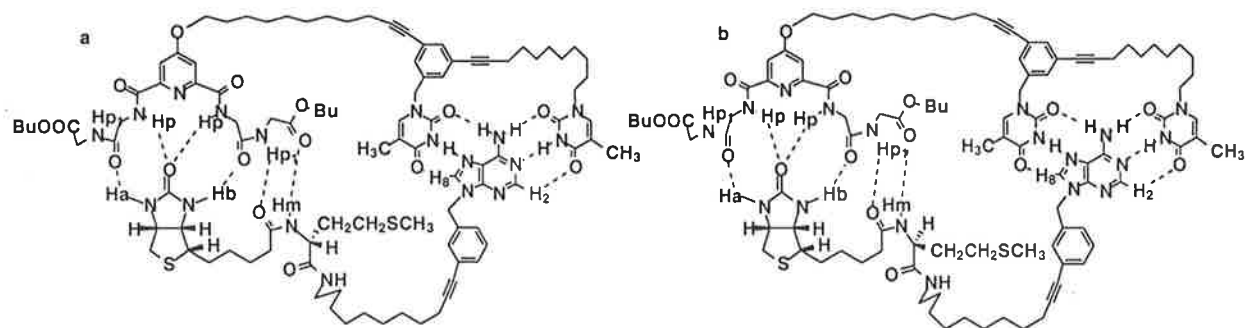


**Figure 165.** Proton chemical shift changes for the complex of biotin adenine Bt-Met(D)-Ade (**152**) (a) and Bt-Met(L)-Ade (**153**) (b) with receptor Re-pt (**133**), [**133**] = 1.0 mM, [**152** or **153**] = 1.0 mM at rt and in CDCl<sub>3</sub> (ppm).

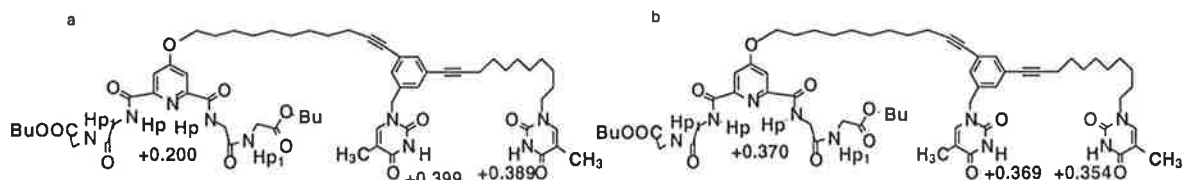


**Figure 166.** Proton chemical shift changes for the complex of biotinyl adenine Bt-Met(D)-Ade (**152**) (a) and Bt-Met(L)-Ade (**153**) (b) with receptor Re-pdigg (**75**), [**75**] = 1.0 mM, [**152** or **153**] = 1.0 mM at rt and in CDCl<sub>3</sub> (ppm).

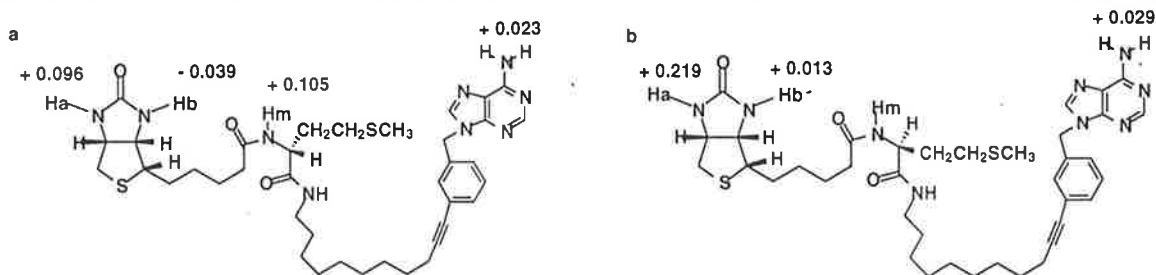
As shown in Figure 167-169, the receptor Re-pdit (**134**) can bind to biotin adenine Bt-Met(D)-Ade (**152**) and Bt-Met(L)-Ade (**153**) by the formation of multiple intermolecular hydrogen bonds. The co-operativity of the binding can be seen by comparing the changes in the chemical shifts with the receptor Re-pdigg (**75**), which lacks the two thymine units (Figure 166). Receptor Re-pdit (**134**), binds Bt-Met(L)-Ade (**153**) more effectively than Bt-Met(D)-Ade (**152**), a trend also observed for receptor **133**.



**Figure 167.** The complexes of biotin adenine Bt-Met(D)-Ade (**152**) (a) and Bt-Met(L)-Ade (**153**) (b) with receptor Re-pdit (**134**).

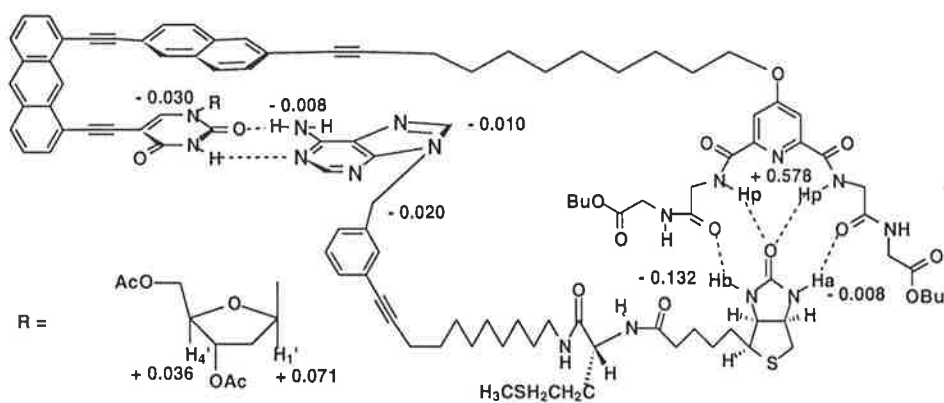


**Figure 168.** The changes of chemical shifts of receptor Re-pdit (**134**) in the complexation with Bt-Met(D)-Ade (**152**) (a) and Bt-Met(L)-Ade (**153**) (b), [**134**] = 1.0 mM, [**152** or **153**] = 1.0 mM at rt and in  $\text{CDCl}_3$  (ppm).

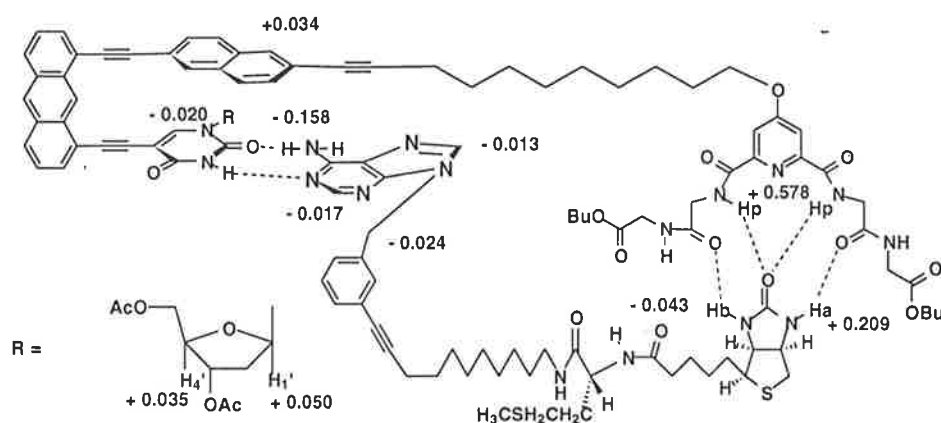


**Figure 169.** The changes of chemical shifts of Bt-Met(D)-Ade (**152**) (a) and Bt-Met(L)-Ade (**153**) (b) in the complexation with receptor Re-pdit (**134**), [**134**] = 1.0 mM, [**152** or **153**] = 1.0 mM at rt and in  $\text{CDCl}_3$  (ppm).

Figure 170 and Figure 171 show binding of the Bt-Met(D)-Ade (**152**) and Bt-Met(L)-Ade (**153**) with the receptor Re-pau (**142**) respectively. The interactions between the receptor and substrates are the multiple hydrogen bonds and  $\pi$ - $\pi$  stacking interactions. The changes of chemical shifts of protons for the ureido moiety in Bt-Met(L)-Ade (**153**) after the binding with receptor Re-pau (**142**) ( $\Delta\text{Ha}$ , + 0.209 ppm;  $\Delta\text{Hb}$ , - 0.043 ppm) are much larger than Bt-Met(D)-Ade (**152**) ( $\Delta\text{Ha}$ , - 0.008 ppm;  $\Delta\text{Hb}$ , - 0.132 ppm), indicating that the receptor Re-pau (**142**) also can selectively bind Bt-Met(L)-Ade (**153**) but not Bt-Met(D)-Ade (**152**).



**Figure 170.** Proton chemical shift changes for the complex of biotinyl adenine Bt-Met(D)-Ade (**152**) with Receptor Re-pau (**142**), [**142**] = 1.0 mM, [**152**] = 1.0 mM at rt and in CDCl<sub>3</sub> (ppm).



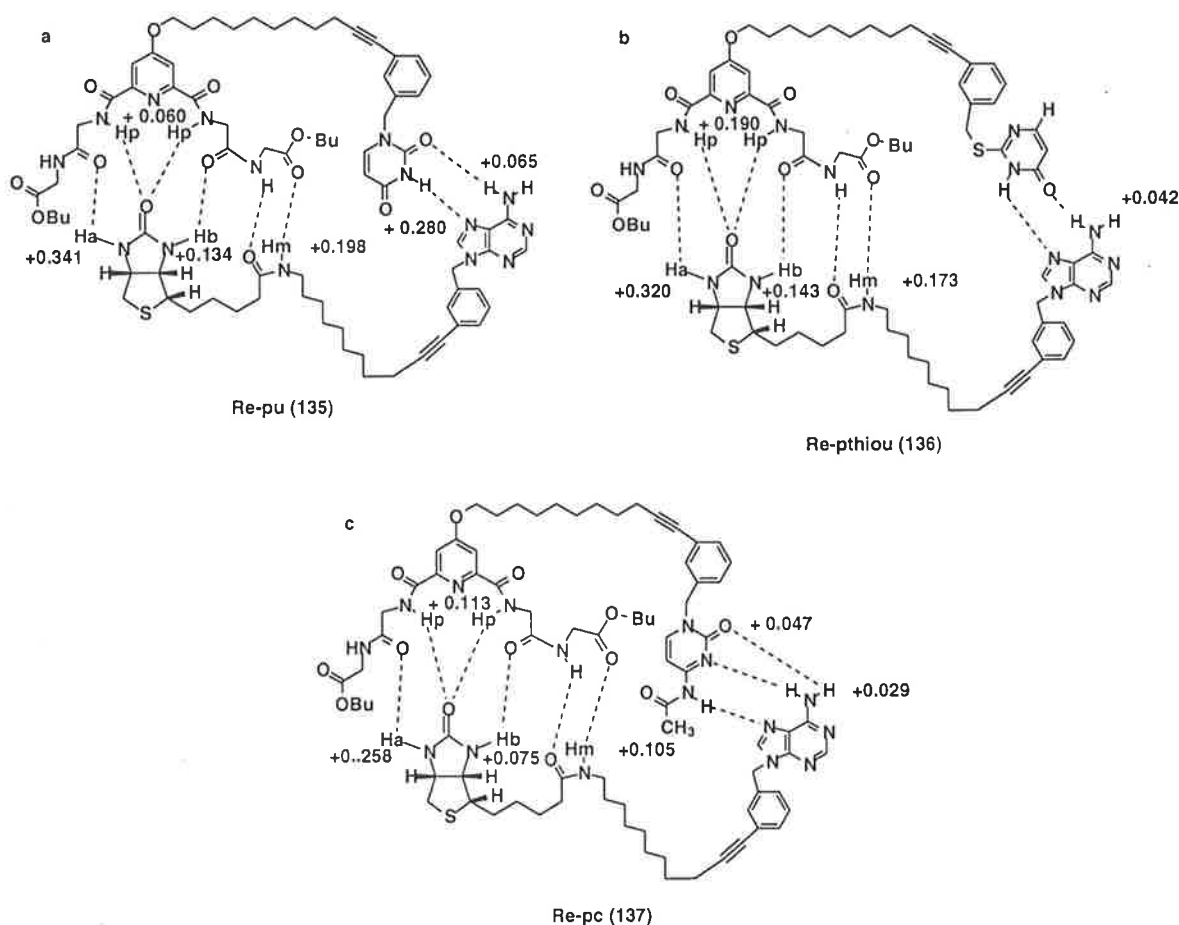
**Figure 171.** Proton chemical shift changes for the complex of biotinyl adenine Bt-Met(L)-Ade (**153**) with receptor Re-pau (**142**), [**142**] = 1.0 mM, [**153**] = 1.0 mM at rt and in CDCl<sub>3</sub> (ppm).

#### 11. 2. 4 Molecular recognition of Bt-Ade (**51**) with other receptors

The molecular recognition of biotinyl adenine Bt-Ade (**51**) with the receptors Re-pu (**135**), Re-pc (**137**) and Re-pthio (**136**) are shown in Figure 172. The interactions between receptor Re-pu (**135**) and Bt-Ade (**51**) are the binding of the biotin amide unit with the tetrapeptide unit in Re-pu (**135**) with six hydrogen bonds and the binding of the adenine with the uracil DNA base pair. The stability of the complex between Re-pu (**135**) and Bt-Ade (**51**) is also comparable to the complex of Re-pt (**133**) with Bt-Ade (**51**) as shown in Figure 159. The binding of the receptor Re-pthiou (**136**) with substrate Bt-Ade (**51**) consists of the interactions of the biotin amide unit of

Bt-Ade (**51**) with the tetrapeptide unit of the receptor and another DNA base pair interaction between adenine and thiouracil. The interaction of Bt-Ade (**51**) with the receptor Re-pc (**137**) includes the hydrogen bonding between tetrapeptide unit and biotin amide unit of Bt-Ade (**51**) and the DNA base cytosine and adenine with base pair hydrogen bonds.

According to the data shown in Figure 172, the binding of receptors Re-thiou (**136**) and Re-pc (**137**) with Bt-Ade (**51**) was not very efficient, compared to the binding of receptor Re-pt (**133**). However, the proton chemical shift changes were larger than those of receptor Re-pdigg (**75**) with Bt-Ade (**51**) (Figure 160). The results show that the DNA base pair interactions, adenine-uracil, adenine-thiouracil and adenine-cytosine are increasing the binding efficiency between the biotin unit and the tetrapeptide unit in the receptors.



**Figure 172.** Proton chemical shift changes for the complexes of biotinyl adenine Bt-Ade (**51**) with the receptor Re-pu (**135**) (a), Re-pthiou (**136**) (b) and Re-pc (**137**) (c), [**51**] = 0.60 mM, [**135**, **136** or **137**] = 0.60 mM at rt and in CDCl<sub>3</sub> (ppm).

---

## Chapter 12

---

# Molecular Reception Catalysis and Biotin Action Mechanisms

### 12.1 Introduction

The ability to characterise the intermolecular interactions between receptors and substrates has led to a better understanding of the mode of action of many enzymes.<sup>70, 75, 278, 279</sup>

Although the structures of bioin dependent enzymes have been recently elucidated, the present details of how the carboxyl group is introduced to NHa of biotin, how the carboxybiotin unit is transferred from one part of the enzyme to another and how the carboxyl group is transferred from the carboxyl biotin unit of the enzyme to a substrate are still not clear.<sup>19</sup>

Very recently, computer modelling and calculations have been applied to the study of the decarboxylation mechanism of carboxybiotin,<sup>90, 280</sup> but the results need be confirmed by experimental evidences.

*Escherichia coli* biotin holoenzyme synthetase, BirA, was reported to possess a biotin and a DNA-binding domain.<sup>19</sup> Kazuta and co-workers reported that Lys-238 seems to interact with the phosphate group of ATP.<sup>281</sup> In an unrelated paper describing a sodium pump, Glu-472 and Lys-480 of the pyrophosphatase were believed to be involved in the recognition of ATP phosphates.<sup>282</sup>

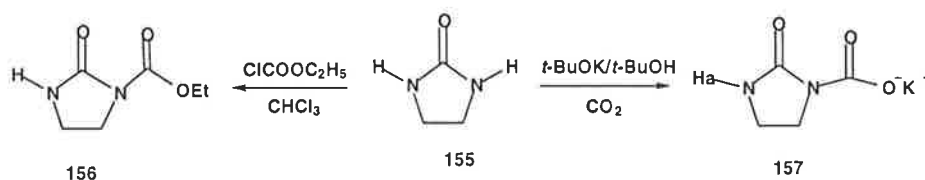
As for the decarboxylation step, Bach and co-worker have reported theoretical results for the study of the influence of electrostatic effects on the activation barrier in the enzymatic reactions,<sup>283</sup> but once again experimental evidences are required to confirm the conclusions.

In this Chapter the mechanism for the carboxylation of NHa of biotin, the transfer of the carboxybiotin unit and the decarboxylation of carboxybiotin are proposed based on the studies reported in earlier Chapters.

## 12.2 Results and Discussion

### 12.2.1 Synthesis

In order to establish a structural basis for these biotin mechanisms and carry out molecular catalysis, *N*-ethoxycarbonyl-2-imidazolidinone (**156**)<sup>284</sup> and potassium *N*-carboxy-2-imidazolidinone (**157**) were prepared as shown in Scheme 35. Neither carboxybiotin nor carboxyimidazolidinone is stable at room temperature, and they both decarboxylate immediately under acidic conditions.<sup>76</sup>



Scheme 35. Synthesis of derivatives of imidazolidinone **155**, **156** and **157**.

### 12.2.2 Molecular recognition of imidazolidinone (**155**) and carboethoxyimidazolidinone (**156**)

Imidazolidinone (**155**) contains one fragment in common with biotin and is often used as an analogue in the study of the action mechanisms, due to its similar geometry, electron distribution and *p*-orbital energies.<sup>90, 280</sup>

The changes in the <sup>1</sup>H NMR chemical shifts of a 1:1 mixture of imidazolidinone (**155**) and receptor Re-pdigg (**75**) are shown in Figure 173, and indicate efficient binding by multiple intermolecular hydrogen bonds.

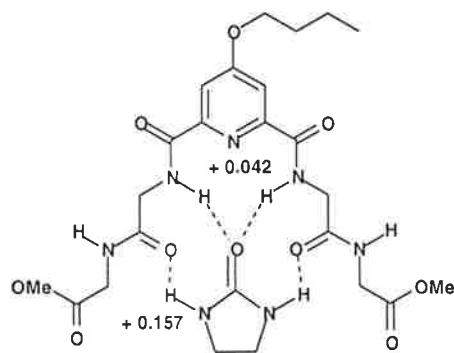
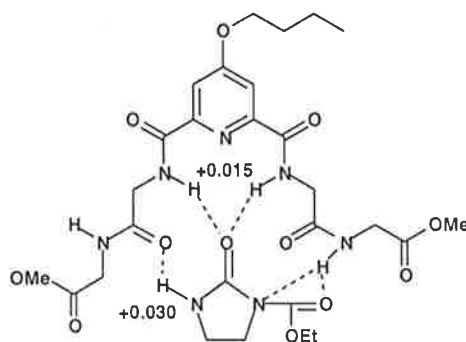


Figure 173. Proton chemical shift changes for the complex of imidazolidinone (**155**) with receptor Re-pdigg (**75**), [**75**] = 10.0 mM, [**155**] = 10.0 mM at rt and in CDCl<sub>3</sub> (ppm).

Carboethoxyimidazolidinone (**156**) is stable in CDCl<sub>3</sub> and was used for binding studies by monitoring the NMR chemical shift changes for a 1:1 mixture with receptor Re-pdigg (**75**) (Figure 174). The proposed binding and the structure of the complex is based on receptors in the

literature.<sup>285</sup> The changes in the proton NMR shifts were small and so, the binding is obviously weaker than binding between the receptor **75** and imidazolidinone (**155**) (Figure 173). Therefore, as an implication, decarboxylation of carboxybiotin to biotin is favorable, since the formation of a more stable complex with biotin by an enzyme will promote the decarboxylation of the carboxybiotin.<sup>75</sup>



**Figure 174.** Proton chemical shift changes for the complex of carboethoxyimidazolidinone (**156**) with receptor Re-pdigg (**75**), [**75**] = 2.0 mM, [**156**] = 2.0 mM at rt and in CDCl<sub>3</sub> (ppm).

### 12. 2. 3 Crystal structure of carboethoxyimidazolidinone (**156**)

The crystal structure of carboethoxyimidazolidinone is shown in Figure 175.<sup>286</sup> The bond length from the nitrogen to the carboxyl carbon (N1-C11, 1.392 Å) is elongated by 0.045 Å, compared to the average for this sort of bond length (1.347 Å) (Figure 176).<sup>287-289</sup> This result supports the theoretical calculations and the possible mechanism of decarboxylation. The elongation of the bond length N1-C11 reflects a possible disruption in the conjugation and lowering of the bond order of the bond, which is favorable for the rotation and decarboxylation.<sup>75</sup>

The bond length of N1-C2 is also elongated due to the carboxyl ester group from the average 1.315 Å in the crystal structure of imidazolidinone hemihydrate **155** (Figure 176a)<sup>290</sup> to 1.411 Å (Figure 176b). The elongation of the bond length reflects the high energy and instability of **156**. Compound **156** is not very stable even in water solution with carbon dioxide bubbles being observed during recrystallization.



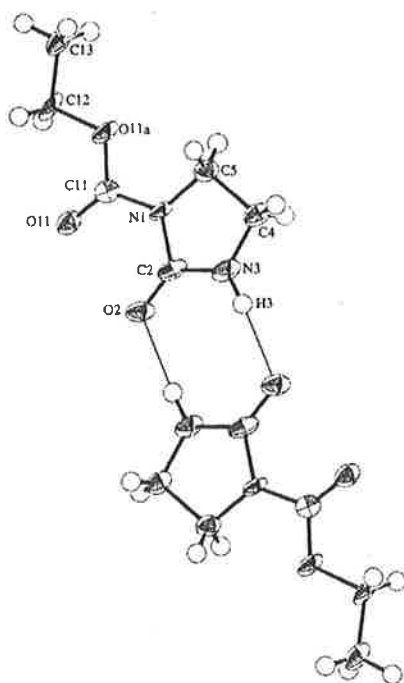


Figure 175. The crystal structure of carboethoxyimidazolidinone (**156**).<sup>286</sup>

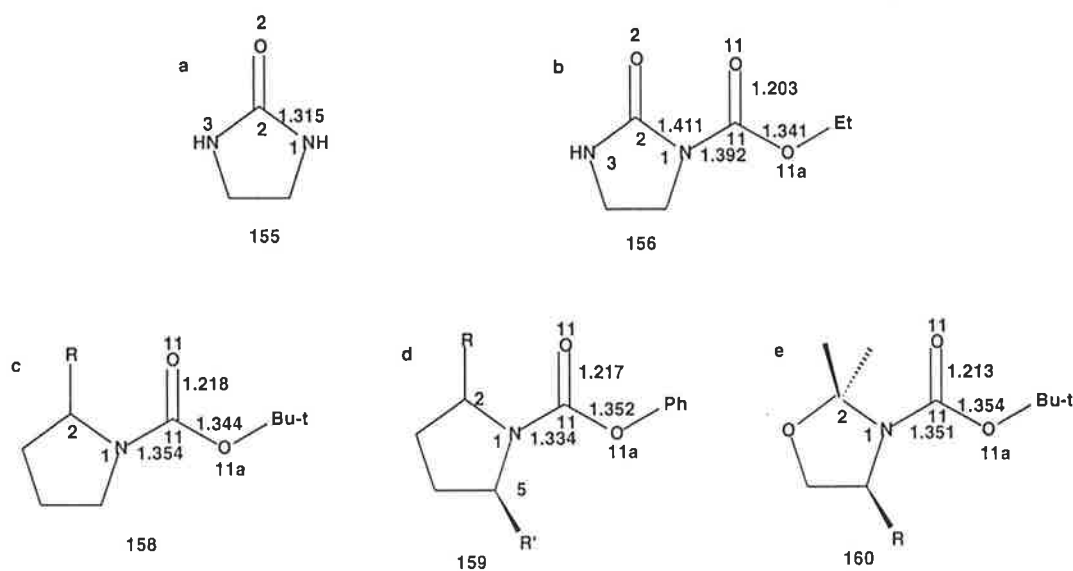


Figure 176. The chemical structures of imidazolidinone (**155**) (a), carboethoxyimidazolidinone (**156**) (b) and *t*-butyl 2-[(hydroxy)(5-hydroxy-1,3-benzodioxol-6-yl)methyl]pyrrolidine-1-carboxylate (**158**), parts of the structures are omitted for clarity (c).<sup>289</sup> (2*S*,2*R*)-*cis*-1-benzoyloxycarbonyl-5-[(2*S*)-hydroxy-2-phenylethyl]-2-proline *t*-butyl ester (PTBEA) (**159**) (d).<sup>287</sup> (1*R*,2*R*)-*N*-benzyl-*N*-[(3-*t*-butoxycarbonyl-2,2-dimethylloxazol-4-yl)(furan-2-yl)methyl]-hydroxylamine (**160**) (e)<sup>288</sup> and selected bond lengths (Å).

Furthermore, the torsional angle C2-N1-C11-O11 (14.6°) (Figure 177) is enlarged, compared to the value in pyrrolidinone **158** shown in Figure 176c (3.3°). The four atoms are not in the same

plane, and the two carbonyl groups are twisted away from each other. There is also a slight distortion from planarity of  $1.1^\circ$  for N1,  $358.9^\circ$  (C2-N1-C11-C5). Therefore, N1 is not in the same plane as C2-C5-C11, but C2 is in the same plane as N3-O2-N1 and C11 is in the same plane of N1-O11-O11a in the crystal structure of carboethoxyimidazolidinone **156** (Figure 175).

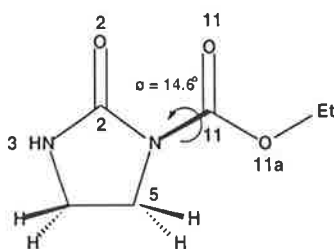


Figure 177. Torsion angle of carboxyl group in carboethoxyimidazolidinone (**156**).

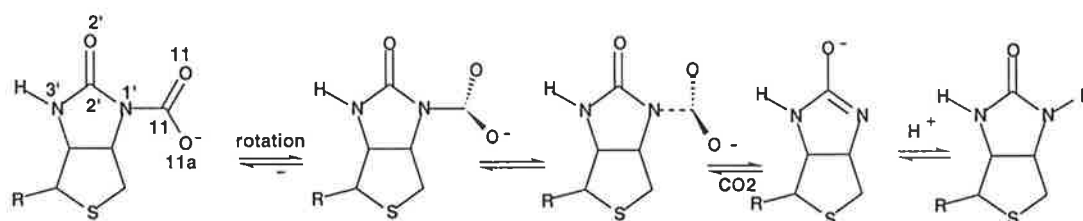
From the crystal structure of **156**, the bond length C11-O11 is  $1.203 \text{ \AA}$ , which is shorter than the average value ( $1.216 \text{ \AA}$ ) for this bond from **158-160**.<sup>287-289</sup> The bond length of C11-O11a in **156** is  $1.341 \text{ \AA}$ , which is also shorter than the average value  $1.348 \text{ \AA}$ . The angle O11-C11-O11a in **156** is  $125.4^\circ$ , which is larger than the average value for this angle in those three literature structures ( $124.1^\circ$ ).<sup>287-289</sup> These results give us the impression that the decarboxylation of carboxyimidazolidinone is impending. The bond length of the carbonyl group in carbon dioxide is only  $1.143 \text{ \AA}$ , so the bond length shortening is already taking place in **156** when a carboxyl group is connected to one of the nitrogens in imidazolidinone.

The shortening of the bond length reflects the increase in electron density and bond order between C11 and O11, or C11 and O11a of the pro-carbon dioxide moiety. The bond angle O-C-O is  $180^\circ$  in  $\text{CO}_2$ , the widening of the bond angle of the carboxyl group also has begun in the carboethoxyimidazolidinone. As reported in the literature, the shortening of bond length (N1-C2), elongation of bond length (N1-C11) and the widening of the bond angle O11-C11-O11a are necessary for the decarboxylation of carboxyimidazolidinone.<sup>90, 280</sup> Therefore, these experimental results provide support for the calculations and the decarboxylation mechanism of carboxybiotin in biotin dependent enzymes (Figure 178).

As reported earlier, the electrostatic binding of an enzyme receptor to the carboxyimidazolidinone ring of carboxybiotin can result in the movement of the exocyclic carboxyl group out of the plane. The enzymic distortion further promotes the decarboxylation.<sup>14, 26, 291</sup>

Therefore, the above results support the mechanism for the decarboxylation of carboxybiotin in the biotin dependent enzymes proposed by Kluger and co-worker as shown in Scheme 36. The first step of the decarboxylation is the formation of a complex between carboxybiotin and an

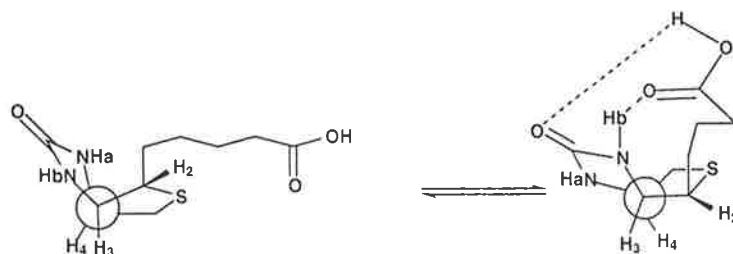
amino acid residue in the active site of the enzyme. This complex is expected to distort further the conformation of the biotin and expose the nitrogen (N-1') to enzyme binding by the electrostatic interaction and hydrogen bonding as shown in Figure 174. The distortion is also going to destroy the resonance preserved in the most stable planar conformation (C2'-N-C11-O11).<sup>75</sup> According to the data of *ab initio* calculation, the perpendicular structure of carboximidazolidinone, where the O11-C11-O11a plane is vertical to the plane of ureido moiety C5-N1-C2, is less stable than the planar one by ca. 5 kcal/mol.<sup>90</sup> The rotation and the binding of nitrogen (N-1') will increase the length of the bond N1-C11. At the same time the angle of the pro-carbon dioxide moiety of the carboxyl group, O11-C11-O11a, will be enlarged. The final step is the departure of the carbon dioxide from carboxybiotin, followed by the recovery of biotin unit from the cyclic urea enolate.



Scheme 36. The mechanism of the decarboxylation of carboxybiotin in biotin dependent enzymes.<sup>75</sup>

#### 12. 2. 4 Hydrogen bonding induced distortion of biotin derivatives

According to the crystal structure of biotin, the ureido ring including the carbonyl oxygen, is not exactly planar, the deviation from the plane of the best fit is 0.03 Å for N-3'.<sup>86</sup> Therefore, the ureido ring is conformationally mobile due to the valeryl side chain because there is an unavoidable interaction of N-3' with C-6 (There is no observable intramolecular hydrogen bonding between Hb and the carboxyl group in the solid state).<sup>86, 292</sup> Although biotin adopts exclusively an *endo* conformation in the crystalline state, in a DMSO-*d*<sub>6</sub> solution and at higher temperature, the inter-conversion from *endo* to *exo* on the NMR time scale was observed, which resulted in the broadening of the NMR peaks of H2, H3, H4, H5a and H5b (Figure 1) due to the changes of the relevant dihedral angles and their chemical environments.<sup>91</sup> In Chapter 2, the intra-molecular hydrogen bonding between the ureido NHb and side-chain carboxyl group of biotin was observed in DMSO-*d*<sub>6</sub>-CDCl<sub>3</sub> solution. The dihedral angles C2'-N3'-C3-C2 and C2'-N'-C3-C4 have changed dramatically after the formation of the hydrogen bond between Hb and the side chain of biotin. The intra-molecular hydrogen bond plays an important role in this change of conformation. Scheme 37 shows the predicted change of conformation of biotin due to rotation around the C3-C4 covalent bond caused by the intra-molecular hydrogen bond.



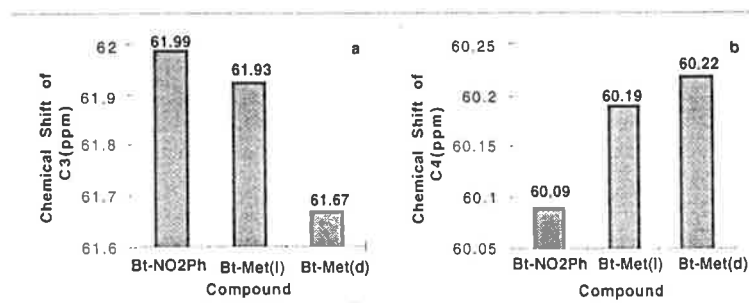
**Scheme 37.** The change of conformation of biotin by the intra-molecular hydrogen bonding concerning Hb from their 3D structures, other hydrogen bonds are omitted for clarity.

The induced change of conformation of biotin in holo-BCCP could be seen in its crystal structure, compared to the NMR structure of apo-BCCP.<sup>21</sup> The multiple interactions between the ureido ring of the biotin moiety and the residue in the protruding thumb of the holo protein appear to confer a strained conformation on the biocytin turn and protect the single tyrosine residue (Tyr 92) from solvent quenching.<sup>21</sup> As a result, the conformational flexibility is attenuated in the biocytin-containing loop, as well as in the protruding thumb with carboxylase and transcarboxylase in the reaction intermediates, which is ready for the following rapid catalytic transfer.

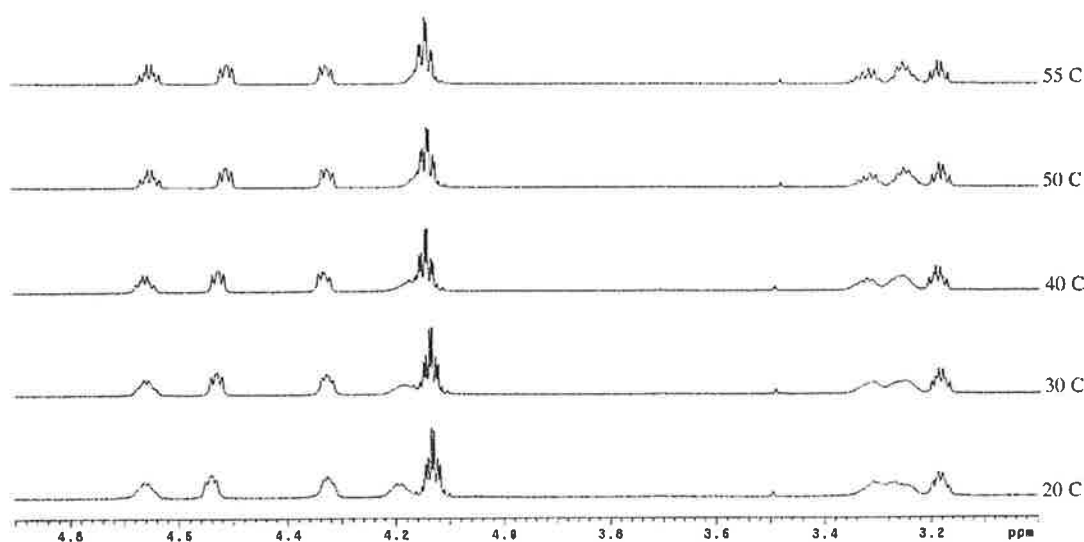
Figure 178 shows the <sup>13</sup>C NMR chemical shifts of carbon C3 and C4 in biotin peptides Bt-Met(D) (**37**), Bt-Met(L) (**38**) and biotin ester **12**. The chemical shifts for C3 moved up-field dramatically with an increase in the strength of intra-molecular hydrogen bond involving Hb but downfield for C4, indicating that the conformation of the biotin ureido ring has been changed because of the intra-molecular hydrogen bonds. It is understandable that <sup>13</sup>C NMR resonances of a carbon vary in different conformations and environments.<sup>293</sup>

As for biotin peptides Bt-Lys(L)-Met(D) (**48**), Bt-Lys(L)-Met(L) (**47**), Bt-Ahx-Met(D) (**50**) and Bt-Ahx-Met(L) (**49**), their NMR spectra at room temperature were shown in Figure 51 and their temperature dependencies were listed in Table 19 at 1 mM in CDCl<sub>3</sub>. The broadening of the NMR signals for H2, H3 and H4 in compound Bt-Lys(L)-Met(L) and Bt-Lys(L)-Met(D) were more obvious than Bt-Ahx-Met(L) and Bt-Ahx-Met(D), which was consistent with their larger temperature dependencies for NHa, Hb and Hc, indicating that the intra-molecular hydrogen bonding interactions play an important role in the changes of the conformations.

Figure 179 shows the temperature-dependent <sup>1</sup>H NMR spectra of the protons H2, H3 and H4 in Bt-Lys(L)-Met(D) (**48**) in CDCl<sub>3</sub> at 1 mM. All these signals gradually sharpened (and separated from one to three signals for H3) when the temperature was raised, which suggests that the broadening of the signals and the changes of the conformation of the biotin ureido unit were greater at low temperature due to stronger intra-molecular hydrogen bonding.



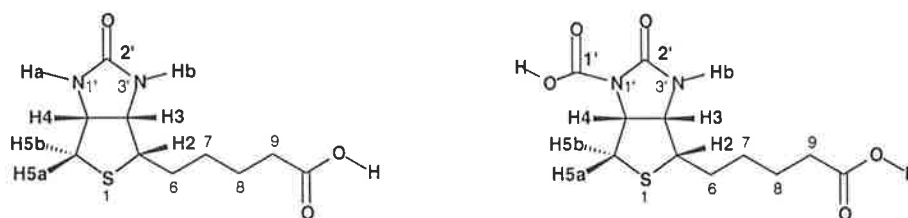
**Figure 178.** <sup>13</sup>C NMR chemical shifts of C3 (a) and C4 (b) in compounds Bt-NO<sub>2</sub>Ph (12) (left), Bt-Met(L) (38) (middle) and Bt-Met(D) (37) (right).



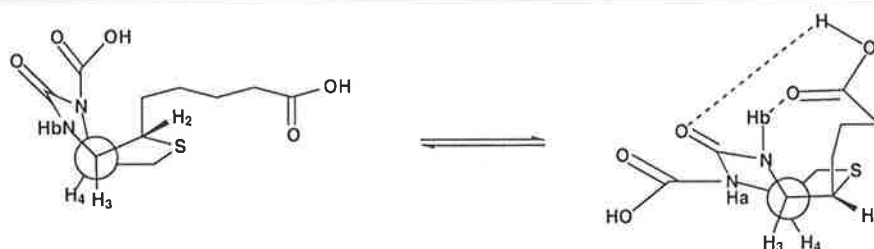
**Figure 179.** Accumulated NMR spectra of 48 at different temperatures from 20 °C - 60 °C at 1 mM in CDCl<sub>3</sub>.

The change of <sup>1</sup>H NMR chemical shift of H5b in Bt-Met(D) was as high as + 0.048 ppm from 20 °C to - 60 °C in CDCl<sub>3</sub> at 1 mM. The increases in <sup>1</sup>H NMR chemical shift for H4 and H5b in Bt-Lys(L)-Met(L) (47) and Bt-Lys(L)-Met(D) (48) were as high as 0.104 ppm and 0.074 ppm respectively from 20 °C to - 60 °C in CDCl<sub>3</sub> and at 1 mM. The results also suggest changes of conformation due to the intra-molecular hydrogen bonding at lower temperature.<sup>15, 293</sup>

Table 41 also shows the changes of the selected dihedral angles C2'-N3'-C3-C2 and C2'-N3'-C3-C4 of the biotin ureido unit after the formation of the intra-molecular hydrogen bonding. As can be seen from Table 41, the dihedral angles Ha-N1-C2'-O2' and Ha-N1'-C4-H4 have been increased by proceeding from an extended conformation of biotin to the intra-molecular hydrogen bonded one. This increased dihedral is favorable for the exposure of the N-1'-Ha to the environment and substitution by a carboxyl group. The changes of the two dihedral angles and conformation for N-1'-carboxybiotin by the intra-molecular hydrogen bonding interactions can also be seen from Table 41 and Scheme 38, according to molecular modelling of carboxybiotin with and without intra-molecular hydrogen bonding.

**Table 41.** Selected dihedral angles ( $^{\circ}$ ) from the molecular modelling structures of biotin and carboxybiotin.

dihedral	biotin (non-H-bonded)	biotin (H-bonded)	carboxybiotin (non-H-bonded)	carboxybiotin (H-bonded)
C2'-N3'-C3-C2	138.2	113.0	147.5	115.5
C2'-N3'-C3-C4	18.2	-7.8	27.9	-6.0
Ha(C1')-N1'-C2'-O2'	3.3	-8.9	10.0	-14.8
Ha(C1')-N1'-C4-H4	-52.6	-56.9	-52.0	-51.9

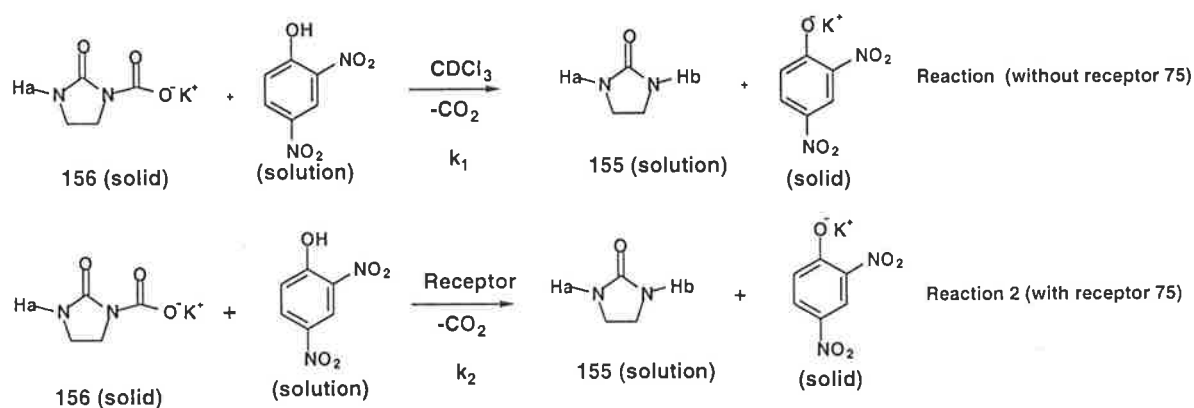
**Scheme 38.** The change of conformation of biotin by the intra-molecular hydrogen bonding concerning Hb from molecular modelling calculations, other hydrogen bonds are omitted for clarity.

It has been proposed that in biotin transcarboxylase the enzyme-induced decarboxylation of carboxybiotin can result from movement of the exocyclic carboxyl group out of the plane of the imidazolidinone ring upon binding to a substrate e.g. acetyl CoA.<sup>14, 291</sup> Hydrogen bonding is expected to distort the conformation and make it more planar as shown in Scheme 38, in which N-COO<sup>-</sup> moiety will be in the envelop lid. The distortion of the conformation results in a strained conformation of carboxybiotin, which is biologically favorable for the following transcarboxylation.<sup>294</sup>

### 12. 2. 5 Receptor catalysis of the decarboxylation of carboxyimidazolidinone

*p*-Nitrophenol was selected as a source of acid to neutralize the basic salt and release the acid form of the carboxyimidazolidinone, which was expected to bind to the tetrapeptide Re-pdigg (**75**), according to the model system of the receptor with ethoxycarboxyimidazolidinone (**156**). If the decarboxylation took place, then the receptor was also expected to bind the product imidazolidinone (**155**). The reactions were monitored by proton NMR for two systems, one in the presence of receptor and another in the absence of receptor.

Scheme 39 shows the reactions for potassium carboxyimidazolidinone (**157**) with and without the receptor Re-pdigg (**75**). As shown in Figure 180, the decarboxylation of the potassium carboxyimidazolidinone (**157**) with the receptor **75** was faster than the control reaction ( $k_2 > k_1$ ), reflecting the effect of binding the substrate to the receptor.



Scheme 39. Reactions for reception catalysis

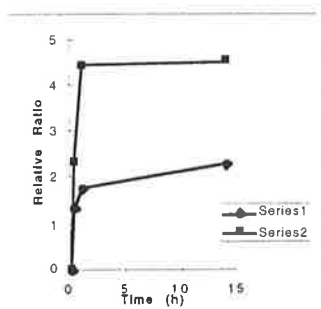
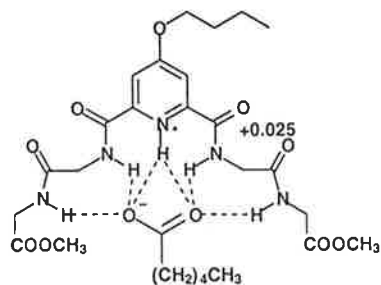


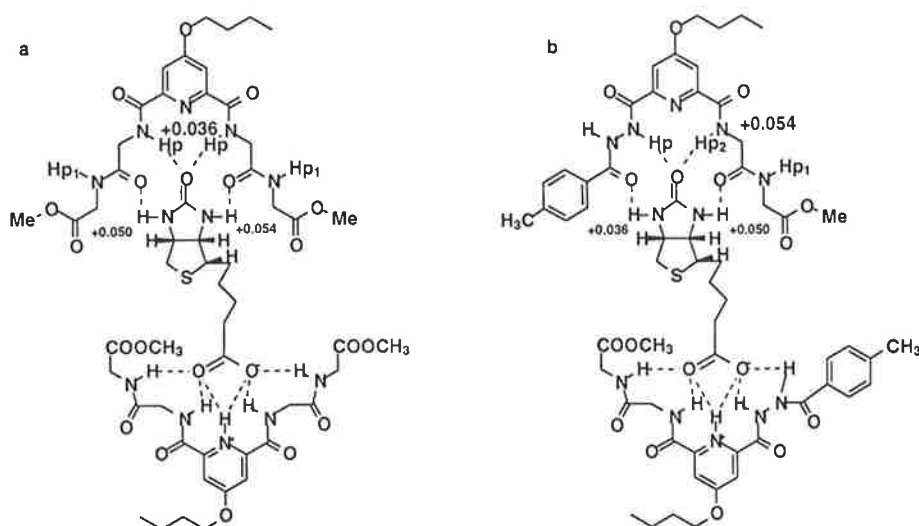
Figure 180. The decarboxylation curves of the decarboxylation of potassium carboxyimidazolidinone (**157**) in  $\text{CDCl}_3$  at rt with receptor Re-pdigg (**75**) (■) and no receptor (♦).

### 12. 2. 6 Molecular recognition of biotin and aliphatic acids.

The interactions between carboxyphosphate and biotin would lead to the formation of carboxybiotin. However, carboxybiotin is a reaction intermediate and unstable (half-life, 70 ms).<sup>295</sup> Therefore, caproic acid was used as a substitute for the carboxyphosphate in the binding of biotin and peptide, which is shown in Figures 181-182. As shown in Figure 181, the nitrogen of the receptor Re-pdigg (**75**) will be protonated, and this proton and four amide protons will form multiple hydrogen bonding with aliphatic carboxylate anions.<sup>74</sup> Figure 182 shows the binding results between whole biotin molecules and the receptors Re-pdigg (**75**) and Re-pdigh (**77**). The results indicate that these receptors can bind to the biotin.



**Figure 181.** Proton chemical shift change for the binding of caproic acid with receptor Re-pdigg (**75**), [caproic acid] = 2.0 mM, [**75**] = 2.0 mM at rt and in  $\text{CDCl}_3$  (ppm).

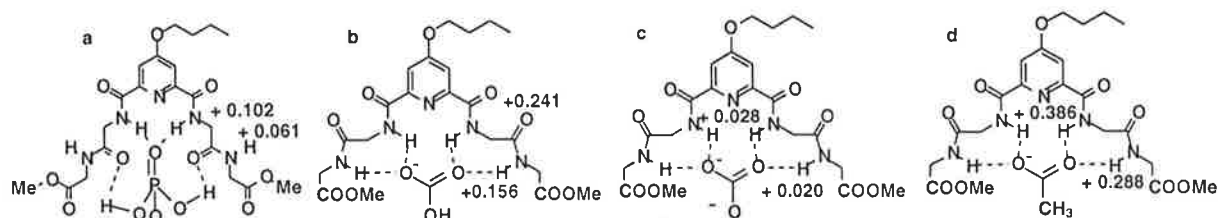


**Figure 182.** Proton chemical shift changes for the complex between biotin (**1**) and receptors **75** or **77**, [**1**] = 5.0 mM, [**75** or **77**] = 5.0 mM at rt and in a mixed solvent 5.0%  $\text{DMSO-d}_6$ - $\text{CDCl}_3$  (ppm).

### 12. 2. 7 Molecular recognition of inorganic substrates $\text{H}_2\text{PO}_4^-$ , $\text{HCO}_3^-$ , $\text{CO}_3^{2-}$ and organic anion $\text{CH}_3\text{COO}^-$

The possible binding of  $\text{H}_2\text{PO}_4^-$ ,  $\text{HCO}_3^-$ ,  $\text{CO}_3^{2-}$  and acetate on mixing with one equivalent of receptor **75** and the changes of chemical shifts of the NH protons in the receptor Re-pdigg (**75**) are shown in Figure 183 in a mixed solvent  $\text{DMSO-d}_6$ - $\text{CDCl}_3$ . The results show that the receptor **75** could bind inorganic substrates  $\text{H}_2\text{PO}_4^-$ ,  $\text{HCO}_3^-$ ,  $\text{CO}_3^{2-}$  and acetate and act as a model for the binding of carboxyphosphate, ATP and AMP during the enzymic carboxylation of biotin.

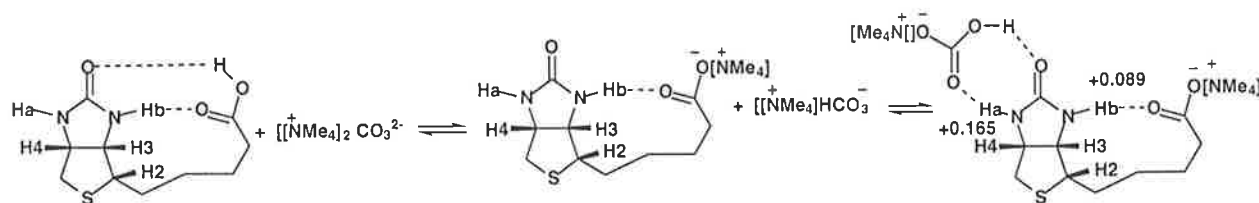




**Figure 183.** Proton chemical shift changes for receptor Re-pdigg (**75**) in the complexation with substrate  $\text{H}_2\text{PO}_4^- + \text{NBu}_4$  (a),  $\text{HCO}_3^- + \text{NBu}_4$  (b),  $\text{CO}_3^{2-} (+\text{NMe}_4)_2$  (c) and  $\text{CH}_3\text{COO}^- + \text{NBu}_4$  (d),  $[\mathbf{75}] = 5.0 \text{ mM}$ ,  $[\text{H}_2\text{PO}_4^- + \text{NBu}_4] = 5.0 \text{ mM}$  at rt and in a mixed solvent 8.7% DMSO- $d_6$ - $\text{CDCl}_3$  (a),  $[\mathbf{75}] = 5.0 \text{ mM}$ ,  $[\text{CO}_3^{2-} (+\text{NMe}_4)_2] = 5.0 \text{ mM}$  at rt and in a mixed solvent 10.0% DMSO- $d_6$ - $\text{CDCl}_3$  (c) and receptor at  $[\mathbf{75}] = 2.0 \text{ mM}$ ,  $[\text{HCO}_3^- + \text{NBu}_4]$  or  $[\text{CH}_3\text{COO}^- + \text{NBu}_4] = 2.0 \text{ mM}$  at rt and in  $\text{CDCl}_3$  (b) and (d) (ppm).

### 12. 2. 8 Binding of bicarbonate $\text{HCO}_3^-$ by biotin and biotin derivatives

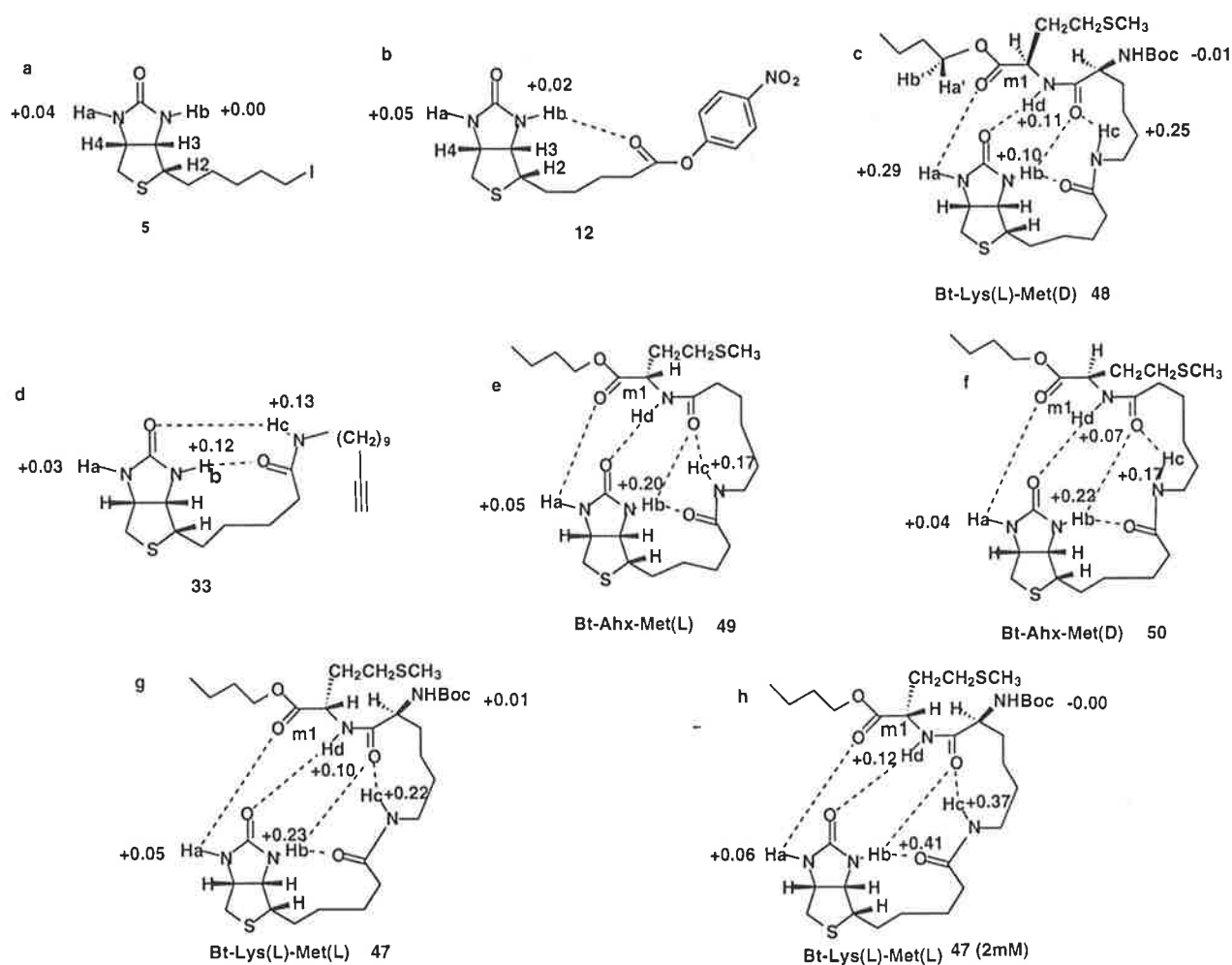
In order to examine the affinity of carbonate for biotin,  $\text{CO}_3^{2-} (+\text{NMe}_4)_2$  was used in the binding study of free biotin in the mixed solvent 10.0% DMSO- $d_6$ - $\text{CDCl}_3$ . In this solution, an equilibrium between carbonate and bicarbonate anions was expected as shown in Scheme 40. The chemical shifts of the NHa and NHb protons in biotin suggested the high affinity of bicarbonate anion to the N1-Ha of biotin in the carboxylation of biotin and biotin dependent enzymes.



**Scheme 40.** Equilibria between carbonate and bicarbonate anions and the proposed binding of biotin by bicarbonate anion. Proton chemical shift changes of biotin NHa and NHb at  $[\text{biotin}] = 5.0 \text{ mM}$ ,  $[[\text{NMe}_4]_2\text{CO}_3^{2-}] = 5.0 \text{ mM}$  at rt and in a mixed solvent 10.0% DMSO- $d_6$ - $\text{CDCl}_3$  (ppm).

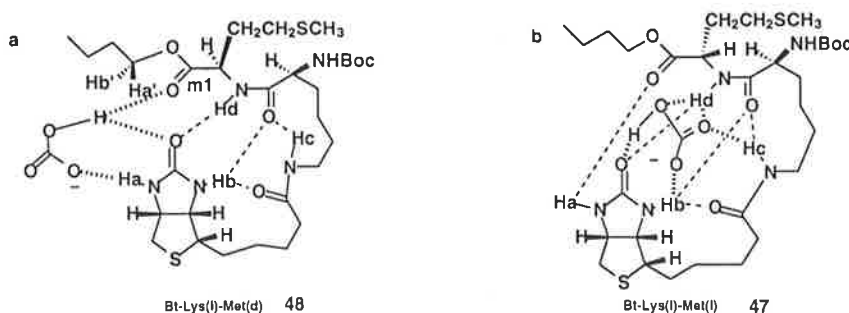
The changes in the proton chemical shifts for the amide NH protons after the binding with bicarbonate anion  $\text{HCO}_3^-$  in  $\text{CDCl}_3$  for biotin derivatives, such as biotin ester and biotin peptides, are arranged in Figure 184. Very little binding was observed for biotinyl iodide **5** as shown by the very small changes in the proton shift for NHb. A minor degree of binding may occur on NHa. The major interaction of the bicarbonate  $\text{HCO}_3^-$  with the biotin ureido group of compound **12** was with the N-1'-Ha as was binding with the more complex **48**. These results are consistent with the known preference for carboxylation at N-1'-Ha.<sup>87</sup>

Compounds **47**, **49** and **50** showed a reversal in the site for binding bicarbonate. The proton shift changes for NHa were very small whilst those for NHb were large. The NH groups in the biotin side chain also showed significant changes in chemical shift consistent with cooperative binding.



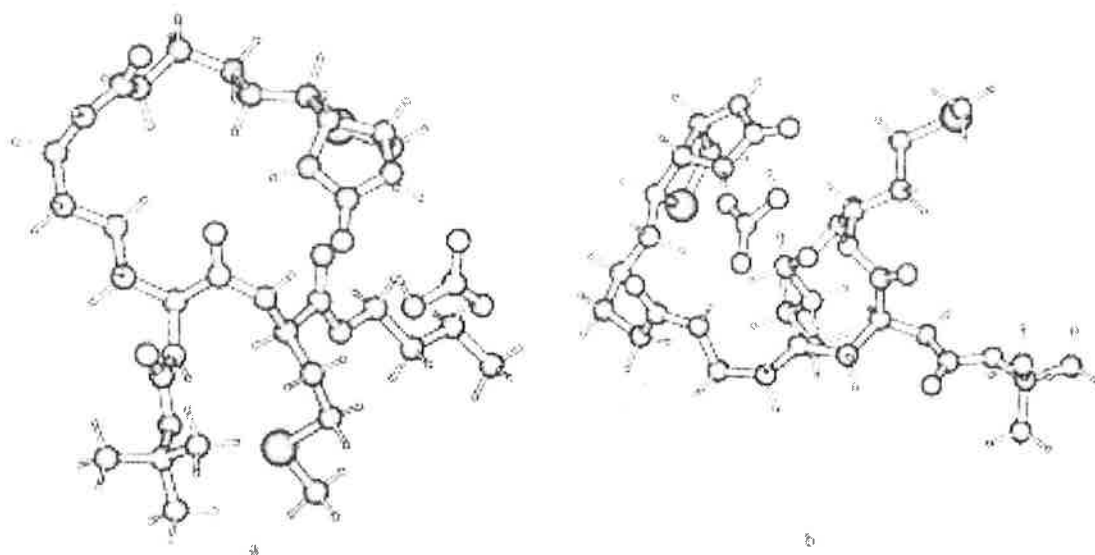
**Figure 184.** The changes of chemical shifts of amide protons after binding with  $[\text{Bu}_4\text{N}^+ \text{HCO}_3^-] = 1.0 \text{ mM}$  in compounds at  $1.0 \text{ mM}$  **5** (a); **12** (b); **48** (c); **33** (d); **49** (e); **50** (f); **47** (g) by comparison to substrates at  $1.0 \text{ mM}$  and rt and in  $\text{CDCl}_3$  (ppm) (those for **47** (h) were at  $2 \text{ mM}$ ).

Biotin peptide Bt-Lys(L)-Met(L) (**47**) is the basic unit of the biotin carrier carboxyl protein (BCCP) and 1.3 subunit of carboxylases, which is the conserved region required for some carboxyl carrier activity.<sup>1</sup> Binding of the bicarbonate anion  $\text{HCO}_3^-$  with Bt-Lys(L)-Met(D) (**48**) was observed on the active side of biotin ureido moiety (N-1'-Ha), however, the binding of the biotin peptide Bt-Lys(L)-Met(L) (**47**) occurred on the N-3'-Hb side (Figure 185). These results were unexpected. A possible explanation is that **48** could form an active site on N-1'-Ha by intramolecular hydrogen bonds (Figure 184), since the temperature dependence  $\Delta\delta\text{H}/\Delta\text{T}$  value for Ha in compound **48** was the largest among **47**, **48**, **49** and **50** (Table 19). Therefore, bicarbonate  $\text{HCO}_3^-$  is expected to bind to the active sites of the compounds **47**, **48**, **49** and **50**.



**Figure 185.** Possible binding sites for  $\text{HCO}_3^-$  in the biotin peptides **48** (a) at N-1'-Ha side and **47** (b) at N-3'-Hb side.

Computer modelling showed the energy for the complex between **48** and bicarbonate  $\text{HCO}_3^-$  (a) in Figure 185a and 186a was  $-191.9$  kcal/mol, however, if the bicarbonate group  $\text{HCO}_3^-$  was at the same position as in **47**, the energy was  $-173.8$  kcal/mol. Therefore, complex (a) in Figure 185 was relatively more stable. Furthermore, the computer modelling showed that the complex between **47** and bicarbonate  $\text{HCO}_3^-$  as described in (b) (Figure 185b and 186b) was  $-181.1$  kcal/mol, lower than the complex between **48** and bicarbonate ( $-161.3$  kcal/mol) when the bicarbonate  $\text{HCO}_3^-$  was in the same position. Therefore, bicarbonate  $\text{HCO}_3^-$  appears to preferentially bind to N-1'-Ha in **48**, but N-3'-Hb in **47**. As a result, assistance from other amino acid residues may be necessary besides the basic peptide unit Bt-Lys(L)-Met(L) for the transport and interaction of bicarbonate  $\text{HCO}_3^-$  on the biologically active side N-1'-Ha of biotin during the carboxylation of biotin containing enzymes.<sup>16</sup>



**Figure 186.** Computer modelling structures of the complexes when  $\text{HCO}_3^-$  in the binding with the biotin peptides **48** (a) at N-1'-Ha side and **47** (b) at N-3'-Hb side.

### 12. 2. 9 A model for the mechanism of formation of biotin-5'-AMP

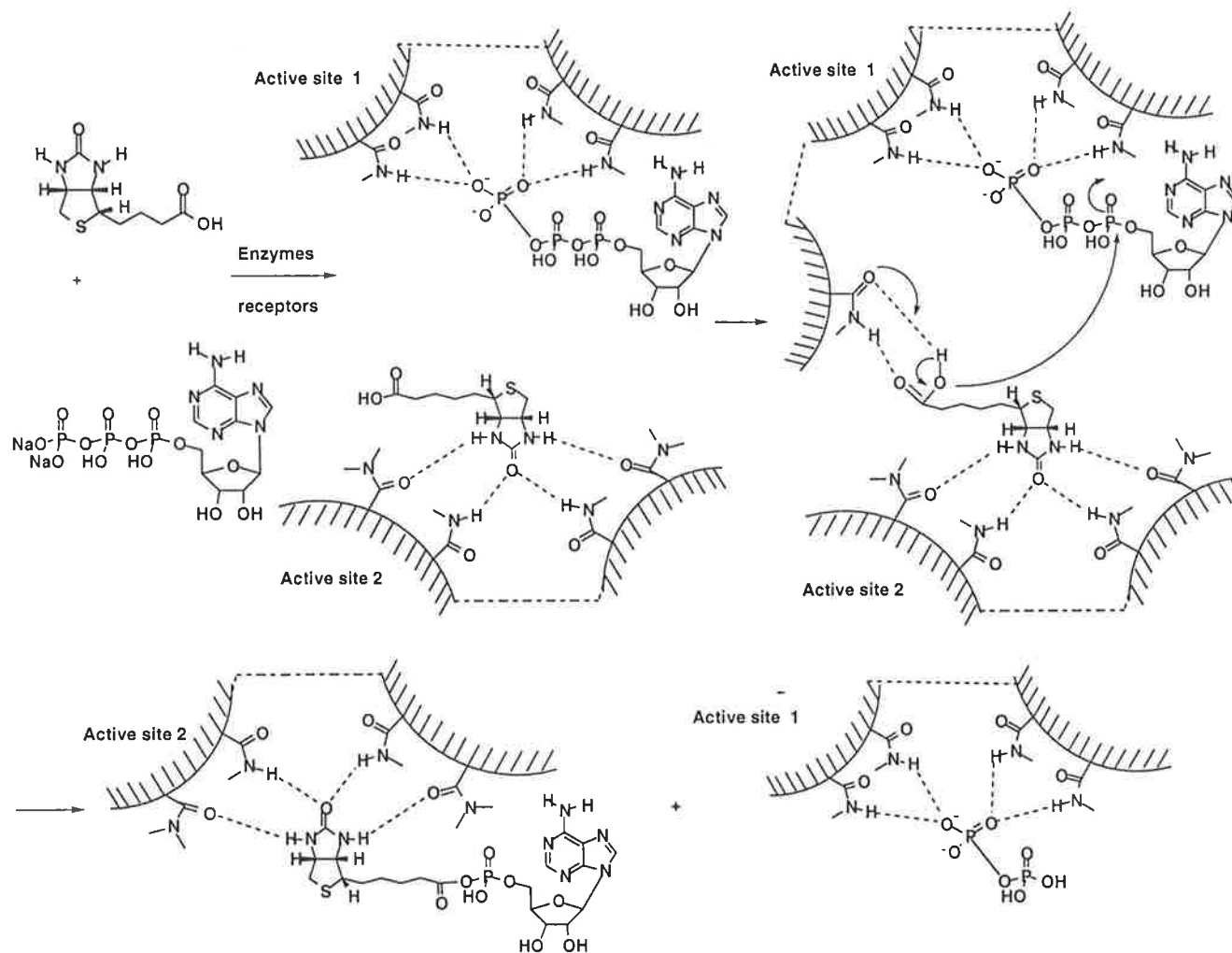
The formation of biotinyl-5'-AMP is activated by the *Escherichia coli* biotin operon repressor, BirA. Biotin-5'-AMP is an intermediate in the post-translational attachment of a biotin unit to a specific lysine residue on the biotin carboxyl carrier protein, a subunit of acetyl-CoA carboxylase. It is believed that BirA collects the biotin and ATP together and catalyses the reaction.<sup>19</sup> Recently, it is reported that the glycine rich region Gly-Gly-Gly-Gly-Arg-Gly at amino acid numbers 163-168 was presumed to be the ATP-binding site of the *E. coli* biotin carboxylase.<sup>296</sup>

The active residues of BirA for the binding of biotin by hydrogen bonds are Arg-116, Ser-89, Thr-90, Gln-112 and Lys-183, in which Lys-183 binds to the carboxyl group at the end of the hydrocarbon tail.<sup>19</sup>

As suggested previously, the tetrapeptide receptor Re-pdigg (**75**), Gly-Gly-Py-Gly-Gly forms a binding pocket for the biotin ureido moiety, hydrogen phosphate, hydrogen carbonate and aliphatic carboxylate. In order to establish a structural basis for the understanding of the interactions in the binding pockets for the binding of biotin, biotin carboxylate, bicarbonate, hydrogen phosphate, ATP, AMP, biotin-5'-AMP, carboxyphosphate, the synthetic receptor Re-pdigg (**75**) (Gly-Gly-Py-Gly-Gly) was used as an analogue for the active site in the enzymatic reactions.

Based on the above assumptions and structural information for the binding of biotin and ATP, a proposed mechanism for the formation of biotin-5'-AMP is outlined in Scheme 41. The receptors for the biotin ureido unit and carboxyl group as well as the phosphate of ATP are outlined in active sites 1 and 2. ATP is bound to active site 1 as is the carboxyl group of biotin whereas the ureido group of biotin is bound to active site 2.

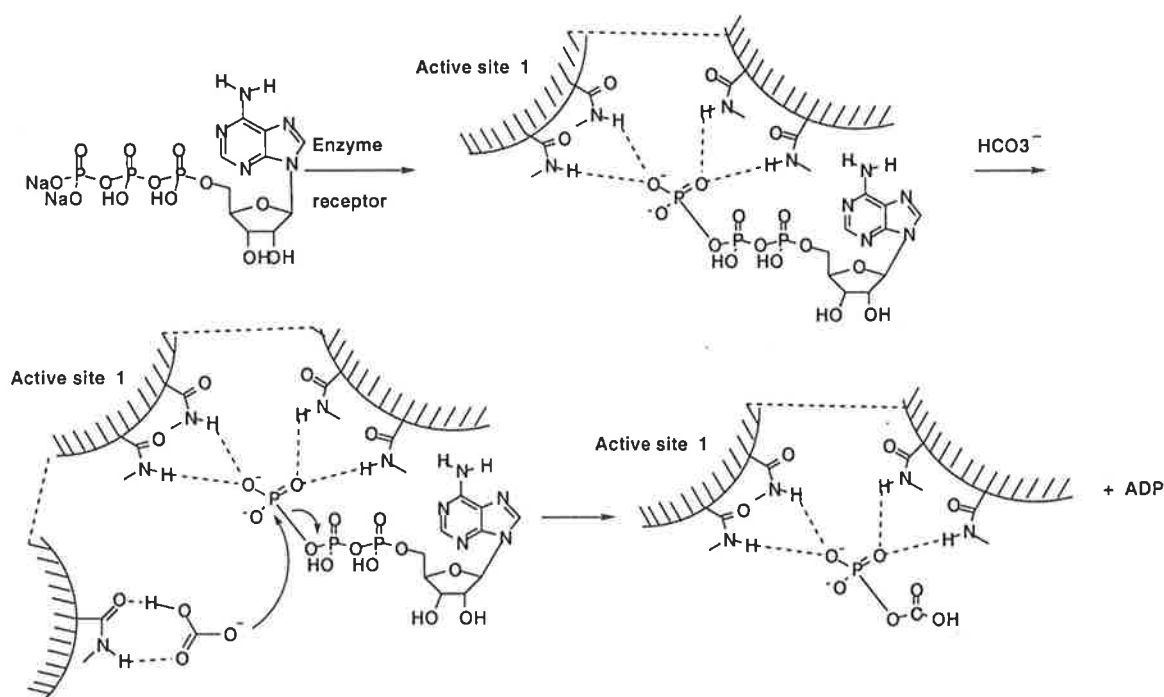
The first step of the biosynthesis of biotin-5'-AMP is believed to be the binding of biotin and ATP. The carboxyl group of biotin is a poor nucleophile, the activation of this group is necessary for the following nucleophilic attack. The binding site for ATP need be close to the activation site for biotin. Therefore, the second step is expected to be the binding of the carboxyl group of biotin at active site 1 for ATP. Then the nucleophilic substitution reaction takes place to form biotin-5'-AMP by the reaction of carboxylate anion with ATP and elimination of pyrophosphate from ATP. Biotin-5'-AMP is still in the active site 2, where it is stabilized by hydrogen bonding. The pyrophosphate bound on the active site 1 should be replaced by a fresh ATP for subsequent reactions.



**Scheme 41.** Proposed mechanism of the formation of biotin-5'-AMP from biotin and ATP under the catalysis of biotin dependent enzymes.

### 12. 2. 10 A model for the mechanism of the formation of carboxyphosphate

Knowles and co-worker reported that carboxyphosphate is the intermediate in the biotin dependent carboxylation, and that it is formed from the phosphorylation of bicarbonate with ATP.<sup>295</sup> Carboxyphosphate is quite unstable, Sauers and co-workers have estimated that its half-life in neutral aqueous solution to be on the order of 70 ms.<sup>295</sup> Therefore the stabilization of carboxyphosphate is necessary by the biotin dependent enzymes for the carboxylation of biotin. However, bicarbonate is a poor electrophile, therefore, activation is also necessary in the formation of the intermediate. The receptor Re-pdigg (Gly-Gly-Py-Gly-Gly) for both bicarbonate and phosphate (Figure 183), is regard as a model for the biotin dependent enzymes in the binding of bicarbonate and ATP, and the following enzymic phosphorylation. The proposed enzymic mechanism based on this hypothesis is shown in (Scheme 42).



**Scheme 42.** Proposed mechanism of the formation of carboxyphosphate from biotin and ATP.

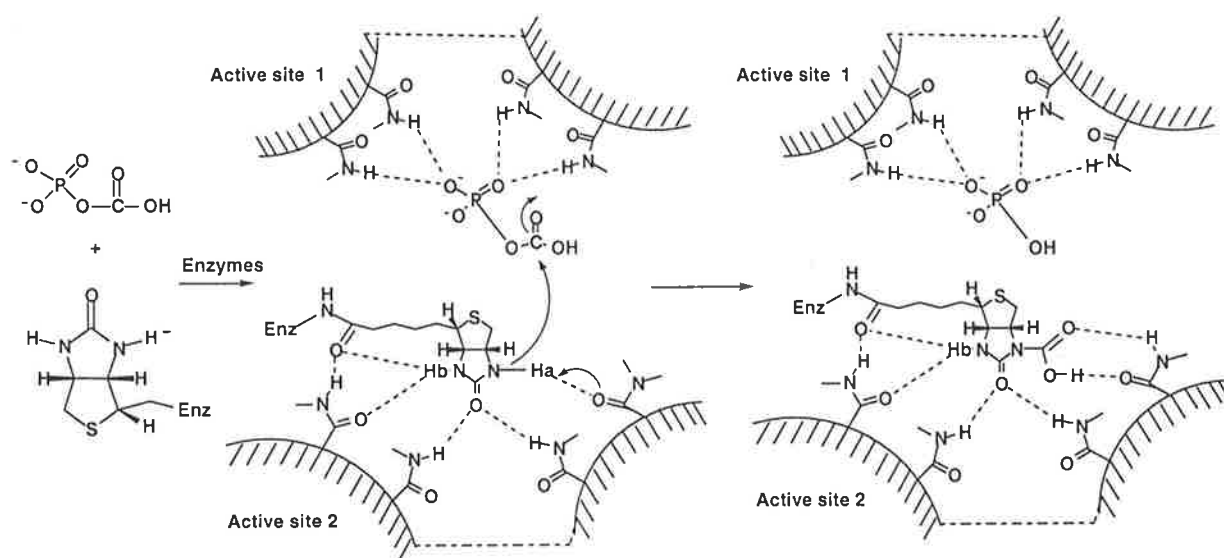
As shown in Scheme 42, ATP is bound to active site 1, followed by the binding of bicarbonate into this active site. The nucleophilic attack and substitution can then take place by the elimination of ADP.

### 12. 2. 11 A model for the mechanism of the carboxylation of biotin by carboxyphosphate

The biotin carboxyl carrier protein (BCCP) is a subunit of acetyl-CoA carboxylase, a biotin dependent enzyme that catalyzes the first step committed step of fatty acid synthesis by intermediate carboxybiotin.<sup>21</sup> A structural study of holo-BCCP showed that biotin was involved in the internal interactions with the residues surrounding it, such as Tyr-92, Thr-94, Pro-95, Ser-96, Pro-97, Ile-117 and Met-124.<sup>25</sup> A tentative identification was carried out by Waldrop and co-workers and the amino acid residues that are believed to form part of active site pocket include His-209, Glu-211, His-236, Glu-241, Glu-276, Ile-287, Glu-296 and Arg-338.<sup>24</sup> Because biotin is a poor nucleophile and the carboxyphosphate is very unstable, the activation of the biotin unit in biotin dependent enzymes and the stabilization of the carboxyphosphate is necessary by the active site of enzymes.

Based on the interaction of the receptor **75** with ATP and biotin (Figure 110-113, 182 and 183), a model for the carboxylation of biotin in the biotin dependent enzymes is proposed as shown in Scheme 43.

The biotin dependent carboxylases are expected to bind both carboxyphosphate and biotin enzyme holo-BCCP and catalyse the carboxylation of biotin unit. The detailed mechanism is expected to be similar to the mechanism provided by Sauers.<sup>297</sup> Because the biotin ureido moiety is a weak nucleophile, the binding of the biotin unit is to improve the basicity of the nitrogen for the following nucleophilic attack by the receptor or active site of the biotin dependent enzymes. The intra-molecular hydrogen bonding involving NHb is also to promote the formation of the complex with enzymes, since it can help to form its own active site. After the reaction, the carboxybiotin is to remain in the active site 2 as shown in Scheme 43.

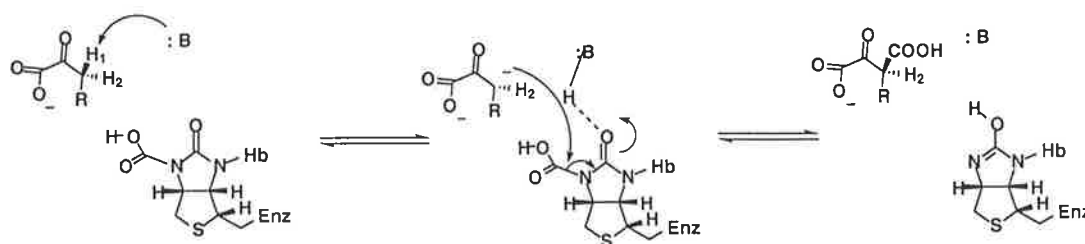


**Scheme 43.** Proposed mechanism of the formation of carboxybiotin from biotin enzyme holo-BCCP and carboxyphosphate, under the catalysis of biotin dependent enzymes.

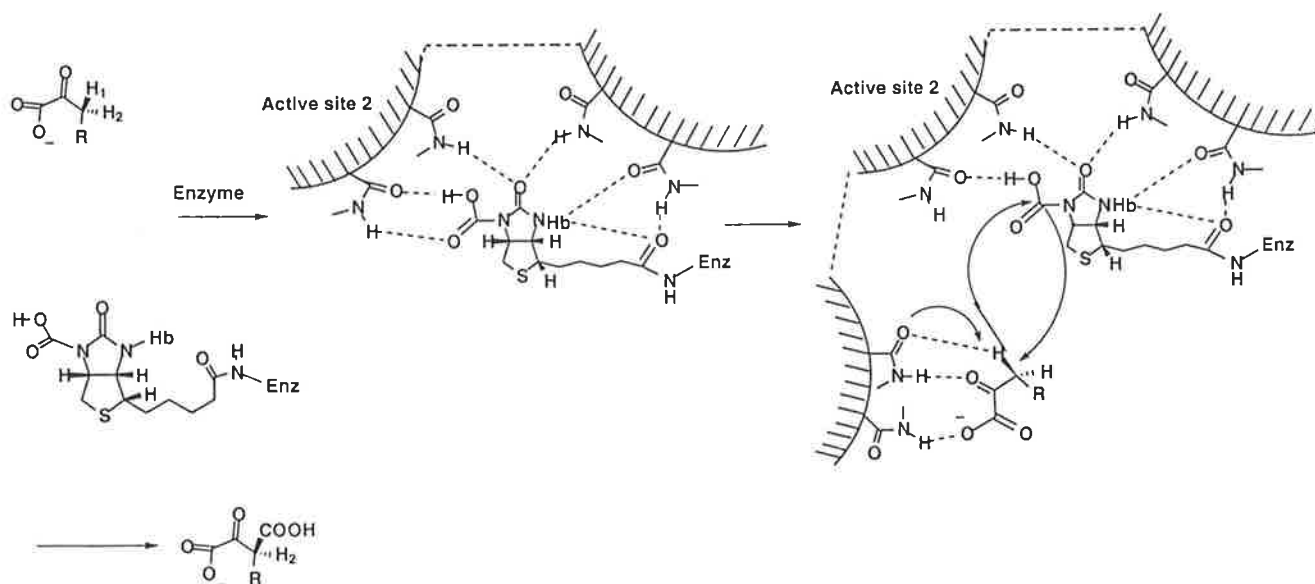
### 12. 2. 12 A model for the mechanism of the transcarboxylation of carboxybiotin and carboxylation of a substrate with the retention of configuration

It is reported that the proton abstraction of propionyl-CoA can be catalysed by both propionyl-CoA carboxylase and transcarboxylase<sup>293, 299</sup> by the electrostatic interaction between the proton to be replaced by the carboxyl group and a basic centre, followed by an attack by the resultant carbanion on the carboxybiotin. The hydrogen bonding between the biotin ureido oxygen and protons in the enzymes is believed to be important as it will increase the electrophilicity of the *N*-carboxyl group and make it more susceptible to nucleophilic attack by the carbanion form of the substrate as shown in Scheme 44.<sup>26</sup> The basis for the proposed mechanism is the observation of the elimination of HF from  $\beta$ -fluoropropionyl-CoA, resulting in the formation of acryl-CoA, however, the binding details between substrate and enzyme are unknown.

Shown in Scheme 45 is a proposed reaction mechanism for the abstraction of protons and the following carboxylation of the substrate with the retention of configuration by biotin carboxylases and transcarboxylases. Substrates such as pyruvate are bound to active site 1. The carboxybiotin unit is expected to be in the adjacent active site 2. For the decarboxylation of carboxyl group from a carboxybiotin or transdecarboxylation of a carboxyl group carboxybiotin unit to a substrate, it is necessary for the substrate pyruvate to enter active site 2. In Scheme 45, the binding of a substrate such as pyruvate in active site 1 will determine the configuration of the complex. Hydrogen bonding between an oxygen atom and the  $\alpha$ -C-H within the complex then promotes the removal of the proton and the formation of the carbon anion. After the formation of the carbon anion, the conformation is fixed, such that the following carboxylation occurs at the position where the pro-*R* or *S* proton was removed. Therefore, the carboxylation occurs with retention of configuration. Furthermore, the binding of the biotin unit with a receptor or enzyme in active site 2 will form multiple electrostatic interaction with the ureido moiety oxygen which are expected to increase the electrophilicity of the pro-chiral proton and promote the nucleophilic attack of the carbon anion and the following decarboxylation.



Scheme 44. The reaction mechanism involving a carbonanion intermediate.<sup>26</sup>



Scheme 45. Proposed mechanism of the transdecarboxylation of carboxybiotin and carboxylation of a substrate with retention of configuration, under the catalysis of biotin dependent enzymes.



## Conclusion

Intra-molecular hydrogen bonding of free biotin was observed in organic solvents by the application of multiple NMR techniques, including 1D NMR at different ratios of solvent  $\text{CDCl}_3$  and  $\text{DMSO-d}_6$ , 2D-NOESY and ROESY. Intra-molecular hydrogen bonding of active biotin esters was also observed, which was confirmed to promote the aminolysis and orient the reaction to occur with stereo-selectivity.

Intra-molecular hydrogen bonding networks in biotin amides and peptides were also revealed by the application of VT NMR and 2D-ROESY techniques. The multiple hydrogen bonds are expected to form active sides for the biotin peptides. The hydrogen bonding induced pro-chiral methylene hydrogens differentiation was observed. The stronger the hydrogen bonds, the better separation will be. The hydrogen bonding promoting hydrophobic interaction between biotin ring and aromatic ring was also observable.

As to biotinyl nucleobases, the intra-molecular hydrogen bonding pair was found to be favorable involving the nucleobases and the NHb of biotin for Bt-Ade(**51**), Bt-Cyt(**52**), Bt-Thy(**53**) and Bt-Ura (**54**). However, the hydrogen bonding pair between thiouracil and the NHa and the carbonyl group of biotin was observed to be favorable for Bt-Thioura (**55**).

Three-centre intra-molecular hydrogen bonding was observed in 2, 6-pyridinedicarboxamide receptors, which resulted in the planar conformation and intermolecular  $\pi$ - $\pi$  stacking interactions. This specific motif and conformation were found to be favorable in the binding of biotin unit in free biotin, biotin esters, biotin amides, biotin nucleobases and biotin peptides and some inorganic substrates, hydrogen phosphate, bicarbonate, carbonate and organic acetate anion.

Some structure-based receptors for adenine were designed and used in the molecular recognition of adenine derivatives through hydrogen bonding and  $\pi$ - $\pi$  stacking interactions. Intra-molecular hydrogen bonding interactions between DNA bases in a series of artificial base pair doublets and triplets were also observed.

The molecular recognition of biotin nucleobases, which are the analogues of biotin-5'-AMP, was then carried out through multiple intermolecular hydrogen bonds (up to 12) and possible  $\pi$ - $\pi$  stacking interactions. The binding of bicarbonate in the active side of biotin peptides was observed. The crystal structure of carboethoxyimidazolidinone suggested the inclination to the

decarboxylation of carboxybiotin. Thus, several models for biotin action mechanism were proposed.

---

## Chapter 13

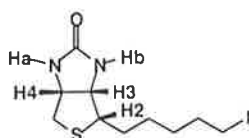
---

### Experimental

All melting points are recorded on a Reichert hot stage apparatus and uncorrected. Reagents were used as obtained from commercial supplies or purified according to the procedures described in the literature.<sup>300</sup> All reactions were performed in oven dried glassware under a nitrogen atmosphere (unless otherwise stated). Proton and carbon NMR spectra were recorded on a Bruker ACP-300 or a Varian 600 spectrometer in CDCl<sub>3</sub> or CD<sub>3</sub>SOCD<sub>3</sub> as a solvent with TMS as an internal standard. Chemical shifts were reproducible within a  $\pm 0.002$  ppm range. CDCl<sub>3</sub> was dried over 4 Å molecular sieves for at least one month before use. Thin layer chromatography was carried out using Merck aluminum sheets precoated with Kieselgel 60 F254, and visualized using either a 250 or 365 nm lamp. Flash chromatography was carried out using Merck Kieselgel 60 (230-400 mesh), and solvents were distilled before use. 2D-COSY, ROESY and NOESY NMR were recorded on Varian 600 NMR spectrometer. Mass spectra were obtained on VG ZAB 2HF mass spectrometer with either electron impact (EI) or fast atom bombardment (FAB) ionization. Accurate mass determinations using EI or Liquid Secondary Ion MS (LSIMS) were made by the Organic Mass Spectrometry Facility at the University of Tasmania. L-CQ mass spectra were recorded on Finnigan Mat spectrometer. Variable temperature NMR experiments were performed under the automatic control of the attachments on the Bruker ACP-300 and Varian-600 spectrometers and the temperature was maintained within a  $\pm 0.02$  °C range. FT-IR experiments were conducted on AT1 Mattison Genesis Series spectrometer.

Compounds **1**, **12**, **15**, **20-25**, **59** were purchased from Sigma or Aldrich and used as received. Compound **2**, **3**, **4**,<sup>93</sup> **6**,<sup>94</sup> **7**, **8**, **9**,<sup>54, 301</sup> **16**,<sup>111</sup> **19**,<sup>112</sup> **24**, **25**,<sup>113</sup> **26**, **27**, **28**, **29**, **30**,<sup>114</sup> **31**, **32**, **33**, **34**, **35**, **143**, **10-undecynyl-1-amine**, **11-iodo-1-undecyne**,<sup>54, 301</sup> **56**, **57**,<sup>302</sup> **4-butoxy-2,6-pyridinedicarboxylic acid**, dibutyl 4-butoxy-2, 6-pyridinedicarboxylate (**81**),<sup>303</sup> were prepared according to the literatures and characterized as mentioned.

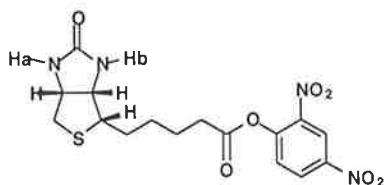
[3aS-(3a $\alpha$ , 4 $\beta$ , 6a $\alpha$ )]-Tetrahydro-4-(5-iodopentyl)-1H-thieno[3, 4-d]imidazol-2(3H)-one (**5**)



[3aS-(3a $\alpha$ , 4 $\beta$ , 6a $\alpha$ )]-Tetrahydro-4-(5-(methylsulfonyl)pentyl)-1H-thieno[3, 4-d]imidazol-2(3H)-one (**4**) (10.0 mg, 0.032 mmol) was dissolved in acetone (2 mL), anhydrous sodium iodide (96 mg, 0.64 mmol) was added. The mixture was stirred overnight at room temperature. The

solvent was removed by a nitrogen stream and the residue was submitted to flash column separation with 8% methanol in dichloromethane as an eluant to give **5** as a light yellow solid 8.0 mg, yield 74%. m.p. 173-176 °C. <sup>1</sup>H NMR (CDCl<sub>3</sub>, 1 mM, rt): δ(ppm) 1.460-1.859 (m, 8 H, CH<sub>2</sub>); 2.768 (d, 1 H, *J* = 12.6 Hz, H5b); 2.984 (dd, 1H, *J* = 12.6 Hz, 5.4 Hz, H5a); 3.149 (m, 1 H, H2); 3.172 (t, 2 H, *J* = 13.8 Hz, CH<sub>2</sub>); 4.340 (m, 1 H, H3); 4.535 (m, 1 H, H4); 4.442 (s, 2 H, NHa + NHb). Calc. for [M+ H]<sup>+</sup> C<sub>10</sub>H<sub>18</sub>N<sub>2</sub>OSi: 341.0203. Found: 341.0192.

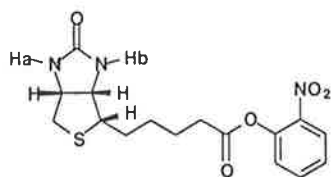
**[3aS-(3aα, 4β, 6aα)]-Hexahydro-2-oxo-1H-thieno[3, 4-d]imidazole-4-pentanoic acid, 2, 4-dinitrophenyl ester (13)**



d-Biotin (**1**) (0.194 g, 0.8 mmol) was dissolved in DMF (2.5 ml) at 80 °C and the solution removed from heating. 2, 4-Dinitrophenol (0.150 g, 0.82 mmol) and DCC (0.186 g, 0.9 mmol) were added and the reaction mixture stirred at room temperature overnight, filtered to remove precipitated DCU and the solvent removed *in vacuo* (oil pump). The residue was purified on silica gel with 6% MeOH, 20% acetone and 74% CH<sub>2</sub>Cl<sub>2</sub> to give **13** as a light yellow solid (0.10 g, 30.5%). m.p. 158-161 °C, decomp. <sup>1</sup>H NMR (CDCl<sub>3</sub>): δ (ppm) 1.558-1.871 (m, 8 H, CH<sub>2</sub>); 2.733 (t, 2 H, CH<sub>2</sub>, *J* = 6.6 Hz); 2.774 (d, 1 H, *J* = 12.6 Hz); 2.993 (dd, 1 H, *J* = 12.6 Hz, 4.8 Hz, H5a); 3.221 (m, 1 H, H2); 4.375 (m, 1 H, H3); 4.528 (s, 1 H, NHa); 4.546 (m, 1 H, H4); 4.715 (s, 2 H, Hb); 7.507 (d, 1 H, Ar, H-6); 8.557 (dd, 1 H, *J* = 8.7 Hz, 2.7 Hz, Ar, H-5); 8.975 (d, 1 H, *J* = 2.7 Hz, Ar, H-3). Calc. for [M+ H]<sup>+</sup> C<sub>16</sub>H<sub>19</sub>N<sub>4</sub>O<sub>7</sub>S: 411.0991. Found: 411.0975.

Compounds **10**, **11**, **13**, **14**, **17** and **18** were prepared in a similar manner as the example described below for **13** except for the difference stated.

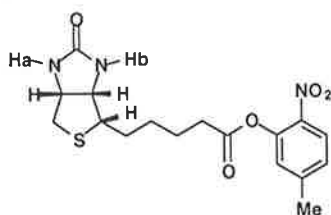
**[3aS-(3aα, 4β, 6aα)]-Hexahydro-2-oxo-1H-thieno[3, 4-d]imidazole-4-pentanoic acid, 2-nitrophenyl ester (10)**



Eluant 10/10/80 acetone/methanol/CH<sub>2</sub>Cl<sub>2</sub>, yield 55%, as a light yellow solid, m.p. 155-156 °C. <sup>1</sup>H NMR (CDCl<sub>3</sub>): δ (ppm) 1.549-1.892 (m, 8 H, CH<sub>2</sub>); 2.707 (m, 3 H, CH, CH<sub>2</sub>); 2.986 (quartet, 1 H, dd, *J* = 12.6 Hz, 4.8 Hz, H5a); 3.243 (m, 1 H, H2); 4.382 (m, 1 H, H3); 4.476 (s, 1 H, NHa); 4.560 (m, 1 H, H4); 4.686 (s, 2 H, Hb); 7.227 (d, 1 H, Ar); 7.439 (dd, 1 H, *J* = 7.2

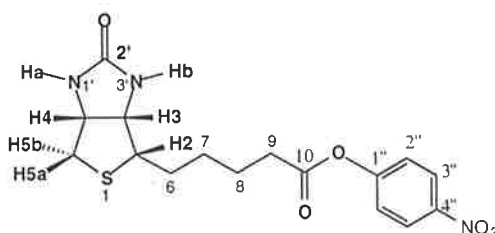
Hz, 1.2 Hz, Ar); 7.674 (dd, 1 H,  $J = 6.9$  Hz, 1.8 Hz, Ar); 8.110 (dd, 1 H,  $J = 8.1$  Hz,  $J = 1.5$  Hz, Ar). Calc. for  $[M+H]^+ C_{16}H_{20}N_3O_5S$ : 366.1140. Found: 366.1112.

**[3aS-(3a $\alpha$ , 4 $\beta$ , 6a $\alpha$ )]-Hexahydro-2-oxo-1H-thieno[3, 4-d]imidazole-4-pentanoic acid, 5-methyl-2-nitrophenyl ester (11)**



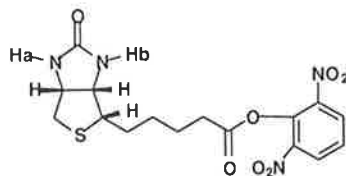
Eluant 10/90 methanol/ $CH_2Cl_2$ , yield 42%, as a light yellow solid, m.p. 162-165 °C.  $^1H$  NMR ( $CDCl_3$ ):  $\delta$  (ppm) 1.547-1.863 (m, 8 H,  $CH_2$ ); 2.453 (s, 3 H,  $CH_3$ ); 2.654-2.759 (m, 3 H, CH,  $CH_2$ ); 2.943 (dd, 1 H, CH,  $J = 12.6$  Hz, 5.1 Hz); 3.220 (m, 1 H, CH); 4.336 (m, 1 H, H3); 4.451 (s, 1 H, NHa); 4.557 (m, 1 H, H4); 4.653 (s, 2 H, Hb); 7.025 (s, 1 H, Ar); 7.169 (dd, 1 H,  $J = 7.2$  Hz, 1.2 Hz, Ar); 7.674 (dd, 1 H,  $J = 6.9$  Hz, 1.8 Hz, Ar); 8.110 (dd, 1 H,  $J = 7.5$  Hz, Ar); 8.033 (d, 1 H, Ar). Calc. for  $[M+H]^+ C_{17}H_{22}N_3O_5S$ : 380.1297. Found: 380.1277.

**[3aS-(3a $\alpha$ , 4 $\beta$ , 6a $\alpha$ )]-Hexahydro-2-oxo-1H-thieno[3, 4-d]imidazole-4-pentanoic acid, 4-nitrophenyl ester (12)**



$^{13}C$  NMR ( $CDCl_3$ , 20 mM, rt) spectrum was assigned by using ghmbc and ghmqc 2D-NMR techniques:  $\delta$ (ppm) C-2', 163.19; C-2, 55.31; C-3, 61.99; C-4, 60.09; C-5, 40.53; C-6, 28.36; C-7, 28.36; C-8, 24.57; C-9, 33.93; C-10, 171.08; C-1'', 145.34; C-2'', 122.44; C-3'', 125.20; C-4'', 155.39.

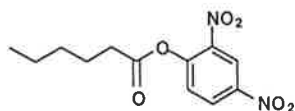
**[3aS-(3a $\alpha$ , 4 $\beta$ , 6a $\alpha$ )]-Hexahydro-2-oxo-1H-thieno[3, 4-d]imidazole-4-pentanoic acid, 2, 6-dinitrophenyl ester (14)**



Eluant 6/20/74 methanol/acetone/ $CH_2Cl_2$ , yield 25% as a light yellow solid, m.p. 146-148 °C, decomp.  $^1H$  NMR ( $CDCl_3$ ):  $\delta$  (ppm) 1.552-1.885 (m, 8 H,  $CH_2$ ); 2.764 (m, 3 H, CH,  $CH_2$ ); 2.947 (dd, 1 H,  $J = 17.7$  Hz, 4.8 Hz, CH); 3.218 (m, 1 H, H2); 4.374 (m, 1 H, H3); 4.498 (s, 1

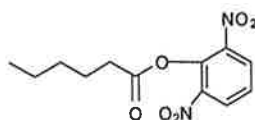
H, NHa); 4.534 (m, 1 H, H4); 4.718 (s, 1 H, NHb); 7.605 (t, 1 H,  $J = 8.4$  Hz, H-4, Ar); 8.335 (d, 2 H,  $J = 8.4$  Hz, H-3 or H-5, phenyl). Calc. for  $[M+H]^+$   $C_{16}H_{19}N_4O_7S$ : 411.0991. Found: 411.0996.

### 2, 4-Dinitrophenylhexanoate (17)



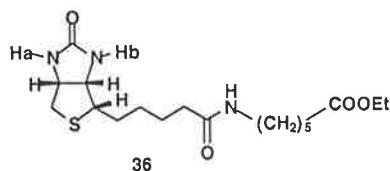
The solvent was  $CH_2Cl_2$  (5 ml). Eluant 50/50  $CH_2Cl_2$ /hexane, yield 62% as a yellow oil.  $^1H$  NMR ( $CDCl_3$ ):  $\delta$  (ppm), 0.944 (t, 3 H,  $J = 7.5$  Hz,  $CH_3$ ); 1.408 (m, 4 H,  $CH_2$ ); 1.813 (m, 2 H,  $CH_2$ ); 2.691 (t, 2 H,  $J = 7.8$  Hz,  $CH_2$ ); 7.486 (d, 1 H,  $J = 8.7$  Hz, H-6, Ar); 8.539 (dd, 1 H,  $J = 9.0$  Hz, 3.0 Hz, H-5, Ar); 8.966 (d, 1 H,  $J = 2.4$  Hz, H-3, Ar).  $^{13}C$  NMR:  $\delta$  (ppm) 13.82, 22.23, 31.10, 33.97, 121.67, 126.63, 128.87, 131.59, 145.03, 148.73, 170.40. Calc. for  $[M]^+$   $C_{12}H_{14}N_2O_6$ : 282.0852. Found: 282.

### 2, 6-Dinitrophenylhexanoate (18)



The solvent was  $CH_2Cl_2$  (5 ml). Eluant 50/50  $CH_2Cl_2$ /hexane, yield 58% as a yellow oil.  $^1H$  NMR ( $CDCl_3$ ):  $\delta$  (ppm) 0.940 (t, 3 H,  $J = 6.9$  Hz,  $CH_3$ ); 1.413 (m, 4 H,  $CH_2$ ); 1.792 (m, 2 H,  $CH_2$ ); 2.702 (t, 2 H,  $J = 7.2$  Hz,  $CH_2$ ); 7.577 (t, 1 H,  $J = 8.4$  Hz, H-4, Ar); 8.323 (d, 2 H,  $J = 8.4$  Hz, H-3, H-5, Ar).  $^{13}C$  NMR:  $\delta$  (ppm) 13.82, 22.23, 23.85, 31.04, 33.75, 126.32, 129.88, 139.02, 143.84, 170.05. Calc. for  $[M]^+$   $C_{12}H_{14}N_2O_6$ : 282.0852. Found: 282.0846.

### [3aS-(3a $\alpha$ , 4 $\beta$ , 6a $\alpha$ )]-Hexahydro-2-oxo-N-(6-aminohexanoic acid ethyl ester)-1H-thieno[3, 4-d]imidazole-4-pentamide (36)

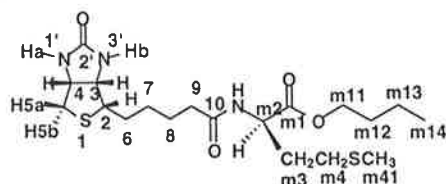


To a stirred solution of biotin *N*-hydroxysuccinimide ester (310 mg, 0.91 mmol) in DMF (4.0 ml) was added ethyl 6-aminohexanoic acid ester hydrochloride (159 mg, 1.0 mmol) and  $NEt_3$  1.0 ml. The mixture was stirred overnight, the solvent was removed *in vacuo* with oil pump, the residue purified by flash chromatography using 10/90 (v/v) MeOH/ $CH_2Cl_2$  as an eluant to give product **36** as a white solid 0.238 mg, yield 67.9%.  $^1H$  NMR ( $CDCl_3$ , 1 mM, rt):  $\delta$  (ppm) 1.211 (t, 3 H,  $J = 6.9$  Hz,  $CH_3$ ); 1.351-1.714 (m,  $CH_2$ ); 2.226 (m,  $CH_2$ ); 2.308 (t, 2 H,  $J = 6.9$  Hz,  $CH_2$ ); 2.754 (d, 1 H,  $J = 13.5$  Hz, H5b); 2.927 (dd, 1 H,  $J = 12.9$  Hz, 5.1 Hz, H5a); 3.287 (m, 3 H, H2+ $CH_2$ ); 4.162 (quartet, 2 H,  $J = 7.2$  Hz,  $CH_2$ ); 4.345 (m, 1 H, H3); 4.507 (m, 1 H, H4); 4.507 (s,

1 H, NHa); 5.060 (s, 1 H, NHb); 5.582 (s, 1 H, NHc). Calc. for  $[M + H]^+ C_{18}H_{31}N_3O_4S$  : 385.2052. Found: 385.2029.

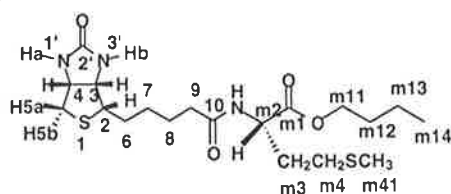
Biotin amides and peptides **37-46** were prepared in a similar manner as the example described below for **39** except for the difference stated.

**[3aS-(3a $\alpha$ , 4 $\beta$ (1R), 6a $\alpha$ )]-Hexahydro-2-oxo-N-(methionine butyl ester)-1H-thieno[3, 4-d]imidazole-4-pentamide (37)**



Eluant 6/9/85 methanol/acetone/ $CH_2Cl_2$  yield 98.6% as a white solid.  $^1H$  NMR ( $CDCl_3$ , 1 mM):  $\delta$  (ppm) 0.943 (t, 3 H,  $J = 7.5$  Hz,  $CH_3$ ); 1.375-1.737 (m, 12 H,  $CH_2$ ); 2.008 (m, 1 H, Hm3b'); 2.105 (s, 3 H,  $CH_3$ ); 2.105 (m, 1 H, Hm3a'); 2.287 (m, 2 H,  $CH_2$ ); 2.520 (t, 3 H,  $J = 7.8$  Hz,  $CH_3$ ); 2.754 (d, 1 H,  $J = 12.6$  Hz, H5b); 2.924 (dd, 1 H,  $J = 12.9$  Hz, 5.1 Hz, H5a); 3.169 (m, 1 H, H2); 4.154 (t, 2 H,  $J = 6.9$  Hz,  $CH_2$ ); 4.343 (m, 1 H, H3); 4.519 (m, 1 H, H4); 4.831 (s, 1 H, NHa); 4.718 (m, 1 H, CH); 5.556 (s, 1 H, NHb); 6.622 (d, 1 H,  $J = 7.2$  Hz, NHc). The peaks of carbons in  $^{13}C$  NMR ( $CDCl_3$ , 25 mM, rt) spectrum was assigned by ghmbc and ghmqc 2D-NMR techniques:  $\delta$ (ppm) C2', 164.08; C2, 55.534; C3, 61.67; C4, 60.22; C5, 40.58; C6, 28.00; C7, 28.00; C8, 25.52; C9, 30.53; C10, 173.13; Cm1, 173.31; Cm2, 51.43; Cm3, 31.74; Cm4, 35.69; Cm41, 15.47; Cm11, 65.52; Cm12, 30.19; Cm13, 19.07; Cm14, 13.66. Calc. for  $[M]^+ C_{19}H_{33}N_3O_4S_2$ : 431.1946. Found: 431.1896.

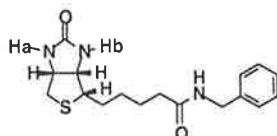
**[3aS-(3a $\alpha$ , 4 $\beta$ (1S), 6a $\alpha$ )]-Hexahydro-2-oxo-N-(methionine butyl ester)-1H-thieno[3, 4-d]imidazole-4-pentamide (38)**



Eluant 6/9/85 methanol/acetone/ $CH_2Cl_2$  yield 94.3% as a white solid.  $^1H$  NMR ( $CDCl_3$ , 1 mM):  $\delta$  (ppm) 0.943 (t, 3 H,  $J = 7.5$  Hz,  $CH_3$ ); 1.351-1.787 (m, 12 H,  $CH_2$ ); 2.017 (m, 1 H, Hm3b'); 2.108 (s, 3 H,  $CH_3$ ); 2.108 (m, 1 H, Hm3a'); 2.270 (t, 2 H,  $J = 6.6$  Hz,  $CH_2$ ); 2.536 (t, 3 H,  $J = 7.8$  Hz,  $CH_3$ ); 2.754 (d, 1 H,  $J = 11.1$  Hz, H5b); 2.950 (dd, 1 H,  $J = 12.9$  Hz, 5.1 Hz, H5a); 3.177 (m, 1 H, H2); 4.159 (t, 2 H,  $J = 6.6$  Hz,  $CH_2$ ); 4.357 (m, 1 H, H3); 4.526 (m, 1 H, H4); 4.609 (s, 1 H, NHa); 4.712 (m, 1 H, CH); 5.492 (s, 1 H, NHb); 6.631 (d, 1 H, NHc). The peaks of carbons in  $^{13}C$  NMR ( $CDCl_3$ , 25 mM, rt) spectrum was assigned by using ghmbc and ghmqc 2D-NMR techniques:  $\delta$  (ppm) C2', 163.97; C2, 55.51; C3, 61.93; C4, 60.19; C5, 40.41; C6,

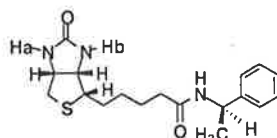
28.20; C7, 28.15; C8, 25.47; C9, 30.21; C10, 172.95; Cm1, 173.26; Cm2, 51.52; Cm3, 31.68; Cm4, 35.63; Cm41, 15.47; Cm11, 65.51; Cm12, 30.53; Cm13, 19.08; Cm14, 13.66. Calc. for  $[M]^+ C_{19}H_{33}N_3O_4S_2$ : 431.1946. Found: 431.1926.

**[3aS-(3a $\alpha$ , 4 $\beta$ , 6a $\alpha$ )]-Hexahydro-2-oxo-N-benzenemethyl-1H-thieno[3, 4-d]imidazole-4-pentamide (39)**



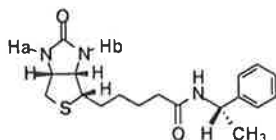
Typically, to a stirred solution of biotin *N*-hydroxysuccinimide ester (34.1 mg, 0.1 mmol) in DMF (2.0 ml) was added benzylamine (10.9  $\mu$ l, 10.7 mg, 0.1 mmol) and  $NEt_3$  (0.015 ml). The mixture was stirred overnight, the solvent was removed *in vacuo* with oil pump, the residue purified by flash chromatography using 10/90 and 25/75 (v/v) MeOH/ $CH_2Cl_2$  as successive eluants to give product **39** as a white solid, 30.3 mg, yield 91.0%.  $^1H$  NMR ( $CDCl_3$ , 1 mM, rt):  $\delta$  (ppm) 1.465-1.746 (m, 8 H,  $CH_2$ ); 2.257 (m, 2 H,  $CH_2$ ); 2.727 (d, 1 H,  $J = 12.9$  Hz, CH); 2.954 (dd, 1 H,  $J = 12.9$  Hz, 5.1 Hz, H5a); 3.169 (m, 1 H, H2); 4.326 (m, 1 H, H3); 4.454 (d, 2 H,  $J = 5.7$  Hz,  $CH_2Ar$ ); 4.506 (m, 1 H, H4); 4.506 (s, 1 H, NHa); 5.102 (s, 1 H, NHb); 5.868 (s, 1 H, NHc); 7.310 (m, 5 H, Ar). Calc. for  $[M]^+ C_{17}H_{23}N_3O_2S$ : 333.1528. Found: 333.1504.

**[3aS-(3a $\alpha$ , 4 $\beta$ (1*R*), 6a $\alpha$ )]-Hexahydro-2-oxo-N-( $\alpha$ -methyl-benzenemethyl)-1H-thieno[3, 4-d]imidazole-4-pentamide (40)**



Eluants 10/90 and 20/80 methanol/ $CH_2Cl_2$ , successively, yield 95.6% as a white solid.  $^1H$  NMR ( $CDCl_3$ ):  $\delta$  (ppm) 1.397-1.747 (m, 6 H,  $CH_2$ ); 1.505 (d, 3 H,  $J = 6.6$  Hz,  $CH_3$ ); 2.222 (m, 2 H,  $CH_2$ ); 2.729 (d, 1 H,  $J = 12.6$  Hz, CH); 2.952 (dd, 1 H,  $J = 12.6$  Hz, 5.1 Hz, H5a); 3.173 (m, 1 H, H2); 4.310 (m, 1 H, H3); 4.456 (s, 1 H, NHa); 4.521 (m, 1 H, H4); 5.012 (s, 1 H, NHb); 5.165 (m, 1 H, CHAr); 5.771 (d, 1 H, NHc); 7.350 (m, 5 H, Ar). Calc. for  $[M]^+ C_{18}H_{25}N_3O_2S$ : 347.1684. Found: 347.1668.

**[3aS-(3a $\alpha$ , 4 $\beta$ (1*S*), 6a $\alpha$ )]-Hexahydro-2-oxo-N-( $\alpha$ -methyl-benzenemethyl)-1H-thieno[3, 4-d]imidazole-4-pentamide (41)**

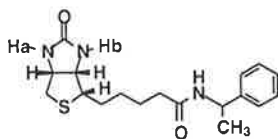


Eluants initially 10/90 and then 20/80 methanol/ $CH_2Cl_2$ , isolated as a white solid, yield 93.2%.  $^1H$  NMR ( $CDCl_3$ ):  $\delta$  (ppm) 1.425-1.769 (m, 6 H,  $CH_2$ ); 1.505 (d, 3 H,  $J = 6.6$  Hz,  $CH_3$ ); 2.204



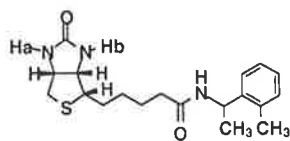
(t, 2 H,  $J = 7.5$  Hz, CH<sub>2</sub>); 2.725 (d, 1 H,  $J = 12.9$  Hz, H5b, CH); 2.950 (dd, 1 H,  $J = 12.9$  Hz, 4.8 Hz, H5a); 3.184 (m, 1 H, H2); 4.296 (m, 1 H, H3); 4.509 (m, 1 H, H4); 4.556 (s, 1 H, NHa); 5.009 (s, 1 H, NHb); 5.165 (m, 1 H, CHAr); 5.779 (d, 1 H, NHc); 7.360 (m, 5 H, Ar). Calc. for [M]<sup>+</sup> C<sub>18</sub>H<sub>25</sub>N<sub>3</sub>O<sub>2</sub>S: 347.1684. Found: 347.1655.

**[3aS-(3a $\alpha$ , 4 $\beta$ (1R, 1S), 6a $\alpha$ )]-Hexahydro-2-oxo-*N*-( $\alpha$ -methyl-benzenemethyl)-1*H*-thieno[3, 4-*d*]imidazole-4-pentamide (42)**



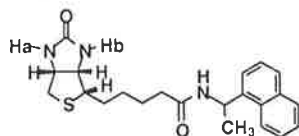
Eluants initially 10/90 and then 20/80 methanol/CH<sub>2</sub>Cl<sub>2</sub>, isolated as a white solid, yield 92.1%. <sup>1</sup>H NMR (CDCl<sub>3</sub>):  $\delta$  (ppm) 1.425-1.769 (m, 6 H, CH<sub>2</sub>); 1.506 (d, 3 H,  $J = 6.9$  Hz, CH<sub>3</sub>); 2.222 (m, 2 H, CH<sub>2</sub>); 2.728 (d, 1 H,  $J = 13.2$  Hz, CH, H5b); 2.949 (dd, 1 H,  $J = 11.7$  Hz, 4.5 Hz, H5a); 3.147 (m, 1 H, H2); 4.294 (m, 1 H, H3); 4.497 (m, 1 H, H4); 4.481 (s, 1 H, NHa); 4.927 (s, 1/2 H, Hb, D-D); 4.994 (s, 1/2 H, Hb, D-L); 5.116 (m, 1 H, CHAr); 5.740 (d, 1 H, NHc); 7.353 (m, 5 H, Ar). Calc. for [M]<sup>+</sup> C<sub>18</sub>H<sub>25</sub>N<sub>3</sub>O<sub>2</sub>S: 347.1684. Found: 347.1656. -

**[3aS-(3a $\alpha$ , 4 $\beta$ (1R, 1S), 6a $\alpha$ )]-Hexahydro-2-oxo-*N*-[ $\alpha$ -methyl-(2-methyl-benzenemethyl)]-1*H*-thieno[3, 4-*d*]imidazole-4-pentamide (43)**



Eluant 12/6/82 methanol/acetone/CH<sub>2</sub>Cl<sub>2</sub> yield 90.3% as a white solid. <sup>1</sup>H NMR (CDCl<sub>3</sub>):  $\delta$  (ppm) 1.408-1.770 (m, 6 H, CH<sub>2</sub>); 1.484 (d, 3 H,  $J = 6.9$  Hz, CH<sub>3</sub>); 2.200 (m, 2 H, CH<sub>2</sub>); 2.376 (s, 3 H, CH<sub>3</sub>); 2.725 (d, 1 H,  $J = 12.6$  Hz, CH, H5b); 2.930 (dd 1 H,  $J = 11.7$  Hz, 5.1 Hz, H5a); 3.143 (m, 1 H, H2); 4.283 (m, 1 H, H3); 4.506 (m, 1 H, H4); 4.506 (s, 1 H, NHa); 4.969 (s, 1/2 H, Hb, D-D); 5.043 (s, 1/2 H, Hb, D-L); 5.304 (m, 1 H, CHAr); 5.697 (d, 1 H, NHc); 7.171 (m, 4 H, Ar). Calc. for [M]<sup>+</sup> C<sub>19</sub>H<sub>27</sub>N<sub>3</sub>O<sub>2</sub>S: 361.1841. Found: 361.1833.

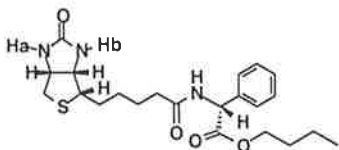
**[3aS-(3a $\alpha$ , 4 $\beta$ (1R, 1S), 6a $\alpha$ )]-Hexahydro-2-oxo-*N*-( $\alpha$ -methyl-naphthalenemethyl)-1*H*-thieno[3, 4-*d*]imidazole-4-pentamide (44)**



Eluant 12/6/82 methanol/acetone/CH<sub>2</sub>Cl<sub>2</sub> yield 87.0% as a white solid. <sup>1</sup>H NMR (CDCl<sub>3</sub>):  $\delta$  (ppm) 1.379-1.679 (m, 6 H, CH<sub>2</sub>); 1.679 (d, 3 H,  $J = 6.9$  Hz, CH<sub>3</sub>); 2.185 (m, 2 H, CH<sub>2</sub>); 2.656 (m, 1 H, H5b); 2.837 (m, 1 H, H5a); 3.068 (m, 1 H, H2); 4.018 (m, 1/2 H, H3, D-L); 4.249 (m, 1/2 H, H3, D-D); 4.362 (m, 1 H, H4); 4.755 (s, 1/2 H, NHa, D-L); 4.795 (s, 1/2 H,

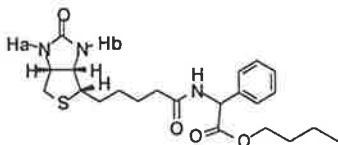
NHa, D-D); 5.653 (s, 1/2 H, NHb, D-L); 5.736 (s, 1/2 H, NHb, D-D); 5.939 (m, 1 H, CHPh); 6.090 (d, 1/2 H,  $J = 8.7$  Hz, NHc, D-L); 6.157 (d, 1/2 H,  $J = 8.1$  Hz, NHc, D-D); 7.426-8.117 (m, 7H, Ar). Calc. for  $[M]^+ C_{22}H_{27}N_3O_2S$ : 397.1841. Found: 397.1829.

**[3aS-(3a $\alpha$ , 4 $\beta$ (1R), 6a $\alpha$ )]-Hexahydro-2-oxo-N-(phenylglycinylyl butyl ester)-1H-thieno[3, 4-d]imidazole-4-pentamide (45)**



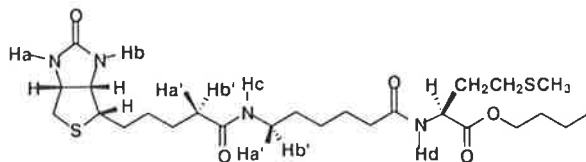
Eluant 12/6/82 methanol/acetone/ $CH_2Cl_2$  yield 91.0% as a white solid.  $^1H$  NMR ( $CDCl_3$ , 1 mM):  $\delta$  (ppm) 0.845 (t, 3 H,  $J = 7.2$  Hz,  $CH_3$ ); 1.280 (m, 2 H,  $CH_2$ ); 1.455-1.747 (m, 8 H,  $CH_2$ ); 2.286 (t, 2 H,  $J = 7.5$  Hz,  $CH_2$ ); 2.722 (d, 1 H,  $J = 13.2$  Hz, H5b); 2.942 (dd, 1 H,  $J = 12.6$  Hz, 5.4 Hz, H5a); 3.132 (m, 1 H, H2); 4.140 (m, 2 H,  $CH_2$ ); 4.275 (m, 1 H, H3); 4.492 (m, 1 H, H4); 4.726 (s, 1 H, NHa); 5.304 (s, 1 H, NHb); 5.608 (d, 1 H,  $J = 7.5$  Hz, CHAr). 6.769 (d, 1 H,  $J = 7.2$  Hz, NHc); 7.363 (m, 5 H, Ar). Calc. for  $[M]^+ C_{22}H_{31}N_3O_4S$ : 433.2052. Found: 433.2042.

**[3aS-(3a $\alpha$ , 4 $\beta$ (1R, 1S), 6a $\alpha$ )]-Hexahydro-2-oxo-N-(phenylglycinylyl butyl ester)-1H-thieno[3, 4-d]imidazole-4-pentamide (46)**



Eluant 12/6/82 methanol/acetone/ $CH_2Cl_2$  yield 93.0% as a white solid.  $^1H$  NMR ( $CDCl_3$ , 1 mM):  $\delta$  (ppm) 0.845 (t, 3 H,  $J = 7.2$  Hz,  $CH_3$ ); 1.280 (m, 2 H,  $CH_2$ ); 1.479-1.747 (m, 8 H,  $CH_2$ ); 2.286 (t, 2 H,  $J = 6.3$  Hz,  $CH_2$ ); 2.717 (d, 1/2 H,  $J = 12.0$  Hz, H5b, D-D); 2.738 (d, 1/2 H,  $J = 12.9$  Hz, H5b, D-L); 2.921 (m, 1 H, H5a); 3.113 (m, 1 H, H2); 4.136 (m, 2 H,  $CH_2$ ); 4.243 (m, 1 H, H3); 4.485 (m, 1 H, H4); 4.614 (s, 1/2 H, NHa, D-L); 4.680 (s, 1/2 H, NHa, D-D); 5.376 (s, 1/2 H, NHb, D-D); 5.565 (s, 1/2 H, NHb, D-L); 5.590 (d, 1/2 H,  $J = 7.5$  Hz, CHAr, D-L); 5.609 (d, 1/2 H,  $J = 7.5$  Hz, CHAr, D-D); 6.724 (d, 1/2 H,  $J = 6.9$  Hz, NHc, D-L); 6.747 (d, 1/2 H,  $J = 6.9$  Hz, NHc, D-D); 7.369 (m, 5 H, Ar). Calc. for  $[M]^+ C_{22}H_{31}N_3O_4S$ : 433.2052. Found: 433.2052.

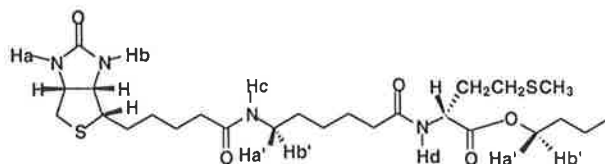
**[3aS-(3a $\alpha$ , 4 $\beta$ (1S), 6a $\alpha$ )]-Hexahydro-2-oxo-N-(6-aminohexanoyl-methionine butyl ester)-1H-thieno[3, 4-d]imidazole-4-pentamide (49)**



To a stirred solution of *N*-hydroxylsuccinimido ester of biotininated 6-aminohexanoic acid (45.4 mg, 0.1 mmol) in DMF (10 ml) at 40-50 °C was added the salt of L-butyl methionine ester hydrochloride (24.2 mg, 0.1 mmol) and NEt<sub>3</sub> (0.030 ml, 0.2 mmol). The reaction mixture was stirred overnight and workup as described for **39** gave crude **49**. Purification of **49** on silica gel with successive eluants 15/5/85 and 25/5/70 methanol/acetone/CH<sub>2</sub>Cl<sub>2</sub> gave pure **49** as a white solid, yield 71.3%. <sup>1</sup>H NMR (600 MHz, CDCl<sub>3</sub>, 1 mM): δ (ppm) 0.945 (t, 3 H, *J* = 7.8 Hz, CH<sub>3</sub>); 1.404-1.803 (m, 16 H, CH<sub>2</sub>); 2.015 (m, 1 H, Hm3b'); 2.105 (s, 3 H, CH<sub>3</sub>); 2.121 (m, 1 H, Hm3a'); 2.294 (m, 2 H, CH<sub>2</sub>); 2.548 (t, 2 H, *J* = 8.4 Hz, CH<sub>2</sub>); 2.731 (d, 1 H, *J* = 12.6 Hz, H5b); 2.950 (dd, 1 H, *J* = 13.2 Hz, 4.8 Hz, H5a); 3.189 (m, 1 H, H2); 3.189, 3.365 (m, 2 H, CH<sub>2</sub>); 4.146 (t, 2 H, *J* = 6.6 Hz, CH<sub>2</sub>); 4.348 (m, 1 H, H3); 4.525 (m, 1 H, H4); 4.609 (s, 1 H, NHa); 4.676 (m, 1 H, CH); 5.541 (s, 1 H, NHb); 6.022 (d, 1 H, NHc); 7.221 (d, 1 H, *J* = 7.8 Hz, NHd). Calc. for [M]<sup>+</sup> C<sub>25</sub>H<sub>44</sub>N<sub>4</sub>O<sub>5</sub>S<sub>2</sub>: 544.2787. Found: 544.2760.

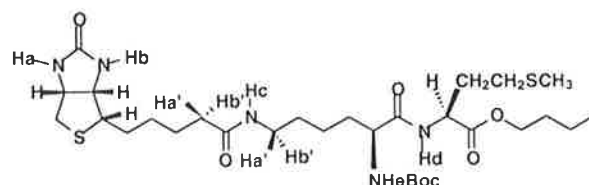
Compounds **47-50** were also prepared in a similar manner. During the preparation compounds **49-50**, *N*-hydroxylsuccinimido ester of biotininated 6-aminohexanoic acid was used as the reactant. Likewise, *N*-hydroxylsuccinimido biocytin was the reactant for the preparation of compounds **47-48**.

**[3aS-(3aα, 4β(1*R*), 6aα)]-Hexahydro-2-oxo-*N*-(6-aminohexanoyl-methionine butyl ester)-1*H*-thieno[3, 4-*d*]imidazole-4-pentamide (**50**)**



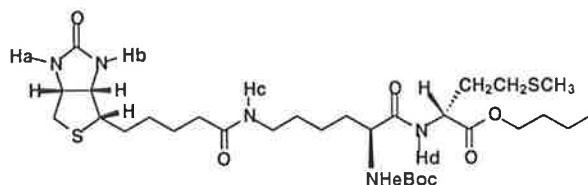
The work-up was the same as that for compound **49**. Eluants were 15/5/85 and 25/5/70 methanol/acetone/CH<sub>2</sub>Cl<sub>2</sub> successively, yield 68.7% as a white solid. <sup>1</sup>H NMR (600 MHz, CDCl<sub>3</sub>, 1 mM): δ (ppm) 0.944 (t, 3 H, *J* = 7.2 Hz, CH<sub>3</sub>); 1.398-1.782 (m, 16 H, CH<sub>2</sub>); 2.033 (m, 1 H, Hm3b'); 2.102 (s, 3 H, CH<sub>3</sub>); 2.119 (m, 1 H, Hm3a'); 2.234 (m, 2 H, CH<sub>2</sub>); 2.557 (m, 2 H, CH<sub>2</sub>); 2.736 (d, 1 H, *J* = 13.2 Hz, H5b); 2.944 (dd, 1 H, *J* = 13.2 Hz, 5.4 Hz, H5a); 3.180 (m, 1 H, H2); 3.255, 3.326 (m, 2 H, CH<sub>2</sub>); 4.140 (m, 2 H, CH<sub>2</sub>); 4.354 (m, 1 H, H3); 4.533 (m, 1 H, H4); 4.687 (m, 1 H, CH); 4.914 (s, 1 H, NHa); 5.151 (s, 1 H, NHb); 5.944 (s, 1 H, NHc); 7.302 (d, 1 H, *J* = 7.2 Hz, NHd). Calc. for [M]<sup>+</sup> C<sub>25</sub>H<sub>44</sub>N<sub>4</sub>O<sub>5</sub>S<sub>2</sub>: 544.2787. Found: 544.2766.

**[3aS-(3aα, 4β(1*S*, 2*S*), 6aα)]-Hexahydro-2-oxo-*N*-(*N*<sup>α</sup>-*t*-butyloxycarbonyl)cynil methionine butyl ester)-1*H*-thieno[3, 4-*d*]imidazole-4-pentamide (**47**)**



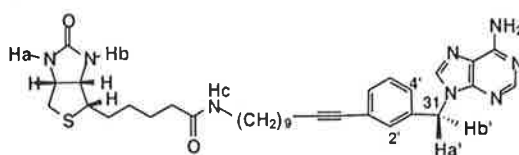
Compounds **47-48** were prepared by using usual manner for the preparation of biotin amides, except that the amine for the amidation was from its hydrochloride salt and generated by using 2 equiv. base  $\text{NEt}_3$ . Eluant was 10/10/80 methanol/acetone/ $\text{CH}_2\text{Cl}_2$ , yield 63.0% as a white solid.  $^1\text{H}$  NMR (600 MHz,  $\text{CDCl}_3$ , 1 mM):  $\delta$  (ppm) 0.938 (t, 3 H,  $J = 7.2$  Hz,  $\text{CH}_3$ ); 1.430 (s, 9 H,  $\text{CH}_3$ ); 1.391-1.849 (m, 16 H,  $\text{CH}_2$ ); 2.027 (m, 1 H, Hm3b'); 2.098 (s, 3 H,  $\text{CH}_3$ ); 2.145 (m, 1 H, Hm3a'); 2.224 (m, 2 H,  $\text{CH}_2$ ); 2.263 (m, 2 H,  $\text{CH}_2$ ); 2.577 (m, 2 H,  $\text{CH}_2$ ); 2.745 (d, 1 H,  $J = 13.2$  Hz, H5b); 2.919 (dd, 1 H,  $J = 12.6$  Hz, 4.8 Hz, H5a); 3.125, 3.429 (m, 2 H,  $\text{CH}_2$ ); 3.198 (m, 1 H, H2); 4.135 (m, 2 H,  $\text{CH}_2$ ); 4.319 (m, 1 H, H3); 4.533 (m, 1 H, H4); 4.683 (m, 1 H, CH); 5.207 (s, 1 H, NHa); 5.312 (s, 1 H, NHb); 5.312 (s, 1 H, NHe); 6.279 (s, 1 H, NHc); 8.018 (d, 1 H,  $J = 7.2$  Hz, NHd). Calc. for  $[\text{M} + \text{H}]^+$   $\text{C}_{30}\text{H}_{54}\text{N}_5\text{O}_7\text{S}_2$ : 660.3498. Found: 660.3500.

**[3aS-(3a $\alpha$ , 4 $\beta$ (1S, 2R), 6a $\alpha$ )]-Hexahydro-2-oxo-N-(N $^\alpha$ -*t*-butyloxycarbonyl)cynyl methionine butyl ester)-1*H*-thieno[3, 4-*d*]imidazole-4-pentamide (**48**)**



Eluant 10/10/80 methanol/acetone/ $\text{CH}_2\text{Cl}_2$ , yield 60.0% as a white solid.  $^1\text{H}$  NMR (600 MHz,  $\text{CDCl}_3$ , 1 mM):  $\delta$  (ppm) 0.938 (t, 3 H,  $J = 7.2$  Hz,  $\text{CH}_3$ ); 1.430 (s, 9 H,  $\text{CH}_3$ ); 1.390-1.781 (m, 16 H,  $\text{CH}_2$ ), 2.049 (m, 1 H, Hm3b'); 2.128 (m, 1 H, Hm3a'); 2.097 (s, 3 H,  $\text{CH}_3$ ); 2.255 (m, 2 H,  $\text{CH}_2$ ); 2.532 (t, 2 H,  $J = 6.6$  Hz,  $\text{CH}_2$ ); 2.780 (d, 1 H,  $J = 12.6$  Hz, H5b); 2.928 (dd, 1 H,  $J = 13.2$  Hz, 4.8 Hz, H5a); 3.195 (m, 1 H, H2); 3.266, 3.299 (m, 2 H,  $\text{CH}_2$ ); 4.134, 4.140 (m, 2 H,  $\text{CH}_2$ ); 4.198 (m, 1 H, CH); 4.325 (m, 1 H, H3); 4.539 (m, 1 H, H4); 4.663 (m, 1 H, CH); 5.203 (s, 1 H, NHa); 5.408 (s, 1 H, NHb); 5.408 [s, 1 H, NHe (at 30 °C, 5.362 ppm for NHe and 5.231 ppm for NHb)]; 6.330 (s, 1 H, NHc); 7.890 (d, 1 H,  $J = 7.2$  Hz, NHd). Calc. for  $[\text{M} + \text{H}]^+$   $\text{C}_{30}\text{H}_{54}\text{N}_5\text{O}_7\text{S}_2$ : 660.3498. Found: 660.3500.

**[3aS-(3a $\alpha$ , 4 $\beta$ , 6a $\alpha$ )]-9-[3-[11-[N-[5-(Hexahydro-2-oxo-1*H*-thieno[3, 4-*d*]imidazol-4-yl)-1-oxopentyl]]-aminoundec-1-ynyl]-benzenemethyl]adenine (**51**)**

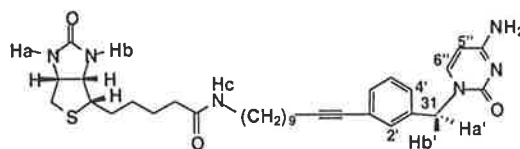


To a stirred suspension of 9-(3'-iodobenzyl)adenine (**58**) (28.4 mg, 0.080 mmol) in piperidine (2 mL) under nitrogen, was added  $\text{Pd}(\text{PPh}_3)_4$  (8.78 mg, 0.0076 mmol),  $\text{PPh}_3$  (4.2 mg),  $\text{ZnCl}_2$  (2.4 mg), NaI (2 mg) and biotin undecynyl amide **33** (30.0 mg, 0.076 mmol) respectively. The resulting suspension was heated at reflux for 2.5 h in oil bath at 110 °C. The solvent was removed *in vacuo* and the residue was purified on silica gel using 15/15/70 (v/v)

MeOH/acetone/CH<sub>2</sub>Cl<sub>2</sub> and 15/15/2.5/62.5 (v/v) MeOH/acetone/NEt<sub>3</sub>/CH<sub>2</sub>Cl<sub>2</sub> as successive eluants to give product as a white solid, 30.3 mg, yield 91.0%. <sup>1</sup>H NMR (CDCl<sub>3</sub>, 1 mM, rt, 600 MHz) δ (ppm) 1.309-1.749 (m, 20 H, CH<sub>2</sub>); 2.175 (m, 2 H, CH<sub>2</sub>); 2.384 (t, 2 H, *J* = 6.6 Hz, CH<sub>2</sub>); 2.736 (d, 1 H, CH, *J* = 13.2 Hz, H5b); 2.948 (dd, 1 H, *J* = 12.6 Hz, 4.8 Hz, H5a); 3.171 (m, 1 H, H2); 3.219 (m, 2 H, NH-CH<sub>2</sub>); 4.347 (m, 1 H, H3); 4.515 (m, 1 H, H4); 4.528 (s, 1 H, NHa); 5.344 (s, 2 H, CH<sub>2</sub>); 5.543 (s, 1 H, NHc); 5.645 (s, 1 H, NHb); 5.931 (s, 2 H, NH<sub>2</sub>); 7.162-7.365 (m, 4 H, Ar); 7.795 (s, 1 H, adenine); 8.373 (s, 1 H, adenine). Calc. for [M + H]<sup>+</sup> C<sub>33</sub>H<sub>45</sub>N<sub>8</sub>O<sub>2</sub>S : 617.3403. Found: 617.3370.

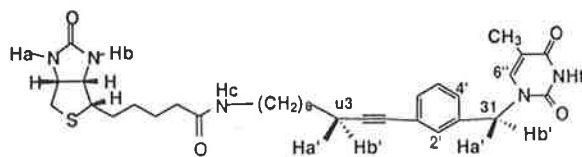
Biotin nucleobases **Bt-Ade (51)**, **Bt-Cyt (52)**, **Bt-Thy (53)**, **Bt-Ura (54)** and **Bt-Thioura (55)** were prepared in a similar manner as the example described below except for the difference stated.

**[3aS-(3aα, 4β, 6aα)]-1-{3-[11-{N-[5-(Hexahydro-2-oxo-1H-thieno[3, 4-d]imidazol-4-yl)-1-oxopentyl]}-aminoundec-1-ynyl]-benzenemethyl}-cytosine (52)**



Eluants 20/80 and 25/10/65 methanol/acetone/CH<sub>2</sub>Cl<sub>2</sub>, isolated as a white solid, yield 66.8%. <sup>1</sup>H NMR (CDCl<sub>3</sub>, 1 mM, rt, 600 MHz): δ (ppm) 1.260-1.946 (m, 20 H, CH<sub>2</sub>); 2.156 (t, 2 H, *J* = 7.2 Hz, CH<sub>2</sub>); 2.406 (t, 2 H, *J* = 6.6 Hz, CH<sub>2</sub>); 2.761 (d, 1 H, *J* = 13.2 Hz, CH, H5b); 2.942 (dd, 1 H, *J* = 12.6 Hz, 4.8 Hz, H5a); 3.163 (m, 3 H, NH-CH<sub>2</sub>+H2); 4.371 (m, 1 H, H3); 4.496 (m, 1 H, H4); 4.782 (d, 1 H, *J* = 15.0 Hz, H31a'); 4.815 (s, 1 H, NHa); 5.071 (d, 1 H, *J* = 15.0 Hz, H31b'); 5.638 (d, 1 H, *J* = 7.2 Hz, cytosine); 6.022 (s, 1 H, NHc); 6.429 (s, 1 H, NHb); 7.165-7.359 (m, 4 H, Ph); 7.206 (d, 1 H, *J* = 7.2 Hz, cytosine); 7.142 (d, 1 H, *J* = 7.8 Hz, Ar); 7.269 (m, 2 H, Ar); 7.311 (s, 1 H, Ar). Calc. for [M + H]<sup>+</sup> C<sub>32</sub>H<sub>45</sub>N<sub>6</sub>O<sub>3</sub>S : 593.3290. Found: 593.3259.

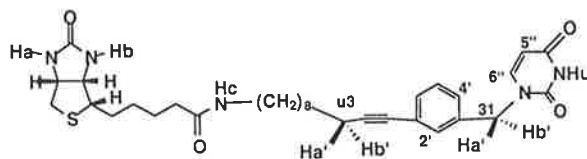
**[3aS-(3aα, 4β, 6aα)]-1-{3-[11-{N-[5-(Hexahydro-2-oxo-1H-thieno[3, 4-d]imidazol-4-yl)-1-oxopentyl]}-aminoundec-1-ynyl]-benzenemethyl}-thymine (53)**



Eluant 10/90 methanol/CH<sub>2</sub>Cl<sub>2</sub>, yield 67.4% as a white solid. <sup>1</sup>H NMR (CDCl<sub>3</sub>, 1 mM, rt, 600 MHz): δ (ppm) 1.258-1.758 (m, 20 H, CH<sub>2</sub>); 1.882 (s, 3 H, CH<sub>3</sub>); 2.214 (m, 2 H, CH<sub>2</sub>); 2.413 (t, 2 H, *J* = 6.6 Hz, CH<sub>2</sub>); 2.749 (d, 1 H, *J* = 13.2 Hz, CH, H5b); 2.948 (dd, 1 H, *J* = 13.2 Hz, 4.8 Hz, H5a); 3.170 (m, 1 H, H2); 3.217 (m, 2 H, NHCH<sub>2</sub>); 4.349 (m, 1 H, H3); 4.521 (m, 1 H, H4); 4.850 (s, 2 H, CH<sub>2</sub> at 31 position); 5.072 (s, 1 H, NHa); 5.761 (s, 1 H, NHc); 5.839 (s, 1 H,

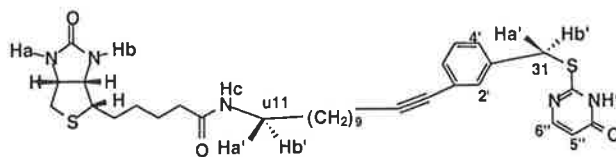
NHb); 6.969 (s, 1 H, thymine); 7.187-7.362 (m, 4 H, Ar); 10.222 (s, 1 H, NH, thymine). Calc. for  $[M + H]^+$   $C_{33}H_{46}N_5S$  : 608.3287. Found: 608.3245.

**[3aS-(3a $\alpha$ , 4 $\beta$ , 6a $\alpha$ )]-1-{3-[11-{N-[5-(Hexahydro-2-oxo-1H-thieno[3, 4-d]imidazol-4-yl)-1-oxopentyl]}-aminoundec-1-ynyl]-benzenemethyl}-uracil (54)**



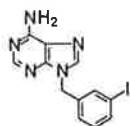
Eluant 10/90 methanol/ $CH_2Cl_2$ , yield 77.0% as a white solid.  $^1H$  NMR ( $CDCl_3$ , 1 mM, rt, 300 MHz):  $\delta$  (ppm) 1.254-1.743 (m, 20 H,  $CH_2$ ); 2.214 (m, 2 H,  $CH_2$ ); 2.200 (m, 2 H,  $CH_2$ ); 2.750 (d, 1 H,  $J = 12.3$  Hz, CH, H5b); 2.964 (dd, 1 H,  $J = 12.9$  Hz, 5.1 Hz, H5a); 3.198 (m, 3 H,  $NH-CH_2+H_2$ ); 4.352 (m, 1 H, H3); 4.501 (m, 1 H, H4); 4.873 (s, 2 H,  $CH_2$  at 31 position); 4.978 (s, 1 H, NHa); 5.694 (d, 1 H,  $J = 8.1$  Hz, uracil); 5.782 (t, 1 H, NHc); 5.855 (s, 1 H, NHb); 7.143 (d, 1 H,  $J = 8.1$  Hz, uracil); 7.183-7.369 (m, 4 H, Ar); 10.522 (s, 1 H, NH, uracil). Calc. for  $[M + H]^+$   $C_{32}H_{44}N_5O_4S$  : 594.3131. Found: 594.3104.

**[3aS-(3a $\alpha$ , 4 $\beta$ , 6a $\alpha$ )]-2-S-{3-[11-{N-[5-(Hexahydro-2-oxo-1H-thieno[3, 4-d]imidazol-4-yl)-1-oxopentyl]}-aminoundec-1-ynyl]-benzenemethyl}-thiouracil (55)**



Eluant 15/5/85 methanol/acetone/ $CH_2Cl_2$ , yield 72.3% as a white solid.  $^1H$  NMR ( $CDCl_3$ , 1 mM, rt, 600 MHz):  $\delta$  (ppm) 1.254-1.694 (m, 20 H,  $CH_2$ ); 2.167 (m, 2 H,  $CH_2$ ); 2.406 (t, 2 H,  $J = 6.6$  Hz,  $CH_2$ ); 2.722 (d, 1 H,  $J = 13.2$  Hz, CH, H5b); 2.894 (dd, 1 H,  $J = 12.6$  Hz, 4.8 Hz, H5a); 3.083 (m, 1 H, H2), 3.238 (m, 2 H,  $NH-CH_2$ ); 4.239 (m, 1 H, H3); 4.296 (d, 1 H,  $J = 13.2$  Hz, H31a'); 4.499 (d, 1 H,  $J = 14.4$  Hz, H31b'); 4.499 (m, 1 H, H4); 6.032 (s, 1 H, NHc); 6.130 (d, 1 H,  $J = 6.6$  Hz, thioiuracil); 6.291 (s, 1 H, NHa); 6.495 (s, 1 H, NHb); 7.190-7.283 (m, 3 H, Ar); 7.446 (s, 1 H, phenyl); 7.269 (m, 2 H, phenyl); 7.886 (d, 1 H,  $J = 6.6$  Hz, thiouracil). Calc. for  $[M + H]^+$   $C_{32}H_{44}N_5O_3S_2$  : 610.2919. Found: 610.2903.

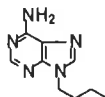
**9-(3-Iodo-benzenemethyl) adenine (58)**



Crude compound **58** was prepared according procedure<sup>304</sup> by the reaction of adenine sodium salt with 3-iodobenzyl bromide in 98.6% yield. Pure compound **58** was got by following the procedure in literature<sup>305</sup> by using toluene and concentrated sulfuric acid to remove possible

impurity in overall 60% yield. M.p. > 200 °C and decomposed. It was pure by checking by TLC. <sup>1</sup>H NMR (CDCl<sub>3</sub>-DMSO-d<sub>6</sub>): δ (ppm) 5.356 (s, 2 H, CH<sub>2</sub>); 7.032 (s, 2 H, NH<sub>2</sub>); 7.105 (t, 1 H, Ar); 7.328 (d, 1 H, Ar); 7.635 (d, 1 H, Ar); 7.710 (s, 1 H, Ar); 8.118 (s, 1 H, 2-C-H); 8.186 (s, 1 H, 8-C-H). <sup>13</sup>C NMR (CDCl<sub>3</sub>-DMSO-d<sub>6</sub>): δ (ppm) 43.96, 92.66, 117.39, 125.43, 128.98, 134.73, 134.99, 137.79, 138.97, 148.16, 151.09, 154.49. Calc. for [M]<sup>+</sup> C<sub>12</sub>H<sub>10</sub>N<sub>5</sub>I: 350.9983. Found: 350.9989.

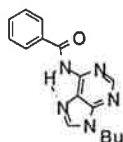
### 9-Butyladenine



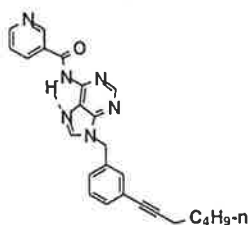
9-Butyladenine was made by a modification to the procedure of Shinkai.<sup>304</sup>

To a three-necked round bottomed flask, was added adenine (2.10 g, 0.0156 mol), NaOH (4.0 g, 0.1 mol) and water (10 ml). After adenine had dissolved in the solution, butyl iodide (7.36 g) and **Aliquat 336** (0.4 g) in hexane (40 ml) was added and stirred under reflux for 48 hours on an oil bath. The crude product was filtered from the solution, washed with water (2 x 10 ml) and hexane (2 x 10 ml). The product was finally recrystallized from toluene, 1.80 g as a white crystal, yield 60.4%. m.p. 135-136 °C. <sup>1</sup>H NMR (CDCl<sub>3</sub>): δ (ppm) 0.966 (t, 3 H, CH<sub>3</sub>); 1.392 (m, 2 H, CH<sub>2</sub>); 1.886 (m, 2 H, CH<sub>2</sub>); 4.204 (t, 2 H, CH<sub>2</sub>); 5.527 (s, 2 H, NH<sub>2</sub>); 7.795 (s, 1 H, 2-C-H); 8.378 (s, 1 H, 8-C-H). <sup>13</sup>C NMR (CDCl<sub>3</sub>): δ (ppm) 13.33, 19.69, 31.92, 43.55, 119.58, 140.33, 150.06, 152.97, 155.83.

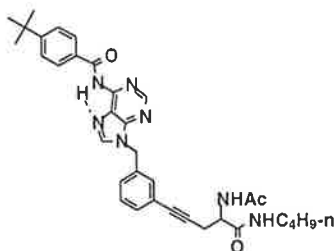
### N-(9-Butyl-9H-6-purinyloxy)benzamide (61)



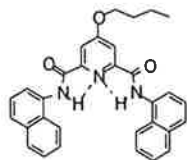
9-Butyladenine (0.143 g, 0.75 mmol), benzoyl chloride (0.105 g, 0.75 mmol) and anhydrous pyridine (1 ml) were stirred together at 100 °C for 1 h. The pyridine was removed *in vacuo*, and the residue was purified by flash chromatography, with methanol/acetone/CH<sub>2</sub>Cl<sub>2</sub> = 1/8.6/26.5 to give product **61** 0.164 g as a white solid, yield 74.4%. m.p. 119-120 °C. <sup>1</sup>H NMR (CDCl<sub>3</sub>): δ (ppm) 0.99 (t, 3 H, CH<sub>3</sub>); 1.44 (m, 2 H, CH<sub>2</sub>); 1.93 (m, 2 H, CH<sub>2</sub>); 4.30 (t, 2 H, CH<sub>2</sub>); 7.51-7.60 (m, 3 H, Ar); 8.01 (s, 1 H, 2'-C-H); 8.04 (d, 2 H, Ar); 8.83 (s, 1 H, 8'-C-H); 8.89 (s, 1 H, NH). <sup>13</sup>C NMR (CDCl<sub>3</sub>): δ (ppm) 13.32, 19.80, 31.90, 43.87, 123.23, 127.92, 128.96, 132.80, 143.00, 149.56, 152.72, 161.30, 164.65. Calc. for [M + H]<sup>+</sup> C<sub>16</sub>H<sub>17</sub>N<sub>5</sub>O: 295.1433. Found: 295.1424.

**N3-{9-[3-(1-Heptynyl)benzyl]-9H-6-purinyl}nicotinamide (62)**

Nicotinic acid (0.083 g, 0.75 mmol) and  $\text{SOCl}_2$  (0.5 ml) were heated at reflux for 4 h. The  $\text{SOCl}_2$  was removed in vacuum. To the residue, was added compound **71** (0.123 g, 0.375 mmol) and pyridine (1 ml) and the mixture stirred at 90 °C for 1 h. The eluant was methanol/ $\text{CH}_2\text{Cl}_2$ /acetone = 1/13.4/13.4. The product was 0.048 g as white solid, yield 30.2%. m.p. 143.5-144 °C.  $^1\text{H NMR}$  ( $\text{CDCl}_3$ ):  $\delta$  (ppm) 0.915 (t, 3 H,  $\text{CH}_3$ ); 1.381-1.585 (m, 6 H,  $\text{CH}_2$ ); 2.382 (t, 2 H,  $\text{CH}_2$ ); 5.422 (s, 2 H,  $\text{CH}_2$ ); 7.237-7.470 (m, Ar); 7.497 (m, 1 H, pyridyl); 8.014 (s, 1H, 2-C-H); 8.327 (d, 1 H, pyridyl); 8.839 (d, 1 H, pyridyl); 8.854 (d, 1 H, pyridyl); 8.949 (s, 1H, NH); 9.246 (s, 1H, 8-C-H). Calc. for  $[\text{M}]^+$   $\text{C}_{25}\text{H}_{23}\text{N}_6\text{O}$ : 424.2011. Found: 424.2002.

**N1-(9-[3-[4-(Acetylamino)-5-(butylamino)-5-oxo-1-pentynyl]benzyl]-9H-6-purinyl)-4-(tert-butyl)benzamide (63)**

Prepared as described for **62** from 4-*t*-butyl benzoyl chloride and compound **72**. The product was got by two separations on silica gel with 7% methanol in  $\text{CH}_2\text{Cl}_2$  as an eluant, yield 20% as a white solid. m.p. 162-164 °C.  $^1\text{H NMR}$  ( $\text{CDCl}_3$ ):  $\delta$  (ppm) 0.870 (m,  $\text{CH}_3$ ); 1.236 (m,  $\text{CH}_2$ ); 1.367 (s, 9 H,  $\text{CH}_3$ ); 2.042 (s, 3 H,  $\text{CH}_3$ ); 2.792-2.957 (m, 2 H,  $\text{CH}_2$ ), 3.317 (m, 2 H,  $\text{CH}_2$ ); 4.543 (m, 1 H, CH); 5.423 (s, 2 H,  $\text{CH}_2$ ); 6.112 (t, 1 H,  $\text{CH}_2$ ); 6.359 (d, 1 H, NH); 7.311 (m, 4 H, Ar); 7.549 (d, 2 H, Ar); 7.978 (d, 2 H, Ar); 7.993 (s, 1 H, 2-C-H); 8.843 (s, 1 H, 8-C-H); 8.916 (s, 1 H, NH). Calc. for  $[\text{M}]^+$   $\text{C}_{34}\text{H}_{39}\text{N}_7\text{O}_3$ : 593.3114. Found: FAB mass spectrum  $[\text{M} + \text{H}]^+$  594.1.

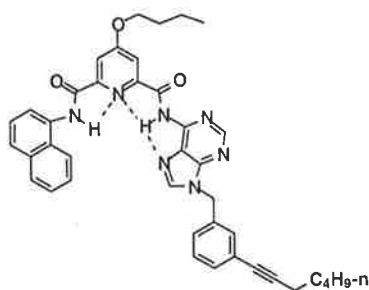
**4-Butoxy-N2, N6-di(1-naphthyl)-2, 6-pyridinedicarboxamide (64)**

4-Butoxypyridine-2, 6-dicarboxylic acid (0.478 g, 2 mmol) and  $\text{SOCl}_2$  (2 ml) were refluxed on an oil bath for 0.5 h, the excess  $\text{SOCl}_2$  was removed *in vacuo*. To the residue was added 1-



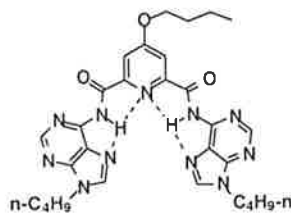
naphthylamine (0.572 g, 4 mmol) and pyridine (2 ml) and stirred at 90 °C for 1 h. The pyridine was removed *in vacuo*. The solid residue was washed with methanol (5 ml) then CHCl<sub>3</sub> (5 ml). The product was isolated in crystalline form 0.35 g, yield 35.7%. m.p. > 230 °C. <sup>1</sup>H NMR (CDCl<sub>3</sub>): δ (ppm) 1.03 (t, 3 H, CH<sub>3</sub>); 1.55 (m, 2 H, CH<sub>2</sub>); 1.90 (m, 2 H, CH<sub>2</sub>); 4.28 (t, 2 H, CH<sub>2</sub>); 7.33-8.12 (m, 6 H, naphthyl); 8.39 (d, 1 H, 2'-C-H); 8.10 (s, 1 H, 3-C-H); 10.32 (s, 1 H, NH). <sup>13</sup>C NMR (CDCl<sub>3</sub>): δ (ppm) 13.64, 18.99, 30.67, 69.00, 112.04, 119.60, 119.99, 125.79, 126.02, 126.12, 126.60, 126.83, 129.14, 131.85, 134.18, 151.11, 161.64, 168.64. Calc. for [M]<sup>+</sup> C<sub>31</sub>H<sub>27</sub>N<sub>3</sub>O<sub>3</sub>: 489.2052. Found: 489.2069.

**4-Butoxy-N2-{9-[3-(1-heptynyl)benzyl]-9H-6-purinyl}-9H-6-pyridinedicarboxamide (65), 6-pyridinedicarboxamide (65)**



Prepared as described for **64**, except that the pyridine free product mixture was dissolved in warm methanol and CH<sub>2</sub>Cl<sub>2</sub> and then chromatographed with methanol/acetone/CH<sub>2</sub>Cl<sub>2</sub> = 1/2/13.4 eluant. The product was recrystallized in methanol to get pure product 0.124 g, yield 37.0%. m.p. 174-175 °C. <sup>1</sup>H NMR (CDCl<sub>3</sub>): δ (ppm) 0.898 (t, 3 H, CH<sub>3</sub>); 1.026 (t, 3 H, CH<sub>3</sub>); 1.322-1.598 (m, CH<sub>2</sub>); 1.889 (m, 2 H, CH<sub>2</sub>); 2.372 (t, 2 H, CH<sub>2</sub>); 4.263 (t, 2 H, CH<sub>2</sub>); 5.431 (s, 2 H, CH<sub>2</sub>); 7.228 (m, 4 H, Ar); 7.542-8.337 (m, naphthyl); 8.435 (d, 1 H, naphthyl); 7.888 (s, 1 H, 2'-C-H); 8.119 (s, 1 H, 3-C-H); 8.943 (s, 1 H, 8'-C-H); 10.398 (s, 1 H, NH); 11.047 (s, 1 H, NH). Calc. for [M]<sup>+</sup> C<sub>40</sub>H<sub>39</sub>N<sub>7</sub>O<sub>3</sub>: 665.3114. Found: 665.3128.

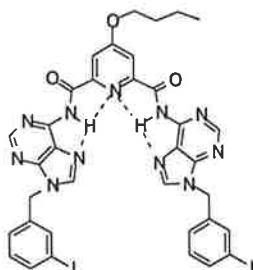
**4-Butoxy-N2, N6-di(9-butyl-9H-6-purinyl)-2, 6-pyridinedicarboxamide (66)**



Prepared as described for **64**, except that the pyridine free product mixture was dissolved in CH<sub>2</sub>Cl<sub>2</sub> and then chromatographed with methanol/acetone/CH<sub>2</sub>Cl<sub>2</sub> = 1/8.6/26.5 as an eluant. The trace water in the product was removed by adding some anhydrous 1-pentane to the solution in CH<sub>2</sub>Cl<sub>2</sub> and removing it *in vacuo*, yield 38.2% as a white solid. m.p. 81-82 °C. <sup>1</sup>H NMR (CDCl<sub>3</sub>): δ (ppm) 1.02 (m, 6 H, CH<sub>3</sub>); 1.43-1.56 (m, 8 H, CH<sub>2</sub>); 1.89 (m, 4 H, CH<sub>2</sub>); 4.23 (t, 2 H, CH<sub>2</sub>); 4.32 (t, 2 H, CH<sub>2</sub>); 8.07 (s, 1 H, 2'-C-H); 8.12 (s, 1 H, 3-C-H); 8.88 (s, 1 H, 8'-C-H); 11.07 (s,

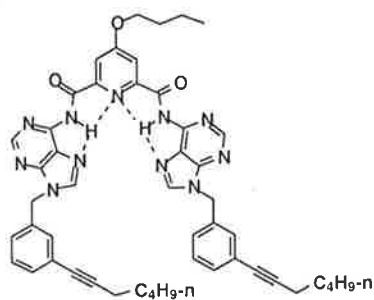
1 H, NH).  $^{13}\text{C}$  NMR ( $\text{CDCl}_3$ ):  $\delta$  (ppm) 13.47, 14.65, 19.04, 19.87, 30.66, 31.95, 43.93, 69.04, 113.20, 143.07, 148.96, 150.26, 152.42, 152.72, 161.28, 168.30. Calc. for  $[\text{M}]^+ \text{C}_{29}\text{H}_{35}\text{N}_{11}\text{O}_3$ : 585.2924. Found: 585.2918.

#### 4-Butoxy-N2, N6-di[9-(3-iodobenzyl)-9H-6-purinyl]-2, 6-pyridinedicarboxamide (67)



Typically, 4-butoxypyridine-2, 6-dicarboxylic acid (0.36 g, 1.5 mmol) and  $\text{SOCl}_2$  (4 ml) were refluxed on an oil bath for 6 h. The  $\text{SOCl}_2$  was removed *in vacuo*. To the residue, was added compound **58** (0.95 g) and anhydrous pyridine (5 ml), and stirred at 90 °C oil bath overnight. Then the pyridine was removed *in vacuo*, and residue was submitted for flash column separation with silica gel with 7% methanol in  $\text{CH}_2\text{Cl}_2$  as eluant twice to get product 0.74 g as a white solid, yield 68%. m.p. 221-223 °C.  $^1\text{H}$  NMR ( $\text{CDCl}_3$ ):  $\delta$  (ppm) 1.01 (t, 3 H,  $\text{CH}_3$ ); 1.55 (m, 2 H,  $\text{CH}_2$ ); 1.87 (m, 2 H,  $\text{CH}_2$ ); 4.23 (t, 2 H,  $\text{CH}_2$ ); 5.42 (s, 2 H,  $\text{CH}_2$ ); 7.11-7.69 (m, 4 H, Ar); 8.04 (s, 1 H, 2'-C-H); 8.12 (s, 1 H, 3-C-H); 8.90 (s, 1 H, 8'-C-H); 11.07 (s, 1 H, NH).  $^{13}\text{C}$  NMR ( $\text{CDCl}_3$ ):  $\delta$  (ppm) 13.61, 18.96, 27.66, 30.60, 46.59, 69.06, 113.31, 123.50, 127.20, 130.94, 136.80, 137.29, 137.95, 142.79, 149.26, 150.29, 152.70, 152.99, 161.35, 168.47. Calc. for  $[\text{M} + \text{H}]^+ \text{C}_{35}\text{H}_{29}\text{I}_2\text{N}_{11}\text{O}_3$ : 906.0626. Found: 906.0626.

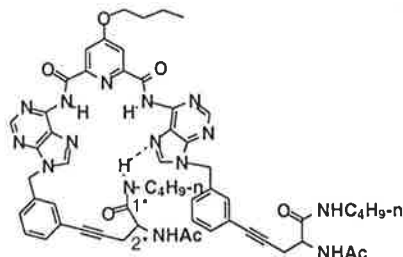
#### 4-Butoxy-N2, N6-di{9-[3-(1-heptynyl)benzyl]-9H-6-purinyl}-2, 6-pyridinedicarboxamide (68)



The procedure was similar to that for **65**. Compound **68** was obtained as a white solid, yield 43%. m.p. 172-174 °C.  $^1\text{H}$  NMR ( $\text{CDCl}_3$ ):  $\delta$  (ppm) 0.91 (t, 3 H,  $\text{CH}_3$ ); 1.01 (t, 3 H,  $\text{CH}_3$ ); 1.38-1.59 (m, 12 H,  $\text{CH}_2$ ); 1.87 (m, 2 H,  $\text{CH}_2$ ); 2.37 (t, 4 H,  $\text{CH}_2$ ); 4.23 (t, 2 H,  $\text{CH}_2$ ); 5.43 (s, 2 H,  $\text{CH}_2$ ); 7.23-7.35 (m, 4 H, Ar); 8.00 (s, 1 H, 2'-C-H); 8.11 (s, 1 H, 3-C-H); 8.90 (s, 1 H, 8'-C-H); 11.04 (s, 1 H, N-H).  $^{13}\text{C}$  NMR ( $\text{CDCl}_3$ ):  $\delta$  (ppm) 13.63, 13.89, 19.04, 19.34, 22.15, 28.32, 30.71, 31.11, 47.11, 69.19, 79.81, 91.85, 113.17, 123.65, 125.32, 126.88, 129.09, 130.83, 131.81, 135.27, 142.96, 148.87, 150.28, 152.69, 152.95, 160.69, 168.61. Calc. for  $[\text{M} + \text{H}]^+$

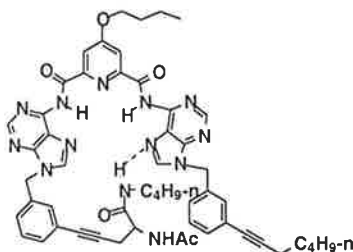
$C_{49}H_{51}N_{11}O_3$ ; 842.4254. Found: 842.4237.

***N*2, *N*6-di(9-{4-[(Acetylamino)-5-(butylamino)-5-oxo-1-pentynyl]benzyl}-4-butoxy-9*H*-6-puriny)-2, 6-pyridinedicarboxamide (69)**



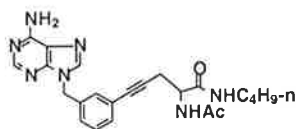
The procedure to prepared **65** was followed, except the eluant was 11% methanol in  $CH_2Cl_2$ . The product from the column was washed with methanol and filtered to get product, yield 18%. m.p. 222-224 °C.  $^1H$  NMR ( $CDCl_3$ ):  $\delta$  (ppm) 0.825 (m, 6 H,  $CH_3$ ); 1.026(t, 3 H,  $CH_3$ ); 1.304-1.564 (m,  $CH_2$ ); 2.749-3.304 (m,  $CH_2$ ); 4.663 (m, 2 H, CH); 5.442 (s, 4 H,  $CH_2$ ); 6.643 (m, 1 H, NH); 6.731 (m, 1 H, NH); 7.294 (m, 8 H, Ar); 8.107 (s, 2 H, 2'-C-H); 8.124 (s, 2 H, 3-C-H); 8.912 (s, 2 H, 8'-C-H); 11.269 (s, 2 H, NH). Calc. for  $[M + H]^+$   $C_{57}H_{63}N_{15}O_7$ : 1070.5112. Found: 1070.5098.

***N*2-(9-{3-[(Acetylamino)-5-(butylamino)-5-oxo-1-pentynyl]-9*H*-6-puriny)-4-butoxy-*N*6-{9-[3-(1-heptynyl)benzyl]-9*H*-6-puriny)-2, 6-pyridinedicarboxamide (70)**



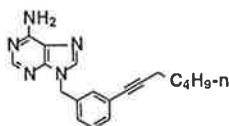
The procedure to prepare **65** was followed. The eluant was 7% methanol in  $CH_2Cl_2$ . The product from the column was treated with acetone. The product **70** was isolated as a white solid, yield 5.3%. m.p. 200-202 °C.  $^1H$  NMR ( $CDCl_3$ ):  $\delta$  (ppm) 0.800 (t, 3 H,  $CH_3$ ); 0.909 (t, 3 H,  $CH_3$ ); 1.010 (t, 3 H,  $CH_3$ ); 1.253-1.864 (m,  $CH_2$ ); 2.378 (t, 2 H,  $CH_2$ ); 2.715-2.994 (m, 2 H,  $CH_2$ ); 3.295 (m, 2 H,  $CH_2$ ); 4.216 (t, 2 H,  $CH_2$ ); 4.643 (m, 1 H, CH); 5.522 (s, 2 H,  $CH_2$ ); 6.560-6.563 (m, 2 H, NH); 7.306 (m, 4 H, Ar); 8.081 (s, 1 H, 2'-C-H); 8.081 (s, 1 H, 3-C-H); 8.965 (s, 1 H, 8'-C-H). Calc. for  $[M + H]^+$   $C_{53}H_{57}N_{13}O_5$ : 956.4683. Found: 956.4697.

**2-(Acetylamino)-*N*1-butyl-5-{3-[(6-amino-9*H*-9-puriny)methyl]phenyl}-4-pentyamide (71)**



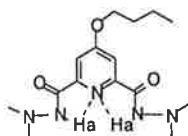
Typically, to a stirred solution of **58** (0.351 g, 1.0 mmol) and 1-*N*-butyl 2-*N*-acetyl-2-propargyl glycine amide (0.210 g, 1 mmol) in piperidine (5 ml) under nitrogen, was added Pd(PPh<sub>3</sub>)<sub>4</sub> (0.052 g, 0.05 mmol), PPh<sub>3</sub> (0.026 g, 0.1 mmol) and copper iodide (0.015 g, 0.1 mmol) respectively. The clear darkened red solution was stirred at reflux temperature for 45 min. The solvent was evaporated *in vacuo* and the residue was purified by column chromatography (20% CH<sub>3</sub>OH/CH<sub>2</sub>Cl<sub>2</sub>). The product **72** was given 0.40 g as a white solid, mp 188-190 °C, yield 93%. <sup>1</sup>H NMR (CDCl<sub>3</sub>): δ (ppm) 0.840 (t, 3 H, CH<sub>3</sub>); 1.255-1.477 (m, 4 H, CH<sub>2</sub>); 2.041 (s, 3 H, CH<sub>3</sub>); 2.754-2.994 (m, 2 H, CH<sub>2</sub>); 3.291 (m, 2 H, CH<sub>2</sub>); 4.534 (m, 1 H, CH); 5.342 (s, 2 H, CH<sub>2</sub>); 6.086 (s, 1 H, NH); 6.352 (d, 1 H, NH); 7.293 (m, 4 H, Ar); 7.777 (s, 1 H, 2-C-H); 8.408 (s, 1 H, 8-C-H). Calc. for [M]<sup>+</sup> C<sub>23</sub>H<sub>27</sub>N<sub>7</sub>O<sub>2</sub>: 434.2304. Found: 434.2300.

### 9-[3-(1-Heptynyl)benzyl]-9H-6-purinamine (72)

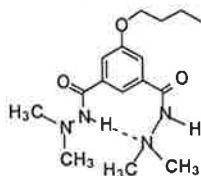


Eluant was 7% CH<sub>3</sub>OH/CH<sub>2</sub>Cl<sub>2</sub>, yield 99% as a white solid, m.p. 147-148 °C. <sup>1</sup>H NMR (CDCl<sub>3</sub>): δ (ppm) 0.914 (t, 3 H, CH<sub>3</sub>); 1.378-1.568 (m, 6 H, CH<sub>2</sub>); 2.377 (t, 2 H, CH<sub>2</sub>); 5.691 (s, 2 H, NH<sub>2</sub>); 7.198-7.307 (m, 4 H, Ar); 7.773 (s, 1 H, 2-C-H); 8.409 (s, 1 H, 8-C-H). <sup>13</sup>C NMR (CDCl<sub>3</sub>): δ (ppm) 13.87, 19.23, 22.10, 28.23, 31.02, 46.78, 73.78, 79.82, 91.62, 119.02, 125.10, 126.92, 129.05, 130.80, 131.66, 135.69, 140.47, 153.44, 155.55. Calc. for C<sub>19</sub>H<sub>21</sub>N<sub>5</sub>: 319.1797. Found: FAB mass spectrum [M + H]<sup>+</sup> 320.

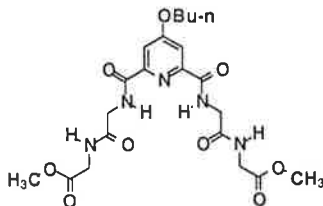
### *N*'2, *N*'2, *N*'6, *N*'6-Tetramethyl-4-butoxy-2, 6-pyridinedicarbohydrazide (73)



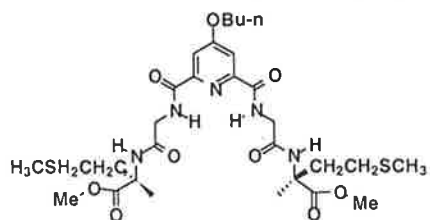
4-Butoxypyridine-2, 6-dicarboxylic acid (0.239 g, 1 mmol) and SOCl<sub>2</sub> (1 ml) were refluxed on an oil bath for 1 h. Then the excess SOCl<sub>2</sub> was removed *in vacuo*. To the residue, was added anhydrous pyridine (2 ml) and *N,N*-dimethyl hydrazine (0.2 ml) and stirred at 60-70 °C on oil bath for one hour. The solution color changed from black to light orange. Then the pyridine was removed *in vacuo*, and residue was submitted for flash column separation with silica gel with eluant 5% methanol in CH<sub>2</sub>Cl<sub>2</sub> firstly and then acetone. The acetone was removed *in vacuo* and extracted with CH<sub>2</sub>Cl<sub>2</sub>. The CH<sub>2</sub>Cl<sub>2</sub> was removed and the product was dried *in vacuo*, 0.198 g as a white solid, yield 61.3%, m.p. 183-185 °C. <sup>1</sup>H NMR (CDCl<sub>3</sub>, 19 mM, rt): δ (ppm) 0.972 (t, 3 H, CH<sub>3</sub>); 1.467 (m, 2 H, CH<sub>2</sub>); 1.799 (m, 2 H, CH<sub>2</sub>); 2.790 (s, 12 H, CH<sub>3</sub>); 4.128 (t, 2 H, CH<sub>2</sub>); 7.838 (s, 2 H, C3-H3); 8.341 (s, 1 H, N-Ha). <sup>13</sup>C NMR (CDCl<sub>3</sub>, 20 mM, rt): δ (ppm) 13.558, 18.922, 30.637, 47.199, 68.791, 111.763, 150.616, 161.184, 167.989. Calc. for [M + H]<sup>+</sup> C<sub>15</sub>H<sub>26</sub>N<sub>5</sub>O<sub>3</sub>: 324.2036. Found: 324.2031.

***N'*1, *N''*1, *N'*3, *N''*3-Tetramethyl-5-butoxy-1, 3-benzenedicarbohydrazide (74)**

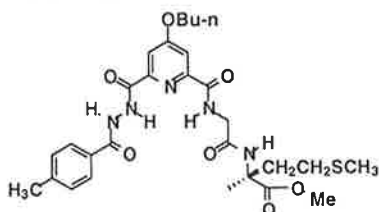
5-Butoxybenzene-1, 3-dicarboxylic acid (0.238 g, 1.0 mmol) and  $\text{SOCl}_2$  (1ml) were heated at reflux on an oil bath for 4 h. The excess  $\text{SOCl}_2$  was removed *in vacuo*. To the residue, was added anhydrous pyridine (2 ml) and *N,N*-dimethylhydrazine (0.2 ml, 2.6 mmol) and stirred at 60-70 °C for 1 h. Pyridine was then removed *in vacuo*, and the residue was submitted to flash chromatography with silica gel with acetone as an eluant to get 0.235 g as a white solid, yield 73%, m. p. 195-197 °C.  $^1\text{H}$  NMR ( $\text{CDCl}_3$ ):  $\delta$  (ppm) 0.982 (t, 3 H,  $J = 7.5$  Hz,  $\text{CH}_3$ ); 1.508 (m, 2 H,  $\text{CH}_2$ ); 1.780 (m, 2 H,  $\text{CH}_2$ ); 2.711 (s, 6 H,  $\text{CH}_3$ ); 4.039 (t, 2 H,  $\text{CH}_2$ ); 6.931 (s, 2 H, NH); 7.391 (d, 2 H,  $J = 1.2$  Hz, H-4, H-6, Ar); 7.607 (t, 1 H,  $J = 1.5$  Hz, H-2, Ar).  $^{13}\text{C}$  NMR:  $\delta$  (ppm) 13.76, 19.17, 31.17, 47.68, 68.40, 116.29, 117.12, 135.40, 159.54, 164.58. Calc. for  $[\text{M}]^+$   $\text{C}_{16}\text{H}_{26}\text{N}_4\text{O}_3$ : 322.2005. Found: 322.2000.

**4-Butoxy-*N*2, *N*6-di(glycinyl glycine methyl ester)-2, 6-pyridinedicarboxamide (75)**

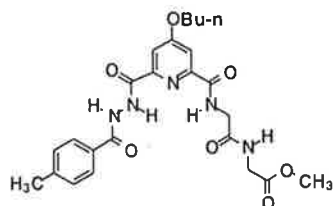
4-Butoxypyridine-2,6-dicarboxylic acid (0.239 g, 1 mmol) and  $\text{SOCl}_2$  (3 ml) were heated on an oil bath for 0.5 h, the excess  $\text{SOCl}_2$  was then removed *in vacuo*. To this residue, was added methyl glycinyl glycine ester hydrochloride (0.365 g, 2 mmol) in hot pyridine (5 ml) solution and the mixture stirred at 90 °C for 1 h. The pyridine was removed *in vacuo* and the residue was submitted to flash column separation with silica gel and eluants ( $\text{CH}_3\text{OH}/\text{CH}_3\text{COCH}_3/\text{CH}_2\text{Cl}_2$ : 5/5/90). The product **75** was got in 34% as a white solid.  $^1\text{H}$  NMR (8.7%  $\text{DMSO-d}_6$ - $\text{CDCl}_3$ , 5 mM, rt, 300 MHz):  $\delta$  (ppm) 0.994 (t, 3 H,  $J = 7.2$  Hz,  $\text{CH}_3$ ); 1.487 (m, 2 H,  $\text{CH}_2$ ); 1.776 (m, 2 H,  $\text{CH}_2$ ); 3.741 (s, 6 H,  $\text{CH}_3$ ); 4.070 (m, 4 H,  $\text{CH}_2$ ); 4.179 (d, 2 H,  $\text{CH}_2$ ); 7.538 (s, 2 H, pyridinyl); 8.092 (t, 2 H, NH); 9.583 (t, 2 H, NH). Calc. for  $[\text{M} + \text{H}]^+$   $\text{C}_{21}\text{H}_{30}\text{N}_5\text{O}_9$ : 496.2043. Found: 496.2026.

**4-Butoxy-N2, N6-di(glycyl D-methionine methyl ester)-2, 6-pyridinedicarboxamide (76)**

Prepared according the procedure for **75**. The product was got in 36%.  $^1\text{H NMR}$  ( $\text{CDCl}_3$ , 1 mM,  $50^\circ\text{C}$ , 300 MHz):  $\delta$  (ppm) 0.992 (t, 3 H,  $J = 7.2$  Hz,  $\text{CH}_3$ ); 1.489 (m, 2 H,  $\text{CH}_2$ ); 1.780 (m, 2 H,  $\text{CH}_2$ ); 2.109 (s, 6 H,  $\text{CH}_3$ ); 2.156 (m, 4 H,  $\text{CH}_2$ ); 2.625 (m, 4 H,  $\text{CH}_2$ ); 3.769 (s, 6 H,  $\text{CH}_3$ ); 4.001 (s, 4 H,  $\text{CH}_2$ ); 4.151 (s, 4 H,  $\text{CH}_2$ ); 4.729 (m, 2 H, CH); 7.376 (s, 2 H, pyridinyl); 7.689 (s, 2 H, NH); 9.183 (t, 2 H, NH). Calc. for  $[\text{M} + \text{H}]^+$   $\text{C}_{27}\text{H}_{41}\text{N}_5\text{O}_9\text{S}_2$ : 580. Found: 580.

**N2-(Glycyl D-methionine methyl ester)-4-butoxy-6-[[2-(4-methylbenzoyl)hydrazino]carbonyl]-2-pyridinecarboxamide (77)**

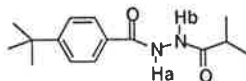
$^1\text{H NMR}$  ( $\text{CDCl}_3$ , 1 mM,  $50^\circ\text{C}$ , 300 MHz):  $\delta$  (ppm) 0.994 (t, 3 H,  $J = 7.2$  Hz,  $\text{CH}_3$ ); 1.487 (m, 2 H,  $\text{CH}_2$ ); 1.772 (m, 2 H,  $\text{CH}_2$ ); 2.426 (s, 3 H,  $\text{CH}_3$ ); 3.715 (s, 3 H,  $\text{CH}_3$ ); 3.953 (t, 2 H,  $J = 6.6$  Hz,  $\text{CH}_2$ ); 4.001 (m, 2 H,  $\text{CH}_2$ ); 4.135 (m, 2 H,  $\text{CH}_2$ ); 7.105 (s, 1 H, pyridyl); 7.236 (d, 2 H, phenyl); 7.712 (s, 1 H, pyridyl); 7.864 (d, 2 H, Ar); 7.376 (s, 2 H, pyridyl); 8.771 (t, 1 H, NH, glycyl); 8.867 (s, 1 H, NH, hydrazine); 10.060 (s, 1 H, NH, glycyl); 12.409 (m, 1 H, NH, hydrazine). Calc. for  $[\text{M}]^+$   $\text{C}_{27}\text{H}_{36}\text{N}_5\text{O}_7\text{S}$ : 574.2352. Found: 574.2344.

**N2-(Glycyl glycine methyl ester)-4-butoxy-6-[[2-(4-methylbenzoyl)hydrazino]carbonyl]-2-pyridinecarboxamide (78)**

4-Butoxypyridine-2, 6-dicarboxylic acid (0.120 g, 0.5 mmol) and  $\text{SOCl}_2$  (2 ml) were heated on an oil bath for 0.5 h, the excess  $\text{SOCl}_2$  was removed *in vacuo*. To this residue, was added methyl glycyl glycine ester hydrochloride (0.091 g, 0.041 mmol) in hot pyridine (5 ml) solution and 4-methylbenzoyl hydrazide (0.064 g, 0.46 mmol) the mixture stirred at  $90^\circ\text{C}$  for 1 h. The pyridine was removed *in vacuo* and the residue was submitted to flash column separation with silica gel and eluant ( $\text{CH}_3\text{OH}/\text{CH}_3\text{COCH}_3/\text{CH}_2\text{Cl}_2$ : 3/10/87). The product was got in 35%.  $^1\text{H NMR}$  (5.0%

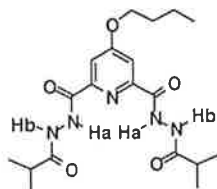
DMSO- $d_6$ - $CDCl_3$ , 5 mM, rt, 300 MHz):  $\delta$  (ppm) 1.002 (t, 3 H,  $J = 7.5$  Hz,  $CH_3$ ); 1.517 (m, 2 H,  $CH_2$ ); 1.807 (m, 2 H,  $CH_2$ ); 2.404 (s, 3 H,  $CH_3$ ); 3.681 (s, 3 H,  $CH_3$ ); 3.939 (m, 2 H,  $J = 5.7$  Hz,  $CH_2$ ); 4.053 (m, 4 H,  $CH_2$ ); 7.261 (d, 2 H,  $J = 8.1$  Hz, Ar); 7.261 (s, 1 H, pyridyl); 7.732 (d, 1 H,  $J = 2.4$  Hz, pyridyl); 7.865 (d, 2 H,  $J = 8.1$  Hz, Ar); 8.047 (t, 1 H, NH); 9.419 (t, 1 H,  $J = 6.3$  Hz, NH); 10.132 (s, 1 H, NH); 11.520 (s, 1 H, NH). Calc. for  $[M + H]^+$   $C_{24}H_{29}N_5O_7$ : 500.2154. Found: 500.2163.

#### *N'*1-[4-(*tert*-Butyl)benzoyl]-2-methylpropanohydrazide (79)

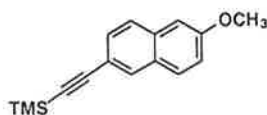


To 4-(*t*-butyl)benzoic acid (0.256 g, 2 mmol) was added  $SOCl_2$  (1.0 ml) and refluxed on an oil bath for 1 h. The  $SOCl_2$  was removed *in vacuo*. To the acid chloride, was added mixture solvent  $NEt_3$ -THF (11 ml, 1/10 (v/v)) and isobutyric hydrazide (0.510 g, 5 mmol), and stirred at 70 °C for 0.5 h. The solvent was removed *in vacuo* and diluted in  $CH_2Cl_2$  and then washed with water. The residue was purified by flash chromatography with methanol/ $CH_2Cl_2$  = 100/5 (v/v) as the eluant to give the product 0.378 g as a white solid, yield 72%. m.p. 133-143 °C.  $^1H$  NMR ( $CDCl_3$ , 20 mM, rt):  $\delta$  (ppm) 1.239 (d, 6 H,  $CH_3$ ); 1.322 (s, 9 H,  $CH_3$ ); 2.582 (m, 1 H, CH); 7.448 (d, 2 H,  $C_6H_2$ ); 7.775 (d, 2 H, Ar); 9.060 (d, 1 H, N-Ha); 9.373 (d, 1 H, N-Hb).  $^{13}C$  NMR ( $CDCl_3$ , 20 mM, rt):  $\delta$  (ppm) 19.172, 31.006, 33.566, 34.939, 125.771, 127.125, 128.619, 156.149, 164.148, 173.817. Calc. for  $[M + H]^+$   $C_{15}H_{23}N_2O_2$ : 263.1759. Found: 263.1761.

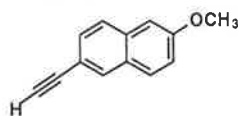
#### *N'*2, *N'*6-Diisobutyryl-4-butoxy-2, 6-pyridinedicarbohydrazide (80)



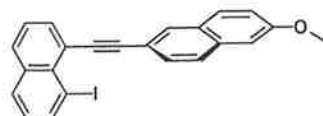
Typically, 4-butoxypyridine-2, 6-dicarboxylic acid (0.478 g, 2 mmol) and  $SOCl_2$  (2 ml) were refluxed on an oil bath for 1 h. The excess  $SOCl_2$  was removed *in vacuo*. To the residue, was added anhydrous pyridine (5 ml) and isobutyric hydrazide (0.510 g, 5 mmol) and stirred at 80 °C oil bath for one hour. The solution color changed from black to light orange. Then the pyridine was removed *in vacuo*, and residue was submitted for flash column separation with silica gel with 5% methanol in  $CH_2Cl_2$  as eluant twice to give the product 0.49 g as a white solid, yield 60.2%, m.p. 191.5-192.5 °C.  $^1H$  NMR ( $CDCl_3$ , 20 mM, rt):  $\delta$  (ppm) 1.003 (t, 3 H,  $CH_3$ ); 1.171 (d, 6 H,  $CH_3$ ); 1.528 (m, 2 H,  $CH_2$ ); 1.749 (m, 2 H,  $CH_2$ ); 2.609 (m, 2 H,  $CH_2$ ); 3.901 (t, 2 H,  $CH_2$ ); 7.002 (s, 2 H, C3-H3); 8.615 (s, 1 H, Ha); 10.283 (s, 1 H, Hb).  $^{13}C$  NMR ( $CDCl_3$ , 20 mM, rt):  $\delta$  (ppm) 13.581, 18.967, 19.263, 30.661, 33.350, 68.743, 110.929, 148.722, 162.278, 167.183, 177.682. Calc. for  $[M + H]^+$   $C_{19}H_{30}N_5O_5$ : 408.2247. Found: 408.2244.

**1-[2-(6-Methoxynaphthyl)]-2-trimethylsilylacetylene (84)**

To a three-neck round flask, were added 6-bromo-2-methoxy-naphthalene (2.371 g, 10 mmol), tetrabutylammonium iodide (11.08 g, 30 mmol),  $\text{NEt}_3$  (8 ml) and DMF (42 ml) under  $\text{N}_2$ . To this solution, was added  $\text{PdCl}_2(\text{PPh}_3)_2$  (0.702 g, 1.0 mmol) and stirred for further 10 min.  $\text{CuI}$  (0.570 g, 3 mmol) was then added and also stirred for further 5 min, finally trimethylsilylacetylene (1.48 g, 2.12 ml, 15 mmol) was injected into with a syringe. The solution was placed onto an oil bath and stirred at 70 °C for 3 h. The resulted solution was diluted with 200 ml  $\text{CH}_2\text{Cl}_2/\text{Hexanes}$  (1/1) after cooling; washed with water, 1N HCl, brine, water consecutively. The solvent was evaporated *in vacuo* and the residue purified on silica gel ( $\text{CH}_2\text{Cl}_2/\text{hexanes}$  (1/3)) to get product 2.57 g as a white solid, yield 100%.  $^1\text{H NMR}$  ( $\text{CDCl}_3$ , 300 MHz):  $\delta$  (ppm) 0.275 (s, 9 H,  $\text{CH}_3$ ); 3.919 (s, 3 H,  $\text{CH}_3$ ); 7.097 (d, 1 H, naphthyl); 7.260 (dd, 1 H, naphthyl); 7.488 (d, dd, 1 H, naphthyl); 7.663 (t, 2 H, naphthyl); 7.924 (s, 1 H, naphthyl). Calc. for  $[\text{M}]^+ \text{C}_{16}\text{H}_{18}\text{OSi}$ : 254.1127. Found: 254.1127.

**1-[2-(6-Methoxynaphthalene)]acetylene (85)**

To a stirred 1-(2-(6-methoxynaphthyl))-2-trimethylsilylacetylene **84** (2.57 g, 10 mmol) solution in THF (10 ml) at 0-5 °C was added dropwisely tetrabutylammonium fluoride hydrate (4.5 g) in THF (10 ml) and then water (1 ml). The solvent was removed *in vacuo* and product was purified on silica gel ( $\text{CH}_2\text{Cl}_2/\text{hexanes}$  (1/3)) to get product 1.44 g as a white solid, yield 79%.  $^1\text{H NMR}$  ( $\text{CDCl}_3$ , 300 MHz):  $\delta$  (ppm) 1.557 (s, 1 H, CH); 3.929 (s, 3 H,  $\text{CH}_3$ ); 7.113 (d, 1 H, naphthyl); 7.180 (d, dd, 1 H, naphthyl); 7.507 (d, dd, 1 H, naphthyl); 7.683 (t, 2 H, naphthyl); 7.950 (s, 1 H, naphthyl). Calc. for  $[\text{M}]^+ \text{C}_{13}\text{H}_{10}\text{O}$ : 182.0732. Found: 182.0729.

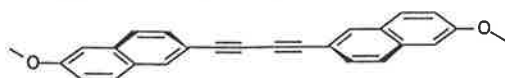
**1-[2-(6-Methoxynaphthyl)]acetynyl-8-iodo-naphthalene (86)**

To a two-neck 250 ml flask were added 1, 8-diiodonaphthalene (0.38 g, 1 mmol), tetrabutylammonium iodide (0.111 g, 0.3 mmol) and  $\text{Et}_3\text{N-DMF}$  (1/5) (5 ml) under  $\text{N}_2$ . To this solution, was added  $\text{PdCl}_2(\text{PPh}_3)_2$  (0.096 g, 0.140 mmol) and the mixture was stirred for 10 min, then  $\text{CuI}$  (0.057 g, 0.3 mmol) and stirred for 10 min. The reaction temperature was raised to 50 °C, then 1-(2-(6-methoxynaphthalene))acetylene **85** (0.181 g, 1 mmol) in DMF (3 ml) was added dropwisely within 1 h with a syringe. The reaction continued for further 2.5 h at 50 °C. The



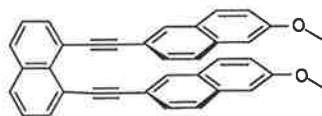
resulted reaction mixture was diluted with  $\text{CH}_2\text{Cl}_2$ , washed with saturated ammonium chloride, fresh water, 0.1N HCl and fresh water consecutively. The solvent was removed *in vacuo* the residue was submitted for flash column separation with  $\text{CH}_2\text{Cl}_2$ /hexanes (1/3) to give product 0.273 g as a yellow solid, yield 63%.  $^1\text{H NMR}$  ( $\text{CDCl}_3$ , 300 MHz):  $\delta$  (ppm) 3.943 (s, 3 H,  $\text{CH}_3$ ); 7.143 (m, naphthyl); 7.463 (t, 1 H, naphthyl); 7.671 (m, naphthyl); 7.982 (d, 1 H, naphthyl); 8.088 (s, 1 H, naphthyl); 8.336 (d, 1 H, naphthyl). Calc. for  $[\text{M}]^+ \text{C}_{23}\text{H}_{15}\text{OI}$ : 434.0169. Found: 434.0160.

**By-product: bis[2-(6-methoxynaphthalene)acetylene]**



This was separated from flash column 0.084 g.  $^1\text{H NMR}$  ( $\text{CDCl}_3$ , 300 MHz):  $\delta$  (ppm) 3.939 (s, 6 H,  $\text{CH}_3$ ); 7.118 (d, 2 H, naphthyl); 7.191 (d, dd, 1 H, naphthyl); 7.540 (d, dd, 1 H, naphthyl); 7.699 (t, 2 H, naphthyl); 8.005 (s, 1 H, naphthyl). Calc. for  $[\text{M}]^+ \text{C}_{26}\text{H}_{18}\text{O}_2$ : 362.1307. Found: 362.1317.

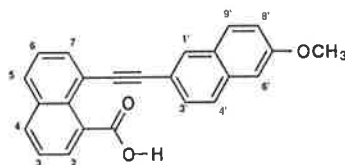
**By-product: 1,8-bis[2-(6-methoxynaphthyl)acetynyl]naphthalene**



**Crystal Structure**

This was separated from flash column 0.068 g.  $^1\text{H NMR}$  ( $\text{CDCl}_3$ , 300 MHz):  $\delta$  (ppm) 3.884 (s, 6 H,  $\text{CH}_3$ ); 6.915 (d, naphthyl); 7.079 (d, 1 H, naphthyl); 7.408 (m, naphthyl); 7.672 (s, naphthyl); 7.873 (d, 1 H, naphthyl); 7.933 (d, 1 H, naphthyl). Calc. for  $[\text{M}]^+ \text{C}_{36}\text{H}_{24}\text{O}_2$ : 488.1776. Found: 488.1778.

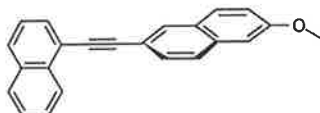
**8-[2-(6-Methoxynaphthyl)]acetynyl-1-naphthoic acid (87)**



To a 2-neck 10 ml flask was added 1-(2-(6-methoxynaphthyl))acetynyl-8-iodo-naphthalene **86** (0.25 g, 0.58 mmol) and anhydrous THF (2 ml). The flask was cooled down to  $-78^\circ\text{C}$  under  $\text{N}_2$  for 5 min. Then butyl lithium (2.5 M in hexanes, 0.58 mmol, 0.3 ml) was added dropwisely through rubber seal with a 1 ml syringe within 5 min. The resulted solution was stirred for further 8 min. Then dry-ice (0.04 g) was added into the solution and let the solution warm up to rt. The THF was removed by  $\text{N}_2$  stream. To the residue, water (1 ml) was added. The solution was washed with ether (2 ml). The resulted clear solution was acidified with 5% HCl. The solid

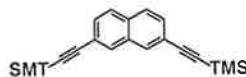
product was filtered and recrystallized from ethanol, 0.080 g as a yellow solid, yield 39%.  $^1\text{H}$  NMR ( $\text{CDCl}_3$ , 600 MHz):  $\delta$  (ppm) 3.960 (s, 3 H,  $\text{CH}_3$ ); 7.116 (s, 1 H, H-6', naphthyl); 7.129 (d, 1 H, H-8', naphthyl); 7.212 (d, 1 H, H-7, naphthyl); 7.287 (t, 1 H, H-6, naphthyl); 7.528 (t, 1 H, H-3, naphthyl); 7.637 (d, 1 H, H-4', naphthyl); 7.695 (m, 2 H, H-8', H-3', naphthyl); 7.895 (m, 3 H, H-5, H-2, H-4, naphthyl); 8.070 (s, 1H, H-1', naphthyl). Calc. for  $[\text{M}]^+$   $\text{C}_{23}\text{H}_{16}\text{O}_3$ : 352.1099. Found: 352.1103.

#### By-product: 1-[2-(6-methoxy-2-naphthyl)-ethynyl]naphthalene



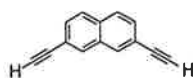
This was separated from flash column.  $^1\text{H}$  NMR ( $\text{CDCl}_3$ , 300 MHz):  $\delta$  (ppm) 3.953 (s, 3 H,  $\text{CH}_3$ ); 7.150 (m, 2 H, naphthyl); 7.744 (m, 1 H, naphthyl); 8.100 (s, 1 H, naphthyl); 8.520 (d, 1 H,  $J = 8.1$  Hz, naphthyl). Calc. for  $[\text{M}]^+$   $\text{C}_{23}\text{H}_{16}\text{O}$ : 308.1201. Found: 308.1198.

#### 2, 7-Bis[1-(2-trimethylsilylethynyl)]naphthalene (89)

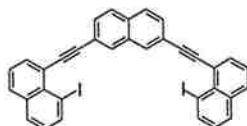


To a three-neck round flask, were added naphthalene-2, 7-diol triflate (2.124 g, 5 mmol), tetrabutylammonium iodide (1.108 g, 3 mmol),  $\text{NEt}_3$  (8 ml) and DMF (42 ml) under  $\text{N}_2$ . To this solution, was added  $\text{PdCl}_2(\text{PPh}_3)_2$  (0.702 g, 1.0 mmol) and stirred for further 10 min and then  $\text{CuI}$  (0.570 g, 3 mmol) was added and also stirred for further 10 min, finally trimethylsilylacetylene (1.48 g, 2.12 ml, 15 mmol) was injected with a syringe. The solution was placed onto an oil bath and stirred at  $70^\circ\text{C}$  for 2 h. The resulted solution was diluted with 200 ml  $\text{CH}_2\text{Cl}_2$ /Hexanes (1/1) after cooling; washed with water, 1N HCl, brine and water consecutively. The solvent was evaporated *in vacuo* and the residue purified on silica gel ( $\text{CH}_2\text{Cl}_2$ /hexanes (1/3)) to get product 1.57 g, yield 98%. Calc. for  $[\text{M}]^+$   $\text{C}_{20}\text{H}_{24}\text{Si}_2$ : 320.1416. Found: 320.1416.

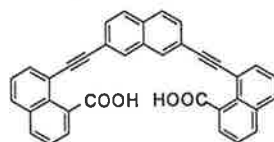
#### 2, 7-Diethynynaphthalene (90)



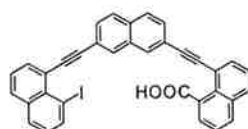
To a stirred solution of **89** (1.54 g, 10 mmol) solution in THF (10 ml) at  $0-5^\circ\text{C}$  was added dropwisely tetrabutylammonium fluoride hydrate 4.5 g in THF (10 ml) and then water (1 ml) and stirred for 0.5 h. The solvent was removed *in vacuo* and product was purified on silica gel ( $\text{CH}_2\text{Cl}_2$ /hexanes (1/3)) to get product 0.757 g as a yellow solid, yield 88%.  $^1\text{H}$  NMR ( $\text{CDCl}_3$ , 300 MHz):  $\delta$  (ppm) 1.557 (s, 1 H, CH); 3.169 (s, 2 H, CH); 7.551 (dd, 2 H,  $J = 8.7$  Hz,  $J = 1.5$  Hz, naphthyl); 7.777 (d, 2 H,  $J = 8.4$  Hz, naphthyl); 7.969 (s, 2 H, naphthyl). Calc. for  $[\text{M}]^+$   $\text{C}_{14}\text{H}_8$ : 176.0626. Found: 176.0619.

**2, 7-Bis{1-[2-(8-iodo-1-naphthylethynyl)]}naphthalene (91)**

To a two-neck 250 ml flask were added 1, 8-diiodonaphthalene (1.60 g, 4.2 mmol), tetrabutylammonium iodide (0.296 g, 0.8 mmol) and Et<sub>3</sub>N-DMF (1/5) (10 ml) under N<sub>2</sub>. To this solution, was added PdCl<sub>2</sub>(PPh<sub>3</sub>)<sub>2</sub> (0.140 g, 0.20 mmol) and stirred for 10 min, then CuI (0.115 g, 0.6 mmol) and stirred for 10 min. The reaction temperature was raised to 50 °C, then **90** (0.352 g, 2 mmol) in DMF (3 ml) was added dropwisely within 1 h with a syringe. The reaction continued for further 2.0 h at 50 °C. The resulted reaction mixture was diluted with CH<sub>2</sub>Cl<sub>2</sub>, washed with saturated ammonium chloride, water, 0.1 N HCl and water consecutively. The solvent was removed *in vacuo* the residue was submitted to flash column separation with CH<sub>2</sub>Cl<sub>2</sub>/hexanes (1/3) to give product 0.38 g as a yellow soild, yield 28%. <sup>1</sup>H NMR (CDCl<sub>3</sub>, 300 MHz): δ (ppm) 7.133 (t, *J* = 6.9 Hz, naphthyl); 7.477 (t, *J* = 5.4 Hz, naphthyl); 7.748 (d, naphthyl); 7.847 (m, naphthyl); 7.984 (d, *J* = 5.7 Hz, naphthyl); 8.167 (s, naphthyl); 8.350 (dd, *J* = 7.5 Hz, *J* = 1.2 Hz, naphthyl). Calc. for [M]<sup>+</sup> C<sub>34</sub>H<sub>18</sub>I<sub>2</sub>: 679.9502. Found: 679.9491.

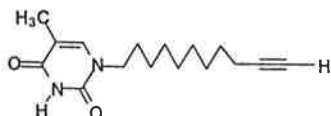
**1, 1'-Bis{8-[1-ethynyl-2-(2, 7-naphthyl)]}naphthalenedicarboxylic acid (93)**

To a 2-neck 50 ml flask was added **91** (0.34 g, 0.50 mmol) and anhydrous THF (10 ml). The flask was put onto dry ice-acetone bath to cool down to -78 °C under N<sub>2</sub> for 5 min. Then butyl lithium (2.5 M in hexanes, 0.58 mmol, 1.2 ml) was added dropwisely through rubber seal with a 1 ml syringe within 5 min. The resulted solution was stirred for further 8 min. Then dry-ice (0.14 g) was added into the solution and let the solution warm up to rt. The THF was removed by N<sub>2</sub> stream. To the residue, water (1 ml) was added. The solution was washed with ether (10 ml). The resulted clear solution was acidified with 5% HCl, extracted with ethyl acetate. The solvent was removed *in vacuo* and products were separated on silica gel (ethyl acetate). A by-product **92** was firstly separated and then product Re-naphthdia **92** as a yellow solid, 0.075 g, yield, 29%. <sup>1</sup>H NMR (DMSO-d<sub>6</sub>-CDCl<sub>3</sub>, 300 MHz): δ (ppm) 7.864 (m, naphthyl); 8.654 (s, naphthyl). Calc. for [M]<sup>+</sup> C<sub>36</sub>H<sub>20</sub>O<sub>4</sub>: 516.1362. Found: 516.1350.

**8-(2-{2-(8-Iodonaphthyl)-1-ethynyl}-2-naphthyl)-1-ethynyl-naphthoic acid (92)**

$^1\text{H NMR}$  ( $\text{CDCl}_3$ , 300 MHz):  $\delta$  (ppm) 7.937 (m, naphthyl). Calc. for  $[\text{M}]^+ \text{C}_{35}\text{H}_{19}\text{O}_2\text{I}$ : 598.0432. Found: 598.0445.

### N-(10-Undecynyl)thymine (95)



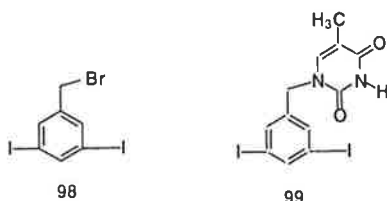
To a solution of thymine (2.54 g, 20 mmol) in DMSO (30 ml), were added anhydrous  $\text{K}_2\text{CO}_3$  and 11-iodo-undecyne (2.78 g, 10 mmol). The mixture was stirred at rt overnight and dilute with 50 ml water, extracted with 20 ml  $\text{CH}_2\text{Cl}_2$  three times, washed with water. The solvent was removed *in vacuo* and the product was purified on silica gel ( $\text{CH}_2\text{Cl}_2$ /ethyl acetate (3/2)) to give 2.05 g as a white solid, yield 74%.  $^1\text{H NMR}$  ( $\text{CDCl}_3$ , 300 MHz):  $\delta$  (ppm) 1.592 (m,  $\text{CH}_2$ ); 1.816 (m,  $\text{CH}_2$ ); 1.947 (s, 3 H,  $\text{CH}_3$ ); 1.956 (t, 1 H, CCH); 2.271 (m, 2 H,  $\text{CH}_2$ ); 3.730 (t, 2 H,  $J = 7.2$  Hz,  $\text{CH}_2$ ); 6.989 (s, 1H, thymine); 8.429 (s, 1H, NH). Calc. for  $[\text{M}]^+ \text{C}_{16}\text{H}_{24}\text{N}_2\text{O}_2$ : 276.1838. Found:

### 11, 11'-Bis[(10-undecynyl)thymine] (96)



To a solution of N-(10-undecynyl)thymine (0.138 g, 0.5 mmol) in THF (2 ml), was added  $\text{PdCl}_2(\text{PPh}_3)_2$  (17 mg, 0.025 mmol),  $\text{CuI}$  (10 mg, 0.05 mmol) and  $\text{I}_2$  (63 mg, 0.25 mmol), and then diisoprylamine (0.5 ml). The resulted solution was stirred for 10 min. The solvent was removed *in vacuo* and the residue was directly submitted to flash column separation with eluant ethyl acetate to give 0.124 g as a white solid, yield 90%.  $^1\text{H NMR}$  ( $\text{CDCl}_3$ , 1 mM, rt, 300 MHz):  $\delta$  (ppm) 1.296 (m,  $\text{CH}_2$ ); 1.505 (m,  $\text{CH}_2$ ); 1.672 (m,  $\text{CH}_2$ ); 1.930 (s, 3 H,  $\text{CH}_3$ ); 2.243 (t, 2 H,  $\text{CH}_2$ ); 3.692 (t, 2 H,  $J = 7.2$  Hz,  $\text{CH}_2$ ); 6.978 (s, 1 H, thymine); 8.650 (s, 1 H, NH). Calc. for  $[\text{M}]^+ \text{C}_{32}\text{H}_{46}\text{N}_4\text{O}_4$ : 550.3519. Found: 550.3503.

### 1-N-(3, 5-Diiodobenzyl)thymine (99)

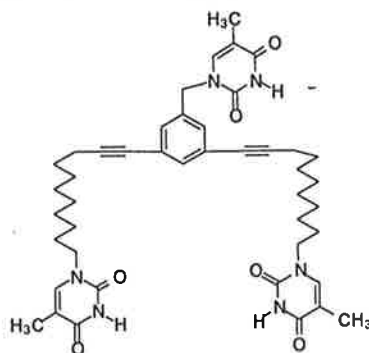


To a solution of 3, 5-diiodotoluene (2.5 g, 7.76 mmol) in  $\text{CCl}_4$  (10 ml), was added NBS (1.54 g, 8.71 mmol) and benzoyl peroxide (80 mg). The mixture was refluxed for 3.5 h with stirring. The resulted mixture was submitted column separation with silica gel (hexanes) without further treatment to give white solid product 3, 5-diiodobenzyl bromide (98) 1.9 g as a white solid.

Some 3, 5-diodotoluene (0.9 g) was recovered. The overall yield is 96%.  $^1\text{H NMR}$  ( $\text{CDCl}_3$ , 300 MHz):  $\delta$  (ppm) 4.311 (s, 2 H,  $\text{CH}_2$ ); 7.696 (d, 2 H,  $J = 1.2$  Hz, phenyl); 7.980 (t, 1 H,  $J = 1.5$  Hz, phenyl). Calc. for  $[\text{M}]^+ \text{C}_7\text{H}_5\text{BrI}_2$ : 422. Found: 422.

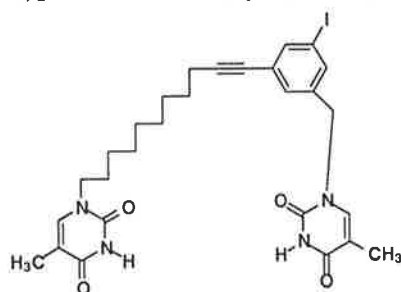
To a solution of thymine (0.43 g, 3.44 mmol) in DMSO (10 ml), were added anhydrous  $\text{K}_2\text{CO}_3$  (0.467 g, 3.44 mmol) and 3, 5-diodobenzyl bromide (**98**) (0.41 g, 0.96 mmol). The resulted mixture was stirred overnight, diluted with water, extracted with  $\text{CH}_2\text{Cl}_2$ , washed with water and purified on silica gel ( $\text{MeOH}/\text{CH}_2\text{Cl}_2$  (5/95)) to give product 0.31 g as a white solid, yield 69%.  $^1\text{H NMR}$  ( $\text{DMSO}-d_6$ - $\text{CDCl}_3$ , 300 MHz):  $\delta$  (ppm) 3.418 (s, 2 H,  $\text{CH}_2$ ); 4.775 (s, 2 H,  $\text{CH}_2$ ); 7.300 (d, 2 H,  $J = 1.2$  Hz, thymine); 7.668 (d, 2 H,  $J = 1.8$  Hz, phenyl); 7.973 (t, 1 H,  $J = 1.5$  Hz, phenyl); 11.257 (s, 1 H, NH, thymine). Calc. for  $[\text{M}]^+ \text{C}_{12}\text{H}_{10}\text{I}_2\text{N}_2\text{O}_2$ : 467.8835. Found: 467.8815.

### 3, 5-Di[(1-undecynyl-11-(N1-thymine)]-1-benzyl-(N1-thymine) (**100**)



To a solution of N-(3, 5-diodobenzyl)thymine (**99**) (138 mg, 0.29 mmol) and  $\text{PPh}_3$  (15 mg) in  $\text{NET}_3/\text{DMF}$  (1/5) (10 ml) under  $\text{N}_2$ , were added  $\text{Pd}(\text{PPh}_3)_4$  (34 mg, 0.029 mmol),  $\text{CuI}$  (11.2 mg, 0.058 mmol) and N-(10-undecynyl)thymine (**95**) (81 mg, 0.29 mmol) respectively. The dark red solution was heated at  $70^\circ\text{C}$  for 1 h. The reaction solvents were removed *in vacuo*. The residue was purified on silica gel ( $\text{MeOH}/\text{acetone}/\text{CH}_2\text{Cl}_2$  (7/10/83)) to give **100** 91.2 mg as a white solid, yield 51% and **101** 19.5 mg also as a white solid, yield 9%. The overall yield was 69%.

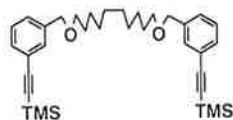
$^1\text{H NMR}$  ( $\text{CDCl}_3$ , 1 mM, rt, 300 MHz):  $\delta$  (ppm) 1.324 (m,  $\text{CH}_2$ ); 1.423 (m,  $\text{CH}_2$ ); 1.672 (m,  $\text{CH}_2$ ); 1.894 (s, 3 H,  $\text{CH}_3$ ); 1.924 (s, 6 H,  $\text{CH}_3$ ); 2.382 (t, 4 H,  $J = 6.9$  Hz,  $\text{CH}_2$ ); 3.694 (t, 4 H,  $J = 7.2$  Hz,  $\text{CH}_2$ ); 4.797 (s, 2 H,  $\text{CH}_2$ ); 6.911 (s, 1 H, thymine); 6.945 (s, 2 H, thymine); 7.199 (s, 2 H, phenyl); 7.370 (s, 1 H, phenyl); 8.851 (s, 2 H, NH); 9.087 (s, 1 H, NH). Calc. for  $[\text{M}]^+ \text{C}_{44}\text{H}_{56}\text{N}_6\text{O}_6$ : 764.4261. Found: 764.4282.

**3-[(1-Undecynyl-11-(N1-thymine)]-5-iodo-1-benzyl-(N1-thymine) (101)**

$^1\text{H}$  NMR ( $\text{CDCl}_3$ , 1 mM, rt, 300 MHz):  $\delta$  (ppm) 1.323 (m,  $\text{CH}_2$ ); 1.431 (m,  $\text{CH}_2$ ); 1.677 (m,  $\text{CH}_2$ ); 1.917 (s, 3 H,  $\text{CH}_3$ ); 1.930 (s, 3 H,  $\text{CH}_3$ ); 2.379 (t, 4 H,  $J = 6.6$  Hz,  $\text{CH}_2$ ); 3.697 (t, 2 H,  $J = 7.2$  Hz,  $\text{CH}_2$ ); 4.780 (s, 2 H,  $\text{CH}_2$ ); 6.943 (s, 1 H, thymine); 6.971 (s, 1 H, thymine); 7.517 (s, Ar); 7.701 (s, Ar); 8.673 (s, 1 H, NH); 8.841 (s, 1H, NH). Calc. for  $[\text{M}]^+$   $\text{C}_{28}\text{H}_{33}\text{IN}_4\text{O}_4$ : 616.1548. Found: 616.1551.

**1, 10-Di[(3-iodobenzyl)oxy]decane (103)**

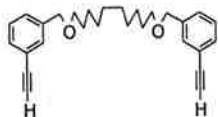
NaH (4.0 g, 60%) was washed with distilled hexanes. To this suspension was added anhydrous THF (20 ml) and a solution of 1, 10-decanediol (1.74 g, 6.6 mmol) in THF (10 ml) dropwisely and stirred for 0.5 h. Then 3-iodobenzyl bromide in THF (10 ml) was also added dropwisely at 0 °C. The resulted solution was stirred at rt for 3 h. Then DMA (20 ml) was added and the suspension was stirred at 50 °C overnight. The excess NaH was decomposed carefully with water. The solution was extracted with dichloromethane, the solvent was removed *in vacuo* and purified on silica gel (hexanes/ $\text{CH}_2\text{Cl}_2$  (4/6)) to give product 1.207 g as a liquid, yield 30%.  $^1\text{H}$  NMR ( $\text{CDCl}_3$ , 300 MHz):  $\delta$  (ppm) 1.283 (m,  $\text{CH}_2$ ); 1.604 (m,  $\text{CH}_2$ ); 3.445 (t, 4 H,  $J = 6.6$  Hz,  $\text{CH}_2$ ); 4.422 (s, 4 H,  $\text{CH}_2$ ); 7.058 (t,  $J = 7.8$  Hz, Ar); 7.299 (d,  $J = 7.5$  Hz, Ar); 7.610 (d,  $J = 6.9$  Hz, Ar); 7.690 (s, Ar). Calc. for  $[\text{M}]^+$   $\text{C}_{24}\text{H}_{32}\text{I}_2\text{O}_2$ : 606.0491. Found: 606.0479.

**1, 10-Dodecan-diol-bis{3-[2-(trimethylsilylethynyl)]-1-benzyl} ether (104)**

To a solution of **103** (1.0 g, 1.64 mmol) and  $\text{PPh}_3$  (43.2 mg, 0.164 mmol) in  $\text{NEt}_3/\text{DMA}$  (1/5) (5 ml) under  $\text{N}_2$ , were added  $\text{Pd}(\text{PPh}_3)_4$  (94.8 mg, 0.082 mmol),  $\text{CuI}$  (31.2 mg, 0.164 mmol) and trimethylsilylacetylene (0.57 ml, 4 mmol) respectively. The dark red solution was heated at 60 °C for 2 h. The reaction solvents were removed *in vacuo*. The residue was purified on silica gel (hexanes/ $\text{CH}_2\text{Cl}_2$  (1/1)) to give **104** 0.90 g as a colorless liquid, yield 100%.  $^1\text{H}$  NMR ( $\text{CDCl}_3$ , 200 MHz):  $\delta$  (ppm) 1.296 (m,  $\text{CH}_2$ ); 1.614 (m,  $\text{CH}_2$ ); 3.449 (t, 4 H,  $J = 6.6$  Hz,  $\text{CH}_2$ ); 4.466 (s, 4 H,  $\text{CH}_2$ ); 7.047 (m, 8 H, Ar).  $^{13}\text{C}$  NMR ( $\text{CDCl}_3$ , 200 MHz):  $\delta$  (ppm) 26.092, 29.377, 29.445,

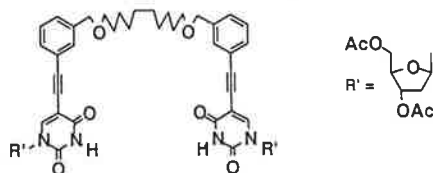
29.665, 70.612, 72.311, 94.070, 105.140, 123.181, 127.741, 128.287, 131.049, 131.132, 138.985.  
Calc. for  $[M]^+$   $C_{34}H_{50}Si_2$ : 546.3349. Found: 546.3345.

### 1, 10-Decan-diol di(3-ethynylbenzyl) ether (105)



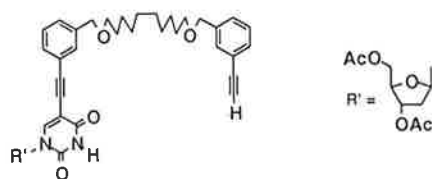
To a stirred solution of **104** (0.90 g) solution in THF (10 ml) at 0-5 °C was added dropwisely tetrabutylammonium fluoride hydrate (1.8 g) in THF (10 ml) and then water (1 ml) and stirred for 0.25 h. The solvent was removed *in vacuo* and product was purified on silica gel ( $CH_2Cl_2$ /hexanes (1/1)) to get product 0.592 g as a colorless liquid, yield 89%. Calc. for  $[M]^+$   $C_{28}H_{34}O_2$ . Found: 402.2557.

### 1, 10-Decan-diol di{3-[5-(3', 5'-di-O-acetyl-2'-deoxyuridine)ethynyl]benzyl} ether (106)



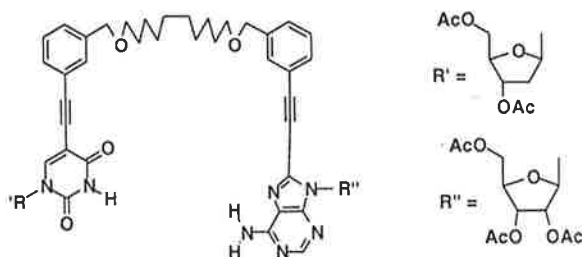
To a solution of diacetyl 5-iododeoxyuridine ester (248 mg, 0.5 mmol) and  $PPh_3$  (26 mg, 0.10 mmol) in  $NEt_3$ /DMA (1/5) (20 ml) under  $N_2$ , were added  $Pd(PPh_3)_4$  (58 mg, 0.05 mmol),  $CuI$  (19 mg, 0.10 mmol) and **105** (320 mg, 0.8 mmol) respectively. The dark red solution was heated at 80 °C for 2 h. The reaction solvents were removed *in vacuo*. The residue was purified on silica gel (MeOH/acetone/ $CH_2Cl_2$  (1/5/70)) to give Re-oc10 (**106**) 60 mg, and by-product **107** (112 mg), the overall yield 57%.  $^1H$  NMR ( $CDCl_3$ , 300 MHz):  $\delta$  (ppm) 1.189 (m,  $CH_2$ ); 1.611 (m,  $CH_2$ ); 2.131 (s, 3 H,  $CH_3$ ); 2.186 (s, 3 H,  $CH_3$ ); 3.453 (t, 4 H,  $J = 6.6$  Hz,  $CH_2$ ); 4.321, 4.388 (m, CH); 4.388 (s, 4 H,  $CH_2$ ); 5.280 (m, CH); 6.354 (m, CH); 7.322 (m, 8H, Ar); 7.904 (s, 2 H, thymine); 8.916 (s, 2 H, NH). Calc. for  $[M]^+$   $C_{54}H_{63}N_4O_{16}$ : 1023.4238. Found: 1023.4190.

### 1, 10-Decan-diol 3-ethynylbenzyl 3-[5-(3', 5'-di-O-acetyl-2'-deoxyuridine)ethynyl]benzyl ether (107)



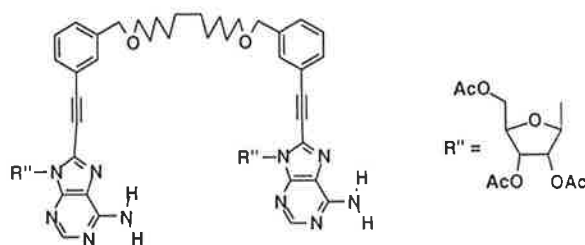
$^1H$  NMR ( $CDCl_3$ , 300 MHz):  $\delta$  (ppm) 1.282 (m,  $CH_2$ ); 1.590 (m,  $CH_2$ ); 2.126 (s, 3 H,  $CH_3$ ); 2.182 (s, 3 H,  $CH_3$ ); 3.460 (m, 4 H,  $CH_2$ ); 4.315, 4.392 (m, CH); 4.382 (s, 2 H,  $CH_2$ ); 4.471 (s, 2 H,  $CH_2$ ); 5.260 (m, CH); 6.339 (m, CH); 7.469 (m, 8 H, Ar); 7.897 (s, 1 H, thymine); 8.359 (s, 1 H, NH).

**1, 10-Decan-diol 3-[8-(2', 3', 5'-tri-O-acetyl-adenosine)ethynyl]benzyl 3-[5-(3', 5'-di-O-acetyl-2'-deoxyuridine)ethynyl]benzyl ether (108)**



To a solution of triacetyl 8-bromoadenosine ester (94.4 mg, 0.20 mmol) and  $\text{PPh}_3$  (13 mg, 0.05 mmol) in  $\text{NEt}_3/\text{DMA}$  (1/5) (5 ml) under  $\text{N}_2$ , were added  $\text{Pd}(\text{PPh}_3)_4$  (29 mg, 0.025 mmol),  $\text{CuI}$  (6 mg, 0.03 mmol) and **107** (110 mg, 0.15 mmol) respectively. The dark red solution was heated at  $80^\circ\text{C}$  for 6 h. The reaction mixture was diluted with water and extracted with ethyl acetate. The solvent was removed *in vacuo* the residue was purified on silica gel (ethyl acetate /  $\text{CH}_2\text{Cl}_2$  (8/1)) to give **108** (29 mg).  $^1\text{H NMR}$  ( $\text{CDCl}_3$ , 300 MHz):  $\delta$  (ppm) 1.271 (m,  $\text{CH}_2$ ); 1.636 (m,  $\text{CH}_2$ ); 2.035 (s, 3 H,  $\text{CH}_3$ ); 2.112 (s, 3 H,  $\text{CH}_3$ ); 2.127 (s, 3 H,  $\text{CH}_3$ ); 2.153 (s, 3 H,  $\text{CH}_3$ ); 2.185 (s, 3 H,  $\text{CH}_3$ ); 3.478 (m, 4 H,  $\text{CH}_2$ ); 4.322, 4.397 (m, CH); 4.472 (s, 2 H,  $\text{CH}_2$ ); 4.521 (s, 2 H,  $\text{CH}_2$ ); 5.230 (m, CH); 5.980 (m, CH); 6.209 (s, 2 H,  $\text{NH}_2$ ); 6.332 (m, CH); 7.420 (m, 8H, Ar); 7.913 (s, 1H, thymine); 8.430 (s, 1 H, adenine); 11.10 (s, 1 H, NH). Calc. for  $[\text{M}]^+$   $\text{C}_{57}\text{H}_{66}\text{N}_7\text{O}_{16}$ : 1104.4566. Found: 1104.4589.

**1, 10-Decan-diol di{3-[8-(2', 3', 5'-tri-O-acetyl-adenosine)ethynyl]benzyl} ether (109)**

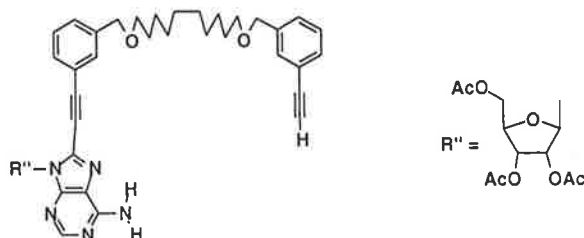


To a solution of triacetyl 8-bromoadenosine ester (201 mg, 0.5 mmol) and  $\text{PPh}_3$  (26 mg, 0.10 mmol) in  $\text{NEt}_3/\text{DMA}$  (1/5) (10 ml) under  $\text{N}_2$ , were added  $\text{Pd}(\text{PPh}_3)_4$  (58 mg, 0.05 mmol),  $\text{CuI}$  (19 mg, 0.10 mmol) and **105** (320 mg, 0.8 mmol) respectively. The dark red solution was heated at  $80\text{--}85^\circ\text{C}$  for 7 h. The reaction mixture was diluted with water and extracted with ethyl acetate. The solvent was removed *in vacuo* the residue was purified on silica gel (acetone/ethyl acetate (1/70)) to give **110** (21 mg), and **109** (80 mg), the overall yield 44%.

$^1\text{H NMR}$  ( $\text{CDCl}_3$ , 300 MHz):  $\delta$  (ppm) 1.298 (m,  $\text{CH}_2$ ); 1.633 (m,  $\text{CH}_2$ ); 2.030 (s, 6 H,  $\text{CH}_3$ ); 2.113 (s, 6 H,  $\text{CH}_3$ ); 2.152 (s, 6 H,  $\text{CH}_3$ ); 3.495 (t, 4 H,  $J = 6.6$  Hz,  $\text{CH}_2$ ); 4.321, 4.380 (m, CH); 4.523 (s, 4 H,  $\text{CH}_2$ ); 5.990 (m, CH); 6.035 (s, 4 H,  $\text{NH}_2$ ); 6.327 (m, CH); 7.560 (m, 8 H, Ar); 8.368 (s, 2 H, adenine). Calc. for  $[\text{M}]^+$   $\text{C}_{60}\text{H}_{69}\text{N}_{10}\text{O}_{16}$ : 1185.4893. Found: 1185.4789.

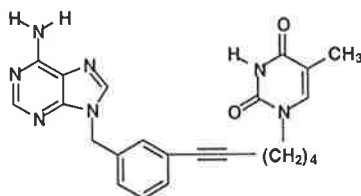


**1, 10-Decan-diol 3-ethynylbenzyl 3-[8-(2', 3', 5'-tri-O-acetyl-adenosine)ethynyl]benzyl ether (110)**



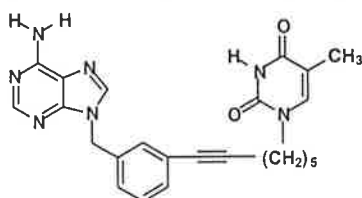
$^1\text{H NMR}$  ( $\text{CDCl}_3$ , 300 MHz):  $\delta$  (ppm) 1.294 (m,  $\text{CH}_2$ ); 1.612 (m,  $\text{CH}_2$ ); 2.030 (s, 3 H,  $\text{CH}_3$ ); 2.112 (s, 3 H,  $\text{CH}_3$ ); 2.152 (s, 3 H,  $\text{CH}_3$ ); 3.478 (m, 4 H,  $\text{CH}_2$ ); 4.377 (m, CH); 4.473 (s, 2 H,  $\text{CH}_2$ ); 4.519 (s, 2 H,  $\text{CH}_2$ ); 5.983 (m, CH); 6.029 (s, 4 H,  $\text{NH}_2$ ); 6.317 (m, CH); 7.426 (m, 8H, Ar); 8.361 (s, 1 H, adenine).

**9-{3-[(6-Hexy-1-nyl)-1-thyminy]-1-benzyl}adenine (111)**

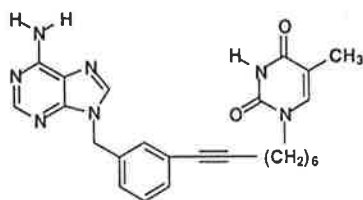


Prepared as described for compound **116**, yield, 68%.  $^1\text{H NMR}$  ( $\text{CDCl}_3$ , 5 mM, rt, 300 MHz):  $\delta$  (ppm) 1.253 (m,  $\text{CH}_2$ ); 1.609 (m,  $\text{CH}_2$ ); 1.901 (s, 3 H,  $\text{CH}_3$ ); 2.456 (t, 2 H,  $J = 6.6$  Hz,  $\text{CH}_2$ ); 3.731 (t, 2 H,  $J = 6.9$  Hz,  $\text{CH}_2$ ); 5.405 (s, 2 H,  $\text{CH}_2$ ); 6.982 (s, 1 H, CH, thymine); 7.145, 7.311 (m, 4 H, Ar); 8.151 (s, 2 H,  $\text{NH}_2$ ); 8.299 (s, 1 H, adenine); 8.345 (s, 1 H, adenine); 10.818 (s, 1 H, NH, thymine). Calc. for  $[\text{M}]^+$   $\text{C}_{23}\text{H}_{23}\text{N}_7\text{O}_2$ : 429.1913. Found: 429.1901.

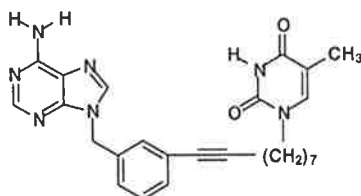
**9-{3-[(7-Hepty-1-nyl)-1-thyminy]-1-benzyl}adenine (112)**



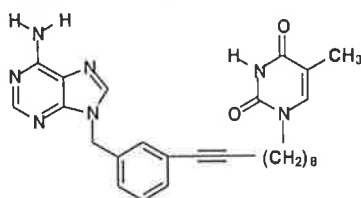
Prepared as described for compound **116**, yield, 70%.  $^1\text{H NMR}$  ( $\text{CDCl}_3$ , 5 mM, rt, 300 MHz):  $\delta$  (ppm) 1.550 (m,  $\text{CH}_2$ ); 1.907 (s, 3 H,  $\text{CH}_3$ ); 2.411 (t, 2 H,  $J = 6.3$  Hz,  $\text{CH}_2$ ); 3.757 (t, 2 H,  $J = 6.9$  Hz,  $\text{CH}_2$ ); 5.375 (s, 2 H,  $\text{CH}_2$ ); 6.246 (s, 2 H,  $\text{NH}_2$ ); 6.983 (s, 1 H, CH, thymine); 7.193, 7.269 (m, 4 H, Ar); 8.072 (d, 1 H,  $J = 2.4$  Hz, adenine); 8.421 (d, 1 H,  $J = 2.4$  Hz, adenine); 11.375 (s, 1 H, NH, thymine). Calc. for  $[\text{M}]^+$   $\text{C}_{24}\text{H}_{25}\text{N}_7\text{O}_2$ : 443.2070. Found: 443.2065.

**9-{3-[(8-Octy-1-nyl)-1-thyminy]-1-benzyl}adenine (113)**

Prepared as described for compound **116**, yield, 74%.  $^1\text{H NMR}$  ( $\text{CDCl}_3$ , 5 mM, rt, 300 MHz):  $\delta$  (ppm) 1.355 (m,  $\text{CH}_2$ ); 1.537 (m,  $\text{CH}_2$ ); 1.651 (m,  $\text{CH}_2$ ); 1.725 (m,  $\text{CH}_2$ ); 1.921 (s, 3 H,  $\text{CH}_3$ ); 2.392 (t, 2 H,  $J = 6.6$  Hz,  $\text{CH}_2$ ); 3.715 (t, 2 H,  $J = 7.2$  Hz,  $\text{CH}_2$ ); 5.345 (s, 2 H,  $\text{CH}_2$ ); 6.222 (s, 2 H,  $\text{NH}_2$ ); 6.976 (s, 1 H, CH, thymine); 7.276, 7.311 (m, 4 H, Ar); 7.975 (s, 1 H, adenine); 8.415 (s, 1 H, adenine); 11.049 (s, 1 H, NH, thymine). Calc. for  $[\text{M}]^+ \text{C}_{25}\text{H}_{27}\text{N}_7\text{O}_2$ : 457.2226. Found: 457.2233.

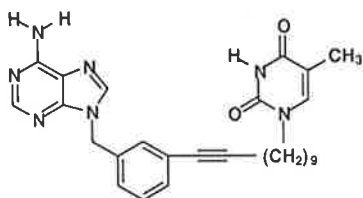
**9-{3-[(9-Undodecy-1-nyl)-1-thyminy]-1-benzyl}adenine (114)**

Prepared as described for compound **116**, yield, 64%.  $^1\text{H NMR}$  ( $\text{CDCl}_3$ , 5 mM, rt, 300 MHz):  $\delta$  (ppm) 1.378 (m,  $\text{CH}_2$ ); 1.530 (m,  $\text{CH}_2$ ); 1.691 (m,  $\text{CH}_2$ ); 1.933 (s, 3 H,  $\text{CH}_3$ ); 2.401 (t, 2 H,  $J = 6.0$  Hz,  $\text{CH}_2$ ); 3.737 (t, 2 H,  $J = 6.6$  Hz,  $\text{CH}_2$ ); 5.338 (s, 2 H,  $\text{CH}_2$ ); 6.437 (s, 2 H,  $\text{NH}_2$ ); 6.984 (s, 1 H, CH, thymine); 7.309 (m, 4 H, Ar); 8.123 (s, 1 H, adenine); 8.408 (s, 1 H, adenine); 12.125 (s, 1 H, NH, thymine). Calc. for  $[\text{M}]^+ \text{C}_{26}\text{H}_{29}\text{N}_7\text{O}_2$ : 471.2382. Found: 471.2382.

**9-{3-[(10-Dodecy-1-nyl)-1-thyminy]-1-benzyl}adenine (115)**

Prepared as described for compound **116**, yield, 66%.  $^1\text{H NMR}$  ( $\text{CDCl}_3$ , 5 mM, rt, 300 MHz):  $\delta$  (ppm) 1.352 (m,  $\text{CH}_2$ ); 1.352 (m,  $\text{CH}_2$ ); 1.446, 1.545, 1.658 (m,  $\text{CH}_2$ ); 1.944 (s, 3 H,  $\text{CH}_3$ ); 2.383 (m, 2 H,  $\text{CH}_2$ ); 3.777 (m, 2 H,  $\text{CH}_2$ ); 5.343 (s, 2 H,  $\text{CH}_2$ ); 6.395 (s, 2 H,  $\text{NH}_2$ ); 6.993 (s, 1 H, CH, thymine); 7.314 (m, 4 H, Ar); 8.076 (s, 1H, adenine); 8.419 (d, 1 H, adenine); 11.942 (s, 1 H, NH, thymine). Calc. for  $[\text{M}]^+ \text{C}_{27}\text{H}_{31}\text{N}_7\text{O}_2$ : 485.2539. Found: 485.2531.

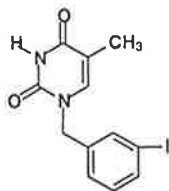
## 9-{3-[(11-Undecy-1-nyl)-1-thyminy]-1-benzyl}adenine (116)



Typically, to a solution of 9-(3-iodobenzyl)-adenine (**58**) (175 mg, 0.5 mmol) and  $\text{PPh}_3$  (26 mg, 0.10 mmol) in piperidine (5 ml) under  $\text{N}_2$ , were added  $\text{Pd}(\text{PPh}_3)_4$  (58 mg, 0.05 mmol),  $\text{ZnCl}_2$  (13.6 g, 0.10 mmol),  $\text{NaI}$  (15 mg) and acetylene compound ( $n = 9$ ) (166 mg, 0.6 mmol) respectively. The dark red solution was heated at reflux (110 °C) for 1 h. The solvent was removed *in vacuo* the residue was purified on silica gel ( $\text{MeOH}/\text{CH}_2\text{Cl}_2$  (9/91)) to give **116** as a white solid (170 mg, 68%).

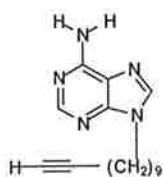
$^1\text{H}$  NMR ( $\text{CDCl}_3$ , 5 mM, rt, 300 MHz):  $\delta$  (ppm) 1.332 (m,  $\text{CH}_2$ ); 1.452 (m,  $\text{CH}_2$ ); 1.562 (m,  $\text{CH}_2$ ); 1.658 (m,  $\text{CH}_2$ ); 1.933 (s, 3 H,  $\text{CH}_3$ ); 2.387 (t, 2 H,  $J = 6.6$  Hz,  $\text{CH}_2$ ); 3.701 (t, 2 H,  $J = 7.5$  Hz,  $\text{CH}_2$ ); 5.302 (s, 2 H,  $\text{CH}_2$ ); 6.490 (s, 2 H,  $\text{NH}_2$ ); 6.988 (s, 1 H, CH, thymine); 7.357 (m, 4 H, Ar); 8.036 (d, 1 H,  $J = 1.8$  Hz, adenine); 8.419 (d, 1 H,  $J = 1.5$  Hz, adenine); 12.287 (s, 1 H, NH, thymine). Calc. for  $[\text{M}]^+$   $\text{C}_{28}\text{H}_{33}\text{N}_7\text{O}_2$ : 499.2696. Found: 499.2702.

## 1-(3-Iodo-1-benzyl)thymine (117)



To a solution of thymine (0.88 g, 7 mmol) in DMSO (15 ml), were added anhydrous  $\text{K}_2\text{CO}_3$  (0.467 g, 3.44 mmol) and 3-iodobenzyl bromide (0.60 g, 2.02 mmol). The resulted mixture was stirred at rt overnight, diluted with water, extracted with  $\text{CH}_2\text{Cl}_2$ , washed with water and purified on silica gel ( $\text{MeOH}/\text{CH}_2\text{Cl}_2$  (5/95)) to give product **117** 0.45 g as a white solid, yield 65%.

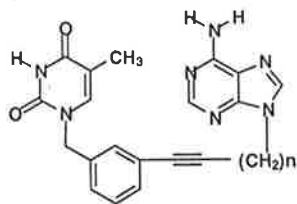
## 9-(11-Undecy-1-nyl)adenine (118)



Crude compound **118** was prepared according procedure<sup>103</sup> by the reaction of adenine sodium salt with 11-iodo-1-undecyne. Pure compound **118** was got by recrystallization in toluene in 20% yield.  $^1\text{H}$  NMR ( $\text{CDCl}_3$ , 2 mM, rt, 600 MHz):  $\delta$  (ppm) 1.276, 1.336, 1.373, 1.896 (m,  $\text{CH}_2$ ); 1.932 (s, 1 H,  $\text{CCH}$ ); 2.169 (m (6 peaks, t, ddd), 2 H,  $J = 4.8$  Hz, 2.4 Hz,  $\text{CH}_2\text{CC}$ ); 4.190 (t, 2 H,

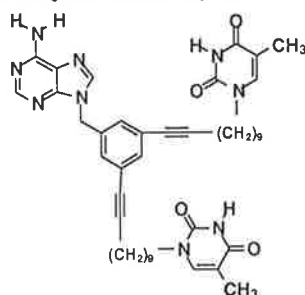
$J = 13.2$  Hz,  $\text{CH}_2$ ); 5.453 (s, 2 H,  $\text{NH}_2$ ); 7.788 (s, 1 H, H8, adenine); 8.379 (s, 1 H, H2, adenine). Calc. for  $[\text{M}]^+ \text{C}_{16}\text{H}_{23}\text{N}_5$ : 285.1953. Found: 285.1950.

### 1-{3-[(11-Undecy-1-nyl)-9-adenyl]-1-benzyl}thymine (119)

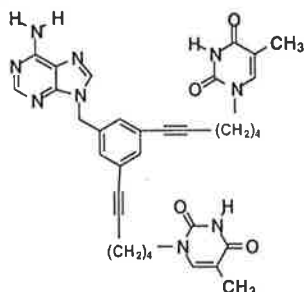


To a solution of N-(3-iodobenzyl)-thymine **117** (171 mg, 0.5 mmol) and  $\text{PPh}_3$  (26 mg, 0.10 mmol) in piperidine (5 ml) under  $\text{N}_2$ , were added  $\text{Pd}(\text{PPh}_3)_4$  (58 mg, 0.05 mmol),  $\text{ZnCl}_2$  (13.6 mg, 0.10 mmol), NaI (15 mg) and compound **118** (130 mg, 0.45 mmol) respectively. The dark red solution was heated reflux (110 °C) for 1 h. The solvent was removed *in vacuo* the residue was purified on silica gel (MeOH/ $\text{CH}_2\text{Cl}_2$  (9/91)) to give **119** (170 mg, 75%).  $^1\text{H}$  NMR ( $\text{CDCl}_3$ , 2 mM, rt, 600 MHz):  $\delta$  (ppm) 1.275, 1.431, 1.538, 1.888 (m,  $\text{CH}_2$ ); 1.914 (s, 3 H,  $\text{CH}_3$ ); 2.383 (t, 2 H,  $\text{CH}_2$ ); 2.383 (t, 2 H,  $J = 5.4$  Hz,  $\text{CH}_2$ ); 4.234 (t, 2 H,  $J = 6.6$  Hz,  $\text{CH}_2$ ); 4.843 (s, 2 H,  $\text{CH}_2$ ); 6.379 (s, 2 H,  $\text{NH}_2$ ); 7.038 (s, 1 H, CH, thymine); 7.192, 7.290, 7.332, 7.445 (m, 4 H, Ar); 8.017 (s, 1 H, H8, adenine); 8.399 (s, 1 H, H2, adenine); 12.452 (s, 1 H, NH, thymine). Calc. for  $[\text{M}]^+ \text{C}_{28}\text{H}_{33}\text{N}_7\text{O}_2$ : 499.2696. Found: 499.2685.

### 9-{3, 5-Di[(11-undecy-1-nyl)-1-thyminy]l}-1-benzyl}adenine (126)



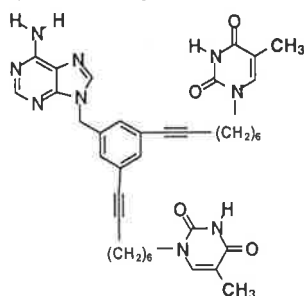
Typically, to a solution of 1-(3, 5-diiodo-1-benzyl)adenine (108 mg, 0.25 mmol) and  $\text{PPh}_3$  (26 mg, 0.10 mmol) in piperidine (5 ml) under  $\text{N}_2$ , were added  $\text{Pd}(\text{PPh}_3)_4$  (58 mg, 0.05 mmol),  $\text{ZnCl}_2$  (13.6 mg, 0.10 mmol), NaI (15 mg) and compound N-(9-undecynyl)thymine (143 mg, 0.50 mmol) respectively. The dark red solution was heated at reflux (110 °C) for 1 h. The solvent was removed *in vacuo* the residue was purified on silica gel (MeOH/ $\text{CH}_2\text{Cl}_2$  (10/90)) to give **126** (129 mg, 67%).  $^1\text{H}$  NMR ( $\text{CDCl}_3$ , 2 mM, rt, 600 MHz):  $\delta$  (ppm) 1.334, 1.539, 1.552, 1.673, 1.890 (m,  $\text{CH}_2$ ); 1.926 (s, 6 H,  $\text{CH}_2$ ); 2.367 (t, 4 H,  $J = 6.6$  Hz,  $\text{CH}_2$ ); 3.691 (t, 4 H,  $J = 7.8$  Hz,  $\text{CH}_2$ ); 5.273 (s, 4 H,  $\text{CH}_2$ ); 6.696 (s, 2 H,  $\text{NH}_2$ ); 6.970 (s, 2 H, CH, thymine); 7.319, 7.331 (m, 4 H, Ar); 8.063 (s, 1 H, H8, adenine); 8.462 (s, 1 H, H2, adenine); 10.941 (s, 2 H, NH, thymine). Calc. for  $[\text{M}]^+ \text{C}_{44}\text{H}_{55}\text{N}_9\text{O}_4$ : 773.4377. Found: 773.4373.

**9-{3, 5-Di[(6-hexy-1-nyl)-1-thyminy]-1-benzyl}adenine (121)**

Yield, 58%.  $^1\text{H NMR}$  ( $\text{CDCl}_3$ , 2 mM, rt, 600 MHz):  $\delta$  (ppm) 1.259, 1.583, 1.893 (m,  $\text{CH}_2$ ); 1.916 (s, 6 H,  $\text{CH}_3$ ); 2.444 (t, 4 H,  $J = 4.8$  Hz,  $\text{CH}_2$ ); 3.739 (t, 4 H,  $J = 7.2$  Hz,  $\text{CH}_2$ ); 5.329 (s, 4 H,  $\text{CH}_2$ ); 6.065 (s, 2 H,  $\text{NH}_2$ ); 6.973 (s, 2 H, CH, thymine); 7.212, 7.291 (m, 4 H, Ar); 8.199 (s, 1 H, H8, adenine); 8.379 (s, 1 H, H2, adenine); 10.093 (s, 2 H, NH, thymine). Calc. for  $[\text{M}]^+$   $\text{C}_{34}\text{H}_{35}\text{N}_9\text{O}_4$ : 633.2812. Found: 633.2793.

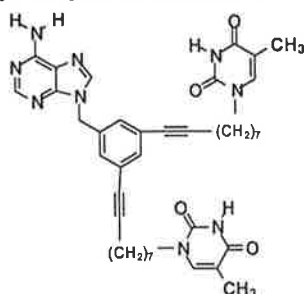
**9-{3, 5-Di[(7-hepty-1-nyl)-1-thyminy]-1-benzyl}adenine (122)**

Yield, 62%.  $^1\text{H NMR}$  ( $\text{CDCl}_3$ , 2 mM, rt, 600 MHz):  $\delta$  (ppm) 1.257, 1.589, 1.731 (m,  $\text{CH}_2$ ); 1.912 (s, 6 H,  $\text{CH}_3$ ); 2.409 (t, 4 H,  $J = 6.6$  Hz,  $\text{CH}_2$ ); 3.760 (t, 4 H,  $J = 6.6$  Hz,  $\text{CH}_2$ ); 5.386 (s, 4 H,  $\text{CH}_2$ ); 6.369 (s, 2 H,  $\text{NH}_2$ ); 6.980 (s, 2 H, CH, thymine); 7.184, 7.274 (m, 4 H, Ar); 8.207 (s, 1 H, H8, adenine); 8.439 (s, 1 H, H2, adenine); 10.443 (s, 2 H, NH, thymine). Calc. for  $[\text{M}]^+$   $\text{C}_{36}\text{H}_{39}\text{N}_9\text{O}_4$ : 661.3125. Found: 661.3131.

**9-{3, 5-Di[(8-octy-1-nyl)-1-thyminy]-1-benzyl}adenine (123)**

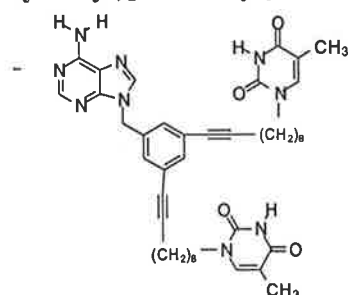
Yield, 61%.  $^1\text{H NMR}$  ( $\text{CDCl}_3$ , 2 mM, rt, 600 MHz):  $\delta$  (ppm) 1.257, 1.358, 1.572, 1.716 (m,  $\text{CH}_2$ ); 1.918 (s, 6 H,  $\text{CH}_3$ ); 2.376 (t, 4 H,  $J = 6.6$  Hz,  $\text{CH}_2$ ); 3.710 (t, 4 H,  $J = 7.2$  Hz,  $\text{CH}_2$ ); 5.310 (s, 4 H,  $\text{CH}_2$ ); 6.322 (s, 2 H,  $\text{NH}_2$ ); 6.965 (s, 2 H, CH, thymine); 7.260, 7.337 (m, 4 H, Ar); 8.025 (s, 1 H, H8, adenine); 8.426 (s, 1 H, H2, adenine); 10.316 (s, 2 H, NH, thymine). Calc. for  $[\text{M}]^+$   $\text{C}_{38}\text{H}_{43}\text{N}_9\text{O}_4$ : 689.3438. Found: 689.3432.

## 9-{3, 5-Di[(9-undodecy-1-nyl)-1-thyminy]-1-benzyl}adenine (124)



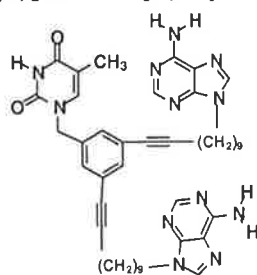
Yield, 69%.  $^1\text{H NMR}$  ( $\text{CDCl}_3$ , 2 mM, rt, 600 MHz):  $\delta$  (ppm) 1.362, 1.451, 1.558, 1.684 (m,  $\text{CH}_2$ ); 1.920 (s, 6 H,  $\text{CH}_3$ ); 2.378 (t, 4 H,  $J = 6.6$  Hz,  $\text{CH}_2$ ); 3.713 (t, 4 H,  $J = 6.6$  Hz,  $\text{CH}_2$ ); 5.312 (s, 4 H,  $\text{CH}_2$ ); 6.480 (s, 2 H,  $\text{NH}_2$ ); 6.965 (s, 2 H, CH, thymine); 7.285, 7.315 (m, 4 H, Ar); 8.144 (s, 1 H, H8, adenine); 8.446 (s, 1 H, H2, adenine); 10.757 (s, 2 H, NH, thymine). Calc. for  $[\text{M}]^+$   $\text{C}_{40}\text{H}_{47}\text{N}_9\text{O}_4$ : 717.3751. Found: 717.3749.

## 9-{3, 5-Di[(10-dodecy-1-nyl)-1-thyminy]-1-benzyl}adenine (125)



Yield, 66%.  $^1\text{H NMR}$  ( $\text{CDCl}_3$ , 2 mM, rt, 600 MHz):  $\delta$  (ppm) 1.322, 1.428, 1.559, 1.684 (m,  $\text{CH}_2$ ); 1.930 (s, 6 H,  $\text{CH}_3$ ); 2.371 (t, 4 H,  $J = 6.6$  Hz,  $\text{CH}_2$ ); 3.727 (t, 4 H,  $J = 7.2$  Hz,  $\text{CH}_2$ ); 5.317 (s, 4 H,  $\text{CH}_2$ ); 6.424 (s, 2 H,  $\text{NH}_2$ ); 6.973 (s, 2 H, CH, thymine); 7.230, 7.340 (m, 4 H, Ar); 8.096 (s, 1 H, H8, adenine); 8.418 (s, 1 H, H2, adenine); 10.582 (s, 2 H, NH, thymine). Calc. for  $[\text{M}]^+$   $\text{C}_{42}\text{H}_{51}\text{N}_9\text{O}_4$ : 745.4064. Found: 745.4056.

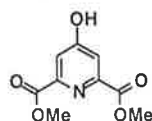
## 1-{3, 5-Di[(11-undecy-1-nyl)-9-adenyl]-1-benzyl}thymine (127)



To a solution of **99** (106 mg, 0.25 mmol) and  $\text{PPh}_3$  (26 mg, 0.10 mmol) in piperidine (5 ml) under  $\text{N}_2$ , were added  $\text{Pd}(\text{PPh}_3)_4$  (58 mg, 0.05 mmol),  $\text{ZnCl}_2$  (13.6 mg, 0.10 mmol), NaI (15 mg) and compound **118** (171 mg, 0.60 mmol) respectively. The dark red solution was heated reflux (110 °C) for 1 h. The solvent was removed *in vacuo* the residue was purified on silica gel (MeOH/ $\text{CH}_2\text{Cl}_2$  (9/91)) to give **127** as a white solid (142 mg, 72%).  $^1\text{H NMR}$  ( $\text{CDCl}_3$ , 2 mM, rt,

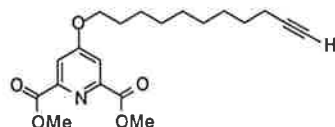
600 MHz):  $\delta$  (ppm) 1.276, 1.318, 1.414, 1.551, 1.890 (m, CH<sub>2</sub>); 1.919 (s, 3 H, CH<sub>3</sub>); 2.371 (t, 4 H,  $J = 7.2$  Hz, CH<sub>2</sub>); 4.214 (t, 4 H,  $J = 7.2$  Hz, CH<sub>2</sub>); 4.784 (s, 2 H, CH<sub>2</sub>); 6.118 (s, 4 H, NH<sub>2</sub>); 7.032 (s, 1 H, CH, thymine); 7.276, 7.355 (m, 4 H, Ar); 7.918 (s, 2 H, H8, adenine); 8.385 (s, 2 H, H2, adenine); 13.175 (s, 1 H, NH, thymine). Calc. for [M]<sup>+</sup> C<sub>44</sub>H<sub>54</sub>N<sub>12</sub>O<sub>2</sub>: 782.4492. Found: 782.4464.

#### Dimethyl 4-hydroxy-2, 6-pyridinedicarboxylate (129)



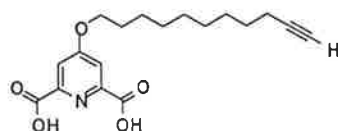
To 4-hydroxy-2, 6-pyridinedicarboxylic acid (2.0 g) in MeOH (20 ml) was added concentrated H<sub>2</sub>SO<sub>4</sub> (2.0 ml) dropwisely and the resulted mixture was refluxed on oil bath for 2 h. The excess methanol was removed *in vacuo* and the residue was treated with saturated NaHCO<sub>3</sub>, washed with water and dried to give 1.87 g as a yellow solid, yield 81.1%. <sup>1</sup>H NMR (DMSO-d<sub>6</sub>-CDCl<sub>3</sub>, 300 MHz):  $\delta$  (ppm) 3.942 (s, 6 H, CH<sub>3</sub>); 7.668 (s, 2 H, pyridine). Calc. for [M]<sup>+</sup> C<sub>9</sub>H<sub>9</sub>NO<sub>5</sub>: 211. Found: 211.

#### Dimethyl 4-(10-undecyloxy)-2, 6-pyridinedicarboxylate (130)



To a solution of compound **129** (0.42 g, 2.0 mmol) in DMSO (5 ml) was added *t*-BuOK (0.448 g, 2.04 mmol) and stirred until it was dissolved. To this vigorous mixture was added 11-iodo-1-undecyne (1.112 g, 4.0 mmol) and stirred for 4 h at rt. The mixture was decomposed with saturated NaHCO<sub>3</sub> (40 ml) and extracted with CH<sub>2</sub>Cl<sub>2</sub> and washed with H<sub>2</sub>O. The solvent was removed *in vacuo* and the residue was purified on silica gel (MeOH/acetone/CH<sub>2</sub>Cl<sub>2</sub> (1/2/97) to give product **130** 220 mg as a liquid, yield 31%. <sup>1</sup>H NMR (CDCl<sub>3</sub>, 300 MHz):  $\delta$  (ppm) 1.339, 1.537 (m, CH<sub>2</sub>); 1.844 (m, 2 H, CH<sub>2</sub>); 1.946 (t, 1 H, CCH); 2.173 (dd, 2 H,  $J = 4.2$  Hz,  $J = 2.4$  Hz, CH<sub>2</sub>CCH); 4.014 (s, 6 H, CH<sub>3</sub>); 4.135 (t, 2 H,  $J = 6.3$  Hz, CH<sub>2</sub>); 7.806 (s, 2 H, pyridyl). Calc. for [M]<sup>+</sup> C<sub>20</sub>H<sub>27</sub>NO<sub>5</sub>: 361.1889. Found: 361.1874.

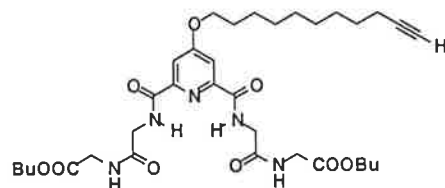
#### 4-(10-Undecyloxy)-2, 6-pyridinedicarboxylic acid (131)



The hydrolysis of compound **130** (200 mg) was carried out by the dissolving in hot methanol (20 ml) firstly and then the addition of solution of KOH (1 g) in methanol (20 ml) and stirring overnight. The excess methanol was removed *in vacuo* and the residue was neutralized with KHSO<sub>4</sub>/H<sub>2</sub>O to give 178 mg product (**131**) as a white solid, yield 96.4%. <sup>1</sup>H NMR (DMSO-d<sub>6</sub>-

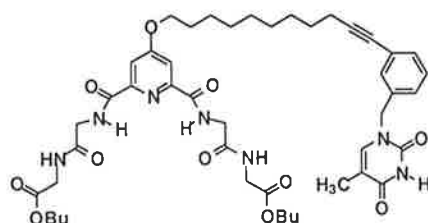
CDCl<sub>3</sub>, 300 MHz):  $\delta$  (ppm) 1.334, 1.498 (m, CH<sub>2</sub>); 1.841 (m, 2 H, CH<sub>2</sub>); 2.172 (m, 2 H, CH<sub>2</sub>); 2.575 (t, 1 H,  $J = 2.1$  Hz, CCH); 4.190 (t, 2 H,  $J = 6.3$  Hz, CH<sub>2</sub>); 7.763 (s, 2 H, pyridyl). Calc. for [M]<sup>+</sup> C<sub>18</sub>H<sub>24</sub>NO<sub>5</sub>: 334.1654. Found: 334.1663.

**4-(10-Undecyloxy)-N2, N6-di(glycylglycine methyl ester)-2, 6-pyridinedicarboxamide (132)**



To compound **131** (35 mg), was added SOCl<sub>2</sub> (2 ml) and reflux for 0.5 h. The excess SOCl<sub>2</sub> was removed *in vacuo*. To the residue was added anhydrous pyridine (2 ml) and butyl glycylglycine ester hydrochloride (86 mg) and stirred at 80 °C for 0.5 h. The solvent was removed *in vacuo* and the residue was purified on silica gel (MeOH/acetone/CH<sub>2</sub>Cl<sub>2</sub> (5/10/85)) to give 44 mg product (**132**) as a liquid, yield 63%. Calc. for [M]<sup>+</sup> C<sub>34</sub>H<sub>52</sub>N<sub>5</sub>O<sub>9</sub>: 674.3790. Found: 674.3790.

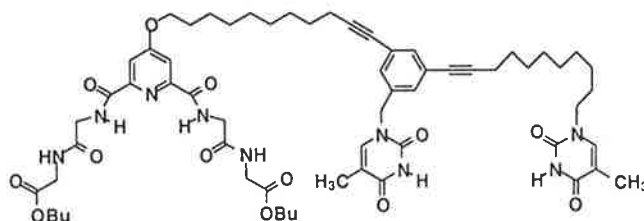
**4-(11-{1-[3-Benzyl-(1-thymine)]}-10-undecyloxy)-N2, N6-di(glycylglycine methyl ester)-2, 6-pyridinedicarboxamide (133)**



To a solution of N-(3-iodobenzyl)thymine **117** (21.0 mg) and PPh<sub>3</sub> (3.8 mg) in NEt<sub>3</sub>/DMF (1/5) (3 ml) under N<sub>2</sub>, were added Pd(PPh<sub>3</sub>)<sub>4</sub> (7.6 mg), CuI (2.4 mg) and **132** (42 mg, 0.062 mmol) respectively. The dark red solution was heated at 70 °C for 2.5 h. The solvent was removed with a N<sub>2</sub> stream at this temperature within 0.5 h, the residue was purified on silica gel (MeOH/acetone/CH<sub>2</sub>Cl<sub>2</sub> (5/10/85)) to give Re-pt (**133**) 49.5 mg, yield 90%. <sup>1</sup>H NMR (CDCl<sub>3</sub>, 1 mM, rt, 300 MHz):  $\delta$  (ppm) 1.432 (m, CH<sub>2</sub>); 1.883 (s, 3H, CH<sub>3</sub>); 2.399 (t, 2 H,  $J = 7.2$  Hz, CH<sub>2</sub>); 3.924 (t, 2 H,  $J = 6.3$  Hz, CH<sub>2</sub>); 4.168 (m, 4 H, CH<sub>2</sub>); 4.839 (s, 2 H, CH<sub>2</sub>); 6.952 (s, 1 H, CH, thymine); 7.285 (m, 5 H, CH, Ar, glycine); 8.081 (s, 2 H, NH, glycine); 8.758 (s, 1 H, NH, thymine); 9.476 (s, 1 H, NH, glycine). Calc. for [M]<sup>+</sup> C<sub>46</sub>H<sub>62</sub>N<sub>7</sub>O<sub>11</sub>: 888.4507. Found: 888.4494.

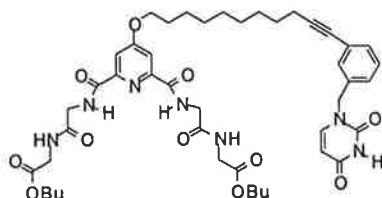


**4-[11-(1-{3-[11-(1-Thymine)undecy-1-nyl]-5-benzyl-(1-thymine)})-10-undecynyloxy]-N2, N6-di(glycinylyl glycine methyl ester)-2, 6-pyridinedicarboxamide (134)**



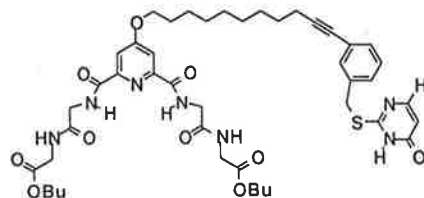
To a solution of Re-bc10 **101** (44.7 mg, 0.0585 mmol) and  $\text{PPh}_3$  (3.4 mg) in  $\text{NEt}_3/\text{DMF}$  (1/5) (4 ml) under  $\text{N}_2$ , were added  $\text{Pd}(\text{PPh}_3)_4$  (6.8 mg),  $\text{CuI}$  (2.2 mg) and **132** (39.4 mg, 0.0585 mmol) respectively. The dark red solution was heated at 70 °C for 70 min. The solvent was removed with  $\text{N}_2$  stream at this temperature within 0.5 h, the residue was purified on silica gel (MeOH/acetone/ $\text{CH}_2\text{Cl}_2$  (5/20/75)) to give Re-pdit (**134**) 68.1 mg as a white solid, yield 94%.  $^1\text{H}$  NMR ( $\text{CDCl}_3$ , 1 mM, rt, 600 MHz):  $\delta$  (ppm) 1.399 (m,  $\text{CH}_2$ ); 1.881 (s, 3 H,  $\text{CH}_3$ ); 1.919 (s, 3 H,  $\text{CH}_3$ ); 2.374 (t, 2 H,  $\text{CH}_2$ ); 3.685 (t, 2 H,  $J = 7.2$  Hz,  $\text{CH}_2$ ); 3.935 (m, 2 H,  $\text{CH}_2$ ); 4.166 (m, 4 H,  $\text{CH}_2$ ); 4.786 (s, 2 H,  $\text{CH}_2$ ); 6.938 (s, 1 H, CH, thymine); 6.968 (s, 1 H, CH, thymine); 7.188 (s, 2 H, phenyl); 7.434 (s, 2 H, CH, pyridine); 7.364 (s, 1 H, Ar); 8.014 (s, 2 H, NH, glycine); 8.911 (s, 1 H, NH, thymine); 9.303 (s, 2 H, NH, glycine); 9.303 (s, 1 H, NH, thymine). Calc. for  $[\text{M}]^+ \text{C}_{62}\text{H}_{84}\text{N}_9\text{O}_{13}$ : 1162.6188. Found: 1162.6180.

**4-(11-{1-[3-benzyl-(1-uracil)]}-10-undecynyloxy)-N2, N6-di(glycinylyl glycine methyl ester)-2, 6-pyridinedicarboxamide (135)**



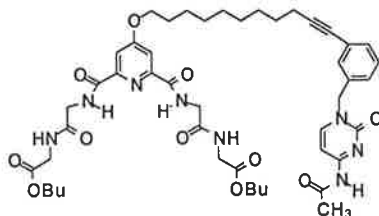
To a solution of N-(3-iodobenzyl)uracil (20.5 mg) and  $\text{PPh}_3$  (3.8 mg) in  $\text{NEt}_3/\text{DMF}$  (1/5) (4 ml) under  $\text{N}_2$ , were added  $\text{Pd}(\text{PPh}_3)_4$  (7.6 mg),  $\text{CuI}$  (2.4 mg) and **132** (42 mg, 0.062 mmol) respectively. The dark red solution was heated at 70 °C for 3 h. The solvent was removed with  $\text{N}_2$  stream at this temperature within 0.5 h, the residue was purified on silica gel (MeOH/acetone/ $\text{CH}_2\text{Cl}_2$  (5/10/85 and 7/10/83)) to give Re-pu (**135**) 49.5 mg as a white solid, yield 90%.  $^1\text{H}$  NMR ( $\text{CDCl}_3$ , 1 mM, rt, 600 MHz):  $\delta$  (ppm) 1.386 (m,  $\text{CH}_2$ ); 2.383 (t, 2H,  $J = 6.6$  Hz,  $\text{CH}_2$ ); 3.930 (t, 2 H,  $\text{CH}_2$ ); 4.165 (m, 4 H,  $\text{CH}_2$ ); 4.864 (s, 2 H,  $\text{CH}_2$ ); 5.693 (d, 1 H,  $J = 7.8$  Hz, CH, thymine); 7.152 (d, 1 H,  $J = 7.8$  Hz, CH, thymine); 7.175, 7.362 (m, 5 H, CH, Ar, pyridine); 7.913 (s, 2 H, CH, glycine); 9.005 (s, 1 H, NH, thymine); 9.400 (s, 2 H, NH, glycine). Calc. for  $[\text{M}]^+ \text{C}_{45}\text{H}_{60}\text{N}_7\text{O}_{11}$ : 874.4350. Found: 874.4356.

**4-(11-{1-[3-Benzyl-(2-S-thiouracil)]}-10-undecyloxy)-N2, N6-di(glycinyl glycine methyl ester)-2, 6-pyridinedicarboxamide (136)**

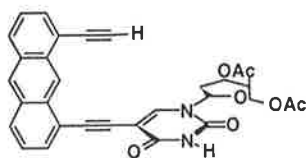


To a solution of S-(3-iodo-benzyl)-thiouracil (21.5 mg) and PPh<sub>3</sub> (3.8 mg) in NEt<sub>3</sub>/DMF (1/5) (4 ml) under N<sub>2</sub>, were added Pd(PPh<sub>3</sub>)<sub>4</sub> (7.6 mg), CuI (2.4 mg) and **132** (42 mg, 0.062 mmol) respectively. The dark red solution was heated at 70 °C for 3 h. The solvent was removed with N<sub>2</sub> stream at this temperature within 0.5 h, the residue was purified on silica gel (MeOH/acetone/CH<sub>2</sub>Cl<sub>2</sub> (5/10/85)) to give Re-pthiou (**136**) 52.5 mg as a white solid, yield 92%. <sup>1</sup>H NMR (CDCl<sub>3</sub>, 1 mM, rt, 600 MHz): δ (ppm) 1.387 (m, CH<sub>2</sub>); 2.390 (t, 2 H, *J* = 7.2 Hz, CH<sub>2</sub>); 3.911 (m, 2 H, CH<sub>2</sub>); 4.165 (m, 4 H, CH<sub>2</sub>); 4.387 (s, 2 H, CH<sub>2</sub>); 6.227 (d, 1 H, *J* = 6.6 Hz, CH, thiouracil); 7.185, 7.362 (m, 5 H, CH, Ar, pyridine); 7.886 (d, 1 H, *J* = 6.6 Hz, CH, thiouracil); 8.100 (s, 2 H, NH, glycine); 9.492 (s, 1 H, NH, glycine). Calc. for [M]<sup>+</sup> C<sub>45</sub>H<sub>60</sub>N<sub>7</sub>O<sub>10</sub>S: 890.4139. Found: 890.4085.

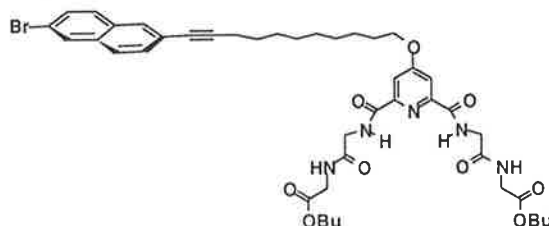
**4-(11-{1-[3-Benzyl-(N-acetyl-1-cytosine)]}-10-undecyloxy)-N2, N6-di(glycinyl glycine methyl ester)-2, 6-pyridinedicarboxamide (137)**



To a solution of N-(3-iodobenzyl)-cytosine (23.0 mg) and PPh<sub>3</sub> (3.8 mg) in NEt<sub>3</sub>/DMF (1/5) (4 ml) under N<sub>2</sub>, were added Pd(PPh<sub>3</sub>)<sub>4</sub> (7.6 mg), CuI (2.4 mg) and **132** (42 mg, 0.062 mmol) respectively. The dark red solution was heated at 70 °C for 5 h. The solvent was removed with N<sub>2</sub> stream at this temperature within 0.5 h, the residue was purified on silica gel (MeOH/acetone/CH<sub>2</sub>Cl<sub>2</sub> (9/7/84, 6/16/78)) to give Re-pc (**137**) 51.5 mg as a white solid, yield 90%. <sup>1</sup>H NMR (CDCl<sub>3</sub>, 1 mM, rt, 600 MHz): δ (ppm) 1.352 (m, CH<sub>2</sub>); 2.285 (s, 3 H, CH<sub>3</sub>); 2.370 (t, 2 H, *J* = 7.2 Hz, CH<sub>2</sub>); 3.893 (m, 2 H, CH<sub>2</sub>); 4.163 (m, 4 H, CH<sub>2</sub>); 5.008 (s, 2 H, CH<sub>2</sub>); 7.190 (d, 1 H, *J* = 8.4 Hz, CH, cytosine); 7.289 (m, 5 H, CH, Ar, pyridine); 7.567 (d, 1 H, *J* = 7.2 Hz, CH, cytosine); 8.093 (s, 2 H, NH, glycine); 9.376 (s, 2 H, NH, glycine); 10.008 (s, 1 H, NH, cytosine). Calc. for [M]<sup>+</sup> C<sub>47</sub>H<sub>63</sub>N<sub>8</sub>O<sub>11</sub>: 915.4616. Found: 915.4654.

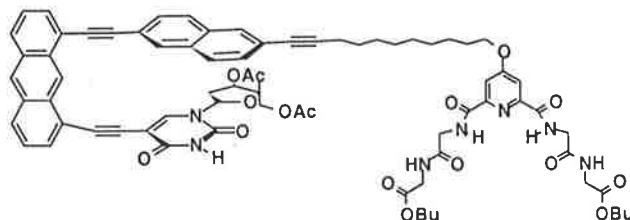
**5-(8-Ethynylanthracyleth-1-ynyl)-3', 5'-di-O-acetyl-2'-deoxyuridine (139)**


To a solution of diacetyl 8-iodo-deoxyuridine ester (349 mg, 0.70 mmol) and  $\text{PPh}_3$  (52 mg, mmol) in  $\text{NEt}_3/\text{DMF}$  (1/5) (5 ml) under  $\text{N}_2$  were added  $\text{Pd}(\text{PPh}_3)_4$  (85 mg),  $\text{CuI}$  (30 mg) and 1, 8-diethynylanthracene (210 mg, 0.93 mmol) respectively. The dark red solution was heated at  $70^\circ\text{C}$  for 3 h. The solvent was removed with a  $\text{N}_2$  stream at this temperature within 0.5 h, the residue was purified on silica gel ( $\text{MeOH}/\text{acetone}/\text{CH}_2\text{Cl}_2$  (1/5/94)) to give 356 mg (**139**) as a yellow solid, yield 85%.  $^1\text{H NMR}$  ( $\text{CDCl}_3$ , 1 mM, rt, 600 MHz):  $\delta$  (ppm) 2.096 (s, 3 H,  $\text{CH}_3$ ); 2.139 (s, 3 H,  $\text{CH}_3$ ); 4.421, 5.283, 6.373 (m, uridine); 7.351, 7.482, 7.608, 7.773, 8.020 (m, 6 H, CH, anthracyl); 8.085 (s, 1 H, uridine); 8.118 (s, 1 H, NH, uridine); 8.469 (s, 1 H, CH, 9-H, anthracyl); 9.499 (s, 1 H, CH, 10-H, anthracyl). Calc. for  $[\text{M}]^+$   $\text{C}_{24}\text{H}_{24}\text{N}_2\text{O}_7$ : 536.1583. Found: .

**4-[11-(6-Bromo-2-naphthyl)-10-undecynoxy]-N2, N6-di(glycylglycine butyl ester)-2,6-pyridinedicarboxamide (141)**


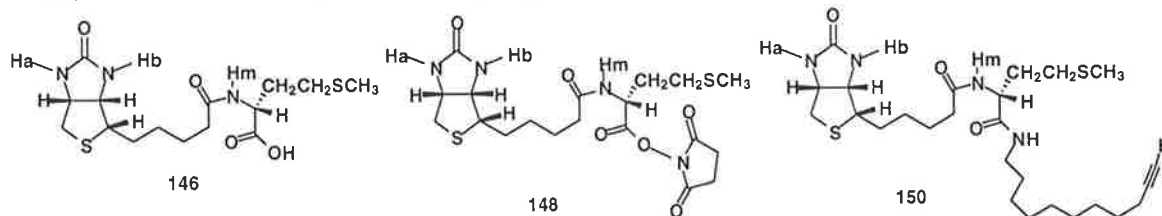
To a solution of 6-bromo-naphthyl triflate (115 mg, 0.324 mmol) and  $\text{PPh}_3$  (10.3 mg) in  $\text{NEt}_3/\text{DMF}$  (1/5) (5 ml) under  $\text{N}_2$ , were added  $\text{Pd}(\text{PPh}_3)_4$  (18.7 mg),  $\text{CuI}$  (6.2 mg) and **132** (109 mg, 0.162 mmol) respectively. The dark red solution was heated at  $70^\circ\text{C}$  for 1.5 h. The solvent was removed with  $\text{N}_2$  a stream at this temperature within 0.5 h, the residue was purified on silica gel ( $\text{MeOH}/\text{acetone}/\text{CH}_2\text{Cl}_2$  (3.3/10.0/86.7)) to give 102 mg (**141**) as a white solid, yield 72%.  $^1\text{H NMR}$  ( $\text{CDCl}_3$ , 1 mM, rt, 300 MHz):  $\delta$  (ppm) 0.868 (t, 3 H,  $J = 7.5$  Hz,  $\text{CH}_3$ ); 1.312 (m,  $\text{CH}_2$ ); 1.623 (m,  $\text{CH}_2$ ); 2.382 (t, 2 H,  $J = 7.2$  Hz,  $\text{CH}_2$ ); 3.843 (t, 2 H,  $\text{CH}_2$ ); 4.099 (m,  $\text{CH}_2$ , glycine); 7.207 (s, 1 H, CH, pyridine); 7.391 (m, 6 H, naphthyl); 8.022 (s, 2 H, NH, glycine); 9.385 (s, 2 H, NH, glycine). Calc. for  $[\text{M}]^+$   $\text{C}_{44}\text{H}_{57}\text{N}_5\text{O}_9\text{Br}$ : 878.3340. Found: 878.3315.

4-{11-[6-(2-{8-[2-(3', 5'-Di-O-acetyl-2'-deoxyuridine)-1-ethynyl]anthracyl}-1-ethynyl)]-10-undecyloxy}-N2, N6-di(glycylglycine butyl ester)-2, 6-pyridinedicarboxamide (142)



To a **141** (39.6 mg, 0.0588 mmol) and  $\text{PPh}_3$  (10 mg) in  $\text{NEt}_3/\text{DMF}$  (1/5) (4 ml) under  $\text{N}_2$ , were added  $\text{Pd}(\text{PPh}_3)_4$  (13.5 mg),  $\text{CuI}$  (3 mg) and **139** (34.9 mg, 0.059 mmol) respectively. The dark red solution was heated at  $70^\circ\text{C}$  for 3 h. The solvent was removed with  $\text{N}_2$  stream at this temperature within 0.5 h, the residue was purified on silica gel ( $\text{MeOH}/\text{acetone}/\text{CH}_2\text{Cl}_2$  (2/20/78)) to give 29 mg **142** (Re-pau) as a yellow solid, yield 42%.  $^1\text{H NMR}$  ( $\text{CDCl}_3$ , 1 mM, rt, 600 MHz):  $\delta$  (ppm) 0.926 (m, 3 H,  $\text{CH}_3$ ); 1.258 (m,  $\text{CH}_2$ ); 1.932 (s, 3 H,  $\text{CH}_3$ ); 2.066 (s, 3 H,  $\text{CH}_3$ ); 2.461 (t, 2 H,  $\text{CH}_2$ ); 4.157 (m,  $\text{CH}_2$ , glycine); 4.818, 5.979 (m, uridine); 7.262 (m, naphthyl, anthracyl); 8.096 (s, 1 H, CH, uridine); 8.210 (s, 2 H, NH, glycine); 8.480 (s, 1 H, CH, 9-H, anthracyl); 9.504 (s, 1 H, CH, 10-H, anthracyl); 9.504 (s, 1 H, NH, glycine). Calc. for  $[\text{M}]^+$   $\text{C}_{75}\text{H}_{80}\text{N}_7\text{O}_{16}$ : 1334.5. Found: 1334.9 (LSIMS).

[3 $\alpha$ S-(3 $\alpha\alpha$ , 4 $\beta$ (1*R*), 6 $\alpha\alpha$ )]-Hexahydro-2-oxo-*N*-[*N*-(10-undecynyl)-methioninamide]-1*H*-thieno[3, 4-*d*]imidazole-4-pentamide (150)

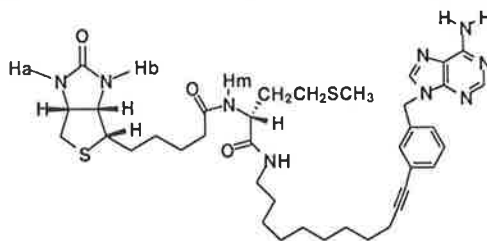


To a stirred solution of **146** (34.1 mg, 0.1 mmol) in DMF (2 ml) was added *N*-hydroxysuccinimide (11.5 mg, 0.1 mmol) and DCC (20.2 mg, 0.1 mmol). This solution was stirred at rt for overnight. The precipitated DCU was removed by filtration.

To the filtrate, was added 10-undecynyl-1-amine (16.7 mg, 0.1 mmol) and stirred at rt overnight.

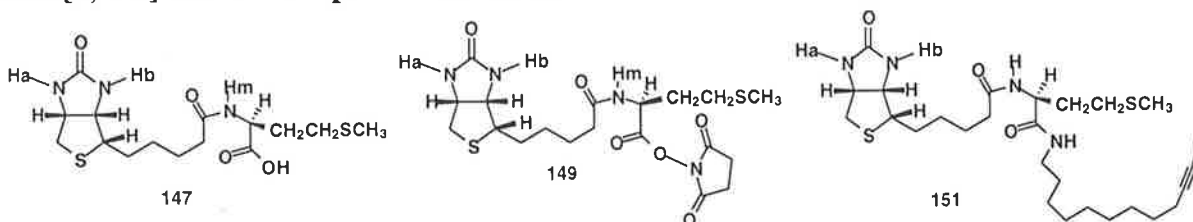
The solvent was removed *in vacuo* and the residue was purified with silica gel ( $\text{MeOH}/\text{acetone}/\text{CH}_2\text{Cl}_2$  (10/10/80)) to give product with 90% yield.  $^1\text{H NMR}$  ( $\text{CDCl}_3$ , 2 mM, rt, 300 MHz):  $\delta$  (ppm) 1.288, 1.654, 2.016, 2.210 (m,  $\text{CH}_2$ ); 1.945 (t, 1 H,  $J = 5.4$  Hz, CCH); 2.106 (s, 3 H,  $\text{CH}_3$ ); 2.527 (m, 2 H,  $\text{CH}_2$ ); 2.768 (d, 1 H,  $J = 12.3$  Hz,  $\text{CH}_2$ ); 2.941 (dd, 1 H,  $J = 12.3$  Hz, 2.4 Hz,  $\text{CH}_2$ ); 3.135, 3.237 (m,  $\text{CH}_2$ ); 4.346 (m, 1 H, H-3 biotin); 4.552 (m, 2 H, H-4 (biotin) and CH (methionine)); 5.977 (s, 1 H, NH, Ha); 6.382 (t, 1 H, NH,  $\text{NHCH}_2$ ); 6.800 (s, 1 H, NH, Hb); 7.756 (d, 1 H,  $J = 8.4$  Hz,  $\text{NHCH}$ ). Calc. for  $[\text{M} + \text{H}]^+$   $\text{C}_{26}\text{H}_{45}\text{N}_4\text{O}_3\text{S}_2$ : 525.2967. Found: 525.2944.

**[3aS-(3a $\alpha$ , 4 $\beta$ (1R), 6a $\alpha$ )]-Hexahydro-2-oxo-N-[N-(11-{1-[3-benzyl-(9-adeninyl)]}-10-undecynyl)-methioninamide]-1H-thieno[3,4-d]imidazole-4-pentamide (152)**



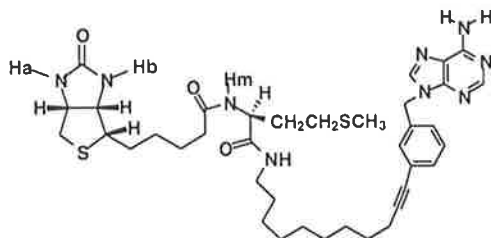
To a 9-(3-iodobenzyl)adenine (35.0 mg, 0.1 mmol) and  $\text{PPh}_3$  (6 mg) in  $\text{NEt}_3/\text{DMF}$  (1/5) (5 ml) under  $\text{N}_2$ , were added  $\text{Pd}(\text{PPh}_3)_4$  (11.5 mg),  $\text{CuI}$  (3.8 mg) and **150** (49 mg, 0.1 mmol) respectively. The dark red solution was heated at 70 °C for 2.5 h. The solvent was removed with a  $\text{N}_2$  stream at this temperature within 0.5 h, the residue was purified on silica gel ( $\text{MeOH}/\text{acetone}/\text{CH}_2\text{Cl}_2$  (10/10/80, 15/10/75) and  $\text{MeOH}/\text{acetone}/\text{NEt}_3/\text{CH}_2\text{Cl}_2$  (20/10/1/69)) to give 37 mg **152** (Bt-Met(D)-Ade) as a white solid, yield 52%.  $^1\text{H}$  NMR ( $\text{CDCl}_3$ , 2 mM, rt, 600 MHz):  $\delta$  (ppm) 1.255 (m,  $\text{CH}_2$ ); 2.006 (m, 2 H,  $\text{CH}_2$ ); 2.080 (s, 3 H,  $\text{CH}_3$ ); 2.237 (m, 2 H,  $\text{CH}_2$ ); 2.378 (t, 2 H,  $J = 6.6$  Hz,  $\text{CH}_2$ ); 2.542 (m, 2 H,  $\text{CH}_2$ ); 2.751 (d, 1 H,  $J = 12.6$  Hz,  $\text{CH}_2$ ); 2.926 (dd, 1 H,  $J = 12.6$  Hz, 24.2 Hz,  $\text{CH}_2$ ); 3.108, 3.226 (m,  $\text{CH}_2$ ); 4.328 (m, 1 H, H-3 biotin); 4.528 (m, 2 H, H-4 (biotin)); 4.602 (m, 1 H, CH (methionine)); 5.361 (quartet, 2 H,  $J = 15.6$  Hz,  $\text{CH}_2$ ); 5.844 (s, 1 H, NH, Ha); 6.264 (s, 2 H,  $\text{NH}_2$ , adenine); 6.722 (s, 1 H, NH, Hb); 6.881 (t, 1 H, NH,  $\text{NHCH}_2$ ); 7.218, 7.295, 7.347 (m, 4 H, Ar); 7.564 (s, 1 H, NHCH); 7.808 (s, 1 H, CH, H-8, adenine); 8.381 (s, 1 H, CH, H-2, adenine). Calc. for  $[\text{M}]^+ \text{C}_{38}\text{H}_{54}\text{N}_9\text{O}_3\text{S}_2$ : 748.3824. Found: 748.3795.

**[3aS-(3a $\alpha$ , 4 $\beta$ (1S), 6a $\alpha$ )]-Hexahydro-2-oxo-N-[N-(10-undecynyl)-methioninamide]-1H-thieno[3,4-d]imidazole-4-pentamide (151)**



$^1\text{H}$  NMR ( $\text{CDCl}_3$ , 2 mM, rt, 300 MHz):  $\delta$  (ppm) 1.288, 1.473, 1.700, 2.001, 2.178 (m,  $\text{CH}_2$ ); 1.953 (t, 1 H,  $J = 4.8$  Hz, CCH); 2.108 (s, 3 H,  $\text{CH}_3$ ); 2.552 (m, 2 H,  $\text{CH}_2$ ); 2.766 (d, 1 H,  $J = 12.9$  Hz,  $\text{CH}_2$ ); 2.970 (dd, 1 H,  $J = 12.9$  Hz, 4.8 Hz,  $\text{CH}_2$ ); 3.199, 3.282 (m,  $\text{CH}_2$ ); 4.369 (m, 1 H, H-3 biotin); 4.549 (m, 2 H, H-4 (biotin) and CH (methionine)); 5.146 (s, 1 H, NH, Ha); 6.471 (s, 1 H, NH, Hb); 6.728 (t, 1 H, NH,  $\text{NHCH}_2$ ); 7.429 (d, 1 H,  $J = 8.4$  Hz, NHCH). Calc. for  $[\text{M} + \text{H}]^+ \text{C}_{26}\text{H}_{45}\text{N}_4\text{O}_3\text{S}_2$ : 525.2967. Found: 525.2910.

[3 $\alpha$ S-(3 $\alpha$ , 4 $\beta$ (1S), 6 $\alpha$ )]-Hexahydro-2-oxo-*N*-[*N*-(11-{1-[3-benzyl-(9-adeninyl)]}-10-undecynyl)-methioninamide]-1*H*-thieno[3, 4-*d*]imidazole-4-pentamide (**153**)



$^1\text{H}$  NMR ( $\text{CDCl}_3$ , 2 mM, rt, 600 MHz):  $\delta$  (ppm) 1.255, 1.418, 1.659 (m,  $\text{CH}_2$ ); 2.009 (m, 2 H,  $\text{CH}_2$ ); 2.082 (s, 3 H,  $\text{CH}_3$ ); 2.226 (m, 2 H,  $\text{CH}_2$ ); 2.388 (t, 2 H,  $J = 7.2$  Hz,  $\text{CH}_2$ ); 2.558 (m, 2 H,  $\text{CH}_2$ ); 2.751 (d, 1 H,  $J = 13.2$  Hz,  $\text{CH}_2$ ); 2.941 (m, 1 H,  $\text{CH}_2$ ); 3.095, 3.209 (m,  $\text{CH}_2$ ); 4.336 (m, 1 H, H-3 biotin), 4.515 (m, 2 H, H-4 (biotin)); 4.624 (m, 1 H, CH (methionine)); 5.266 (s, 1 H, NH, Ha); 5.387 (quartet, 2 H,  $J = 14.8$  Hz,  $\text{CH}_2$ ); 6.432 (s, 2 H,  $\text{NH}_2$ , adenine); 6.559 (s, 1 H, NH, Hb); 7.121 (t, 1 H, NH,  $\text{NHCH}_2$ ); 7.241, 7.284, 7.345 (m, 5 H, CH, Ar, NH,  $\text{NHCH}$ ); 7.826 (s, 1 H, CH, H-8, adenine); 8.376 (s, 1 H, CH, H-2, adenine). Calc. for  $[\text{M}]^+$   $\text{C}_{38}\text{H}_{54}\text{N}_9\text{O}_3\text{S}_2$ : 748.3824. Found: 748.3789.

#### Decarboxylation of potassium carboxyimidazolidinone

Typically, to two NMR tubes were added powder of potassium carboxyimidazolidinone (2.0 mg), 2, 4-dinitrophenol (2.0 mg) respectively. To one of the tubes was added receptor Re-pdigg (**75**) (5.0 mg). To both of the NMR tubes were added the solvent  $\text{CDCl}_3$  (1.0 ml) with internal standard TMS simultaneously. After the addition, the NMR tubes were covered with NMR lids and shaken for 10min. Then NMR spectra of the both samples were determined. The relative amount of the imidazolidinone (**155**) for each system was measured with an internal standard.

## Bibliography

1. Wood, H. G.; Kumar, G. K. *Ann. N. Y. Acad. Sci.* **1985**, *447*, 1.
2. Mahapatra, S.; Halfen, J. A.; Wilkinson, E. C.; Pan, G.; Wang, X.; Young, V. G. Jr.; Cramer, J. C.; Que, L. Jr.; Tolman, W. B. *J. Am. Chem. Soc.* **1996**, *118*, 11555.
3. Zang, Y.; Dong, Y.; Que, L. Jr.; Kauffman, K.; Munck, E. *J. Am. Chem. Soc.* **1995**, *117*, 1169.
4. Marquet, A.; Florentin, D.; Ploux, O.; Bui, B. T. S. *J. Phys. Org. Chem.* **1998**, *11*, 529.
5. Bonjour, J. -P. *Ann. N. Y. Acad. Sci.* **1985**, *447*, 97.
6. Alban, C.; Dounce, R. *Exp. Biol. Semin. Ser.* **1998**, *67*, 29.
7. Midla, L. T.; Hoblet, K. H.; Weiss, W. P.; Moeschberger, M. L. *Am. J. Vet. Res.* **1998**, *59*, 733.
8. Ezerskaya, A. V.; Maltsev, V. S. *Veterinariya (Moscow)* **1998**, *47* (CA: 129, 81071f).
9. Watanabe, T.; Fukui, T. *Food Addit. Contam.* **1998**, *15*, 619.
10. Moro, M.; Pelagi, M.; Fulci, G.; Paganelli, G.; Dellabona, P.; Casorati, G.; Siccardi, A.; Corti, A. *Cancer Res.* **1997**, *57*, 1922.
11. Wilbur, D. S.; Hamlin, D. K.; Pathare, P. M.; Weerawarna, S. A. *Bioconjug. Chem.* **1997**, *8*, 542.
12. Zhu, H.; Jain, R. K.; Baxter, L. T. *J. Nucl. Med.* **1998**, *39*, 65.
13. Samols, D.; Thornton, C. G.; Murtif, V. L.; Kumar, G. K.; Haase, F. C.; Wood, H. G. *J. Biol. Chem.* **1988**, *263*, 6461.
14. Knowles, J. R. *Ann. Rev. Biochem.* **1989**, *58*, 195.
15. Reche, P.; Li, Y.-L.; Fuller, C.; Eichhorn, K.; Perham, R. N. *Biochemistry* **1998**, *589*.
16. Champman-Smith, A.; Morris, T. W.; Wallace, J. C.; Cronan, J. E. Jr. *J. Biol. Chem.* **1999**, *274*, 1449.
17. Hoagland, M. B.; Keller, E. B.; Zamecnik, P. C. *J. Biol. Chem.* **1956**, *218*, 345.
18. Lane, M. D.; Rominger, K. L.; Young, D. L.; Lynen, F. *J. Biol. Chem.* **1962**, *239*, 2858.
19. Wilson, K. P.; Shewchuk, L. M.; Brennan, R. G.; Otsuka, A. J.; Matthews, B. W. *Proc. Natl. Acad. Sci. U. S. A.* **1992**, *89*, 9257.
20. Li, S.-L.; Cronan, J. E. Jr. *J. Biol. Chem.* **1992**, *267*, 855.
21. Yao, X.; Wei, D.; Soden, Jr. C.; Summers, M. F.; Beckett, D. *Biochemistry* **1997**, *36*, 15089.
22. Lane, D. L.; Rominger, K. L.; Young, D. L.; Lynen, F. *J. Biol. Chem.* **1964**, *239*, 2865.
23. Fall, R. R. *Methods Enzymol.* **1979**, *62*, 390.
24. Waldrop, G. L.; Rayment, I.; Holden, H. M. *Biochemistry* **1994**, *33*, 10249.
25. Athappilly, F. K.; Hendrickson, W. A. *Structure* **1995**, *3*, 1407.
26. Goodall, G. J.; Prager, R.; Wallace, J. C.; Keech, D. B. *FEBS Lett.* **1983**, *163*, 6.

27. Williams, D. H.; Westwell, M. S. *Chem. Soc. Rev.* **1998**, *27*, 57.
28. Grabowski, S. J. *Tetrahedron* **1998**, *54*, 10153.
29. Steiner, T. *J. Chem. Soc., Chem. Commun.* **1995**, 1331.
30. Gellman, S. H.; Dado, G. P.; Liang, G.-B.; Adams, B. R. *J. Am. Chem. Soc.* **1991**, *113*, 1164.
31. Dill, K. A. *Biochemistry* **1990**, *29*, 7151.
32. Diaz, E.; Galeazzi, E.; Nava, J. L.; Muchowski, J. M.; Guzman, A.; van Calsteren, M. R.; Jankowski, K. *Mag. Res. Chem.* **1995**, *33*, 581.
33. Krauthauser, S.; Christianson, L. A.; Powell, D. R.; Gellman, S. H. *J. Am. Chem. Soc.* **1997**, *119*, 11719.
34. Gardner, R. R.; Gellman, S. H. *J. Am. Chem. Soc.* **1995**, *117*, 10411.
35. Pfeifer, M. E.; Robinson, J. A. *J. Chem. Soc., Chem. Commun.* **1998**, 1977.
36. Yang, J.; Gellman, S. H. *J. Am. Chem. Soc.* **1998**, *120*, 9090.
37. Holmes, D. L.; Smith, E. M.; Nowick, J. S. *J. Am. Chem. Soc.* **1997**, *119*, 7665.
38. Hartzoulakis, B.; Rutherford, T. J.; Ryan, M. D.; Gani, D. *Tetrahedron Lett.* **1996**, *37*, 6911.
39. Griffiths-Jones, S. R.; Maynard, A. J.; Sharman, G. J.; Searle, M. S. *J. Chem. Soc., Chem. Commun.* **1998**, 789.
40. Gellman, S. H. *Acc. Chem. Res.* **1998**, *31*, 173.
41. Yavari, I.; Shaabani, A.; Soliemani, H.; Nourmohammadian, F.; Bijanzadeh, H. R. *Mag. Res. Chem.* **1996**, *34*, 1003.
42. Westley, J. *Enzyme Catalysis*, Harper and Row, New York, **1969**.
43. Boyer, P. D., Ed., *The Enzymes*, 3rd edn, Academic Press, New York, **1970**.
44. Dixon, M.; Web, E. C. *Enzymes*, Longmans, **1964**.
45. Fersht, A. *Enzyme Mechanism and Structure*, Freeman, San Francisco, **1977**.
46. Hartsuck, J. A.; Lipscombe, W. N. *The Enzymes* **1971**, *3*, 1.
47. Bender, M. L. *Mechanisms of Homogeneous Catalysis*, Wiley, New York, **1971**.
48. Hanessian, S.; Yang, H.; Schaum, R. *J. Am. Chem. Soc.* **1996**, *118*, 2507.
49. Hulst, R.; Broxterman, Q. B.; Kamphuis, J.; Formaggio, F.; Crisma, M.; Toniolo, C.; Kellogg, R. M. *Tetrahedron: Asymmetry* **1997**, *8*, 1987.
50. Prestat, G.; Marchand, A.; Lebreton, J.; Guingant, A.; Pradere, J.-P. *Tetrahedron: Asymmetry* **1998**, *9*, 197.
51. Freitag, S.; LeTrong, I.; Klumb, L.; Stayton, P.; Stenkamp, R. E. *Protein Science* **1997**, *6*, 1157.
52. Falzone, C. J.; Wright, P. E.; Benkovic, S. J. *Biochemistry* **1994**, *33*, 439.
53. Bibbius, K. B.; Boeuf, H.; Varmus, H. E. *Mol. Cell Biol.* **1993**, *13*, 7278.
54. Crisp, G. T.; Gore, J. *Tetrahedron* **1997**, *53*, 1523.
55. Hampson, I. N.; Hampson, L.; Dexter, T. M. *Nucleic Acid Res.* **1996**, *24*, 4832.
56. Loew, R.; Rausch, T. *BioMethods (Basel)* **1996**, *7*, 201.



57. Dumas, S.; Horellou, P.; Helin, C.; Mallet, J. *J. Chem. Neuroanat.* **1992**, *5*, 11.
58. Blow, D. M. *Acc. Chem. Res.* **1976**, *9*, 145.
59. Kraut, J. *Science (Washington DC)*, **1988**, *242*, 533.
60. Frey, P. A. *Science* **1995**, *269*, 104.
61. Frey, P. A.; Tobin, J. B.; Whitt, S. A. *Science* **1994**, *164*, 1887.
62. Cassidy, C. S.; Lin, J.; Frey, P. A. *Biochemistry* **1997**, *36*, 4576.
63. Neuvonen, H.; Neuvonen, K. *J. Chem. Soc., Perkin Trans. 2* **1998**, 1665.
64. Philips, D. C. *Scientific American*, **1986**.
65. Blake, C. C. F.; Johnson, L. N.; Mair, G. A.; Orth, A. C. T.; Philips, D. E.; Sorma, V. R. *Proc. Roy. Soc. B* **1967**, *167*, 378.
66. Vernon, C. A. *Proc. Roy. Soc. B.* **1967**, *167*, 389.
67. Lipscomb, W. N. *Tetrahedron* **1974**, *30*, 1725.
68. Lipscomb, W. N. *Proc. Nat. Acad. Sci.* **1973**, *70*, 3797.
69. Deavin, A.; Mathias, A. P.; Rabin, B. R. *Biochem. J.* **1966**, *101*, 146.
70. Kato, T.; Takeuchi, T.; Karube, I. *J. Chem. Soc., Chem. Commun.* **1996**, 953.
71. Thoden, J. B.; Holden, H. M.; Wesenberg, G.; Raushel, F. M.; Rayment, I. *Biochemistry* **1987**, *26*, 6305.
72. Post, L. E.; Post, D. J.; Raushel, F. M. *J. Biol. Chem.* **1989**, *265*, 9942.
73. Hibi, T.; Nishioka, T.; Kato, H.; Tanizawa, K.; Fukui, T.; Katsube, Y.; Oda, J. *Nat. Struct. Biol.* **1996**, *3*, 16.
74. Nishizawa, S.; Buhlmann, P.; Iwao, M.; Umezawa, Y. *Tetrahedron Lett.* **1995**, *36*, 6483.
75. Kluger, R.; Tsao, B. *J. Am. Chem. Soc.* **1993**, *115*, 2089.
76. Rahil, J.; You, S.; Kluger, R. *J. Am. Chem. Soc.* **1996**, *118*, 12495.
77. Yeo, W.-S.; Hong, J.-I. *Tetrahedron Lett.* **1998**, *39*, 3769.
78. Rana, V. S. et al. *J. Org. Chem.* **1996**, *61*, 3578.
79. Kuroda, Y.; Lintuluoto, J. M.; Ogoshi, H. *J. Chem. Soc., Perkin Trans. 2* **1997**, 333.
80. Weber, P. C.; Ohlendorf, D. H.; Wendoloski, J. J.; Salemme, F. R. *Science* **1989**, *243*, 85.
81. Livnah, O.; Bayer, E. A.; Wilchek, M.; Sussman, J. L. *Proc. Natl. Acad. Sci. U. S. A.* **1993**, *90*, 5076.
82. Artymiuk, P. J.; Poirrette, A. R.; Rice, D. W.; Willett, P. *Nat. Struct. Biol.* **1996**, *3*, 128.
83. Prasadarao, N. V.; Wass, C. A.; Stins, M. F.; Shimada, H.; Kim, K. S. *Infect. Immun.* **1999**, *67*, 5775.
84. Nomoto, K.; Yokokura, T.; Tomita, N. *Biosci. Microflora.* **1998**, *17*, 115.
85. Kaser, M. R.; Skouteris, G. G. *Peptides (N. Y.)* **1997**, *18*, 1441.
86. DeTitta, G. T.; Edmonds, J. W.; Stallings, W.; Donohue, J. *J. Am. Chem. Soc.* **1976**, *98*, 1920.
87. Fry, D. C.; Fox, T. L.; Lane, M. D.; Mildvan, A. S. *J. Am. Chem. Soc.* **1985**, *107*, 7659.
88. Tonan, K.; Adachi, K.; Ikawa, S. *Spectrochim. Acta Part A* **1998**, *54*, 989.

89. Reddy, D. V.; Shenoy, B. C.; Carey, P. R.; Sonnichsen, F. D. *Biochemistry* **1997**, *36*, 14676.
90. Musashi, Y.; Hamada, T.; Sakaki, S. *J. Am. Chem. Soc.* **1995**, *117*, 11320.
91. DeTitta, G. T.; Blessing, R. H.; Moss, G. R.; King, H. F.; Sukumaran, D. K.; Roskwitalski, R. L. *J. Am. Chem. Soc.* **1994**, *116*, 6485.
92. Guchhait, R. B.; Polakis, S. E.; Hollis, D.; Fenselau, C.; Lae, M. D. *J. Biol. Chem.* **1974**, *249*, 6646.
93. Islam, I.; Ng, K.; Chong, K. T.; McQuade, T. J.; Hui, J. O.; Wilkinson, K. F.; Rush, B. D.; Ruwart, M. J.; Borchardt, R. T.; Fisher, J. F. *J. Med. Chem.* **1994**, *37*, 293.
94. Knappe, J.; Ringelmann, E.; Lynen, F. *Biochem. Z.* **1961**, *335*, 168.
95. Fry, D. C.; Fox, T.; Lane, M. D.; Dilavan, A. S. *Ann. N. Y. Acad. Sci.* **1985**, *447*, 140.
96. Dado, G. P.; Gellman, S. H. *J. Am. Chem. Soc.* **1993**, *115*, 4228.
97. Tsang, K. Y.; Diaz, H.; Graciani, N.; Kelly, J. W. *J. Am. Chem. Soc.* **1994**, *116*, 3988.
98. Sawada, M.; Takai, Y.; Yamada, H.; Hyrayama, S.; Kaneda, T.; Tanaka, T.; Kamada, K.; Sasaki, S.; Nakashima, S.; Nagatsugi, F.; Tanaka, Y.; Hisatome, M.; Maeda, M. *Tetrahedron Lett.* **1995**, *36*, 9521.
99. Schiner, P. D.; Klassen, J. S.; Strittmatter, E. F.; Williams, E. R. *J. Am. Chem. Soc.* **1998**, *120*, 9605.
100. Leiserowitz, L. *Acta Cryst.* **1976**, *B32*, 775.
101. Turi, L.; Dannenburg, J. J. *J. Am. Chem. Soc.* **1994**, *116*, 8714.
102. Holtzberg, F.; Post, B.; Fankuchen, I. *Acta Cryst.* **1953**, *6*, 127.
103. Johnson, J. F.; Cole, R. H. *J. Am. Chem. Soc.* **1951**, *73*, 4536.
104. Tominaga, M.; Konishi, K.; Aida, T. *J. Am. Chem. Soc.* **1999**, *121*, 7704.
105. Camarero, J. A.; Pavel, J.; Muir, T. W. *Angew. Chem. Int. Ed.* **1998**, *37*, 347.
106. Mammen, M.; Choi, S.-K.; Whitesides, G. M. *Angew. Chem. Int. Ed.* **1998**, *37*, 2754.
107. Hanessian, S.; Gomtsyan, A.; Simard, M.; Roelens, S. *J. Am. Chem. Soc.* **1994**, *116*, 4495.
108. Mildvan, A. S.; Scrutton, M. C.; Utter, M. F. *J. Biol. Chem.* **1966**, *241*, 3488.
109. Retey, J.; Lynen, F. *Biochemistry* **1965**, *342*, 256.
110. Rose, I. A.; O'Connell, E. L.; Solonon, F. *J. Biol. Chem.* **1976**, *251*, 902.
111. Haberfield, P.; Cincotta, J. J. *J. Org. Chem.* **1990**, *55*, 1334.
112. Higuchi, K.; Yamashina, T.; Ishikawa, K.; Hirata, H. *Yukagaku* **1987**, *36*, 16 (CA 107: 197844k).
113. Ingersoll, A. W. *Org. Syn. Col. Vol. II* **1944**, 503.
114. Patel, R. P.; Price, S. *J. Org. Chem.* **1965**, *30*, 3575.
115. Kumar, G. A.; McAllister, M. A. *J. Org. Chem.* **1998**, *63*, 6968.
116. Wallet, J.-C.; Molins, E.; Miraultlles, C. *J. Phy. Org. Chem.* **1998**, *11*, 751.
117. Nassar, A. M. G.; Abou-Ali, S. A. *J. Chin. Chem. Soc.* **1985**, *32*, 467.

118. Lesniewski, B.; Przybyszewski, B.; Pawlak, Z. *J. Chem. Soc., Faraday Trans. 1* **1986**, 80(7), 1769.
119. Pife, T. H. *Bioorganic Chemistry*, Van Tamelen, E. E., Ed., Academic Press, New York, **1978**, Vol I, pp 93-116.
120. Page, M. I.; Williams, A. *Enzyme Mechanisms*, Pressed by The Royal Society of Chemistry; London, **1987**, pp159.
121. Menger, F. M.; Smith, J. H. *J. Am. Chem. Soc.* **1972**, 94, 3824.
122. Castro, E.; Ureta, C. *J. Org. Chem.* **1990**, 55, 1676.
123. Hirata, H.; Nakasato, S. *Yukagaku* **1986**, 35, 438 (CA 107: 7538t).
124. Hirata, H.; Takao, Y.; Higuchi, K. *Yukagaku* **1991**, 40, 406 (CA 115: 66995c).
125. Adalsteinsson, H. A.; Bruice, T. C. *J. Am. Chem. Soc.* **1998**, 120, 3440.
126. Mizutani, T.; Takagi, H.; Ueno, Y.; Horiguchi, T.; Yamamura, K.; Ogoshi, H. *J. Phy. Org. Chem.* **1998**, 11, 737.
127. Menger, F. M.; Smith, J. H. *Tetrahedron Lett.* **1970**, 48, 4163.
128. Caminati, W.; Moreschini, P.; Rossi, I.; Favero, P. G. *J. Am. Chem. Soc.* **1998**, 120, 11144.
129. Dugas, H.; Penney, C. *Bioorganic Chemistry*, Springer-Verlag; New York, **1981**.
130. Retey, J.; Robinson, J. A. *Stereospecificity in Organic Chemistry*, Verlag Chemie; Weinheim, **1982**.
131. Wong, C-H.; Whitesides, G. M. *Enzymes in Synthetic Organic Chemistry*, Elsevier Science Ltd.; Oxford, **1994**.
132. Jones, J. *Asymmetric Synthesis*, Morrison, J. D. Ed. Academic Press; New York, **1985**, 5, 309.
133. Mattson, A.; Orrenius, C.; Ohrner, N.; Unelius, C. R.; Hult, K.; Norin, T. *Acta Chem. Scand.* **1996**, 50, 918.
134. Julia, S.; Masana, J.; Vega, J. C. *Angew. Chem. Int. Ed.* **1980**, 19, 929.
135. Julia, S.; Guixer, J.; Masana, J.; Rocas, J.; Colonna, S.; Annuziata, R.; Molinari, H. *J. Chem. Soc., Perkin Trans. 1* **1982**, 1317.
136. Colonna, S.; Molinari, H.; Banfi, S.; Julia, S.; Masana, J.; Alvarez, A. *Tetrahedron* **1983**, 39, 1635.
137. Budt, K. -H.; Vatele, J. M.; Kishi, Y. *J. Am. Chem. Soc.* **1986**, 108, 6080.
138. Lasterra-Sanchez, M. E.; Roberts, S. M. *J. Chem. Soc., Perkin Trans. 1* **1995**, 1467.
139. Lasterra-Sanchez, M. E.; Felter, M. E.; Mayan, U.; Roberts, S. M.; Thornton, S. R.; Todd, C. J. *J. Chem. Soc., Perkin Trans. 1* **1996**, 343.
140. Miyazawa, T.; Higashi, K.; Otomatsu, T.; Yamada, T.; Kuwata, S. *Chem. Express* **1990**, 5, 77.
141. Miyazawa, T.; Yamada, T.; Kuwata, S. *Chem. Express* **1991**, 6, 173.
142. Jeong, T. M.; Park, K. H. *Taehan Huahakhoe Chi* **1988**, 32, 588 (CA 111: 154326h)

143. Drabowicz, J.; Dudzinski, B.; Mikolajczyk, M.; Colonna, S.; Gaggero, N. *Tetrahedron: Asymmetry* **1997**, *8*, 2267.
144. Tait, A.; Colorini, E.; Bella, M. D. *Tetrahedron: Asymmetry* **1997**, *8*, 2199.
145. Molander, G. A.; Bobbitt, K. L. *J. Am. Chem. Soc.* **1993**, *115*, 7517.
146. Tamai, Y.; Koike, S.; Ogura, A.; Miyano, S. *J. Chem. Soc., Chem. Commun.* **1991**, 798.
147. Denmark, S. E.; Marble, L. K. *J. Org. Chem.* **1990**, *55*, 411.
148. Magnus, N.; Magnus, P. *Tetrahedron Lett.* **1997**, *38*, 3491.
149. Thomas, E. J. *J. Chem. Soc., Chem. Commun.* **1997**, 411.
150. Nordstrom, K.; Moberg, C. *Tetrahedron Lett.* **1994**, *35*, 7267.
151. Carey, J. S.; Thomas, E. T. *J. Chem. Soc., Chem. Commun.* **1994**, 283.
152. Stanway, S. J.; Thomas, E. T. *Tetrahedron Lett.* **1995**, *36*, 3417.
153. Evans, D. A.; Coleman, P. J.; Cote, B. *J. Org. Chem.* **1997**, *62*, 788.
154. Gruttadauria, M.; Thomas, E. J. *J. Chem. Soc., Perkin Trans. I* **1995**, 1469.
155. Bartok, M.; Felfoldi, K.; Torok, B.; Bartok, T. *J. Chem. Soc., Chem. Commun.* **1998**, 2605.
156. Heaton, N. J.; Bello, P.; Herrondon, B.; Campo, A. del; Jimenez-Barbero, J. *J. Am. Chem. Soc.* **1998**, *120*, 12371.
157. Li, Z. -H.; Bulychev, A.; Kotra, L. P.; Massova, I.; Mobashery, S. *J. Am. Chem. Soc.* **1998**, *120*, 13003.
158. Artymiuk, P. J.; Rice, D. W.; Poirrette, A. R.; Willett, P. *Nat. Struct. Biol.* **1994**, *1*, 760.
159. Curran, T. P.; Chandler, N. M.; Kennedy, R. J.; Keaney, M. T. *Tetrahedron Lett.* **1996**, *37*, 1933.
160. Kessler, H. *Angew. Chem., Int. Ed. Engl.* **1982**, *21*, 2177.
161. Stevens, E. S.; Sugawara, N.; Bonora, G. M.; Toniolo, C. *J. Am. Chem. Soc.* **1980**, *102*, 7048.
162. Wunningham, M. J.; Sogah, D. Y. *J. Am. Chem. Soc.* **1994**, *116*, 11173.
163. Gerlt, J. A.; Gassman, P. G. *J. Am. Chem. Soc.* **1993**, *115*, 11552.
164. Clark, P. L.; Liu, Z. -P.; Rizo, J.; Gierasch, L. M. *Nature Struct. Biol.* **1997**, *4*, 886.
165. Smith, S. O.; Smith, C. S.; Bormann *Nature Struct. Biol.* **1996**, *3*, 252.
166. Shenoy, B. C.; Xie, Y.; Park, V. L.; Kumar, G. K.; Beegen, H.; Wood, H. G.; Samols, D. *J. Biol. Chem.* **1992**, *267*, 18407.
167. Green, N. M. Avidin. In *Advances in Protein Chemistry*, edited by Anfinsen, C. B.; Edsall, J. T.; Richards, F. M. pp. 85-133. New York: Academic Press, **1975**.
168. Green, N. M. *Biochem. J.* **1963**, *89*, 585.
169. Morpurgo, M.; Hofstetter, H.; Bayer, E. A.; Wilchek, M. *J. Am. Chem. Soc.* **1998**, *120*, 12734.
170. Bateman, W. G. *J. Biol. Chem.* **1916**, *26*, 263.
171. McCormick, D. B. *Nutr. Rev.* **1975**, *33*, 97.
172. Gelb, M. H.; Heimbrook, D. C.; Sligar, S. G. *Biochemistry* **1982**, *21*, 370.
173. Groves, J. T.; Viski, P. *J. Am. Chem. Soc.* **1989**, *111*, 8537.

174. Shaphiro, S.; Piper, J. V.; Capspi, E. *J. Am. Chem. Soc.* **1982**, *104*, 2301.
175. Wackett, L. P.; Kwart, L. D.; Gibson, D. T. *Biochemistry* **1988**, *27*, 1360.
176. Boyd, D. R.; Sharma, N. D.; Stevenson, P. J.; Chima, J.; Dalton, H. *Tetrahedron Lett.* **1991**, *32*, 3887.
177. Boyd, D. R.; Sharma, N. D.; Bowers, N. I.; Goodrich, P. A.; Groocock, M. R.; Blacker, A. J.; Clarke, D. A.; Howard, T.; Dalton, H. *Tetrahedron: Asymmetry* **1996**, *7*, 1559.
178. Herichs, P. M.; Rodger, C. A.; Caulfield, T.; Guo, P. *Mag. Res. Chem.* **1995**, *33*, 905.
179. Clayden, J.; Darbyshire, M.; Pink, J. H.; Westlund, N.; Wilson, F. X. *Tetrahedron Lett.* **1997**, *38*, 8587.
180. Alvarez-Ibarra, C.; Arias-Perez, M. S.; de Andres, A.; Balcazar, J. L. *Mag. Res. Chem.* **1986**, *24*, 568.
181. Hoye, T. R.; Koltun, D. O. *J. Am. Chem. Soc.* **1998**, *120*, 4638.
182. Orme-Johnson, N. R.; Light, D. R.; White-Stevens, R. W.; Orme-Johnson, W. H. *J. Biol. Chem.* **1979**, *254*, 2103.
183. Nakajin, S.; Shinoda, M.; Haniu, M.; Shively, J. E.; Hall, P. F. *J. Biol. Chem.* **1984**, *259*, 3971.
184. Peters, P.; Peters, J. *J. Mol. Struct.* **1980**, *68*, 255.
185. Eisenberg, M. A. *Ann. N. Y. Acad. Sci.* **1985**, *447*, 335.
186. Cronan, J. E. *Cell* **1989**, *58*, 427.
187. Barker, D. F.; Campbell, A. M. *J. Biol. Chem.* **1982**, *257*, 15167.
188. Howard, P. K.; Shaw, J.; Osuka, A. J. *Gene* **1985**, *35*, 321.
189. Prakash, O.; Eisenberg, M. A. *Proc. Natl. Acad. Sci. U. S. A.* **1979**, *76*, 5592.
190. Cronan, J. E. *J. Biol. Chem.* **1986**, *263*, 10332.
191. Mrksich, M.; Dervan, P. B. *J. Am. Chem. Soc.* **1995**, *117*, 3325.
192. Agback, P.; Baumann, H.; Knapp, S.; Ladenstein, R.; Hard, T. *Nat. Struct. Biol.* **1998**, *5*, 579.
193. Huc, I.; Rebek, Jr. J. *Tetrahedron Lett.* **1994**, *35*, 1035.
194. Lonergan, D. G.; Deslongchamps, G. *Tetrahedron* **1998**, *54*, 14041.
195. Crisp, G. T.; Jiang, Y.-L. *Tetrahedron* **1999**, *55*, 549.
196. Nowick, J. S.; Pairish, M.; Lee, I. Q.; Holmes, D. L.; Ziller, J. W. *J. Am. Chem. Soc.* **1997**, *119*, 5413.
197. Zushi, S.; Kodama, Y.; Nishihata, K.; Umemura, K.; Nishio, M.; Uzawa, J.; Hirota, M. *Bull. Chem. Soc. Jpn.* **1980**, *53*, 3631.
198. Dunham, S. U.; Dunham, S. U.; Turner, C. J.; Lippard, S. J. *J. Am. Chem. Soc.* **1998**, *120*, 5395.
199. Weber, D. C.; Wendoloski, J. J.; Pantoliano, M. W.; Salemme, F. R. *J. Am. Chem. Soc.* **1992**, *114*, 3179.
200. Bhat, B.; Neelima; Leonard, N. J.; Robinson, H.; Wang, H. -J. *J. Am. Chem. Soc.* **1996**, *118*, 3065.

201. Mink, D.; Deslongchamps, G. *Tetrahedron Lett.* **1996**, *37*, 7035.
202. Conn, M. M.; Deslongchamps, G.; Mendoza, J. de; Rebek, Jr. J. *J. Am. Chem. Soc.* **1993**, *115*, 3548.
203. Amosova, O.; George, J.; Fresco, J. R. *Nucleic Acids Res.* **1997**, *25*, 1930.
204. Rothman, J. H.; Richards, W. G. *J. Chem. Soc., Chem. Commun.* **1995**, 1589.
205. Strobel, S. A.; Doucette-Stamm, L. A.; Riba, L.; Housman, D. E.; Dervan, P. B. *Science* **1991**, *254*, 1639.
206. Zimmerman, S. C.; Schmitt, P. *J. Am. Chem. Soc.* **1995**, *117*, 10769.
207. Rana, V. S.; Ganesh, K. N. *Nucleic Acids Res.* **2000**, *28*, 1162.
208. Czernecki, S.; Hoang, A.; Valery, J.-M. *Tetrahedron Lett.* **1996**, *37*, 8857.
209. Hunter, C. A.; Sanders, J. K. M. *J. Am. Chem. Soc.* **1990**, *112*, 5525.
210. Hildbrand, S.; Blaser, A.; Parel, S. P.; Leumann, C. J. *J. Am. Chem. Soc.* **1997**, *119*, 5499.
211. Durand, M.; Thuong, N. T.; Maurizot, J. C. *J. Biol. Chem.* **1992**, *267*, 24394.
212. Umemoto, K.; Sarma, M. H.; Gupta, G.; Luo, J.; Sarma, R. H. *J. Am. Chem. Soc.* **1990**, *112*, 4539.
213. Kessler, D. J.; Pettitt, B. M.; Cheng, Y.-K.; Smith, S. R.; Jayaraman, K.; Vu, H. M.; Hogan, M. E. *Nucleic Acids Res.* **1993**, *21*, 4810.
214. Zhou-Sun, B.; Sun, J.; Gryaznov, S. M.; Liquier, J.; Garestier, T.; Helene, C.; Taillandier, E. *Nucleic Acids Res.* **1997**, *25*, 1782.
215. Cheng, Y.-K.; Pettitt, B. M. *J. Am. Chem. Soc.* **1992**, *114*, 4465.
216. Wilson, C. C.; Tollin, P. *Acta Cryst.* **1986**, *C42*, 697.
217. Mande, S.; Lalitha, H. N.; Rakakumar, S.; Viswamitra, M. A. *Nucleosides & Nucleotides* **1992**, *11*, 1089.
218. Kohwi, Y.; Kohwi-Shigematsu, T. *Proc. Nat. Acad. Sci. U. S. A.* **1988**, *85*, 3881.
219. Chaudhuri, N. C.; Kool, E. T. *J. Am. Chem. Soc.* **1995**, *117*, 10434.
220. Lyon, P. A.; Reese, C. B. *J. Chem. Soc., Perkin Trans. 1* **1974**, 2645.
221. Crisp, G. T.; Jiang, Y.-L.; Pullman, P.; De Sari, C. *Tetrahedron* **1997**, *53*, 17489.
222. Cozzi, F.; Cinquini, M.; Annuziata, R.; Siegel, J. S. *J. Am. Chem. Soc.* **1993**, *115*, 5330.
223. Jorgensen, W. L.; Severance, D. L. *J. Am. Chem. Soc.* **1990**, *112*, 4768.
224. Green, N. M. *Adv. Protein Chem.* **1975**, *29*, 84.
225. de la Mare *Pure, Appl. Chem.* **1984**, *56*, 1755.
226. Pouchert, C. J.; Behnke, J. *The Aldrich Library of <sup>13</sup>C and <sup>1</sup>H FT NMR spectra.*, Ed. Vol. 1 p472 and 481. Pressed by Aldrich Chemical Company Inc, **1993**.
227. Izquierdo, M. C.; Stein, R. L. *J. Am. Chem. Soc.* **1990**, *112*, 6054.
228. Schall, O. F.; Gokel, G. W. *J. Org. Chem.* **1996**, *61*, 1449.
229. Appella, D. H.; Christianson, L. A.; Klein, D. A.; Powell, D. R.; Huang, X.; Barchi, J. J.; Gellman, S. H. *Nature* **1997**, *387*, 381.
230. Seebach, D.; Ciceri, P. E.; Overhand, M.; Jaun, B.; Rigo, D.; Oberer, L.; Hommel, U.;

- Seela, F.; Debelak, H.; Reuter, H.; Kastner, G.; Mikhailopulo, I. A. *Tetrahedron* **1999**, *55*, 1295.
231. Herman, D. M.; Baird, E. E.; Dervan, P. B. *J. Am. Chem. Soc.* **1998**, *120*, 1382.
232. Parks, M. E.; Baird, E. E.; Dervan, P. B. *J. Am. Chem. Soc.* **1996**, *118*, 6147.
233. Travins, J. M.; Etkorn, F. A. *J. Org. Chem.* **1997**, *62*, 8387.
234. Frankel, D. A.; O'Brien, D. F. *J. Am. Chem. Soc.* **1994**, *116*, 10058.
235. Rowan, A. E.; Nolte, R. J. M. *Angew. Chem. Int. Ed. Engl.* **1998**, *37*, 63.
236. Hanabusa, K.; Yamada, M.; Kimura, M.; Shirai, H. *Angew. Chem. Int. Ed. Engl.* **1996**, *35*, 1949.255.
237. Sommerdijk, N. A. J. M.; Buynsters, P. J. A. A.; Pistorius, A. M. A.; Wang, M.; Feiters, M. C.; Nolte, R. J. M.; Zwanenburg, B. *J. Chem. Soc., Chem Commun.* **1994**, 1941.
238. Lovinger, A. J.; Nuckolls, C.; Katz, T. J. *J. Am. Chem. Soc.* **1998**, *120*, 264.
239. Clark, T. D.; Buehler, L. K.; Ghadiri, M. R. *J. Am. Chem. Soc.* **1998**, *120*, 651.
240. Palasin, S.; Chin, D. N.; Simanek, E. E.; MacDonald, J. C.; Whitesides, G. M.; McBride, M. T.; Palmore, G. T. R. *J. Am. Chem. Soc.* **1997**, *119*, 11807.
241. Adams, H.; Carver, F. J.; Hunter, C. A.; Morales, J. C.; Seward, E. M. *Angew. Chem. Int. Ed. Engl.* **1996**, *35*, 1542.
242. Liao, R. -F.; Lauher, J. W.; Fowler, F. W. *Tetrahedron* **1996**, *52*, 3153.
243. Chaney, J. D.; Goss, C. R.; Folting, K.; Santarsiero, B. D.; Hollingsworth, M. D. *J. Am. Chem. Soc.* **1996**, *118*, 9432.
244. Smith, E. M.; Holmes, D. L.; Shaka, H. A. J.; Nowick, J. S. *J. Org. Chem.* **1997**, *62*, 7906.
245. Bausch, M. J.; David, B.; Dobrowolski, P.; Guadalupe-Fasano, C.; Gostowski, R.; Selmarten, D.; Prasad, V.; Vaughn, A.; Wang, L.-H. *J. Org. Chem.* **1991**, *56*, 5643.
246. Bordwell, F. G.; Fried, H. E.; Hughes, D. L.; Lynch, T.-Y.; Satish, A. V.; Whang, Y. E. *J. Org. Chem.* **1990**, *55*, 3330.
247. Kopple, K. D.; Ohnishi, M.; Go, A. *J. Am. Chem. Soc.* **1969**, *91*, 4246.
248. Rose, G. D.; Gierasch, L. M.; Smith, J. A. *Adv. Protein Chem.* **1985**, *37*, 1.
249. Curm, T. P.; Chanddler, N. M.; Kennedy, R. J.; Keaney, M. T. *Tetrahedron* **1996**, *52*, 1933.
250. Iwahashi, H.; Kyogoku, Y. *J. Am. Chem. Soc.* **1977**, *99*, 7761.
251. Platts, J. A.; Howard, S. T.; Wozniak, K. *J. Chem. Soc., Chem. Commun.* **1996**, 63.
252. Derewenda, Z. S.; Lee, L.; Derewenda, U. *J. Mol. Biol.* **1995**, *252*, 248.
253. Martinez-Martinez, E. J.; Padilla-Martinez, I. I.; Brito, M. A.; Geniz, E. D.; Rojas, R. C.; Saavedra, J. B. R.; Hopfl, H.; Tlahuextl, M.; Contreras, R. *J. Chem. Soc., Perkin Trans. 2* **1998**, 401.
254. Kohmoto, S.; Koyano, I.; Kawatsuji, T.; Kasimuru, H.; Kishikawa, K.; Yamamoto, M.; Yamada, K. *Bull. Chem. Soc. Jpn.* **1996**, *69*, 3261.

255. Flory, P. J. *Conformation of Biopolymers* Ed. Ramachandran, G. N. Academic Press, New York, **1967**.
256. Gallo, E. A.; Gellman, S. H. *J. Am. Chem. Soc.* **1993**, *115*, 9774.
257. Crisp, G. T.; Jiang, Y.-L.; Tiekink, E. R. T. *Acta Cryst.* **1998**, *C54*, 436.
258. Crisp, G. T.; Jiang, Y.-L.; Tiekink, E. R. T. *Z. Kristallogr.* **1998**, *213*, 389.
259. Crisp, G. T.; Jiang, Y.-L.; Tiekink, E. R. T. *Z. Kristallogr.* **1998**, *213*, 41.
260. Baxter, N. J.; Williamson, M. P.; Lilley, T. H.; Haslam, E. *J. Chem. Soc., Faraday Trans. 1* **1996**, *92*, 231.
261. Prat, F.; Houk, K. N.; Foote, C. S. *J. Am. Chem. Soc.* **1998**, *120*, 845.
262. Aradi, F. *Mag. Res. Chem.* **1990**, *28*, 1040.
263. Kessler, H. *Angew. Chem. Int. Ed. Engl.* **1982**, 512.
264. Weast, R. C.; Astle, M. J.; Beyer, W. H. *CRC Handbook of Chemistry and Physics*, 64th ed CRC press Inc.: Florida **1988**.
265. Sawada, M.; Takai, Y.; Yamada, H.; Hirayama, S.; Kaneda, T.; Tanaka, T.; Kamada, K.; Mizooku, T.; Takeuchi, S.; Ueno, K.; Hirose, K.; Tobe, Y.; Naemura, K. *J. Am. Chem. Soc.* **1995**, *117*, 7726.
266. Liu-Gonzalez, M.; Sanz-Ruiz, F.; Gonzalez-Rosende, M. E.; Lozano-Lucia, O.; Zaballo-Garcia, E.; Sepulveda-Arques, J. *Acta Cryst.* **1997**, *C53*, 490.
267. Heroux, A.; Brisse, F. *Acta Cryst.* **1997**, *C53*, 1318.
268. Ray, J. K.; Mahato, T. K.; Chinnakali, K.; Fun, H. -K. *Acta Cryst.* **1997**, *C53*, 1621.
269. Stivers, J. T.; Pankiewicz, K. W.; Watanabe, K. *Biochemistry* **1999**, *38*, 952.
270. Zimmerman, S. C.; Wu, W.; Zeng, Z. *J. Am. Chem. Soc.* **1991**, *113*, 196.
271. Williams, K.; Askew, B.; Ballester, P.; Buhr, C.; Jeong, K. S.; Rebek, Jr. J. *J. Am. Chem. Soc.* **1989**, *111*, 1090.
272. Chen, C.-T.; Siegel, J. S. *J. Am. Chem. Soc.* **1994**, *116*, 5959.
273. Lonergan, D. G.; Riego, J.; Deslongchamps, G. *Tetrahedron Lett.* **1996**, *37*, 6109.
274. Lonergan, D. G.; Riego, J.; Deslongchamps, G.; Tomas, S. *Tetrahedron Lett.* **1998**, *39*, 7861.
275. Liu, Q.; Burton, D. J. *Tetrahedron Lett.* **1997**, *38*, 4371.
276. Bisson, A. P.; Hunter, C. A.; Morales, J. C.; Young, K. *Chem. Eur. J.* **1998**, *4*, 845.
277. Rao, P.; Ghosh, S.; Maitra, U. *J. Phy. Chem. B* **1999**, *103*, 4528.
278. Kennan, A.; Whitlock, H. W. *J. Am. Chem. Soc.* **1996**, *118*, 3027.
279. Mori, K.; Murai, O.; Hashimoto, S.; Nakamura, Y. *Tetrahedron Lett.* **1996**, *37*, 8523.
280. Gao, D.; Pan, Y.-K. *J. Org. Chem.* **1999**, *64*, 1151.
281. Kazuta, Y.; Tokunaga, E.; Aramaki, E.; Kondo, H. *FEBS Lett.* **1998**, *427*, 377.
282. Scheiner-Bobis, G.; Schreiber, S. *Biochemistry* **1999**, *38*, 9198.
283. Bach, R. D.; Canea, C.; Glukhovtsev, M. N. *J. Am. Chem. Soc.* **1999**, *121*, 6542.
284. Caplow, M.; Yager, M. *J. Am. Chem. Soc.* **1967**, *89*, 4513 (CA, 75: 48977a).
285. Tipton, P. A.; Cleland, W. W. *J. Am. Chem. Soc.* **1988**, *110*, 5866.



286. Crisp, G. T.; Jiang, Y.-L.; Tiekink, E. R. T. *Z. Kristallogr.* **2000**, *215*, 85.
287. Soave, R.; Roversi, P.; Destro, R. *Acta Cryst.* **1997**, *C53*, 933.
288. Merino, P.; Merchán, F. L.; Teiero, T.; Lanaspá, A. *Acta Cryst.* **1996**, *C52*, 2536.
289. Bocelli, G.; Cantoni, A. *Acta Cryst.* **1995**, *C51*, 993.
290. Kapon, M.; Reisner, G. M. *Acta Cryst.* **1989**, *C45*, 780.
291. Thatcher, G. R. J.; Poirier, R.; Kluger, R. *J. Am. Chem. Soc.* **1986**, *108*, 2699.
292. Chen, C.-S.; Parthasarathy, R.; DeTitta, G. T. *J. Am. Chem. Soc.* **1976**, *98*, 4983.
293. Suarez, C.; Tafazzoli, M.; True, N. S.; Gerrard, S. *J. Phy. Chem.* **1995**, *99*, 8170.
294. Clarkson, J.; Carey, P. R. *J. Phys. Chem.* **1999**, *103*, 2851.
295. Ogita, T.; Knowels, J. R. *Biochemistry* **1988**, *27*, 8028.
296. Kondo, H.; Shiratsuchi, K.; Yoshimoto, T.; Masuda, T.; Kitazono, A.; Tsuru, D.; Anai, M.; Sekiguchi, M.; Tanabe, T. *Proc. Natl. Acad. Sci. U. S. A.* **1991**, *88*, 9730.
297. Sauers, C. K.; Jencks, W. P.; Groh, S. *J. Am. Chem. Soc.* **1975**, *97*, 5546.
298. Stubbe, I. A.; O'Connell, E. L.; Solomon, F. *J. Biol. Chem.* **1977**, *251*, 8338.
299. Stubbe, J.; Fish, S.; Abeles, R. H. *J. Biol. Chem.* **1980**, *255*, 236.
300. Perrin, D. D.; Armerego, W. L. F., Eds.; *Purification of Laboratory Chemicals*, 3rd ed.; Pergamon Press plc: Oxford, **1988**.
301. Crisp, G. T.; Gore, J. *Synth. Commun.* **1997**, *27*, 2203.
302. Nowick, J. S.; Cao, T.; Noronha, G. *J. Am. Chem. Soc.* **1994**, *116*, 3285.
303. Inouye, M.; Miyake, T.; Furusyo, M.; Nakazumi, H. *J. Am. Chem. Soc.* **1995**, *117*, 12416.
304. Shinkai, I.; Zwan, M. C. V.; Harter, F. W.; Reamer, R. A.; Tull, R. J.; Weinstock, L. M. *J. Heterocyclic Chem.* **1981**, *18*, 197.
305. Weinstock, L. M.; Tull, R. J.; Douglas, A. W.; Shinkai, I. *J. Org. Chem.* **1980**, *45*, 5419.
306. Higashijima, T.; Tasumi, M.; Miyazawa, T.; Miyoshi, M. *Eur. J. Biochem.* **1978**, *89*, 543.
307. Zhang, X.; Takegoshi, K.; Hikichi, K. *Macromolecules* **1991**, *24*, 5756.